ABSTRACT

FACULTY OF ENGINEERING AND APPLIED SCIENCE

AERONAUTICS AND ASTRONAUTICS

Doctor of Philosophy

IMPROVED WIND TUNNEL TESTING AND DATA REDUCTION METHODS USING A MAGNETIC SUSPENSION SYSTEM

by Talat Abdel-Gawad DIAB

Improved techniques and data reduction methods for aerodynamic force measurements are proposed and tested. The model levitation and force measurements are provided by the magnetic suspension and balance system of Southampton University. Quasi-static and dynamic forces and moments are measured at low tunnel air flow speeds.

A systematic study of the incidence ramp technique established limitations set by the model aerodynamic properties, balance dynamics and data reduction methods. A simple relationship between the maximum ramp rate, the aerodynamic flow response time and the required data smoothing was obtained. This relationship was verified experimentally. The aerodynamic forces on several slender models were measured using slow incidence ramp rates. The effect of ramp rate on various aerodynamic characteristics was studied using an AGARD-G planform model. The results compare favourably with published work. The drag force is found to exhibit very slow response. It requires correction even at the lowest ramp rate. The results of the ramp testing show finer aerodynamic details than conventional point-by-point testing. The set of data points for a single test display a high degree of self consistency. They demonstrate the potential for a reduced cost per data point from wind-tunnel testing.

The novel method of digital covariance zero crossing for accurate determination of the frequency response of linear dynamic systems is

proposed. The method is particularly useful for low frequency sinusoidal signals distorted by heavy superimposed noise. It is shown that the accuracy of calculated joint dynamic properties of two signals depends on their record length, or number of oscillation cycles. A relationship between the signal-to-noise ratios, minimum record length and required accuracy is obtained. A verification of the method is provided by a simple digital simulation.

The method has been applied to or considered for:

(i) the measurement of roll damping derivative at constant incidence,

(ii) the measurement of roll damping derivative with ramped incidence,

(iii) multi-degree of freedom systems for the measurement of combined pitch and heave derivatives.

IMPROVED WIND TUNNEL TESTING AND DATA REDUCTION METHODS USING A MAGNETIC SUSPENSION SYSTEM

by TALAT A. DIAB

A Thesis Presented for the Degree of

DOCTOR OF PHILOSOPHY

in the

FACULTY OF ENGINEERING AND APPLIED SCIENCE

UNIVERSITY OF SOUTHAMPTON

July 1976

TO MY WIFE

AND MY FAMILY

CORRIGENDA

Page	line	Present	Change to
9	7t	$\frac{1}{4}$	quarter of a
9	10t	various effects	various nonlinear effects
33	8b	displacement-transients free, one	one which is free from displacement transients
68	5t	45^{o}	1 decade/decade
114	1b	maximum force	maximum balance force
133	9t	is	is listed under 'Computer Program listing' and is
171	6t	insert a new sentence	Table 7.4 gives a sample of computer output.
176	10t	low $\lvert\dot{\alpha}\rvert$	low $\lvert\dot{\alpha}\rvert$, see fig. 7.26
199	12t	the search	there should be a search

N.B. t denotes lines from top of page.
b denotes lines from bottom of page.

INDEX OF CONTENTS

ACKNOWLEDGEMENTS

It is with pleasure that the author wishes to express his profound sense of gratitude to the following.

To the MoD for financial support of the research contract monitored by Mr. R. Fail.

To Prof. G.M. Lilley for providing the opportunity for carrying out research at the Department of Aeronautics and Astronautics and his continuous and generous help.

To Drs M. Judd and M.J. Goodyer for their supervision, understanding and unfailing support. Their discussions on the subject have undoubtedly been an impetus for continuation and a source of inspiration. Drs Goodyer and Judd have provided a tremendous source of encouragement at numerous critical stages of this research.

To the workshop technicians for providing excellent services in terms of high quality workmanship.

To the wind-tunnel and aircompressor staff for their cooperation.

To the electronics laboratory team for their expert advice and building various electronic devices needed and especially Mr. F. Littler who built the ramp function generator.

And finally to Mrs. A. Lampard for the neat and efficient typing which was often carried out at a short notice.

SYMBOLS

CHAPTER 1

R_N	Reynolds number = $\frac{U\ell}{\nu}$
U	free stream velocity
ℓ	model characteristic length
ν	fluid kinematic viscosity

CHAPTER 2

C	damping coefficient
DOF	degree of freedom
F	forcing torque
I	moment of inertia
k	stiffness
ℓ	model characteristic length
R_N	Reynolds number = $U\ell/\nu$
T	Thomson number = $t_r U/\ell$
t	time
t_r	flow response time
U	flow speed
α	incidence
ζ	damping ratio
θ	pitch displacement
ν	fluid kinematic viscosity
ϕ	phase angle
ω	frequency, rad/sec.
ω_n	undamped natural frequency, rad/sec.
$(\dot{})$	derivative with respect to time
$(\hat{})$	amplitude

CHAPTER 3

a indicial aerodynamic coefficient, see equation 3.6

b_1, b_2 calibration contants, equation 3.27

$[B]$ inverse calibration matrix

B_1, B_2 calibration constants, equation 3.18

B_R calibration constant

$B_{R\Phi}$ $\frac{\partial B_R}{\partial \Phi}$ } equation 3.86

B_{R2} calibration constant, equation 3.94

c, C, C_1, C_2, c' damping coefficients

$[C]$ damping coefficient matrix

C_a mean aerodynamic chord

C_r

$C_{x\dot{x}}$ autocovariance of x

$C_{x\dot{y}}$ covariance of x and y signals, x may be roll displacement Φ, incidence α, lateral heave displacement z and y may be α, ω, lateral force Z, pitching moment, etc.

e_1-e_6 constants

f_{WN} white noise bandwidth

F amplitude of lateral force for combined heave and pitch osc.

$F(t)$, F_α, $F_{\dot{\alpha}}$ aerodynamic force, stiffness and damping coefficient.

g, g' function of time and its derivative

$[G]$ force matrix defined in equation 3.115

h amplitude of lateral heave oscillation

$[H]$ response matrix defined in equation 3.115

I electromagnet coil current

I' roll current at zero roll displacement

$j = \sqrt{-1}$

J model mass moment of inertia, about longitudinal axis for roll oscillation and about pitch axis for combined heave and pitch oscillation

k, K, k_1, k_2, K' stiffness

$[k]$ stiffness matrix defined in 3.133

k_{11}, k_{12}, k_{22} constants that correspond to balance force and moment components

K_c calibration constant

ℓ characteristic length of model

ℓ_A, ℓ_G, ℓ_{GO}, ℓ_{OR} defined in figure 3.16

ℓ_p dimensionless oscillatory roll damping derivative

L lift force

L_α $\dfrac{\partial L}{\partial \alpha}$

ΔL step change in lift force

ΔL_{ss} steady state change in lift force

m, m' mass

$[m]$ inertia matrix defined in 3.133

$\hat{m}_q = \dfrac{Mq}{\rho U S C a^2}$

$\hat{m} = \dfrac{M\omega}{\rho U S C a}$

$\hat{m}_{\dot{\omega}} = \dfrac{M}{\rho S C a^2}$

} dimensionless stability derivations

M pitching moment oscillation amplitude, roll torque

$M'(t)$ pitching moment

$(Ma)_G$ aerodynamic pitching moment about mass centre

$(M_m)_G$ magnetic pitching moment about mass centre

$M_q = \dfrac{\partial M'}{\partial q}$

$M_\omega = \dfrac{\partial M'}{\partial \omega}$

$M_{\dot{\omega}} = \dfrac{\partial M'}{\partial \dot{\omega}}$

n number of samples in an averaging interval

$n(t)$ random noise signal

$n_1(t)$, $n_2(t)$ white noise random variables

N number of points to be measured in a staircase test

N_s sampling rate

$p = \frac{d\phi}{dt}$ roll rate

$[P]$ defined in equation 3.111

q pitch rate

Q_{in}, Q_{quad} in phase and quadrature components

R_x correlation coefficient

S wing reference area

s model semispan

t time

t_{bal} balance response time

t_{lag} ramp response time lag $\frac{2\zeta}{\omega_n}$

t_o ramp starting time

t_R ramp duration

t_{RS} flow response time

Δt piecemeal averaging interval

Δt_{min} minimum averaging interval

$\Delta_1 t$ time resolution of averaged results

T signal record time duration

T_{RS} dimensionless flow response time

U flow speed

V_α, V_F, V_M, V_Z voltage signal corresponding to incidence lateral (heave) force, pitching moment and lateral heave.

V_ϕ, V_R voltage signals corresponding to roll displacement and roll current

w_B perturbation flow velocity along lateral axis at mass centre

$x(t) = \bar{X} \sin \omega t$

$\bar{x}$ average of x(t) over an interval T

x_B, x_{OM}, x_{GP}, x_{MO}, x_{MP}, x_{GM} defined in figure 3.16

$y(t) = \bar{Y} \sin \omega t$

$\bar{y}$ average y(t) over an interval T

z heave displacement

z_B, z_P, z_M defined in figure 3.16

$\hat{z}_q = \dfrac{Zq}{\rho USCa}$

$\hat{z}_\omega = \dfrac{Z\omega}{\rho USCa}$

$z_{\dot{\omega}} \quad \dfrac{Z\dot{\omega}}{\rho SCa}$

} dimensionless stability derivatives

Z lateral force

Z_a aerodynamic force

Z_m magnetic force

$Z_q = \dfrac{\partial Z}{\partial q}$

$Z\omega = \dfrac{\partial Z}{\partial \omega}$

$Z_{\dot{\omega}} = \dfrac{\partial Z}{\partial \dot{\omega}}$

α model angle of incidence

α_{ss} steady state change in incidence

$\Delta\alpha$ change in incidence

$\Delta\alpha_{ramp}$ ramp range of incidence

$\Delta\alpha_{trans}$ transients corrupted incidence range

$\dot{\alpha}$ incidence rate

$\beta_x, \beta_y,$ signal to noise ratios of x and y signals

γ_1 relative error in covariance estimate

δ_s sampling interval

Δ_o, Δ errors in ramp response at the start and later on respectively

ϵ	bias error in averaged results for piece-meal averaging, phase angle in dynamic testing
ζ	damping ratio
η_H	fraction of a harmonic amplitude residual in the piecemeal averaging
η_n	defined in equation 3.82
η_{trans}	fraction of ramp results corrupted by transient effects
θ	pitch displacement.
ν	tolerable fractional error in step response of aerodynamic lift force
ξ	dummy time variable
ρ	air density
σ	standard deviation
τ	time constant, covariance lag (indep. variable of covariance estimate)
$(\tau_{int})_{min}$	minimum lag interval before use of zero crossing starts
τ_{min}	minimum lag
τ_{zc}	value of time lag at a zero crossing
ϕ	phase angle, roll displacement
$\chi_1, \chi_2, \chi_3, \chi_4$	phase angles
$\Psi_1, \Psi_2, \Psi_3, \Psi_4$	phase angles
ω	oscillation frequency
ω_1, ω_2	oscillation frequencies - combined heave and pitch testing
ω_c	lowest frequency of the harmonic components contributing a zero average
ω_{max}	effective highest frequency contributing to averaging
ω_n	natural frequency
Ω	non-dimensional excitation frequency = $\frac{\omega Ca}{U}$

subscripts

i,j	1,2,.....n
a	aerodynamic
m	magnetic
act	actual
ref	reference
+	$\dot{\alpha} > 0$
-	$\dot{\alpha} < 0$
$(^{\bullet})$	$\frac{d}{dt}$
$(\hat{})$	amplitude
sinc x	$= \frac{\sin x}{x}$

CHAPTER 4

t_p	pause duration	figure 4.12
t_R	ramp duration	figure 4.12

CHAPTER 5

D	drag force
[G]	calibration, matrix, p.122
$(G)_{dyn}$	dynamic calibration constant
$(G)_{st}$	static calibration constant
I_A, I_F	lateral aft and lateral forward currents less bias respectively
I_D, I_R	drag and roll currents respectively
L	lift force
M	pitching moment
T	roll torque
α	angle of incidence
ζ	damping ratio

ω forced oscillation frequency

ω_n natural frequency of a balnce force loop

CHAPTER 6

C_a mean aerodynamic chord

C_D drag force coefficient = $\frac{D}{\frac{1}{2}\rho U^2 S}$

C_L lift force coefficient = $\frac{L}{\frac{1}{2}\rho U^2 S}$

C_e rolling moment coefficient = $\frac{T}{\frac{1}{2}\rho U^2 Ss}$

C_M pitching moment coefficient = $\frac{M}{\frac{1}{2}\rho U^2 SCa}$

$C_{\phi R}$ covariance estimate of roll displacement and torque signals

$C_{\phi\phi}$ autocovariance of roll displacement

D aerodynaic drag force

$\{F\}$ force vector

$\{G_1\}$ direct calibration matrix

$\{G_2\}$ interaction calibration matrix

$\{I\}$ electromagnet coil currents vector

$j = \sqrt{-1}$

$[K_{IV}]$ current - voltage calibration matrix

ℓ_p dimensionless oscillatory roll damping derivative

L aerodynamic lift force

m integer, zero crossing number

M aerodynamic pitching moment

n_a number of successive points for approximate inverse calibration matrix calculation

N_c number of lags per cycle oscillation

N_s sampling rate

p roll rate

s	model semispan
S	using reference area
T	roll torque
U	flow speed
$\{V\}$	voltage signals vector
$V_A, V_D, V_F, V_R, V_X, V_\alpha$	Voltage signals correponding to lateral aft less bias, drag, lateral forward less bias, roll currents, axial displacement and incidence angle respectively
X_{CP}	centre of pressure location behind extended wing centre line apex
α	incidence
δ	change in incidence
ε	phase angle of oscillation signals
ε_{cal}	phase angle corresponding to calibration signals
ρ	air density
τ	lag variable
ω	forced oscillation frequency
Ω	dimensionless oscillation frequency $\frac{\omega C_a}{U}$

CHAPTER 7

Same as for Chapter 3

C_A	Aerodynamic coefficient
q	Dynamic head of flow
h	Dynamic head, cm. methylated spirits

APPENDIX A

A_{ir} force calibration tensor (3 x 6)

$\vec{B}$ magnetic field strength

B_{ir} moment calibration matrix (3 x 6)

C_f, C_m scalar constants

C_{sr} augmented force calibration tensor (6 x 6)

$D_{rs} = C_{sr}^{-1}$

f_i force vector 3 x 1

$\vec{\delta f}$ force on elemental magnet δm

F_s augmented force vector (6 x 1)

G_{rs} total calibration matrix (6 x 6)

h_{ir} i^{th} component of field due to a unit current in r^{th} coil

$\vec{H}$ magnetic field due to B

H_c coercive strength

I_D drag current

I_r r^{th} coil current

$I^x_{r,s} = \frac{\partial Ir}{\partial x_s}$

$I^F_{r,s} = \frac{\partial Ir}{\partial Fs}$

$I^{xF}_{r,t,s} = \frac{\partial^2 Ir}{\partial x_t \partial F_s}$

m magnetization intensity

$\vec{\delta m}$ magnetic moment of an elemental magnet

μ_i moment vector

$\vec{\delta M}$ moment acting on the elemental magnet

X_s displacement vector (6 x 1)

$(\Delta x)_{drift}$ axial position drift

α angle of incidence

δ_{rs} Kronecher's delta = 1 for r=s, 0 otherwise

μ_{ij} permeability tensor

μ_o homogeneous permeability intensity

$[\Delta]$ error in calibration matrix $|G|$

APPENDIX B

$[A]$ force calibration matrix 6 x 6

$[B]=[A]^{-1}$ inverse force calibration matrix 6 x 6

$[B_1], [B_2], [B_3], [B_4]$ components of partitioned matrix $[B]$, see B.4

$\{F\}$ augmented force vector 6 x 1

$[P]$ system impedance matrix 6 x 6

$[P_1], [P_2], [P_3], [P_4]$ components of partitioned $|P|$ see B.4

$\{V\}$ current signal 6 x 1

$\{V_1\}, \{V_2\}$ components of partitioned vector $\{V\}$

$\{X\}$ displacement vector 6 x 1

$\{X_1\}, \{X_2\}$ components of partitioned $\{X\}$ vector

1. INTRODUCTION

In the history of mechanical powered flight the Wright Brothers are credited with two major achievements. First, they pioneered mechanical flight by making and successfully flying the first powered aircraft. Second, they devised (what has remained) an extremely effective methodology for aircraft design using wind-tunnel testing on suitable models. Ever since the Wright Flyer, wind-tunnel testing has been universally established as the most convenient experimental means of collecting basic and applied aerodynamic information on the ground. This information is essentially needed in early stages of project studies and during the course of design and development of a new aircraft. The amount of time and the cost of necessary wind-tunnel testing for newly designed aircraft have grown over the years as shown in Figure 1.1 [Harper (1968), de Meritte (1973)]. The data in the figure is for American aircraft since the evolution of mechanical flight, and forecasts a requirement for wind-tunnel testing time in the order of, or greater than, 10,000 hrs. for a new design.

Wind-tunnel testing of aircraft models is a form of experimental ground simulation of actual flight. A theoretical counterpart is computer simulation. A vast variety of wind-tunnels have been built over the years for general or special purpose testing. The degree of simulation achievable is limited by the tunnel capabilities and the method of testing. The accuracy of test results can generally be assessed and the confidence level in data can be established. No matter how high that confidence level, differences between wind-tunnel test results and flight test results exist which are mainly attributable to imperfections of the simulation technique. These differences can be due to:

i) small size model, scale (or Reynolds number) effects,

ii) tunnel wall interference

iii) model support interference

iv) flow unsteadiness, nonuniformity, turbulence and background noise levels.

Improvements in a simulation technique can be accomplished through efforts in two distinct areas:

i) hardware improvements, involving the development of new facilities and instrumentation, and

ii) software innovations, involving procedure of testing and data monitoring, collection, reduction and analysis.

Economic factors set serious limitations on the development of large test facilities in general. Compromise between the extreme of perfect simulation (required) and the cost of a less perfect, but perhaps acceptable, facility and methods of testing to provide a reasonable turnout of results seems to be inevitable in most cases.

The progressive growth in size and speed of airliners has demanded larger sized wind-tunnels, but rarely during the past two decades have new and larger tunnels been commissioned. Hence there has been a worsening trend in Reynolds number (R_N) simulation. On the larger vehicles, local areas of the flow which depend strongly on viscous effects (and hence R_N) are common occurrences and do not have an accurately predictable behaviour. These could have important consequences relevant to the operation of control surfaces, on high incidence flight, on supercritical flow and on the stability derivatives. Wind-tunnels of the sizes to fully simulate flight values of Reynolds number would be very expensive and complex installations to build and operate [Lukasiewicz (1973), Küchemann (1972)]. Improvements on R_N simulation are exemplified by the systems recently proposed and under development. Short duration ($\sim$ 10 seconds run time) high R_N large wind-tunnels of several configurations

are preferred at present to continuous operation tunnels for economical reasons [Lukasiewicz (1973)], while continuous operation cryogenic tunnels offering the same range of R_N but of smaller size and cost are being validated [Goodyer and Kilgore (1972)]. For productivity to be acceptable the short duration facilities require the development of special instrumentations and software testing techniques.

Improvements in the quality of simulation by the elimination of support interference through the development of magnetic suspension systems, have been achieved, although still confined to small size tunnels and models [Tournier and Laurenceau (1957)]. A powerful combination would seem to be the magnetic suspension system and the cryogenic tunnel.

Demands on the quality of wind-tunnel test results depend on the nature and objectives of the test concerned. Data of the qualitative type may suffice for preliminary, or project, study of a new aeroplane and basic aerodynamic testing, whilst during design, development and modification stages detailed quantitative data is often of prime interest. It is in the latter case that higher precision of test results and lower cost of testing have to be maintained consistently. High precision (i.e. fine resolution) is required when measuring the aerodynamic effects of minor configuration changes and when accurate determination of the onset of incipient local secondary flow is desired. A convenient index specifying the cost of testing is the cost per useful data point measured [Lilley (1963)]. This index is however linked to the overall initial as well as running costs and data productivity of the facility. Means of improving the data productivity, for the purpose of cutting down the cost per data point are therefore of practical interest. In practice, a large part of the airplane design schedule is paced by the aerodynamic configuration development program. The overall cost of building an aircraft, however, increases with the time required for the testing program. Appropriate test techniques can cut the wind tunnel testing program time

and result in a considerable cost saving. Wilson and Maddox (1969) claim a significant cost saving in the aerodynamic development of the C-5 airplane by developing and using a technique of simultaneous measurement of forces and pressures on the model.

More often than not, in routine testing, aerodynamic characteristics over a range of variables (e.g. incidence) are of more interest than a single data point. This underlines the need for the definition of a parameter that will indicate the quality of data points at the stage of assessing test results. This qualitative property is called 'self consistency of data points'. Self consistency of a set of data points over a range of the independent variable (e.g. incidence) obtained in a single test may be regarded as the counterpart of the repeatability used to indicate the joint properties of data points collected in different runs at the same conditions. Self consistency is more related to the software technique of testing in contrast to repeatability which depends more on the state of statistical control of the test and hence to a large extent on the hardware. In view of modern system reliability concepts both self consistency and repeatability add up to form the ultimate level of confidence (or degree of reliability) of test results. It is important, however, to appreciate that the cost of improvements on the former (self-consistency) can be in general much less expensive than on the latter for a given simulation technique designed to provide data results with a certain degree of reliability. Therefore poorer quality hardware components than would be required for the highest repeatability levels may be adequate for achieving a certain level of confidence in the final results if appropriate software techniques producing a high degree of self consistent results are adopted.

Systematic evaluation of the effect of various parameters involved in a test technique is of great practical interest for the purposes of:

i) establishing possible limitations and accuracy bounds of resulting measurements

ii) enhancing the efficiency of its use

iii) possibly reducing the amount of trial and error often resorted to.

Two software techniques for aerodynamic force testing are investigated in this work. One is for the measurement of steady forces and the other is for the measurement of dynamic stability derivatives. The measurement of aerodynamic forces while the model is steadily pitching has been proved a useful practical technique for increasing the data turnout of short duration wind tunnels. At suitably low pitch rates quasi-steady aerodynamic data can be extracted from the moving model measurements. The relationships between pitch rate, test duration, aerodynamic characteristics, incidence resolution and accuracy requirements are of direct interest. For the dynamic stability derivative measurements, very accurate and precise information is required on amplitude and phase relations between the forces and displacements of a model forced into harmonic oscillation. Very often the force and displacement signals are noise corrupted. The use of digital correlation methods in the extraction of these data for a single and multi-degree of freedom oscillation is investigated. The relationship between test duration, frequency of oscillation, signal/noise ratio and sampling rate is important.

The six-component magnetic suspension and balance system (MSBS) of Southampton University and its wind tunnel have been used for the development and study of both techniques. The model consisted of AGARD-G planform wings attached to a slender fuselage. The model exhibits linear and non-linear aerodynamic characteristics depending on incidence

and the state of boundary layers on the wings. A Marconi Myriad Mk II digital computer was used for the first stage of data reduction while complementary stages were performed on an ICL 1907 computer.

The MSBS provides a useful tool for assessing and developing test techniques involving controlled model motions for the following reasons.

i) absence of mechanical support flow interference

ii) ease with which various motions can be imparted to a magnetically levitated model achieved by feeding appropriate 'error' signals in the control system loops.

iii) the potential accuracy and dynamic load range of the magnetic balance as compared with mechanical balances.

Magnetic suspension systems of d-c type suffer, however, from limitations on the dynamic response owing to the relatively low natural frequencies of suspension and to the inevitable force interactions.

The techniques described above are not only suitable for short duration wind tunnel testing but can also have considerable potential in improving the utility of conventional continuous operation tunnels. Two examples are included to illustrate this statement. Flow unsteadiness often causes problems of consistency of results in V/STOL aircraft testing at very low speeds in open circuit tunnels whose inlets and exhausts are subject to atmospheric flow disturbances. The wind can change direction in as short a time as one minute and so force data over a range of incidence must be collected in this short duration for good self consistency. The incidence sweep (or ramp) technique provides an efficient method of testing. Tedious (and often very expensive) efforts are generally spent in order to calibrate and perform a complex experiment (e.g. force testing in a large continuous operation wind tunnel at

moderate and high flow speeds), whilst maintaining good statistical control over long periods of time. In addition the associated power consumption may be significant. Simplification of testing methods and possibly savings can be achieved by utilising appropriate short duration test routines of the ramp kind. Similarly suitable techniques for the measurement of dynamic oscillatory derivatives in short test durations are equally important. Most of the existing techniques are of the free oscillation type. Novel forced oscillation techniques using suitable correlation methods of data reduction presented in this thesis offer means that may complement or replace free oscillation ones in short duration tunnels. A combination of forced oscillation technique and incidence sweep can be a powerful method for measurement of the stability derivatives in short to moderate test durations.

Chapter 2 of this thesis reviews some of the relevant methods that have been used (and still are in use) for aerodynamic steady force and dynamic stability measurements in wind tunnels. Proposed techniques are introduced and theoretically assessed in Chapter 3. Linear and nonlinear aerodynamics are discussed. Chapter 4 describes the wind tunnel and magnetic suspension and balance system developed at Southampton University. Generalised force-current relations are developed and discussed in Appendix A. Calibration methods to provide the corresponding calibration constants in these relations are briefly described in Chapter 4. The slender winged model used in this investigation is described in Chapter 5. The data acquisition, reduction and analysis methods are explained in Chapter 6. The main results of the investigation and discussions of the effect of various parameters on the characteristics of the proposed techniques are presented in Chapter 7. Conclusions and suggestions for further work are given in Chapter 8.

2. SURVEY OF PRESENT TEST TECHNIQUES

For aerodynamic load measurement in a wind-tunnel, the model has to be supported in the flow field of the test section and the forces transmitted outside the tunnel. These force data are usually obtained, whether directly or indirectly, in a form that requires some manipulation before extracting the relevant aerodynamic loads. A complementary part to an actual wind-on test is therefore its data reduction method. In conventional wind tunnels the complete aircraft model is mechanically supported as compared with the magnetically levitated model in magnetic suspension tunnels. The testing technique depends on the specific purposes of the particular test. However, for many years it has been found convenient to classify testing under two broad categories:

i) steady testing, which provides static aerodynamic characteristics for the general shape of the aircraft, and

ii) dynamic testing, which permits the study and measurement of stability, flutter and control derivatives of the aircraft and its components.

In general the type of test and accuracy requirements specify the most suitable type of support. During various phases of design, manufacture and development of an aircraft the nature and quality of aerodynamic data required may vary quite widely. While at one stage data of ultimate accuracy and precision may be very important, at another stage, particularly the preliminary stage, data of a less accurate nature may suffice certain specific purpose. Sometimes the wind-tunnel type, speed range and load dynamic range of available instrumentation and economic requirements decide the test technique that can be used with a particular model.

This chapter presents a review of a selection of test techniques that have been developed in both areas of testing considered above. The

associated data reduction methods and the limitations are highlighted.

2.1 Steady-force-testing techniques

Ever since wind tunnels were first used for aerodynamic measurement and flow studies, the continuous flow method of testing has been employed. However, most of the developments in such testing in the first half-century of mechanical flight were directed towards the hardware side. Distinct software techniques have reportedly been developed only over the past ¼ century or so. Among the factors promoting the development of new techniques or improvements over an established one might be more accurate data requirement, interaction of various effects, optimum utilisation of the tunnel, reduction of testing cost, etc.

In continuous operation wind tunnels no strict limitation was imposed on the test run time, i.e. economic factors were not the prime factor. Models could be held steadily in the flow field for a long time and so truly steady measurements could be made. High speed testing in addition to the need for six-component force measurement gave rise to the development of the sting support as an improvement over the older mechanical means of support.

Intermittent operation wind tunnels provided very economic facilities for testing at high speeds but with relatively short test duration. The short test duration provided an impetus to the development of advanced test techniques so that higher rates of data acquisition from these tunnels could be achieved. If the model was moved automatically in a pre-arranged program after the flow has been established in the tunnel test section, and the force and moment signals recorded, then a large number of data points can be obtained from a single run. Lukasiewicz (1955) reported the application of a pitch ramping technique for an intermittent operation supersonic wind tunnel where flow

duration can be as short as 15 seconds. His technique consists of driving the model into either a continuous constant pitch rate or in staircase steps over the required incidence range during flow onset, fig. 2.1. The model is driven by an external 'incidence gear' and electrical signals from the balance outputs are directly recorded on a paper chart recorder. The system of balance and recorder had a time constant less than a second. For small signals, the established frequency bandwidth was 0 to 20 Hz. Lukasiewicz argues that so long as the linear velocities due to model rotation are small compared with the free stream velocity, such motion should not affect the measured aerodynamic characteristics appreciably. This condition is given by

$$\frac{\dot{\alpha}\ell}{2U} << 1. \qquad 2.1$$

where $\dot{\alpha}$ is the pitch rate, ℓ is a characteristic length of the model and U is the free stream velocity. A rate no greater than 1^{o}/sec was considered suitable for initial tests. Linear aerodynamic characteristics were assumed and so the steady ramp case was only used to provide the lift and moment curve-slopes while the staircase case provided a discrete point picture of the steady characteristics. Fig. 2.2. shows an example of the measurement obtained using this technique. Damping in the balance caused a time lag in the response as shown in Fig. 2.3. The inertia of the driving system caused a further jump towards the end of the range. Static incidence calibration was used to establish the incidence scale for the ramp case. This could be in error at high pitch rates since the damping in the system might significantly upset the correspondence between the indicated steady and ramped incidences.

Tanney (1959) developed a suitable data reduction method for the above system on a three-component force balance. Incidence sweep rates

were used in the range 0.7 to 3.3°/sec. Chart recorders with good ramp function response were used. The test data was digitised after being presented on self balancing potentiometers. Filtering the data was effected simultaneously or immediately after the test run. A digitised reading was punched every .16 sec. on paper tape or cards. Temporary storage is essential because of the slow rate of punching operation, for which purpose a small digital computer was used.

The technique of incidence sweep has also been used in low speed VTOL/STOL wind tunnel testing [Emslie (1963)]. The flow in the working section of a continuous operation open circuit low speed tunnel tends to be extremely sensitive to external winds during the time of testing at the very low tunnel speeds often required for V/STOL work. The external wind changes direction, most of the time unpredictably. To avoid or reduce the effect of corresponding flow unsteadiness on force measurements a complete set of force-incidence data points would be required in a short duration, of the order of one minute. Both the continuous sweep and staircase incidence functions were applied to the model during the test. Quasi-steady data points were obtained from the continuous sweep case while the staircase served to provide checkpoints on the steadiness of these data points. Unlike the Lukasiewicz method, only a few of the staircase points are required at key incidence settings. Based on this, a versatile system has been developed over the years and used for supersonic as well as low speed testing, [Emslie (1973)]. Routine sweep rates vary from 0.5 °/sec. to 3.0 °/sec., over a range of about 30°, depending on the flow speed. The criterion for deciding the sweep rate is that the flow response time is about the same as the time required by fluid particles to traverse 5 - 10 chords at free stream velocity. Position and force signals (e.g. strain-gauge balance output) are heavily filtered (sometimes with a low pass cut-off at 2.0 Hz) to suppress the noise. The signals are then electronically amplified,

temporarily stored magnetically, digitized, displayed visually, read on digital voltmeters and punched on tape, for subsequent computer analysis. The digital data is punched at a rate of 3 to 10 points per second. This allows a specific test incidence data resolution of the order 1^{o} to 0.05^{o} if required. The filter is recognised as a very important and decisive factor in the system. This technique has been used for the measurement of both linear and nonlinear aerodynamic properties of complete aircraft models. It should be noted that the staircase test is used for fixing the right sweep rate for the continuous sweep test. However, there appears to be no reported systematic study of the effect of sweep rate on the quality of data obtained.

Accurate simulation of transonic flight requires the development of high Reynolds number (R_N) test facilities. Short duration tunnels seem to be most suitable on economical grounds. Currently proposed tunnels for the $R_N = 10^8$ range have running times of the order of a few seconds. For increased tunnel productivity, advanced test techniques (software type) are needed [Pugh (1973)].

Starr and Schaeler (1973) have produced a preliminary study of the parameters affecting the force and pressure measurements on moving models in a pilot high Reynolds number transonic tunnel. Flow duration available for testing was in the range of 100 m.sec. The flow response time t_r is expressed non-dimensionally as the Thompson number T defined as

$$T = \frac{t_r U}{\ell} \qquad 2.2$$

For a certain model and flow field T is constant. They designed an experiment to measure values of T for various flow fields on a 15-degree cone model, 3.5 in. long. The cone attitude was changed from -4^{o} to $+4^{o}$ in 4 to 6 m.sec. and the exact instant at which the model reached the limit

attitudes was precisely recorded using electrical contacts. They measured the differential pressure at symmetrical points on the windward and leeward sides of the model surface, at a distance 2.9 in. from the apex, using a fast response differential pressure transducer. The time it takes the differential pressure to settle down after the model has reached each of the limit attitudes is measured and non-dimensionalised as in equation 2.2. At a flow Mach number of 0.85 they found $T \simeq 1.7$. This agrees with published results for impulsively started flows on flat plates and wedges in laminar and turbulent flows at subsonic and supersonic velocities. For laminar boundary layers

$$T \simeq 2 \text{ to } 4,$$

and for turbulent boundary layers

$$T \simeq 1 \text{ to } 2,$$

and published results for experiments on an oscillating aerofoil in transonic flow give

$$T < 5$$

Fig. 2.4 summarises these results. The values of T established can be used to calculate the flow response time for the full scale tunnel. They do given an indication of being short enough to allow the model in the full scale tunnel to be swept over a large sector of the required attitude range.

Recently van Nunnen (1973) considered the test time requirement for steady force measurement using a continuous incidence sweep. As in the case considered by Starr and Schueler, van Nunnen's work is mainly directed towards application to large high R_N short duration tunnels. He stresses the need for sweep-up and sweep down in the same run and argues that rates of the order of 2^o/sec. are appropriate over an incidence range of 10^o. This defines a required run time of the order of 10 seconds. The

criterion for the selection of the sweep rate would be the extent of hysteresis in the lift-incidence characteristic. This hysteresis tends to increase with faster sweep rates as shown schematically in Fig. 2.5.

In all the work described above there appears no systematic study of the effect of the various parameters defining the incidence sweep technique on the quality of measured data. The majority of the relevant information resides in the experience of the field workers. One of the purposes of this thesis is to present a systematic study of the incidence sweep technique and investigate the possibility of its further potential applications.

2.2 Dynamic stability derivative measurements

Development of methods for the measurement of aerodynamic stability derivatives for rigid models has been rather slower than for the measurement of steady forces. Apparently the following two reasons are mainly responsible for this;

i) the slow recognition of the relative importance of prior knowledge (i.e. at the design stage) of the dynamic derivatives as compared with static derivatives, and

ii) the difficulty associated with dynamic measurements both in hardware and software techniques.

With the advent of high speed aircraft and missiles, increased emphasis has been placed on performance and dynamic stability problems since advanced missions demand precise control not only in small disturbances from level flight but also in large scale manoeuvres. In addition, recent developments in instrumentation and data handling systems have helped a great deal in the practical realisation of new ideas.

Dynamic stability derivative measurement in a wind tunnel involves supporting the model (whether it is a 2-D, a half or a complete aircraft model) in the test section and allowing it to describe certain motions

in one or more degrees of freedom. In some cases an external force is applied to maintain or support this motion. Derivatives are then extracted from observation of model motion (and applied force, if any) using a simple mathematical model.

At present three distinct types of movements are employed; continuous rotation, sinusoidal oscillation and pure random motion. A classification of the methods used for stability derivative measurement in wind tunnels is shown in Fig. 2.6. Most of the methods in use fall under one or a combination of these headings. Since the derivatives for complete aircraft models are of main interest here, the following review is confined as far as possible to these types of model.

Free motion methods

These methods employ the decayed continuous rotation or decayed oscillation in a single degree of freedom or a combination of several degrees of a model suitably suspended in the airflow.

For the free rotation case, accurate measurement of the angular velocity is required. Derivatives like the roll damping ℓ_p can be measured in this way. Care, however, should be taken to ensure that damping in the bearing is low and that the derivative measured is linear over the range of angular velocities considered.

The decaying free oscillation method is the most widely used technique for stability derivative measurement, and the simplest, at least as far as hardware is concerned, [Jones (1935)]. The model is initially disturbed either by release from a displaced attitude or by applying an impulse and the subsequent motion is then observed. Provided that the model has positive damping and the amplitude of oscillation is not too large, observation of the amplitude and frequency of a few cycles of the motion with wind on can be compared with similar data from a vacuum test to

provide both damping and static derivatives. For reasonable accuracy of measurement of stability derivatives:

i) precise measurement of natural frequency of oscillation and logarithmic decrement are required,

ii) transients pertaining to the initial disturbances have to be eliminated,

iii) the nonlinearities associated with large amplitudes of displacements must be absent, and

iv) the noise on the displacement signal must be sufficiently small.

In general, several cycles of oscillation are required for the analysis. These can usually be obtained by adjusting the natural frequency of oscillation of the system. There are a few methods of data reduction and analysis particularly suitable for the free oscillation method. They range from hand smoothing and plotting the time response of the displacement on a semi log scale and calculating the logarithmic decrement and frequency, to the use of automatic devices like the dampometer and logarithmic circuit [Bratt (1960)] capable of accuracies of about 2%. Orlick-Rukemann (1963) developed a travel summation method capable of accuracies of the order of 1%.

Fully automatic facilities have been developed for sensing, recording and analysing free oscillation data of complete models in short duration testing, [Orlick-Rukemann (1960)]. Multi-degree of freedom testing of slender missile models in wind tunnels using the free oscillation method have been considered by Nicolaidis and Eikenberry (1970). For such cases a sophisticated mathematical model and a complicated method of data reduction are unavoidable.

In almost all the cases considered above the data analysis is carried out in the time domain.

Flow induced forced motion

Stability derivatives can be obtained from a model response to unsteady flow. Turbulent flows and sinusoidal flow can be quite well reproduced in the wind tunnel.

Response of models to turbulent flow is a random motion. Provided the turbulence has a flat frequency spectrum in the range of frequency of interest, the spectrum of the displacement gives the magnitude of the frequency response function of the system and hence natural frequency and damping ratio can be found [Lundgren (1971)]. Two aspects, however, appear to cause uncertainty in the results from this method. One is the degree of flatness of the turbulence and force spectra and the other is the sharpness of the resonance or damping ratio of the system. The lower the damping the sharper is the peak and the larger is the error in the spectral density. Lundgren relied on results from a decayed free oscillation method for confirmation of the random excitation method results. Judd (1963) used a similar excitation method on a 2-D aerofoil, but used a completely different kind of analysis. A random signal with a flat spectrum has an impulse auto correlation function. The auto-correlation function of the aerofoil response to turbulence is identical with the impulse response in the time domain of a free oscillation test. By observation of the cross over points and the amplitude decay of the auto correlation function, damping and static derivatives can be extracted.

It is necessary to distinguish between loads generated by an unsteady flow and those resulting from unsteady model motion in a steady flow. Gilman and Bennet (1966) used a vertical sinusoidal gust generated in a wind tunnel for studying the frequency response function of an aircraft model. The model was cable mounted to improve flight simulation. Flow angles and model c.g. accelerations were measured and the acceleration

frequency response function determined over a range of frequencies. Although their main interest was in flutter derivative measurement, stability derivatives can be measured by Gilman and Bennet's method if the model is regarded as rigid and the mathematical model suitably simplified.

Externally forced motion methods

In these methods, the model is maintained in steady motion under the action of an external force. Derivatives are obtained from measurements of both the force applied to and displacement of the model using an appropriate mathematical model. Although more complicated hardware is required for this type of measurement than for free motion methods, it possesses several advantages, notably:

i) independence of the motion from the specific model aerodynamic and dynamic characteristics,

ii) greater degree of control is maintained, e.g. frequency and amplitude are constant in a forced oscillation, and

iii) more precise measurements can be obtained.

The simplest of these methods is the forced continuous rotation method. In this case the external torque maintaining a constant angular velocity balances the aerodynamic and bearing frictional torques. Measurement of the applied torque and angular velocities in wind-on and vacuum states can be used to find the relevant damping derivative, e.g. roll damping derivative ℓ_p. If lateral forces can be measured when the model is set at incidence, lift and magnus forces can be measured as well [Platou (1965)].

Forced oscillation methods consist of forcing the model externally into a constant amplitude constant frequency sinusoidal motion in one or more degrees of freedom about suitable pivots in the support. Instantaneous force and displacement signals are measured and analysed for

the required stability derivatives.

The mathematical model for a single degree of freedom small amplitude angular oscillation, Fig. 2.7, is given by

$$I\ddot{\theta} + c\dot{\theta} + k\theta = F \qquad 2.3$$

For harmonic oscillation, in general, the displacement and torque are given by

$$\theta = \hat{\theta}\, e^{i\omega t} \qquad 2.4$$

$$F = \hat{F}\, e^{i\omega t}$$

Substituting in 2.1 and reducing gives

$$\frac{\hat{F}}{\hat{\theta}} = k - \omega^2 I + i\omega c \qquad 2.5$$

$$= \left|\frac{\hat{F}}{\hat{\theta}}\right| \angle \phi$$

where $\phi = \tan^{-1} \dfrac{\omega c}{k - \omega^2 I}$ is the phase angle between the torque and the displacement. The undamped natural frequency of the system is

$$\omega_n = \sqrt{\frac{k}{I}} \qquad 2.6$$

Equation 2.3 shows that the damping can be determined from a measurement of $\hat{F}/\hat{\theta}$ at the test frequency. This requires either measurement of the amplitude ratio $|\hat{F}/\hat{\theta}|$ and phase difference or the inphase and quadrative component of the forcing torque relative to the displacement.

Equation 2.3 subject to 2.4 can be represented by a vector diagram as shown in Fig. 2.8a. Three categories of testing can be identified depending on the ratio of oscillation frequency to the system undamped natural frequency as shown in Fig. 2.8a- c.

Forcing a model to oscillate at $\omega/\omega_n \gg 1$, Fig. 2.8c, is ruled out on the following grounds:

i) an extra strength requirement is imposed on the model and support in order to reduce aeroelastic distortions,

ii) the domination of the measurements by the inertia terms (unless the oscillating model system is dynamically balanced),

iii) corruption of the signals by the tunnel vibration and flow induced random noise, and

iv) the extremely small phase angles require extra precision instruments.

Forced resonance oscillation (i.e. at $\omega = \omega_n$) requires a form of displacement feedback associated with the input excitation. The form of feedback, sometimes becomes quite complex [Beam (1956)]. This type of testing, however, does not require very accurate phase measurement since at $\omega = \omega_n$, $\phi = 90^o$ and can be set easily because $\frac{d\phi}{d\omega}$ is a maximum. In addition the amplitude of oscillation is close to the maximum obtainable with a given excitation level. The maximum occurs actually at $\omega = \omega_n\sqrt{1 - 2\zeta^2}$ where ζ is the ratio of system damping to the critical. At the condition $\omega = \omega_n$, the applied force equals the damping force. When the system resonant frequency is high, signals become vulnerable to noise corruption as explained earlier and the corresponding identification of the resonant condition may become difficult. Testing at frequencies close to but not exactly equal to resonant frequencies can give rise to a beating effect. Most of the present forced oscillation test facilities have some provision for resonance force testing.

Testing at low frequencies, $\omega/\omega_n < 1$, demands very precise measurement of the phase angle ϕ for reasonable damping measurement accuracy. It does not, in general, require the degree of sophistication demanded for a forced resonance system and is characterised by an absence of aeroelastic effects on the measured derivatives.

The presence of noise on the measured signals hampers very much the accuracy of phase measurement in low frequency forced oscillation testing. Most of the recently developed methods are of the analog type. These include the electronic trigger circuits, gated counter-chronographs, special a.c. bridges and resolved component indicators (RCI). The latter (RCI) works on the wattmeter principle, employed by Bratt & Wight (1944) to reduce the great labour of manual reduction previously employed, [Bratt and Scruton (1938)]. The majority of the methods mentioned above rely on the availability of a reasonably clean reference signal at the oscillation frequency. In the RCI method this reference signal, of a fixed amplitude, and a 90° phase shifted version of it are multiplied by the measured signal. The resulting products are filtered and read on d-c damped microammeters as the in-phase and quadrature parts. The use of a reference signal at the fundamental frequency and the averaging of the modulated signal effectively filters all higher order harmonics. Part of this signal is still due to the fraction of the noise spectrum imposed on the signals at this fundamental frequency. Braslow, Wiley and Lee (1962) have developed a system for the measurement of lateral dynamic stability derivatives, at transonic and supersonic speeds at resonant and non-resonant frequencies, which relied on the RCI for monitoring and reading the relevant components. Automatic digital equipment was used to digitize, acquire and record the RCI readings.

Thompson and Fail (1962) report a derivative measuring system capable of pitch-heave displacements, and later, developed a three-degree-of freedom system for simultaneous measurement of yaw, roll and sideslip derivatives [Thompson and Fail (1966)]. Instead of using strain gauge for the measurement of forces and displacements, as used in most earlier systems, they used accelerometers for the displacement signals. Three

accelerometers are arranged to give accelerations in the three degrees of freedom and the system is excited by an electromagnetic shaker. The equipment is compact and particularly suited for slender model bearing.

Excitation is made in each mode separately and close to the relevant natural frequency (e.g. 5 Hz for yaw, 8 Hz for side slip and 13 Hz for roll) to ensure a reasonably large oscillation amplitude at a reasonable phase angle without the need for an excessive excitation force. A mathematical model of 3-D of freedom oscillation is assumed valid for small oscillations. The acceleration signals and force excitation signals are fed into a resolver of the wattmeter type, all referred to a common clean signal drawn from the oscillator. The in-phase and quadrature components of all the signals and the frequency of oscillation (measured by an electronic counter), are recorded on a punched tape and read on a teletype. For each data point three sets of readings are made, one for each mode of oscillation. These results and tunnel conditions plus calibration constants are fed into a digital computer which solves the equations of motion comprising the mathematical model and produces the required derivatives. A layout of this system of data handling is shown in Fig. 2.9.

There was large scatter in the results of lateral derivatives on a slender winged model at low speeds measured using this system. The scatter did not obscure the trend of the data but is expected to increase further as the testing flow speed goes up. The background noise on the signals is considered partly responsible for the scatter of data. In other words it is the low value of signal-to-noise ratio resulting from the small amplitudes of motion (of the order of 1^{o}) employed.

In the operation of the RCI, there are at least two causes of error arising from the analog reduction of noisy signals;

i) the presence of various harmonics which need to be filtered, and

ii) the presence of correlated noise on both the reference and measured signal affects the d-c reading and cannot be eliminated with such equipment.

One possible way of improving the accuracy of measurement of the derivatives is by recording all the raw signals in digital form so that reference signals can be generated numerically at the oscillation frequency. In this case the reference signal is almost pure, but a very large number of digital samples per cycle would be required [private discussion with Fail].

Another possible technique for improvement is to transform the data reduction to the correlation domain. This method is introduced and described in the next chapter and represents the second topic of this thesis.

3. PROPOSED TECHNIQUES OF TESTING AND DATA ANALYSIS

In view of the importance of wind tunnel force testing on aircraft models and its impact on the overall design and development programs, new and improved techniques of testing are in demand. Justification for such demand, as applied to existing test facilities, can be the reduction of the cost of wind tunnel testing per data point, shortening the duration of wind tunnel test programs, attainment of test results with a higher degree of self consistency and/or attainment of more accurate results. As regards new and future test facilities, where economy dictates short duration types of wind tunnels, the demand becomes a necessity.

A modern wind tunnel normally has a digital computer comprising the principal element of its total data reduction and analysis system. Therefore software techniques which can best satisfy the requirements and limitations stated above and make better use of a suitable data analysis system can be very useful. Two types of force testing are presented and assessed in this chapter. The first deals with steady aerodynamic force measurements and the second with dynamic stability derivative measurements. These are discussed from the general point of view but the application to the magnetic suspension and balance system are investigated specifically.

3.1 Steady Aerodynamic Testing Method - Incidence Sweep Technique

One of the problems present in some wind-tunnel testing is the short wind-on time of operation. This determines the number of obtainable data points if truly static aerodynamic data is required. The number of runs required in order to determine a complete range of model characteristics may be very large either because of the number of data points sought or because of the low degree of reproducibility of test conditions. This problem is alleviated if the model is made to describe certain motions while the wind is on and the measurements instantaneously analysed or

recorded for later analysis. Analogue methods of data reduction and analysis may be necessary for the instantaneous (on-line) analysis case, while completely digital methods can be used for the later (off-line) analysis. The simplest kind of motion in the case of longitudinal aerodynamic measurements is the pitch ramp. In this case the model incidence is made to change from a starting value to a final value at a constant rate. Fig. 3.1 shows a typical incidence sweep (ramp) time function. The negative rate of incidence sweep is included for a reason to be discussed later. The time history of the pitch attitude and force signals are filtered, digitized at a suitable equispaced sampling interval for digital analysis, then averaged over short time intervals and the averaged values corrected for dynamic effects.

The main parameter in the pitch ramping method is the value of the pitch rate, which is simply the incidence range covered divided by the ramp duration. Factors affecting this ramp rate (e.g. model size, flow speed and balance limitations), are therefore relevant and need investigation. Other features of the method are the filter type and setting, sampling rate of digitizing and averaging interval required in relation to the quality of results sought. The latter feature is the controlling factor in the degree of smearing of aerodynamic force details.

A systematic study of this technique would require the theoretical estimation of the possible limitations on the values of the parameters involved and the development of test routines for the experimental results required to verify the theoretical predictions.

Naturally while the model is in motion relative to the free stream any force measurement will contain unsteady as well as static effects. Indeed, three kinds of transients affect the measurements:

i) aerodynamic transients,

ii) displacement transients, and

iii) balance transients.

Measured results have got to be either insignificantly affected by or corrected for these transients in order to recover the steady or quasi-steady quantities required. It is important, before pursuing further details of the technique, to define the quality of the aerodynamic forces involved and the transients taking place.

3.1.1 Aerodynamic transients - flow response time

A model in a real fluid flow sets up an associated vorticity field which is responsible for the fluid forces acting on it. Unlike other flow properties, shed vorticity is transported at a finite velocity, i.e. of the order of the free stream velocity U, [Lighthill (1963)].* Consequently following a change in model attitude, the vorticity field of the flow adjusts itself to a new steady pattern in a finite time. This time of 'adjustment' is called the flow response time, t_{RS}. If a characteristic length for the model is known as ℓ and flow speed U, a dimensionless quantity can be formed as

$$T_{RS} = \frac{t_{RS}U}{\ell} \qquad 3.1$$

This response time is governed by the conditions inside the boundary layer where the vorticity is produced and the presence of sharp edges on the model configuration causing the formation of free vortices. As a result it is affected by other flow phenomena influencing the boundary layer, e.g. onset or presence of a flow separation, transition from a laminar to turbulent boundary layer, shock-wave boundary layer interaction ... etc. The process

.....

* Lighthill (1963) states that change in the vorticity distribution gives rise to an almost instantaneous change in the pressure distribution and hence the aerodynamic forces.

through which such adjustment takes place is generally a complex one and its time history is the aerodynamic transient which is normally studied in the form of the position step response and called 'indicial aerodynamics'.

Consider the case of a model, having linear aerodynamic characteristics, in a flow and receiving a sudden plunging motion at time t_o, fig. 3.2. Shortly after the start of motion the aerodynamic effect is a transient one, known as the Wagner effect, and depends on the time elapsed since t_o. The usual definition of linear aerodynamic derivatives ceases to be meaningful during this transient period. Eventually at an appropriately long time, t greater than $t_o + t_{RS}$, the aerodynamic effect approaches the steady state value. This value can then be regarded as independent of the past history. This steady state value is achieved exactly in supersonic flow but can only be approached asymptotically for subsonic flow since the starting vortex and wake affect the flow indefinitely upstream. Therefore, so long as the observation time is longer than t_{RS} from the change in position the aerodynamic forces depend only on the instantaneous values of the position and its derivatives. A useful representation of the change in an aerodynamic force component, say linear lift force, may take the form

$$\Delta L \sim L_\alpha \Delta\alpha + L_{\dot\alpha} \Delta\dot\alpha + L_{\ddot\alpha} \Delta\ddot\alpha \qquad 3.2$$

where the subscripts indicate partial derivatives and the dots derivatives w.r.t. time. The derivatives L_α, $L_{\dot\alpha}$, $L_{\ddot\alpha}$ etc. are called quasi-steady derivatives and are of major interest in aeronautics. Transient effects, however, may be of interest in special applications such as aircraft flutter and short period oscillation and ship unsteady motion.

In the case of steady pitch ramping the aerodynamic transients are partly due to the step in pitch rate. Hence, these are less severe than for the plunging motion case. Correspondingly, one can safely conjecture

a shorter flow response time. In a ramp response, on the other hand, the steady state output (force) always lags the input (displacement). This lag can be argued as due in part to the indicial effect, but it has been shown, [Etkin (1956)], that for relatively long times from the start of motion this lag is simply related to the usual damping derivative. Therefore t_{RS} can be regarded as a conservative upper estimate for the pitch ramp case.

Similar flow patterns around similar models but of different sizes, or at different flow speeds, should have the same dimensionless flow response time T_{RS}. The flow response time T_{RS} for the same model, however, can appreciably change when the flow pattern does. An example of this is the classical case of a high aspect ratio wing at low incidence as compared with the same wing at a stalled condition where in the latter the dependence on the flow Reynolds number is stronger. A similar example is witnessed in the supercritical wing with the associated onset of shock-boundary layer interactions. In the examples just cited, it can be shown that the aerodynamic phenomena are nonlinear and the model-flow system may possess a hysteresis effect. In these cases the flow response time is larger than in the linear aerodynamics case. It is convenient to group the types of aerodynamic characteristic into three groups

i) linear aerodynamics case, for example high aspect ratio winged models at low and moderate incidences,

ii) nonlinear aerodynamics (no-hysteresis) case, e.g. slender winged aircraft models at moderate incidences

and

iii) nonlinear aerodynamics with hysteresis cases, as in case (i) at stalling incidences.

Although a single ramp leg of the kind suggested in fig. 3.1 suffices for group (i), the full function is required in order to confirm the linearity of group (i) and is necessary to provide aerodynamic information in groups (ii) and (iii).

Measurement of t_{RS} can be obtained by observation of the incidence step response, i.e. the indicial admittance, of the model in the flow field or by observation of a terminated ramp response since a pure step may be difficult to generate.

Examples of T_{RS} for a variety of flow fields have been described earlier, section 2.1, and are given in fig. 2.4.

Measurements free from aerodynamic transients are therefore essential for two reasons:

i) in order that measured steady or quasi-steady characteristics can be meaningful, and

ii) if transients occur there is no simple way for correcting them.

It is necessary therefore in pitch ramp testing to discard the first t_{RS} length of data following the start of the model ramp as being corrupted by the aerodynamic transients, where t_{RS} corresponds to the longest flow response time corresponding to flow patterns that may form on the model during an overall incidence excursion. For a ramp rate of $\dot{\alpha}$, t_{RS} corresponds to an incidence range of

$$\Delta\alpha_{\text{trans}} \sim \dot{\alpha}\ t_{RS} \qquad 3.3$$

Since a ramp duration may be fixed, e.g. by tunnel test duration, the fraction of transient corrupted data is

$$\eta_{\text{trans.}} = \frac{t_{RS}}{t_R} = \frac{T_{RS}}{t_R}\ \frac{\ell}{U} \qquad 3.4$$

where t_R is the ramp duration. It follows that, for the largest useful output from a ramp test,

$$\Delta \alpha_{trans.} = \eta_{trans.} \Delta \alpha_{ramp} \qquad 3.5$$

must be kept as small as possible. In addition to this there is a steady state error in the aerodynamic characteristics associated with the incidence time rate. In the case of the linear lift force this amounts to $L_{\dot{\alpha}} \times \dot{\alpha}$ (from equation 3.2) and is schematically shown in fig. 3.3. Although this can be corrected for, as will be shown later, it is preferable to keep the correction as small as possible. At this stage only arbitrary limits can be set on $\dot{\alpha}$. However, later in this section more definite limits are discussed.

This establishes the aerodynamic transient limitations on the motion and the corresponding loss in the incidence range.

It is interesting to consider the use of a staircase pitch variation (fig. 3.4) in the hope of achieving steady state dwell durations. Since t_{RS} is independent of the amplitude of pitch step, it appears necessary to allow on each step of the staircase a minimum time interval of t_{RS} before a 'static' measurement can be taken. If N points are to be measured during t_R, a duration of $N.t_{RS}$ would be lost. Therefore it is conceivable that the use of a staircase function may be limited to several data points in a certain incidence range. The advantage of the staircase over the pitch ramp lies in measuring strongly nonlinear aerodynamic forces since the staircase displacement case provides results with essentially the same quality as in the linear case while the ramp function can produce locally distorted aerodynamic characteristics.

Finally, the question of the aerodynamic limitation on the maximum pitch rate has to be answered. Dore (1966) has found that the indicial

subsonic aerodynamic lift change on a wing can be fairly well approximated by

$$\Delta L(t) \simeq \Delta L_{SS}(1 - a\, e^{-t/\tau}) \qquad 3.6$$

where

$\Delta L(t)$ is the actual change in lift at time t following a step incidence change at t = 0, ΔL_{SS} is the corresponding steady state change, a and τ are constants depending on the flow pattern and model geometry. Clearly the steady-state condition is only reached asymptotically. If the steady state is assumed to take the approximate value $\Delta L(t) = \Delta L_{SS}(1 - \nu)$, where ν is a small positive number, then the time $t = t_{RS}$ and

$$\nu = a\, e^{-t_{RS}/\tau} \ll 1. \qquad 3.7$$

If $a/\nu > 1$.

$$\tau = \frac{t_{RS}}{\ell n(a/\nu)} \qquad 3.8$$

The derivative of the lift force w.r.t. time is obtained from equation 3.6 as

$$\frac{d\Delta L}{dt} = \frac{a}{\tau}\, \Delta L_{SS}\, e^{-t/\tau} \qquad 3.9$$

At large values of time t the differential coefficient can be approximated by a difference form and we get

$$\delta(\Delta L) \sim \frac{a}{\tau}\, \Delta L_{SS}\, e^{-t/\tau}\, \delta t \qquad 3.10$$

The time rate of change of the measured lift force component, when transient free, at constant pitch rate is given by

$$\frac{d(\Delta L)_{meas}}{dt} = \dot{\alpha}\, \frac{\partial L}{\partial \alpha} \qquad 3.11$$

since $\alpha \sim \dot{\alpha} t$. In difference form, this becomes,

$$\frac{\delta(\Delta L_{meas})}{\delta t} \simeq \dot{\alpha} \quad (\overline{\frac{\partial L}{\partial \alpha}}) \qquad 3.12$$

where $(\overline{\quad})$ indicates average over δt.

For a small transient effect on the measured lift force, the changes in lift force measured in an interval δt and the corresponding transient change in the same interval must be related by

$$\frac{\delta(\Delta L)_{meas.}}{\delta(\Delta L)_{act.}} << 1. \qquad 3.13$$

Substitution from equations (3.8), (3.10), (3.12) into (3.13) gives

$$\dot{\alpha} \quad (\overline{\frac{\partial L}{\partial \alpha}}) << \quad \frac{\nu \, \Delta L}{t_{RS}} \quad \ell n (\frac{a}{\nu}) \qquad 3.14$$

where the subscript 'SS' has been dropped.

When $\quad \overline{L}_{\alpha} \neq 0$

$$\dot{\alpha}_{max} = \frac{\Delta L}{\overline{L}_{\alpha}} \left[\frac{\nu}{t_{RS}} \ell n \frac{a}{\nu} \right] \qquad 3.15$$

This establishes the permissible upper limit of the ramp rate. Similar forms can be obtained for the other force components. This result is a fairly general one since equation (3.11) is valid for both linear and nonlinear lift forces. Equation (3.15) serves two purposes:

i) to estimate the maximum pitch rate for testing if the aerodynamic characteristics are roughly known, or

ii) to check the freedom of various measured force components at a certain pitch rate from significant transient effects.

The quantity in the square brackets of equation (3.15) is a function of the aerodynamic transient characteristics and the specified ν (permissible relative error in aerodynamic force) and defined t_{RS}. Later in this chapter methods of estimating and measuring this quantity will be discussed.

3.1.2 Balance and displacement transients

A linear force balance can in general be regarded a form of low pass filter. The measurement of a time varying force is therefore always affected by the characteristics of the balance system used. The cut-off frequency, beyond which large attenuation of signal harmonics takes place, is close to the balance natural frequency of oscillation where the balance is regarded as a second order system. Associated with the amplitude attenuation is a phase shift which is relatively large at high frequencies. The natural frequency depends on some kind of ratio of stiffness to inertia of the moving parts, as well as the control system properties. In order that a measurement can be reasonably free from balance transients, the highest frequency content required for the force component must be small compared with the balance natural frequency. Unlike aerodynamic transients, balance transients can be corrected for if the balance characteristics are precisely known a priori.

Appreciable displacement transients, however, can complicate the picture by introducing undesirable higher order motion derivatives, thereby affecting both the aerodynamic forces and their measurements. It is therefore important that the achieved form of motion be as close as possible to the ideal, i.e. displacement-transients free, one.

The particular case of the magnetic suspension and balance system is considered. The situation is slightly more involved in this kind of balance than in a strain gauge balance because the model comprises a link in the control system of the balance. The block diagram of the actual control system for one degree of freedom small motion can be represented by the diagram shown in fig. 3.5. Consider an equivalent second order system representing the motion of the model under

the influence of the electromagnet current in one degree of freedom. The differential equation of motion of the model is then given by

$$J\ddot{\theta} + c\dot{\theta} + k\theta = F(t) = F_m(t) + F_a(t) \qquad 3.16$$

where θ is the model pitch attitude displacement, J is the model inertia, c is damping (e.g. due to eddy currents in the model) and k is the balance stiffness. F(t) is the total instantaneous external force acting on the model and is the addition of two parts, the magnetic force $F_m(t)$ and the instantaneous aerodynamic force increment $F_a(t)$ due to incidence $\alpha(t)$. The instantaneous aerodynamic force increment, which in this case represents the pitching moment about model C.G., can be represented in the time domain by the function

$$F_a(t) \simeq F_\alpha\, \alpha(t) + F_{\dot{\alpha}}\, \dot{\alpha}(t) \qquad 3.17$$

where F_α and $F_{\dot{\alpha}}$ are the aerodynamic stiffness and damping coefficients at the reference values $\alpha = 0$ and $\dot{\alpha} = 0$. F_α and $F_{\dot{\alpha}}$ are constant only for the linear aerodynamic case considered here. The magnetic force is related to the electromagnet coil current and model position for small displacements through the relation,

$$F_m(t) = B_1\, I(t) + B_2\, \bar{I}\, \theta(t) \qquad 3.18$$

where I(t) is the instantaneous current, $\bar{I}$ is the current at the reference condition, and B_1 and B_2 are constants. Since θ can be taken equal to α, by substitution from equations 3.17 and 3.18 into 3.16 we get

$$J\ddot{\alpha} + (c - F_{\dot{\alpha}})\dot{\alpha} + (k - B_2\, \bar{I} - F_\alpha)\alpha = B_1\, I \quad . \qquad 3.19$$

It is important at this stage to identify the physical picture and

nature of forces acting on the model. With reference to fig. 3.5, an error signal inserted in the control circuit causes a magnetic force which drives the model to change its position. Therefore, through the action of model finite inertia this force component leads the displacement. Consequent upon the model displacement the aerodynamic forces acting on the model will change, but this part of the force lags the displacement. The magnetic field acts to stabilise the model position through the feedback. The result of this sequence of events is that the magnetic force, in terms of the measured electric currents in the coils, can either lead or lag the displacement signal. The nature of the phase relationship between the net aerodynamic force and the measured current is determined by model inertia, system characteristics and the model aerodynamic transfer function. A schematic of the vector diagram for a sinusoidal low frequency forced oscillation is shown in fig. 3.6. The phase relations are shown exaggerated to emphasise the complex nature of the dynamics involved.

If the error signal is a ramp function, the steady state ramp response lags the force signal and a region of transients is set at the ramp start. For the ideal case of a second order system with a natural undamped frequency $\omega_n \left(= \sqrt{\frac{k - B_2 \bar{I} - F_\alpha}{J}} \right)$, damping ratio $\zeta \left(= \frac{c - F_{\dot{\alpha}}}{2 \omega_n J} \right)$ and the input current $I = \dot{I}t$, the α response for $t \geq 0$ becomes

$$(k - B_2 \bar{I} - F_\alpha) \frac{\alpha}{\dot{I}} = (t - \frac{2\zeta}{\omega_n}) + \frac{e^{-\zeta\omega_n t}}{\omega_n \sqrt{1-\zeta^2}} \sin(\omega_n \sqrt{1-\zeta^2}\, t + \phi) \qquad 3.20$$

where $\tan \phi = \frac{2\zeta\sqrt{1-\zeta^2}}{2\zeta^2 - 1}$.

At large values of t, α reaches its steady state condition $\alpha_{(ss)}$ given

$$(k - B_2 \bar{I} - F_\alpha)\alpha_{(ss)} = \dot{I}\,(t - \frac{2\zeta}{\omega_n}) \qquad 3.21$$

which clearly indicates that $\alpha_{(ss)}$ lags I by the time $\frac{2\zeta}{\omega_n}$ $\left(= \frac{c - F_{\dot{\alpha}}}{k - B_2 \bar{I} - F_\alpha}\right)$.

Therefore it is necessary to shift the current signal in time, fig. 3.7, by this amount, if it is significant, in order to recover a measure of the 'static' data. This can be done in practice easily if the damping and stiffness terms in equation 3.19 are known, or by curve fitting the current response to a straight line, after allowing for a short transient period. The intersection with the datum, relative to the incidence ramp start, then gives the required time lag. The latter is only reliable if the two signals under consideration (i.e. current and incidence) are purely linearly related.

The other important feature of the ramp response is the presence of the initial transient given by the last term of equation 3.20. It can be shown that the transient subsides to a small fraction of the steady state error, Δ/Δ_o, in a time given by

$$t_{bal.} \sim \frac{1}{\zeta\omega_n} \ln(\frac{\Delta_o}{\Delta}) \qquad 3.22$$

where $\Delta_o = \dfrac{\dot{\alpha}}{\omega_n\sqrt{1-\zeta^2}}\, e^{-2\zeta^2}$ (see fig. 3.7)

Δ_o clearly varies linearly with $\dot{\alpha}$ and so $t_{bal.}$ increases only as the logarithm of $\dot{\alpha}$ but varies inversely with ω_n indicating a stronger dependence on the latter. It is necessary to ensure that $t_{bal.} \leq t_{RS}$ in order that clean aerodynamic effect can be recovered. If this condition is not satisfied, the initial transients would inevitably corrupt the measured data. Assuming an arbitrary but reasonable value for Δ

say $\Delta = 0.1\ \Delta_o$ then

$$t_{RS} \geq \frac{1}{\zeta\omega_n} \ln 10 = \frac{2.303}{\zeta\omega_n} \qquad 3.23$$

or

$$\omega_n \geq \frac{2.303}{\zeta\ t_{RS}} . \qquad 3.24$$

If the initial transient error is specified as 0.1 of the steady state error instead, an alternative form to equation(3.24)would be given by

$$\omega_n \geq \frac{1}{\zeta\ t_{RS}} \left[1.6 + \ln \left(\frac{1/\zeta}{\sqrt{1-\zeta^2}} \right) - 2\zeta^2 \right] . \qquad 3.25$$

Equation(3.24) gives a conservative estimate of the minimum natural frequency of the balance system which leads to measurements requiring no balance correction. From equation (3.24) the time lag in the steady state response would be given by

$$t_{lag} \leq \frac{2}{2.303}\ \zeta^2\ t_{RS} . \qquad 3.26$$

The quality of the response can be judged from observation of the incidence signal as a function of time. If $\alpha = \dot{\alpha}t$ a steady state relation can be established between α and the current I since $\ddot{\alpha} = 0$. Before doing that, equation (3.19) requires slight rearrangement for it to be useful for the direct evaluation of static forces. In a similar way to that for the force-current relationships developed in Appendix A, it is possible to show that a change in the force F_m is related to a change in the current I by:

$$F_m = (b_1 + b_2\,\alpha)I \qquad 3.27$$

where b_1 and b_2 are related to B_1 and B_2 defined in equation 3.18. Hence rearranging and substituting for $\dot{\alpha}$ = const. into equation (3.19) we get

$$(c - F_{\dot{\alpha}})\dot{\alpha} + (k - F_{\alpha})\alpha = B_1 I + B_2 \bar{I}\,\alpha \qquad 3.28$$

If the lag t_{lag} is negligible, then by performing wind-on and wind-off tests at the same $\dot{\alpha}$ equation (3.28) can be applied twice and the two sets of results differenced at the same values of α to obtain the net aerodynamic effect which is then given by

$$-\dot{\alpha} F_{\dot{\alpha}} - F_{\alpha}\,\alpha = (b_1 + b_2\,\alpha)I \qquad 3.29$$

where I indicates the net current change due to aerodynamic forces. This result can be arrived at intuitively for the 'almost static' cases. When the lag time is appreciable, some means of correcting, e.g. by shifting I(t) curves appropriately, is required before carrying out the subtraction operation leading to equation(3.29).

For the nonlinear aerodynamic case, the correction is expected to be more subtle. The main difficulty in the nonlinear case is expected to be found in attempts to separate the true nonlinearities from the transients. For the pure ramp incidence test, i.e. $\dot{\alpha}$ = const, equation (3.29) remains valid for the nonlinear aerodynamic case but with the terms $F_{\alpha}.\alpha$ and $I.\alpha$ replaced by the general functions $F(\alpha)$ and $I(\alpha)$ respectively. In this case the linearity of incidence with time indicates a prevailing constant phase relationship between the current signal and the acting aerodynamic force. The time lag between the current

signal and displacement depends on the local first derivative of current with respect to time, or the derivative of the aerodynamic force with respect to incidence. The transients, however, depend as well on higher derivatives in addition to the overall previous history since the instant of start of excitation. Precise details of the transients in such a case are difficult to estimate for the general case. Resort must therefore be made to approximate methods. One method of treating a nonlinear function is by considering it to be made up of linearised segments i.e. by carrying out a piecewise linearisation. The linearised portions are joined at instants fixed by the suitably chosen instants of occurrence of a set of equivalent pulses in the diagram of second derivative. An alternative way of estimating the overall corrections can be followed in practice through the observation of small step response at critically nonlinear regions in the performance range.

The practical situation of pitch ramp testing can involve the measurement of several force components e.g. lift force, pitching moment and drag force. In a multicomponent balance these force components need to be measured simultaneously. Each component is measured in the form of an electrical signal in a control system, the system having its own natural frequency of oscillation. In general these natural frequencies are not equal; hence the transients, lags and distortions of various force components are not the same. If times longer than the flow response time t_{RS} are observed then the aerodynamic effects are regarded as occurring simultaneously. Balance correction, consequently, should be applied to each component separately. In addition, initial transients may persist for a relatively long time in force components having the lowest balance natural frequency and damping in this component. Care should therefore be taken to ensure that such conditions do not arise, so that

the overall accuracy of the results is maintained.

In conclusion, it is worth emphasising that balance output signals at frequencies much higher than its natural frequency (s) are of no significance to the measured aerodynamic forces for the various reasons previously discussed.

3.1.3 Basic details of the proposed technique of testing

The previous two sections have defined the limitations imposed by the required quality of aerodynamic measurement and the effects of balance transients on the method of constant pitch ramp testing. Other features of the technique, which require consideration, include the estimation of:

i - a suitable averaging interval for the data,

ii - the filter bandwidths and required sampling rate of digital data,

iii - the dynamic correction of data.

Since the model displacement and various current components are measured as analogue voltage signals which contain a certain amount of superimposed noise (e.g. due to power supply and control system imperfections), it is necessary to filter and digitize the data for digital analysis. To reduce the noise and quantity of data further, piece-meal averaging is suggested. Averaged digital data is then corrected for the effect of averaging interval and dynamic effects in order to recover the original analogue mid-range values. Balance dynamic effects are then introduced to correct for lags between various components and finally static force calibration relations are applied to obtain the aerodynamic forces and moments.

Piece-meal averaging of analogue data

Consider a continuous time varying function g(t), e.g. a force or a displacement signal, as shown in the sketch. By subdividing the time axis into short intervals of time Δt, the best estimate (time average)

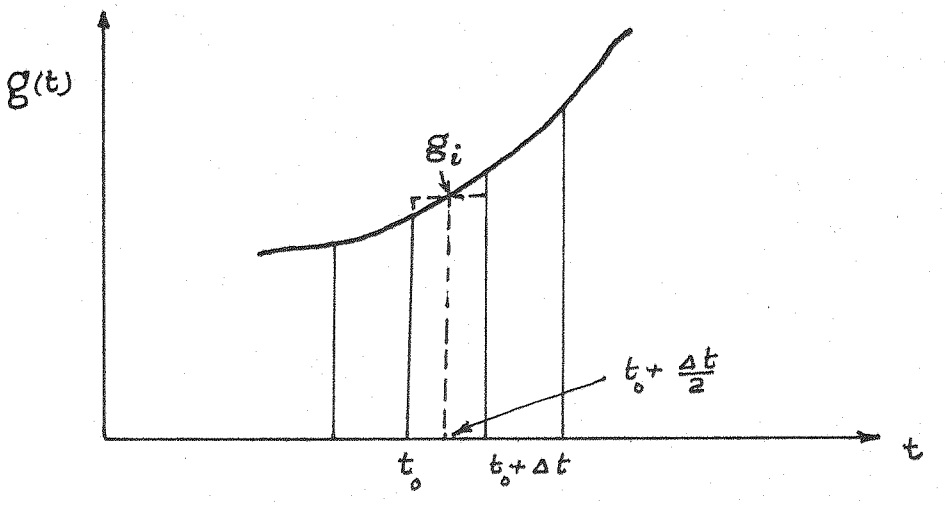

and variance of the function in any interval t (e.g. interval i) can be calculated as follows.

$$\left.\begin{aligned} \bar{g}_i &= \frac{1}{\Delta t} \int_{t_o}^{t_o+\Delta t} g(t)\, dt \\ \sigma_{g_i}^2 &= \frac{1}{\Delta t} \int_{t_o}^{t_o+\Delta t} g^2(t)\, dt - (\bar{g}_i)^2 \end{aligned}\right\} \quad 3.30$$

A new independent variable ξ is defined by

$$\xi = t - \left(t_o + \frac{\Delta t}{2}\right)$$

valid in the range

$$-\frac{\Delta t}{2} \leq \xi < \frac{\Delta t}{2} .$$

The function $g(t)$ ($\equiv g(\xi)$) can be expanded for small values of ξ in the interval Δt using a Taylor's series as follows,

$$g_i(t) = g_i(\xi) = g_i(o) + \xi\, g_i'(o) + \frac{\xi^2}{2!} g''(o) + \ldots \qquad 3.31$$

where the primes indicate differentiation with respect to time. Substituting into equations (3.30) and evaluating the corresponding integrals gives:

$$\left.\begin{aligned} \overline{g}_i &= g_i + \frac{(\Delta t)^2}{24} g_i''(o) + O(\Delta t)^3 \\ \sigma^2_{g_i} &= \frac{(\Delta t)^2}{12} g_i'^2 + \frac{(\Delta t)^2}{60} g_i''^2 + O(\Delta t)^6 \end{aligned}\right\} \qquad 3.32$$

Since at the middle of the interval the value of the function is g_i, the averaging process recovers this value within an error of

$$\varepsilon_i \approx \frac{(\Delta t)^2}{24} g_i'' \qquad 3.33$$

which has a standard deviation of

$$\sigma_{g_i} \simeq \frac{\Delta t}{\sqrt{12}} |g_i'| \qquad 3.34$$

This error term shows that piecemeal averaging necessarily displaces the, essentially nonlinear, estimate of the function towards the centre of curvature by an amount varying as $(\Delta t)^2$. For purely linear functions ε_i is identically equal to zero and no correction is necessary. For nonlinear functions, if a good estimate of the second derivative of the function is available, ε_i can be corrected for. This can be easily estimated from an approximate knowledge of g_i over successive intervals.

Overlapping the averaging intervals can improve data resolution. If intervals are allowed to overlap each other, the discrete values of g_i would be separated by $\Delta_1 t$, representing the time resolution of averaged results. At the i^{th} point a good estimate of g_i'' is given by

$$g_i'' \approx \frac{g_{i+1} - 2g_i + g_{i-1}}{(\Delta_1 t)^2} \qquad 3.35$$

Therefore the correction to be added to the averaged data points $\bar{g}_i$ is

$$-\varepsilon_i = -\frac{1}{24}\left(\frac{\Delta t}{\Delta_1 t}\right)^2 (g_{i+1} - 2g_i + g_{i-1}) \qquad 3.36$$

which is correct to within a standard deviation = $\sqrt{6}\,\sigma_g$. Equation (3.34) can be used as a basis for establishing a criterion limiting the resolution of the averaged data in the noise free function case. The criterion is that a change in the value of the function between two successive points (after averaging over intervals Δt long) must be at least equal to the standard deviation σ_g. In the current notation this leads to

$$(g')^2 (\Delta_1 t)^2 \geq \frac{(\Delta t)^2}{12} (g')^2 \qquad 3.37$$

Provided that $g' \neq 0$ an expression for the minimum value of $(\Delta_1 t/\Delta t)$ can be obtained from equation (3.37) and is given by

$$\left(\frac{\Delta_1 t}{\Delta t}\right)_{min} = \sqrt{\frac{1}{12}} = 0.29 \qquad 3.38$$

If $g' = 0$ the function possesses a local extremum. In this case a value of $\Delta_1 t/\Delta t < 1.0$ has no particular advantage over $\Delta_1 t/\Delta t = 1.0$, therefore the latter value is regarded reasonable. A value of $\Delta_1 t/\Delta t > 1.$ is of

no interest to the present work since it implies dropping part of the data deliberately. It is obvious that the presence of noise in the practical situation, being added to the function g, can greatly increase the variance and hence add a positive quantity to the RHS of equation (3.37). This results in an increase in $(\Delta_1 t/\Delta t)_{min}$ by an amount related to the ratio of the noise standard deviation to the local derivative of the function.

In order to study the effect of noise present on the data the harmonic content of g(t) is considered, i.e. the equivalent Fourier series terms. If g(t) contains a sinusoid component, $x = x_o \sin \omega t$, where ω is the frequency of the sinusoid, it can be shown that piecemeal averaging causes an attenuation of this component by the factor $\text{sinc} \frac{\omega \Delta t}{2} = \sin(\frac{\omega \Delta t}{2})/(\frac{\omega \Delta t}{2})$ and the error term is

$$\varepsilon_i = x_i \left[1 - \text{sinc} \frac{\omega \Delta t}{2} \right] \qquad 3.39$$

where x_i is the actual value of the function at the middle of Δt. The quantity in the square brackets is always positive since $\text{sinc} \frac{\omega \Delta t}{2} \leq 1.0$ and is shown in fig. 3.8. At very small values of $\frac{\omega \Delta t}{2}$, i.e. for $\omega << \frac{2}{\Delta t}$

$$\varepsilon_i \simeq x_i \frac{(\omega \Delta t)^2}{24} \qquad 3.40$$

while at large values of $\frac{\omega \Delta t}{2}$, i.e. for $\omega >> \frac{2}{\Delta t}$

$$\varepsilon_i \simeq x_i \left[1 - \frac{2}{\omega \Delta t} \right] \qquad 3.41$$

Equation (3.41) indicates that the piecemeal averaging at a constant interval width Δt in effect filters the high frequency content of the

original data while low frequency parts suffer only a slight attenuation as shown by equation (3.40). It follows that the shorter the averaging interval Δt, the broader is the corresponding frequency spectrum included. Since in this work interest lies in recovering the low end of the frequency spectrum with the least error, the result obtained in equation (3.40) deserves a closer look. The lowest frequency of the harmonic component with a vanishing average in the interval Δt is $\omega_c = \frac{2\pi}{\Delta t}$ and the frequency contributing maximum numerical value to the average is $\frac{\omega_c}{2}$. At frequencies higher than ω_c the contribution of a particular harmonic will have a maximum value of $\frac{2A}{\omega\ \Delta t}$ where A is the amplitude of this harmonic. If this is to be kept within a fraction of A, say η_H A, then

$$\omega \geq \frac{2}{\Delta t\ \eta_H} \quad . \qquad 3.42$$

This equation establishes a relationship between the permissible averaging interval and the effective highest frequency contributing to the averaged data of the noise corrupted function. The minimum averaging interval width is given by

$$\Delta t_{min} = \frac{2}{\eta_H\ \omega_{max}} \quad . \qquad 3.43$$

Less quantitative relationships limiting the largest Δt can be thought of. On a qualitative basis, it can be argued that averaging causes a smearing of the details of the function and therefore the maximum degree of smearing must be related to the longest allowable interval. Overlapping of the averaged intervals improves the recovery of the original function and hence reduces the degree of smearing. In the absence of suitable quantitative estimates reliance must be placed on the incidence interval corresponding to the averaging time interval as a convenient index in the

incidence sweep test for fixing a reasonable time interval.

Piecemeal averaging of digital data

In digitizing analogue data, two types of error can arise:

i - quantisation error - improper conversion of the amplitude of signals, and

ii - discretisation or sampling error - affecting the frequency content of signals.

The first type is mainly related to the number of binary digital bits, i.e. precision, and accuracy of the Analogue-to-Digital Converter (ADC), while the second type is associated more closely with the sampling rate. Signal amplification before digitisation can easily reduce the quantisation error to an insignificant value and so will not be considered any further. In connection with the second type, statistical sampling theories indicate that in the digitised data only frequencies up to $\frac{2\,N_s}{5}$ can be identified, where N_s is the sampling rate. The presence of higher frequencies in the analogue signal causes aliasing. In order to reduce aliasing, higher frequency components must be appropriately filtered before digitising. This requires a low-pass filter for a single signal acquisition, or a set of phase matched filters for phase related multi-signal simultaneous acquisition, with a cut-off frequency set at about $2\,N_s/5$ or less.

Consider the continuous function of time g(t) being represented by discrete values uniformly spaced at an interval $\delta_s = \frac{1}{N_s}$ as shown in the sketch below.

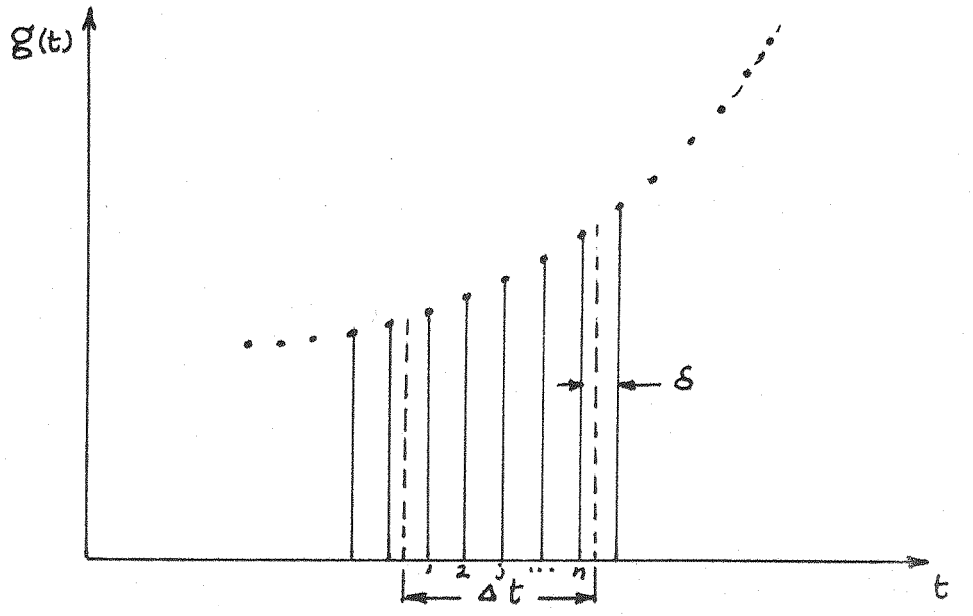

The averaging interval Δt will therefore contain n samples since $\Delta t = n\delta_s$. If n is an odd number then mid-range is at the value $j = \frac{n+1}{2}$ where j is the sample number. The original function at the j^{th} point in the inverval Δt, can be obtained by substituting $\xi = (j - \frac{n+1}{2})\delta_s$ in equation (3.31) which gives the j^{th} value in the i^{th} interval as

$$g_j \simeq g_{\frac{n+1}{2}} + (j - \tfrac{n+1}{2})\delta_s\, g'_{\frac{n+1}{2}} + (j - \tfrac{n+1}{2})^2 \frac{\delta_s^2}{2!}\, g''_{\frac{n+1}{2}} \qquad 3.44$$

where $j = 1,2,\ldots n$. For simplicity the subscript $\frac{n+1}{2}$ is going to be replaced by i without loss of generality. Taking the mean and variance of the discrete values yields

$$\left.\begin{aligned} \overline{g}_i &= g_i + \frac{\delta_s^2}{2n} \sum_1^n (j - \tfrac{n+1}{2})^2\, g''_i \\ \sigma^2_{g_i} &= \frac{\delta_s^2}{n} \sum_1^n (j - \tfrac{n+1}{2})^2\, g'^2_i \quad . \end{aligned}\right\} \qquad 3.45$$

It can be shown that when n is an odd integer,

$$\sum_1^n (h - \tfrac{n+1}{2})^2 = 2 \sum_1^{\frac{n-1}{2}} j^2$$

The error in the average value is therefore given by

$$\varepsilon_i = \frac{\delta_s^2}{n} \left(\sum_{1}^{\frac{n-1}{2}} j^2 \right) g_i'' \qquad 3.46$$

Substituting for δ_s in terms of Δt, the error and variance

$$\left.\begin{aligned} \varepsilon_i &= (\Delta t)^2 \left[\frac{1}{n} \sum_{1}^{\frac{n-1}{2}} j^2 \right] g_i'' \\ \sigma_g^2 &= (\Delta t)^2 \left[\frac{2}{n^3} \sum_{1}^{\frac{n-1}{2}} j^2 \right] g_i'^2 \end{aligned}\right\} \qquad 3.47$$

Comparing these expressions for ε_i and σ_g^2 with the results obtained for the analogue case (equation 3.33 and 3.34), it is found that the displacement of the piecemeal averaged value is several times as much for low values of n but decreases asymptotically to the analogue value as n becomes very large. An expression for the correction term to be added to the averaged data in order to recover the original time functional variation is obtained in a similar way to that of the analogue case equation (3.36) and is given by

$$-\varepsilon_i = -\left(\frac{\Delta t}{\Delta_1 t}\right)^2 \left[\frac{\sum_{1}^{\frac{n-1}{2}} j^2}{n^3} \right] (g_{i+1} - 2g_i + g_{i-1}) \qquad 3.48$$

If n_1 is the number of samples separating the averaged interval midpoints then the correction term and variance are given by

$$\left.\begin{aligned} -\varepsilon_i &= -\left[\frac{1}{n_1 n} \sum_{1}^{\frac{n-1}{2}} j^2 \right] (g_{i+1} - 2g_i + g_{i-1}) \\ \sigma_{g_i}^2 &= \left[\frac{2}{n_1 n} \sum_{1}^{\frac{n-1}{2}} j^2 \right] (g_{i+1} - g_i)^2 \end{aligned}\right\} \qquad 3.49$$

So far data correction formulae contained finite difference estimates of the derivatives g' and g". When the signal at hand is noise corrupted the uncertainty of the averaged data and the standard deviation become larger, hence the finite difference estimates of the derivatives becomes unreliable. In this situation derivatives are best numerically evaluated using a suitable local least squares fit of the averaged data.

Effect of piecemeal averaging on the balance transients

It has already been shown that piecemeal averaging displaces the actual curve towards its centre of curvature. When this is applied to the transients of a ramp response the result is an attenuation of the amplitude of the transient. Therefore the condition of reaching an error Δ, equation (3.22), is achieved earlier i.e. $t_{bal.}$ is actually reduced. This in effect reduces the allowable minimum natural frequency of the balance. The relative shortening is given by

$$-\frac{\omega_n (\Delta t)^2}{24 \ln(\Delta_o/\Delta)} \qquad 3.50$$

for the digital data. It can be shown that when $\Delta t = \frac{2\pi}{\omega_n\sqrt{1-\zeta^2}}$ the value of $t_{bal.}$ reduces to an insignificant value.

Correction of the data for damping derivatives

The instantaneous aerodynamic lift force acting on a slowly moving model is a function of the instantaneous values of incidence and pitch rate and can be given by

$$L = L(\alpha , \dot{\alpha}) = g(t) \qquad 3.51$$

In general this is a nonlinear function in α and $\dot{\alpha}$. The change in lift force following small changes in α and $\dot{\alpha}$ from reference values α_{ref} and $\dot{\alpha}_{ref}$ (=0) can be expressed using a Taylor's expansion as follows,

$$\Delta L = \frac{\partial L}{\partial \alpha} \Delta\alpha + \frac{\partial^2 L}{\partial \alpha^2} \frac{(\Delta\alpha)^2}{2!} + \ldots + \frac{\partial L}{\partial \dot{\alpha}} \dot{\alpha} + \ldots + \frac{\partial^2 L}{\partial \alpha \partial \dot{\alpha}} \Delta\alpha \, \Delta\dot{\alpha} + \ldots$$

$$\simeq \Delta L(\alpha, \dot{\alpha}_{ref}) + \Delta\dot{\alpha}\left(\frac{\partial L}{\partial \dot{\alpha}} + \Delta\alpha \frac{\partial^2 L}{\partial \alpha \partial \dot{\alpha}} \right). \qquad 3.52$$

When $\dot{\alpha}_{ref} = 0$ the first term on the RHS of the last equation represents the static lift and the second, bracketed, quantity represents the damping contribution. For a continuously moving model the instantaneous incidence is given by

$$\alpha = \alpha_{ref} + \int_{t_{ref}}^{t} \dot{\alpha}(u) \, du \qquad 3.53$$

Changing the independent variables α, $\dot{\alpha}$ in equation (3.52) to the single variable t, the time, and making use of equation (3.51) and the last equation we get, provided that $\dot{\alpha}$ is continuous,

$$\frac{\partial L}{\partial \dot{\alpha}} = \frac{\partial t}{\partial \dot{\alpha}} \frac{dg}{dt} = - \frac{(t - t_{ref})}{\dot{\alpha}} \frac{dg}{dt}$$

$$\frac{\partial^2 L}{\partial \alpha \, \partial \dot{\alpha}} = - \frac{1}{\dot{\alpha}^2} \frac{dg}{dt} - \frac{(t - t_{ref})}{\dot{\alpha}^2} \frac{d^2 g}{dt^2} \qquad 3.54$$

For the pure pitch ramp case, $\dot{\alpha}$ exhibits discontinuities at the start and at the termination of the ramp while it remains, in the ideal case, constant in between. Equation (3.52) reduces to

$$\Delta L = \Delta L(\alpha, \dot{\alpha}_{ref}) + \Delta\dot{\alpha} \frac{\partial}{\partial\dot{\alpha}} L(\alpha,\dot{\alpha})\Big|_{\dot{\alpha}_{ref}} \qquad 3.55$$

Since the step change in ramp rate $\Delta\dot{\alpha}$ = const, at least two values of $\Delta\dot{\alpha}$ must be applied successively in a testing (in the absence of information about $L_{\dot{\alpha}}(\alpha)$) in order to be able to estimate the second quantity in the last equation. This is easily achieved by reversing the ramp after a pause as suggested earlier and then interpolating the aerodynamic force at every incidence value for $\dot{\alpha} = \dot{\alpha}_{ref}$ by using the values for the two equal but opposite sign cases of $\Delta\dot{\alpha}$. The static force at a certain value of incidence is therefore given by the average of the two ramp

$$\Delta L(\alpha) = ((\Delta L)_+ + (\Delta L)_-)/2 \qquad 3.56$$

where the subscripts + and - correspond to measured forces under positive and negative ramp rates respectively. It is implicitly assumed in the last equation that the aerodynamic force is of a nonhysteretic nature. If the aerodynamic characteristic possesses a hysteresis additional information about the region and extent of occurrence of this hysteresis would be required before a successful damping correction can be applied.

A byproduct of equation (3.55) and the ramp testing is a measure of the damping derivative, since

$$2\,\Delta\dot{\alpha} \frac{\partial L}{\partial\dot{\alpha}} = (\Delta L)_+ - (\Delta L)_- \quad .$$

Although this is true in principle, in practice it is not a proposition worth pursuing. The reason lies in the fact that unless $\dot{\alpha}$ is very large the static part comprises the major part of the measured force signals. This in turn renders the dynamic part of the signals affected strongly by the noise present hence it has a relatively larger uncertainty.

3.1.4 Self consistency of a performance test

In practice the reliability of a certain measurement depends on the hardware and software complexity, degree of redundancy of the test facility and the test duration. The longer the testing time or separation between two data points the lower is the reliability of measurement. Higher reliability of measurement results in better repeatability of the experiment. Favourable conditions can only be realised if the experiment (and facility) are statistically well-controlled.

If data points to cover a certain performance range in an experiment are taken in a single test run over a relatively short duration then a high degree of repeatability or 'self consistency' of the data points is found to exist. It is possible then to draw a demarcation between repeatability and self consistency. A test run may provide a set of highly self consistent data points over a performance range while single data points obtained in various runs may not enjoy high repeatability. It can be argued that in a single test run over a short duration of time the total error in each data point is a purely random error while it is likely that from different test runs other types of error can add to this. The relative error in the first case between any two data points is just $\sqrt{2}$ times the random error in either, but in the latter case it may be several times higher.

Pitch ramp testing in a magnetic suspension system, as proposed

here, offers a good example of a complex system where only a fair degree of statistical control can be maintained on measurements. Electronic noise and drift, position (optics) drift, amplifier intermittency etc. can cause a greater amount of uncertainty in a measurement than would be caused by purely stationary random noise. Since the drift and intermittency are slowly varying functions of time it is clear that the shorter the test duration the greater is the self consistency of widely spaced data points in the performance range of testing, i.e. range of incidence. It must however be emphasized that the pitch ramp testing as presented here contains a certain degree of dynamic effect but, as discussed earlier, this can be reduced to a very small value.

3.2 Dynamic stability derivative measurement techniques

Very often the measurement of oscillatory dynamic derivatives in wind-tunnels at low frequency parameters and small amplitudes of oscillation is of interest. This is generally the case with forced oscillation testing. In this kind of testing, signals proportional to displacement and force are observed and analysed for the required derivatives. If both signals are pure contrived sinusoids, then methods of deterministic analysis are sufficient to provide the required information on dynamic derivatives. In practice, however, system random noise (which can only be statistically specified) inevitably corrupts the signals to varying extents. This noise could be flow induced, due to wind-tunnel vibration or of electrical or electronic origin. Such noise can seriously affect the accuracy of testing particularly if the signal to noise ratio is low or moderate. Particularly in existing magnetic suspension systems there is a great deal of power supply noise on the current signals (the force indication) although the noise may not be fundamental to such systems. The noise is present everywhere in the

control loop stabilising the model. Means of filtering this noise from the signals are therefore required before clean signals can be recovered. Hence it becomes natural to seek statistical methods of data analysis for filtering and/or providing the required information directly. There is a host of methods of statistical data analysis that may be used. The most important are:

i - spectral analysis method,

ii - signal averaging method,

iii - direct correlation methods (zero lag),

iv - correlation methods using reference clean signals (zero lag),

v - correlation methods using numerically generated clean signals (zero lag).

When signals contain a contrived sinusoid component their frequency spectral distribution will feature sharp peaks at the sinusoid frequency. Spectral methods of analysis will produce poor accuracy unless the signal duration is very long and the spectral resolution of analysis is very narrow, owing to the poor coherence of analysis at the sinusoid frequency. Signal averaging methods require similarly long test durations as well as precise knowledge of the frequency of the sinusoid part and a sampling rate which is an integral value of the sinusoid period. Correlation methods, however, can be applied to both deterministic and random signals and so offer great potential and deserve investigation in depth. Direct correlation methods suffer inaccuracies if the noise on the two signals is correlated in part. In addition, a moderately long signal duration is required. Correlation methods using reference clean signals can improve on the previous method but would require twice the analysis effort. Methods of correlation using numerically generated sinusoids can be very useful particularly with short duration signals,

i.e. of about one cycle of oscillation length, however extreme precision on the frequency is needed.

It is well known that correlation methods, if exploited appropriately, can recover hidden sinusoidal signals when correlation coefficients are observed at moderate lags (i.e. time delays), i.e. further from zero lag. The method of level crossings of the correlation functions away from the zero lag axis offers a means of estimating the required signal properties to better accuracy than the various methods listed above, without necessitating the strict limitations imposed by any of them. This method is presented and discussed in the following sections following an adequate mathematical model representation of the oscillating model.

3.2.1 Single degree of freedom testing - fixed incidence

Consider a model in the flow of a wind-tunnel working section. The model and wind axis systems are defined in figure 3.9. The model is forced into a sinusoidal oscillation in roll about its longitudinal axis X at a small roll displacement ϕ. When the model is kept at a fixed incidence, its dynamics can be adequately represented by a second order damped system. The mathematical model is therefore given by the differential equation

$$J\ddot{\phi} + C\dot{\phi} + K\phi = M(t) \qquad 3.57$$

where J is the moment of inertia about the X-axis, C is the total damping, K is the total roll stiffness and M(t) is the applied roll torque. When M is sinusoidal with a frequency ω which is smaller than the system natural frequency ω_n then the vector diagram representing the motion is very much the same as the one shown in fig. 2.8.a. High frequency testing has the disadvantages discussed earlier in chapter 2. In addition,

for a magnetic suspension balance low frequency testing is particularly advantageous in order to minimise the otherwise significant eddy current contribution to damping in a conducting model.

Let the torque and displacement be given by:

$$\left.\begin{aligned} M(t) &= \hat{M}\, e^{j\omega t} \\ \phi(t) &= \hat{\phi}\, e^{j\omega t} \end{aligned}\right\} \qquad 3.58$$

Applying these equations to equation (3.57) gives

$$\left.\begin{aligned} \frac{\hat{M}(\omega)}{\hat{\phi}(\omega)} &= (K - J\omega^2) + j\omega C \\ &= \left| \frac{\hat{M}(\omega)}{\hat{\phi}(\omega)} \right| < \varepsilon \end{aligned}\right\} \qquad 3.59$$

where

$$\tan \varepsilon = \frac{\omega C}{K - J\omega^2}$$

$\hat{M}(\omega)/\hat{\phi}(\omega)$ is (some kind of) a frequency response function and can be written in the following form

$$\frac{\hat{M}(\omega)}{\hat{\phi}(\omega)} = Q_{in} + j\, Q_{quad.} \qquad 3.60$$

where Q_{in} is the component of $\hat{M}(\omega)$ in-phase and Q_{quad} the corresponding component in quadrature with the displacement signal. Equations (3.59) and (3.60) give

$$\begin{aligned} \omega C &= Q_{quad.} \\ &= \left| \frac{\hat{M}(\omega)}{\hat{\phi}(\omega)} \right| \sin \varepsilon \end{aligned} \qquad 3.61$$

It is clear from the above result that in order to measure the damping derivative accurately, accurate estimates are needed for the torque-displacement frequency response function (magnitude and phase angle) and the frequency of oscillation.

The measured voltage signals corresponding to the forcing torque and displacement are generally corrupted with noise which can affect the accuracy of damping measurement for two reasons:

(i) displacement signal is usually deliberately kept small in order to avoid nonlinear effects,

(ii) in low frequency testing the phase angles are usually very small.

By far the most widely used method nowadays works on the wattmeter principle, section 2.2. Methods and instrumentation based on the wattmeter principle provide reasonable accuracies so long as phase differences are large e.g. close to 90^{o} , i.e. when $\omega \not\approx \omega_n$ hence extreme precision is not required. The wattmeter method is a form of real time analysis where the product of the two signals is averaged over long times, providing the covariance function at zero lag, and this average is heavily filtered to read an effectively d.c. signal. The presence of correlated noise on both signals contributes an error to this d.c. signal no matter how long the averaging time or how heavy the filtering. The next sections illustrate this and provide a closer look at the details of the signals.

3.2.2 Correlation (covariance) method - (Sine wave + noise)

Let the two signals $x(t)$ and $y(t)$, $0 \leq t \leq T$ represent two stationary random variables with zero means. These can be regarded as the output and input signals of a linear system or the displacement and force (or

torque) signal in a forced oscillation testing. The autocovariance function of x(t) is defined as

$$C_{xx}(\tau) = \lim_{T\to\infty} \frac{1}{T} \int_0^T x(t)\, x(t+\tau)\, dt$$

and of y(t) as

$$C_{yy}(\tau) = \lim_{T\to\infty} \frac{1}{T} \int_0^T y(t)\, y(t+\tau)\, dt \qquad 3.62$$

where τ is the time lag or shift. The covariance of x(t) and y(t) is defined as

$$C_{xy}(\tau) = \lim_{T\to\infty} \frac{1}{T} \int_0^T x(t)\, y(t+\tau)\, dt \qquad 3.63$$

When $\tau = 0$ the variances associated with the pair of records are

$$\sigma_x^2 = C_{xx}(o)$$

$$\sigma_y^2 = C_{yy}(o) \qquad 3.64$$

The correlation functions (or correlation coefficients) are defined in association with the auto-covariance and covariance functions as:

$$R_{xx}(\tau) = \frac{C_{xx}(\tau)}{C_{xx}(o)}$$

$$R_{yy}(\tau) = \frac{C_{yy}(\tau)}{C_{yy}(o)} \qquad 3.65$$

$$R_{xy}(\tau) = \frac{C_{xy}(\tau)}{\sqrt{C_{xx}(o)C_{yy}(o)}}$$

The first two equations of (3.65) define the autocorrelation coefficient of the single records and the third defines the cross correlation coefficients.

The auto covariance function (or cutocorrelation coefficient) and power spectral density function represent a Fourier transform pair. The cross correlation coefficient (or covariance function) and the cross spectrum form a similar pair.

In practice T is finite and so only approximations to the auto covariance and covariance functions defined in equations (3.62) and (3.63) are obtained:-

$$\left.\begin{aligned} \hat{C}_{xx}(\tau) &= \frac{1}{T-|\tau|} \int_{\frac{|\tau|}{2}}^{T-\frac{|\tau|}{2}} x(t-\tfrac{\tau}{2})\, x(t+\tfrac{\tau}{2})\, dt \\ \hat{C}_{xy}(\tau) &= \frac{1}{T-|\tau|} \int_{\frac{|\tau|}{2}}^{T-\frac{|\tau|}{2}} x(t-\tfrac{\tau}{2})\, x(t+\tfrac{\tau}{2})\, dt \end{aligned}\right\} \qquad 3.66$$

The integration limits are suitably modified to allow for the shortening of the records used in the calculation of the covariances following a time shift between multiplicants. It can be shown that these approximate covariance functions are the best estimates for the exact covariances, [Bendat (1958)].

Consider first the case of two pure sinusoidal records given by

$$\left.\begin{aligned} x &= \overline{X} \sin \omega t \\ y &= \overline{Y} \sin(\omega t+\varepsilon) \end{aligned}\right\} \qquad 3.67$$

$$0 \leq t \leq T$$

The averages of these records are

$$\left.\begin{aligned} \bar{x} &= \bar{X}\,\frac{1-\cos\omega T}{T} = \bar{X}\sin\frac{\omega T}{2}\left(\frac{\sin\frac{\omega T}{2}}{\frac{\omega T}{2}}\right) \\ \bar{y} &= \bar{Y}\sin\left(\frac{\omega T}{2}+\varepsilon\right)\left(\frac{\sin\left(\frac{\omega T}{2}\right)}{\left(\frac{\omega T}{2}\right)}\right) \end{aligned}\right\} \qquad 3.68$$

From the quantities in brackets it can be seen that the averages tend to zero as ωT tends to infinity irrespective of the precise value of ωT. But these averages can be zero when $\frac{\omega T}{2} = m\pi$, $m = 1,2,\ldots$, i.e. when T is precisely equal to an integral multiple of the period of oscillation.

The unbiased autocovariance estimates are obtained by evaluation of the integrals in equation 3.66, leading to

$$\begin{aligned} \hat{C}_{xx}(\tau) &= \frac{\bar{X}^2}{2}\left\{\cos\omega\tau - \cos\omega T\,\frac{\sin\omega(T-\tau)}{\omega(T-\tau)}\right\} - \bar{x} \\ \hat{C}_{yy}(\tau) &= \frac{\bar{Y}^2}{2}\left\{\cos\omega\tau - \cos(\omega T+\varepsilon)\,\frac{\sin\omega(T-\tau)}{\omega(T-\tau)}\right\} - \bar{y} \qquad 3.69 \\ \hat{C}_{xy}(\tau) &= \frac{\bar{X}\,\bar{Y}}{2}\left\{\cos(\omega\tau+\varepsilon) - \cos(\omega T+\varepsilon)\,\frac{\sin\omega(T-|\tau|)}{\omega(T-|\tau|)}\right\} - \bar{x}\,\bar{y} \end{aligned}$$

Equations (3.69) show that the auto covariance and covariance functions of the sinusoids are sinusoidal in the time lag τ at the same basic frequency ω and are given by the first terms on the RHS of the equations. The additional terms can be regarded as error terms which depend on the record length and the value of τ. These error terms tend identically to zero if

$$\left.\begin{aligned} \omega T &= 2m\pi \\ \omega\tau &= m\pi \end{aligned}\right\} \quad 3.70$$

where m takes the values 1,2,3,... ∞. The first of these two conditions imply that the record length of the signals should be an integral number of cycles of oscillation. The value of m = 1 is particularly significant since at $\tau = 0$ exact estimates of the variances of the signals and phase angle can be obtained using a single cycle record length. This is not easy to realise in practice, no matter what record lengths are resorted to for an accurate estimate of ε from $\hat{C}_{xy}(o)$. This occurs because error terms vanish as $1/\omega T$. An alternative method of calculating the phase angle is by observation of the zero crossings of the cross covariance estimate. The full importance of this method will be recognised later in this section. Ideally, if the first of conditions 3.70 holds, then

$$\hat{C}_{xy}(\tau) = \frac{\overline{X}\,\overline{Y}}{2}\left[\cos(\omega\tau+\varepsilon) - \cos\varepsilon\,\frac{\sin\omega(T-\tau)}{\omega(T-\tau)}\right] \quad 3.71$$

for $\tau > 0$. The LHS of this equation goes to zero when

$$\cos(\omega\tau_{zc}+\varepsilon) = \frac{\sin\omega(T-\tau_{zc})}{\omega(T-\tau_{zc})}\cos\varepsilon \quad 3.72$$

This is a complex expression for precise evaluation of τ_{zc}. If we consider the further approximation $\omega(T-\tau_{zc}) >> 1$, then:

$$\cos(\omega\tau_{zc}+\varepsilon) \simeq 0 \quad 3.73$$

or

$$\omega\,\tau_{zc} + \varepsilon = \frac{2m+1}{2}\,\pi$$

which yields

$$m = \frac{\omega}{\pi} \tau_{zc} + \left(\frac{\varepsilon}{\pi} - \frac{1}{2}\right) \qquad 3.74$$

where m = 0, ± 1, ± 2, ± 3, ... etc. and the subscript 'zc' indicates zero crossing. If τ_{zc} is plotted against m as in fig. 3.10, a straight line is obtained (equation 3.74) whose slope equals twice the frequency (in cps) of the signal, and intersection with the m-axis gives the quantity $\frac{\varepsilon}{\pi} - \frac{1}{2}$ from which the phase can be readily obtained. Obviously a number of cycles of the original signal is needed to satisfy the condition $T >> \tau$ and hence allow a range of lags large enough to contain a small number of zero crossings.

The simplest form of noise is a band limited white noise having a uniform power spectral density from d.c. up to the highest frequency f_{WN} and zero everywhere else. The auto covariance function for a zero mean (or average) record of the white noise can be obtained from the spectrum function and is given by

$$\hat{C}_{nn}(\tau) = \sigma_n^2 \frac{\sin 2\pi f_{WN} \tau}{2\pi f_{WN} \tau} \qquad 3.75$$

where σ_n^2 is the noise variance. It is clear from this equation that $\hat{C}_{nn}$ has a maximum at $\tau = 0$ and oscillates with peaks that reduce for other values of τ at a rate of $1/(2\pi\tau f_{WN})$. Fig. 3.11 shows a typical auto covariance function of band limited noise.

Consider now the case of sine wave plus noise. Let

$$\left.\begin{aligned} x_1(t) &= x(t) + n_1(t) = \overline{X} \sin \omega t + n_1(t) \\ y_1(t) &= y(t) + n_2(t) = \overline{Y} \sin (\omega t + \varepsilon) + n_2(t) \end{aligned}\right\} \qquad 3.76$$

$$\text{with} \qquad 0 \leq t \leq T$$

where n_1 and n_2 are random variables representing the noise added to the respective signals and satisfy certain conditions as follows:

i) both random variables are stationary,

ii) both have zero averages,

iii) each has a relatively wide spectrum, and

iv) neither of them correlated significantly with the sinusoids.

It is convenient at this stage to define the signal to noise ratio as the ratio of useful signal amplitude to noise standard deviation

$$\beta_x = \frac{\overline{X}}{\sigma_{n1}}$$
$$\beta_y = \frac{\overline{Y}}{\sigma_{n2}} \qquad 3.77$$

where σ_{n1} and σ_{n2} are the standard deviations of the random variables n_1 and n_2. The auto covariance and covariance of x_1 and y_1 are obtained by substitution into equations 3.66 to give:

$$\hat{C}_{x_1x_1}(\tau) = \hat{C}_{xx}(\tau) + \hat{C}_{n1n1}(\tau) \qquad 3.78$$

and

$$\hat{C}_{x_1y_1}(\tau) = \hat{C}_{xy}(\tau) + \hat{C}_{n1n2}(\tau) \qquad 3.79$$

If the noise random variables have any appreciable degree of correlation, $\hat{C}_{n1n2}$ will be nonzero and the estimate of $\hat{C}_{x_1y_1}(\tau)$ will be in error by this amount. In addition to the conditions already imposed on n_1 and n_2, it is assumed further that they are both of white noise type but may be of different bandwidths. In view of these assumptions it seems reasonable to suggest that a better recovery of the clean signals is obtained where τ is sufficiently different from zero.

The form of $\hat{C}_{n_1n_2}(\tau)$ is not an obvious one to predict since the degree of correlation of the two random variables is not yet well defined. In a qualitative way n_2 can be thought of as the sum of two parts. The first part is due to extraneous noise added to the signal at the output and is independent of n_1. The other part is related to n_1 through the dynamic properties of an assumed linear physical system representing the measuring system. Correspondingly the covariance of the two variables n_1 and n_2 peaks at a lag value, which is related to the system's input-output phase lag at its natural frequency, and then falls off as the lag value τ changes from this. The maximum error in $\hat{C}_{x_1y_1}(\tau)$ due to correlated noise will lie close to the peak just described and smaller errors are to be expected elsewhere. In order to estimate the rate at which such decay takes place it is necessary to estimate $\hat{C}_{n_1n_2}(\tau)$ using the oscillation system characteristics. Although generalised expressions involving convolution integrals can be written down for $\hat{C}_{n_1n_2}(\tau)$ it is preferred here to resort to a simplified analogy for a rough estimate of decay rate. It is known that the response to white noise of bandwidth ω_c, of a second order system having a natural frequency ω_n and a damping ratio ζ, has an exponentially decaying cosine form for its auto covariance function. This can be shown to have the form

$$C(\tau) \simeq \frac{\sigma_{n1}^2}{8} \frac{\omega_n^2}{\omega_c} e^{-\zeta\omega_n\tau} \cos(\omega_n\sqrt{1-\zeta^2}\,\tau) \qquad 3.80$$

which possesses a rate of amplitude decay of

$$-\frac{\sigma_{n1}^2}{8} \frac{\omega_n^2}{\omega_c} e^{-\zeta\omega_n\tau} \qquad 3.81$$

where σ_{n1}^2 is the variance of the noise. The covariance of the input

and output has an amplitude which is smaller than the autocovariance function amplitude and decays at a rate which is at least equal to the one associated with the output autocovariance function. Actually the amplitude reduces to the fraction η_n in a delay interval of

$$\frac{1}{\zeta\omega_n} \ln \frac{1}{\eta_n} \qquad 3.82$$

where

$$\eta_n = \frac{\text{amplitude of covariance}}{(\sigma_{n1}^2\ \omega_n/8\zeta\ \omega_c)}$$

If an arbitrary value of $\eta_n = 1/10$ is chosen, the corresponding minimum lag interval is therefore estimated to be,

$$(\tau_{int})_{min} \sim \frac{1}{\zeta\omega_n} \ln 10 = \frac{2.303}{\zeta\ \omega_n} \qquad 3.82a$$

This lag interval must be allowed for on both sides of the lag value at which the peak of the covariance function occurs before reasonably clean covariance functions can be expected to occur. This result establishes part of the lower limit on the lag values. The upper limit is decided by two factors:

i) truncation effect of the periodic signal on the covariance function, i.e. finite record length effect, and

ii) the numerical error in $\hat{C}_{x1y1}(\tau)$ when τ gets closer to T.

From equation (3.69) it can be shown that the truncation error reduces to less than 1% for T larger than 10 periods of oscillation. The numerical error incurred in $C_{x1y1}(\tau)$ increases as τ increases because of the effective shortening of the record to $T - |\tau|$ with the following

two consequences:

i) as τ increases the error terms in (3.69) increase following a $\frac{\sin \omega(T-\tau)}{\omega(T-\tau)}$ behaviour as shown in fig. 3.12,

ii) as τ increases the error in the estimate of $C_{n1n2}(\tau)$ increases and the uncertainty associated with it increases owing to the reduction in the number of degrees of freedom of the analysis. Bendat and Piersol (1966) show that the standard deviation of the covariance function varies as

$$\frac{1}{\sqrt{\omega_c(T-|\tau|)}} \left| C^2_{n1n2}(\tau) + C_{n1n1}(o) + C_{n2n2}(o) \right|^{\frac{1}{2}}$$

Inspection of the $\frac{\sin x}{x}$ tables show that the first part can be kept to within 1% of its maximum value if $\omega(T - |\tau_{max}|) \geq 100$, or a minimum difference of about 16 periods of oscillation between the record length and the maximum lag to be used. Alternatively, since interest lies in τ_{zc} values, this same term can be shown to produce an error in an estimate of the angle ε, using a single value of τ_{zc}, of the order of $\frac{\sin \omega(T-\tau)}{\omega(T-\tau)}$. If several points (e.g. 8 points) are used to fit a straight line to the τ_{zc} values, the error in ε can be kept to within $1/10^{o}$ if $T-|\tau|$ corresponds to 16 periods of oscillation. The effect of the error from the second part on $C_{x1y1}(\tau)$ depends on the signal to noise ratios defined in equation (3.77). The amplitude of the noise covariance function can be approximately given by:

$$C_{n1n2}(\tau) = \frac{\bar{X}\,\bar{Y}}{2\beta_x\beta_y} e^{-\zeta(\omega_n\tau+\varepsilon)} \qquad 3.83$$

which peaks at $\omega_n\tau = -\varepsilon$. The relative error in the overall covariance estimate reduces to less than γ_1 (of its maximum value, $\bar{\bar{X}}\bar{\bar{Y}}/2$) if the lag is larger than

$$|\tau_{min}| \geq \frac{1}{\zeta\omega_n} \ln\left(\frac{1}{\gamma_1\beta_x\beta_y}\right) \qquad 3.83a$$

from the lag value corresponding to the peak of the covariance estimate. For realisable values of $|\tau_{min}|$, $\gamma_1\beta_x\beta_y$ must be less than 1. As an example, using the typical values $\gamma_1 = 0.005$, $\beta_x = 50$ and $\beta_y = 2$, the corresponding value of $|\tau_{min}|$ should be larger than or equal to $0.85/\zeta\omega_n$. The latter value is already smaller than the value estimated earlier using equation 3.82a. An illustration of the behaviour of equations 3.82a and 3.83a is shown in fig. 3.13a. Values of γ_1, η_n and $|(1/\zeta)(\omega/\omega_n)|$ are taken as parameters. It is interesting to notice that the change-over from the limiting condition of equation 3.82a to that of equation 3.83a occurs at a value of $\beta_x\beta_y = \frac{\zeta_n}{\gamma_1}$ and is independent of the balance dynamic characteristics. When $|\tau| >> \tau_{min}$ the standard deviation of the noise variance estimate varies as

$$\sqrt{\frac{\bar{X}\,\bar{Y}}{2}} \; \frac{1}{\sqrt{\beta_x\beta_y\,\omega_c(T-|\tau|)}} \; .$$

The condition that this quantity be within a small fraction γ_2 of the signals covariance peak value is given by

$$(T - |\tau_{max}|) \geq \frac{1}{\gamma_2^2\beta_x\beta_y}\left(\frac{\omega}{\omega_c}\right) \qquad 3.84$$

This relationship compliments the results arrived at previously from consideration of the truncation effect alone. Equation (3.84) provides a limitation on record length set by noise characteristics. Its importance becomes clearer when dealing with signals having particularly poor values of signal to noise ratios. The behaviour of this relationship is illustrated graphically in fig. 3.13b where the term $(1/\gamma_2^2).(\omega/\omega_c)$ is taken as a parameter. Notice that both axes are logarithmic for

convenience. For favourable values of $\beta_x\beta_y$ the graph shows that the dominant factor in deciding $(T-\tau_{max})$ is the truncation error while for poorer $\beta_x\beta_y$, equation (3.84) sets the limits. The changeover corresponds to $\beta_x\beta_y = 0.01\ (\omega/\omega_c)\ 1/\gamma_2^2$ and the slope of the lines corresponding to equation (3.84) is 45^o. In order to realize the accuracy postulated by the assumption of numerical values for η_n, γ_1 and γ_2 appropriate to a particular system and particular noise characteristics, the record length and range of lags to be calculated must satisfy all the inequalities of equations (3.82-3.84).

The overall record length can be estimated from a combination of equations (3.82) to (3.84) and having τ_{max} corresponding to

$$\omega\,\tau_{max} \simeq \omega\tau_{min} + 2\pi\,N_{zc}$$

where N_{zc} = No. of cycles used for the τ_{zc} calculation. This yields

$$\omega T \geq 2\pi\,N_{zc} + \frac{1}{\zeta}\frac{\omega}{\omega_n} \times \max\{\ln\ \frac{1}{\eta_n}\ ,\ \ln\frac{1}{\gamma_1\beta_x\beta_y}\}$$

$$+ \max\{100,\ \frac{1}{\gamma_2^2\beta_x\beta_y}\ \frac{\omega}{\omega_c}\}\ . \qquad 3.85$$

Families of characteristics can be constructed for various selections of parameters included in this equation which defines the minimum record length. Fig. 3.14 illustrates the case with $\eta_n = 0.1$, $\gamma_1 = \gamma_2 = 0.01$, $N_{zc} = 2$ while $(\omega/\omega_n)/\zeta$ and (ω/ω_c) are taken as parameters. It is clear from the graph that the last term in equation (3.85) is the most critical for the useful range of applications. Since the interest lies in keeping the record length as short as possible one must select the parameters such that one operates as near as possible to the base line.

This corresponds to a record length of about 20 cycles of oscillation for signals with $\beta_x\beta_y > 20$. It can therefore be inferred that such a record should suffice for the accurate determination of amplitudes of covariance and autocovariance of the two signals and their phase difference. The zero crossing of the covariance function should be observed over about two cycles and at distances about two cycles from the zero lag condition.

3.2.3 Aspects of digital computation of covariance functions

In order that analogue signals can be digitally analysed, they must be first transformed into discrete sequences by use of an analogue to digital converter, see chapter 6. The formulation given in previous sections in the continuous form can be easily replaced by the corresponding discrete form, simply by changing the integrals into summations and suitably defining the sequence ordering. Since the points that form a sequence are separated by one sampling interval, the unit for a discrete time shift (or the covariance time-lag resolution) can only be taken as this sampling interval. Covariance calculation does not cause any distortion of the frequency of the sinusoid signal. It follows, therefore, that the number of samples per cycle of the sinusoid in the original signal is the same as the number of lag values comprising a cycle of the corresponding sinusoid in the covariance function. In the following, a lag value is used to denote the time shift between the original signals, which is the product of a lag point 'number' and the sampling interval.

Computation of the discrete covariance of signals can be carried out in two says. First, direct computation is achieved by averaging the product pairs of shifted sequences corresponding to original signals. This method is referred to as the slow covariance method. Second, the discovery of efficient and fast Fourier transform computer algorithms

[Cooley and Tukey (1965)], led to the development of high speed convolution methods, [Stockham (1966)], for efficient calculation of discrete covariance estimates. The latter method provides a real advantage over the former only if the whole range of lags is to be computed. In addition, the high speed convolution method imposes strict limitations on the number of samples comprising the signals in order to obtain linear convolution instead of circular one. For the purpose of the present investigation, however, interest in covariance estimates centres round locations where C_{xy} either attains an extremum value (e.g. a peak or a trough) or crosses the zero value. One therefore needs only to calculate the covariance functions at individual lag values near these locations. It is therefore obvious that the direct method must be used.

A rough estimate of the starting values is obtained through an initial calculation of the covariance function over a range of lags covering slightly over half a period of the sinusoid. From the graph of C_{xy} against τ one may estimate the value of τ_{zc} corresponding to the first occurrence of zero crossing on the positive lag side, i.e. $m = 0$ in fig. 3.11. The m-th zero crossing occurs at a lag approximately $\frac{m\pi}{\omega}$ away from the one just obtained. However, as a result of the noise effect on the covariance function it is necessary to carry out the computation at several lag values around the predicted one. From this set of values of covariance estimates an accurate value for the m-th zero crossing lag may be obtained. Similarly for extrema determination, a computation of the covariance estimate at a set of lag values centred about a value $\frac{\pi}{2\omega}$ from a zero crossing occurrence is required. An accurate estimate of the particular value of covariance extremum may be obtained from observation of the change of the covariance along the set of points corresponding to various lags. It is interesting

to note here that covariance estimates for short record lengths may result in a biased estimate as a result of the variation of the mean values with record length involved in the actual computation. It can be shown that for the autocovariance function this error is unidirectional, therefore the peaks and absolute values of troughs must be combined in an averaging process in order to get a better estimate of the unbiased autocovariance amplitude.

When signal to noise ratios are particularly poor, the smoothing operation inherent in the determination of τ_{zc} or the extrema of C_{xy} or C_{xx}, can be a very useful feature of the technique. The smoothing operation acts as a form of local filtering at an intermediate stage in the analysis of data. Methods of implementing this form of smoothing in the data analysis method are described in chapter 6.

3.2.4 Covariance analysis applied to the roll damping measurement

Since the measured torque signal is found from the electric current in the respective field coils of the roll control loop, it is appropriate at this stage to modify the mathematical model to allow the introduction of the measured quantities. The moment acting on an oscillating magnetically suspended model is given by

$$\left.\begin{aligned} M(t) &= M_m(t) + M_a(t) \\ \text{where} \quad M_m &= B_R I + B_{R\phi} I' \phi \\ \text{and} \quad M_a &= M_\phi \phi + M_{\dot\phi} \dot\phi \end{aligned}\right\} \qquad 3.86$$

Subscripts m, a, R, ϕ denote magnetic, aerodynamic, magnetic roll torque and roll displacement derivatives and I' is the roll current at zero displacement. The dot denotes a time derivative. M_ϕ is normally small and is neglected in the present analysis. Substitution of equations (3.86) into equation (3.57) and modifying the coefficients

gives:-

$$J\ddot{\phi}(t) + C'\dot{\phi}(t) + K'\phi(t) = B_R I(t) \qquad 3.87$$

where

$$C' = C - M_{\dot{\phi}}$$

$$K' = K = B_{R\phi} I'$$

Multiplying both sides of equation (3.87) by $\phi(t+\tau)$ and averaging over the interval $T-|\tau|$ yields

$$J\ddot{\hat{C}}_{\phi\phi}(\tau) + C'\dot{\hat{C}}_{\phi\phi}(\tau) + K'\hat{C}_{\phi\phi}(\tau) = B_R \hat{C}_{I\phi}(\tau) \qquad 3.88$$

By analogy with equation (3.61), in the case of periodic auto-covariance and covariance functions at a frequency ω, the following results can be obtained

$$C'\omega = B_R \left| \frac{\hat{C}_{I\phi}}{\hat{C}_{\phi\phi}} \right|^* \sin\varepsilon \qquad 3.89a$$

and

$$K' - J\omega^2 = B_R \left| \frac{\hat{C}_{I\phi}}{\hat{C}_{\phi\phi}} \right|^* \cos\varepsilon \qquad 3.89b$$

The asterisks indicate a best estimate. In the presence of inevitable noise it is necessary to calculate the RHS of the two equations above from computations of the covariance functions. The zero crossings and the peaks of the covariance functions of the roll current and displacement signals at the appropriate range of lags defined in the previous section are used to estimate the amplitude of the clean periodic part of $\hat{C}_{I\phi}(\tau)$ and the phase angle ε. The peaks of the auto-covariance function of the displacement signal in the same range of lags can be used to estimate the amplitude of $\hat{C}_{\phi\phi}$. A convenient estimate of the signal to noise ratio is obtained from the spectra of the signals. The integrated

power spectrum of a signal (i.e. the cumulative frequency spectrum) containing a sinusoid shows a steep rise at the sinusoid frequency as shown in the illustration below. The square root of the ratio of the sinusoid variance to the rest of signal energy, i.e. $\sqrt{\frac{A}{\sigma^2-A}}$, gives the required signal to noise ratio. Signal to noise ratios are required in order to confirm that the range of lag values chosen at conditions where noise covariance estimates are reduced to 1/10 their maximum value is sufficient to enhance the effective signal to noise ratio to a reasonable magnitude. If the signal to noise ratio turned out to be very poor, e.g. $\beta_x\beta_y$ less than 20 then the use of formulae (3.83) to (3.85) in conjunction with figs. 3.13 and 3.14 should be consulted for the suitable estimates of record length and lag range.

If the tests are carried out wind-on and then wind-off and results subtracted it can be shown that

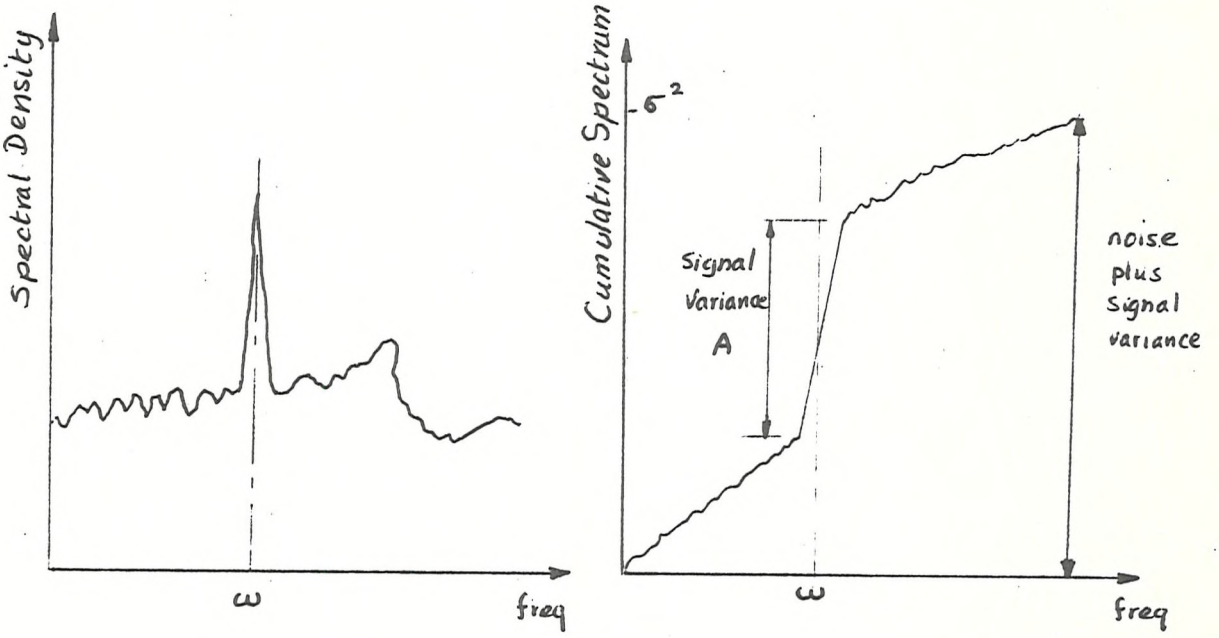

Power Spectral Distribution Cumulative Spectrum

$$-M_{\dot{\phi}}^{*}\,\omega = B_R\left[\left\{\left|\frac{\hat{C}_{I\phi}}{\hat{C}_{\phi\phi}}\right|^{*}\sin\varepsilon\right\}_{ON} - \left\{\left|\frac{\hat{C}_{I\phi}}{\hat{C}_{\phi\phi}}\right|^{*}\sin\varepsilon\right\}_{OFF}\right] \qquad 3.90a$$

$$-B_{R\phi}(I'_{ON} - I'_{OFF}) = B_R\left[\left\{\left|\frac{\hat{C}_{I\phi}}{\hat{C}_{\phi\phi}}\right|^{*}\cos\varepsilon\right\}_{ON} - \left\{\left|\frac{\hat{C}_{I\phi}}{\hat{C}_{\phi\phi}}\right|^{*}\cos\varepsilon\right\}_{OFF}\right] \qquad 3.90b$$

Equation(3.90a) is evaluated for the aerodynamic roll damping term $M_{\dot{\phi}}^{*}$. This quantity is conveniently defined as

$$\omega\, M_{\dot{\phi}}^{*} = \rho\, U\, S\, s^2\, \ell_p\, \omega\ . \qquad 3.91$$

where ρ, U are the air density and wind speed; S, s are the wing reference area and semi-span respectively and ℓ_p is the nondimensional roll damping derivative. It follows that

$$-\ell_p = \frac{B_R\, K_c}{\rho\, U\, S' s^2\, \omega^{\pi}}\left[\left\{\left|\frac{\hat{C}_{I\phi}}{\hat{C}_{\phi\phi}}\right|^{*}\sin\varepsilon\right\}_{ON} - \left\{\left|\frac{\hat{C}_{I\phi}}{\hat{C}_{\phi\phi}}\right|^{*}\sin\varepsilon\right\}_{OFF}\right] \qquad 3.92$$

where K_c is an additional calibration factor accounting for the fact that the current and displacement signals are measured as voltage signals. This constant factor can be taken to absorb other factors pertinent to the specific data handling method, e.g. analogue magnetic recording and reproducing gain variations ... etc.

3.2.5 Roll damping measurement at varying incidence

The variation of the dynamic stability derivatives with incidence is often of considerable interest. Owing to the large range of uncertainty associated with the measured derivatives it is desirable to collect all information relevant to the variation of the particular derivative with incidence from a single test run. One way of doing this is to follow a procedure similar to that outlined in section 3.1, i.e. by changing the incidence at a very slow rate compared with the frequency of oscillation and by carrying out the covariance analysis

on signal intervals over a short duration (hence short incidence range). In view of the arguments put forward in section 3.1.4 this method should lead to a more self consistent measurement of the derivative, provided that the variability of the analysis is not significantly affected by the nonstationary nature of the signals associated with varying incidence.

The method based on the level crossings of the covariance function suggests that about 20 cycles of oscillation should be taken as the minimum analysis interval of the signals for the constant incidence case. Before extending the arguments any further it is necessary to assess the effects of the constant pitch rate on the kind of data to be obtained, i.e. the derivatives to be measured, and the analysis method.

From the aerodynamic point of view, cross coupling derivatives due to combined pitch rate, incidence and roll rate all contribute to measured damping. For slender winged configurations with small fins these cross coupling derivatives can be neglected (owing to the conditions stated above on the relative magnitude of $\dot{\alpha}$ and ω). In general, however, ℓ_p is a function of incidence. Incidence is a function of time by virtue of the finite pitch rate. Thus ℓ_p is necessarily a function of time. If this time dependence is weak enough, the mathematical model of oscillation may still be represented by a second order differential equation similar to equation 3.87, the only difference being that C', K' contain weakly-time-varying parts. The presence of any significant coupling between the roll and pitch control loops of the balance will add another time varying part to C and K. This effect is expected to be relatively small for at least two reasons. The first is that $\dot{\alpha}$ is very small compared with balance natural frequencies, and the second is that the tare effect is to be subtracted from the wind-on measurement at the same incidence values and rates.

Naturally the first step is to investigate the effect of pitch rate, $\dot{\alpha}$, on the covariance estimates of the signals involved and hence on the results obtained by utilisation of these covariance functions. A mathematical model of this oscillation with time varying amplitudes will produce an ordinary differential equation with variable coefficients. Unlike the case with constant coefficients, there exists no general analytical solution for this type of equation. Resort therefore must be made to alternative methods of solution, or techniques of data reduction. These alternative methods include:

i) approximate solutions, e.g. assuming expansions involving small parameters,

ii) simulation method using either analogue or digital methods,

iii) use of specially modified data analysis methods.

The first method necessitates that the coefficients must contain only weak time varying parts. The advantage of this method is the possibility of obtaining approximate analytic solutions valid over certain orders of magnitude of the time varying parts. In addition it provides the opportunity for establishing direct relationships among the various parameters involved. The second method, does not impose the same limitation on the nature of the time varying coefficients, but the relationships among the various parameters and the solutions can only be inferred from the repeated numerical solution of the system of equations. This method offers a very wide potential for assessing sophisticated novel techniques or may be coupled with a variety of data analysis methods and hence used to assist in selection of an appropriate method. The third type of methods is completely oriented towards developing special data reduction techniques for accurate calculation of phase and amplitude information of the measurement signals. One example of these consists of carrying out the covariance calculation in

two steps by use of a clean constant amplitude (and same length) reference version of the sinusoid signal signal driving the model oscillations. This method in effect causes a partial filtering of the main signals with the clean one and hence the covariance estimate will contain weaker time varying parts than if covariance was obtained directly from the signals. Another example in the same class of methods consists of utilising a numerically generated signal of a single period length at the sinusoid precise frequency as the reference for carrying out the covariance. Only single period of the measurement signals is required, hence the advantage of short testing time, and the calculation of covariance at zero lag is sufficient. In the latter method the degree of precision of frequency value and computer storage and arithmetic precision must be high. In this section the results of analysis of an approximation valid up to first order in time varying amplitude are given.

In the case of time varying incidence, the overall record length of the signals corresponding to the total range of swept incidence, is broken into a number of subrecords of length T seconds, which corresponds to an incidence interval of $\dot{\alpha}T$. Successive subrecords of each signal may overlap and hence the incidence resolution of the results may be enhanced. Each pair of subrecords, corresponding to displacement and current signals, can be analysed separately by the covariance methods. Taking the origin of time at the middle of subrecord then the damping and stiffness coefficients, equation (3.87), can be assumed to be given by

$$\left.\begin{aligned} C &= C_o(1 + e_1\,\dot{\alpha}t) \\ K &= K_o(1 + e_2\,\dot{\alpha}t) \end{aligned}\right\} \qquad 3.93$$

where C_o and K_o are the damping coefficient and stiffness at the middle

of the interval, e_1 and e_2 are small constants. Account of the time varying amplitude and phase angle of the current signal may be taken by assuming the current signal to be given by

$$I = \hat{I}(1 + e_3 \dot{\alpha}t)\left|\sin \omega t + B_{R2}(1 + e_4 \dot{\alpha}t)\cos \omega t\right| \qquad 3.94$$

where e_3, e_4 and B_{R2} are constants. Substitution from equations (3.93) and (3.94) into (3.87) gives

$$J\ddot{\phi} + C_o(1+e_1\dot{\alpha}t)\dot{\phi} + K_o(1+e_2\dot{\alpha}t)\phi = B_R\hat{I}(1+e_3\dot{\alpha}t)\left|\sin \omega t + B_{R2}(1+e_4\dot{\alpha}t)\cos \omega t\right| \qquad 3.95$$

Only an approximate solution for this equation may be sought. Since the perturbation terms, comprised of $\dot{\alpha}t$, are assumed to be very small compared with unity, they can be regarded as comprising a long period variation while the sinusoid terms represent a short period variation. It may therefore be reasonable to assume that the solution is approximately given by

$$\phi \simeq \phi_o(t) + e_5(\dot{\alpha}t)\phi_1(t) + e_6(\dot{\alpha}t)^2\phi_2(t) + \ldots \qquad 3.96$$

where e_5 and e_6 are constants. The short period time variation is contained in the successive approximations of the functions $\phi_n(t)$ while the long period variation indicated by the $\dot{\alpha}t$ term is taken as a small parameter. By substitution of (3.96) into (3.95) and regarding the differentiation as acting on the short period parts only, an equation is obtained that contains terms of various orders of magnitude in $(\dot{\alpha}t)$. Equating coefficients of terms of the same order and retaining only the zero and first order results will give the following constant coefficients linear differential equations:

$$J\ddot{\phi}_o + C_o\dot{\phi}_o + K_o\phi_o = B_R(\sin\omega t + B_{R2}\cos\omega t)$$

$$e_5\left[J\ddot{\phi}_1 + C_o\dot{\phi}_1 + K_o\phi_1\right] = B_R\{e_3\sin\omega t + B_{R2}(e_2+e_4)\cos\omega t\} - C_o e_1\dot{\phi}_o - K_o e_2\phi_o \qquad 3.97$$

Suitable forms for ϕ_o and ϕ_1 are:

$$\phi_o = \hat{\phi}_o \sin\omega t$$
$$\phi_1 = \hat{\phi}_1 \sin\omega t\ . \qquad 3.98$$

These solutions lead to relationships among the constants e_1, e_2, e_3, e_4, e_5 and frequencies involved as follows:

$$e_1 = e_3 + e_4 - e_5$$
$$e_2 = \frac{e_3 - e_5}{1 - (\omega/\omega_n)^2} \qquad 3.99$$

where $\omega_n = \sqrt{K_o/J}$, the natural frequency corresponding to the basic constant coefficient model. These equations are valid for the case where $\dot{\alpha}T << 1$. The approximate solution is therefore

$$\phi \simeq \hat{\phi}\sin\omega t(1 + e_5\dot{\alpha}t)\ . \qquad 3.100$$

where $\hat{\phi} = \hat{\phi}_o$ and $\hat{\phi}_1/\hat{\phi}_o$ is absorbed in e_5. The covariance functions for ϕ and I can be shown to be given up to second order in $\dot{\alpha}\tau$ by:

$$\hat{C}_{\phi\phi}(\tau) = \frac{\hat{\phi}^2}{2}\left[1 - \left(\frac{e_5\dot{\alpha}\tau}{2}\right)^2\right]\left[\cos\omega\tau - \text{sinc}\,\omega(T-\tau)\right] + O\left(\frac{\dot{\alpha}}{\omega}\right)^2 - \bar{\phi}^2 \qquad 3.101a$$

$$\hat{C}_{\phi I}(\tau) \approx \frac{\hat{I}\,\hat{\phi}}{2}\Big[\{1 + \frac{e_3-e_5}{2}\dot{\alpha}\tau - \frac{e_3\,e_5}{4}(\dot{\alpha}\tau)^2\}\{\cos\omega\tau - \operatorname{sinc}\omega(T-\tau)\}$$

$$- B_{R2}\{1 + (e_3+e_4-e_5)\frac{\tau\dot{\alpha}}{2} - \frac{e_4\,e_5}{4}(\dot{\alpha}\tau)^2 + \frac{e_4 e_5}{12}(\dot{\alpha}(T-\tau))^2\}\sin\omega\tau$$

$$+ B_{R2}\left(\frac{e_3+e_4+e_5}{2}\frac{\dot{\alpha}}{\omega}\right)\{\operatorname{sinc}\omega(T-\tau) - \cos\omega(T-\tau)\}\Big]$$

$$+ O\left(\frac{\dot{\alpha}}{\omega}\right)^2 - \bar{\phi}\,\bar{I} \qquad 3.101b$$

where O( ) signifies of an order of magnitude of. It is important to notice in the last equation that terms containing (e_3-e_5) and $(e_3+e_4-e_5)$ are linear in $\dot{\alpha}\tau$. Substitution from equations (3.99) gives

$$\hat{C}_{\phi I}(\tau) \approx \frac{\hat{I}\,\hat{\phi}}{2}\Big[\{1 + \frac{e_2\,\dot{\alpha}\tau}{2(1-(\omega/\omega_n)^2)} - O(\dot{\alpha}\tau)^2\}\{\cos\omega\tau - \operatorname{sinc}\omega(T-\tau)\}$$

$$- B_{R2}\{1 + \frac{e_1\,\dot{\alpha}\tau}{2} - O(\dot{\alpha}\tau)^2\}\sin\omega\tau$$

$$+ B_{R2}\left((\frac{e_1}{2} + e_5)\frac{\dot{\alpha}}{\omega}\right)\{\operatorname{sinc}\omega(T-\tau) - \cos\omega(T-\tau)\}\Big] + O\left(\frac{\dot{\alpha}}{\omega}\right) - \bar{\phi}\,\bar{I}$$

3.102

The last equation indicates the manner in which the component of the cross covariance function, which is in phase with the autocovariance function leading term, has been affected by $\dot{\alpha}$. It changes in a similar way to the change in the stiffness K as a result of the pitch rate. Similarly the quadrature component suffers a change similar to that of the damping coefficient. These resemblances are only true if terms of order $(\dot{\alpha}\tau)^2$ and $(\dot{\alpha}/\omega)^2$ are negligible. Consequent to the assumed behaviour of the phase angle in the time domain, the phase angle obtained from the covariance estimates in the lag domain will depend on the lag value. After algebraic manipulation and considering $\dot{\alpha}\tau$, $\dot{\alpha}/\omega$, phase angle to be small, the covariance function can be shown to reduce to

the appropriate form

$$\hat{C}_{\phi I} \simeq \frac{\hat{I}\,\hat{\phi}}{2}\left[1 + \frac{e_1\,\dot{\alpha}\tau}{2} + \frac{e_4+e_5}{2}\,\frac{\dot{\alpha}}{\omega}\,\varepsilon\,\cos\,\omega T\right]\cos(\omega\tau + \varepsilon_s) \qquad 3.103$$

where ε_s is the phase angle between the shifted, i.e. lagged, time varying amplitude records and ε is the phase angle for constant amplitude records. It can be shown that ε_s is given by

$$\tan\,\varepsilon_s \simeq \tan\,\varepsilon\left[1 + \frac{e_4\,\dot{\alpha}\tau}{2} + \frac{e_3+e_4+e_5}{2}\,\frac{\dot{\alpha}}{\omega}\,\frac{\sin(\omega T+\varepsilon)}{\cos\,\varepsilon}\right]$$

and for small angles ε_s and ε, this yields

$$\varepsilon_s \simeq \varepsilon\left[1 + \frac{e_4\,\dot{\alpha}\tau}{2} + \frac{e_3+e_4+e_5}{2}\,\frac{\dot{\alpha}}{\omega}\,\sin(\omega T+\varepsilon)\right] \qquad 3.104$$

It is useful to define an effective phase angle, ε_{so}, which corresponds to zero lag covariance. From the covariance above it can be clearly seen that the introduction of $\dot{\alpha}$ combined with sinusoid frequency ω and a finite record length causes a bias in the measured effective phase angle. The values of the lags for zero crossings of the covariance function suffer a similar linear shift. From the equations above, for small τ, zero crossings of $\hat{C}_{\phi\tau}$ occur at:

$$\omega\tau_{zc} + \varepsilon_{so} + \varepsilon\,\frac{e_4\dot{\alpha}}{2}\,\tau_{zc} = \frac{2m+1}{2}\,\pi$$

or

$$m = \frac{\omega\tau_{zc}}{\pi}\left(1 + \frac{\varepsilon e_4}{2}\,\frac{\dot{\alpha}}{\omega}\right) - \frac{\pi}{2} + \varepsilon\left(1 + \frac{e_3+e_4+e_5}{2}\,\frac{\dot{\alpha}}{\omega}\,\frac{\sin\omega T+\varepsilon}{\cos\,\varepsilon}\right)$$

A close examination of this equation shows that the zero crossing characteristic at nonzero values of $\frac{\dot{\alpha}}{\omega}$ is related to that corresponding to constant incidence. If both are presented on the same graph they

intersect at a fixed point, which might be called the pivot point, whose coordinate is given by

$$\left[\omega\tau_{zc}\right]_{pivot} = - \left|\frac{e_3+e_4+e_5}{e_4}\right| \sin(\omega T+\varepsilon) \qquad 3.106$$

The implication of this result is that within linear perturbation all zero crossing characteristics of the covariance function for records of same length but of varying $\dot{\alpha}/\omega$ pass through a single point.

When the oscillatory test is repeated for two different values of $\dot{\alpha}$ and the corresponding phase angles calculated from the covariance zero crossings, the phase angle corresponding to constant incidence can be obtained by interpolation or extrapolation.

In the practical situation, the noise present on the signals introduces further errors. The error effect of stationary random noise has been dealt with in section 3.2.3. In the present case, the part of the noise in the displacement and current signals which is correlated, is necessarily nonstationary. It is reasonable to regard the remaining part of the noise to be stationary. The nonstationary part has a weak time varying effect caused by the varying damping coefficient and stiffness of the dynamic model considered. An estimation of the covariance function of a signal plus noise in this condition is required. Sveshnikov (1966) has shown methods for obtaining solutions to nonhomogeneous differential equations with time varying coefficients having a linear function of a random variable as its RHS. When the linear function is replaced by a deterministic function multiplying the random variable particular integrals can still be obtained. The main results show that the autocovariance function of a random variable multiplied by a deterministic function is equal to the square of the

function times the autocovariance of the random variable. Though this might be reasonably true for the case of infinitely long records, it can only be an approximation for finite length records. Hence the variability of the autocovariance estimate as a result of finite record length is increased at least by the square of the deterministic function. Applying this result to the present case, it can be seen that for a weak time varying deterministic function $(1 + e_6\dot{\alpha}t)$ multiplying the noise term, where e_6 is a constant, the autocovariance function of the broad band noise is

$$\sigma_n^2(1 + e_6\dot{\alpha}t) \sin \omega_c\tau \ .$$

This can further be approximated to the form

$$\sigma_n^2(1 + 2e_6\dot{\alpha}t) \sin \omega_c\tau \ . \qquad 3.107$$

This is clearly a biased estimate since it does not decay to zero as τ increases indefinitely but tends to the value $2\sigma_n^2 e_6\dot{\alpha} \sin \omega_c\tau$. However, since such a change is a slow one, it amounts at the most to approximately $(1 + 0.4e_6\dot{\alpha}T)$ times the mid interval constant incidence case, if lags up to 20% of the record length T are allowed. The effect of noise covariance on the covariance zero crossings of the signal plus noise is going to be larger than on the amplitudes. If the test is repeated at more than one value of $\dot{\alpha}$ and results interpolated for $\dot{\alpha} = 0$, as has already been suggested earlier, there should be an improvement in the final result.

The effect of variability in the statistical properties of the noise is difficult to assess analytically. Digital simulation appears to be very promising in establishing the limiting conditions on $\dot{\alpha}$ for a certain signal-to-noise ratio and certain damping against incidence performance. It is therefore suggested that in the absence of quanti-

tative data on the nonstationary noise behaviour, data reduction should be carried out as with the clean signals.

3.2.6 Two-degree-of-freedom oscillation testing

In addition to the methods of measurement of oscillatory derivatives for models forced in a single degree of freedom oscillation interest lies in multidegree of freedom excitation as well. An airplane in free flight seldom, if ever, oscillates in a single degree of freedom as a result of the general disturbances it meets in flight, the lack of its structural (hence inertial) symmetry or the existence of aerodynamic cross derivatives. In particular the measurement of oscillatory cross derivatives in wind tunnels requires consideration of multidegree of freedom oscillation systems. It is therefore of interest to explore the possibility of extension of the previous techniques to multidegree of freedom testing. The relative simplicity of the means of imparting arbitrary controlled motion to magnetically levitated models in a magnetic suspension system is an advantage that merits utilisation in this respect. The simplest form of a multidegree of freedom forced oscillation system comprises a combined pitch and heave two-dimensional oscillation. In this section the basic theory for 2-degree-of-freedom (2-DOF) forced oscillation is presented. A method for measurement of system parameters utilising covariance estimates is described. Finally the application to a combined pitch and heave forced oscillation of a magnetically suspended model is given.

3.2.6.1 Measurement of parameters of 2-degree of freedom oscillatory systems

Consider the linear system shown in figure 3.15 which consists of a mass m suspended on two linear springs k_1 and k_2 and two dashpots

with damping coefficients C_1 and C_2. Point O on the mass is taken as the origin for the axes and is restrained to move along the z-axis only. The mass is induced into oscillation translationally along the z-axis and rotationally about O by the action of force Z(t) and torque M(t) respectively. The equations of motion for small oscillation of this system can be written in matrix form as follows, |Thomson (1965)|

$$[m]\begin{Bmatrix}\ddot{z}(t)\\ \ell\ddot{\theta}(t)\end{Bmatrix} + [c]\begin{Bmatrix}\dot{z}(t)\\ \ell\dot{\theta}(t)\end{Bmatrix} + [k]\begin{Bmatrix}z(t)\\ \ell\theta(t)\end{Bmatrix} = \begin{Bmatrix}Z(t)\\ \frac{M}{\ell}(t)\end{Bmatrix} \qquad 3.108$$

where $[m]$, $[c]$ and $[k]$ are the inertia, damping coefficient and stiffness 2 x 2 matrices respectively, while $\begin{Bmatrix}Z(t)\\ \frac{M}{\ell}(t)\end{Bmatrix}$ and $\begin{Bmatrix}z(t)\\ \ell\theta(t)\end{Bmatrix}$ are the forcing and response vectors and ℓ is a system characteristic length. The latter multiplies $\theta(t)$ and the torque is divided by ℓ in order to maintain dimensional homogeneity in the equation. The elements of $[m]$, $[c]$ and $[k]$ can be easily expressed in terms of the system properties. In general these matrices are not diagonal as a result of various couplings caused by the choice of the coordinate system. If the excitation is harmonic at a frequency ω, the response is also harmonic. It is convenient to assume that the variables take the form given below.

$$\begin{aligned} z(t) &= h\, e^{j(\omega t+\chi_1)} \\ \ell\theta(t) &= \ell\alpha\, e^{j(\omega t+\chi_2)} \\ Z(t) &= F\, e^{j(\omega t+\chi_3)} \\ M(t) &= M\, e^{j(\omega t+\chi_4)} \end{aligned} \qquad 3.109$$

where h, α, F, M are the amplitudes and χ_1, χ_2, χ_3 and χ_4 are the phase angles of z(t), θ(t), Z(t) and M(t) respectively. Substituting these

into equation 3.108 yields

$$[P]\begin{Bmatrix} h\, e^{j\chi_1} \\ \ell\alpha\, e^{j\chi_2} \end{Bmatrix} e^{j\omega t} = \begin{Bmatrix} F\, e^{j\chi_3} \\ \frac{M}{\ell}\, e^{j\chi_4} \end{Bmatrix} e^{j\omega t} \qquad 3.110$$

where

$$[P] = -\omega^2[m] + j\omega[c] + [k] \qquad 3.111$$

which is a 2 x 2 matrix with complex elements.

Dividing equation 3.110 by z(t) where $h \neq 0$ we get

$$[P]\begin{Bmatrix} 1.0 \\ (\frac{\ell\alpha}{h})e^{j(\chi_2-\chi_1)} \end{Bmatrix} = \begin{Bmatrix} (\frac{F}{h})e^{j(\chi_3-\chi_1)} \\ (\frac{M}{\ell h})e^{j(\chi_4-\chi_1)} \end{Bmatrix} \qquad 3.112$$

This represents two complex scalar equations in four complex unknowns (the elements of $[P]$). If excitation is repeated at the same frequency but with different forcing vector which is not proportional to the first one, then a similar equation to 3.112 can be written. In this case however one may normalise the variables with respect to the other displacement i.e. $\theta(t)$. The resulting equation takes the form

$$[P]\begin{Bmatrix} (\frac{h}{\ell\alpha})_2 e^{j(\psi_1-\psi_2)} \\ 1.0 \end{Bmatrix} = \begin{Bmatrix} (\frac{F}{\ell\alpha})e^{j(\psi_3-\psi_2)} \\ (\frac{M}{\ell^2\alpha})e^{j(\psi_4-\psi_2)} \end{Bmatrix} \qquad 3.113$$

where ψ_1, ψ_2, ψ_3, ψ_4 are the phase angles corresponding to z, θ, Z, M respectively. Combining the force vectors and the response vectors from equations 3.112 and 3.113 to form force matrix $[G]$ and response matrix $[H]$ we get

$$[P]\ [H] = [G]$$

where

$$[G] = \begin{bmatrix} \left(\frac{F}{h}\right)_1 e^{j(\chi_3-\chi_1)} & \left(\frac{F}{\ell\alpha}\right)_2 e^{j(\psi_3-\psi_2)} \\ \left(\frac{M}{h\ell}\right)_1 e^{j(\chi_4-\chi_1)} & \left(\frac{M}{\ell^2\alpha}\right)_2 e^{j(\psi_4-\psi_2)} \end{bmatrix} \qquad 3.115$$

and

$$[H] = \begin{bmatrix} 1.0 & \left(\frac{h}{\ell\alpha}\right)_2 e^{j(\psi_1-\psi_2)} \\ \left(\frac{\ell\alpha}{h}\right)_1 e^{j(\chi_2-\chi_1)} & 1.0 \end{bmatrix}$$

By inverting matrix $[H]$ and post multiplying both sides of equation 3.114 by the inverse we get

$$[P] = [G]\,[H]^{-1} \qquad 3.116$$

The inverse matrix can only exist if the original matrix of the displacement vectors is nonsingular i.e. if its columns (or rows) are linearly independent. It follows therefore that the excitation vectors must be linearly independent as has already been postulated. The development of $[H]$ must be made as close as possible to 1.0. This can be realised exactly if in either excitation cases the response in a coordinate to an excitation vector is zero. Equation 3.116 is sufficient to determine all elements of $[P]$ and hence system parameters provided that a reasonably accurate estimate of the amplitude ratios and phase differences shown in matrices $[G]$ and $[H]$ is available. An attractively simple case can be seen to result when forcing is chosen such that only a single displacement is excited at a time. In this case $[H]$ is equal to unity matrix and

$$[P] = [G] \qquad 3.117$$

The importance of this case is not only in relative simplicity of the analysis but in data collection as well since number of measurements is reduced by one.

In practice difficulties may arise in the computation of $[H]$ and $[G]$ owing to the presence of measurement and system noise on the signals. The technique of using covariance estimate can be used to extract the useful sinusoid parts from the noisy signals with higher fidelity. The covariance formulation of the problem is presented next.

Let $z(t)$ be the response component with the larger amplitude or higher signal to noise ratio. Multiply equation 3.108 by $z(t)$ and average the time shifted products over an indefinitely long period of time. This gives

$$[m]\begin{Bmatrix} C_{zz}^{\cdot\cdot}(\tau) \\ \\ C_{z\ell\theta}^{\cdot\cdot}(\tau) \end{Bmatrix} + [c]\begin{Bmatrix} C_{zz}^{\cdot}(\tau) \\ \\ C_{z\ell\theta}^{\cdot}(\tau) \end{Bmatrix} + [k]\begin{Bmatrix} C_{zz}(\tau) \\ \\ C_{z\ell\theta}(\tau) \end{Bmatrix} = \begin{Bmatrix} C_{zZ}(\tau) \\ \\ C_{zM}(\tau) \end{Bmatrix} \qquad 3.118$$

where $C_{zz}(\tau)$, $C_{z\ell\theta}(\tau)$ etc. are complex covariance functions.
If the forced oscillation is sinusoidal in time as assumed in equation 3.109 it can be shown that the complex covariance functions ** are similarly sinusoidal, with the same frequency, in the shifted time. In

---

** In this section complex covariance is taken to represent covariance of complex variables [Sveshnikov (1966)] . For the complex variables $W(t) = U(t) + jV_1(t)$ and $S(t) = U_2(t) + jV_2(t)$ One can define the complex auto covariance function

$$C_{WW}(\tau) = \underset{T \to \infty}{Lt} \frac{1}{T} \int_{-T/2}^{T/2} W^*(t)\, W(t+\tau)dt$$

and the complex covariance

$$C_{WS}(\tau) = \underset{T \to \infty}{Lt} \frac{1}{T} \int_{-T/2}^{T/2} W^*(t)\, S(t+\tau)dt$$

where (*) denotes complex conjugate.

addition equation 3.118 reduces to the algebraic equation

$$[P] \begin{Bmatrix} C_{zz}(\tau) \\ \\ C_{z\theta\ell}(\tau) \end{Bmatrix} = \begin{Bmatrix} C_{zZ}(\tau) \\ \\ C_{z\frac{M}{\ell}}(\tau) \end{Bmatrix} \qquad 3.119$$

The autocovariance and covariance functions are given by

$$\begin{aligned} C_{zz}(\tau) &= h^2 e^{j\omega\tau} \\ C_{z\theta\ell}(\tau) &= h\alpha\ell\, e^{j(\omega\tau+\chi_2-\chi_1)} \\ C_{zZ}(\tau) &= Fh\, e^{j(\omega t+\chi_3-\chi_1)} \\ C_{z\frac{M}{\ell}}(\tau) &= \frac{M}{\ell} h\, e^{j(\omega t+\chi_4-\chi_1)} \end{aligned} \qquad 3.120$$

Substitution into equation 3.119 and dividing both sides with respect to $C_{zz}(\tau)$ yields

$$[P] \begin{Bmatrix} 1 \\ \\ (\frac{\alpha\ell}{h}) e^{j(\chi_2-\chi_1)} \end{Bmatrix} = \begin{Bmatrix} (F/h) e^{j(\chi_3-\chi_1)} \\ \\ (M/h\ell) e^{j(\chi_4-\chi_1)} \end{Bmatrix} \qquad 3.121$$

which is identical to 3.112. Similarly if excitation is repeated at the same frequency but with a force vector that is linearly independent of the previous one and the covariance is taken w.r.t. the largest and/or cleanest amplitude response component, say $\theta(t)$, another equation equivalent to 3.113 results. Force and displacement matrices can be formed and considerations regarding the latter matrix remain unaltered. It remains to solve equation 3.116 for the elements of $[P]$.

The problem reduces to the calculation (digital) of the covariance functions $C_{zz}(\tau)$, $C_{z\ell\theta}(\tau)$, $C_{zZ}(\tau)$ and $C_{z\frac{M}{\ell}}(\ell)$ for the first excitation case and $C_{\ell\theta z}(\tau)$, $C_{\ell\theta\ell\theta}(\tau)$, $C_{\ell\theta Z}(\tau)$ and $C_{\theta M}(\tau)$ for the second, at suitable ranges of lag values, and then calculate the amplitude and phase angles involved. The advantages of this method become clearer when noise present on the practical signals are introduced. The response of a multidegree of freedom system to ideal white noise random processes has been considered by Meirovitch (1967). It can be shown that the response autocovariance functions resemble the impulse response function of the system in its decay rate and dependence on the system resonant frequencies. Owing to the existence of more than one resonant frequency, the response covariance functions consist of the addition of two exponentially decaying cosine functions at the resonant frequencies. If the frequencies are close to each other, this may have the same effect as an effective modulation or beating of the covariance functions with a low frequency component. Careful examination of the covariance estimates is necessary in the following conditions:

(i) either the system damping is very small, or

(ii) beat frequency is comparable with test frequency, or

(iii) signal to noise ratio is poor.

The effect of the covariance estimates of the noise is likely to be a reduction in the accuracy of the results obtained by the covariance zero crossing method. The estimation of the minimum lag value preceding the range of lags for zero crossing calculation and hence the minimum record length for signals with particularly poor signal/noise ratio becomes a laborious task. It suffices, however, at this stage to highlight some

possible precautions against possible sources of errors.

A conservative estimate of the minimum lag value may be obtained by consideration of the smaller of the beat frequency or lowest resonant frequency and the lowest damping of the two degrees of freedom. This implies use of longer record lengths than might be predicted from a more precise analysis. Fig. 3.13 and 3.14 can be used for fixing other parameters. Another alternative might be to resort to another method of covariance estimation, e.g. use of single cycle numerically generated signals, at least for confirmation of accuracy purposes.

The analysis given above can be extended to multidegree of freedom systems, but the number of force excitation vectors required equals the number of degrees of freedom allowed. The number of measured quantities increases similarly since number of measured quantities has to be 2 x (no. of degrees of freedom involved in the oscillation).

3.2.6.2 Application to combined heave and pitch oscillatory derivative measurements

A symmetric model in a symmetric magnetic balance can simulate reasonably well the case of symmetric longitudinal oscillations of an aircraft in free flight. In general this is a three degree of freedom (3-DOF) motion system comprising the axial, lateral heave and pitching motions. A model describing the longitudinal symmetric oscillations completely must allow for the three kinds of motion. Consider the airplane model shown in figure 3.16. When oscillations are of small amplitude and low frequency and the aerodynamic flow pattern is stable, the equations of motion in the plane of symmetry can be linearised. Babister (1961) has given the equations of motion for longitudinal small oscillations in pitch and heave. The disturbances relative to wind

axes are taken w, θ corresponding to velocities along the z axis and angular displacement about the y-axis. In a magnetic balance, the stiffness of the system to positional displacement necessitates the use of the lateral displacement z instead of w as the first independent variable.

Fig. 3.16a shows a model undergoing oscillations in the horizontal plane which consists of translational oscillation along the z-axis as well as rotation about point O'. X-axis is pointing horizontally forward and Y-axis is vertically downward which would be normal to the plane of the page. Certain key points in the system require definition. These are

(i) Optical position system centre, about which pitch displacement calibration is made, O

(ii) Model pitch centre, P, distance $\ell_{O'}$ ahead of base

(iii) Model mass centre which is ℓ_G ahead of base

(iv) Magnetic balance pitching moment centre, x_{OM} from O

(v) Aerodynamic centre of model, distance ℓ_A from base

(vi) Centre of model pure rotation, if it exists, distance ℓ_{OR} from O.

By virtue of its design, the control system of the MSBS forces the model pitching oscillation in the horizontal plane about a point in the plane normal to tunnel axis through the optics centre. Since model axial position is fixed then points O and P are only laterally separated for small oscillation. Lateral displacement is taken here to represent a z-component displacement. The mass and aerodynamic centres are properties of the model and are located in it. The magnetic pitching moment centre is a property of the balance and model combination, and

is here chosen on the tunnel axis at a point corresponding to the moment calibration centre. The centre of pure rotation is a hypothetical point in the X-Z plane; the conditions for existence and location of a pure rotation centre will be discussed later.

In order to study model dynamics in suspension it is useful to define two sets of axes. Tunnel axis system OXZ with optics centre as origin and body axis system GX_BZ_B with mass centre as origin and x_B along fuselage axis pointing forward. The following geometrical relationships can be written among various displacements following a model positional disturbances, fig. 3.16b. First

$$z_B = z_P \cos\theta + \ell_{GO} \sin\theta \qquad 3.122a$$

where z_B is the model lateral displacement along Z_B axis; z_P is the lateral displacement of model pitch centre along tunnel Z-axis; θ is the angular pitch displacement and ℓ_{GO} is the distance between centre of mass and optics centre. For small displacements

$$z_B \sim z_P + x_{GP}\,\theta \qquad 3.122b$$

where $x_{GP} \simeq \ell_{GO}$ is the axisl distance of mass centre ahead of pitch centre. Second, displacements along the tunnel Z-axis at magnetic balance moment centre axial location z_M is related to z_P and θ as follows

$$z_M = z_P - x_{MO} \tan\theta \sim z_P - x_{MP}\,\theta \qquad 3.123$$

where x_{MO} is the axial distance of magnetic centre ahead of optics centre and is approximately equal to x_{MP} which represents the axial distance of the magnetic centre ahead of pitch centre. Differentiating equations 3.122 and 3.123 w.r.t. time yields

$$\dot{z}_B \sim \dot{z}_P + x_{GP}\,\dot{\theta}$$
$$\dot{z}_M \sim \dot{z}_P - x_{MP}\,\dot{\theta} \qquad 3.124$$

The perturbation flow velocity along Z_B, up to first order in the displacements and their velocities, is given by

$$w_B \sim U\theta + \dot{z}_B = U\theta + \dot{z}_P + x_{GP}\,\dot{\theta} \qquad 3.125$$

where U is the free stream undisturbed tunnel flow velocity. Differentiating this w.r.t. time gives

$$\dot{w}_B \sim U\,\dot{\theta} + \ddot{z}_P + x_{GP}\,\ddot{\theta} \qquad 3.126$$

The equations of model motion in small perturbation referred to a body axis system are given by

$$m\,\ddot{z}_B = Z_a(t) + Z_m(t)$$
$$J\,\ddot{\theta} = (M_a(t))_G + (M_m(t))_G \qquad 3.127$$

where m,J are the model mass and moment of inertia about the centre of mass; $Z_a(t)$ and $Z_m(t)$ are the lateral components of aerodynamic and magnetic forces acting on the model; $(M_a(t))_G$ and $(M_m(t))_G$ are the aerodynamic and magnetic pitching moments about the mass centre respectively. The aerodynamic force and moment following small amplitude oscillatory motion referred to body axis system are given by

$$Z_a(t) = Z_{ao} + Z_{\dot{w}}\,\dot{w}_B + Z_w\,w_B + Z_q\,\dot{\theta} + Z_\theta\,\theta$$
$$M_a(t) = M_{ao} + M_{\dot{w}}\,\dot{w}_B + M_w\,w_B + M_q\,\dot{\theta} + M_\theta\,\theta \qquad 3.128$$

where Z_{ao} and M_{ao} correspond to the aerodynamic lateral force and pitching moment about the mass centre in the nonoscillatory mean position condition; $Z_{\dot{w}}$, Z_w, Z_q, Z_θ, $M_{\dot{w}}$, M_w, M_q, M_θ are the aerodynamic force and moment oscillatory derivatives relative to body axis system, e.g. $Z_\theta = \frac{\partial Z}{\partial \theta}$, they are evaluated at the mean position; w_B and θ are functions of time; and $q = \frac{d\theta}{dt} = \dot{\theta}$. The instantaneous magnetic force and moments acting on the model following small amplitude motions can be assumed to be given by

$$Z_m(t) = Z_{mo}(1 + k_{11} z_M + k_{12}\theta) + Z_{m\dot{z}}\,\dot{z}_M + Z_{mq}\,\dot{\theta} + Z(t)$$

$$(M_m(t))_M = M_{mo}(1 + k_{21} z_M + k_{22}\theta) + M_{m\dot{z}}\,\dot{z}_M + M_{mq}\,\dot{\theta} + M(t)$$

where Z_{mo} and M_{mo} are the steady magnetic force and moment about the magnetic centre; k_{11}, k_{12}, k_{21} and k_{22} are constants that correspond to balance force and moment stiffnesses with respect to displacements z_M and θ; $Z_{m\dot{z}}$, Z_{mq}, $M_{m\dot{z}}$ and M_{mq} are the balance equivalent viscous damping coefficients; $Z(t)$ and $M(t)$ are the force and moment excitation terms. The magnetic pitching moment can be transferred to the mass centre using the relation

$$(M_m(t))_G = (M_m(t))_M + x_{GM}\,Z_m(t) \qquad 3.130$$

where x_{GM} is the axial distance of mass centre ahead of magnetic centre. In practice position measurement is referred to pitch centre, therefore it is required to transfer variables in all quantities to z_p and θ. Substitution of equation 3.125 into 3.128 and 3.124 into 3.129 then 3.129 into 3.130 and finally into equation 3.127 and rearrangement results in a set of two equations each of which has two parts. One arises from the mean or steady state conditions and the second involves

only the disturbance variables. The steady state parts, where all disturbances vanish, give

$$Z_{ao} + Z_{mo} = 0$$
$$M_{ao} + M_{mo} + x_{GM} Z_{mo} = 0 \qquad 3.131$$

The remaining parts involve only the disturbance variables and take the form:

$$(m-Z_{\dot{w}})\ddot{z}_P-(Z_w+Z_{m\dot{z}})\dot{z}_P+Z_{ao}k_{11}z_P+x_{GP}(m-Z_{\dot{w}})\ddot{\theta}-(Z_q+UZ_{\dot{w}}+x_{GP}Z_w+x_{MP}Z_{w\dot{z}}+Z_{mq})\dot{\theta}$$
$$-(Z_\theta+UZ_w-Z_{ao}(k_{11}x_{MP}+k_{12}))\theta = Z(t) \qquad 3.132a$$

$$-M_{\dot{w}}\ddot{z}_P-(M_w+M_{m\dot{z}}+x_{GM}Z_{m\dot{z}})\dot{z}_P+(k_{21}M_{ao}+c_{GM}Z_{ao}(k_{11}-k_{21}))z_P+(J-x_{GP}M_{\dot{w}})\ddot{\theta}$$
$$-(M_q+UM_{\dot{w}}+x_{GP}M_w+x_{MP}M_{m\dot{z}}+M_{mq}+x_{GM}(x_{MP}Z_{m\dot{z}}+Z_{mq}))\dot{\theta}$$
$$-(M+UM_w-M_{ao}(k_{21}x_{MP}+k_{22})-x_{GM}Z_{ao}((k_{11}1k_{21})x_{MP}+(k_{12}-k_{22})))\theta$$
$$= M(t) + x_{GM}Z(t) \qquad 3.132b$$

The following 2 x 2 matrices can be defined:

$$[m] = \begin{bmatrix} m-Z_{\dot{w}} & x_{GP}(m-Z_{\dot{w}}) \\ -M_{\dot{w}} & J-x_{GP}M_{\dot{w}} \end{bmatrix} \qquad 3.133a$$

$$[c] = \begin{bmatrix} -(Z_w + Z_{\dot{mz}}) & -(Z_q + UZ_{\dot{w}} + x_{GP}Z_w + x_{MP}Z_{\dot{wz}} + Z_{mq}) \\ -(M_w + M_{\dot{mz}} + x_{GM}Z_{\dot{wz}}) & -(M_q + UM_{\dot{w}} + x_{GP}M_w + x_{MP}M_{\dot{wz}} + M_{mq} + x_{GM}(x_{MP}Z_{\dot{wz}} + Z_{mq})) \end{bmatrix}$$

3.133b

$$[k] = \begin{bmatrix} Z_{ao}k_{11} & -(Z_\theta + UZ_w - Z_{ao}(k_{11}x_{MP} + k_{12})) \\ k_{21}M_{ao} + x_{GM}Z_{ao}(k_{11} - k_{21}) & -(M_\theta + UM_w - M_{ao}(k_{21}x_{MP} + k_{22}) \\ & -x_{GM}Z_{ao}((k_{11} - k_{21})x_{MP} + (k_{12} - k_{22}))) \end{bmatrix}$$

3.133c

and the equations of motion reduce to

$$[m]\begin{Bmatrix} \ddot{z}_P \\ \ddot{\theta} \end{Bmatrix} + [c]\begin{Bmatrix} \dot{z}_P \\ \dot{\theta} \end{Bmatrix} + [k]\begin{Bmatrix} z_P \\ \theta \end{Bmatrix} = \begin{bmatrix} 1 & 0 \\ x_{GM} & 1 \end{bmatrix}\begin{Bmatrix} Z(t) \\ M(t) \end{Bmatrix} \qquad 3.134$$

The appearance of the square matrix on the RHS of this equation is a consequence of the axis shift. Apart from this square matrix, equation 3.134 is similar in form to equation 3.108. If direct measurements of the displacement and force vectors were available, methods of data reduction described in section 3.2.6.1 can be directly applied. In practice, however, these are obtained in the form of precalibrated voltage signals (see chapter 4). In view of the coordinate system chosen it can be seen that

$$\theta(t) = \alpha(t) \qquad 3.135$$

where α is the angle of incidence. The displacement vector can be

rewritten as

$$\begin{Bmatrix} z_p \\ \theta \end{Bmatrix} = \begin{bmatrix} \frac{\partial z}{\partial V_z} & 0 \\ 0 & \frac{\partial \alpha}{\partial V_\alpha} \end{bmatrix} \begin{Bmatrix} V_z \\ V_\alpha \end{Bmatrix} \qquad 3.136$$

where V_z and V_α are the voltage signals corresponding to lateral heave and pitch displacements. The matrix in equation 3.136 above is the position calibration matrix with elements corresponding to position calibration constants which can be determined experimentally (see chapters 4 and 5). The forces are related to the relevant electromagnet currents through a more complex calibration matrix. The complexity is caused by the magnitude of coupling present among various force components and by the dynamic effects (see appendix A and B). If the oscillation frequency is chosen to be low compared with the system resonant frequencies, the static force calibration matrix amy be assumed valid. Corrections due to dynamic effects may be applied following a similar procedure to suggestions in chapters 4, 5 and appendix A, but extended to the multidegree of freedom system. In this case at least approximate measurements of resonant frequencies of the oscillating system are required. The other difficulty arises from the fact that the balance-model combination contains a certain degree of static and (perhaps dynamic) force coupling (or interaction) between the observed and nonobserved force components. Quantitative estimation of the effects of static force coupling is given in appendix B. In the absence of coupling, the balance-model oscillating system can be excited to perform the desired oscillation without imparting any force disturbance to other modes. Coupling results in a certain amount of unwanted forced

excitation. The relevant control loops of the balance react to this disturbance in order to reduce the model position errors in these degrees of freedom with respect to the undisturbed value. The effectiveness depends on several factors:-

- frequency of oscillation
- magnitude and nature of coupling
- resonant frequency and damping of this mode of control.

Although the model may not suffer an apparent significant displacement in this coupled mode, its force indication will certainly be in error. A position servo-control system's ability to maintain a model position is lowest when the disturbance frequency is close to its resonant frequency. In this case, the actual model displacements in the undesired modes may also become significant. The remaining cause of undesired mode displacements is the existence of position interaction, but this can be largely eliminated (see ch.4). If sufficient precautions, or corrections, are taken then the relationship between force and measured current signals can be written as:

$$\begin{Bmatrix} Z(t) \\ \\ M(t) \end{Bmatrix} = [B] \begin{Bmatrix} V_F(t) \\ \\ V_M(t) \end{Bmatrix} \qquad 3.137$$

where $|B|$ is the inverse calibration matrix; V_F and V_M are the electromagnet current signals. Matrix $[B]$ contains any field-position interactions present at the mean incidence and lateral heave positions. Substitution of equations 3.135 - 3.137 into equation 3.134 and applying the methods of section 3.2.6.1 yields

$$[P]\begin{bmatrix} \frac{\partial z}{\partial V_z} & 0 \\ 0 & \frac{\partial \alpha}{\partial V_\alpha} \end{bmatrix}\begin{bmatrix} 1.0 & (\frac{C_{\alpha z}}{C_{\alpha\alpha}})_2 \\ (\frac{C_{z\alpha}}{C_{zz}})_1 & 1.0 \end{bmatrix} = \begin{bmatrix} 1 & 0 \\ x_{GM} & 1 \end{bmatrix}[B]\begin{bmatrix} (\frac{C_{zZ}}{C_{zz}})_1 & (\frac{C_{\alpha Z}}{C_{\alpha\alpha}})_2 \\ (\frac{C_{zM}}{C_{zz}})_1 & (\frac{C_{\alpha M}}{C_{\alpha\alpha}})_2 \end{bmatrix}$$

3.138

where the subscripts 1,2 correspond to measurements with excitation cases 1,2 respectively and the complex covariances

C_{zz} = autocovariance of V_z

$C_{\alpha\alpha}$ = autocovariance of V_α

$C_{z\alpha}$ = covariance of V_z and V_α

$C_{\alpha z}$ = covariance of V_α and V_z

C_{zZ} = covariance of V_z and V_F

C_{zM} = covariance of V_z and V_M

$C_{\alpha Z}$ = covariance of V_α and V_F

$C_{\alpha M}$ = covariance of V_α and V_M

Matrices $[H]$ and $[G]$ can then be rewritten as

$$[H] = \begin{bmatrix} 1.0 & (\frac{C_{\alpha z}}{C_{\alpha\alpha}})_2 \\ (\frac{C_{z\alpha}}{C_{zz}})_1 & 1.0 \end{bmatrix} \qquad 3.139a$$

$$[G] = \begin{bmatrix} (\frac{C_{zZ}}{C_{zz}})_1 & (\frac{C_{\alpha Z}}{C_{\alpha\alpha}})_2 \\ (\frac{C_{zM}}{C_{zz}}) & (\frac{C_{\alpha M}}{C_{\alpha\alpha}})_2 \end{bmatrix} \qquad 3.139b$$

When excitation vectors (comprising the columns of $[G]$) are chosen to be linearly independent, columns of $[H]$ are linearly independent and the

inverse matrix $[H]^{-1}$ exists and equation 3.138 reduces to

$$[P] = \begin{bmatrix} 1 & 0 \\ x_{GM} & 1 \end{bmatrix} [B] [G] [H]^{-1} \begin{bmatrix} \frac{\partial z}{\partial V_z} & 0 \\ 0 & \frac{\partial \alpha}{\partial V_\alpha} \end{bmatrix}^{-1} \qquad 3.140$$

which can be solved for the elements of $[P]$. Note that the elements of $[P]$ may contain small interaction terms caused by other effects e.g. aerodynamic asymmetries, (see Appendix B). $[P]$ principally consists of inertia, magnetic and aerodynamic terms. Since interest is in measurement of aerodynamic effects it is necessary either to have precise estimates of the inertia and magnetic terms or alternatively repeat the whole test at same test frequency and model mean positions once again in evacuated tunnel working section. The latter can be replaced by repeating the test just in wind-off conditions. The net aerodynamic effects can be extracted as follows

$$[P]_{aero.} = [P]_{wind\text{-}on} - [P]_{wind\text{-}off} \qquad 3.141a$$

$$= \begin{bmatrix} 1 & 0 \\ x_{GM} & 1 \end{bmatrix} [B] \left(([G][H]^{-1})_{W\text{-}on} - ([G][H]^{-1})_{W\text{-}off} \right) \begin{bmatrix} \frac{\partial z}{\partial V_z} & 0 \\ 0 & \frac{\partial \alpha}{\partial V_\alpha} \end{bmatrix} \qquad 3.141b$$

Therefore

$$[k] + \omega^2 \begin{bmatrix} Z_w^{\cdot} & x_{GP} Z_w^{\cdot} \\ M_w^{\cdot} & x_{GP} M_w^{\cdot} \end{bmatrix} - j\omega \begin{bmatrix} Z_w & Z_q + UZ_w^{\cdot} + x_{GP} Z_w \\ M_w & M_q + UM_w^{\cdot} + x_{GP} M_w \end{bmatrix} = [P]_{aero} \qquad 3.142$$

where matrix $[k]$ retains the same form as in equation 3.133c. Since this is a complex equation, the real and imaginary parts on both sides

can be equated and the aerodynamic derivatives obtained. The full utilisation of this equation however, requires a knowledge of the magnetic stiffness coefficients k_{11}, k_{12}, k_{21}, and k_{22}. In arriving at equation 3.142 it has been implicitly assumed that either there is no change in balance damping or that such damping is very small compared with aerodynamic damping. If interest lies mainly in the measurement of damping derivatives, equating imaginary parts of both sides of equation 3.142 leads to

$$-\omega \begin{bmatrix} Z_w & Z_q + UZ_{\dot{w}} + x_{GP} Z_w \\ M_w & M_q + UM_{\dot{w}} + x_{GP} M_w \end{bmatrix} = \text{Imag} \left([P]_{aero} \right) \qquad 3.143$$

which does not require a knowledge of the balance stiffnesses. Furthermore if test is repeated at different frequencies and the real parts of $[P]_{aero}$ are plotted against ω^2 the slopes provide estimates for $Z_{\dot{w}}$ and $M_{\dot{w}}$. Therefore without knowledge of balance stiffness it should be possible to measure M_q, $M_{\dot{w}}$, M_w, Z_q, $Z_{\dot{w}}$, Z_w explicitly, but the demand on accuracy of covariance estimates increases. In fact if the wind-off case is replaced by a set of testing at a different oscillation frequency then the difference between the determined P matrix from each case is independent of the balance condition. It can be shown that up to first order

$$(\omega_2^2 - \omega_1^2) \begin{bmatrix} Z_{\dot{w}} & x_{GP} Z_{\dot{w}} \\ M_{\dot{w}} & x_{GP} M_{\dot{w}} \end{bmatrix} - j(\omega_2 - \omega_1) \begin{bmatrix} Z_w & Z_q + UZ_{\dot{w}} + x_{GP} Z_w \\ M_w & M_q + UM_{\dot{w}} + x_{GP} M_w \end{bmatrix} = [P]_{\omega_2} - [P]_{\omega_1}$$

3.144

where ω_1 and ω_2 correspond to the wind-on test frequencies with the model at the same mean positions. Although, in principle, higher accuracy can be achieved if ω_2 and ω_1 are widely separated, the range of frequency available within the framework of the simplified model presented here is rather limited.

In both testing methods described above, two different excitations in two stages (corresponding to two frequencies) i.e. four sets of wind-on testing records are needed. This requires a relatively long wind-on testing time. A reduction of testing time can be achieved, at least in principle, if the features of testing are more efficiently utilised. Since two different frequencies of oscillation are required and sinusoids of different frequencies are not correlated over sufficiently long record lengths, error signals feeding model oscillation can be chosen to be composed of the addition of two sinusoids of different frequencies. Clean reference signals corresponding to the different sinusoids are recorded. The analysis is more complex than previous cases since covariance must be carefully carried out in two stages. In the first stage covariance is taken with respect to one of the reference sinusoids and the calculated covariances form the elements of the first columns of the first of two sets of matrices $([H]_{\omega_1}, [G]_{\omega_1})$ and $([H]_{\omega_2}, [G]_{\omega_2})$ while covariances with respect to the other reference signal form the elements of the first columns of the second set. With the test repeated at different force configuration but same frequencies, the remaining columns of the matrices above can be calculated. Although testing time can be halved, strict limitations on the record length and amplitudes may seriously affect the achievable accuracy of this method.

Introducing suitable nondimensionalised forms of the derivatives

[Babister (1961)] using the mean aerodynamic chord as the characteristic length we get

$$\frac{c_a}{\rho U^2 S}[\bar{k}] + \Omega^2\begin{bmatrix}\hat{z}_{\dot{w}} & x'_{GP}\hat{z}_{\dot{w}}\\ \hat{m}_{\dot{w}} & x'_{GP}\hat{m}_{\dot{w}}\end{bmatrix} - j\Omega\begin{bmatrix}\hat{z}_w & \hat{z}_q+\hat{z}_{\dot{w}}+x'_{GP}\hat{z}_w\\ \hat{m}_w & \hat{m}_q+\hat{m}_{\dot{w}}+x'_{GP}\hat{m}_w\end{bmatrix} = \frac{c_a}{\rho U^2 S}[P]_{aero}$$

3.145

where c_a, S are the mean aerodynamic chord and wing reference area; ρ air density; and the oscillatory derivatives are given by

$$\hat{z}_{\dot{w}} = \frac{Z_{\dot{w}}}{\rho S c_a}\ , \qquad \hat{m}_{\dot{w}} = \frac{M_{\dot{w}}}{\rho S c_a^2}\ ,$$

$$\hat{z}_w = \frac{Z_w}{\rho U S c_a}\ , \qquad \hat{m}_w = \frac{M_w}{\rho U S c_a}\ ,$$

$$\hat{z}_q = \frac{Z_q}{U S c_a}\ , \qquad \hat{m}_q = \frac{M_q}{\rho U S c_a^2}\ ,$$

and

$\Omega = \frac{\omega c_a}{U}$. It should be noted that, in order for equation 3.145 to be dimensionally compatible, matrices [H] and [G] should be modified to take the form

$$[H] = \begin{bmatrix} 1. & c_a\left(\frac{C_{\alpha z}}{C_{\alpha\alpha}}\right)_2 \\ c_a\left(\frac{C_{z\alpha}}{C_{zz}}\right)_1 & 1. \end{bmatrix}$$

3.146

$$[G] = \begin{bmatrix} \left(\frac{C_{zZ}}{C_{zz}}\right)_1 & c_a\left(\frac{C_{\alpha Z}}{C_{\alpha\alpha}}\right)_2 \\ c_a\left(\frac{C_{zM}}{C_{zz}}\right)_1 & c_a^2\left(\frac{C_{\alpha M}}{C_{\alpha\alpha}}\right)_2 \end{bmatrix}$$

In summary the technique presented here involves forcing the model in oscillation, at a preselected frequency, twice in wind-on and recording 2 position and 2 force signals each time. The shole test is repeated wind-off or at a different frequency and similar recording is carried out. The covariance estimates are then digitally calculated for selected pairs of signals and amplitude ratio and phase differences obtained. Matrix $[H]$ and $[G]$ are then obtained for wind-on and wind-off or other frequency case then $[P]_{aero}$ is obtained. In order to determine the acceleration derivatives $\hat{z}_{\dot{w}}$, $\hat{m}_{\dot{w}}$ in absence of balance stiffnesses, repeating the wind-on test at two different frequencies of oscillation is necessary and sufficient.

In the mathematical model assumed, the axial displacement and force are assumed to be zero. The first of these can be realised in practice if the model is sufficiently restrained in the axial direction and no significant coupling exists between the axial and other force components. In a mechanical suspension and balance system, this can usually be achieved independent of the model construction or stiffnesses in the lateral plane i.e. the heave and pitch. There is however a difficulty in generating the desired model motion in a simple way. In a fixed configuration MSBS, for a certain model the ratio between the stiffnesses in the lateral and axial motions is approximately fixed. If this ratio is small the representation of the oscillatory system by a 2-DOF model

may require reexamination. However, the ease with which model motions can be imparted in a magnetic balance may balance this shortcoming.

In practice, two additional important factors can affect the accuracy of test results. These are the nonlinearity and noise. In order to minimise the effect of the first, the amplitudes of oscillation are kept small. The consequence of this, however, is a reduction in the signal to noise ratio. A compromise has to be reached. Fortunately, in the present case, the displacement signals are expected to be cleaner than in the case of roll displacement (see sec. 3.2.4). This permits physical oscillations of the order of 2 deg. p-p in pitch and 3 mm. p-p in lateral heave to produce reasonable amplitude and clean signal.

3.2.6.3 Alternative test techniques for measurement of aerodynamic oscillatory derivatives

The mathematical model used in the previous section was developed for the full 2-DOF system. It is useful to explore the possibility of simplification of the mathematical model and hence reduction in the number of measurements. If the test is carried out such that only pure pitching oscillation about the mean position takes place, then the mathematical model reduces to a set of two differential equations in θ and two excitation terms which can be obtained from equations 3.132 by setting $z_p = \dot{z}_p = \ddot{z}_p = 0$. If the number of measurements is restricted to two at a time then simultaneous recording of θ and $Z(t)$ in wind-on then wind-off can yield a measurement of the aerodynamic force derivatives. In absence of information about balance stiffness, a repetition of the test at another frequency of oscillation is required in order to separate the acceleration force derivative. Similarly repeating for θ and $M(t)$ can yield the moment derivatives. The latter case, however,

requires a knowledge of the force derivatives since the original moment equation contains a term resulting from the axis of moments shift.

If only lateral heave oscillation is imparted to the model (i.e. model undergoing plunging oscillation) then the equation simplifies since θ can be set = 0. Two pairs of signals can be used to obtain information on the derivatives involved. z and Z can lead to the measurement of $\hat{z}_w$ and $\hat{z}_{\dot{w}}$ while z and M can lead to $\hat{m}_w$ and $\hat{m}_{\dot{w}}$. The latter pair z,M requires the information of $\hat{z}_w$ and $\hat{z}_{\dot{w}}$ for its final determination.

A combination of these two types of testing can offer a simplification in the procedure of conducting the actual testing and a reduction of the number of measured quantities. Quantitative effect of noise is difficult to assess. The general comments presented in section 3.2.6.1 remain valid. These quantitative effects, however, can be most effectively obtained from a suitable digital simulation.

4. THE WIND-TUNNEL AND MAGNETIC BALANCE

4.1 The wind-tunnel

The wind-tunnel used in this investigation is a 6" x 8" induction type tunnel. It is a modified version of the 3" x 9" NPL tunnel [Holder & North (1949)]. It has a return circuit, but with an adjustable relief valve such that the tunnel stagnation pressure can be kept close to atmospheric pressure. The working section is horizontal, rectangular and closed. It measures at the centre-line 6" x 8.2" (0.15 m x 0.21 m) and is 16 in. (0.4 m) long. The working section was originally located 0.3 m ahead of the injector section. However, for improved performance and the provision of a larger working space, this distance was increased to about .9 m by displacing the injector further downstream of the working section. An easily removable wooden section is used to join the end of the test section to the injector section. The return circuit is similarly lengthened such that continuity is maintained. The tunnel has a set of 4 screens placed just ahead of the contraction section.

4.1.1 Tunnel drive and speed control

The compressed air supply to the injector is fed from the 250 psig pressure line through a manually controlled valve. A constant pressure regulating valve was found unnecessary (and sometimes unsatisfactory) for test runs at very low injection pressures and manual control was used throughout.

4.1.2 Speed and flow characteristics

The wind-tunnel is theoretically capable of establishing a steady airflow in its working section at speeds from zero up to M = 1.8. In practice, however, difficulties were experienced in attempts to achieve

the high performance limit for reasons pertaining to the inefficiency of mixing of the tunnel flow and injector air. Since the stagnation pressure is close to the ambient atmospheric pressure, the working section dynamic head and Reynolds number/metre at 15°C are directly related to the Mach number as in fig. 4.1. The series of tests considered here were concerned only with incompressible flow. The dynamic head of the flow in the test section was calibrated against static pressure tapping located just ahead of the test section and at the beginning of the contraction. It is shown in fig. 4.2, and is accurate to within ± .5%.

4.1.3 Turbulence level and flow angularity

A hot wire probe was inserted in the middle of the test section and the rms value for the air speed fluctuation was measured with the wire axis in two perpendicular positions normal to the tunnel axis. At a tunnel flow speed of about 30 m/s the turbulence level was found to be about 0.12%. Recently, independent and more detailed measurements have confirmed this figure and show that most of the energy content resides in the high frequency band. The latter is consistent with expected upstream acoustical influence of the injector noise.

Because of the low speeds involved and the tunnel working section aspect ratio (depth/width), the tunnel flow is expected to be less angularly inclined to the centre line in the horizontal plane than in the vertical. Yawmeter measurements showed that the flow is parallel to the centre line to within ± 0.1° in the vertical plane.

4.1.4 Flow transparency

The model position sensing system, as will be described later in this chapter, uses the airflow in the test section as a medium for the passage of light beams across the model to photocells. The presence of

fine solid or liquid particles in the flow field reduces the transparency of the medium and causes refraction, diffraction or attenuation of the light beam during a wind-on test, which in turn could cause a positional error or drift. The particles are carried into the tunnel circuit with the compressed air. To avoid this effect, the direct solution would be the installation of an air filter just prior to the air injector. Owing to the absence of such filter, at that time, care has been taken to run the tunnel regularly for long periods without the model in and inspect various glass windows and mirrors in the test section for any visible deposits. A satisfactory state is assumed reached when the position signals obtained from approximately half-masked sensors indicate differences less than 0.1^{o} or 0.1 mm between wind-on and wind-off cases with the flow duration approximately 50% longer than intended test run to follow. It was found that several such attempts were necessary until satisfactory state is achieved.

4.2 The magnetic suspension and balance system

Magnetic suspension of models provides a support-free means of flight simulation in wind-tunnels and a balance for the measurement of aerodynamic forces acting on the model. Several systems have been developed since the first French system [Tournier and Laurenceau (1957)]. These systems are reported in the proceedings of the two conferences held at Ohio [Daum (1966)] and at Southampton [Judd and Goodyer (1971)].

The Southampton University MSBS is a d.c. system; i.e. the magnetic fields involved vary only at low frequencies. The model position is controlled in all six degrees of freedom. Because all support currents are monitored it also forms a six-component balance. It is mounted

on the test section of the wind-tunnel described in 4.1 above.

4.2.1 Basic principles of the magnetic suspension

A model containing magnetic material experiences forces and moments when placed in a magnetic field. These forces are related to the spatial field distributions, e.g. forces are proportional to field gradients and moments are proportional to field strengths near the model. Earnshaw's theorem shows that a system made up solely of a ferromagnetic material and a steady magnetic field is inherently unstable in at least one degree of freedom. A form of feedback from the model position to control the field is necessary to produce complete stability. This is realised in the Southampton system by monitoring the model position, modifying the gain and phase of the position signal and feeding it back to the power supplies energizing the field electromagnet coils. The system is in effect a position control servo in each of its degrees of freedom. Levitation is achieved by maintaining a powerful enough field to produce a force that equalises the gravitational force on the model.

When external forces act on a magnetically levitated model the fields will automatically adjust by the action of feedback, in order to generate additional equalising forces. Unless a form of integral feedback is present, this action results in a steady state error in the model position. If this force is constant in a test condition, and in absence of integral feedback, correction due to steady state errors can be made by manually trimming the position setting. Integral feedback, however, causes a slowing of the dynamic response of the system. The change in the fields following an external force can be force calibrated and the system used as a balance. The achievable accuracy of the balance rests mainly on the accuracy of the appropriate force

calibration. Owing to their wide load dynamic range, magnetic balances possess great potential applications. Beams (1971) states that under comparable conditions the load to precision ratio, LPR, for a magnetic balance approaches 10^{10} while a comparable microbalance, at the present, is limited to 2×10^{8}.

4.2.2 Description of the Southampton MSBS

The layout of the electromagnets around the test section is sketched in fig. 4.3. It consists of three pairs of horse-shoe electromagnet coils, two horizontal and one vertical above the test section, and a doughnut coil wound round the test section near the upstream end. The vertical pair (lift magnet) generates the necessary field to levitate the model and take up forces in the vertical plane. The lateral pairs supply the field required to balance external forces on the model in the horizontal plane. They contain three sets of winding sections. The main one is fed from the controllable lateral currents power supplies which is unidirectional. The second is fed from a constant current power supply and forms the lateral bias current. Bias current is necessary in order to offset the magnetic field in the test section and so allow the controllable field to balance both positive and negative lateral forces. The third set of winding sections are separately fed from an independently controlled current supply, the roll power supply. The current in these winding sections acts to generate a field distribution necessary for augmenting any roll stiffness (present to some extent in all degrees of freedom) and balancing external roll torques. The drag force is taken by the doughnut coil field.

The power supplies are six independent controlled units each comprising a thyristor controlled 3-phase silicon-controlled-rectifier. All the power supplies generate a unidirectional current i.e. current

is either positive or negative. The current signals contain ripples having a fundamental frequency of 150 Hz.

Position sensing is achieved by a passive optical system. Nearly parallel light beams from miniature filament d.c. bulbs shine across the edge of the model from one side and are received at the other side on a photo-conductor, silicon solar cell. Linear displacement of the model edge changes the beam area and consequently the amount of light falling on the photo-cell. This gives rise to a signal proportional to the respective displacement. Both the source and cell are located outside the test section and unattached to it. For this reason and to enable observation of the model during testing, small glass windows on the side walls and a whole thick completely glass floor are provided in the test section. A schematic of a pair of position sensors is shown in fig. 4.4. Two such units, one at the front and one at the rear of the fuselage, are used to sense model pitch, yaw, vertical heave and lateral heave. Reference to fig. 4.3 shows that the model is levitated wings vertical instead of the conventional horizontal wings. Therefore pitch angle, i.e. incidence, is taken in the horizontal or lateral plane. For the roll displacement sensing a slightly different arrangement is used, fig. 4.5. A light beam from a source under the test section is reflected by a mirror fixed in the test section roof and made to pass through a special window in the model fin having equi-spaced inclined vanes before being received by the respective photo-cell, [Goodyer (1968)]. Model roll displacement changes the width of the beam and so produces a signal at the cell output which is approximately proportional to the roll displacement provided the latter is small. Axial position can be monitored by a beam cutting the blunt base of the fuselage or by a beam intersection with the conical nose of the model.

In the latter case a beam of light, again reflected from the tunnel roof, passes across the conical nose and is received through a circular arc slit to a condensing lens and finally to the photo-cell. The width of the slit and its location are chosen such that a length of about 4 mm of the model located about 15 mm downstream of the apex is monitored. The radius of the slit is chosen such that model pitching (in lateral plane) causes the minimum of axial displacement.

The output signals of the 6 photo-cells are amplified and combined, where required, to form signals directly proportional to conventional displacements e.g. pitch, yaw, vertical and lateral heave motions. These signals are then passed through phase lead-lag networks, re-combined and fed to the power amplifiers at appropriate gain. The power amplifiers feed the required currents to the electro-magnet coils. A schematic of the feedback circuit for the lateral control modes is shown in fig. 4.6. Circuits are wired on standard plug-in cards and mounted in suitable racks in the control cabinet.

Model displacement signals and currents in the coils are monitored and displayed on suitable meters housed in the control panel . Current signals are in addition amplified and filtered (i.e. conditioned) for recording and for reading directly on DVM's. Filtering is necessary in order to reduce the amplitude of spikes noise which might otherwise cause errors later in the data reduction and analysis processes. Fig. 4.7 shows the current-signal conditioning circuits.

4.2.3 System capability and limitations

Maximum allowable currents in the coils, at present, are 100 amps in the drag coil and 35 amps in each of the other coil sections. These limit the maximum force capability on a typical 0.3 kg. model containing

a 0.25 kg. Alcomax permanent magnet to about 5N in the axial and lateral planes and about half as much in the vertical plane. When drawing the maximum currents in all coils, the system dissipates about 22 kW, while at a normal suspension wind-off condition it dissipates about 2 kW. This limits the suspension time to less than one hour without the use of coil cooling.

For the model tested (see chap. 5) the natural frequency of suspension varies from one degree of freedom to the other and varies with the gains of the feedback control loops. In pitch and yaw, typical natural frequencies are in the region 18-20 Hz, in lateral and vertical heave about 13-15 Hz. In roll the natural frequency is as low as 5-8 Hz and in axial motion it is about 2 Hz. Slight control over the natural frequency is obtained by adjusting the phase and gain margins of the respective loops.

4.3 MSBS calibration

The accuracy of any measurement depends on the accuracy of the calibrations involved. In the case of the MSBS two separate calibrations are usually involved, position or optics calibration and force calibration.

4.3.1 Position calibrations

From time-to-time, calibrations in all modes of motion are carried out. However, to illustrate typical techniques the two calibrations most closely associated with this work will be described.

For incidence calibration the model is mounted in a rig which is designed to allow model rotation about a fixed vertical axis. This allows the model only freedom to pitch in the horizontal plane. A mirror on the rotating model mount reflects the image of a hairline onto

a scale thereby optically magnifying the angular displacements. The rig is first used to check the optical interactions among various displacements and then readings of the incidence on the scale are taken against the DVM reading of the incidence voltage signal. Fig. 4.8 shows a typical incidence calibration and the associated untrimmed interactions present. The estimated accuracy of this method of incidence calibration is about 0.05 degree (3').

Roll attitude calibration is carried out by monitoring the displacements of two points on the trailing edges of the wings, while the model is magnetically suspended, using a travelling microscope. As the model undergoes roll displacement the selected points undergo lateral displacements which can be accurately measured by the traverse of the microscope. Lateral displacements of the chosen points can be related to the model roll displacement which can therefore be plotted against the roll attitude voltage signal. Fig. 4.9 shows a typical result of this form of calibration. The accuracy of this method is of the order of half-a-minute of roll displacement. An advantage of this calibration method is that it can be easily repeated with the model at incidence in order to determine the minimum incidence-roll interaction.

4.3.2 Force and moment calibration

The objective of these calibrations is to obtain the necessary numerical values for the constants in the force calibration relations, Appendix *A*. Calibrations are carried out by applying external forces to the magnetically suspended model through a system of strings and pulleys and monitoring the resultant current signals. Two groups of calibration constants are sought. The direct calibration constants and the interaction calibration constants. The former are obtained from the force-current characteristics with the model at a fixed nominal (e.g. zero)

incidence, while in the latter variations of these with model incidence are determined. As discussed in Appendix A the interaction calibration constants are of a smaller magnitude than the direct ones and can only be determined with reduced accuracy.

4.4 Other devices used

4.4.1 The incidence ramp-function generator

In order to drive the model into the required form of motion, either an incidence sweep or staircase motion, an 'error' signal has to be fed into the control loop circuit. Ramp function can be easily generated using a fixed amplitude integrating operational amplifier network followed by an amplitude, or range, setting amplifier. Fig. 4.10 shows an initial design of a circuit built into the model control console to produce such ramp functions with independent amplitude and duration settings. Two operations of the switch are necessary for the combined ramp-up and ramp-down. This added greatly to work load during a wind-on test, although it served well in the initial stages of testing.

A specially designed portable ramp function generator was therefore built. It has a more sophisticated circuit, Fig. 4.11, which generates voltage functions as shown in fig. 4.12, in response to a single pressing of the push button. The sweep time t_{swp} can be set at any value between 0.1 sec and 220 sec upon adjustment of a calibrated potentiometer, and the pause time t_p can be set to 1, 2, 5 or 10 seconds values. This device proved to be useful because of the wide range of sweep times available and the need for only a single pressing of a switch. Being portable, it enabled more attention to be paid to tunnel flow and model behaviour. The device performance was repeatable over most of its operating range.

4.4.2 The magnetometer

It has been well established that precise measurement of the model magnetisation is necessary at the time of force and moment calibration and prior to each set of test runs. All force and moment components are scaled by the magnetisation intensity of the model. A simple and reasonably precise device was constructed which is based on the induction principle. The integrated emf induced in a search coil following the displacement of a nearby magnet is related to its intensity of magnetisation, [Parker and Studders (1962)]. If the model is held at a precise location relative to the coil and made to execute the same displacement every time then the integrated emf signal is proportional to the intensity of magnetisation of the model. A small air-cored coil 1 in. inside dia. x 2 in. outside dia. x 1 in. long permanently fixed to a perspex tube and frame is bolted to the incidence calibration rig in a position close to but, just behind the model tail. This allows the model to rotate horizontally in the rig over a range limited by mechanical stops. The signal from the coil is amplified using a differential op-amp and then integrated and read on a DVM. To increase the magnitude of the generated emf signal a soft iron core is inserted into the coil. Integrator drift is the main source of error in this device. A low offset current instrumentation type op-amp would have been the most suitable type for use in the integrator but was not available at the time. However, by strictly following the same procedure every time the device is used, very accurate measurements could be obtained. Fig. 4.13 shows a schematic of the magnetometer layout and circuit.

The accuracy achievable in terms of precision and day to day repeatability is about ± .5%.

5. THE MODEL AND ASSOCIATED DATA

In order to develop the test techniques presented here a complete aircraft winged model was constructed. A special interest exists in the AGARD-G dynamic testing model. This is a slender wing model specially designed for dynamic calibration of test facilities. The exact AGARD-G model configuration is not immediately suitable for suspension in the MSBS unless extensive modifications to the position sensing system are introduced. A compromise model was constructed and built, fig. 5.1. It has a slender circular cylindrical fuselage with AGARD-G planform wings attached to it. The cylindrical fuselage reduces greatly the problems of suspending the model and calibrating the position sensing system.

This chapter presents a description of the model and its associated calibration data. This data consists of model position displacement calibration data, static force (and moment) calibration constants and some qualitative information on dynamic behaviour of model in suspension.

5.1 Model description

Fig. 5.2 shows the sections of the model and its main dimensions. The fuselage is a 16 mm dia. Dural shell, containing a slide fit space for a $\frac{1}{2}$ in dia. x 6 in long round bar Alcomax III magnet. This is the main magnet, magnetised along its length and secured in position inside the Dural fuselage by a screwed cap with O-ring. The O-ring serves to hold the magnet securely inside the shell. The Dural nose is conical near the apex, smoothly faired to the fuselage diameter and is fixed to it through a brass connector. The wings are constructed of Dural with cut-outs housing the roll magnets. The latter are Platinax II magnets in the form of short strips and cylinders which are magnetised normal to the wing plane and in opposite senses in each wing. The magnets are held by Araldite in cut-outs in the wings. Although the main magnet produces

some roll stiffness owing to the nonhomogeneity of its material, these wing magnets are essential in order to allow control over roll attitude, [Goodyer (1967)]. The wings are glued to the fuselage and the corners between the wing roots and the fuselage are smoothly faired with the adhesive. A Dural fin containing the inclined grid window is similarly glued to the fuselage at right angles to the wing plane.

5.2 Model geometrical data

The main geometric characteristics may be summarised as follows:

Wing planform area	$= 60.63 \times 10^{-4}$ m^2
" semispan	= 37.3 mm
" centre line chord	= 143.9 mm
Model length	= 204 mm
Mean geometric chord	= 81.2 mm
Mean aerodynamic chord	= 97.9 mm
Wing root thickness	= 5.64 mm

5.3 Position calibration data

Optical position calibration can vary slightly from day to day for a variety of reasons including contamination of the optical path of the light beams and drift in the voltage supply to the light sources. Continuous monitoring of the supply voltage has been maintained throughout. Recalibrations of the most important position signal, the incidence signal and its associated interactions, is carried out immediately prior to and after a set of test runs. Fig. 5.3 shows two typical sets of calibrations taken at two different dates. Incidence values and corresponding signals are taken every $\frac{1}{2}$ degree interval covering the range -3° to $+9^{\circ}$ and the values are recorded for further use in data reduction and analysis. The calibrations are good to within $\pm 0.05^{\circ}$.

Fig. 5.4 shows an example of the roll position calibration at two different values of incidence showing the absence of significant incidence-roll optical interaction.

5.4 Steady force calibration data

For the measurements reported here major interest of steady force testing lies in the aerodynamic forces acting on the model. These comprise lift force L, drag force D and pitching moment *M*. Due to the shape and distribution material in this model and the MSBS magnetic field spatial distribution, a significant interaction on these forces was found originating from the roll torque. It was therefore decided to include the aerodynamic roll torque T in these measurements. Thus four components are involved. Correspondingly it is necessary to measure changes in four currents. During the applications of force combinations corresponding to changes in L, D, *M* and T, either in the calibration process or in wind-on testing, the currents in the suspension electromagnets were found to remain substantially constant. This formed a sufficient evidence to justify neglection of their effects. The four monitored currents are:

i) net lateral forward current I_F, which is the lateral forward current less bias current,

ii) net lateral aft current I_A, which is the lateral aft current less bias current,

iii) the drag current I_D

iv) the roll current I_R

Two sets of force-current calibration constants are determined. First is the set of 16 direct calibration constants pertaining to force-current relationships at model fixed position e.g. at nominal (zero)

incidence. Second set corresponds to the variation of those constants with model major displacement during testing e.g. during incidence change as a result of ramping. These add another 16 calibration constants to be determined. Following the discussions and conclusions of Chapter 4 and Appendix A these two sets of force-current calibration constants can be made unique for the model containing this particular magnet shape if their dependence on the state of magnetisation of the model is eliminated. The constants so obtained need only be determined once. They form the elements of the matrix G_{rs} in equation A.17. G_{rs} is a 4 x 4 matrix. Each element of G_{rs} is the sum of a direct and α times an indirect calibration constant. α is the model incidence displacement from nominal. If m is the magnetic moment of the model then the elements of G_{rs} are as follows:

$$G_{11} = m \frac{\partial I_F}{\partial L} + m\alpha \frac{\partial}{\mu\alpha} \left(\frac{\partial I_F}{L}\right) = G'_{11} + \alpha G''_{11}$$

$$G_{12} = m \frac{\partial I_F}{\partial D} + m\alpha \frac{\partial}{\partial \alpha} \left(\frac{\partial I_F}{\partial D}\right) = G'_{12} + \alpha G''_{12}$$

$$G_{13} = m \frac{\partial I_F}{\partial M} + m\alpha \frac{\partial}{\partial \alpha} \left(\frac{\partial I_F}{\partial M}\right) = G'_{13} + \alpha G''_{13}$$

$$G_{14} = m \frac{\partial I_F}{\partial T} + m\alpha \frac{\partial}{\partial \alpha} \left(\frac{\partial I_F}{\partial T}\right) = G'_{14} + \alpha G''_{14}$$

$$G_{21} = m \frac{\partial I_A}{\partial L} + m\alpha \frac{\partial}{\partial \alpha} \left(\frac{\partial I_A}{\partial L}\right) = G'_{21} + \alpha G''_{21}$$

$$G_{22} = m \frac{\partial I_A}{\partial D} + m\alpha \frac{\partial}{\partial \alpha} \left(\frac{\partial I_A}{\partial D}\right) = G'_{22} + \alpha G''_{22}$$

$$G_{23} = m \frac{\partial I_A}{\partial M} + m\alpha \frac{\partial}{\partial \alpha} \left(\frac{\partial I_A}{\partial M}\right) = G'_{23} + \alpha G''_{23}$$

$$G_{24} = m \frac{\partial I_A}{\partial T} + m\alpha \frac{\partial}{\partial \alpha} \left(\frac{\partial I_A}{\partial T}\right) = G'_{24} + \alpha G''_{24}$$

$$G_{31} = m \frac{\partial I_D}{\partial L} + m\alpha \frac{\partial}{\partial \alpha} \left(\frac{\partial I_D}{\partial L}\right) = G'_{31} + \alpha G''_{31}$$

$$G_{32} = m \frac{\partial I_D}{\partial D} + m\alpha \frac{\partial}{\partial \alpha} \left(\frac{\partial I_D}{\partial D}\right) = G'_{32} + \alpha G''_{32}$$

$$G_{33} = m \frac{\partial I_D}{\partial M} + m\alpha \frac{\partial}{\partial \alpha} \left(\frac{\partial I_D}{\partial M}\right) = G'_{33} + \alpha G''_{33}$$

$$G_{34} = m \frac{\partial I_D}{\partial T} + m\alpha \frac{\partial}{\partial \alpha} \left(\frac{\partial I_D}{\partial T}\right) = G'_{34} + \alpha G''_{34}$$

$$G_{41} = m \frac{\partial I_R}{\partial L} + m\alpha \frac{\partial}{\partial \alpha} \left(\frac{\partial I_R}{\partial L}\right) = G'_{41} + \alpha G''_{41}$$

$$G_{42} = m \frac{\partial I_R}{\partial D} + m\alpha \frac{\partial}{\partial \alpha} \left(\frac{\partial I_R}{\partial D}\right) = G'_{42} + \alpha G''_{42}$$

$$G_{43} = m \frac{\partial I_R}{\partial M} + m\alpha \frac{\partial}{\partial \alpha} \left(\frac{\partial I_R}{\partial M}\right) = G'_{43} + \alpha G''_{43}$$

$$G_{44} = m \frac{\partial I_R}{\partial T} + m\alpha \frac{\partial}{\partial \alpha} \left(\frac{\partial I_R}{\partial T}\right) = G'_{44} + \alpha G''_{44}$$

Examples of the results of a force calibration carried out according to section 4.3 are shown in fig. 5.5 to 5.10 and the derived coefficients are listed in table 5.1.It is clear from the figures that the linearity is well preserved for the direct calibration constants while in the indirect calibrations some cases tend to be more nonlinear than would be acceptable according to the arguments put forward in the force-current formulation. One simple way of accounting for these nonlinearities is to add another set of interaction calibration constants which varies with the square of the incidence. This means that the interaction effect is taken as a quadratic rather than a linear function of incidence. Table 5.1shows the quadratic interaction terms in addition to the linear interaction terms. The practical situation, however, includes various sources of experimental error. Notable among these are:

- the friction in the pulleys,
- the degree of imprecision in force application,
- the presence of noise on the signals, and
- the possible electronic drift during the calibration run, particularly in the current di-ferential amplifiers.

The accuracy of the calibration data can be easily assessed, in the practical sense, by applying a known combination of external forces and moments to the model, recording the changes in the relevant four currents and incidence. The changes in the currents and incidence are converted into forces and moments using the calibration data and equation A.19 rewritten here for convenience

$$\Delta F_s = m \left[G_{rs}\right]^{-1} \Delta I_r \qquad 5.1$$

where the single subscripted variables denote vectors. A comparison of the calculated values with actual values indicates the errors incurred by the calibration data. By repeating this over several force, moment and incidence combinations a sample of the statistical behaviour of the rrror can be obtained. The errors in various force and moment components are listed in table 5.2

5.5 Dynamic calibration constants

In order to analyse the results of unsteady measurements on a magnetically levitated model undergoing continuous time motion, accurate information on the dynamics of model position sensing and of balance force (and torque) dynamic response and the degree of coupling in both is required. The latter is referred to as interaction to signify it as being unwanted.

The frequency response of the position sensing system is practically flat up to a relatively high natural frequency e.g. of the order

100-300 Hz, [Goodyer, (1968)]. The precise value for a certain displacement component is dictated by the time constant of the low pass filter on the first stage of electronic amplification of the optical sensor signal. The lowest value above corresponds to the axial position displacement. These values, therefore, confirm that static position calibration is sufficiently good to convert low frequency (e.g. 1-2 Hz) time varying position signals into physical displacements.

The application of sinusoidal force to a model in magnetic levitation without changing the suspension stiffness or mass is very difficult both in realisation and means of extraction of the relevant calibration constants. This, however, is not necessary when the oscillation frequencies are very low compared with the balance natural frequency. As has been mentioned earlier, ch. 3, it is reasonable to assume that the response of a dynamic balance can be approximated by that of a second order system. Therefore the force calibration constant at low frequency oscillation $(G)_{dyn}$ in a certain degree of freedom can be obtained from the corresponding static calibration constant $(G)_{st}$ using the approximate formula (valid for $\omega/\omega_n << 1.$):

$$(G)_{dyn.} \simeq \frac{(G)_{st}}{1 - (1-2\zeta^2)(\omega/\omega_n)^2} \qquad 5.2$$

where ω, ω_n are the testing frequency and balance natural frequency in that force component and ζ is the effective damping ratio. Typical values of roll oscillation testing frequency of 1.-2. Hz with a natural frequency of 12.-15. Hz, i.e. a ratio $\omega/\omega_n \simeq 0.16 - 0.06$, results in $(G)_{dyn} \simeq 1.026(G)_{st}$ to $1.0036(G)_{st}$ for a lightly damped system. ω_n for roll component may change with incidence in which case a correction must be applied to the dynamic calibration constant. This, however,

was found unnecessary for incidence values less than 6^{o}. The static roll torque calibration constant is given in table 5.1 as C'_{44}. Fig. 5.11 shows a typical roll torque calibration result. For the lateral heave and pitch oscillation similar results hold. The relevant calibration constants are listed and given in table 5.1.

The other important aspect of the unsteady testing is the interaction resulting from imperfection in position sensing system and electromagnet coils layout. This interaction can cause unwanted excitation of other components. The first of these is curable over most of the linear range but tends to get worse as the suspended model approaches either of the ends of the particular displacement range. This is cured through a trial and error process involving careful tailoring of the optical position sensing until the situation is achieved where the required component of displacement causes only insignificant changes in other components of model displacement. For a roll angular displacement of about 8^{o} of this model, the associated linear displacement was less than 0.2 mm and angular displacement less than 0.1 degree in other degrees of freedom. Force component interactions resulting from coil layout can not be easily controlled. The evidence of its existence is observed as the model oscillates in unwanted components of motion in the levitated wind-off mode, while it is forced to oscillate in certain components provided that the position interaction is minimal. For the AGARD-G winged model severe interaction between roll oscillation and lateral (as well as axial) motion were noted at high incidence, i.e. greater than 6 deg. A comparison of the interaction detected in the case of this model with other models suggests that the low roll torque stiffness of the present model might be partly responsible for the interaction observed. The low roll torque stiffness is caused by

locating most of the roll magnets close to the model axis and the generally low magnetic moment of these magnets.

6. DATA REDUCTION AND ANALYSIS METHODS AND TEST PROCEDURES

The techniques of data reduction and analysis described here were originally developed for specific use on the MSBS and an exploratory version was presented at the Second International Symposium on Electromagnetic Suspension, 1971. A detailed version and improvements on these techniques are presented in this chapter with a view to it aimed at general applicability to other test facilities.

About the time of beginning this work a digital computer in the data analysis centre of the ISVR*, of Southampton University was made available to other users, Appendix C. The MSBS had just been moved to its new location and the modernisation of its data acquisition and analysis was required. This demanded a search for suitable techniques for data handling making best use of the digital computer. Prior to that, manual data acquisition was used involving direct reading of currents from meters at discrete incidence settings and the use of resolved component indicators for the reduction of forced oscillation test results. Manual data handling proved to be laborious and required very long test run times. A long test run time is a drawback in complex systems, like the MSBS, unless statistical control over the experiment is strictly maintained. In particular drift in subsystem characteristics, e.g. position drift, proved to be a serious problem that could significantly affect the accuracy of results. Another problem was the lack of self consistency in a set of data points. Hand smoothing and joining a set of discrete data points is a good means of noise filtering, but involves a great deal of human judgement. Fine aerodynamic details may get unnecessarily smeared out in this process. An alternative way

* Institute of Sound and Vibration Research.

to avoid this is to measure more closely spaced data points in those doubtful areas if known a priori or in later tests. This results in long testing and analysis times and high cost penalties. The other alternative is to acquire automatically all data points in analog or digital form for the full range of test independent variable (e.g. incidence) in a single test run, with a simultaneous rough monitoring of the measured quantities, and perform the appropriate analysis in digital form. The test run time should be long enough to retain a predominant steadiness of all data but reasonably short to reduce the chance of subsystem drift in the acquired results. The latter approach has potential application in general test facilities and so was pursued further.

In this chapter the system of data acquisition, reduction and analysis for the incidence sweep tests is described and test procedure highlighted. The application of the data reduction methods and test procedures for the several forced oscillation techniques presented in chapter 3 is described.

6.1 Steady incidence sweep data reduction method

A block diagram of the data acquisition, reduction and analysis for the steady incidence sweep testing is shown in fig. 6.1. The system makes use of a multichannel FM tape recorder, a storage scope, a set of filters, a pulse insertion unit, a pair of analog to digital converters attached to the Myriad II computer with graphical and punched tape output units and the ICL 1907 digital computer.

The magnetic tape recorder is an Ampex 1300A FM 14 channel type, using the 3-M and Ampex instrumentation tapes. The recorder is a low noise type (S/N ratio 43 db at 60 ips) and frequency range 0 - 40 kHz at its top tape speed, 60 ips. The input-output linearity is within

± 0.7% with an input signal up to 1.0 Volt rms. Tape speeds are reproducible to within a good degree of accuracy. Other recording characteristics satisfy the IRIG specifications.

The variables in a test run, in the form of voltage signals V_α, V_F, V_A, V_D, V_R and V_X (corresponding to incidence, lateral forward less bias and lateral aft less bias currents, drag current, roll current and axial position signal respectively) and a suitable timing signal are first recorded on the magnetic tape. The timing signal is a -0.24 to +1.2 Volt stop lasting at the high level about 14 seconds, initiated by a press button. This signal serves to identify the start of test run data for each record. At the time of recording, the signals on the magnetic tape are simultaneously monitored on an X-Y type storage oscilloscope. On the screen of the scope 4 traces can be temporarily retained for observation and possible photographic record. These give an analog (and unfiltered) picture of the variation of the current signals V_F, V_A, V_D and V_R with the signal V_α which is roughly proportional to the incidence α. The storage scope traces have two purposes. The first of these is to check that the MSBS is performing satisfactorily since only limited time is available for direct model observation; and the second is to monitor the output stages of the currents differential operational amplifiers. The latter has been found necessary because of the low reliability of these amplifiers owing to their continuous subjection to common mode large amplitude spikes present on all currents. In earlier attempts using an Ampex 1300 tape recorder it was possible to observe all the 4 currents measured, but with the Ampex 1300A only two can be simultaneously monitored owing to the limited number of modules available at the time. Care is taken that the recorded signals lie within the linear range of the recorder, and

that the minimum effect of the recorder (e.g. mains interference) on the signals is achieved.

Out of the recorded test run cases, a batch is selected for digital analysis. There are two possible means of data acquisition on the Myriad computer. Repeated single (or two) channel data acquisition and multiplexed data acquisition. In the former case several tape runs are required in order to digitize and acquire all the test run data, while in the latter a single tape run is sufficient. Following is a listing of the relative merits and drawbacks of both types of acquisition:

Repeated two channel acquisition

Advantages

i) Short setting-up time,

ii) Three reproduce modules are sufficient,

iii) A single dual filter is sufficient,

iv) Data points are simultaneously acquired,

v) Maximum sampling rate is the ADC maximum value.

Disadvantage

i) Several tape runs are required and hence a relatively long computer time is required.

Multiplexed acquisition

Advantages

i) Single tape run and hence a shorter computer time is required.

ii) Particularly useful in on-line digital data analysis.

Disadvantages

i) Long setting-up time for recorded data analysis.

ii) Seven reproduce modules are required.

iii) Six phase matched filters are required.

iv) Data points are time shifted.

v) Maximum sampling rate is 1/7th the ADC maximum value.

The multiplexed acquisition was therefore abandoned because of the limited number of modules available for the Ampex 1300A, absence of enough good quality filters and the large setting up time.

The timing signal was passed in a pulse insertion unit (PIU) in order to generate a square pulse of large amplitude (approximately 10 Volts). Since this pulse is used essentially to trigger the ADC unit, the pulse width is chosen to be $\geq \frac{1.5}{N_s}$ seconds where N_s is the sampling rate of the ADC. It is clear in this case that a random time shift between the data of each acquisition exists which can be as large as $1/N_s$ seconds. As will be shown later this has no significant effect on the quality of steady data sought provided that piecemeal averaging is taken over a large enough number of samples. The choice of the filter setting and sampling rate of the ADC have been discussed earlier in chapter 3. The quantization error has a maximum amplitude of ± 5 mV and appears as a random error on the digital signals. To reduce its relative effect on the accuracy, the analogue signals are amplified about 10 times and the precise amplification factor is digitally corrected for later on.

Digital data corresponding to each variable is then acquired by the Myriad II computer and stored as a data file. The first stage of data reduction applied to the data files consists of dividing the numbers in the data files into equal length (successive or overlapping) intervals and calculating the average value and standard deviation of each group, i.e. piecemeal averaging. These two values take as reference coordinate the centre point of each respective time interval. The length of the averaging interval and spacing depend on the ramp rate, required incidence resolution and sampling rate as presented in chapter 3. The reduced data files are graph plotted for inspection and further

reduction and/or editing. The second stage involves editing the data files in order to select the best of the two records taken successively in the test run, and drop the unnecessary constant value data points. Modified data files are then graph plotted and the average parts merged into a single data file which is then punched on a paper tape. A sample program of this data reduction stage is shown in fig. 6.2.

Paper tapes are taken for the third and final stage of analysis to the main computer (ICL 1907). The program for this analysis is prepared according to the flow chart of fig. 6.3. It features reading the paper tape data and reading constants relevant to model geometry, test conditions, flow conditions, force calibration constants, position and recording calibration constants. The main data is read in the sequence wind-off then wind-on. The data files are read in the sequence wind-off then wind-on. The wind-off data files, now considered as vectors are least-squares fitted to the incidence signal in polynomials of the form

$$y_i = a_{o_i} + a_{1_i} x + a_{2_i} x^2 + a_{3_i} x^3 + \ldots \qquad 6.1$$

where y_i represents the wind-off signal of the i^{th} variable, x represents the incidence signal and a_{o_i}, a_{1_i}, ... constants (polynomial coefficients). Corresponding wind-on expressions for y_i are calculated using the polynomial coefficients, and these in turn are subtracted from wind-on data for the same incidence values. It is likely that some positional drift may have occurred in the axial position control system; a correction for this is provided by recording the axial position signal V_X at a point in the loop with minimal and regular drift properties. A static calibration provides the variation of drag current against that position signal from which a calibration constant

can be worked out. This is used to correct the drag current against the drift in such position signal between wind-on and wind-off runs. The equation depicting this correction is

$$\delta V_D = - \frac{\partial V_D}{\partial V_X} \delta V_X \qquad 6.2$$

where δV_X is the position signal drift and δV_D is the corresponding drag current signal correction. In this way the wind-on data is tare corrected. The tape recorder, filters and ADC may introduce some offset and gain errors and corrections for these are referred to as data handling calibration constants. A method of obtaining these calibration constants is presented later in this section. The wind-on data is corrected for these data handling calibration constants. The incidence signal calibration points are least squares fitted to a polynomial of degree 3 and the polynomial is used to translate V_α into actual incidence.

The next stage in the analysis is the conversion of voltage signals into forces and moments using the results of the force calibrations. The force-current relationship is derived in Appendix A and can be rewritten here as

$$[G] \{F\} = \{I\} = [K_{IV}] \{V\} \qquad 6.3$$

where $[K_{IV}]$ is the current voltage signal calibration matrix (diagonal matrix) and $[G]$ is the force calibration matrix. $[G]$ is composed of two parts:-

$$[G] = [G_1] + \alpha [G_2]$$

where $[G_1] = \frac{\partial V_i}{\partial F_j}$ and $[G_2] = \frac{\partial^2 V_i}{\partial \alpha \partial F_j}$

The force vector is therefore given by

$$\{F\} = [G]^{-1} \{V\} \qquad 6.4$$

It is necessary therefore to determine $[G]$ and then calculate its inverse in order to find the values of $\{F\}$ at each point. There are two ways of doing this numerically. One is the direct method just described leading to the exact values, but this takes a relatively long computation time. The other is an approximate method based on the possibility of modification of the inverse of a square matrix following small changes in its elements without the need to recalculate the new matrix. In the latter case if $[G]$ and $[G']$ are the calibration matrices corresponding to α and α' $[= \alpha + \delta]$ then their inverses are related by the exact formula, [Householder, (1953)],

$$[G']^{-1} = [G]^{-1} \left\{ 1. - \delta [G_2] \; (1. + \delta [G]^{-1} [G_2])^{-1} [G]^{-1} \right\} \qquad 6.5$$

However, since δ is very small, retaining only terms up to first order gives

$$[G']^{-1} \simeq [G]^{-1} \left\{ 1. - \delta [G_2] [G]^{-1} \right\} \qquad 6.6$$

The advantage of using this approximate method is the saving on computation time. Both the exact and approximate methods have been included in the program. The exact method is adopted for the first point in the file then the approximate method is followed for the next batch of points (e.g. five), after which the exact method is resorted to again in order to check on the last point. If the cumulative error in each force component has not exceeded 0.5%, approximate method is retained. If not, the exact method must be used. A less arbitrary choice of the number of points sufficient for the approximate method can be determined as follows. The difference between the exact and

approximate formulae can be limited to an a priori fixed small number say 0.005. Therefore in a number of points n_a the inequality

$$n_a \delta \left[G^{-1} G_2^{-1}\right] \leq 0.005 \qquad 6.7$$

must be satisfied. Since G includes σ then the above formula should be applied at both extreme values of α and the lowest of the two nearest integer values of n_a must be taken. If this value of n_a turns out to be of the order of half the number of points in the file or larger, there would be no need to resort to the exact formula beyond the first point in the file. Otherwise the method suggested earlier is retained.

The next part of the analysis consists of converting the force components just obtained into the coefficient forms C_L, C_M, C_D, C_ℓ as defined in the nomenclature and then the wind tunnel interference corrections are applied. The latter follow methods suggested by Garner et al (1966).

Additional computations are used to find the centre of pressure position X_{CP} according to the equation

$$X_{CP} = X_{CM} + C_a \frac{C_M}{C_L} \qquad 6.8$$

where X_{CM} is the reference centre of moments and C_a is the mean aerodynamic chord. When C_L becomes very small the values of X_{CP} are meaningless so a value for $C_{L_{min}}$ is numerically specified to avoid this. If C_M values orresponding to small values of C_L are fitted into a polynomial e.g.

$$C_M = a_o + a_1 C_L + a_2 C_L^2 \qquad 6.9$$

using least squares method, then (dC_M/dC_L) can be obtained immediately as $a_1 + 2a_2 C_L$ which can be substituted for C_M/C_L in equation 6.8.

In this case the division by small number is bypassed and a regular expression results. However, the calculated X_{CP} should be understood to represent the aerodynamic centre of the model having linear aerodynamic behaviour.

The aerodynamic coefficients are then tabulated against incidence and fed into the ICL graph plotter producing graphs of the format

$C_L - \alpha$ $\qquad$ $C_D - C_L$

$C_M - C_L$ $\qquad$ $C_D - C_L^2$

$\frac{C_D - C_{Do}}{C_L^2} - C_L$ $\qquad$ $X_{CP} - \alpha$

$\frac{X_{CP}}{C_R} - C_L$ $\qquad$ $C - \alpha$

This concludes the data reduction method.

The data handling calibration is achieved by recording known signals, e.g. square waves with a period of about 30 seconds, fig. 6.4, on all tape channels used just prior to collecting test run data. These calibration signals are reduced on the Myriad computer using similar settings of filters and ADC just prior to a test run data acquisition session. The d-c shift and gain factor are calculated for each channel using the interval averaging and checking the standard deviation parts to ensure freedom from any transients.

6.1.1 Test procedure and test format

The procedure followed in carrying out the incidence sweep tests can be summarised as follows:

a) Carry out incidence calibration and trim the optics amplifiers, if necessary, with power supply voltage to light sources set to the nominal.

b) Record laboratory temperature and pressure.

c) Record the calibration signals on various tracks of the magnetic tape.

d) Connect the tape recorder input leads to the current and position signals of interest and the output leads to the storage scope inputs.

e) Measure and record model intensity of magnetization.

f) Suspend the model and switch on the integrators in all degrees of freedom. Seal the tunnel circuit.

g) Check that the ramp function generator amplitude sweeps the model over the required incidence range.

h) Select the sweep time t_R and pause time t_P and make sure that the model is steady in suspension at a nominal starting incidence value approximately -1° to -2°.

i) Take a set of wind-off recordings by pressing the timing signal once and the ramp function generator once for every sweep cycle required.

j) Repeat h and i for the various sweep rates required.

k) Take the tunnel speed up to a steady value and maintain as constant a value as possible manually. Repeat h-j for same rates of sweep as in wind-off case. Record the manometer reading and flow temperature.

l) Bring the tunnel speed down to zero and record a wind-off case, or a set of cases similar to i-j if coils are not excessively overheated.

m) Switch off the integrators and remove the model from suspension.

n) Identify the acceptable test run cases on tapes.

6.2 Methods of dynamic stability derivatives data reduction

Unlike the previous data reduction method for steady aerodynamic characteristic measurements where dynamic effects on the signals were of secondary importance, in the present case the dynamic behaviour of the signals is of primary interest. The techniques of derivative measurement presented here consist of forcing the model in harmonic oscillations and measuring the dynamic relationships (i.e. relative amplitudes and phase difference) between signals representing the excitation (force) and response (displacement) of the model. The three techniques of dynamic measurement presented in chapter 3 reduce, at the data reduction and analysis stage, to one of determining the above relationship for a pair (or pairs) of signals relevant to the particular measurement, e.g. roll torque and roll displacement in case of roll damping measurement. This section presents the methods followed in collecting and reducing the data. A description of the detailed method of application of the covariance zero crossings for determining the dynamic relationship between two signals follows.

6.2.1 Oscillatory roll damping measurement - constant incidence

A block diagram of the data acquisition, reduction and analysis system is shown in fig. 6.5. Equipment used is much the same as those used for the steady data reduction method, (see sec. 6.1 and fig. 6.1). The additional instrument used is a low frequency oscillator. There are some differences in the number of channels utilised for recording and also differences in the kind of data reduction and analysis required and in the need for careful filtering of signals.

The roll position signal V_ϕ and partially filtered and d-c compensated roll current signal V_R are recorded on magnetic tape. D-c compensation of V_R is achieved by passing it through a unit gain differencing

op-amp and then subtracting a d-c signal. This is found to be more efficient than utilising heavy high pass filtering which would have resulted in significant changes in the phase angles. A reference signal from the oscillator and the timing reference signal are simultaneously recorded. The frequency of the oscillator is read on an electronic timer counter and the constant incidence setting on a DVM. Care is taken to separate the channels containing the data to be cross correlated in order to minimise the effect of recorder inter-channel cross talk. Signals are monitored on the screen of an oscilloscope in order to ensure that levels are large enough but within the dynamic range of the recorder (i.e. 1.0V rms). The wind-tunnel flow head is set at a constant value while a recording is being made.

At the computation stage, prior to digital analysis, the analogue signals to be cross-correlated are passed through a pair of dual phase matched filters with calibrated phase and gain characteristics. The analogue data is reproduced at a conveniently higher tape speed. A high pass mode of filtering using high quality filters can now be safely used to eliminate the remaining d-c offset of the signals before digitizing. In order to ensure a minimisation of the quantization error the signals are duly analogue amplified. The cut-off frequency of the filters is chosen to correspond to 1/16 Hz in signal real time. The low pass end of the filters, i.e. anti-aliasing frequency, and ADC sampling rate are appropriately chosen such that about 180 samples per cycle of test frequency are obtained. Signals are then digitized and acquired by the Myriad computer. Although about 20 cycles of oscillation are required for analysis, about 60 cycles are stored. This amounts to about 10 thousand samples per signal.

Owing to the dynamic characteristics of the data handling equipment (e.g. tape recorder and filter-cum-amplifiers) involved it is necessary to calibrate the system. This calibration is achieved by recording two identical pure sinusoids (of the same frequency as test signal) on the channels to be used for data recording. An op-amp buffer stage is needed because of the relatively high output impedance of the low frequency oscillators. At the data reduction stage these calibration signals are analysed in exactly the same manner as the main signals; amplitude ratios and any phase differences between the channels are calculated. Analysis of the calibration signals recorded at various stages during a full test session provides information on the variability of the data handling system.

A flow chart of the digital analysis carried on the two signals in order to obtain the ratio of their amplitudes and phase difference is shown in fig. 6.6. Digital signals corresponding to approximately 20 cycles of oscillation are first 'normalised' by extracting the mean values. The discrete covariance $C_{\phi R}$ of the signals V_{ϕ} and V_R is calculated over a lag range extending over about 0.6 of the period of recorded test frequency. The lag number corresponding to the first zero crossing τ_{z_1} and the precise number of lags per period N_C are determined. These values are used to predict the first approximation to the location of successive zero crossings. The covariance of V_{ϕ} and V_R is calculated over a range given by:

$$\tau_{z_1} + m\frac{N_C}{2} - p \leq \tau \leq \tau_{z_1} + m\frac{N_C}{2} + p$$

where p is a small integer, say 4, and m is the zero crossing number. The resulting covariance amplitudes are plotted against the lag values

in order to confirm that the zero crossing has actually occurred within the range of lags used and the value of τ_z is then obtained by interpolation. If the range of lags is biased to one side of the zero crossing a correction to τ_{z_1} may be introduced. Values of m and the correspinding τ_z are stored. m is changed to take values $-8 \leq m \leq -4$ and $4 \leq m \leq 8$ and the resulting set of 10 pairs of values of m and τ_z are punched on paper tape. Linear least squares fitting of m and τ_z produces a straight line slope $\frac{\omega}{\pi}$, where ω is the test frequency in rad/sec, and intersects the $m = -\frac{1}{2}$ line at a value of τ such that $\varepsilon = \omega\tau$ where ε is the phase lead of V_R over V_ϕ.

For determination of the amplitudes the covariance is calculated again at values of lag $\tau_{z_1} + (m+\frac{1}{2})N_c/2-p \leq \tau \leq \tau_{z_1} + (m+\frac{1}{2})N_c/2+p$. For each m the resulting set of points are used to determine the local extreme value (peak or trough). This can be repeated for the values of m used before, and the average modulus of these extrema is taken to represent the best estimate of the amplitude $\hat{C}_{\phi R}$. For determination of the amplitude of $C_{\phi\phi}$, the auto-covariance of the displacement signal V can be calculated as in the case of $C_{\phi R}$ but with $\tau_{z_1} = 0$ and $4 \leq m \leq 8$. The average of the resulting extrema yields the best estimate of the amplitude $\hat{C}_{\phi\phi}$. The ratio of $C_{\phi R}$ and $C_{\phi\phi}$ is given by

$$\frac{C_{\phi R}}{C_{\phi\phi}} = \frac{\hat{C}_{\phi R}}{\hat{C}_{\phi\phi}} e^{j\varepsilon}$$

where $j = \sqrt{-1}$ and ε is the phase difference. This ratio is in error because of the dynamic characteristics of the data handling system. In order to correct for this, the procedure outlined above is repeated using the calibration signals. The resulting ratio of covariance to auto-covariance of calibration signals corresponds to the amplification ratio of the two recording channels and the phase angle $\varepsilon_{cal.}$ corresponds to

the phase difference at the test frequency. If the results for the main signals are corrected, the result is

$$\left[\frac{C_{\phi R}}{C_{\phi\phi}}\right]_{cor.} = \left[\frac{\hat{C}_{\phi R}}{\hat{C}_{\phi\phi}}\right]_{sig.} \Big/ \left[\frac{\hat{C}_{\phi R}}{\hat{C}_{\phi\phi}}\right]_{cal.} e^{j(\varepsilon-\varepsilon_{cal.})}$$

The quadrature component of the expression above can be introduced into equation 3.90a and the damping term is obtained. When this is repeated for wind-off and the corresponding damping is subtracted from the wind-on, the difference gives the aerodynamic damping as follows:

$$\text{aerod. damping} = \left[\frac{\hat{C}_{\phi\phi}}{C_{\phi R}}\right]_{cal.} \left(\left\{ \left[\frac{\hat{C}_{\phi R}}{\hat{C}_{\phi\phi}}\right] \sin(\varepsilon-\varepsilon_{cal.}) \right\}_{w.on} - \left\{ \left[\frac{\hat{C}_{\phi R}}{\hat{C}_{\phi\phi}}\right] \sin(\varepsilon-\varepsilon_{cal.}) \right\}_{w.off} \right)$$

$$= \omega\, C_{aero}$$

The nondimensional roll oscillatory derivative ℓ_p can be obtained readily from this equation using the flow and model geometry parameters, ρ (air density), U (flow velocity), S (wing area) and semispan s as given by equation 3.92.

The data reduction method described above is then repeated for other incidences α, and the results of ℓ_p are graph plotted against α.

Due to inherent variability in the analysis as a result of noise in the signals, a repetition of the analysis for different parts of the record can be taken as a check on the degree of precision of the data reduction method.

Main points in test procedure

a. Check that the model roll displacement calibration is free from incidence displacement interference over the range of incidence and roll oscillation amplitude.

b. Check that in the wind-on state the model is properly aligned with the free stream, so that at zero roll angle the fin does not generate any significant aerodynamic side force or yawing moment over the range of incidence of interest.

c. A check is made that the current signal has a sufficiently large dynamic range in both wind-on and wind-off states. Various settings of d-c compensation are determined.

d. Calibration signals are recorded on tape for about two minutes.

e. Model roll displacement and balance roll current signals, a reference version of the oscillation signal and the timing pulse signal are recorded for the wind-off case. Record lengths corresponding to about 60 cycles of oscillation are taken.

f. Set tunnel flow at constant speed and record speed head, air temperature and ambient pressure. Check that model roll oscillation is accompanied by a suitable roll current level at the required incidence. Record about 60 cycles of oscillations on tape and record down the incidence setting.

g. Repeat e) and f) for the set of incidence values of interest then record another set of calibration signals.

h. Data on tape is reproduced on an oscilloscope and edited if necessary.

i. The digital data reduction method described earlier in this section is then followed.

6.2.2 Oscillatory roll damping measurement - ramped incidence

In this case the model incidence is driven by a slow ramp function while undergoing forced roll oscillation. The incidence displacement is generated by the ramp function generator which was used in the steady aerodynamic characteristic measurement technique (see ch. 5). The

longest ramp time available is 220 sec. This is used to drive the model over a range of incidence of about 6-8 degrees.

The data collection method is only slightly different from the case of constant incidence, fig. 6.5. The number of continuous measurements is increased by one, the incidence signal. A suitable setting of the d-c compensator on the roll current signal is selected. Several wind-on runs are necessary before signal recording in order to confirm the absence of any significant signal distortion as a result of limited tape recorded dynamic range. Signals are then recorded for the required wind-on test runs at various ramp rates and incidence range.

Data digitization and digital analysis required some minor modifications owing to the nonstationary nature of the signals. Acquisition is taken in two steps. The first involves the speed up of the V_ϕ and V_R signals. The second step involves the acquisition of incidence and reference signals. In the first step the filters are set to high-pass followed in series by a low-pass in order to reduce the nonstationary effect. The high pass setting corresponded to a cut-off frequency of 1/16 Hz in signal real time. The low pass setting corresponded to a frequency permitting non aliased digitization of the signals into approximately 150 samples per cycle of oscillation.

The incidence signal is piecemeal averaged with an averaging interval corresponding to a record length of about 20 periods of roll oscillation and an overlap of 10 periods. The covariance zero crossing calculation between V_ϕ and V_R over lengths of the digitized record corresponding to approximately 20 periods of oscillation is carried out as in the previous section. An overlap of about 10 periods provides a means of increasing the resolution of damping measured. In addition, the covariance is carried out with respect to the reference signal in

order to check the results obtained at several points within the incidence range. In this case the analysis time per point is approximately twice that of the direct covariance. The procedure is applied to the wind-on and wind-off cases with the same incidence at record mid-range. Corrections for dynamic interference of the recording, filtering and digitization on the signals are obtained by application of the covariance zero crossing method to a pair of calibration signals. The difference between corrected quadrature components of current-displacement covariance in wind-on and wind-off states at the same incidence yields the aerodynamic damping. The test procedure is the same as described in the previous section.

6.2.3 Pitch and heave oscillatory derivative measurement

Data collection and reduction method for this type of testing is basically similar to that in fig. 6.5, but there are small differences resulting from the number of measurements to be made. There are now more than two signals to be analysed dynamically, namely pitch displacement, heave displacement, force and moment current signals. Six signals are recorded simultaneously on the tape. Four correspond to the main signals above; additionally, a reference oscillation signal and the timing pulse are recorded. Calibration signals of pure sinusoid form at the test frequencies are recorded on the four main channels in order to correct as before for the dynamic properties of the data handling system. Precautions about signal amplitudes at the recording stage are similar to those previously taken. At the data digitization stage there are two options available, either to

i. carry out the data acquisition of the four main signals simultaneously without filtering via a multiplexer (corrections for the phase shift due to multiplexing can be applied during the analysis), or

ii. carry out the data acquisition of a pair of signals at a time, meaning that one of the signals will have to be used each time. In this case high quality phase matched filters can be used and the phase relationships between all of the simultaneously acquired signals are preserved.

It has been found more reliable to follow the second option in view of its practical simplicity. The number of rounds of acquisition in the general case of simultaneous pitch and heave displacements is six for the two forcing conditions. The use of two test frequencies made a total of 12 rounds. When one of the displacements is maintained zero at every forcing condition, the number of acquisition rounds reduces to 8. Signal amplification and low pass filters are set constant throughout. About 60 periods of oscillation (150 samples per period) are digitized and disc stored.

The covariance zero crossing method (section 6.2.1), was applied to each pair of simultaneously digitized signals corresponding to a certain model position, forcing condition and test frequency. Records approximately 20 periods long are first normalised and the ratio of the covariance of current and displacement signals to the autocovariance of the displacement signal is obtained. Repeating for the calibration signals on the same pair of channels provides correction factors for the ratio. The corrected covariance ratios of the two currents and repetitions for the second forcing case provides the elements of the matrices $[H]$ and $[G]$ and hence the matrix product $[G]\ [H]^{-1}$ is formed (see equations 3.139, 3.140, 3.145). The whole process is repeated for the other test frequency. Using the model geometric, calibration and flow data, the aerodynamic characteristics can be obtained from equation 3.141 and 3.144 in non-dimensional form as follows

$$(\Omega_2^2 - \Omega_1^2)\begin{bmatrix} \hat{z}_{\dot{w}} & x'_{GP}\,\hat{z}_{\dot{w}} \\ \hat{m}_{\dot{w}} & z'_{GP}\,\hat{m}_{\dot{w}} \end{bmatrix} - j(\Omega_2-\Omega_1)\begin{bmatrix} \hat{z}_w & \hat{z}_q+\hat{z}_{\dot{w}}+x'_{GP}\,\hat{z}_w \\ \hat{m}_w & \hat{m}_q+\hat{m}_{\dot{w}}+x'_{GP}\,\hat{m}_w \end{bmatrix}$$

$$= \frac{C_a}{\rho U^2 S}\begin{bmatrix} 1 & 0 \\ x'_{GM} & 1 \end{bmatrix}[B]\left([G][H]_{\omega_2}^{-1} - [G][H]_{\omega}^{-1}\right)\begin{bmatrix} \frac{\partial z}{\partial V_z} & 0 \\ 0 & \frac{\partial \alpha}{\partial V_\alpha} \end{bmatrix}$$

where symbols have the same meaning as in chapter 3. It follows that the oscillatory derivatives are obtained by equating the real and imaginary parts of the equation.

Main points in the test procedure

a. Check that model oscillations at the required test frequencies in pitch and heave are not significantly coupled with other modes of motion in wind-off and wind-on conditions.

b. Repeat (a) for all required mean model positions.

c. Select signal amplitude to comply with tape recording requirements. If the mean model position corresponds to large d-c signals, then some form of d-c compensation or subtraction must be employed.

d. Record the calibration signals on the main signal channels.

e. Set the tunnel dynamic head at a constant value.

f. Apply a pure pitch oscillation to the model at one frequency and record pitch displacement, force and moment current signals, a reference signal and the timing pulse signal. Ensure that the model heave oscillation is negligible compared with pitch. Record about 150 cycles of oscillations.

g. Repeat test with a pure heave oscillation at same frequency as (f).

h. Repeat (f) and (g) at another frequency but at the same mean model attitude.

i. Repeat (f) - (h) for other model mean positions.

j. Again record the calibration signals.

k. Apply the data reduction method described earlier.

7. RESULTS AND DISCUSSIONS

Following the conception and development of the test techniques presented in the previous chapters, several winged models have been aerodynamically tested. These models have the common feature of a slender wing configuration and differ only slightly from the main model (i.e. the AGARD-G winged model) presented in chapter 5. The models include:

i) a cropped-delta wing on a 24.0 mm (0.94 in.) diameter fuselage,

ii) a cropped-delta wing on a 16.0 mm (0.63 in.) diameter fuselage,

iii) a pure delta wing supplied by NASA, Langley Field.*

All models fall within the same range of wing aspect ratio and total planform area. The experience gained in carrying out tests on these models will be discussed in the following section.

The techniques of testing presented in the previous chapters featured model movement while collecting the relevant measurements. Such motions affect the model stability in suspension as well as the analysis parameters. These aspects, in addition to confirmatory checks on the overall system, are discussed in section 7.2.

Section 7.3 presents the quasi-steady aerodynamic test results obtained using the incidence ramp method and the main model (i.e. the AGARD-G winged model). Detailed discussion of the various parameters involved is included, together with the effect of incidence ramp rate on the results is given.

Dynamic measurements of the oscillatory roll damping derivative are presented in section 7.4 as well as comparisons with published data. Difficulties associated with combined pitch and heave oscillatory testing are discussed in the same section.

---

* From now on this model will be referred to as the RAK model, since it has been supplied by R.A. Kilgore.

Overall error bounds and accuracy assessment of the results due to uncertainty and fluctuations in airflow characteristics, technique parameters and digital data reduction are discussed in section 7.5.

7.1 Preliminary testing results

7.1.1 The first application results

It has already been mentioned that, prior to undertaking this investigation, the data reduction method was completely manual. This involved model magnetic suspension in the MSBS and direct reading of the DVM voltage signals that correspond to the various coil currents and model positions. The model is held at a fixed incidence in wind-on then wind-off conditions for as long a time as is sufficient to achieve a stationary set of readings. Very often some kind of visual averaging, or smoothing, is found essential. This averaging, applied to a measurement involving several simultaneous readings is reasonably good only while the balance and measurement system comprise a reasonably statistically controlled process. The MSBS has been shown before to contain several sources of weaknesses that reduce its statistical controllability. Figures 7.1a and 7.1b illustrate the results of three sets of lift force and drag force measurements on the 70^{o} cropped delta winged model. The three sets are nominally exact repetitions and data reduction is manual. The figures show random scatter as well as shifts due to systematic effects. Careful and detailed investigation of the system indicated that among the most probable causes, model position drift and operational amplifier output intermittency and noise were prominent. In order to cure the system expensive hardware modifications would be necessary. Such modifications may add to the complexity of the whole system which may reduce the overall system reliability. Short duration testing emerged

as an alternative solution that may result in measurements relatively insensitive to such weaknesses. It proved then timely since a development of a digitized data reduction system was required.

Contrived model motion during testing, with the motion both stepwise (i.e. staircase) and continuous (i.e. ramp) were roughly evaluated. The stepwise technique was rejected for ultimate adoption due to uncertainty about the effects of the many velocity discontinuities. On the other hand it was regarded as a means of confirming the continuous motion data at key points in a ramp since a slow step process can be regarded as a quasi-steady point-by-point.

Sets of measurements of static characteristics for a slender cropped delta wing model of aspect ratio 1.18 (model (ii)) and for first time on the AGARD-G wing model, were taken by the old method of point-by-point measurement and with an incidence ramp at a rate approximately equal to 0.1 deg/sec. over an 8 degrees range. These incidence ramp results were tape recorded and later-on filtered, digitized and piecemeal averaged over 0.1 deg. intervals. The reduced results were then compared with the results from point-by-point (manual) measurements. Typical results were reported at a conference [Abdel-Kawi et al, (1971)]. Fig. 7.2 shows a typical case with wings having transition strips near the leading edges. The circles correspond to point-by-point results while the continuous line corresponds to the incidence ramp case as obtained from the computer graph plotter. There is evidently very good agreement between the two methods. The continuous line data in this figure corresponds to two incidence ramps corresponding to a positive and a negative ramp rate of the same magnitude. The absence of any significant hysteresis is a sufficient indication of the quasi-static nature of data obtained at this ramp rate. It is of interest to compare the testing time required in the two methods. The time required for a

set of 15-20 points in the point-by-point case is about 35-45 minutes, while the time required for the whole length of incidence ramp excursion is about 1.5 minutes. The testing time for each point of the former method is therefore comparable with the time required for a whole ramp excursion. Fig. 7.3 shows the lift force coefficient for the AGARD-G model where the wings are clean i.e. without transition strips. Fine detail is clearly evident on this figure such as the plateau for α between 1.7^{o} and 1.9^{o}. This is regarded as evidence that the MSBS is capable of high resolution (of lift and angle of attack in this case), but also that the steady ramp method can highlight detail, in particular small discontinuities, which might not have been detected in conventional testing using discrete changes of angle of attack. Alternatively in conventional testing the small discontinuity might appear in a few points but be interpreted as noise and therefore ignored. The fact that the flow Reynolds number is ganerally low, $3.x\ 10^{5}$ - $4.x\ 10^{5}$ based on the wing mean aerodynamic chord, renders the prevailing laminar boundary layer over the front parts of the model very sensitive to model geometric details and surface condition. Therefore such aerodynamic results may only have limited practical importance.

The data reduction involved the digitization of the analogue (tape recorded) signals, application of simple calibration relations and graph plotting. It was found necessary to retain a simple data reduction method at this stage. One reason for this was the limited programming facility available to users of the Myriad computer.

Dynamic derivative measurements were confined to the measurement of the roll damping derivative. The in-plane and quadrature components of the model displacement and rolling moment current signals were measured with respect to a reference signal of the same frequency using a resolved component indicator. Owing to the low frequency of the signal

and the low signal to noise ratio it was difficult to get a reasonably repeatable set of measurements. Heavy analogue filtering of the dynamic signals using high quality filters improved the measurements but required a long settling time and hence testing time. A first attempt towards digital analysis involved the computation of the spectra of the two signals. The dynamic transfer function between the moment and displacement signals was obtained from the quotient of their cross-spectrum and displacement spectrum. The method was rejected owing to the need for a long record length to obtain reasonable resolution and hence accurate phase information at the excitation frequency. The method might have worked if the spectra were rather flat over a range of frequencies.

Correlation analysis was then seen as a promising alternative. The quadrature component required is directly obtained from the zero shift cross covariance of the two signals involved. This component is directly related to the damping of the oscillating system. When signals are reasonably clean, i.e. of high signal to noise ratios, and records are reasonably long, the results obtained from this method compare favourably with those obtained following the manual method, i.e. using a resolved component indicator. For signals with moderate to low signal to noise ratios the agreement is less favourable since both methods are prone to large errors in such circumstances. Therefore it was found necessary to look for improvements in the covariance estimates by investigating the nonzero shift covariances. This was encouraged and motivated by the property that in a pure noise signal values covary less effectively if they are sufficiently widely separated in time.

7.1.2 RAK delta wing model results

The results of the preliminary investigation together with a current interest in slender delta wings suggested the application of the technique to the measurement of aerodynamic characteristics on delta wing models and to compare the results with measurements obtained elsewhere, [Vlajinac et al (1971)] , [Davenport and Huffman (1971)] and [Stephens et al (1972)]. A sketch of the RAK model is shown in fig. 7.4. Wings of basically flat plate cross section are shown, but another model where the wing cross section is a circular arc on the same fuselage, has also been tested.

Steady aerodynamic data were obtained from incidence ramp testing. In order to select a suitable ramp rate, lift and drag measurements were examined with the ramp rates varying from 0.16 deg/sec. to 0.045 deg./sec. in wind-on at a flow speed ranging from 22.4 to 40 m/s. The conclusion arrived at was that a ramp rate of 0.08 deg./sec. or less was sufficient to ensure quasi-static aerodynamic force measurements. This was then adopted for the rest of the test program on these models. Sets of measurements were obtained for the following conditions [Diab (1972)]:

i) wing surfaces clean and with transition strips,

ii) different flow dynamic head values and hence R_N,

iii) two wing cross sections, and

iv) varying digital piecemeal averaging interval during the data reduction.

The tape recorded test data were analogue filtered, digitized, reduced digitally and the results plotted. Although the digital analysis was kept reasonably simple the effects of varying the analogue filter cut-off frequency, sampling rate and piecemeal averaging period were investigated in detail. It was found convenient and reasonable to use a sampling rate equivalent to 62.5 samples per second and to average the data every second of real time. The one second value was found adequate

to show the required aerodynamic details. This corresponds to data incidence steps of 0.08 deg. For a range of incidence ramp from -0.5^{o} to $+6.0^{o}$ a record results in a total number of digitised points of 9.5 K. The total analysis time from the start of digitization until the final graphs is about 25 minutes per case. A typical set of results is shown in figures 7.5 to 7.10. It is important to note that continuous curves shown in the graphs do not imply infinite resolution. This representation has merely been chosen to indicate that results are obtained using a continuously varying incidence. Since the resolution is high (i.e. $\pm$ 0.04 deg.) it therefore seems justifiable to join the successive points by straight lines. The details of the force variations taking place during incidence intervals of the order of the resolution above suffer the largest inaccuracies. Fig. 7.5 shows a complete set of results for a model with clean wings while fig. 7.6 shows a similar set with transition strips on the same wings. A comparison of the results for the flat plate wings with those of Vlajinac et al (1971) and Davenport and Huffman (1971) shows the following:

i) The lift coefficient is higher than given by Vlajinac and in particular the lift coefficients at incidence values of 2^{o} and 4^{o} in the present results are 0.052 and 0.123 respectively compared to 0.0494 and 0.1069 respectively in Vlajinac et al (1971). Consequently the lift curve slope of the present results at zero incidence appears to be closer to the potential flow prediction [Polhamus (1971)].

ii) The present data includes a change in sign of the lift coefficient, hence the accurate location of the zero-lift incidence is possible. The zero lift incidence appears to agree with results of Davenport and Huffman (1971).

iii) Incidence resolution of the present data is ± 0.04° as compared to the results of Vlajinac et al (1971) and Davenport and Huffman(1971)of2°, hence the new technique is more powerful in showing small details on the lift curve.

Comparison of the results of the clean wings with those having transition strips (≠ 35 grit size) shows distinctly the existence of an aerodynamic hysteresis near 0.5 to 1.0 deg. of incidence, fig. 7.7. A plausible physical reason for the occurrence of such hysteresis might be the complex wing-body interaction in a prevailing laminar boundary layer. A similar phenomenon has been observed and reported in conjunction with earlier measurements in the same facility [Judd and Goodyer (1969)] and elsewhere [Kirby and Hepworth (1971)] . An important consequence of the addition or removal of the transition strip is a shift in the whole lift characteristic relative to the incidence scale. In particular the zero lift incidence appears to shift by about +½° as transition strips of 3. mm width are fixed to the model at about 20 mm behind the sharp leading edges of the clean wing. It is hard to determine the causes of this phenomenon, but since the Reynolds number is very low, ∿ 3. x 10^5, it is suspected that it may be a viscous effect. When incidences are referred to the respective zero-lift values then for same incidence increment but above 1° the lift coefficient of the clean wing is consistently 0.025 higher than that of the other wing. This effect may be attributed to a formation of some additional lift-producing vortices following a separation at a sharp corner when incidence increases through 1°. The initiation of these vortices may be triggered-off by viscous effects, hence the onset of a hysteresis loop as discussed above, but their growth is of a potential flow nature. The drag coefficient behaviour is more regular and has the expected form.

C_D is consistently higher for the wings with transition strips than for the clean wings case. The effect of surface condition on the aerodynamic pitching moment is the elimination of an apparent plateau at the incidence range of 0.5 - 1.0 deg. following the addition of the transition strips. Viscous effects of the flow on the aerodynamic characteristics C_L and C_D is illustrated in fig. 7.8. Although the Reynolds number is low the variation of the lift coefficient with Reynolds number, particularly near 1^o incidence and also at high incidence can be clearly seen. It must be emphasised that although the ramp rate is constant the effective or nondimensionalised ramp rate (i.e. $\dot{\alpha}C/U$) increases as U decreases (or R_N decreases) therefore rendering different dynamic effects. The hysteresis loop appears to move slowly towards higher incidences as R_N decreases. Viscous effects are however more pronounced on the drag coefficient. The drag coefficient reduces consistently as the Reynolds number increases. Fig. 7.9 shows the effect of wing cross section on the lift and drag coefficients where both wings, one the flat plate and the other the circular arc cross section, have transition strips. The transition strips are reproduced as near as possible on both. Finally fig. 7.10 illustrates the repeatability of the measurements. It contains the data on the RAK model from 4 different runs superimposed. The repeatability is clearly very good for C_L-α and C_D-C_L characteristics.

In order to carry out oscillatory roll derivative measurements, detailed examination of the covariance estimates was required. In particular the effect of the analog filter cut-off frequency, sampling rate and record length were investigated over the range of test frequencies of interest (i.e. 1. to 3.0 Hz.). Sampling rate dictates the maximum cut-off frequency that the analog filter can be set to. The cut-off frequency of the analog filter represents the bandwidth of

the noise corrupting the signal. A cut-off frequency of 40 Hz (real time) or 20 to 30 times test frequency whichever is lower was employed. This cut-off is sufficiently below the mains frequency which in most cases was detected in the signals. Maximum sampling rate is then decided by the required covariance lag resolution and computation time that can be tolerated. A value of 125 samples/sec. is found reasonable for the 1.0 Hz testing frequency. In order to assess the effect of record length on the covariance estimate several oscillatory roll test recordings were analysed with varying analysis record length. A typical result for RAK flat plate model (for $\alpha = 0$) is shown in fig. 7.11. This figure illustrates the autocovariance of the displacement and current signals for wind-on and wind-off cases. Both signals are normalised i.e. bias-free and divided by their respective standard deviations. It is clear that at least about 60 cycles of oscillation would be required before the covariance estimates achieve their asymptotic values within 1/2%. For the case illustrated this would amount to an angular error of about $\frac{1}{4}$ to $\frac{1}{2}$ deg. of phase difference between the wind-on and wind-off case. It is significant however to notice that the difference between the two covariance graphs for wind-on and wind-off becomes more or less constant for record lengths above 20-30 cycles. This evidence suggested the choise of 20 cycles for the record length to be used in calculating covariances and in the application of the zero crossing method. Covariance estimates for lag values further away from system lag yet much shorter than record length are calculated. The zero crossing of these covariances allows the utilization of more than a single value of covariance to estimate the phase angle. Details of the method are standardized and have been given in sections 3.2 and 6.2. Results of the application of this method to the measurement of oscillatory roll damping having roll displacement amplitudes about 2 deg. at a selection of values of incidence are shown in fig. 7.12. The nondimen-

sional oscillatory roll derivative ℓ_p for the RAK Model with flat plate and circular arc cross section wings is plotted and compared with published results for similar geometries [Boyden (1970)]. Agreement is very good for zero incidence but is progressively poorer as incidence changes from zero. There are several reasons which may account for the differences. First, it is possible that the differences are caused by differences in configurations, e.g. the RAK model has a fin and fuselage while Boyden's model has none but must have had means to support the model in the testing section, most probably a sting. The present measurements are however free from support interference. Secondly, it is possible that the discrepancy may result from differences in axis systems since the present measurements are obtained with respect to wind axes while Boyden's are shown with respect to body axes. A correction of the present results requires a knowledge of the term $\ell_v' \sin \alpha$ where ℓ_v' is the roll derivative due to side slip. The third possible cause of error may be the data reduction technique. At an incidence of 4^o, ℓ_p for the flat plate wing appears to depart from the trend indicated by the rest of the values which were in closer agreement with Boyden's results. Repetition of the test three times consistently reproduced the same value with a scatter of about 3-4%. It is not clear what might be the cause of this apparent error, although one may conjecture that the noise on the signals must have been very heavy at this incidence value and so much more careful choice of the analysis record should have been made. The other possibility is a systematic error in the testing technique at this value. A logical remedy for this is the use of a testing technique where the incidence is continuously ramped in incidence while the model is forced into a roll oscillation.

The general accuracy of the results discussed in this section is

limited by the strict adherence to simple calibration and data reduction methods. The pitching moment coefficient is the least accurate of the steady aerodynamic characteristics discussed above [Diab (1972)]. Wind tunnel wall interference has also been neglected. Tunnel wall interference corrections are not significant except possibly for drag coefficient and roll damping derivative results. Since a magnetic suspension system is used the results are clearly free from support aerodynamic interference.

7.2 Confirmation of overall system dynamic characteristics

The systematic investigation of the techniques of testing forming the subject of this investigation required the detailed identification and when possible the measurement of certain system properties. These include details about the characteristics and behaviour of the MSBS in wind-off and wind-on states. Most important among these characteristics are:

i) the stability of the model in suspension in the wind-on condition, particularly when the model is moving,

ii) severity of the coupling or interaction among various components (or degrees of freedom) of the balance due to the nature of the position sensing system and the field coil arrangement,

iii) the change in the dynamic behaviour of the balance and model combination due to the action of aerodynamic forces.

(i) and (iii) above can be qualitatively assessed and may be quantitatively measured, through the observation of the change in the natural frequency and effective damping of the various degrees of freedom. Further due to the lack of a fail-safe mechanism in the system, the appearance of a spurious transient signal often caused a loss of model control

followed by free flight ending with some form of model damage. In addition to geometric distortions resulting from this damage, the magnetic moment of the model changes. This necessitated the adoption of a careful sequence of repairs and checks in order to reduce the effect on repeatability. A comprehensive test of performance of the overall system with the wind on was carried out at regular intervals prior to force calibration and data recording.

A frequency response measurement of the complete open loop system (excluding the model) is very useful in assessing the stability of the MSBS but is time consuming and impractical for routine checks. Furthermore it is difficult to relate wind-off to wind-on results. Alternatively the step response is a simple test to carry out and could be very informative if the imperfections in the step signal, which are unavoidable in practice, can be tolerated. This was therefore adopted as the standard quick dynamic test. Typical oscillograms of responses of various force components due to a step input in the feedback loop of the MSBS are shown in fig. 7.13 - 7.15 in wind-on and wind-off cases. The top traces in fig. 7.13 and 7.14 are the model incidence signals while the other three traces correspond to lift force, pitching moment and drag force signals. The excitation signal was injected into the control loop at the same point as the ramp signal would be injected. Therefore the dynamic responses obtained were relevant to the ramp testing technique. The response times due to step excitation were found to vary a great deal depending on the mean incidence, the flow and the sense of application of the step. Additional information that can be extracted from these oscillograms are the natural frequencies and effective damping of various modes of motion.

In wind-off conditions fig. 7.13 (a) and (c) and fig. 7.14 (a) and (c) show the effect of the starting incidence value on the dynamic

responses of the incidence signal V_α, lift force signal V_F, pitching moment signal V_M and drag force signal V_D. Settling time for V_α seems to reduce regularly from about 200 ms at zero incidence to about 100 ms at an incidence of 4.1 degrees. The settling time of V_F follows a similar pattern over the same range of incidence and amounts to about 1 to 2 times that of V_α. The wind-off natural frequency of the balance lift force signal can be estimated from such traces and is about 10 to 20 Hz over the range of incidence considered. The pitching moment signal response, however, is more dependent on incidence. V_M response seems to consist of two parts, an exponential decay on which is superimposed a heavily damped sinusoid part. The latter tends to behave like an impulse response which gets more definite with α increasing as evidenced by fig. 7.14 (c) and (d). The natural frequency of this component is close to that of the V_F signal. The response time however is estimated to be 2-3 times that of V_α. Similar to the behaviour of V_M, the drag force signal is strongly dependent on incidence. From fig. 7.14 (a) and (c) and 7.14 (a) and (c) the effective damping appears to reduce as incidence increases and possibly reaches a minimum at mid α range. As evidenced by static force calibration, the drag current required to hold the model at the same position varies nonlinearly with incidence for incidences less than about 3½ degrees but remains constant above that incidence. Following a change in incidence the amount of change in drag current depends on the initial and final incidences. At the high incidence (α = 4.1 deg.) it can be seen, fig. 7.14 (c), that a step does not cause any detectable transient in the drag current. It is therefore only logical to deduce that the dynamic response of the drag current signal is strongly affected by the nonlinearities of the V_D axial displacement characteristic. The wind-off natural frequency of this loop is about 5-10 Hz while the response time can be estimated to vary between 2-5 times that of V_α. Fig. 7.13(b) illustrates the consequences of

applying a negative step. Comparison of this figure with 7.13(a) shows the effect of nonlinearity (of the static characteristics) on both the natural frequency and damping of various force component indications. In particular the drag current appears to suffer the largest changes.

The effect of aerodynamic forces on the performance of the MSBS can be extracted from the oscillograms of fig. 7.13(d), 7.14(b) and (d) at progressively increasing incidence setting. The conclusions about natural frequencies and settling time remain substantially similar to the wind-off case. The effective damping and the amplitudes of the transients are, however, different.

Eddy current effects in the behaviour described above is difficult to assess quantitatively but may only be qualitatively estimated. Eddy currents affect the step response in two major ways, namely in contributing to the effective damping and in promoting dynamic coupling among various balance components. The severity of both effects depends on the steady state rise in various currents and associated gradients. The major conclusions however remain unchanged.

The phenomena described above are quite tolerable for a point-by-point measurement. For the ramp testing investigation however it is necessary to cut down on the settling times. Careful 'optimization' of the phase leads of various control loops improved the lift force and pitching moment step responses while it improved the drag signal only marginally. The settling time for the former components is brought to the same order as V_α while that of the latter is reduced to about 3 times that of V_α, fig. 7.15. The dynamic response levels were checked and maintained during the test program since this policy appeared to render the MSBS rather less susceptible to interferences.

Dynamic coupling among various components of the balance was observed in a similar manner to that of the step transient observation. In this case the suspension currents and roll current response to the step excitation in the incidence control loop were monitored. The suspension currents did not indicate noticeable dynamic transients while the roll current appears to be much more sensitive. Since model position interaction has been ruled out as a possible cause, interaction must be attributed to the electromagnets mutual inductances and the model eddy currents. This phenomenon had not been as obvious when testing earlier models. One reason suggested for the present strength of interaction is the low roll suspension stiffness caused by the spatial distribution and low magnetic moment of the roll control magnets mounted in the model wings as compared with other models. Monitoring the roll current and/or roll position during ramp testing is important since the roll control loop has a low natural frequency and is generally lightly damped.

As a general conclusion to this section, it can be stated that a correction to allow for the transients is difficult to implement with a great deal of certainty. Effective damping ratio and natural frequency of oscillation of various balance force components estimated from step response can be used to realign various force components in the ramp response measurements.

7.3 Aerodynamic data - steady characteristics

The knowledge gained from the preliminary results discussed in the previous sections were put to use in the development of the incidence ramp technique presented in section 3.1. The systematic study of this technique necessitated planning a comprehensive set of calibrations and measurements. The purposes are to cover reasonably wide ranges of the

incidence ramp rate parameter and various types of aerodynamic characteristics, and to ensure reasonable accuracy of the results.

Certain limitations were set by the MSBS, model and flow on the ranges of variables involved. For example the incidence range is limited to about 9^{o}, -1.5 to +7.5 deg. Incidence ramp rate is limited by aerodynamic considerations. The lowest value of ramp rate for transient-corrupted aerodynamic measurement can be estimated from equation 3.15. In that equation assuming $\nu = 0.05$, $a = 0.5$ and an averaging interval of 0.2 deg. of incidence (i.e. corresponding to $\Delta L/\bar{L}_{\alpha} = 0.2$ deg) then

$$\dot{\alpha}_{max} = \frac{1.8\sqrt{h}}{T_{RS}}$$

where T_{RS} is the nondimensional flow response time (chap. 3) and h is the flow dynamic head in cm of methylated spirit. Adopting $T_{RS} = 2$ (reasons will be discussed later) and h = 16 cm gives an estimate of $\dot{\alpha}_{max} = 3.6$ deg/sec. Alternatively, judging by the balance dynamic behaviour discussed in the previous section a maximum incidence ramp rate of $\sim$ 15 deg/sec. appears to be feasible, at least for lift force measurement. Therefore, for the purpose of this investigation an $\dot{\alpha}_{max}$ = 20 deg/sec. is chosen as the largest value for the testing program. The minimum value of ramp rate is taken arbitrarily for reasonable test duration to be about 0.05 deg/sec. which is slow enough to ensure the accurate recovery of the static aerodynamic effects. Limitation on the balance natural frequency and damping can be theoretically estimated from equations 3.24 or 3.26. By making use of equation 3.15 the balance natural frequency ω_n and damping ratio ζ in a single component are given by

$$\omega_n \zeta \geq 100\ \dot{\alpha}_{max} \qquad \text{rad/sec.}$$

For a typical damping ratio of 0.1 and the value of $\dot{\alpha}_{max}$ estimated from equation 3.15, the balance would need to have a natural frequency of 570 Hz. This appears to be an overestimation of the requirement and is certainly not reflected by the step responses of fig. 7.13, 14, 15 discussed in sec. 7.2. A limitation is imposed similarly on the flow dynamic head. The maximum value is limited by the available electro-magnet coil current (balance force capacity) when the model is subject to the worst combination of aerodynamic forces. This consideration allows a maximum dynamic pressure corresponding to 20 cm. methylated spirits (1560 N/m²). The lowest value causes the largest errors in the measurements, ref. sec. 7.5, and results in an effective increase in the nondimensional ramp rate i.e. $\dot{\alpha}c/U$.

Following is a list of the conditions and the range of numerical values of variables adopted in the testing program:

- Incidence ramp rate

  0.05, 0.125, 0.25, 0.5, 1.0, 2.5, 5.0, 10.0, 20.0 deg/sec.

- Flow dynamic head range

  5.0 to 20. cm methylated spirits.

- Wing surface condition

  Clean and with ≠ 35 grit transition strips.

Additional confirmatory tests were carried out for the purposes of checking the freedom of measured aerodynamic data from yaw, vertical heave and roll effects resulting either from position interaction, magnetic field coupling or aerodynamic cross coupling. Several repeats of a wind-on test were carried out before recording in order to ensure a reasonable level of confidence in the test data. In particular, the problem of one person maintaining the tunnel head constant and observing the model visually, monitoring its position and the force signals and

taking records was responsible for a high rejection ratio of the records. Table 7.1 shows a list of the recorded test runs (on magnetic tape). For practical reasons only a selection of the cases were analysed, with the result that only 20 cases (two for each ramp rate value) for each wing surface condition were chosen for digitization and further data reduction.

Since the incidence ramp is variable among the set of records chosen, the settings of the analogue low pass 'antialiasing' filters and the sampling rates have to be selected and adjusted. The criterion followed here is to fix the incidence averaging interval to about 0.2 deg. Equation 3.43 provides a means of estimation of the filter cut-off frequency. Assuming the contribution of the highest harmonic component to be attenuated to 1/10 of its amplitude (i.e. $\eta_H = 0.1$) then the cut-off frequency of the filter is

$$f_{lp} = 16\ \dot{\alpha} \qquad \text{Hz}$$

where $\dot{\alpha}$ is in deg/sec. Alternatively, for a sufficient statistical accuracy of the averages, the number of degrees of freedom (i.e. maximum frequency x interval time length) of the averaging process must have a reasonable value, say ≥ 5. For the incidence averaging interval assumed earlier, the corresponding filter cut-off frequency is $\sim 25\ \dot{\alpha}$ Hz. A reconciliation of these two figures may be achieved by observing that they combine into a concise form relating η_H and the number of degrees of freedom of the averaging process i.e. no. of degrees of freedom $\times\ \eta_H = 1/\pi$. The cut-off frequency is taken to be $25\ \dot{\alpha}$ Hz for $\dot{\alpha} \geq 1$ and a constant at 25 Hz for $\dot{\alpha} < 1$. The corresponding sampling rate is taken to be 2.5 times this value. The digitized number of samples per record,

the record comprising positive and negative ramp excursions plus three pauses as shown in fig. 3.1 and 4.13, amounted to about 12000 samples for the slowest ramp rate up to about 19000 samples for the highest. For slow ramp rates, pairs of consecutive records are digitized in a single acquisition period while for high ramp rates each individual record is digitized separately. Piecemeal averaging of the two records is carried out and results plotted for inspection and editing. The limitation of the incidence resolution of the averaged data is provided by equation 3.38. A resolution of between 0.06 and 0.1 deg. is possible and corresponds to an overlap factor between successive averaging intervals of 0.7 to 0.5 respectively. The degree of interaction with the computer data reduction, exemplified by the editing process, is rather lengthy owing to the absence of an online display, or soft graphic, facility. Editing, however, provided the opportunity to remove unwanted, or 'redundant', data lengths and also allowed the selection of records for further reduction. The total number of points per record is then chosen to vary from 185 points for the slow ramp to about 450 points o for the fastest. The number of cases for each wing condition is therefore reduced to 10. Each selected case is punched on paper tape. The rest of the data reduction process including the application of force, displacement and data handling calibrations, the application of various corrections and the data presentation is carried out on the University's central computer following the procedure given in section 6.1. It is worth commenting, however, that the alternative method of inverse calibration matrix correction, due to small changes incidence, which was adopted for the purpose of saving on computation time did not in the event lead to significant savings. This is thought to be a consequence of the relatively small number of points comprising each case.

In the remaining part of this section the results of tests on wings with and without transition strips are presented and discussed. Discussions related to the 'optimum' ramp rate and general discussions then follow .

7.3.1 Aerodynamic results - wings with transition strips

With transition strips applied, the flow pattern is assumed to be turbulent and stable over the incidence range. This stabilising effect has however a more subtle influence on the flow field than that. Certain secondary flow phenomena peculiar to fine model details, and which may be attributed to scale effects, may become very sensitive to the details of the transition strip itself. Examples of sensitive flows are:

i) the formation of secondary vortices at high incidence on slender wings with sharp leading edges (a function of wing thickness too),

ii) the flow at wing-body junctions, and

iii) the flow over the crevices and bumps on the lifting surface as experienced on practical aeroplanes.

A largely turbulent boundary layer on the configuration shortens and, to a large extent, fixes the flow response time than if boundary layer was laminar. Assuming an equivalent flat plate with turbulent boundary layers for the model planform, the nondimensional response time from fig. 2.4 is 2.0. The maximum ramp rate based on equation 3.15 falls in the range of 2.2 - 4. deg/sec. for the flow dynamic head range of 6. - 20. cm methylated spirit. The validity of the flat plate assumption, however, is subject to experimental verification.

The requirement of fixing an averaging time interval with a minimum length equal to the period of the transients of the slowest responding force component (e.g. drag force) while incidence interval is kept con-

stant at 0.2 deg. leads to a maximum balance-transients-free ramp rate of 1.2 deg/sec. Therefore for ramp rates less than that figure the contribution of balance transients are expected to be very small.

Computer graphic representation of the results of these cases are presented in fig. 7.16 - 7.23 covering incidence ramp rates 0.125, 0.25, 0.5, 1.0, 2.5, 5, 10 deg/sec. respectively. The Reynolds number is 0.37 million based on wing centre line chord.

The general form of the results for a reasonably low incidence ramp rate of 0.125 deg/sec., fig. 7.16-(a)-(e), suggests that the data is reasonably free from any significant dynamic effect. This is evidenced by the closeness of the results from the up and down ramp excursions. The force and moment calibration precision is represented by the bar denoting 'resolution' on the graphs for comparison purposes. Although the Reynolds number is low, it is of interest to explain the aerodynamic aspects of these results. C_L varies linearly with incidence over the range $-1\frac{1}{2}^{\circ}$ to $+2.5^{\circ}$. For higher values of incidence the lift is nonlinear, having a slight hollow in the lift curve between $\alpha = +2.5$ and 4.1 deg., followed by the gradual nonlinear rise characteristic of the leading edge vortex effect. This suggests that in spite of the sharp leading edges of the wings, attached flow prevails at low incidences and flow separation associated with the formation of leading edge vortices is delayed. This delay is caused by the existence of the body extending ahead of the wing apex. Similar phenomena have been observed by Kirby and Hepworth (1971). In this reference, however, the delay amounted to about 5° for a range of wing thicknesses and wing body combinations. An indication, although with uncertainty, of the existence of the hollow mentioned earlier can be detected in that reference at the transition region, from linear to nonlinear lift. It is possible that in such circumstances the hollow is a consequence of the interaction between the

forebody vortices and the wing vortices, probably the formation of the latter causing a premature breakdown of the former. It is interesting to compare this result with the results obtained in the same facility on the RAK model described in sec. 7.1.2. Owing to the presence of the body the delay in the formation of the wing leading edge vortices is clear, but owing to the lack of a forebody the hollow is absent.

It is interesting also to compare the linear lift curve slope found in the present measurement with that of the reference above. Kirby and Hepworth obtained for their pure gothic wing (sharp leading edges, aspect ratio 1.385) linear normal force slopes at zero incidence of 1.66 per rad. for a 4% thickness wing and 1.6 per rad. for a 9% thickness wing. Using the empirical formula due to Peckham (1958), the normal force slope for the present model can be predicted from Kirby and Hepworth's results. For a model comprised of the wings of the present model extending to the centre line, but without body, the normal force slopes should be 1.33 for 4% thickness and 1.285 for 9% thickness wings when the thickness distributions are the same as that of Kirby and Hepworth. The wings of the present model have a different thickness distribution, hence slightly different leading edge thickness angles, but the overall thickness to chord ratio is 4.83%. The measured lift curve slope at zero incidence is found to be 1.26 per rad. By taking the drag at zero lift into account a normal force slope of 1.302 per rad. results. This is in good agreement with the Kirby and Hepwroth results in spite of the difference in R_N and surface conditions. It should be noted that a conclusion of that reference was that for a mid-wing configuration the presence of the body produced no detectable effect on the lift curve slope at zero incidence. Therefore the results obtained in the present measurement seem to have a good accuracy.

Fig. 7.16(b) shows the drag coefficient variation with lift coefficient. It can be seen that there is a slight separation between the ramp up and ramp down of incidence. It is important to distinguish between two kinds of differences, namely those that take place in the range $0. < C_L < 0.05$ and those that occur elsewhere. The former differences have mainly aerodynamic origins while the latter may be attributed to dynamic effects of the testing or to some other systematic error. It can be seen that the latter difference is of the order of the difference between the starting and finishing points of the test which suggests that in this test run there is a possibility of a drift having occurred in the drag force loop. It has been argued earlier that in the range of C_L indicated above, any vortex system present in the flow field may be due to the body or the wing thickness distribution, and hence may have a strong viscous dependence. It is likely, therefore that the hysteresis is a genuine aerodynamic effect. Comparison of the drag coefficient of the present model with other measurements can best be carried out by considering the lift dependent drag parameter, $(C_D - C_{D_o})/C_L^2$. This parameter was found to be twice as large as the values obtained by Kirby and Hepworth. Moreover within the incidence range of the test the drag parameter does not appear to approach a constant value as would be expected for such a slender model. This result is corroborated by the $C_D - C_L^2$ graph fig. 7.16(c) which demonstrates a nonlinear behaviour. In view of the low R_N, no definite conclusion can be drawn about the overall drag properties of this model.

Pitching moment and centre of pressure location are illustrated in fig. 7.16(d) and (e) respectively. The separation between the results corresponding to the two ramp excursions is of the order of the difference between the start and end conditions and is less than 0.0005 (or 3.0 g.cm.

of moment) which is smaller than the moment resolution of the balance. There is a tendency for the centre of pressure to move forward at high incidence. At the zero lift incidence the centre of pressure lies at 0.53 of the centre-line chord from the wing apex. This can be compared with Kirby & Hepworth's results. Interpolation of their results for the present model geometry gives $X_{CP}/C_r \simeq .54$. The present results are seen to be in good agreement with that value inspite of the differences between the two configurations. It is interesting to notice that the centre of pressure is independent of the flow dynamic head. The difference between the two curves corresponding to ramp up and ramp down in fig. 7.16 (e) may be attributed to either aerodynamic hysteresis or errors in the data reduction technique. The apparent step in X_{CP}/C_r at $\alpha = 2^o$ is a consequence of the data reduction method. At that incidence a changeover from calculation of aerodynamic centre to that of centre of pressure (sec. 6.1) takes place. This is detectable in varying amounts in most of the centre of pressure results reported here.

The effect of $\dot{\alpha}$ on the measured aerodynamic characteristics can be inferred from the observation of the results at progressively increasing $|\dot{\alpha}|$ fig. 7.16 to 7.22. In general it can be seen that the positive and negative ramp rate data begin to separate significantly for $|\dot{\alpha}|$ 1.0^o/sec. The apparent separation in the lift coefficient characteristic at $\dot{\alpha} = 0.25$ deg/sec., fig. 7.17 (a) is believed to be a dynamic flow fluctuation effect since it is not correlated with a significant hysteresis on the X_{CP}/C_r characteristic. The effect of $|\dot{\alpha}|$ on the amount of hysteresis change in lift coefficient is shown in fig. 7.23. Effects at four incidence values are considered, e.g. 0.0, 3.0, 5.4 and 6.6^o. It can be clearly seen that there is a marked change in the magnitude of the hysteresis depending on the incidence and pitch rate. A pattern of systematic change can however be obtained if the hysteretic component of

C_L is replaced by $C_L/C_{L_{\alpha}} \times \dot{\alpha}$), which is called here the 'lift parameter', fig. 7.24. According to the theory of sec. 3.1 this parameter is equivalent to ζ/ω_n or the ramp response time lag of a second order system. With linear aerodynamics and in the absence of any transients the resulting change of lift parameter with $\dot{\alpha}$ should be a constant line parallel to $\dot{\alpha}$ axis. Fig. 7.24 however shows clearly that the lift parameter starts at a constant value for very small $\dot{\alpha}$, gradually increases, achieves a prominent peak particularly for large incidences near $|\dot{\alpha}| \simeq 5$ deg/sec., and then starts decreasing and presumably achieves the level corresponding to $\alpha = 0$ asymptotically. No attempt has been made to deduce a physical reason for the occurrence of such peaks, or the subsequent reduction in lift parameter at large $\dot{\alpha}$. The constancy of the lift parameter at all incidences at low values of $\dot{\alpha}$ is sufficient evidence for the absence of aerodynamic transients corrupting the quasi-static results, hence simple corrections can be applied to account for different lag values. The gradual increase in lift parameter is an evidence of dynamic corruption. Fig. 7.24 provides a conformation on the aerodynamic response time since it suggests that transients start affecting the measurements at $|\dot{\alpha}| > 2.0$ deg/sec. which agrees well with the prediction given earlier. The noise on the lift curve, however, increases as $\dot{\alpha}$ increase . This is a consequence of the shortening of the piecemeal averaging interval. A remedy could be the use of a more sophisticated 'filtering' algorithm.

The effect of $|\dot{\alpha}|$ on C_D is much more prominent, fig. 7.16 - 7.22. In considering this data it is essential to break down the drag into constituent parts, namely zero lift drag or minimum drag and drag due to lift. The change in the minimum drag value, taken as the average of ramp up and ramp down condition, with $\dot{\alpha}$ is shown in fig. 7.25. The strong dependence of $C_{D_{min}}$ on $\dot{\alpha}$ is characteristic of viscous effects and the reduction in its value can only be a confirmation of the fact that

with increasing $\dot{\alpha}$ the flow approaches the fully turbulent state. This result is significant since it suggests that as far as indicated forces are concerned a further correction due to C_D inaccuracy, even at very small incidence ramp rates, may be necessary. The drag due to lift, or the drag parameter $(C_D - C_{D_{min}})/C_L^2$, appears to decrease relatively slightly with increasing $|\dot{\alpha}|$ at high incidence. This would be expected since lift variations resulting from high $\dot{\alpha}$ arise from potential wake adjustment.

The moment coefficient and centre of pressure are also strongly dependent on $|\dot{\alpha}|$, particularly at low $|\dot{\alpha}|$. Apart from the increase in variability of C_M and X_{CP}/C_r with increase in $|\dot{\alpha}|$, the global trend remains relatively unaltered. The moment coefficient at zero incidence, however, decreases gradually from -0.003 at $|\dot{\alpha}|$ = 0.125 deg/sec. to -0.017 at 0.25 deg/sec. and then increases gradually with $|\dot{\alpha}|$. This corresponds to a change in the aerodynamic centre of about 2% of the centre line chord. The static stability about mid chord at zero lift appears to change from a value of approximately zero at 0.125 deg/sec. to a stable value in the range of $|\dot{\alpha}| \sim 0.5 - 1.$ deg/sec. but reduces back to near zero at high pitch rates.

7. 3.2 Aerodynamic results - clean wings

Previous testing in this facility has shown that clean slender wing models exhibit pronounced nonlinearities in their aerodynamic characteristics at low incidences and low flow Reynolds numbers. They may be caused by thickness and/or wing-body interference effects and are referred to in the following discussion as secondary effects. Therefore in addition to the determination of the steady aerodynamic characteristics of the clean wing AGARD-G planform model, the same measurements can be useful as a severe test of the validity of the

incidence ramp testing.

An estimation of the flow response time is much more involved in this laminar flow case since the vortex system is much more complex and it is possible that some of the secondary phenomena have a much longer response time than the predominant flow. It is likely that a complex pattern over a model would have a longer response time than the flow over a flat plate with a laminar boundary layer. Following a similar process to that pursued in the previous section and assuming a nondimensional flow response time of 4., the associated maximum permissible ramp rate is estimated to be 1.1 to 2. deg/sec. for the range of flow dynamic head considered before.

Further reduced measurements relevant to the AGARD-G planform model with clean wings have been obtained and computer graphics of some of the results are shown in fig. 7.27 - 7.32 for incidence ramp rates of 0.05, 0.125, 0.25, 0.5, 2.5 and 20. deg/sec. respectively. The Reynolds number is 0.33 million which is slightly lower than used in the tests with transition strips.

At very low ramp rates e.g. 0.05 deg/sec.,test duration is relatively long. In this case the measurements become sensitive to fluctuations in the manually controlled tunnel flow dynamic head. In addition, the probability of spurious interference on the measurements is high. This is clearly demonstrated by the results for $|\dot{\alpha}|$ = 0.05 deg/sec., fig. 7.27 (a0 to (e). The separation between the ramp up and ramp down C_L curves near $\alpha = 3^o$ and between $\alpha = 4.2^o$ and 6.6^o, fig. 7.27 (a) are most probably flow dynamic head fluctuations since they are absent in the X_{CP}/C_r graph, fig. 7.27 (e). There is clearly spurious interference in the drag coefficient at $C_L = -0.045$ (or $\alpha = -1.0^o$), fig. 7.27 (b), and another one on the moment coefficient at $C_L = +0.17$ or ($\alpha = 6.6^o$), fig. 7.27 (d).

This is clearly an indication of a state of reduced statistical control of this test. At higher ramp rates the test duration is shorter and the chances of interferences of the kinds mentioned above are very much reduced. Consider the results for $|\dot{\alpha}|$ = 0.125 deg/sec., fig. 7.28 (a) to (e). This set of results indicates the 'static' nature of the data. For the drag coefficient, however, the separation between the two ramp excursions is comparable with the balance drag force resolution, and there is insufficient evidence that this is an aerodynamic effect. For this ramp case, the lift coefficient, fig. 7.28 (a), is very different to the equivalent case with a transition strip, fig. 7.16 (a). Since the Reynolds numbers for the two cases are very close, the only possible cause of the differences is the effect of the transition strips. With clean wings the flow is expected to be predominently laminar. A first look at fig. 7.28 (a) suggests that C_L-α is more or less linear in the incidence range -1.4 to +1.8 deg. with a slight waviness. In a point-by-point measurement this waviness may be completely attributed to experimental errors. The lift curve slope corresponding to this linear range is about 2.0 per rad. This value is nearly 60% higher than the corresponding value for the wings with transition strips. A closer look at the C_L-α curve reveals a great deal more information in this low incidence range. It can be seen that around the zero lift incidence C_L has a definite linear trend in the range -0.2 to +0.5°. The lift slope of this part is only 1.65 per rad. or 30% above the corresponding wing with transition strips. At higher incidence there is clear evidence of a nonlinearity, similar to that associated with the formation of the lift generating vortex systems. At α = 1.5 deg. yet another vortex system may have formed, however its effect does not appear to persist for long. The interaction of this vortex system with the previous one appears to

lead to a gradual cancellation of their resultant effect on lift starting at an incidence of +1.8 deg. At an incidence of about 3^{o} the lift curve slope starts to increase again which indicates the formation of more powerful lift generating vortices. It is suggested that the earlier two vortex systems are akin to the separation on the body surface and/or on the aft parts of the wings while the latter is a wing leading edge separation type vortex. This is supported by measurements and observations reported by Kirby & Hepworth (1971) and Kirby & Kirkpatrick (1969). In the former reference it was concluded that wing thickness and body presence cause a delay in the formation of the leading edge vortex system. Flow visualisation along the model surface in the latter reference provided a corroboration of the thickness effect at low incidence and a clear indication of the reduction in lift curve slope of a 16% thick delta wing at an incidence between 2^{o} and 4^{o} with free transition. Evidence was provided in the same reference of the effect of R_N on the reduction of lift curve slope. Further evidence is required in addition to that on fig. 7.28 (a) in order to support the possibility of the vortex systems explained above. This is provided by the pitching moment and centre of pressure results.

The pitching moment about the mid-centre line chord and the centre of pressure results are shown in fig. 7.28 (d) and 7.28 (e) respectively. These two figures indicate a statically stable model ($d C_m/d C_L < 0$) with an aerodynamic centre at zero lift at .70 of the centre line chord behind wing apex which is consistent with nonseparated flow. The conclusion of this is that the aft parts of the model form the main lift force generating parts. For incidences above 1.8 deg. (or $C_L > .08$) the moment reverses trend to a statically unstable (i.e. $d C_m/d C_L > 0$) situation and the centre of pressure moves forwards indicating that the

forward parts are contributing more predominantly to the total lift. The kinks on the moment graph coincide with the key incidence values quoted above. The fine details yielded by the slow ramp testing can therefore be utilised to obtain more precise information about complex flow patterns than hitherto in conventional testing.

The drag coefficient is shown in fig. 7.28 (b). C_{D_o} is about ½ of that shown in fig. 7.16 (b), another confirmation of laminar flow. Although there is a certain amount of remnant noise on the drag curve, more than on the lift or moment curves, the kinks shown on the graph occur at the key incidence values. Two important features of the drag behaviour deserve comment. One is the slight asymmetry of C_D about $C_L = 0$ for which the only plausible explanation is small asymmetries n in the model configuration. The other is the occurrence of valleys, or local minima of C_D, at nonzero incidence. The most significant one is at $C_L \sim 0.07$ or $\alpha \sim 1.8^o$. Several possibilities can explain this phenomenon. The cancellation of the effects of various vortex systems in this range of incidence, as argued in conjunction with the reduction in local lift curve slope, may be rather associated with annihilation of some of them in favour of the remaining ones. Such annihilation, or vortex breakdown, is usually accompanied by a reduction in the drag force slope at least in the low R_N range [Kirby & Kirkpatrick (1969)]. The alternative possibility is the effect of the blunt base of the fuselage. The latter could be responsible at least in part for this phenomenon since the vortices generated on the model finally interact with the base wake. The drag due to lift expressed in the form of the drag parameter, or the drag variation with C_L^2 fig. 7.28 (c), did not approach an expected constant value or linear behaviour with C_L^2. This is difficult to explain, but it agrees with the findings related to wings with transition strips.

The changes of the aerodynamic characteristics with $|\dot{\alpha}|$ can be obtained from fig. 7.27 - 7.32 for progressively increasing $|\dot{\alpha}|$. These changes are similar to those for the case of wings with transition strips.

7.4 Oscillatory derivative results

As a verification of the estimated optimum record length for application to the covariance zero crossing method, a limited digital simulation has been carried out. A block diagram of the simulation is shown in fig. 7.33. A numerically generated sine wave of frequency 2.0 Hz and sampled at 180 samples/cycle is taken as the input to the second order system represented by the box. Noise (1) and noise (2) are different parts of a uniform random sequence, each having zero average.

Ideally when the noise is absent, the output signal Y is an attenuated (or magnified) and phase shifted version of the input signal X dependent on the system transfer function at this frequency. The purpose of the simulation was to introduce various amounts of noise into the signals, apply the zero crossing covariance method to signals X and Y and then to compute the quadrature component of Y with respect to X for a range of record lengths around those predicted from fig. 3.13 and 3.14. The results showed an excellent agreement with prediction for a specified accuracy of 0.5% in the quadrature component magnitude. In fact for a system phase difference of 12^{o} the following phase differences between the X and Y variables at different signal-to-noise ratios, but with a constant record length of 20 cycles, were obtained:

Signal-to-Noise ratio		Phase angle	error
Input	Output	(^{o})	(^{o})
∞	∞	11.96	-.04
7.54	1.72	11.92	-.08
7.54	0.262	12.92	+.92

It is clear from these limited results that the prediction of the theory is of the right order.

The technique of covariance zero crossing presented in section 3.2 has been applied to the measurement of oscillatory aerodynamic derivatives for the AGARD-G wing model. The procedure followed is that given in section 6.2. Flow dynamic head and amplitude of oscillation are chosen such that the dynamic range of the electromagnet currents corresponding to oscillation do not exceed the coil capacity. A convenient value for the dynamic head of 10.5 cm. methylated spirit (820 N/m^2) was used. The low closed-loop stiffness of the roll control is mainly responsible for the choice of a low dynamic head. The 'optimum' amplitude setting is chosen from observation of several test runs, and the linearity of the response is checked by digital analysis of a set of recordings at different amplitudes of oscillation but constant incidence and flow dynamic head. Fig. 7.34 illustrates a typical linearity check. The standard deviation of the roll displacement signal σ_ϕ is shown as the abscissa while the quantity $(\sigma_R/\sigma_\phi).(C_{\phi R}/C_{\phi\phi})$ is proportional to the amplitude of the cleaned roll current signal relative to displacement signal and ε/π is the phase difference between the two signals. The linearity is well established for the range of displacement measured upto about 1.8°. Below 0.5° or above 2° of roll oscillation amplitude, marked signal distortions could be observed. Throughout the program of testing the amplitude is kept down to about $1.0 - 1.6^\circ$. The general outcome is a set of results at low flow Reynolds number i.e. 3.64×10^5 based on the wing centre line chord, and low rolling frequency parameter, 0.013 to 0.03. The frequency parameter is $\omega s/U$ where ω is the oscillation frequency in rad/sec., s the semispan and U is the flow speed.

The effect of noise on the length of record used for the estimation of the covariance functions has been investigated for this model and the

conclusion remains substantially the same as that of section 7.12, namely that a minimum record length of 20 cycles is necessary for a reasonable accuracy of various estimated covariances.

180 samples per cycle of oscillation is regarded as a reasonable compromise between the accuracy obtainable with the present signal-to-noise ratio and precision of analysis. The sampling rate chosen is related to the number of samples per cycle and oscillation frequency. Fig. 7.35 illustrates typical plots of digitized roll displacement and roll current signals, in a wind-on test. Trace (a) corresponds to the displacement while the other two correspond to current signals. The top current signal (b) is a typical signal heavily polluted with noise while (c) is only lightly polluted but rather distorted.

The spectra of pairs of the signals, e.g. roll displacement and roll current signals taken in wind-on or wind-off at constant incidence setting were digitally computed and the signal to noise ratio was estimated. These signal-to-noise ratios were introduced into the charts of fig. 3.13 and 3.14 together with various frequency ratios and accuracy requirements to determine the suitable analysis record length. Typical values of the signal to noise ratios obtained for different incidence setting are shown in the following table.

α (°)	-1	0	1	1.75	3	3.5	4.4	5.2	6.	6.9
$\beta_x = (S/N)_{disp.}$	19	18	22	26	21	28	28	25	18	12
$\beta_y = (S/N)_{curr.}$	1.9	2.2	3.4	6.9	3.1	6.1	6.4	4.9	1.5	4.5
$\beta_x\beta_y$	36 *	40	75	180	65	170	180	120	27 *	54 *
min. length of record (cycles) from figs 3.13 and 3.14.	20	20	20	20	20	20	20	20	20	20

(S/N denotes signal-to-noise ratio)
(* indicates distortion present)

Except for the incidences -1 and 6° the signal-to-noise ratios appear to be good and the figure of 20 cycles for minimum record length is confirmed.

Table 7.3 shows the list of cases of oscillatory derivative measurements which have been recorded. Owing to the large volume of computation required, see below, only a few of these records were selected for further reduction.

A the data reduction stage there is a great deal of interaction with the computer, (see sec. 6.2.1) and consequently the computation time is long. The limited programming facility on the available computer, Myriad Mk II, has hampered attempts to produce more extensive results. To illustrate the volume of computation involved per each data point consider a 20 cycle record. These are sampled at 180 samples/cycle giving 7200 samples. The covariances are computed at 8 lag values around each zero crossing and 4 lag values around each peak or trough. If 10 zero crossings, 10 covariance peaks and 5 auto-covariances are calculated then the total number of lag values is about 140. This represents a considerable amount of computation per record.

7.4.1 Oscillatory roll damping - constant incidence results

Oscillatory roll damping derivatives of the AGARD-G wing model have been measured at constant incidence settings, at two different oscillation frequencies and for two different wing surface conditions. For the practical reasons cited earlier, only a few cases were analysed.

The tape recorder was checked for its gain and phase accuracy and was found acceptable. The wind-off signal-to-noise ratio product ($\beta_x \beta_y$) was found to be higher than 60 over most of the incidence range except near or above 6.0° and near or less than -1.0°. Typical values for wind-on signals are shown in the table above. These are regarded in general to be acceptable except for high incidence and they can be

analysed with a standard 20 cycle record length. Detailed examination of the signals with poorer signal-to-noise ratios or at extreme incidence suggests that the distortion of the sinusoid rather than the added noise is more serious. The correction of the rolling moment calibration constant (obtained statically) due to dynamic effects has been estimated before, see (sec. 5.5) and is small.

Reduced results for different cases are shown in fig. 7.36 in the form of the variation of ℓ_p with incidence. ℓ_p is compared on the same graph with results of recent RAE measurements on the standard AGARD-G wings [Fail (1973)] , NASA results on 74° delta wings [Boyden (1970)] and earlier measurements in the same facility on a cropped delta wing model [Abdelkawi et al (1971)] . It must be noted that Fail's and Boyden's results are given in a body axis system i.e. $\ell_p + \ell_v \sin \alpha$

Present results for the wings with transition strips for oscillation frequencies of 1.0 Hz and 2.0 Hz agree and have the same trend in the range of their overlap. A few points were found to lie outside the trend e.g. at $\alpha = 6$ and frequency 1.0 Hz and $\alpha = 6.9°$ and frequency 2.0 Hz. It was found that in such cases the signal-to-noise ratio of the displacement and/or the roll current signals were smaller than normal.

Certain differences can be noticed between the present data and the published ones. The present data appears to have a peak at zero incidence. It is interesting to notice that earlier measurement in the same facility [Abdelkawi et al (1971)] exhibit a similar behaviour in the low incidence range, i.e. near zero incidence. Fail's and Boyden's data approach a minimum at zero incidence. The existence of differences between the sources of data is not surprising in view of detail differences in configurations, methods of support, and of course Reynolds number. It has been shown in the steady force measurements that the presence of a body delays the onset of the sharp leading edge vortices. The immediate

consequence of this on ℓ_p for the present model is the delay in the gradual increase in the magnitude of ℓ_p with increasing incidence. For this model, the zero-lift incidence occurs at $\alpha = 0.2^o$ (see sec. 7.3.1). It is therefore reasonable to claim that the technique described in this thesis is providing valid data. A physical interpretation of the troughs occurring at $\alpha = -\frac{1}{2}^o$ and $\alpha = +1^o$ is in order. The products of the signal to noise ratios at these incidences are 32 and 72 respectively which indicates a high degree of confidence in the data. Having established the credibility of the results at other incidences it is therefore most likely that these troughs are genuine. The reducing magnitude of ℓ_p in the vicinity of zero incidence, where the major contribution is expected to be of a potential flow nature, can only be attributed to an asymmetric vortex pattern of viscous origin, similar to a thickness effect, which dominates the outboard sections of the wing. This is consistent with lift measurements discussed in sec. 7.3.1. The presence of the larger fin is likely to be the prime reason that the ℓ_p value obtained at zero incidence in the present results is larger than Fail's results. The effect of the fin at other values of incidence is to contribute partly to the values of ℓ_p obtained.

With clean wings at zero incidence and again at incidences above about $4\frac{1}{2}^o$ the oscillatory roll damping derivative is in good agreement with data taken with transition strips. In the intermediate range of incidence, however, the pattern of the two sets of results is markedly different, and can only indicate a sensitivity of ℓ_p to wing surface condition.

It has been noticed that measurements at a certain fixed incidence following a decrease in incidence are of much lower signal-to-noise ratio

and so are less reliable than the rest of the points. Examples of these points are shown in fig. 7.36 with arrows pointing towards decreasing incidence at $\alpha = 1.75^{o}$ and 4.35^{o}. In this range of incidence the lift curve slope indicates a strongly nonlinear behaviour. Despite the low signal-to-noise ratio, it is possible that the data reflects a real aerodynamic phenomenon and that there is more than one state of equilibrium of the flow pattern, the final state depending on the starting conditions of the incidence and its speed of variation.

It is reasonable to conclude that the present technique provides a useful alternative method for measurement of dynamic derivatives when the oscillatory system can be described reasonably by a linear model. The closest approach to this is achieved for the value obtained for ℓ_p at zero incidence where it is expected that any model would behave to a large extent linearly. An examination of the wind-off model oscillations gives a good indication of any likely distortion in signals, which in practice occurred at extremes of incidence.

7.4.2 Oscillatory roll damping with ramped incidence

Measurement of the oscillatory roll damping derivative has been carried out with the model incidence smoothly changing following the procedure of sec. 6.2.2. The incidence ramp duration is set at about 220 sec. for a single ramp, or 455 sec. for a full ramp test which includes a ramp up, a ramp down and three pauses of 5 sec. each. Different incidence ranges were selected in order to vary the ramp rates. The number of records taken on magnetic tape is shown in table 7.3. Owing to the large amount of computation needed per single record, only one single ramp case has been selected for digitizing and further data reduction. This corresponds to an incidence range of 8.8^{o} and hence a ramp rate of about 0.04 deg/sec. The wings have transition strips. The

flow dynamic head is set at the same value as in the previous set of tests for measurement of ℓ_p on the wings with the same surface condition but at constant incidence. The frequency of oscillation is 2. Hz, the number of samples per cycle is 180, the antialiasing filter is set to 40 Hz and the high pass filter to 0.0625 Hz. There are 162000 samples for each signal. Using the same analysis record length of 20 cycles fixes the incidence interval width. For the present case this corresponds to $\sim 0.4^{\circ}$. Although overlapping successive intervals can improve the incidence resolution, only contiguous intervals were used in order to reduce the volume of computation involved. Fig. 7.37 shows a breakdown of the computation details at different points along the record length. Although the test covers two full ramps, the record was delayed relative to the starting point of the ramp. The standard deviation of the displacement signal is σ_ϕ, the current signal σ_R, the covariance of the current and displacement signals $\hat{C}_{\phi R}$, the amplitude ratio of the effective or cleaned current signal $\frac{\sigma_R}{\sigma_\phi}\frac{\hat{C}_{\phi R}}{\hat{C}_{\phi\phi}}$ and the phase difference $\frac{\varepsilon}{\pi}$. It can be seen that a few points departed relatively widely from the trend set by neighbouring points. It is believed that these points are caused by spurious effects in the data reduction method. Modified replacement points are flagged. The reduced results plotted against mid interval incidence are shown in fig. 7.38.

The results of the incidence ramp test show two changes as compared with the constant incidence measurements. The first is that the data points in the incidence ramp case are more self consistent. The value of ℓ_p obtained at a constant incidence setting of $\alpha = 6.9^{\circ}$ is clearly out of the general trend and test repetitions either at the same incidence or in the neighbourhood would be mandatory in order to establish the local trend of ℓ_p. For the ramped incidence case, values of ℓ_p at a

certain incidence relative to that at any other nearby incidence is correct to within a controllable small systematic error introduced by the effect of $\dot{\alpha}$ and computation errors. The second is a direct confirmation of the effect of the direction of change of $\dot{\alpha}$. It can be seen from the graph that in the incidence range $2.5^{o} < \alpha < 4.3^{o}$ the resulting points for both signs of $\dot{\alpha}$ coincide while elsewhere there is a difference amounting to about 5%. The agreement between the incidence ramp and constant incidence measurement is only fair, particularly in the incidence range where the roll damping characteristic exhibits a strong curvature close to zero incidence. This is partly caused by the averaging process (see sec. 3.1) and partly due to the bias effect of $\dot{\alpha}$ on the covariance estimate which is proportional to $\dot{\alpha}^2$. There is a possibility of a field interaction (a balance effect) at high incidences introducing errors. Analysing more cases at different values of $\dot{\alpha}$ seems to be the only logical means for resolving these problems.

In conclusion, it can be stated that there is clear evidence supporting the higher self consistency of the data obtained from combined incidence ramp and roll oscillation. Details of the presence of any hysteretic aerodynamic effects may probably be more easily obtained from these tests than from conventional tests. The agreement between incidence ramp results and constant incidence results is only fair, partly as a consequence of the use of a relatively high incidence ramp rate. Because of the volume of computation involved the incidence resolution of the reduced data points is kept to the width of the analysis, or averaging, interval. With a more efficient computation algorithm, however, the incidence resolution can be improved a great deal.

7.4.3 Two degree of freedom forced oscillation

The method developed in section 3.2.6 and procedure given in 6.2.3 were applied to measurements with a combined pitch and heave oscillation.

The test was repeated at convenient oscillation frequencies of 1. and 2. Hz. The low dynamic head was set at 10.5 cm. methylated spirits. Sets of recordings were taken at different mean incidences in wind-on and wind-off states. The test runs were of an exploratory nature in order to assess the accuracy of the data reduction method and the postulated mathematical oscillation model.

The relevant signals V_α, V_h, V_F, V_A, V_R and V_ϕ - which correspond to incidence, heave, forward coil current, aft coil current, roll current and roll attitude signals respectively - are observed and occasionally the drag current and axial position signals. It was clear that a strong interaction among various modes of motion was present. The most serious one is the interaction from the roll mode into a combined pitch and heave oscillation. Nevertheless recorded signals were taken for further investigation.

Fig. 7.39 shows a set of digitized signals obtained for a combined pitch and heave forced oscillation at frequency 2. Hz and amplitudes of 1^o and 2. mm. of the pitch and heave respectively. The filter setting is the same as in the case of forced roll oscillation and the sampling rate is chosen in order to yield 180 samples per oscillation cycle.

Strong nonlinearities are found to dominate the signals. This is characterised by an apparent distortion of modulation of the signals. The modulation appears to exhibit a beat having a period of about 4 - 6 times the oscillation period. It is possible that such modulation is caused by the nonlinearity of model aerodynamics coupled with the strong roll - longitudinal mode interactions. The consistency of the beating along the record length (of at least 240 cycles) rules out the possibility of a transient interaction from the balance but leaves the phenomenon difficult to explain. The distortion of the signals is, most probably,

caused by the relatively large amplitudes of oscillation.

The presence of such nonlinearity on the signals throws a great doubt on the validity of the linear mathematical model assumed in developing the theory of section 3.2.6 and the technique was not tested further. In addition the strong interaction from other modes of motion necessitates an increase in the order of the oscillatory system, i.e. instead of a two degree of freedom oscillation perhaps a four degrees would be more appropriate if the unmodified MSBS system is used. The result of this would be a very complex mathematical model. Such a measure is not justified within the scope of the present investigation. Alternatively a simple way to reduce the interaction between the roll and longitudinal modes is by increasing the model-balance roll stiffness. This could be done by replacing the roll magnets by more powerful ones i.e. having larger $(BH)_{max}$ e.g. samarium cobalt or equivalent magnets.

7.5 Overall accuracy assessment and general discussions

Measurement uncertainty is caused by several factors, and most important among these are the following:

i) balance calibration errors,

ii) flow dynamic head fluctuations,

iii) model geometrical errors,

iv) suspension system nonstationarity,

v) oscillation frequency (for forced oscillation testing) errors,

vi) error in data collection and digitizing,

vii) errors due to data reduction and analysis.

These are mainly random errors, provided that the contribution of each source to the total error is very small. In addition there are two main sources of systematic error. The first is caused by the dynamic effect on the steady aerodynamic data resulting from the finite ramp rate in

ramp testing, and then by the associated mathematical model assumed for the model in dynamic testing. The second is the error in the wind tunnel wall correction applied to the aerodynamic data. These two sources of error are independent of the statistical control of the measurement technique adopted. An overall error assessment therefore requires estimating each of the above errors and combining them in a cumulative way.

An accurate estimate of the random errors can only be determined in a statistical form which dictates the need for a sufficiently large number of test repetitions under the same running conditions. Careful observation, however, has lead to a reliable rough estimate of these errors from a limited number of experiments. Out of the variety of possible sources of random errors listed above the most significant ones are (i) and (ii). Assuming a similar error probability distribution for both of these sources, then the probable total error in a measured aerodynamic characteristic (or derivative) is given by:

$$\delta C_A = \frac{\delta F}{Sq} \sqrt{1 + \left(C_A \frac{S\delta q}{\delta F}\right)^2}$$

where the aerodynamic force $F = qSC_A$ and q, S, C_A are the flow dynamic head, wing reference area and the aerodynamic coefficient respectively. δC_A, δF, δq are the probable errors in the respective quantities. This relationship can be graphically illustrated in a variety of ways. Fig. 7.40 shows several possibilities for fixed balance error δF (= 1.0 gm force) and flow dynamic head error δq (= 8 N/m^2 or 1 mm methylated spirit). In this figure (a) and (b) illustrate the absolute error in 'normalised' and explicit forms respectively, while (c) and (d) illustrate the corresponding relative error in a similar manner as a function of the magnitude of the aerodynamic coefficient with q as a parameter for the explicit

forms. It is clear that the error reduces as the dynamic head q (and consequently the Reynolds number) increases. The absolute error, however, increases as the measured coefficient increases (e.g. lift coefficient at large incidence). The significance of the contribution of the dynamic head error to the total error depends on the magnitude of the factor $C_A \frac{S\delta q}{\delta F}$. If this factor is much larger than unity then the error is dominated by the dynamic head error and is more conveniently expressed in relative form, while if it is much less than unity the major contributor is the balance force error and is then more conveniently expressed in absolute form. Similar sets of graphs can be constructed for different values of δF corresponding to lift force, pitching moment and drag force.

8. CONCLUSIONS

8.1 General conclusions

A study of new techniques of aerodynamic testing and data reduction is introduced in this thesis. The aim is to produce accurate data with a minimum of tunnel run time. The first technique consists of continuous incidence ramp while collecting quasi-static aerodynamic data. In the second technique covariance zero crossings are used for the accurate determination of quadrature components of a forced oscillation system and hence for the determination of aerodynamic oscillatory derivatives. Thirdly a combination of the two techniques above has been considered. Finally, extension of the second technique to more degrees of freedom is considered. Proposed procedures of testing and data reduction are presented.

The theoretical basis for the ramp technique has been laid. Aerodynamic balance and data reduction limitations have been derived and a relationship between the ramp rate, flow response time and data smoothing obtained. This indicates that the product of nondimensional model aerodynamic lift force response time and the nondimensional ramp rate is equal to the incidence averaging interval multiplied by a constant. The constant is related to the indicial property of the model and accuracy requirement for achieving the steady state. Balance dynamic effects account for transients and time lags in force components, mainly at the start and end of the incidence range. Digital data reduction method is introduced and a piecemeal averaging over contiguous or overlapping short intervals of the signals is proposed as a first step smoothing. The accuracy of the method is assessed in terms of the noise on the signals and recommendations about sampling rates and filter setting made.

The concept of self consistency of data points in a single test is introduced as a valid and useful qualitative measure of merit.

The six-component magnetic suspension and balance system of Southampton University has been used as a facility for the application of the incidence ramp technique to the measurement of aerodynamic characteristics of an AGARD-G winged model. In spite of the slow dynamic response of the balance and a roll-longitudinal mode interaction, a range of measurements have been made. Results for the lift coefficient and pitching moment coefficient variation with incidence agree with published results on comparable models in spite of the low Reynolds number of the present tests (0.37 million based on wing centre line chord). The present results, however, show fine aerodynamic details owing to the continuous incidence variation. The details revealed in this way may be easily missed or mistaken for noise in conventional point-by-point measurement. The results of a single test demonstrate the high degree of self consistency of data points over the range of incidence covered. This is reinforced by an agreement between points corresponding to positive and negative ramp rate which is better than the force resolution of the balance.

Study of the effect of ramp rate on measured results, for the range 0.05 to 20 deg/sec., produced at least two important conclusions. Firstly the predicted maximum allowable ramp rate was experimentally verified. Secondly, there is a need to correct viscous drag even at the lowest ramp rate. Independent measurement of the minimum drag at constant incidence is therefore important.

The optimum range of incidence ramp rates can be predicted and depends on the facility for the lowest value, and on the model aerodynamic properties, balance dynamic behaviour and data reduction method for the highest value. The application of the technique to aerodynamic

measurement in short duration facilities or continuous facilities which do not necessarily enjoy the highest degree of statistical control, is recommended.

The measurement of oscillatory aerodynamic derivatives from forced oscillation testing requires accurate comparison of the dynamic properties of two time varying signals. A novel technique using the digital covariance zero crossing is introduced and assessed as an efficient means of data reduction particularly for relatively short record lengths. The accurate determination of amplitude ratio and phase angle of two sinusoidal waves in the presence of noise is demonstrated. Relationships defining minimum zero crossing lag of interest and record length are derived and related to the degree of corruption on the two signals and the required accuracy of the result. It is shown that the product of the signal-to-noise ratios of the two signals, which forms the first important parameter of the method, can be used to define a minimum record length. Convenient charts are constructed for this process. For signals with a product of signal to noise ratios of about 25 or greater a minimum record length of 20 cycles suffices. In digitizing the signals, the number of samples per cycle of oscillation is found to be the second most important parameter, particularly in determining of the phase angle.

The method is applied to the measurement of aerodynamic oscillatory roll damping derivatives on the AGARD-G winged model at constant incidences using the magnetic suspension and balance system. Oscillatory roll displacement and roll current signals were analysed by this method and results compared with relevant published data. The present measurements reveal interesting variations of ℓ_p with incidence in the vicinity of zero incidence for the case of wings with transition strips. The roll damping reaches a peak at an incidence very close to zero, has two minima,

one on each side of the zero incidence, and then conforms with the expected trend at higher incidences. It is suspected that this phenomenon is a combination of viscous effects and model asymmetry. At extreme incidence values, however, the results appear to depart from the trend of other data. It was found that the signals were severely distorted at such incidences, which produces an effective reduction in the signal to noise ratio and systematic error in the results. In such conditions, the linear mathematical model of the oscillation is not valid.

The effect of continuously changing incidence while forcing the model in roll oscillation has been considered theoretically and experimentally. The mathematical model for the system still consists of a second order differential equation but with time varying coefficients. Results of measurement of ℓ_p in a 0.04 deg/sec. incidence ramp test are analysed by the method outlined above. As expected the signal-to-noise ratio of the records are better than for the case of constant incidence. The limited results obtained are compared with constant incidence measurement. The ramp results again demonstrate fine detail and indicate the self consistency of the results. An apparent systematic difference with the point by point results suggests that the ramp rate may be too high or the dynamic correction is inadequate. Further simulation study is required to resolve this.

Extension of the covariance zero crossing method to a two-degree-of-freedom system has been considered theoretically for combined pitch and heave motion. Some practical balance difficulties are met in applying this method for the measurement of pitch and heave derivatives. It is believed that nonlinearities and distortions of the displacement and current signals coupled with interactions from the other modes of motion renders the balance not particularly suited for testing according to the

simplified theory and procedure proposed.

General conclusions to be drawn are as follows. Certain viable techniques for yielding high quality data from wind tunnel testing have been introduced, tested and applied to aerodynamic measurements. The resulting measurements are characterised by a high degree of self consistency. The techniques could lead to considerable reduction in the time and cost of testing per data point. The digital data reduction adopted here involved more than one computer system, which often caused errors. A single integrated system is therefore strongly recommended. Further investigation is however, necessary in order to design a high reliability system to match the particular wind tunnel.

8.2 Suggestions for further work

In the work presented earlier, certain aspects of the techniques investigated have not been extensively assessed. The viability of these methods can be greatly enhanced when knowledge about following aspects can be obtained.

On the balance side improved calibration results are essential; the dynamic effects of force calibrations are of particular importance. Means of improving the frequency response characteristics of the balance would enhance the range of testing.

On the aerodynamic side accurate knowledge on the following is often required:

i) sensitivity of aerodynamic details to flow statistical perturbations

ii) effect of secondary phenomena on flow response time, particularly relevant to complex configurations

iii) standardization of a step response of various configurations.

On the data reduction side it is strongly recommended that the digital system used for the data reduction must incorporate sufficient programming facility for carrying limited digital simulation of the testing conditions and possible variations in the testing procedures. Algorithms are required for efficient digital filtering to replace the present piecemeal averaging but must be suitable for incorporation in a digital on line preprocessor which carries out the first part of data reduction in the incidence ramp case. This appears to be within the capacity of commercially available systems. On the covariance zero crossing method knowledge in two aspects is needed. Firstly the possibility of application of high speed convolution methods can reduce the computation time to a great extent. Secondly the search for more efficient methods for extracting phase angle from a set of covariance zero crossing lags of two signals plus noise.

8.3 Applications to conventional test facilities

The techniques of testing, data reduction and analysis presented in this thesis require some modification for application in conventional facilities. The essential hardware comprises a model moving mechanism, a digital computer and a set of peripherals for monitoring data at various stages of testing and data reduction as well as for producing final results in the desired form(s). The motion equipment should be capable of driving the model into various kinds of time varying displacements, e.g. linear and angular, as well as combinations of selected modes. A reliable means of precise model position monitoring either as part of the motion driving gear or independently, for preference, is necessary.

For a significant part of this work the intermediate stage computer acted as a digital preprocessor on the data. Digital preprocessors with

a wide variety of fixed and flexible configurations are now relatively cheap. A digital preprocessor is a device designed to do only a specific digital computation on data on-line and so is faster than a mini computer.

A fully integrated system then would consist of a mini computer, a digital preprocessor and ancillary equipment, e.g. model driving gear, position monitoring systems etc., and peripheral devices, e.g. storage oscilloscopes and VDU.

When the aerodynamic characteristics of the model are unknown before hand or known to possess strong hysteresis it is necessary to repeat the test at more than one ramp rate value for the quasi-steady state testing and more than one frequency and oscillation amplitude for the dynamic testing. From these results extrapolation or interpolation for zero ramp rate may be obtained. The importance of the technique however is in the self consistency of a set of data points, even when the flow phenomena may be unsteady in nature. The increasing availability of powerful, fast and cheap mini computers should be an encouraging impetus for utilization of sophisticated test techniques. The importance of mini computers in conjunction with digital preprocessors is that, with a carefully designed reduction system, data from the facility can be acquired on-line, digitally reduced and analysed, possibly in real time and the results produced in a comprehensible form e.g. displayed on a VDU. The flexibility of these mini computers is exemplified by the ease of interfacing with a wide variety of peripheral devices [Korn (1973)] and ease of operator interaction. In addition the short time lapse between test time and final results would facilitate decision taking about the course of the program. On-line digital analysis can by-pass several of the intermediate stages used in this investigation e.g. magnetic tape recording, tape recording static and dynamic calibration.

APPENDIX A

FORCE-CURRENT RELATIONS

The forces and moments acting on a magnetically levitated model at any instant of time depends on:

i) shape and state of magnetization of the magnets in the model,

ii) magnetic field spatial distribution (or currents in various coils if the model is magnetically saturated),

iii) model position relative to the electromagnets, and

iv) characteristics of the feedback control system in the case of unsteady motion.

It is not practical to attempt to calculate theoretically the exact forces on a general finite model in a non-uniform magnetic field, even for the steady case, let alone the unsteady one. The difficulty arises from the complex nature of the magnetic field distribution due to several finite size electromagnet coils with mutual interactions among them and the finite extent and irregularity of the magnetic material in the model. In view of this fact it has been widely accepted that force and moment calibrations should be conducted. The force-current relations need to be appropriately formulated and the calibration constants experimentally obtained.

Acting as a balance every practical system involves a certain degree of force interaction between various modes. So more reliable equations expressing this interaction, and yet be capable of further extension, would increase both the confidence of the translation of measured signals into forces and moments and increase the precision of the balance.

A.1 Magnetic force relations for the steady case

The first case considered is that of a stationary (non-moving) model. The relationships between forces on the model, field distribution, intensity of magnetization and model position and orientation are found. To

establish these relationships, the permanent magnetic material is assumed to be made up of a distribution of non-interacting infinitesimal magnetic dipoles. The elemental force and moment vectors acting on the elemental dipole of magnetic moment δm are given by

$$\vec{\delta f} = C_f \, \vec{\delta m} . \nabla (\vec{B})$$
$$\vec{\delta M} = C_m \, \vec{\delta m} \times \vec{B} \qquad \text{A.1}$$

where $\vec{\delta f}$ and $\vec{\delta M}$ are the force and moment vectors acting on $\vec{\delta m}$, $\vec{B}$ is the magnetic field strength at the location of $\vec{\delta m}$ and C_f and C_m are scalar constants. Equations A.1 are true only so long as the field $\vec{H}$ due to $\vec{B}$ has a magnitude less than the coercive field H_c of $\vec{\delta m}$. Rewriting these equations in tensor form, for reasons that will become clear later, we get

$$\delta f_i = C_f \, \delta m_j \frac{\partial}{\partial x_j} B_i = C_f \, \delta m_j \, B_{i,j}$$
$$\delta M_i = C_m \, (\delta m_j \, B_k - \delta m_k \, B_j) \qquad \text{A.2}$$

Cartesian tensor notations are followed; repeated subscripts in the same term denote summation, i,j,k take the values 1,2,3 only while r,s,t (to be introduced and used later) take the values 1,2, ... 6; and differentiation is indicated by a comma in the subscripts.

The magnetic field H_i at a point in the test section, generated by various electromagnets, is related to the currents in the respective coils through the equation.

$$H_i = h_{ir} \, I_r \qquad \text{A.3}$$

where I_r is the instantaneous current vector with 6 independently controlled current components. The second order tensor h_{ir} has components that depend on the construction of the coils and on the relative positions of the point under consideration. The magnetic field B_i (flux density)

affecting the model magnetic material is related to this generated field H_i through

$$B_i = \mu_{ij} \; H_j \qquad \text{A.4a}$$

where μ_{ij} is the permeability tensor of the medium. For a homogeneous medium and a saturated magnet μ_{ij} reduces to a scalar value, therefore

$$B_i = \mu_o \; H_i \qquad \text{A.4b}$$

Substitution from A.4b and A.3 into equation A.2 and integration over the volume of the whole magnetic material gives

$$\begin{aligned} f_i &= C_f \int_m dm_j \; h_{ir,j} \; I_r \\ \mu_i &= C_m \int_m (dm_j \; h_{k\,r} \; I_r - dm_k \; h_{jr} \; I_r) \end{aligned} \qquad \text{A.5}$$

where the coefficients C_f and C_m now incorporate the permeability constant.

In equations A.5, I_r is independent of the state of magnetization and position of the magnet. The integrals over dm can be transformed to volume integrals since the net characteristics of a magnet can be expressed as the product of its magnetic moment magnitude and a unit vector which depends solely on the shape of the magnet. Therefore these equations can be rewritten as

$$\begin{aligned} f_i &= m \; A_{ir} \; I_r \\ \mu_i &= m \; B_{ir} \; I_r \end{aligned} \qquad \text{A.6}$$

where m is the magnetic moment magnitude, the 2-D tensors (matrices) A_{ir} and B_{ir} are 3 x 6 and completely dependent on the geometry of the coils and test section, model magnet shape and its position relative to the coils. They may be expressed as:

$$A_{ir} = C_f \int \frac{dm_j}{m} \; h_{i_{r,j}}$$

$$B_{ir} = C_m \int \left(h_{k_r} \frac{dm_j}{m} - h_{jr} \frac{dm_k}{m} \right) \qquad \text{A.7}$$

Equations A.6 can be combined in the form of an augmented general force vector F_s with the first three components corresponding to the usual cartesian force components and the latter to the moments about the respective axes. Similarly the position vector is, implicitly, augmented to include all displacements in the six-degrees of freedom. It should be noted that angular displacements are taken to be small in order to validate the vectorial representation. The force-current relations then take the compact form

$$F_s = m \, C_{sr} \, I_r \qquad \text{A.8}$$

where

$$C_{sr} = A_{ir} \qquad s = i = 1,2,3$$

$$C_{sr} = B_{jr} \qquad s - 3 = j = 1,2,3$$

By analogy with the simple case of a magnet in the field of a single electromagnet coil, the component C_{rs} dependence on the component of the position vector between the magnet and the s^{th} coil takes the form

$$C_{rs} \propto \left(\frac{1}{\chi_s}\right)^{n_{rs}} \qquad \text{A.9}$$

where $n_{rs} > 1$. n_{rs} varies widely depending on r and s.

Provided that C_{sr} is a non singular matrix, its inverse exists, therefore

$$I_r = \frac{1}{m} \, D_{rs} \, F_s \qquad \text{A.10}$$

where

$$D_{rs} \, C_{sr} = [1]$$

Equation A.10 shows the manner in which the coil current vector (the directly measured variable) varies with the model magnetization, external forces on the model and medium characteristics including coil construction,

shape and co-ordinates of the magnet. It is important to notice the linear relationship between I_r and F_s.

Consider now the effect of variation in m, F_s and model displacements x_s from a reference condition on the indicated current vector I_r. Applying a generalised Taylor's theorem to equation A.10 and retaining only terms up to 2nd order, the following are obtained:

$$\Delta I_r \simeq {}^{x}I_{r,s}\ \Delta x_s + {}^{F}I_{r,s}\ \Delta F_s - I_r \frac{\Delta m}{m} + \frac{1}{2}\Big[{}^{xx}I_{r,t,s}\ \Delta x_t\ \Delta x_s + 2\ {}^{xF}I_{r,t,s}\ \Delta x_t\ \Delta F_s - 2\ {}^{x}I_{r,s}\ \Delta x_s \frac{\Delta m}{m} + 2\ I_r \left(\frac{\Delta m}{m}\right)^2 - 2\ {}^{F}I_{r,s}\ \Delta F_s \frac{\Delta m}{m}\Big] \qquad \text{A.11}$$

where the superscripts denote the independent variable of differentiation i.e. x and F denote position vector and force vector respectively. Re-arranging and grouping the terms gives

$$\Big[{}^{F}I_{r,s}\ (1 - \frac{\Delta m}{m}) + {}^{xF}I_{r,t,s}\ \Delta x_t\Big]\ \Delta F_s \simeq \Delta I_r + I_r\ \frac{\Delta m}{m}\ (1 - \frac{\Delta m}{m}) - \Big[{}^{x}I_{r,s}\ (1 - \frac{\Delta m}{m}) + \frac{1}{2}\ {}^{xx}I_{r,t,s}\ \Delta x_t\Big]\ \Delta x_s \qquad \text{A.12}$$

If the variation of m is represented completely, equation A.12 reduces to

$$\Big[m\ {}^{F}I_{r,s} + m\ {}^{xF}I_{r,t,s}\ \Delta x_t\Big]\ \Delta F_s \simeq (m + \Delta m)\ \Delta I_r + m I_r\ \frac{\Delta m}{m} - \Big[m\ {}^{x}I_{r,s} + \frac{1}{2}\ m\ {}^{xx}I_{r,t,s}\ \Delta x_t\Big]\ \Delta x_s \qquad \text{A.13}$$

This is the most general form for the steady force-current-displacement relationship of a magnetic balance of the d-c type with a model containing a permanent magnet. Second and third order tensors multiplied by m represent the universal calibration constants for the balance and magnet shape. The universality applies because the constants are independent of the state

of magnetization of the model magnet. This is maintained so long as during force application $[\vec{H}]$ is less than magnet coercive force H_c.

An important consequence of this result is that force calibration constants for a certain model, having a certain shape of magnet and reasonably strongly magnetised, need only be measured once.

The importance of equation A.13 becomes clear when the proper physical meanings are associated with the various terms present. The elements of the matrix $m\, I^{F}_{r,s}$ $\left(= m \frac{\partial I_r}{\partial F_s} = D_{rs} \right)$ represent the direct calibration constants. For an ideally uncoupled system

$$m\, I^{F}_{r,s} = m\left[I^{F}_{r,s} \right] \delta_{rs} \qquad \text{A.14}$$

where δ_{rs} is the Kronecker's delta which takes the value 1 if r = s and zero otherwise. The elements of this matrix are obtained from direct force and moment incremental changes with the currents while the model positions are held fixed.

The tensor $m\, I^{xF}_{r,t,s}$ (in general 6 x 6 x 6) represents the position-force interaction calibration constants. Its elements are of the form

$$m \quad \frac{\partial^2 I_r}{\partial F_s \partial x_t} = \frac{\partial}{\partial x_t} \left(m \frac{\partial I_r}{\partial F_s} \right)$$

These are second order derivatives which represent the rate of change of the direct calibration constants with model orientation or displacement from a nominal reference condition. This set of calibration constants is a measure of the degree of non-uniformity of the field and the spatial distribution of field gradients in the vicinity of the model. In general the variation of I_r with x_t is non-linear; however for small displacements Δx_t, such exact behaviour can be approximated by a linear variation bearing in mind that the effect on the overall force determination is of second order compared with the direct calibration constants.

The matrix $m\, I^{x}_{r,s}$ $\left(= m \frac{\partial I_r}{\partial x_s} \right)$ which is 6 x 6 represents the stiffness matrix of the suspension and balance system. The elements of this matrix are only constant for small displacements owing to the current-displacement non-linearity. The second order of this non-linearity is expressed by the third order tensor $m\, I^{xx}_{r,t,s}$ $\left[= \frac{\partial}{\partial x_t} \left(m \frac{\partial I_r}{\partial x_s} \right) \right]$ whose elements represent the degree of change of the stiffness with the displacement.

If one is to measure the external forces acting on a model by conducting a single test (i.e. a wind-on test) all these factors have to be taken into account and drastic restrictions have to be imposed on the model displacements in order to reduce errors introduced as a result of using equation A.13. Later on it will be shown that such restriction on a single test and the close restriction on displacement are not necessary.

The last term in A.13 represents the effect of change of model magnetization on the net change of current vector ΔI_r. This is linearly related to the values of the currents I_r with the model levitated free from external forces apart from gravity. The values of $m\, I_r$ are again independent of model magnetization but can be shown to be related to the model weight.

A.2 Use of the steady force calibration relation

Equation A.13 as presented above requires the determination of 510 calibration constants before it can be directly applied. In practice, however, by following proper routines of testing such a large number of constants would not be required.

Force calibrations are carried at a certain data whilst actual tests may well be conducted at a later date. Between these two dates, model magnetization could have changed. So if model position has not changed, which can be easily checked from the optics calibration, equation A.13 can be applied with $F_s = \Delta x_s = 0$ to give:

$$(m + \Delta m)\ \Delta I_r = - m\ I_r\ \frac{\Delta m}{m} \qquad \text{A.15}$$

which gives ΔI_r in terms of Δm, I_r, m. So if the intensity of model magnetization is independently but accurately measured, equation A.14 above serves as a means of confirmation of the universality of the calibration constants.

Between two measurements taken with the model at the same position and unchanged state of magnetization, equation A.13 can be applied to each case and, after the two equations have been subtracted, the following is obtained:

$$\left[m\ I^{F}_{r,s} + m\ I^{Fx}_{r,s,t}\ \Delta x_t \right] \Delta F_{s_{net}} = m'\ \Delta I_{r_{net}} \qquad \text{A.16}$$

where m' is the intensity of magnetization as measured just before the tests and which may be different from the calibration value m. If only one component of displacement is allowed, e.g. pitch, then equation A.15 reduces to

$$\left[m\ I^{F}_{r,s} + m \frac{\partial}{\partial \alpha} (I^{F}_{r,s}).\alpha \right] \Delta F_s = m'\ \Delta I_r \qquad \text{A.17}$$

The LHS of this equation becomes a 6 x 6 matrix. So

$$G_{rs}\ \Delta F_s = m'\ \Delta I_r \qquad \text{A.18}$$

where

$$G_{rs} = m \frac{\partial I_r}{\partial F_s} + m\alpha \frac{\partial^2 I_r}{\partial \alpha \partial F_s} \qquad \text{A.19}$$

Therefore only 72 calibration constants, the elements of G_{rs}, are required to determine the net forces acting on the model between the two tests. If G_{rs} is non-singular, equation A.17 can be modified to give an explicit expression for ΔF_s as

$$\Delta F_s = m'\ G^{-1}_{rs}\ \Delta I_r \qquad \text{A.20}$$

Many of the calibration constants are almost zero. The larger the number of vanishing elements the higher the degree of uncoupling between various degrees of freedom and the higher the degree of symmetry of the coil layout. In addition, for a certain prescribed accuracy of force measurement, a few more constants prove too small to have a significant effect.

It should be noted that owing to the wide range of variation of n_{rs}, equation A.9, some current components may display stronger dependence on the model displacement. In such cases an improvement on the accuracy of the calibration relations is achieved by the inclusion of second order terms in the displacement variation. Equation A.19 can therefore be modified to take the form

$$G_{rs} = m \frac{\partial I_r}{\partial F_s} + m\alpha \frac{\partial^2 I_r}{\partial \alpha \partial F_s} + m\alpha^2 \frac{\partial^3 I_r}{\partial \alpha \partial \alpha \partial F_s} \qquad \text{A.21}$$

The determination of the additional term in this equation, however, dictates higher precision requirement of the calibration procedure.

An additional use of equation A.13 is in the assessment of the changes in current resulting from model positional drift caused by possible contamination of the optical path of the position sensing system or a drift in the characteristics of the optics operational amplifiers. An example of this is the drift in axial position which, although small compared with tunnel dimensions, could seriously hamper the accuracy of measurement of small drag forces if the axial stiffness is large. So by application of equation A.13 and noting that $\Delta F_s = 0$ and drifts in axial position affects only drag currents up to 1st order, then

$$m\,(\Delta I_D)_{drift} = m \frac{\partial I_D}{\partial x} (\Delta x)_{drift} \qquad \text{A.22}$$

The constant $m \frac{\partial I_D}{\partial x}$ can be easily measured when the model is suspended wind-off by displacing the model forward and backward in several steps and plotting I_D against x (or the axial displacement signal).

A.3 Extension to the dynamic case

For the time dependent case, corresponding to time varying external force and/or time varying displacement, no longer can each coil be treated separately. The time varying field generated by one coil will cause a time varying flux linking other coils and inducing an emf and vice versa. The previous formulation must then be modified to consider the current vector as made up of a d.c. part and a time varying part. The latter is a product of the induction coefficient matrix with the time rate of change of the current vector. Model motion induces another emf in the coils which has to be included in the current vector. Temporal field variations set up eddy currents in the conducting parts of the model and cause non-linear damping forces. It is clear that the general dynamical form of the force-current relations is not easy to arrive at. Fortunately, in the case of interest here, i.e. that of small model velocities and oscillation frequencies, eddy current effects can be neglected. The effort required to develop the general equations does not seem to be justified at present.

A.4 Accuracy of force measurements

Force measurements using a magnetic balance are affected by three main sources of inaccuracy:

i) Errors in the calibration relations, due to the truncation of what essentially is an infinite series equation A.11,

ii) Errors due to inaccuracy of the determination of the elements of the calibration matrix,

iii) Errors due to the noise present on the measured current signals.

To a large extent the first source of errors can be compensated for by accurate force calibrations. The second and third types of error can be estimated from the calibration relations, equation A.20.

If the calibration matrix is in an error of $[\Delta]$, and the measured current signal is in an error of $\{\delta I\}$ then the error in $\{F\}$, i.e. $\{\delta F\}$ can be shown to be given by

$$\{\delta F\} = m\,([G]^{-1}\{\delta I\} - [G]^{-1}([\Delta](1 - [G]^{-1}[\Delta])^{-1}[G]^{-1}))\{I + \delta I\}) \qquad \text{A.23}$$

where in the previous equation the matrix $[\Delta]$ is assumed a perturbation over $[G]$, hence the direct method of evaluation of inverse matrix due to Householder (1954) has been applied. If $[\Delta]$ is taken such that $||[G]^{-1}|\cdot|[\Delta]|| << 1$ equation A.23 reduces to

$$\{\delta F\} \sim ([G]^{-1}\{\delta I\} - [G]^{-1}([\Delta][G]^{-1})\{I\}) \qquad \text{A.24}$$

The first term shows directly the relation between errors on the measured current signals and resulting error in force components. This is an absolute error, i.e. it does not depend on magnitude of force or current measured. The second term, however, depends on the level of forces, or currents, measured. By selecting the maximum force to be encountered during testing, a numerical procedure can be established which can provide estimates of the errors $\{\delta F\}$ due to small perturbation on each element of $[G]$. The elements of $[G]$, at this stage, need to be known only roughly, e.g. only direct calibration constants obtained. The desired accuracy of the force measurement and the results of the numerical procedure can be used to set the accuracy prerequisite on the elements of $[G]$. Consequently the important interaction calibration constants can be singled out and necessary calibration procedures carried out for their determination.

Appendix B

Relationship between rigid body and constrained oscillation testing

A rigid body oscillating without constraints in 6-DOF* can be realised in wind-tunnel testing using a 6-component balance (e.g. this MSBS). The static force-current calibration relation for a 6-component balance is given by (App. A)

$$[A]\ \{F\} = \{V\} \qquad \text{B.1a}$$

where $[A]$ is a 6 x 6 matrix whose elements correspond to the balance-model calibration constants; $\{F\}$ and $\{V\}$ are both 6-component vectors corresponding to the magnetic forces and electromagnet coil currents respectively. In actual fact the off diagonal elements of $[A]$ are nonzero as a result of force coupling inherent in the system. In certain cases, e.g. well designed balances, these elements may be very small compared with the diagonal elements, thereby indicating a close approximation to an orthogonal or uncoupled forcep system. Multiplying equation B.1a by the inverse matrix $[A]^{-1}$ gives

$$\{F\} = [A]^{-1}\ \{V\} \qquad \text{B.1b}$$

For a very low frequency sinusoidal oscillation, these equations may still be valid for converting dynamic current signals into corresponding dynamic forces.

The dunamic response of a model following a general small force disturbance represented by the vector $\{F\}$, which has 6 components, can be expressed through the 6-component displacement vector $\{X\}$. In general $\{X\}$ and $\{F\}$ are related through 6 linear ordinary differential

---

* (DOF) degress-of-freedom.

equations. In the case of harmonic small amplitude oscillations these reduce to a set of 6 linear complex algebraic equations qhich can be written in matrix form as

$$[P]\ \{X\} = \{F\} \qquad \text{B.2}$$

where $[P]$ is a 6 x 6 matrix consisting of the system impedances. Combining equations B.2 and B.1b gives

$$[P]\ \{X\} = [B]\ \{V\} \qquad \text{B.3}$$

By virtue of the conditions imposed on equations C.1 and C.2, the oscillation must have both small amplitude and low frequency. The elements of $[P]$ in B.3 can be obtained using six excitations at same frequency in which the set of vectors $\{V\}$ are linearly independent. An accurate measure of $\{V\}$ and $\{X\}$ in each case is then taken and substituted into B.3. The resulting set of equations can then be solved for $[P]$. This involves the measurement and observation of 12 signals 6 times. This is hardly justified in most cases owing to the complexity of the hardware as well as the data reduction method that might be needed.

In practice, however, the full 6-DOF case is seldom required. Various restraints on degrees of freedom, symmetries pertinent to model or excitation can be utilised to reduce the number of measurements in an experiment. However, no matter how carefully the experiment is conducted, the existence of force coupling exhibited by the off-diagonal elements of $[A]$ (and $[A]^{-1}$) will cause a systematic error in the measurements if the effect of such coupling is not taken into account. To consider this analytically let the vector $\{X\}$ be split into two smaller dimension sub-vectors $\{X_1\}$ and $\{X_2\}$ such that

$$\{X\} = \begin{Bmatrix} X_1 \\ \cdots \\ X_2 \end{Bmatrix}$$

Similarly for the currents vector

$$\{V\} = \begin{Bmatrix} V_1 \\ \cdots \\ V_2 \end{Bmatrix}$$

and the matrices P and B can be suitably partitioned in a manner that renders the resulting submatrices compatibly multiplicable with the corresponding subvectors as required by equation B.3. This equation can be rewritten as

$$\left[\begin{array}{c|c} P_1 & P_2 \\ \hline P_3 & P_4 \end{array}\right] \left\{\begin{array}{c} X_1 \\ \hline X_2 \end{array}\right\} = \left[\begin{array}{c|c} B_1 & B_2 \\ \hline B_3 & B_4 \end{array}\right] \left\{\begin{array}{c} V_1 \\ \hline V_2 \end{array}\right\} \qquad \text{B.4}$$

The usefulness of this partitioning arises in the design of a particular test with a limited number of DOF and hence limited measurement. As an example, for pitch and heave testing $\{X_1\}$ could have elements corresponding to incidence angle and lateral heave displacement while the corresponding current vector $\{V_1\}$ represents the pitching moment and lateral force. $\{X_2\}$ represents the remaining displacements, axial, vertical heave, yaw and roll and $\{V_2\}$ the other currents. In this case $[P_1]$ represents the reduced system impedance. It is obvious from equation B.4 that unless $[B_2]$, $[B_3]$, $[P_2]$ and $[P_3]$ are all identically zero, errors in the measurement of $[P_1]$ from consideration of $\{V_1\}$ and $\{X_1\}$ alone will occur. Expanding equation B.4 gives

$$\begin{aligned} [P_1]\{X_1\} + [P_2]\{X_2\} &= [B_1]\{V_1\} + [B_2]\{V_2\} \\ [P_3]\{X_1\} + [P_4]\{X_2\} &= [B_3]\{V_1\} + [B_4]\{V_2\} \end{aligned} \qquad \text{B.5}$$

If the system can be constrained such that either $\{X_2\}$ or $\{V_2\}$ is zero, simplification of these equations can be achieved. Since current signals are usually difficult to observe owing to their contamination with noise while displacement signals are much cleaner, constraints are applied to the displacements in the undisturbed modes. Assuming that $\{X_2\} = 0$ can be achieved experimentally, then equations B.6 reduce to:

$$\begin{aligned} [P_1]\ \{X_1\} &= [B_1]\ \{V_1\} + [B_2]\ \{V_2\} \\ [P_3]\ \{X_1\} &= [B_3]\ \{V_1\} + [B_4]\ \{V_2\} \end{aligned} \qquad \text{B.6}$$

These equations show that in this case $\{V_2\}$ can only be zero if $[B_3]$ and $[P_3]$ are also zero. A simplification can result, however, if $[B_2]$ is zero, when

$$[P_1]\ \{X_1\} = [B_1]\ \{V_1\} \qquad \text{B.7}$$

and the $[P_1]$ obtained from this is exactly the same as that from the larger number of DOF oscillation. When $[B_2] \neq [0]$, $\{V_2\}$ must be eliminated from equation B.6. After applying some matrix algebra the equations reduce to

$$([P_1] - [B_2]\ [B_4]^{-1}\ [P_3])\ \{X_1\} = ([B_1] - [B_2]\ [B_4]^{-1}\ [B_3])\ \{V_1\} \qquad \text{B.8}$$

If balance force coupling is very small the second term on the RHS may be regarded as a second order contribution compared to the first and its neglect leads to

$$([P_1] - [B_2]\ [B_4]^{-1}\ [P_3])\ \{X_1\} \simeq [B_1]\ \{V_1\} \qquad \text{B.9}$$

This equation shows that another correction due to $[P_3]$ is required. Physically $[P_3]$ could represent aerodynamic coupling or gravitational coupling effects. Only in cases where these coupling terms in conjunction with balance coupling terms corresponding to $[B_2]$ are known to be very small can further approximation of B.6 be considered and it then becomes similar to equation B.7.

Since this is a dynamic situation it is important to notice that the approximations considered above may not in general lead to a uniform error on the determined values of the elements of $[P_1]$. This is caused by the fact that these elements are not necessarily of the same order of magnitude, neither are the elements of $[P_3]$ and calibration matrices. Hence smaller value elements of $[P_1]$ will suffer the largest inaccuracy if the corresponding elements in the second terms of both sides of equation B.8 are not zero or very much smaller than the rest of the terms.

For a carefully calibrated balance, a good estimation of $[B]$ is available while reasonable values may be obtained for the critical elements of $[P_3]$. Hence an accurate determination of $[P_1]$ (i.e. oscillating system parameters and aerodynamic derivatives) may be obtained from a limited number of DOF oscillation test.

APPENDIX C

The Myriad Mk II computer system

The data analysis centre of ISVR has a Marconi Myriad Mk II digital computer, Mercer (1973), which is presently available to all users. The centre's main activity is in statistical data analysis. The computer has a 16 K words core store, a 2×10^6 work disc store, two analog to digital converters (each 12 bits and samples at up to 40000 samples/sec and one with a 24 channels multiplexer input), an incremental graph plotter, a control typewriter and paper tape reader and punch. A control language modelled upon Fortran, developed by the centre is used. Data is handled as a block, with a single name, comprising a data file. Associated with each data file is a control block which contains information on the statistical properties of the data file. The system has available a library of fixed statistical analysis algorithm subroutines which can be called during the course of analysis to execute the required operation.

REFERENCES

Abdel-Kawi, S.,Diab, T., Goodyer, M., Henderson, R. and Judd, M. (1974)
'Aerodynamic data acquisition with the University of Southampton magnetic balance'
Paper O Proc. Second Int. Symp. on Electromagnetic Suspension, Southampton.

Babister, A.W. (1961)
Aircraft stability and control
Pergamon Press.

Beam, B.H. (1956)
'A wind tunnel test technique for measuring the dynamic rotary stability derivatives at subsonic and supersonic speeds'.
NACA-R-1258

Beams, J.W. (1971)
'Some remarks on servocontrolled magnetic suspensions at the University of Virginia'
Introductory, Paper, Proc. Second Int. Symp. Electromag. Suspension, Southampton.

Bendat, J.S. (1958)
Principles and Applications of Random Noise Theory
J. Wiley & Sons.

*
Boyden, R.P. (1970)
'Theoretical and experimental studies of the effects of leading edge vortex flow on the roll damping of slender wings'
AIAA Paper No. 70-540.

Braslow, A.L., Wiley, H.G., and Lee, C.Q. (1962)
'A rigidly forced oscillation system for measuring dynamic stability parameters in transonic and supersonic wind tunnels'.
NACA-TN-D1231

Bratt, J.B. (1960)
'Wind tunnel testing for the measurement of oscillatory derivatives'.
A.R.C. R & M 3319.

Bratt, J.B. and Scruton , C. (1938)
'Measurement of pitching moment derivatives for an aerofoil oscillating about the half-chord axis'.
A.R.C. R & M - 1921

Bratt, J.B. and Wight, K.C. (1944)
'The development of an automatic electric balance for research on aerodynamic stability'
Phil. Mag., 35, p.588.

Cooley, J.W. and Tukey, J.W. (1965)
'An algorithm for the machine calculation of complex Fourier Series'.
Math. of Comp., 19, p.297.

Daum, F.L. (Ed.) (1966)
Summary of ARL Symposium on magnetic wind tunnel model suspension and balance systems.
ARL, Ohio.

Davenport, E.E. and Huffman, J.K. (1971)
'Experimental and analytical investigation of subsonic longitudinal and lateral aerodynamic characteristics of slender sharp edge 74° swept wings'.
NASA-TN-D-6344.

Diab, T.A. (1972)
'Results of steady aerodynamic testing of delta wing configurations'.
Unpublished rep., comm. to R.A. Kilgore, NASA, Langley Field, Va.

Dore, B.D. (1966)
'The unsteady forces on finite wings in transient motion'.
A.R.C., R & M - 3456.

Emslie, K. (1963)
'VSTOL Test facilities'.
BAC Rep. AX286.

Emslie, K. (1973)
Private communication.

Etkin, B. (1956)
'Aerodynamic transfer functions: an improvement on stability derivatives for unsteady flight'
Univ. Toronto, UTIA Rep. No. 42.

Fail, R.A. (1973)
'Results of RAE measurements of oscillatory derivatives on AGARD model G'
Unpublished work.

Garner, H.C., Rogers, E.W.E., Acum, W.E.A. and Maskell, E.C. (1966)
'Subsonic wind tunnel wall corrections'.
AGARDograph 109, Ch.5.

Gilman, J. and Bennett, R.M. (1966)
'A wind tunnel technique for measuring frequency response function for gust load analyses'.
J.A., 3, p.535.

Goodyer, M.J. (1967)
'Roll control techniques on magnetic suspension systems'.
The Aero. Quart., 18, p.22.

Goodyer, M.J. and Kilgore, R.A. (1972)
'The high Reynolds Number cryogenic wind tunnel'.
AIAA Seventh Aerod. Testing Conf., Palo Alto, Calif.
Also, AIAA J., 11, (1973)

Goodyer, M.J. (1968)
'The magnetic suspension of wind tunnel models for dynamic testing'.
Ph.D. Thesis, Southampton Univ.

Harper, C.W. (1968)
'Prospects in aeronautics research and developments'.
J.A., 5, p.417.

Holder, D.W. and North, R.J. (1949)
'The 9" x 3" NPL Induced Flow High Speed Wind Tunnel'
N.P.L., TP-285.

Householder, A.S. (1953)
'Principles of numerical analysis'.
McGraw-Hill Co.

Jones, B.M. (1935)
in Aerodynamic Theory, vol. V, Ed. by W.F. Durand, Dover Co.

Judd, M. (1963)
'The measurement of stability derivatives from the response to a randomly varying aerodynamic force'.
ARC 24970.

Judd, M. and Goodyer, M.J. (Ed.) (1971)
'Proc. Second Int. Symp. on Electromagnetic Suspension', Southampton University.

Kirby, D.A. and Hepworth, A.G. (1971)
'Low speed wind tunnel tests on some slender airbus configurations'.
A.R.C. R & M 3747.

Kirby, D.A. and Kirkpatrick, D.L.I. (1969)
'An experimental investigation of the effect of thickness on the subsonic longitudinal stability characteristics of delta wings of 70° sweep back'.
A.R.C. R & M 3673.

Korn, G.A. (1973)
Minicomputers for engineers and scientists.
McGraw Hill Inc.

Küchemann, D. (Ed.) (1972)
'Fluid motion problems in Wind Tunnel design'.
AGARD-R-602.

Lighthill, M.J. (1963)
in Laminar Boundary Layers, Ed. L. Rosenhead
C.U.P.

Lilley, G.M. (1963)
'The role played by wind tunnels in modern aeronautics'.
J. Roy. Aer. Soc., 67, p.463.

Lukasiewicz, J. (1955)
'Development of large intermittent wind tunnels'.
J. Roy. Aer. Soc., 59. p.259.

Lukasiewicz, J. (1973)
'Aerodynamic test simulation: Lessons from the past and future prospects'.
AGARD-R-603.

Lundgren, S. (1971)
Unpublished

Meirovitch, L. (1967)
Analytical methods in vibrations.
McMillan, New York.

Mercer, C.A. (1973)
'Development of data analysis in sound and vibration'.
JSV, 28, p.631.

de Meriette, F.J. (1973)
'Aeronautical facilities for the seventies'.
Lecture at NASA Headquarters, Washington D.C.

Nicolaides, J.D. and Eikenberry, R.S. (1970)
Unpublished

van Nunnen, J.W.G., Coupry, G. and Forsching, H. (1973)
'Minimum required times to perform instationary measurements in transonic wind tunnels'.
AGARD-R-601.

Orlick-Rukeman, K.J. (1960)
'Methods of measurement of aircraft dynamic stability derivatives'.
Can. Aero. Inst. J., 6, Oct.

Orlick-Rukemann, K.J. (1963)
'Travel summation and time summation methods of free oscillation data analysis'.
AIAA J., 1, p.1698

Parker R.J. and Studders, R.J. (1962)
Permanent magnets and their applications.
J. Wiley & Sons.

Peckham, D.H. (1958)
'Low speed wind tunnel tests on a series of uncambered slender pointed wings with sharp edges.'
A.R.C., R & M 3186.

Platou, A.S. (1965)
'Magnus characteristics of finned and non finned projectiles'.
AIAA J., 3, p.83.

Polhamus, E.C. (1971)
'Prediction of vortex lift characteristics by a leading edge suction analogy'.
J. A., 8, p.193.

Pugh, P. (1973)
Private Communication.

Starr and Schueler, C.J. (1973)
'Experimental studies of a Ludwieg tube high R_N transonic tunnel'.
AIAA paper No. 73-212.

Stephens, T., Covert, E., Vlajinac, M. and Gilliam, G. (1972)
'Recent developments in a wind tunnel magnetic balance'.
AIAA - paper No. 72-164.

Stockham, T.G., Jr. (1966)
'High speed convolution and correlation'.
AFIPS Conf. Proc., 28, p.229.

Sveshnikov, A.A. (1966)
Applied methods of the theory of random functions.
Pergamon Press, London.

Tanney, J.W. (1959)
'Force and pressure measuring systems for intermittent wind tunnels'.
NAE (Can), Quart. Bull. (1), Rep DME/NAE

Thompson, J.S. and Fail, R.A. (1962)
'Oscillatory derivative measurements on sting mounted wind-tunnel models: Methods of test and results for pitch and yaw on a cambered ogee wing at Mach numbers up to 2.6'.
A.R.C. R & M 3355.

Thompson, J.S. and Fail, R.A. (1966)
'Oscillatory derivative measurements on sting-mounted wind tunnel models at R.A.E., Bedford'.
AGARD-CP-17 ρ.437.

Thomson, W.T. (1965)
Vibration Theory and Applications
Allen & Unwin, London.

Tournier, M. and Laurencaau, P. (1957)
'Suspension magnétique dime maquette en soufflerie'.
La Rech. Aero., Nr.59, p.21.

Vlajinac, M., Stephens, T., Gilliam, G., Pestas, N. and Covert, E. (1971)
'Subsonic static characteristics of slender wing configuration using a magnetic suspension and balance system'.
NASA-CR-1796.

Wilson, F.M., Jr. and Maddox, B.W. (1969)
'Some recent innovations in wind tunnel testing techniques'.
S.A.E. paper 69-0677.

---

* Bendat, J.S. and Piersol, A.G. (1966)
'Measurement and Analysis of Random Data'
J. Wiley & Sons.

Table 5.1

MODEL FORCE AND MOMENT CALIBRATION CONSTANTS

$$G_{rs} = \left[m \frac{\partial I_r}{\partial F_s}\right] + \left[m \frac{\partial}{\partial \alpha} \left(\frac{\partial I_r}{\partial F_s}\right)\right] \alpha + \left[m \frac{\partial^2}{\partial \alpha^2} \left(\frac{\partial I_r}{\partial F_s}\right)\right] \alpha^2$$

Force vector $\equiv \{L \quad M \quad D \quad T\}'$

Current vector $\equiv \{ I_F \; I_A \; I_D \; I_R\}'$

$m = 9.37$

Component	Direct Calibration Constant x 10^3	Interaction Calibration Constant	
		Linear with α x 10^4	Quadratic with α x 10^5
G_{11}	-3.445	-0.744	1.85
G_{12}	-0.328	0.0063	0.022
G_{12}	-0.530	3.98	-0.885
G_{14}	0.904	-9.94	4.84
G_{21}	3.650	-1.036	2.175
G_{22}	-0.317	0.009	0.014
G_{23}	-0.240	-2.03	11.5
G_{24}	-0.553	-7.4	-1.0
G_{31}	-1.050	-0.0556	-1.53
G_{32}	-0.040	0.023	-0.067
G_{33}	-21.20	0	0
G_{34}	0.00	6.46	-5.27
G_{41}	0.540	24.7	-50.2
G_{42}	-0.105	-0.063	0.283
G_{43}	-1.68	-0.226	4.21
G_{44}	50.25	5.55	-4.52

Table 5.2

ACCURACY OF FORCE AND MOMENT MEASUREMENTS

Resolution of measurements using the calibration constants of Table 5.1 are:

Lift force	±.5	gm
Pitching moment	±4	gm.cm
Drag force	±.5	gm
Roll torque	±1	gm.cm

Table 7.1

TAPE RECORDED STEADY RAMP TESTS

WINGS WITH TRANSITION STRIPS

Record Number	Type/Flow cm. Meth.	$\dot{\alpha}$ (deg/sec)	Date
76	CAL	-	22.8
77	0	.125	"
79	0	1.25	"
81	0	2.5	"
83	0	.25	"
85	0	2.0	"
87	0	1.0	"
89	0	.50	"
91	11.2	.125	"
93	"	1.25	"
95	"	2.50	"
97	"	.25	"
99	"	2.0	"
101	"	1.0	"
103	"	.50	"
106	CAL	-	23.8
107	0	2.0	"
109	0	2.5	"
111	0	4.	"
113	0	5.	"
115	0	8.	"
117	5.	2.	"
119	"	2.5	"
121	"	4	"
123	"	5.	"
125	"	8.	"
127	10.0	2.	"
129	"	2.5	"
131	"	4.0	"
133	"	5.0	"
135	"	8.0	"
137	15.0	2.	"
139	"	2.5	"
141	"	4.0	"
143	"	5.0	"
145	"	8.0	"

Record Number	Type/Flow cm. Meth	$\dot{\alpha}$ (deg/sec)	Date
148	0	2.0	23.8
149	0	2.5	"
150	0	4.0	"
151	0	5.0	"
152	0	8.0	"
153	CAL	-	28.9
154	11.5	20.0	"
156	"	.05	"
158	"	12.5	"
160	"	.125	"
162	"	10.	"
164	"	.25	"
166	"	8.	"
168	"	.5	"
170	"	5.0	"
172	"	1.	"
174	"	4.0	"
176	"	1.25	"
178	"	2.5	"
180	"	2.	"
182	11.5	.5	"
184	15.3	.5	"
186	19.1	.5	"
187	7.6	.5	"
188	3.8	.5	"
189	0	.5	"

Table 7.2

TAPE RECORDED STEADY RAMP TESTS

CLEAN WINGS

Record Number	Type/flow	$\dot{\alpha}$ (deg/sec)	Date
210	CAL	-	1.10
211	12.	20	"
212	"	.05	"
213	"	12.5	"
214	"	.125	"
215	"	10.0	"
216	"	.25	"
217	"	8.	"
218	"	.5	"
219	"	5.	"
220	"	1.	"
221	"	4.	"
222	"	1.25	"
223	"	2.5	"
224	12.	2.	"
225	12.	.5	"
226	10.	.5	"
227	8.	.5	"
228	6.	.5	"
229	4.	.5	"
230	14.	.5	"
231	0.	.5	"
232	0	20.	"
233	"	12.5	"
234	"	.125	"
235	"	10.	"
236	"	.25	"
237	"	8.	"
238	"	.5	"
239	"	5.	"
240	"	1.	"
241	"	4.	"
242	"	1.25	"
243	"	2.5	"
244	"	2.	"
245	"	1.	"
246	"	.05	"
247	CAL	-	"

Table 7.3

TAPE RECORDED OSCILLATORY DYNAMIC TESTS

Record Number	Type/flow cm. Meth	Transition	Osc.freq (Hz)	α (deg)	$\dot{\alpha}$ (deg/sec)	Date
1001	CAL	-	1.	-	-	15.9
1002	CAL	-	1.5	-	-	"
1003	CAL	-	2.0	-	-	"
1004	CAL	-	2.5	-	-	"
1005	10.5	fixed	1.0	-.9	-	26.9
1006	"	"	"	-.5	-	"
1007	"	"	"	0	-	"
1008	"	"	"	1.0	-	"
1009	"	"	"	3.0	-	"
1010	"	"	"	6.0	-	"
1011	0.0	"	"	-1.0	-	"
1012	"	"	"	- .5	-	"
1013	"	"	"	0.0	-	"
1014	"	"	"	+1.0	-	"
1015	"	"	"	+3.0	-	"
1016	"	"	"	+6.0	-	"
1017	CAL	"	"	-	-	"
1021	10.5	"	2.0	-	0.04	27.9
1022	"	"	"	-	0.02	"
1023	"	"	"	-	0.02	"
1024	"	"	"	0.0	-	"
1025	0.0	"	"	"	-	"
1027	"	"	"	-	.02	"
1028	" "	"	"	-	..04	"
1029	10.5	"	"	-	0.08	"
1030	"	"	"	-	0.08	"
1031	"	"	"	-	0.16	"
1032	"	"	"	-	0.16	"
1033	"	"	"	-1.5	-	"
1034	"	"	"	-1.8	-	"
1035	"	"	"	+ .9	-	"
1036	"	"	"	+7.0	-	"
1037	"	"	"	6.1	-	"
1038	"	"	"	5.3	-	"
1039	"	"	"	4.4	-	"
1040	"	"	"	3.6	-	"
1041	"	"	"	2.7	-	"
1042	"	"	"	1.8	-	"

Table 7.3 (continued)

Record Number	Type/flow cm.Meth	Transition	Osc.freq (Hz)	α (deg)	$\dot{\alpha}$ (deg/sec)	Date
1043	0	fixed	2.	-	.16	28.9
1044	0	"	"	-	.08	"
1045	0	"	"	-1.5	-	"
1046	0	"	"	- .8	-	"
1047	0	"	"	+ .9	-	"
1048	0	"	"	7.	-	"
1049	0	"	"	6.1	-	"
1050	0	"	"	5.3	-	"
1051	0	"	"	4.4	-	"
1052	0	"	"	3.6	-	"
1053	0	"	"	2.7	-	"
1054	0	"	"	1.8	-	"
1056	0	"	1.	0.0	-	"
1057	0	"	1.5	0.0	-	"
1058	0	"	2.0	0.0	-	"
1059	0	"	2.5	0.0	-	"
1060	10.5	"	2.0	0.0	-	"
1061	"	"	2.0	0.0	-	"
1062	"	"	2.0	0.0	-	"
1063	"	"	2.0	0.0	-	"
1064	"	"	2.0	0.0	-	"
1065	"	"	2.5	0.0	-	"
1066	"	"	1.5	0.0	-	"
1067	"	"	1.0	0.0	-	"
1068	"	"	3.0	0.0	-	"
1069	"	"	3.0	4.4	-	"
1070	"	"	2.0	4.4	-	"
1071	0	"	2.0	0.0	-	"

Table 3 (continued)

Record Number	Type/flow cm.Meth	Transition	Osc.freq (Hz)	α (deg)	$\dot{\alpha}$ (deg/sec)	Date
1078	8.4	-	2.0	-	-	1.10
1079	"	free	"	0.0	-	"
1080	"	"	"	-1.4	-	"
1081	"	"	"	-0.8	-	"
1082	"	"	"	-0.4	-	"
1083	"	"	"	0	-	"
1084	"	"	"	+ .45	-	"
1085	"	"	"	+ .90	-	"
1086	"	"	"	+1.8	-	"
1087	"	"	"	+7.0	-	"
1088	"	"	"	+1.8	-	"
1089	"	"	"	+5.3	-	"
1090	"	"	"	+4.4	-	"
1091	"	"	"	+3.6	-	"
1092	"	"	"	+2.7	-	"
1093	"	"	"	+1.8	-	"
1094	"	"	"	0.	-	"
1095	9.8	"	"	0.	-	"
1096	7.0	"	"	0.	-	"
1097	5.6	"	"	0.	-	"
1098	4.2	"	"	0.	-	"
1099	0	"	"	0.	-	"
1100	0	"	"	-1.4	-	"
1101	0	"	"	-0.8	-	"
1102	0	"	"	+0.9	-	"
1103	0	"	"	+-.7	-	"
1104	0	"	"	+4.4	-	"
1105	0	"	"	+6.1	-	"
1106	0	"	"	+7.0	-	"

Table 7.4

A sample computer result of
a steady incidence sweep test

MAGNETIC SUSPENSION SYSTEM (MSBS)

STEADY AERODYNAMICS TESTING ** DATA REDUCTION

APPROX. AGARD-C WING MODEL

WING REF. AREA = 60.65 SQCM MEAN AEROD. CHORD = 9.79 CM ASPECT RATIO = 0.92

SURFACE CONDITION :: WITH TRANS STRIPS

FLOW SPEED = 39.3 M/S DYNAMIC HEAD = 923.83 N/SQM

MACH NO. = 0.114 TEST REYNOLDS NO. = 0.37 MILLION

INCIDENCE RAMP RATE = 0.050

TABLE OF RESULTS

I	ALFA	CL	CD	CM	XCP	XPP	CLSQ	2CD/CLSQ	CR	IND
1	-1.740	-0.041597	0.038448	-0.005544	5.937751	0.412650	0.001730	2.584523	-0.000228	0
2	-1.740	-0.041597	0.038448	-0.005544	5.937751	0.412650	0.001730	2.584523	-0.000228	0
3	-1.740	-0.038046	0.038163	-0.005147	7.109603	0.494066	0.001447	5.031260	-0.000299	0
4	-1.754	-0.038118	0.038048	-0.005521	5.401476	0.444855	0.001453	2.940622	-0.000250	0
5	-1.756	-0.038062	0.037914	-0.005500	5.397657	0.5750?8	0.001446	2.793671	-0.000255	0
6	-1.686	-0.036224	0.037782	-0.004908	4.625569	0.521305	0.001312	3.052893	-0.000167	0
7	-1.585	-0.034002	0.037401	-0.004220	5.534248	0.384570	0.001156	3.135557	-0.000065	0
8	-1.477	-0.031580	0.036456	-0.003520	5.489709	0.381495	0.000994	2.676650	0.000150	0
9	-1.378	-0.029204	0.036056	-0.003053	5.080386	0.422542	0.000853	3.377161	0.000256	0
10	-1.270	-0.026978	0.036307	-0.003297	5.220472	0.432594	0.000728	3.478653	0.000395	0
11	-1.164	-0.024874	0.036240	-0.003181	5.817969	0.404305	0.000619	4.466595	0.000527	0
12	-1.058	-0.022761	0.036131	-0.002723	5.500623	0.362253	0.000518	4.547421	0.000612	0
13	-0.951	-0.020416	0.035778	-0.002567	5.551086	0.386750	0.000417	4.803419	0.000691	0
14	-0.835	-0.018213	0.035313	-0.001780	5.780034	0.401670	0.000332	4.633545	0.000757	0
15	-0.728	-0.015959	0.035092	-0.001683	5.036523	0.419494	0.000255	5.169598	0.000842	0
16	-0.617	-0.013769	0.034554	-0.001423	5.724067	0.467274	0.000190	4.105337	0.000891	0
17	-0.515	-0.011527	0.034405	-0.001515	5.104999	0.424253	0.000133	3.231392	0.000935	0
18	-0.407	-0.009365	0.033926	-0.001354	5.133618	0.426242	0.000088	1.735652	0.000970	0
19	-0.298	-0.007372	0.033596	-0.000729	5.284585	0.367240	0.000055	-3.278624	0.001005	0
20	-0.186	-0.005270	0.033630	-0.000501	4.200438	0.291900	0.000028	#.###900	0.001021	0
21	-0.076	-0.003110	0.033120	0.000127	4.660073	0.324377	0.000010	#.###900	0.001059	0
22	0.037	-0.000992	0.032046	0.001208	5.470602	0.450077	0.000001	#.###900	0.001057	0
23	0.148	0.001114	0.032387	0.001467	5.317185	0.377954	0.000001	#.###900	0.001070	0
24	0.251	0.003242	0.036694	0.000124	#.649032	0.670537	0.000011	#.###900	0.001118	0
25	0.361	0.005441	0.047347	-0.000854	#.706588	0.674259	0.000050	#.###900	0.001135	0
26	0.465	0.007640	0.047712	-0.000956	5.160681	0.567108	0.000058	#.###900	0.001202	0
27	0.573	0.010024	0.047399	-0.000816	5.623862	0.460310	0.000100	#.###900	0.001187	0
28	0.680	0.012355	0.047499	-0.000775	5.257346	0.433450	0.000155	#.###900	0.001164	0
29	0.787	0.014465	0.046919	-0.000327	5.173402	0.429145	0.000209	#.###900	0.001147	0
30	0.893	0.016552	0.046402	-0.000084	5.357512	0.441801	0.000274	#.###900	0.001151	0
31	1.001	0.018824	0.046942	0.000101	5.112838	0.424795	0.000354	#.###900	0.001167	0
32	1.100	0.021114	0.046965	-0.000026	5.430293	0.446858	0.000446	#.###900	0.001139	0
33	1.209	0.023096	0.046881	0.000326	5.150737	0.427431	0.000553	#.###900	0.001149	0
34	1.318	0.025664	0.046776	0.000525	5.313326	0.369377	0.000656	#.###900	0.001140	0
35	1.427	0.027704	0.046437	0.001043	5.046523	0.420239	0.000787	#.###900	0.001117	0
36	1.534	0.030158	0.046366	0.001208	5.420763	0.446615	0.000948	#.###900	0.001144	0
37	1.637	0.032259	0.046587	0.001701	5.630567	0.401552	0.001040	#.###900	0.001165	0
38	1.740	0.034767	0.046416	0.001538	5.860145	0.476755	0.001205	#.###900	0.001087	0
39	1.850	0.036756	0.046457	0.001963	5.600757	0.433141	0.001351	#.384016	0.001084	0
40	1.950	0.039119	0.046011	0.002015	5.636750	0.391714	0.001530	#.520017	0.000921	0

TABLE OF RESULTS (CONT.)

I	ALFA	CL	CD	CM	XCP	XPP	CLSQ	@CD/CLSQ	CR	IND
41	2,067	0,041236	0,046012	0,002241	5,424539	0,376966	0,001700	7,666754	0,000983	0
42	2,182	0,043109	0,046344	0,002676	5,587578	0,457769	0,001855	6,870562	0,000980	0
43	2,293	0,045159	0,046495	0,003082	5,520959	0,453576	0,002037	6,237249	0,000979	0
44	2,400	0,047414	0,046450	0,003594	5,455038	0,448459	0,002248	5,638120	0,000968	0
45	2,504	0,049536	0,046050	0,003927	5,417166	0,446055	0,002454	5,327668	0,000951	0
46	2,611	0,051545	0,046030	0,004895	5,263564	0,435411	0,002657	4,913334	0,000956	0
47	2,718	0,053624	0,046047	0,005291	5,229335	0,432893	0,002875	4,476422	0,000952	0
48	2,824	0,055800	0,046082	0,005482	5,233595	0,433189	0,003114	4,208363	0,000961	0
49	2,928	0,057907	0,046099	0,006474	5,100741	0,423957	0,003353	3,915607	0,001041	0
50	3,036	0,060270	0,047043	0,006910	5,073123	0,422038	0,003553	3,651519	0,001070	0
51	3,139	0,062065	0,046053	0,007677	5,984746	0,415876	0,003855	3,540846	0,001086	0
52	3,243	0,064517	0,046008	0,008588	5,877015	0,408410	0,004162	3,085001	0,001111	0
53	3,344	0,066551	0,046796	0,009149	5,849592	0,405504	0,004429	2,939880	0,001184	0
54	3,454	0,068726	0,046061	0,009722	5,810557	0,403771	0,004724	2,726022	0,001228	0
55	3,557	0,070805	0,046379	0,010365	5,763886	0,400548	0,005024	2,548347	0,001292	0
56	3,660	0,073455	0,046072	0,010870	5,740691	0,399353	0,005395	2,390534	0,001395	0
57	3,760	0,076025	0,046092	0,011287	5,744000	0,399027	0,005780	2,269392	0,001527	0
58	3,864	0,078544	0,047458	0,011933	5,708055	0,396668	0,006169	2,217870	0,001655	0
59	3,960	0,080613	0,047031	0,011585	5,788502	0,402259	0,006495	2,162907	0,001741	0
60	4,065	0,083470	0,048001	0,011538	5,842183	0,405969	0,006967	2,041687	0,001859	0
61	4,166	0,086394	0,048353	0,011866	5,850757	0,406585	0,007464	1,979953	0,001921	0
62	4,267	0,089327	0,048024	0,012726	5,800673	0,403104	0,007979	1,885952	0,002009	0
63	4,367	0,092583	0,049091	0,013038	5,810753	0,404222	0,008572	1,856722	0,002150	0
64	4,469	0,095417	0,050482	0,013573	5,802779	0,403251	0,009104	1,815031	0,002281	0
65	4,571	0,098448	0,050716	0,013538	5,869020	0,407854	0,009692	1,768489	0,002630	0
66	4,670	0,100973	0,051356	0,013741	5,845741	0,406077	0,010195	1,743921	0,002577	0
67	4,777	0,104057	0,052208	0,014096	5,869187	0,407866	0,010828	1,702283	0,002755	0
68	4,882	0,106891	0,052758	0,014558	5,866093	0,407373	0,011425	1,678890	0,002962	0
69	4,985	0,109735	0,053224	0,015317	5,828928	0,405058	0,012042	1,640048	0,003161	0
70	5,085	0,112645	0,054559	0,015584	5,840970	0,405905	0,012689	1,622187	0,003400	0
71	5,185	0,115342	0,054691	0,015904	5,845518	0,406221	0,013304	1,587183	0,003605	0
72	5,290	0,118015	0,055750	0,016628	5,810010	0,404170	0,013927	1,576369	0,003865	0
73	5,391	0,120862	0,056330	0,016856	5,830021	0,405144	0,014608	1,544040	0,004119	0
74	5,492	0,123809	0,057288	0,017198	5,833508	0,405525	0,015329	1,535882	0,004465	0
75	5,591	0,126467	0,057796	0,018044	5,790637	0,402953	0,015994	1,501872	0,004749	0
76	5,690	0,129277	0,059078	0,018572	5,769012	0,402274	0,016713	1,513948	0,005097	0
77	5,790	0,131607	0,059879	0,019079	5,776793	0,401445	0,017335	1,505746	0,005476	0
78	5,891	0,134939	0,061017	0,019891	5,756344	0,399746	0,018209	1,496076	0,005920	0
79	5,990	0,137360	0,062067	0,020427	5,737638	0,398863	0,018869	1,497310	0,006325	0
80	6,085	0,139266	0,063726	0,020398	5,761490	0,400381	0,019395	1,544256	0,006761	0

TABLE OF RESULTS (CONT.)

I	ALFA	CL	CD	CM	XCP	XPP	CLSQ	@CD/CLSQ	CR	IND
81	6,185	0,142221	0,064059	0,021857	5,690919	0,395477	0,020227	1,526875	0,007240	0
82	6,286	0,144753	0,065735	0,022718	5,656798	0,393245	0,020948	1,526619	0,007704	0
83	6,389	0,147151	0,067031	0,023075	5,660292	0,393549	0,021623	1,535829	0,008137	0
84	6,474	0,149149	0,068473	0,023616	5,645326	0,392309	0,022245	1,559756	0,008577	0
85	6,576	0,151464	0,069056	0,024502	5,611977	0,389991	0,022947	1,572521	0,009103	0
86	6,677	0,153658	0,070490	0,025065	5,598543	0,389058	0,023611	1,576176	0,009618	0
87	6,775	0,156560	0,072079	0,025471	5,604735	0,389349	0,024511	1,595321	0,010212	0
88	6,870	0,158505	0,074417	0,026460	5,561195	0,386452	0,025124	1,607699	0,010757	0
89	6,971	0,160455	0,075968	0,026989	5,540806	0,385602	0,025745	1,638872	0,011305	0
90	7,072	0,163197	0,077984	0,027735	5,551700	0,386413	0,026653	1,659880	0,011958	0
91	7,150	0,165388	0,079864	0,027816	5,550861	0,386300	0,027585	1,664727	0,012605	0
92	7,143	0,166066	0,079843	0,027819	5,555486	0,386066	0,027577	1,670507	0,012545	0
93	7,143	0,165993	0,079697	0,026092	5,556682	0,386478	0,027554	1,673884	0,012532	0
94	7,109	0,165308	0,079329	0,027602	5,560839	0,386458	0,027327	1,666985	0,012349	0
95	7,009	0,162609	0,077919	0,027051	5,566894	0,386858	0,026442	1,665681	0,011682	0
96	6,911	0,160677	0,075729	0,025837	5,621260	0,390637	0,025817	1,625022	0,011100	0
97	6,811	0,158161	0,074035	0,025039	5,643574	0,392326	0,025015	1,609397	0,010477	0
98	6,712	0,155756	0,072196	0,024258	5,670570	0,394063	0,024294	1,585871	0,009908	0
99	6,612	0,153600	0,070815	0,023221	5,713390	0,397178	0,023593	1,569946	0,009378	0
100	6,514	0,151090	0,068719	0,022032	5,767779	0,400819	0,022825	1,530698	0,008825	0
101	6,419	0,148460	0,067019	0,022183	5,756508	0,398374	0,022040	1,508528	0,008344	0
102	6,319	0,146110	0,065094	0,021575	5,749798	0,399569	0,021348	1,504504	0,007868	0
103	6,217	0,142911	0,063357	0,020767	5,772838	0,401170	0,020464	1,497374	0,007338	0
104	6,116	0,140392	0,062238	0,020135	5,791353	0,402437	0,019710	1,480618	0,006865	0
105	6,018	0,137860	0,061442	0,019510	5,807953	0,403610	0,018950	1,449394	0,006400	0
106	5,916	0,134907	0,059039	0,018846	5,827811	0,404990	0,018200	1,421063	0,005927	0
107	5,815	0,132081	0,057754	0,018085	5,854907	0,406873	0,017446	1,384608	0,005486	0
108	5,712	0,129360	0,057029	0,017631	5,861314	0,407319	0,016759	1,384129	0,005099	0
109	5,611	0,126523	0,056004	0,017287	5,857814	0,407075	0,016003	1,388570	0,004745	0
110	5,504	0,122030	0,055514	0,017704	5,739165	0,400220	0,014873	1,446232	0,004395	0
111	5,402	0,120602	0,054271	0,016405	5,863825	0,407493	0,014547	1,429572	0,004108	0
112	5,293	0,117547	0,054269	0,015754	5,882999	0,408826	0,013827	1,481743	0,003858	0
113	5,190	0,114529	0,052704	0,015388	5,880064	0,408642	0,013117	1,447803	0,003568	0
114	5,088	0,111635	0,052453	0,015028	5,877471	0,408441	0,012452	1,482637	0,003317	0
115	4,986	0,108510	0,051200	0,014787	5,863075	0,407441	0,011774	1,477879	0,003089	0
116	4,884	0,105845	0,050426	0,014278	5,874321	0,408257	0,011203	1,530296	0,002864	0
117	4,784	0,104009	0,050427	0,013827	5,893910	0,409584	0,010618	1,527980	0,002737	0
118	4,678	0,101052	0,050122	0,013470	5,909790	0,410687	0,010212	1,601390	0,002573	0
119	4,574	0,098008	0,049763	0,012894	5,907424	0,410525	0,009506	1,655331	0,002422	0
120	4,469	0,095114	0,049523	0,012491	5,909723	0,410583	0,009047	1,760861	0,002279	0

TABLE OF RESULTS (CONT.)

I	ALFA	CL	CD	CM	XCP	XPP	CLSQ	BCD/CLSQ	CR	IND
121	4,554	0,092416	0,048738	0,012158	5,907492	0,410528	0,008541	1,775277	0,002120	0
122	4,258	0,089466	0,048560	0,011813	5,902693	0,410174	0,008004	1,847082	0,002020	0
123	4,158	0,086776	0,048353	0,011468	5,901626	0,410140	0,007550	1,933137	0,001941	0
124	4,056	0,084076	0,047928	0,011586	5,869551	0,407891	0,007089	1,987913	0,001859	0
125	3,956	0,081186	0,047205	0,010864	5,865349	0,408989	0,006591	2,037452	0,001738	0
126	3,849	0,078375	0,046976	0,010426	5,893117	0,409529	0,006143	2,083839	0,001613	0
127	3,748	0,075568	0,046077	0,010444	5,842361	0,406001	0,005711	2,154167	0,001486	0
128	3,643	0,073069	0,045927	0,009813	5,880681	0,408664	0,005359	2,276005	0,001375	0
129	3,536	0,070510	0,045736	0,009550	5,897142	0,409808	0,004972	2,403750	0,001267	0
130	3,429	0,067816	0,045402	0,009135	5,870600	0,408381	0,004599	2,484624	0,001165	0
131	3,321	0,065621	0,045085	0,008795	5,885342	0,408849	0,004306	2,626550	0,001119	0
132	3,217	0,063316	0,044776	0,008375	5,900283	0,410027	0,004003	2,744314	0,001062	0
133	3,114	0,061047	0,044443	0,008108	5,895129	0,409668	0,003727	2,862643	0,001050	0
134	3,001	0,058521	0,044334	0,007249	5,986771	0,415759	0,003425	3,082945	0,000945	0
135	2,896	0,056268	0,043804	0,007082	5,963239	0,414402	0,003166	3,167963	0,000915	0
136	2,787	0,054257	0,044081	0,006566	5,010154	0,417652	0,002942	3,503323	0,000793	0
137	2,677	0,052329	0,043893	0,005962	5,070150	0,422247	0,002738	3,621747	0,000841	0
138	2,567	0,050053	0,043748	0,005075	5,204752	0,431046	0,002505	3,780685	0,000712	0
139	2,458	0,048185	0,044099	0,004547	5,271423	0,435818	0,002322	4,446513	0,000932	0
140	2,355	0,046099	0,044288	0,004065	5,352008	0,440028	0,002125	4,946697	0,000957	0
141	2,245	0,043919	0,044206	0,003622	5,387792	0,443905	0,001927	5,407729	0,000940	0
142	2,134	0,041780	0,043915	0,003236	5,436859	0,447315	0,001745	5,808607	0,000922	0
143	2,025	0,039779	0,043691	0,002822	5,379950	0,373589	0,001584	5,259704	0,000919	0
144	1,917	0,037625	0,043748	0,002474	4,994605	0,347089	0,001415	7,044917	0,000949	0
145	1,807	0,035390	0,043652	0,002037	5,193524	0,360912	0,001252	8,044776	0,001022	0
146	1,695	0,033106	0,044008	0,001286	5,099949	0,354409	0,001095	9,335555	0,001095	0
147	1,587	0,030845	0,044436	0,000990	5,536434	0,384742	0,000951	9,999900	0,001094	0
148	1,480	0,028651	0,044301	0,000549	5,366602	0,442571	0,000820	9,999900	0,001097	0
149	1,374	0,026310	0,044284	0,000499	7,798017	0,541756	0,000693	9,999900	0,001071	0
150	1,265	0,023750	0,044391	0,000496	8,769077	0,609387	0,000564	9,999900	0,001079	0
151	1,159	0,021454	0,044001	0,001567	8,962982	0,622852	0,000460	9,999900	0,001089	0
152	1,049	0,019195	0,044031	0,002067	8,257861	0,573471	0,000368	9,999900	0,001087	0
153	0,941	0,017066	0,043906	0,002170	8,472323	0,449779	0,000291	9,999900	0,001064	0
154	0,835	0,014915	0,043872	0,001438	5,873744	0,408182	0,000222	9,999900	0,001096	0
155	0,724	0,012691	0,043589	0,000920	5,556404	0,385852	0,000161	9,999900	0,001104	0
156	0,615	0,010405	0,043752	0,000880	5,780982	0,471785	0,000108	9,999900	0,001118	0
157	0,509	0,008365	0,043823	0,000710	7,218574	0,501658	0,000070	9,999900	0,001144	0
158	0,397	0,005997	0,043917	0,001068	7,440566	0,517621	0,000056	9,999900	0,001152	0
159	0,288	0,003649	0,043953	0,000942	7,351081	0,510847	0,000013	9,999900	0,001162	0
160	0,179	0,001346	0,043980	0,001115	7,313659	0,508385	0,000002	9,999900	0,001147	0

TABLE OF RESULTS (CONT.)

I	ALFA	CL	CD	CM	XCP	XPP	CLSQ	BCD/CLSQ	CR	IND
161	0,064	=0,000995	0,043481	0,000859	5,250001	0,454329	0,000001	9,999900	0,001127	0
162	=0,046	=0,003326	0,043393	0,001183	5,929121	0,412051	0,000011	9,999900	0,001112	0
163	=0,161	=0,005718	0,044200	0,000037	5,509472	0,382868	0,000053	9,999900	0,001098	0
164	=0,270	=0,008000	0,044315	=0,000094	5,266529	0,365707	0,000064	9,999900	0,001096	0
165	=0,384	=0,010489	0,044025	=0,000776	5,007069	0,417447	0,000110	9,999900	0,001060	0
166	=0,490	=0,012851	0,045041	=0,000698	5,108700	0,450089	0,000165	9,999900	0,001014	0
167	=0,597	=0,015051	0,045638	=0,001095	5,904189	0,479652	0,000227	9,999900	0,000962	0
168	=0,705	=0,017555	0,045948	=0,001077	5,343096	0,440938	0,000308	9,999900	0,000908	0
169	=0,811	=0,019864	0,046260	=0,001056	5,654444	0,461045	0,000395	9,999900	0,000822	0
170	=0,922	=0,022431	0,046754	=0,001529	5,715966	0,397079	0,000503	9,999900	0,000761	0
171	=1,031	=0,024644	0,046977	=0,001645	5,075101	0,352683	0,000607	9,999900	0,000675	0
172	=1,145	=0,027211	0,047378	=0,002537	4,909514	0,341175	0,000740	9,999900	0,000575	0
173	=1,250	=0,041597	0,048113	=0,003184	5,445769	0,447934	0,001750	8,286100	0,000446	0
174	=1,355	=0,041597	0,048343	=0,003784	5,304597	0,438125	0,001750	8,416846	0,000310	0
175	=1,355	=0,041597	0,048343	=0,003784	5,304597	0,438125	0,001750	8,416846	0,000310	0

THE HYSTERESIS PRESENT ON THE TEST RESULTS IS AS FOLLOWS

INCIDENCE IS TAKEN AS THE INDEPENDENT VARIABLE WHILE VALUES OF K CORRESPOND TO VARIOUS CHARACTERISTICS

K = 1 FOR CL , =2 FOR CM ,=3 FOR CD , =4 FOR CR ,=5 FOR XCP

K	AV	RMS	OV	%AV	%RMS
1	0,000896	0,001884	0,207985	0,430810	0,905843
2	=0,000073	0,000959	0,033436	=0,219724	2,870668
3	=0,000599	0,005584	0,047310	=1,266637	11,380592
4	0,000021	0,000049	0,012864	0,166467	0,382918
5	=0,017579	0,845254	5,502150	=0,319501	15,361931
6	=0,001516	0,005588	0,047310	=3,204033	11,727348
7	=0,000525	0,001050	0,033436	=0,973194	3,141304
8	=0,018227	0,821668	5,502150	=0,332367	14,932940

MAIN – COMPUTER PROGRAM

STEADY RAMP TESTS

```
0007            MASTER MSBS AERODYNAMIC MEASUREMENTS
0008      C     AERODYNAMIC DATA REDUCTION FROM MEASURMENTS ON MAGNETIC SUSPENSION
0009      C     SYSTEM (MSBS) OF THE UNIVERSITY OF SOUTHAMPTON
0010      C     I**    STEADY AERODYNAMIC CHARACTERISTICS
0011      C     -*****
0012            DIMENSION XC(185,12),X(185),Y(185),W(185),CDLSQ(185),REC(10)
0013            DIMENSION ALFA(185),CL(185),CM(185),XCP(185),CD(185),CR(185)
0014            DIMENSION BDIR(4,4),BINT(4,4),ALF(25),VALF(25),C(10),A(10),B(4)
0015            DIMENSION BAUX(4,4),BAXU(4,4),Z(150,ZY(10),BINTA(4,4),BINTB(4,4)
0016            REAL INTMAG,INTMAGO
0017      C     INTMAG IS THE INTENSITY OF MAGNETISATION INDEX ( THE INTEGRATED
0018      C     E.M.F. VOLTAGE SIGNAL ) ( MAGNETOMETER READING)
0019      C     ***************************************
0020            DATA S,CA,CRM,XCM,AR/60.63,9.787,14.39,4.96,0.92/
0021      C     UNITS OF S : SQCM : CA,CR,&XCM ARE ALL IN CMS
0022            DATA A0,A1,A2,A3/0.0,84.3,0.0,0.0/
0023            DATA INTMAGO,EPS1,EPS2/9.37,0.02,0.00005/
0024      C     ************************************************************
0025            MTPT=185
0026            READ(1,105) IMOUSE
0027      C     IMOUSE IS AN INDEX SELECTING THE ALGORITHM OF DATA REDUCTION
0028      C        IMOUSE = 0 FOR DIRECT EVALUATION OF EXACT FORCES AT EACH PT
0029      C        IMOUSE = 1 FOR EVALUATION USING HOUSEHOLDER'S APPROX. METHOD
0030            NFM=4
0031      C     NFM IS THE NUMBER OF FORCES AND MOMENTS TO BE REDUCED
0032            PI=3.14159
0033            PII=PI*PI
0034            CRM2=CRM/2.
0035            READ (1,104) ((BDIR(I,J),I=1,NFM),J=1,NFM),((BINTA(I,J),I=1,NFM),
0036           *   J=1,NFM),((BINTB(I,J),I=1,NFM),J=1,NFM)



0037      C     UNITS OF BDIR(I,J) & BINT(I,J) ARE VOLT/GRAM(FORCE)
0038      C     IF UNITS ARE IN VOLTS/NEWTON CHANGE THE CONST.IN QS TO  0.0001
0039            READ (1,116) VDX
0040      C     VDX IS THE STATIC AXIAL FORCE SIGNAL=AXIAL DISPLACEMENT SIGNAL
0041      C     CALIBRATION COEFFICIENT
0042            READ (1,106)  NALF,NPA
0043      C     NALF = NO. OF PTS. COMPRISING THE INCIDENCE CALIBRATION CHARACT.
0044      C        NPA  :  ORDER OF POLYNOMIAL OF INCIDENCE CALIBRATION CHAR.
0045            READ (1,111) ( ALF(I),VALF(I) ,I=1,NALF)
0046            READ(1,105) ICASE
0047            DO 100 ICAS=1,ICASE
0048            READ(1,114)  PITRATE,TMSPACE
0049            READ (1,135) RHO,H,T,PA
0050      C     RHO = TUNNEL MANOMETER LIQUID DENSITY IN GM/C.C.
0051      C     H = TUNNEL MANOMETER HEIGHT DIFFERENCE IN CMS OF METHYLATED SPIRIT
0052      C     T = ROOM TEMP DEG CENTIGRADE
0053      C     PA = ATMOSPHERIC PRESS.   MM.  HG.
0054            READ(1,105) IDFDT
0055      C     PAR. IDFDT=1 IF WIND ON AND WIND OFF CALIB. (RECORING.)
0056      C        ARE DIFFERENT :  OTHERWISE  =0
0057            READ (1,107) (C(J),J=1,6),CREC
0058            IF(IDFDT.EQ.1)  READ(1,107) (REC(J),J=1,6),RCREC
0059            READ(1,119) INTMAG
0060            READ (1,102) MO,M,NAV,NINT,NV,NP
0061      C        MO  :  NO. OF POINTS WIND=OFF
0062      C        M   :  NO. OF POINTS WIND=ON
0063      C        NAV :  NO. OF SAMPLES IN AVERAGING INTERVAL
0064      C        NINT:  NO. OF SAMPLES SEPARATING EACH TWO CONSECUTIVE AVERAGED
0065      C                 POINTS
0066      C        NV  :  NO. OF VARIABLES REDUCED FROM RECORDING
0067      C        NP  :  ORDER OF POLYNOMIAL USED TO FIT THE WIND=OFF DATA BY LS
0068            NE = 2*NV
0069            INTMAG=INTMAG/INTMAGO
0070            WRITE(2,2001)
0071            WRITE(2,2002) S,CA,CRM,XCM,AR
0072            WRITE(2,2002) A0,A1,A2,A3
0073            WRITE(2,2002) PITRATE,TMSPACE
0074            WRITE(2,2003) ((BDIR(I,J),J=1,4),I=1,4)
0075            WRITE(2,2003) ((BINTA(I,J),J=1,4),I=1,4)
0076            WRITE(2,2003) ((BINTB(I,J),J=1,4),I=1,4)
0077            WRITE(2,2002) VDX
0078            WRITE(2,2004) NALF,NPA
0079            WRITE(2,2002) (ALF(I),VALF(I),I=1,NALF)
0080            WRITE(2,2002) RHO,H,T,PA
0081            WRITE(2,2004) MO,M,NAV,NINT,NV,NP
0082            WRITE(2,2002) (C(J),J=1,NV),CREC
0083            IF(IDFDT.EQ.1) WRITE(2,2002) (REC(J),J=1,6),RCREC
```

```
C     ***********************************************************
      NC=0
      DO 110 K=1,NAV/2
  110 NC=NC*K*K
      FNV=NAV
      FN1=N1+T
      FNC=NC
      CFN=FNC/FNV/FN1/FN1
      NV1=1
      KL=0
      MR=40
    2 CONTINUE
      DO 60 J=NV1,NV*NV1=1
      READ (1,108) (XC(I,J),I=1,MR)
C     DATA READ IN THE ORDER WIND OFF THEN WIND ON
C     FILES IN THE ORDER VALFA, VF , VM , VD , VR , VX
   60 CONTINUE
C     ***************************************
C     DATA CORRECTION DUE TO AVERAGING AND DIGITIZING ERRORS
C        LEAST SQUARES METHODIS ADOPTED
      IF(NV1,NE,1) GO TO 3001
      DO 3005 I=1,6
 3005 A(I)=XC(175-I,6)
      IF(NV1,EQ,1) CALL RARG(XC,MTPT,12,MD)
      GO TO 3002
 3001 CALL RARG2(XC,MTPT,12,A,6,M)
 3002 CONTINUE
      LS=3
      LS1=LS*1
      LSM=MR=LS
      DO 115 J=NV1,NV*NV1=1
      DO 135 I=LS1,LSM
      CALL SMTH(XC,MTPT,12,MR,I,J,LS,DERV)
      CFDR=CFN*DERV
      IF(I,NE,LS1) GO TO 126
      K1=1
      K2=I
      GO TO 128
  126 IF(I,NE,LSM) GO TO 127
      K1=I
      K2=MR
  128 DO 130 K=K1,K2
  130 Y(K)=XC(K,J)=CFDR
      GO TO 135
  127 Y(I)=XC(I,J)=CFDR
  135 CONTINUE
      DO 140 I=1,MR

  140 XC(I,J)=Y(I)
  115 CONTINUE
      KL=KL*1
      MR=4
      IF(KL,EQ,2)  GO TO 3
      NV1=7
      GO TO 2
    3 CONTINUE
      XC(1,6)=XC(2,6)
      XC(1,7)=XC(2,7)
C     ***********************************************************
      QMAN=RHO*H
      QCAL=QMAN*64,3
      V   = SQRT(2,0*QCAL)
      TA  = 273,0+T
      DEN = 0,4642*PA/TA
      Q   = DEN*QCAL
C     TRUE  DYNAMIC HEAD
      VM  =,0493*V/SQRT(TA)
C     TRUE  REYNOLDS NUMBER
      RN  = 0,00317*V*CRN*PA*(TA*114,0)*TA**(=2,5)
      QS=2*S*0,0102
      QSC= QS*CA
      QSC1=QS*3,73
      WRITE(2,2004)
      WRITE(2,201)
      WRITE(2,202)
      WRITE(2,203)
      WRITE(2,204) S,CA,AR
      WRITE(2,205)
      WRITE(2,206) V,Q
      WRITE(2,207)VM, RN
      WRITE(2,231) PITRATE
      WRITE(2,209)
      DO 5 I=1,40
    5 X(I) = XC(I,1)
      NMAX = NP *1
      DREC=REC(1)/C(1)
      DO 10 J=2,NV
      DO 15 I=1,MD
   15 Y(I) = XC(I,J)
      IND=0
C     POLYNOMIAL CURVE FITTING OF THE WIND-OFF DATA USING LEAST
C     SQUARES TECHNIQUE UP TO ORDER=NP
      CALL LSQC(X,Y,MD,A,NP,IND,RES)
      NJV=NV*J
      DREC(J)=REC(J)/C(J)
```

```
                DO 25 I=1,M
                XCNV=AC(I,/)
                IF(IDPDT.EQ.1)  XCNV=XCNV*DREC
                SUM=A(1)
                DO 30 K = 2,NMAX
             30 SUM=SUM+A(K)*XCNV**(K-1)
                IF(IDPDT.EQ.1)  SUM=SUM/DRECJ
             25 XC(I,J)=(XC(I,NJV)-SUM)/C(J)
C       WIND OFF DATA HAS BEEN SUBTRACTED
C       CORRECTION DUE TO AMPEX D.C GAIN IS APPLIED
             10 CONTINUE
                DO 405 I=1,M
C       CORRECTION OF DRAG SIGNAL FOR AXIAL POSITION DRIFT
            405 XC(I,4) = XC(I,4) - VDX*XC(I,5)
                NMAXA = NPA+1
                IND=0
                CALL  LSQC(VALF,ALF,NALF,A,NPA,IND,RES)
C  FIND  THE  INCIDENCE  CALIBRATION  EQUATION
                N=NFM
                NA = N*N
                IN = 1
                DDF=PITRATE*TMSPACE
C       INCIDENCE RESOLUTION OF PITCH RAMP TEST, ALONG CONST. PITCH RATE
                IF(IHOUSE.EQ.0) GO TO 304
                AMAX=0.
                AMIN=100.
                CCCCC=C(1)
                DO 305 I=1,M
                SUM=A(1)
                XCXX=(XC(I,7)-CREC)/CCCCC
                DO 315 K=2,NMAXA
            315 SUM=SUM+A(K)*XCXX**(K-1)
                ALFA(I)=SUM
                IF(AMAX.LT.SUM)  AMAX=SUM
                IF(AMIN.GT.SUM)  AMIN=SUM
            305 CONTINUE
C       CALCULATION OF 'NA1' & 'NA2'  AND FINDING 'NINV'
                WRITE(2,241)
                ABCD=AMAX
                IAI=0
            306 DO 310 I=1,N

                DO 310 J=1,N
            310 BAUX(I,J)=BDIK(I,J)*ABCD*(BINTA(I,J)*ABCD*BINTB(I,J))
                ACCUR=0.00001
                CALL FPMGEIN(N,ACCUR,Z(1),W(1),DET,NRR)
                IF(NRR.EQ.128)  WRITE(2,242) ABCD,ACCUR,IRANK



                DO 320 I=1,N
                DO 320 J=1,N
                SUM=0.
                DO 325 K=1,N
            325 SUM=SUM+BAUX(I,K)*(BINTA(K,J)*ABCD*BINTB(K,J))
                ZY(I+N*(J-1))=SUM
            320 CONTINUE
                CALL FPDET(ZY,N,NA,D,ID,W,IT)
                DETER=D*2.**ID
                NAAA =IFIX(0.005/DDF/ABS(DETER))
                IF(IAI.GT.0)  GO TO 311
                NA1=NAAA
                IAI=IAI+1
                ABCD=AMIN
                GO TO 306
            311 NA2=NAAA
                NA3=(4*M)/10
                NINV=MIN0(NA1,NA2,NA3)
                IF(NINV.LT.NA3)  WRITE(2,243) NINV
                IF(NINV.GE.NA3) NINV =M
C
                EPS10=0.00001
                IR=1
                DO 330 I=1,M
                IF(I.EQ.1) GO TO 333
                IF(NINV.EQ.M) GO TO 331
                NIRA=NINV*IR
                IA=(I/NIRA)*(NIRA/I)
                IF(IA.EQ.0) GO TO 331
            333 CONTINUE
                XC(I,6)=0.0
                AXF=ALFA(I)
                DO 335 J=1,N
                IF(I.EQ.1) B(J)=0.
                DO 335 K=1,N
            335 BAUX(J,K)=BDIK(J,K)*AXF*(BINTA(J,K)*AXF*BINTB(J,K))
                ACCUR=0.00001
                CALL FPMGEIN(N,ACCUR,Z(1),W(1),DET,NRR)
                DO 340 J=1,N
                SUM=0.
                DO 345 K=1,N
            345 SUM=SUM+BAUX(J,K)*XC(I,K+1)
                IF(ABS(SUM).LT.EPS10) GO TO 340
                IF(ABS((SUM-B(J))/SUM).GT.0.005.AND.I.NE.1)  WRITE(2,244) I
            340 B(J)=SUM
                GO TO 332
C
```

```
C     ***********************************
C     HOUSEHOLDER'S APPROXIMATE FORMULA FOR MODIFYING THEINVERSE CALIBR,
C     MATRIX IS GIVEN BY :
C             BAUX=BAUX L1,*DALF*BINT*BAUXJ
C
      331 DEN=ALFA(I)=ALFA(I-1)
          XC(I,0)=1,0
          DO 350 J=1,N
          SUM1=0,
          DO 355 K=1,N
          SUM2=0,
          DO 360 L1=1,N
          SUM3=0,
          DO 365 L=1,N
      365 SUM3=SUM3+(BINTA(L1,L)+AXF*BINT3(L1,L))*BAUX(L,K)
      360 SUM2=SUM2+BAUX(J,L1)*(((L1/K)*(K/L1))-DEN*SUM3)
          BAUX(J,K)=SUM2
      355 SUM1=SUM1+SUM2*XC(I,K-1)
      350 B(J)=SUM1
          DO 370 J=1,N
          DO 370 K=1,N
      370 BAUX(J,K)=BAUX(J,K)
      332 CONTINUE
          GO TO 332
      305 CONTINUE
      350 CONTINUE
C
C     ***********************************
C
      304 CONTINUE
          IF(IHOUSE.EQ.1) GO TO 301

          CCCCC=C(1)
          IA2=0
          DO 35 I=1,M
          SALF=A(1)
          XYZ=(AC(1,7)-CREC)/CCCCC
          DO 505 K=2,NMAXA
      505 SALF=SALF+A(K)*XYZ**(K-1)
          ALFA(I)=SALF
          DO  40  K=1,N
          B(K)    = AC(I,K+1)
          DO  40  L=1,N
       40 Y(K+N*(L-1))=BDIR(K,L)+SALF*(BINTA(K,L)+SALF*BINTB(K,L))
C     Y  IS  THE  TOTAL  FORCE & MOMENT  CALIB  MATRIX  INCLUDING  THE
C     DIRECT  AND  INTERACTION  (DUE  TO  INCIDENCE )  PARTS
C     ELEMENTS  OF  VECTOR  B  REPRESENT  THE  NET  AERODYNAMIC  LIFT



C     PITCHING  MOMENT  AND  DRAG  FORCES  ACTING  ON  THE  MODEL
      CALL F4SOLVE( Y,B,N,NA,N ,IN,D,ID,IT,W)
      IF(IT.EQ.-1)  WRITE(2,253) D,ID
  302 CONTINUE
      DO 400 JKL=1,N
  400 B(JKL)=INTMAG*B(JKL)
      CL(I) = 1.0/QS*B(1)
      CM(I) = 1.0/QSC*B(2)
C     THIS IS THE MOMENT COEFF. @ THE CENTRE OF MOMENT OF THE FORCE
C     CALIBRATION .
C     THE MOMENT COEFF. ABOUT HALF ROOT CHORD IS  :
      CM(I)=CM(I)-CL(I)*(CRH2-XCM)/CA
      CD(I) = 1.0/QS*B(3)
      CR(I)=1./QSC1*B(4)
      IF(IHOUSE.EQ.1) GO TO 303
   55 CONTINUE
  301 CONTINUE
C     DATA CORRECTION DUE TO AERODYNAMIC DYNAMIC EFFECTS
      CLMX=0.
      CLMN = 1.0
      DO 120 I=1,M-1
      GO TO 121
      IF(I.NE.1)  GO TO 121
      TP11=CL(I)
      TP21=CM(I)
      TP31=CD(I)
      TP41=CR(I)
      GO TO 120
      TP22=CM(I)
      TP32=CD(I)
      TP42=CR(I)
      TP13=CL(I+1)
      TP23=CM(I+1)
      TP33=CD(I+1)
      TP43=CR(I+1)
      TP14=TP12
      TP24=TP22
      TP34=TP32
      TP44=TP42
      CL(I)=5,*(TP13-TP12)+TP11
      CM(I)=5,*(TP23-TP22)+TP21
      CD(I)=5,*(TP33-TP32)+TP31
      CR(I)=5,*(TP43-TP42)+TP41
      TP11=TP14
      TP21=TP24
      TP31=TP34
      TP41=TP44
```

```
      141 CONTINUE
          ABLM=ABS(CL(I))
          IF(ABLM.GT.CLMN)  GO TO 41
          CLMN=ABLM
          KM=I
       41 IF(CLMX.LT.ABLM)  CLMX=ABLM
      140 CONTINUE
C     TUNNEL WALL CORRECTION
C     LEAST SQUARES CL-ALFA CURVE FIT TO FIND A ROUGH ESTIMAT OF
C                                          DCL/DALFA
C     FOR PURPOSE OF TUNNEL WALL CORRECTION
          NCLF=5
          CALL LSQC(ALFA,CL,M,A,NCLF,0,RES)
          U1=A(2)
          U2=A(3)
          U3=A(4)
          U4=A(5)
          U5=A(6)
          AFMX=-10.
          AFMN=10.
          DO 125 I=2,M-1
          ALX=ALFA(I)
          IF(ALX.GT.AFMX) AFMX=ALX
          IF(ALX.LT.AFMN) AFMN=ALX
          CLZ=CL(I)
          DALF=0.03535*CLZ
          DCD=0.023*CLZ*CLZ
          DCLF=U1+ALX*(2.*U2+ALX*(3.*U3+ALX*(4.*U4+ALX*(5.*U5))))
          DCM=0.00351*CLZ*DCLF
          ALFA(I)=ALFA(I)+DALF
          CD(I)=CD(I)+DCD
          CM(I)=CM(I)+DCM
      125 CONTINUE
C     A 'FALSE' CORRECTION TO THE END POINTS
          ALFA(1)=ALFA(2)
          ALFA(M)=ALFA(M-1)
          CL(1)=CL(2)
          CL(M)=CL(M-1)
          CD(1)=CD(2)
          CD(M)=CD(M-1)
          CM(1)=CM(2)
          CM(M)=CM(M-1)
          CR(1)=CR(2)
          CR(M)=CR(M-1)
C
          CDMIN=(CD(KM)+CD(KM+1)+CD(KM-1)+CD(KM+2)+CD(KM-2))/5.
C
          EPS1=AMAX1(EPS1,(CLMX/4.0))
          DO 45 I=1,M
          IF(I.LE.2.OR.I.GE.M-2)  GO TO 44

          IF(ABS(CL(I)).GT.EPS1)  GO TO 42
          DCLM=CL(I+2)-CL(I-2)
          DDD=PII*AR*DDF/144.
          IF(ABS(DCLM).LT.DDD)  DCLM=SIGN(DDD,DCLM)
C     THIS MAKES SURE THAT A REASONABLE ESTIMATE OF  '@CM/@CL'  AT COND.
C     WHEN  CL  IS ALMOST CONSTANT
          XAVSL=(CM(I+2)-CM(I-2))/DCLM
C     THIS IS AN APPROX. TO THE AVERAGE SLOPE @CM/@CL AT SMALL CL
C     THE RESULTING CENTRE IS THE AERODYNAMIC CENTRE
          XCP(I)=CRM2-CA*XAVSL
          GO TO 43
       44 IF(ABS(CL(I)).LT.EPS1)  CL(I)=SIGN(EPS1,CL(I))
       42 XCP(I)=CRM2-CA*CM(I)/CL(I)
C     LOCATION OF C.P. FROM THE  WING APEX
       43 CONTINUE
          IF(ABS(XCP(I)).GT.25.)  XCP(I)=SIGN(25.0,XCP(I))
          SCL=CL(I)*CL(I)
          IF(SCL.GT.EPS2)  GO TO 46
          DCD       = (CD(I) -CDMN)/EPS2
          GO TO 47
       46 DCD      =(CD(I)-CDMIN)/SCL
       47 IF(ABS(DCD).GT.9.9999)  DCD=SIGN(9.9999,DCD)
          CDLSQ(I)=DCD
       45 CONTINUE
          MST=1
          MDEL=20
          WRITE(2,210)
       51 MPIN=MST+MDEL
          IF(MST.GT.1)  WRITE(2,219)
          WRITE(2,214)
          DO 50 I=MST,MPIN
          SCL=CL(I)*CL(I)
          XPP=XCP(I)/CRM
          DCD = CDLSQ(I)
          SCR=CR(I)
          LFR=IFIX(XCP(I)*10)
          WRITE(2,215)I,ALFA(I),CL(I),CD(I),CM(I),XCP(I),XPP,SCL,DCD,SCR,LFR
          GO TO 50
          WRITE(4,217)I,ALFA(I),CL(I),CD(I),CM(I),XCP(I),XPP,SCL,DCD,SCR
       50 CONTINUE
          MST=MPIN+1
          IF(MPIN.GE.M)  GO TO 52
          MDEL=M-MST
```

```
      IF(MDEL.GT.39)  MDEL=39
      GO TO 21
   22 CONTINUE
      WRITE(6) W/PITRATE
      WRITE(6) ALFA
      WRITE(6) CL
      WRITE(6) CD
      WRITE(6) CM
      WRITE(6) XCP
      WRITE(6) CDLSQ
      WRITE(6) CR
C
C  CHECK ON HYSTERESIS EFFECT
      CALL HYSTER(1,M,ALFA,CL)
      CALL HYSTER(2,M,ALFA,CM)
      CALL HYSTER(3,M,ALFA,CD)
      CALL HYSTER(4,M,ALFA,CR)
      CALL HYSTER(5,M,ALFA,XCP)
      CALL HYSTER(6,M,CL,CD)
      CALL HYSTER(7,M,CL,CM)
      CALL HYSTER(8,M,CL,XCP)
 1005 CONTINUE
  102 FORMAT(5I0)
  103 FORMAT(4F0.0)
  104 FORMAT(8F0.0/8F0.0/8F0.0/8F0.0/3F0.0/8F0.0)
  106 FORMAT(2I0)
  107 FORMAT(10F0.0)
  108 FORMAT(10F0.0)
  111 FORMAT(12F0.0)
  114 FORMAT(2F0.0)
  116 FORMAT(F0.0)
  119 FORMAT(F0.0)
  201 FORMAT(1H1,41H MAGNETIC   SUSPENSION SYSTEM    (MSBS)              )
  202 FORMAT(1HO,50H STEADY AERODYNAMICS TESTING ** DATA REDUCTION     )
  203 FORMAT(1HO,42H APPROX, AGARD-G WING   MODEL                      )
  204 FORMAT(1HO,19H WING REF. AREA =         ,F6.2,3X,4HSQC",8X,
     1   21 H MEAN AEROD. CHORD =     ,F6.2,3X,2HCM,8X,15HASPECT RATIO =
     2  ,F6.2)
  206 FORMAT(1HO,15H FLOW SPEED =  ,F6.1,3X,5HM/S,9X,14HDYNAMIC HEAD = ,
     1      F7.2,4X,3HN/SQM )
  207 FORMAT(1HO,12H MACH NO. =  ,F6.3,8X,23HTEST REYNOLDS NO. =      ,
     1    F6.2,4X,7HMILLION         )
  208 FORMAT(1HO,45H SURFACE CONDITION :: WITH TRANS STRIPS           )
  209 FORMAT(/////////)
  212 FORMAT(1H1,/50X,'TABLE   OF    RESULTS'/)
  214 FORMAT(1HO,1X,'I',4X,'ALFA', 9X,'CL',11X,'CD',11X,'CM',11X,
     1   'XCP',10X,'XPP',9X,'CLSQ',8X,'CD/CLSQ',8X,'CR',4X,'IND'/)



  216 FORMAT(1H ,I3,2X,F7.3,8(3X,F10.5),5X,I1)
  217 FORMAT(10X,I3,9(2H   ,F10.5,1H   ))
  219 FORMAT(1H1,/45X,'TABLE    OF    RESULTS (CONT.)'/)
  231 FORMAT(1HO,'INCIDENCE RAMP RATE  = ',F10.3)
  241 FORMAT(1H1)
  242 FORMAT(1H ,'AT ALFA =',F10.5,2X,'MATRIX IS SINGULAR WITH DET. <',
     1   F11.7,2X,'AND RANK = ',I10)
  243 FORMAT(1H ,'THE NUMBER OF CONSECUTIVE POINTS THAT CAN BE CALCULATE
     1D BEFORE NEEDING A CHECK WITH THE EXACT FORMULA =',I5,2X,'PTS')
  244 FORMAT(1H ,'ERROR RESULTING FROM USE OF APPROXIMATE INVERSE CALIBR
     1ATION MATRIX IS > 0.5# AT THE',I5,'-TH POINT')
  248 FORMAT(////2X,'COEFF. OF POLYNOMIAL OF LS CURVE FITTING OFINCIDENCE
     1  CALIBRATION UP TO DEGREE',I4)
  249 FORMAT(1H1,'COEFF. OF POLYNOMIAL CURVE FITTING OF WIND OFF DATA
     1AS FUNCTIONS OF ALFA UP TO DEGREE',I4,3X,'IN THE SEQUENCE VF,...,VX
     2'/// 9X,'A0',13X,'A1',13X,'A2',13X,'A3',13X,'A4',13X,'A5',13X,'A6'
     3,5X,'RESIDUAL')
  251 FORMAT(1HO,8F15.5)
  253 FORMAT(1HO,30X,'THE CALIBRATION MATRIX IS SINGULAR WITH A DETERMI
     1 ',4X,F10.5,5('**',I3)
  291 FORMAT(1HO,I5,5X,5F15.8)
 2001 FORMAT(1HO,'  INPUT    DATA  '//)
 2002 FORMAT(1HO,(20X,8F12.5))
 2003 FORMAT(1HO,4(10X,4F16.9/))
 2004 FORMAT(1HO/10X,8I10)
 2006 FORMAT(1HO,3(20X,A8/))
      STOP
      END



      SUBROUTINE HYSTER(K,M,X,Y)
      DIMENSION X(M),Y(M)
      N=M/2
      IF(1+2*N.EQ.M) M=M-1
      YMX=-1000.
      YMN=1000.
      DO 5 I=1,M
      IF(YMX.LT.Y(I)) YMX=Y(I)
      IF(YMN.GT.Y(I)) YMN=Y(I)
    5 CONTINUE
      DYMYMX=YMN
      AV=0.0
      SQ=0.0
      KJ=0
```

```
      DO 15 J=1,N
      XO=X(J)
      I1=M-5*J
      I2=M+1-J
      KK=0
    1 DO 10 I=I1,I2
      H=XO-X(I)
      IF(I.EQ.I1) GO TO 10
      IF(G*H.LE.0.0) GO TO 6
   10 G=H
      IF(KK.EQ.0) GO TO 7
      KJ=KJ-1
      GO TO 15
    7 I1=N+1
      I2=M
      KK=KK+1
      GO TO 1
    6 Z=(G*Y(I)-H*Y(I-1))/(G-H)
      YZ=Y(J)-Z
      AV=AV+YZ
      SQ=SQ+YZ*YZ
      KJ=KJ+1
   15 CONTINUE
      FKJ=FLOAT(KJ)
      AV=AV/FKJ
      FSQKJ=SQ/FKJ-AV*AV
      IF(FSQKJ.GE.0.) RMS=SQRT(FSQKJ)
      FAV=AV*100./OV
      FRMS=RMS*100./OV
      IF(K.EQ.1) WRITE(2,201)
      IF(K.EQ.1) WRITE(2,202)
      WRITE(2,203) K,AV,RMS,OV,FAV,FRMS
  201 FORMAT(1H1,30X,'THE HYSTERESIS PRESENT ON THE TEST RESULTS IS AS
     *FOLLOWS'///5X,'INCIDENCE IS TAKEN AS THE INDEPENDENT VARIABLE WHIL
     *E VALUES OF  K  CORRESPOND TO VARIOUS CHARACTERISTICS'//10X,'K = 1
     *  FOR  CL ,=2  FOR  CM ,=3 FOR  CD ,  =4  FOR  CR ,=5 FOR  XCP'/)
  202 FORMAT(1HO,25X,'K',8X,'AV',12X,'RMS',13X,'OV',12X,'%AV',12X,'%RMS'
     *)
  203 FORMAT(1HO,25X,I3,5F15.6)
      RETURN
      END

      SUBROUTINE  LSQC(X,Y,M,A,N,IND,RES)
      DIMENSION  X(M),Y(M),A(10)
      N1=N+1
      CALL EQ2ACF(X,Y,M,A,N1,RES)
      RETURN
      END


      SUBROUTINE  CARA(X,Y,N)
      DIMENSION  X(N),Y(N),A(10)
      CALL LSQC(X,Y,N,A,4,0,R)
      WRITE(2,201) (A(I),I=1,4)
  201 FORMAT(1HO,'THE COEFF OF POL. FITTING OF CD(CL) ARE'///10X,4F15.6)
      RETURN
      END

      SUBROUTINE SMOOTH(Z,M,N,K,MM,L)
      DIMENSION Z(M,N),X(25),Y(25),A(10)
      NO=1
      IF(K.GT.6) NO=7
      M1=1
    1 M2=M1+L-1
      DO 5 I=M1,M2
      II=I-M1+1
      X(II)=Z(I,NO)
    5 Y(II)=Z(I,K)
      CALL LSQC(X,Y,L,A,3,0,R)
      AO=A(1)
      A1=A(2)
      A2=A(3)
      A3=A(4)
      DO 10 I=M1,M2
      ZZ  =Z(I,NO)
   10 Z(I,K )=AO+ZZ*(A1+ZZ*(A2+ZZ*A3))
      IF((MM-M2).LT.L) GO TO 2
      M1=M2+1
      GO TO 1
    2 CONTINUE
      RETURN
      END


      SUBROUTINE SMTH(X,K,M,NA,I,J,LS,A)
      DIMENSION  X(M,N),Y(20),Z(20),B(10)
      LS1=LS+1
      LL=LS1+LS
      DO 5 II=1,LL
      JK=II-LS1
      Y(II)=JK
    5 Z(II)=X(I+JK,J)
      CALL LSQC(Y,Z,LL,B,2,0,R)
      A=B(1)
      RETURN
      END
```

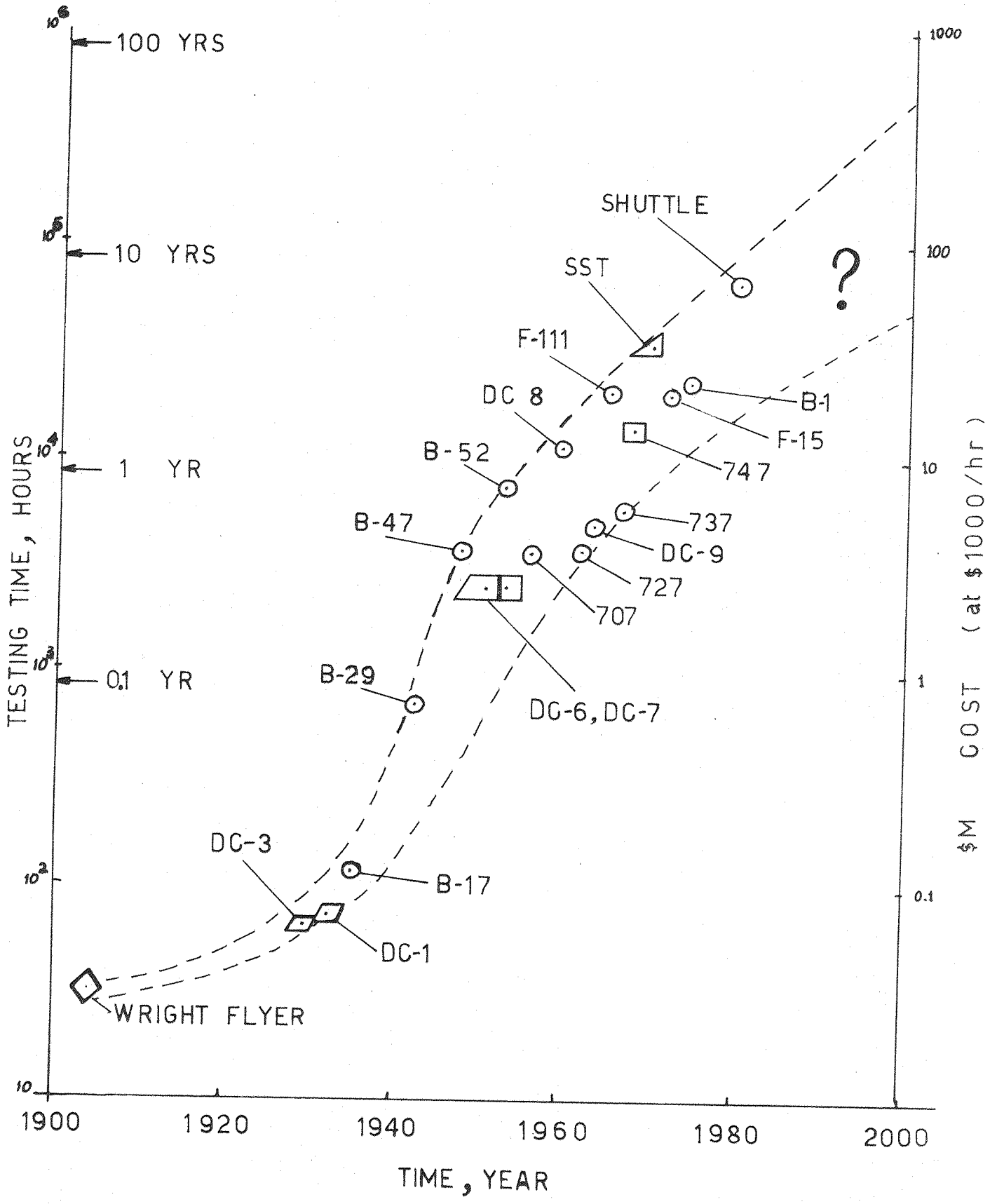

FIG. 1.1 TREND IN WIND TUNNEL TESTING

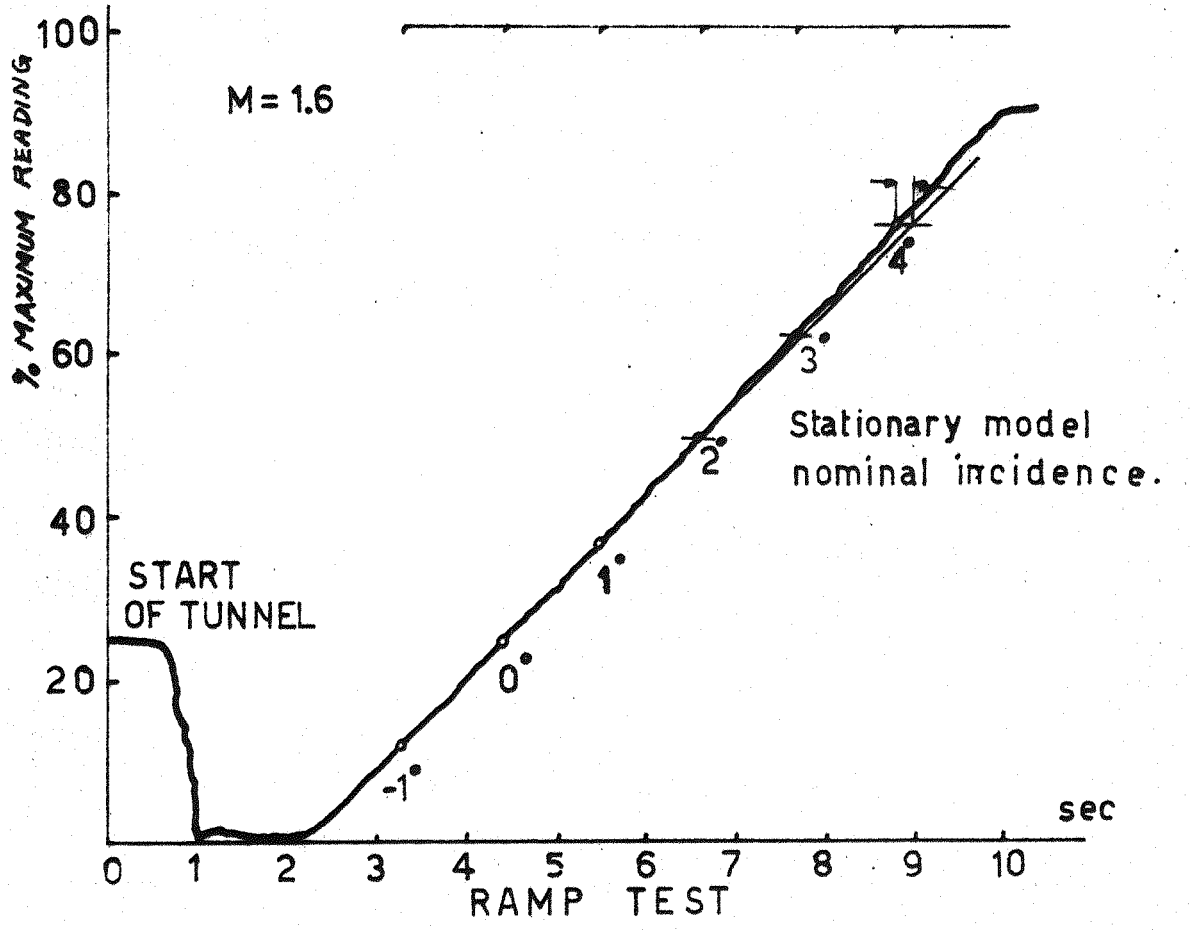

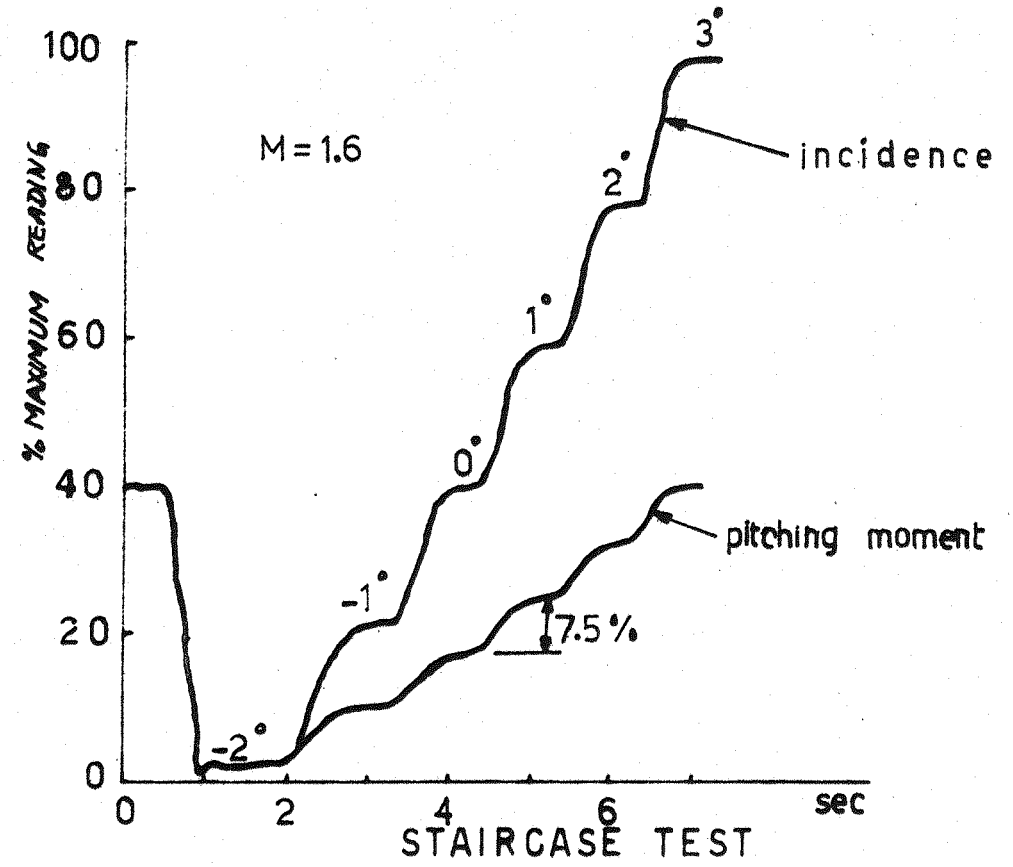

FIG. 2-1 INCIDENCE AND PITCHING MOMENT
[Ref. LUKASIEWICZ (1955)]

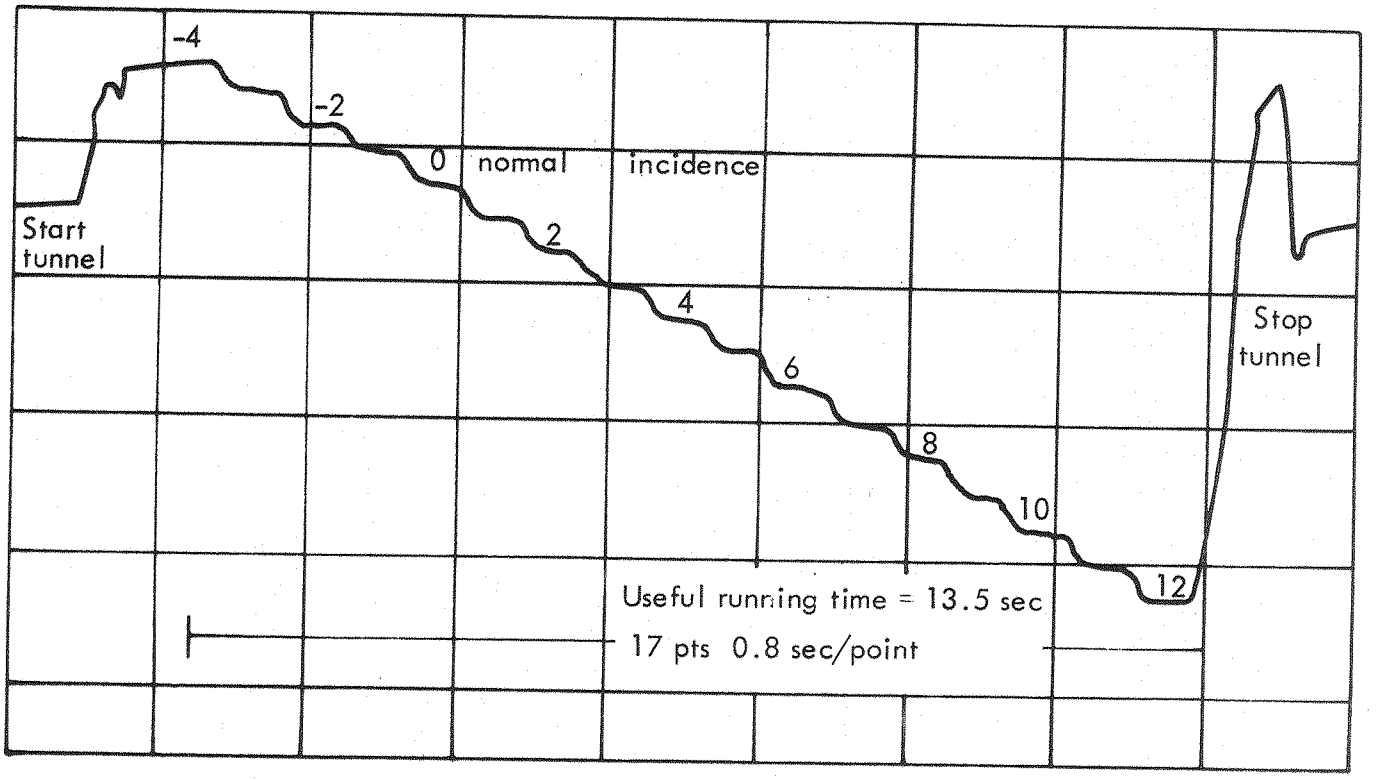

FIG. 2.2. TYPICAL RECORD OF NOMINAL FORCE OBTAINED ON A DELTA WING HALF MODEL . M = 1.22 [Lukasiewicz (1955)]

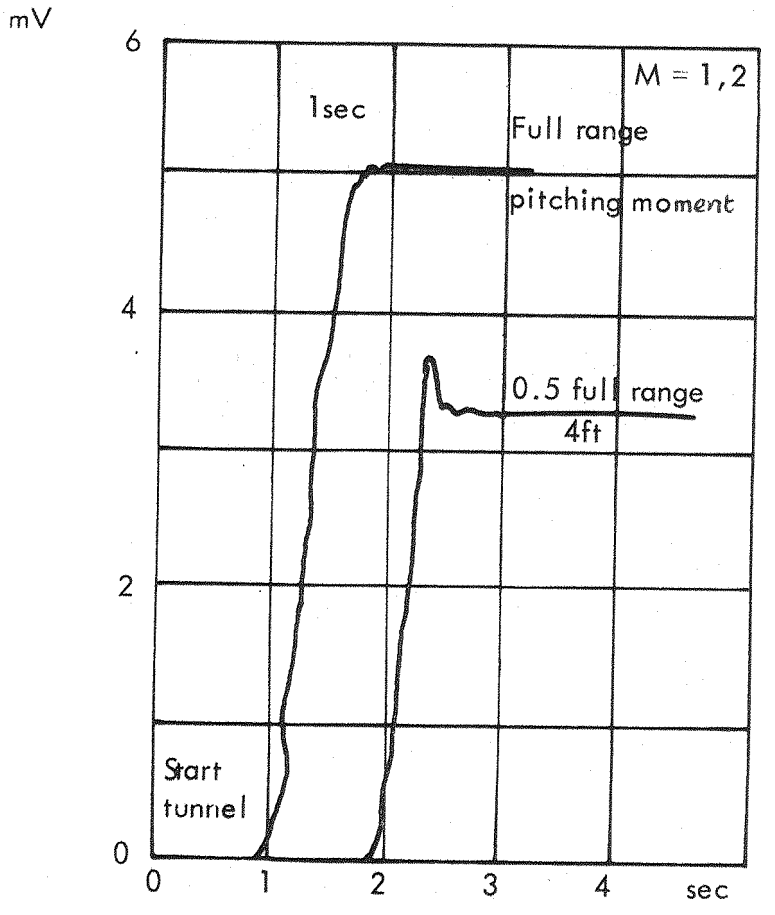

FIG. 2.3. RECORDER RESPONSE TO STRAIN GUAGE BALANCE OUTPUT FROM Lukasiewicz (1955)

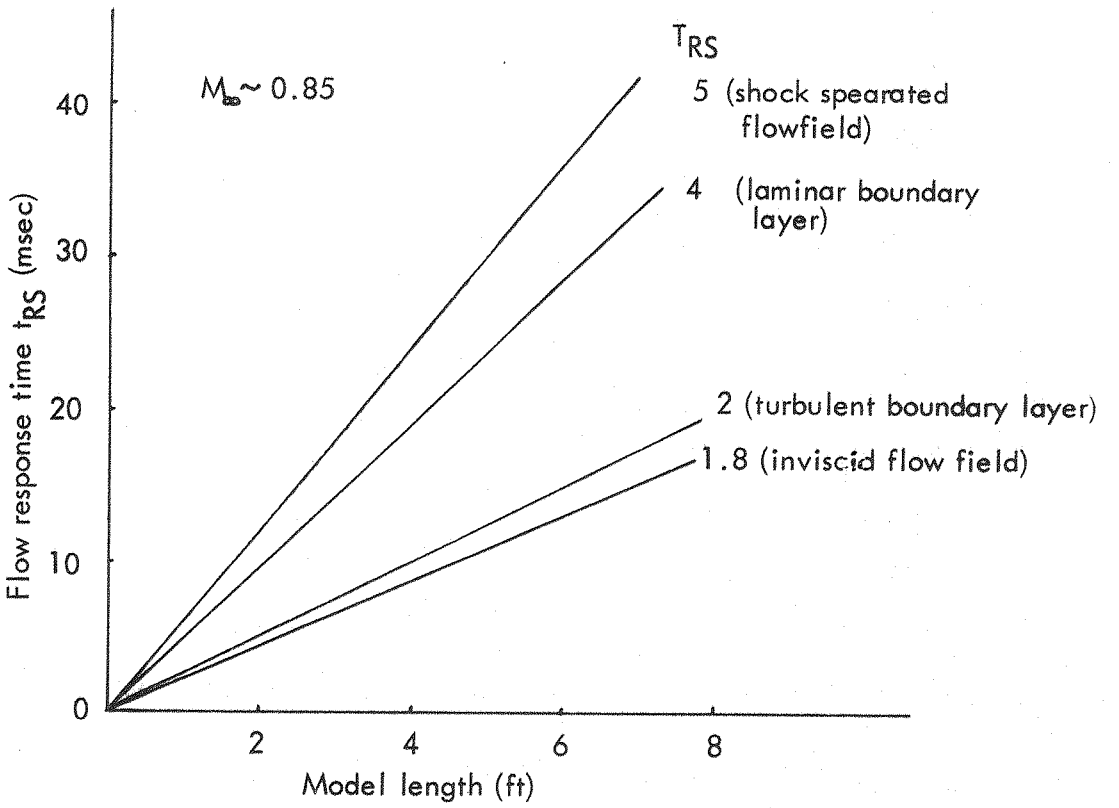

FIG. 2.4. FLOW RESPONSE TIME FOR VARIOUS FLOW PATTERNS.

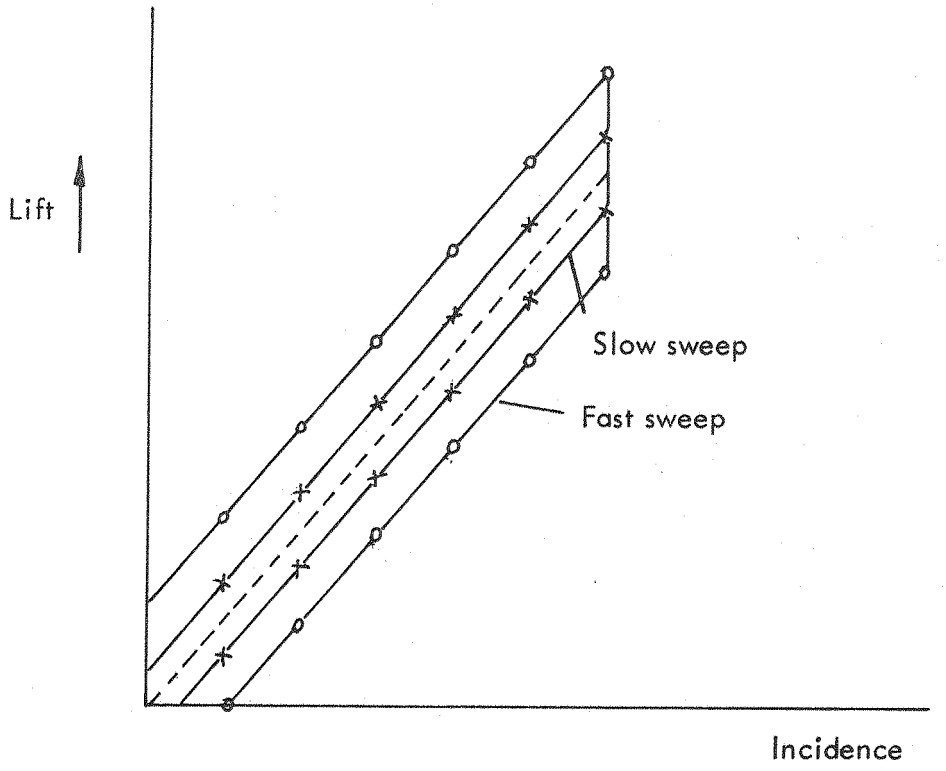

FIG. 2.5. A SCHEMATIC OF THE EFFECT OF INCIDENCE SWEEP RATE ON MEASURED FORCE.

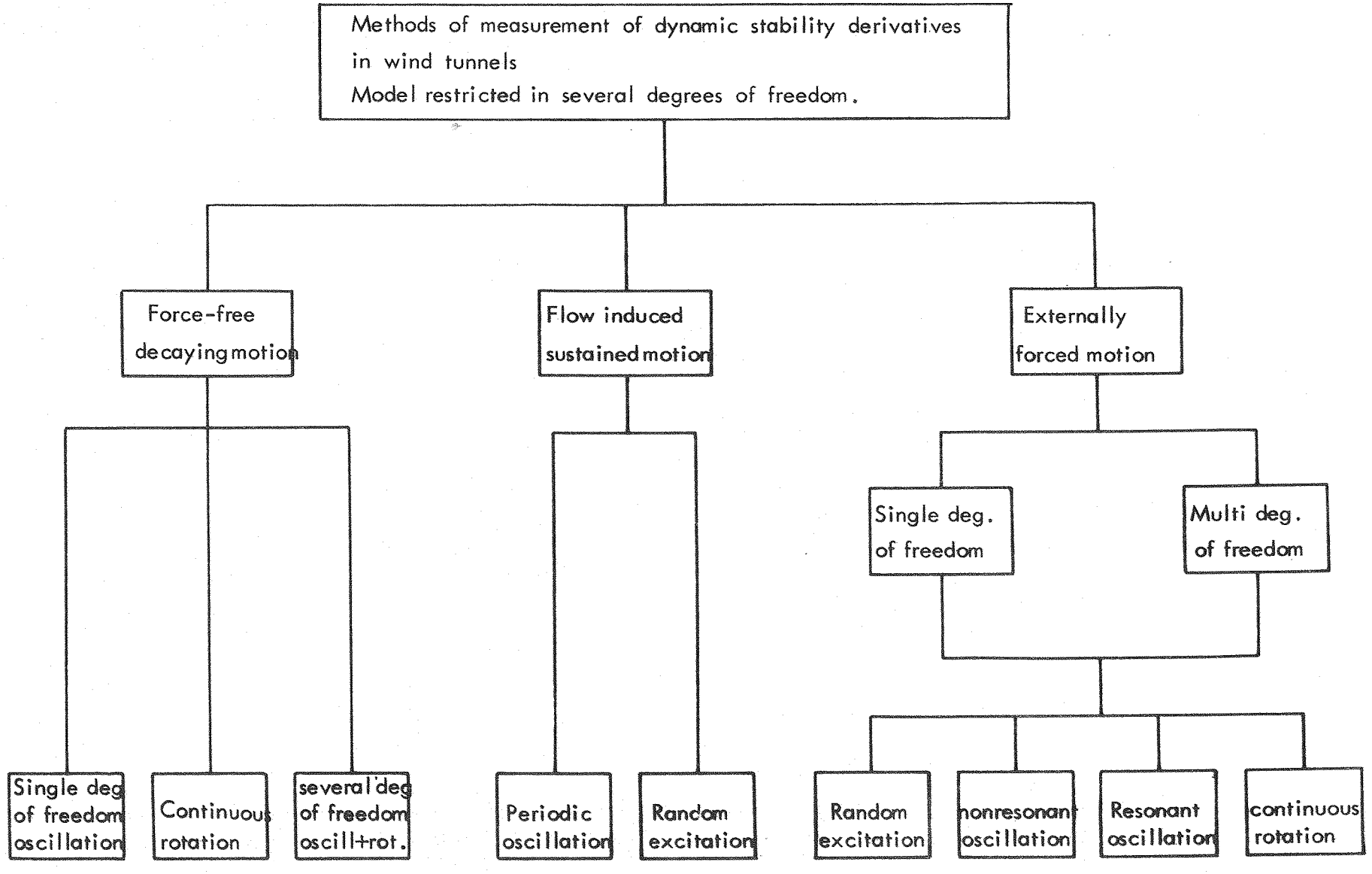

FIG. 2.6. METHODS FOR DYNAMIC STABILITY DERIVATIVE MEASUREMENT IN WIND TUNNELS.

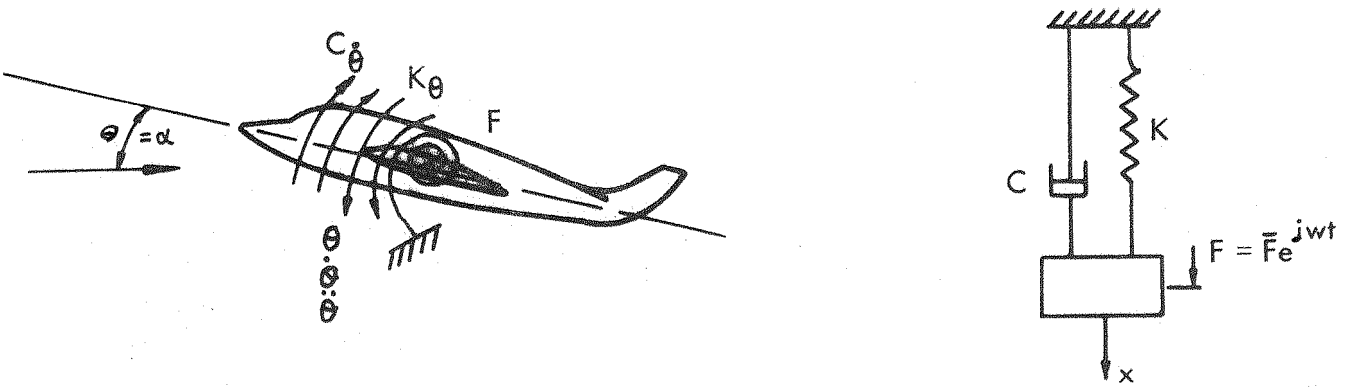

FIG. 2.7. A MODEL UNDERGOING PURE PITCHING OSCILLATION AND EQUIVALENT 2nd ORDER SPRING-MASS DASHPOT SYSTEM.

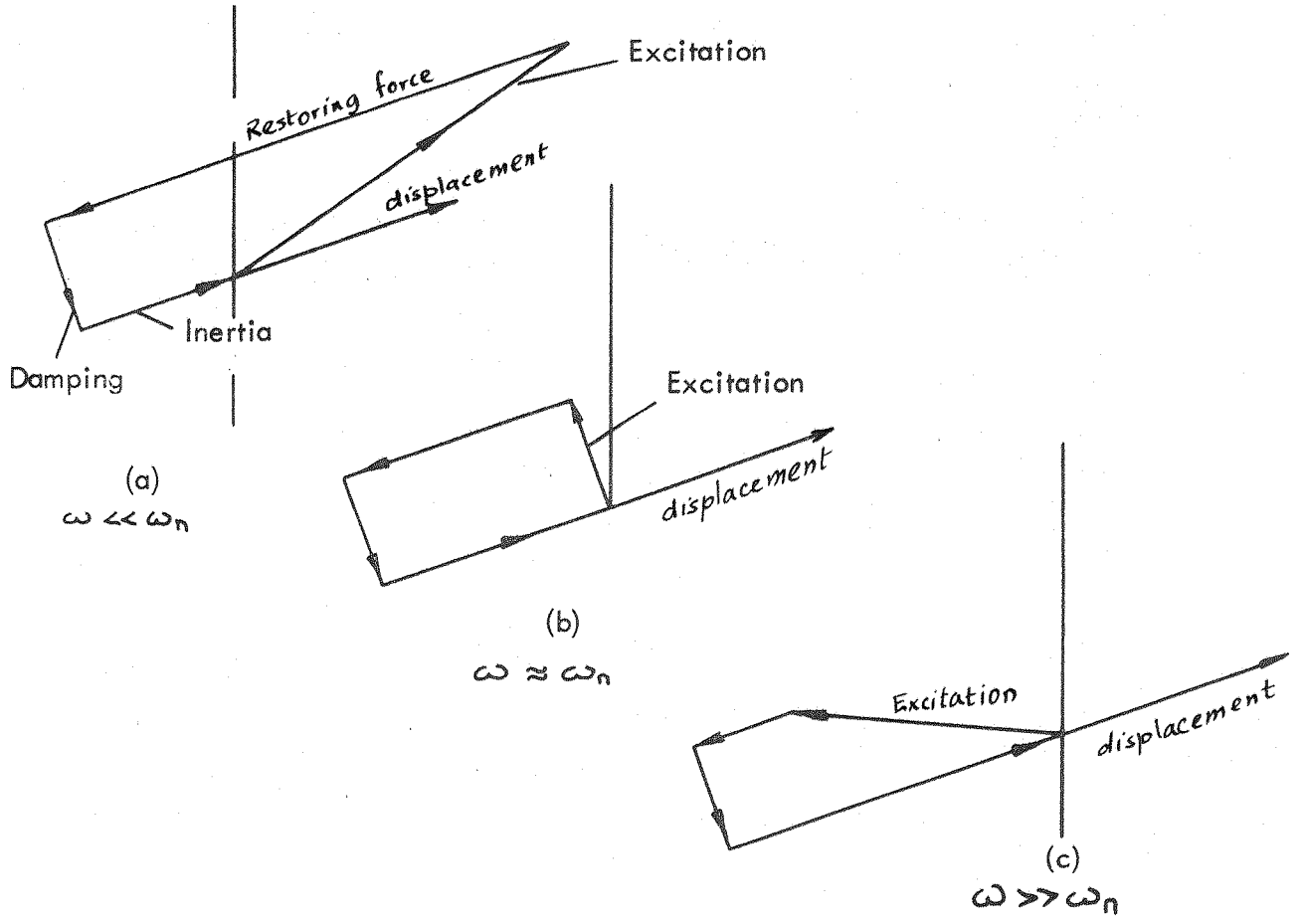

FIG. 2.8. INSTANTANEOUS VECTOR DIAGRAMS OF FORCES ACTING ON SINUSOIDALLY OSCILLATING MODEL.

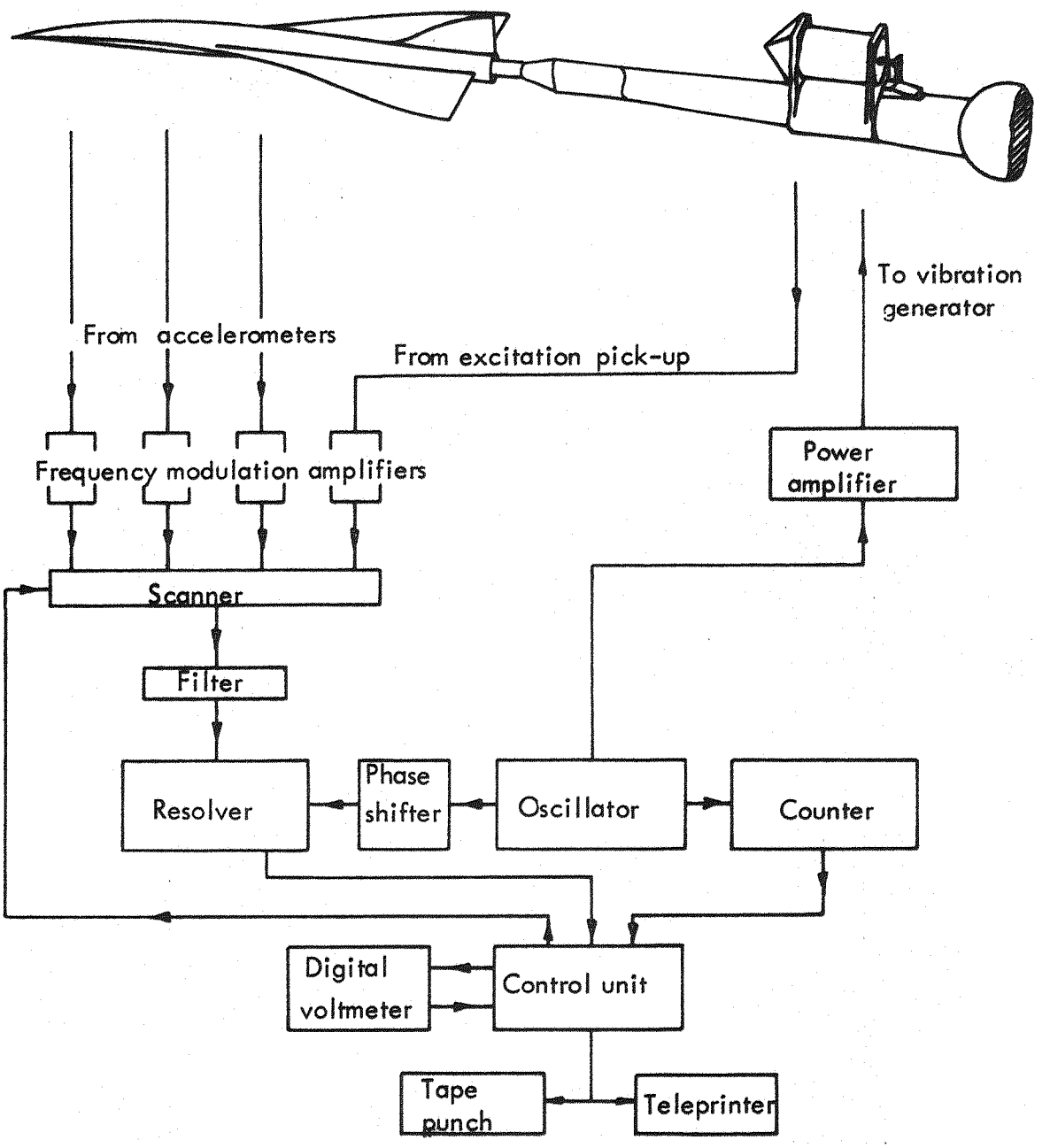

FIG. 2.9. LAYOUT OF EQUIPMENT USED BY THOMPSON & FAIL (1966)

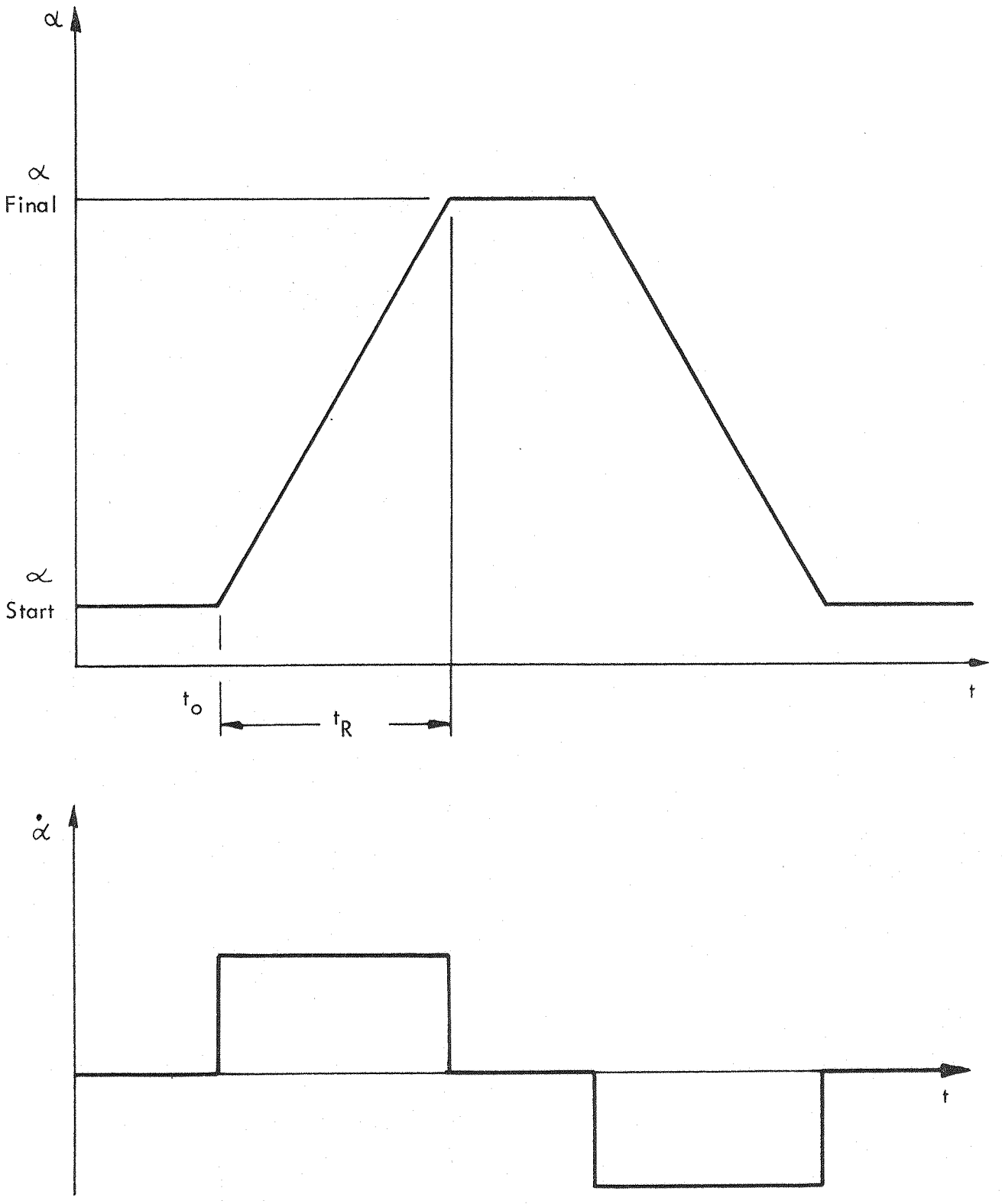

FIG. 3.1. THE INCIDENCE RAMP FUNCTION AND ASSOCIATED PITCH RATE.

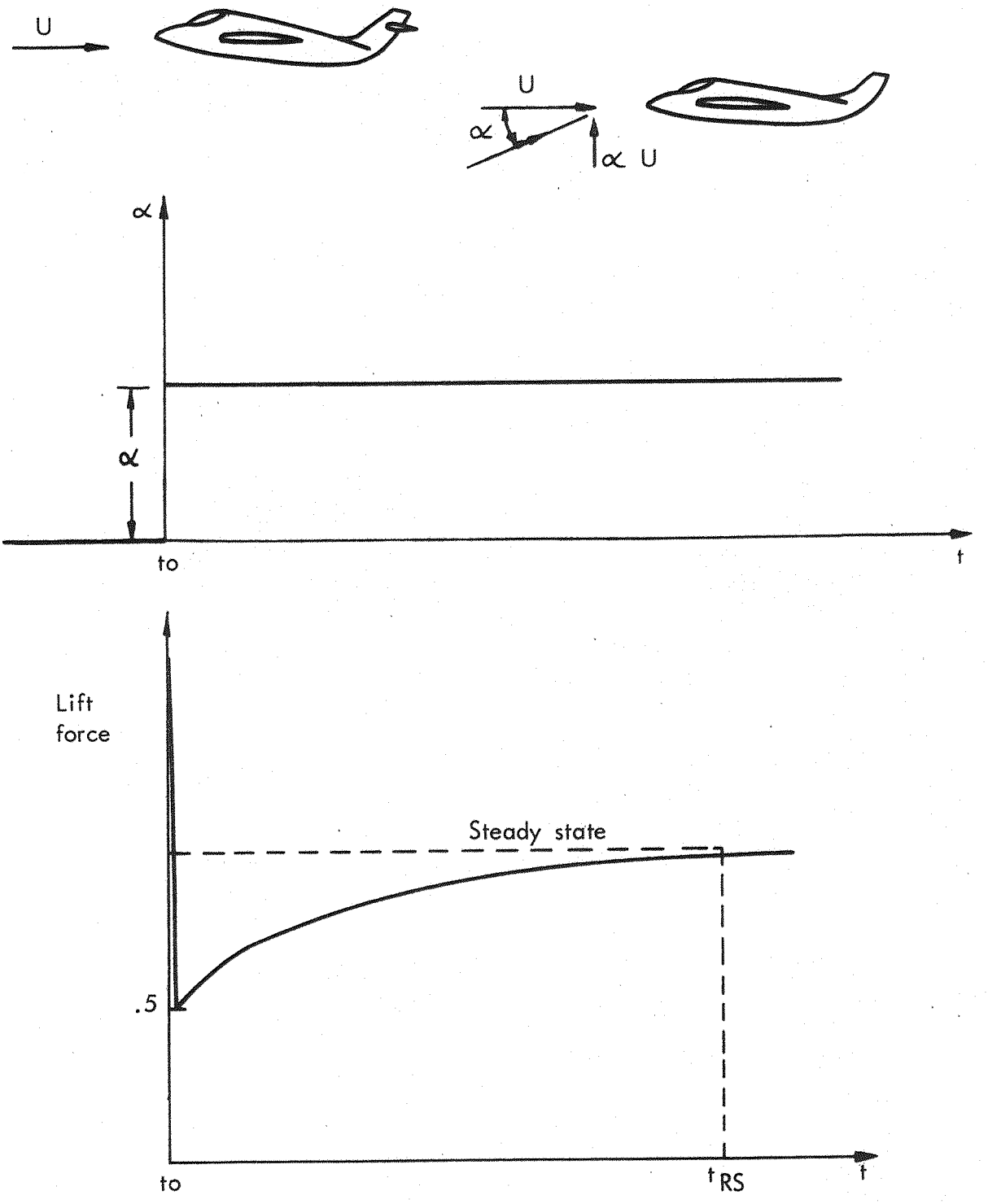

FIG. 3.2. INDICIAL LIFT FORCE VARIATION.

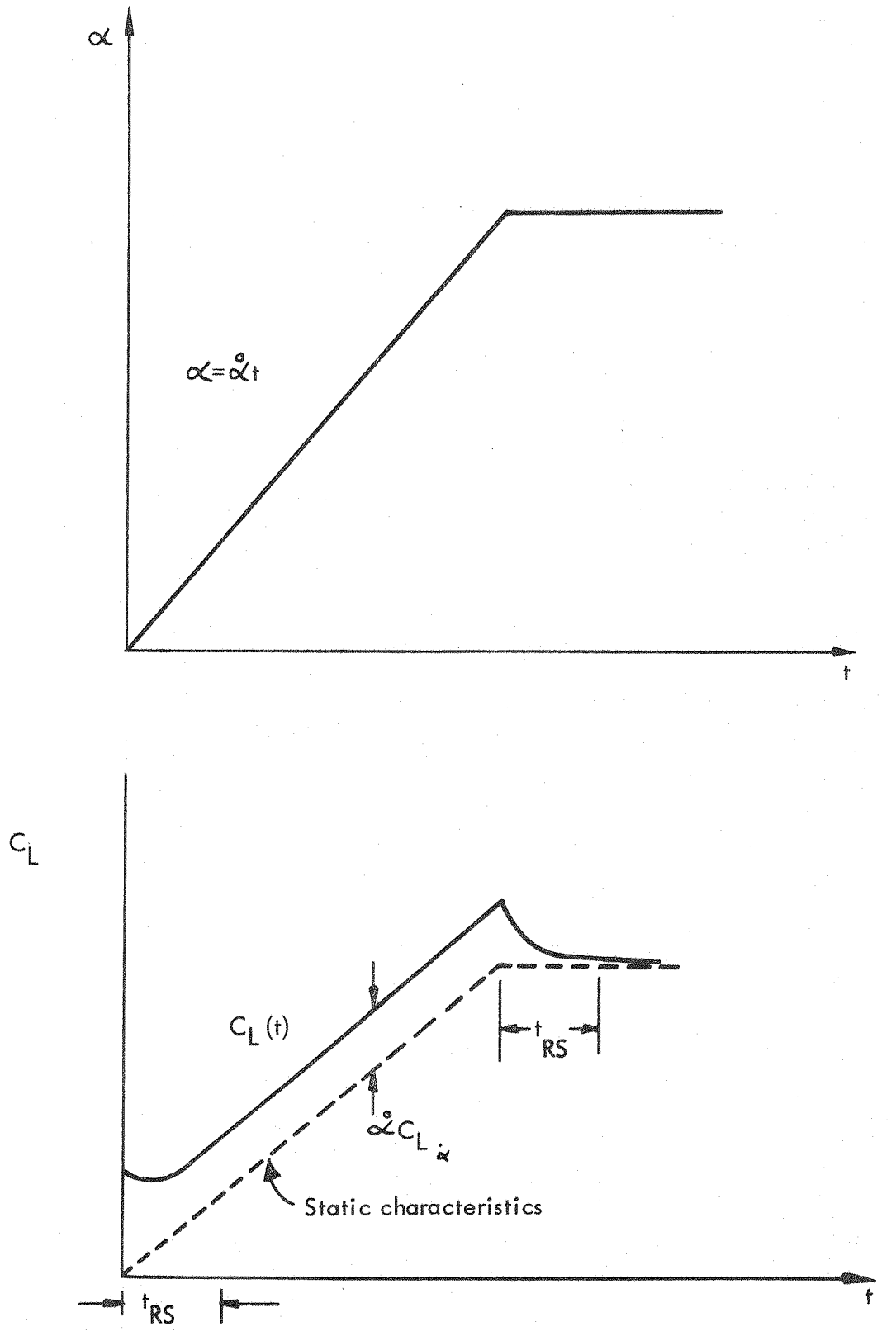

FIG. 3.3. AERODYNAMICS FORCE RESPONSE TO A SLOW PITCH RAMP.

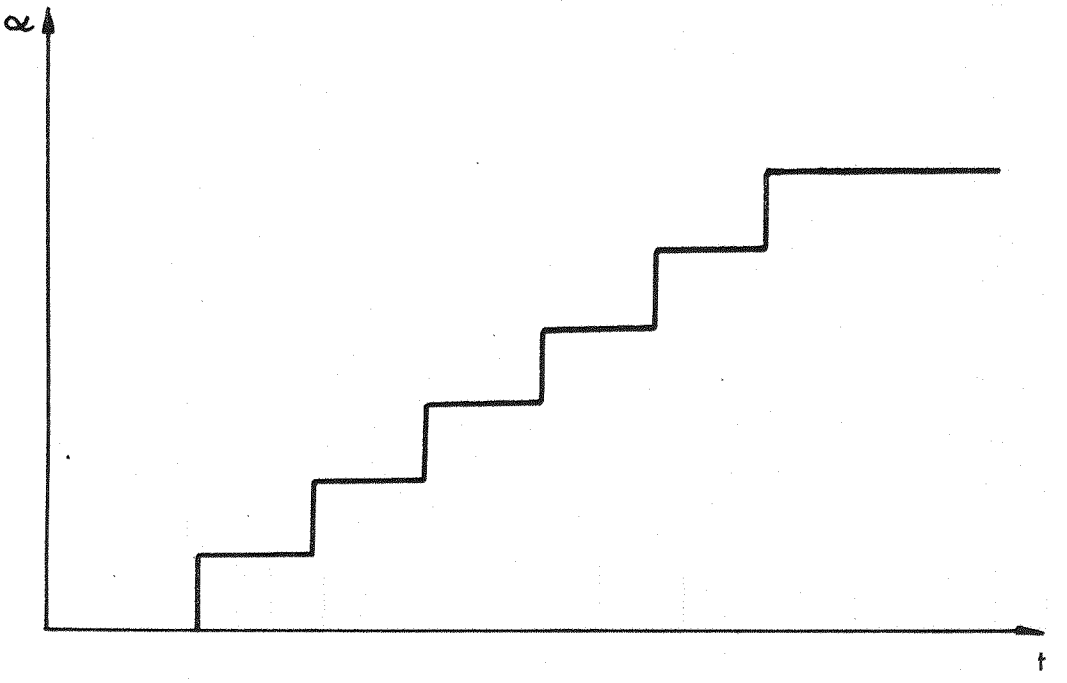

FIG. 3.4. STAIRCASE INCIDENCE FUNCTION.

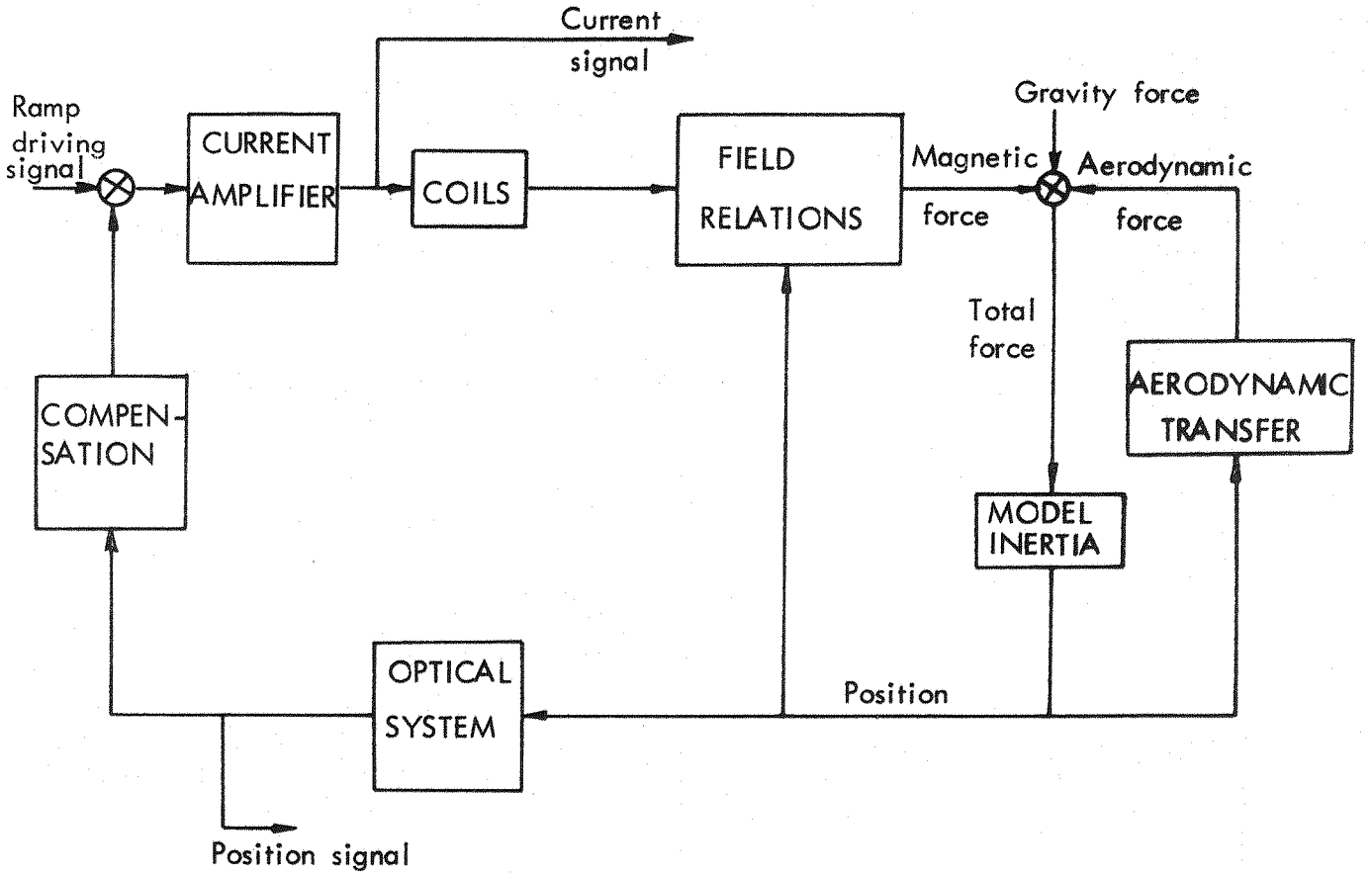

FIG. 3.5. A SINGLE DEGREE OF FREEDOM CONTROL LOOP OF A MAGNETIC BALANCE FOR STABILIZING MODEL AND MEASURING LINEAR AERODYNAMIC EFFECT.

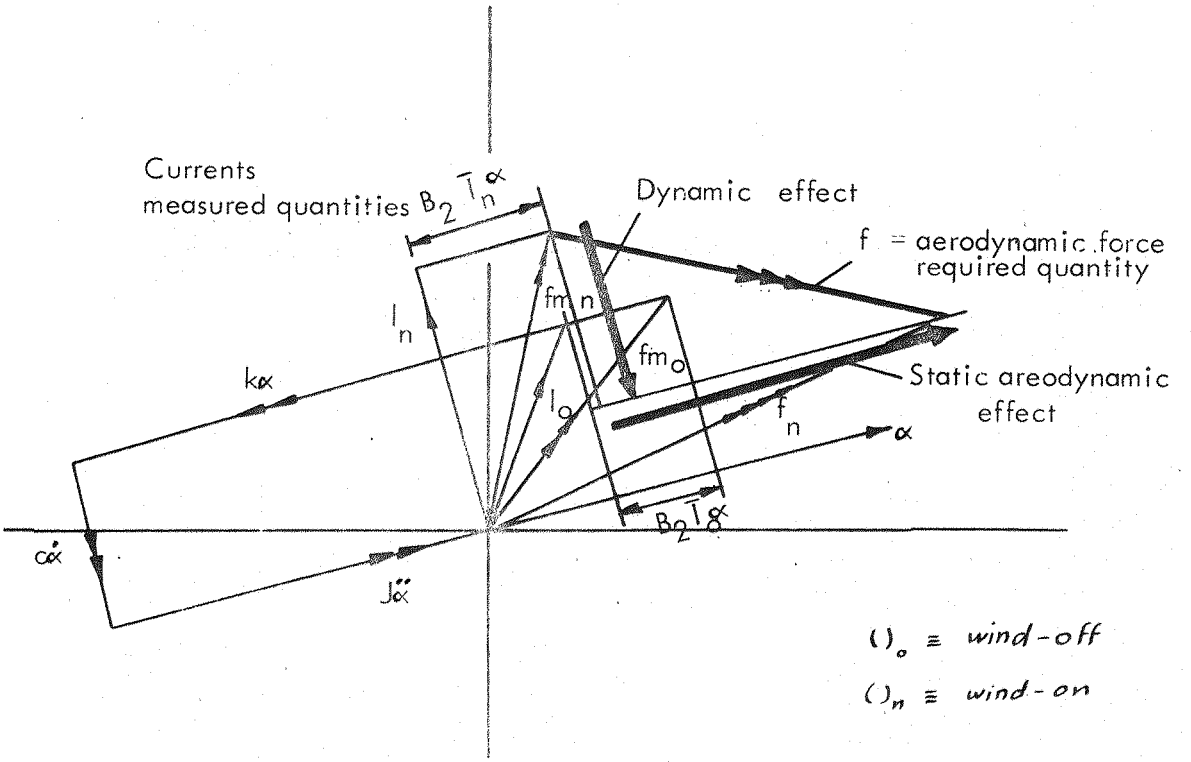

FIG. 3.6. INSTANTANEOUS FORCES VECTOR DIAGRAM FOR OSCILLATORY MOTION.

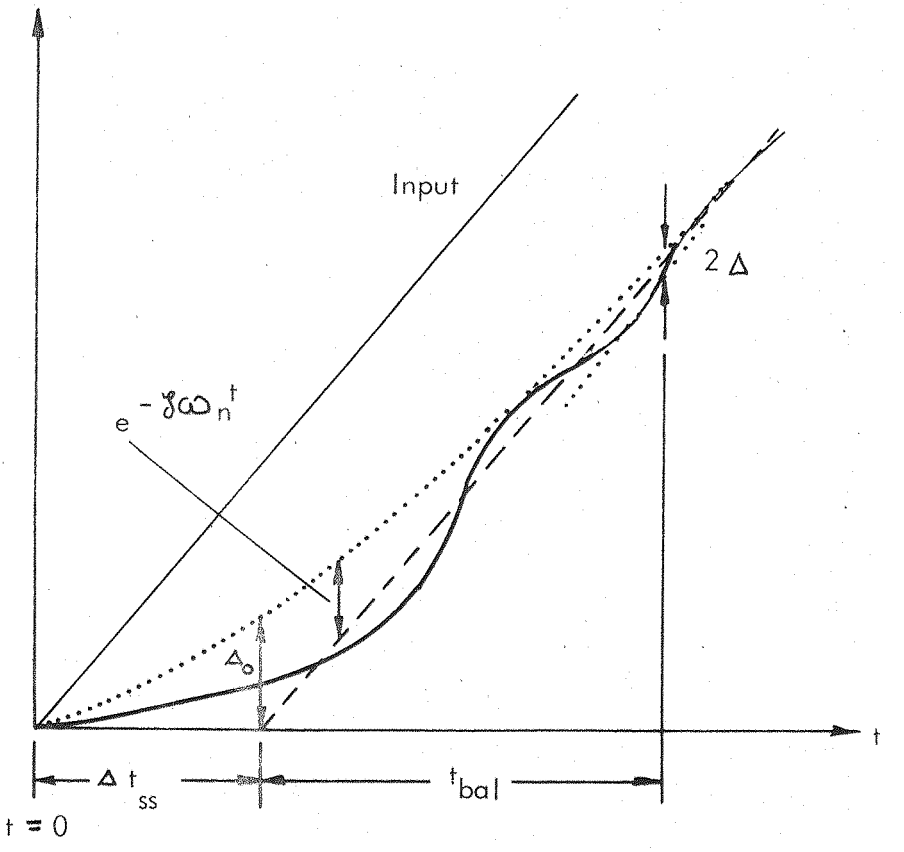

FIG. 3.7. RAMP RESPONSE OF A SECOND ORDER SYSTEM.

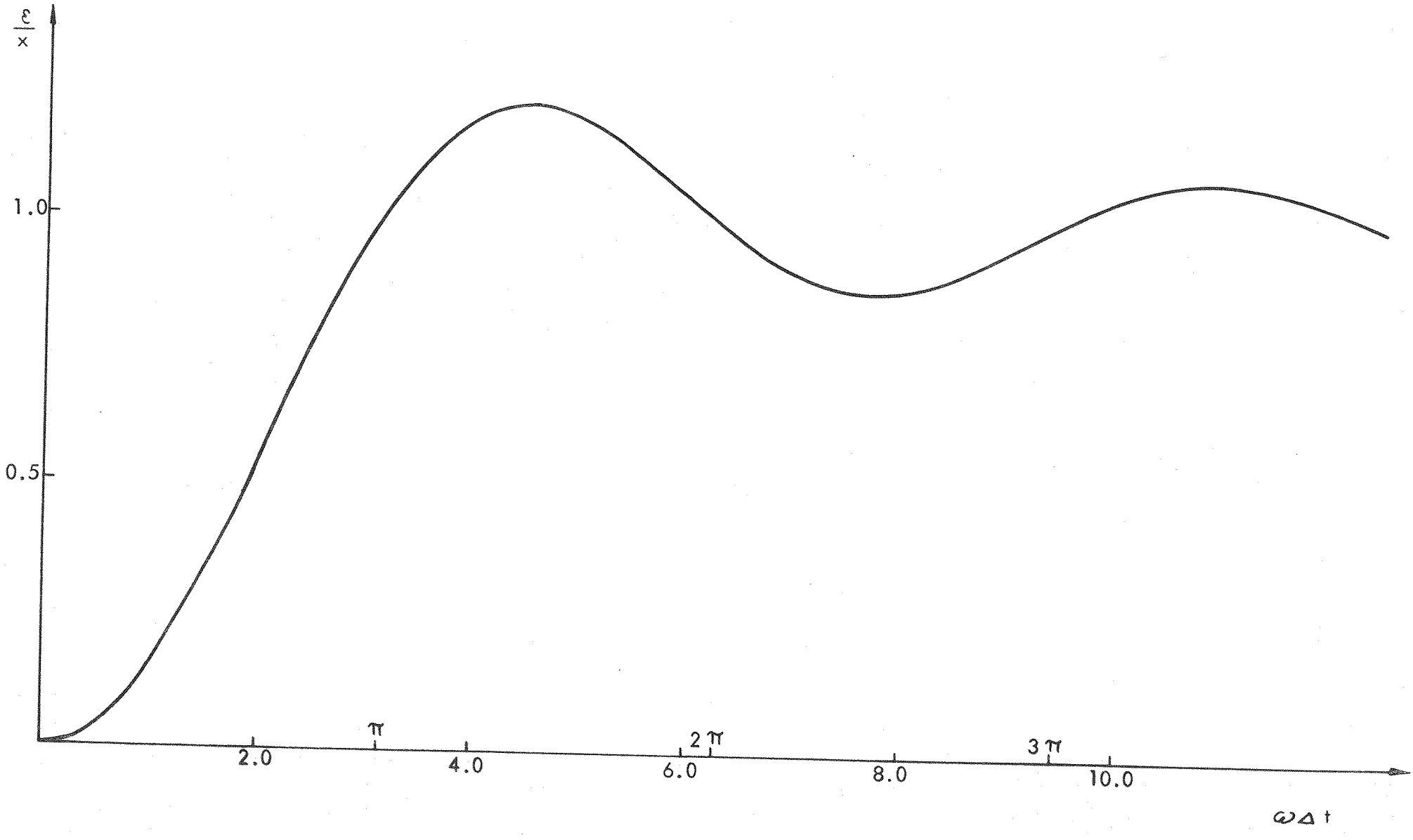

FIG. 3.8. THE ERROR ASSOCIATED WITH PIECE MEAL AVERAGING OVER AN INTERVAL Δ t OF A FUNCTION

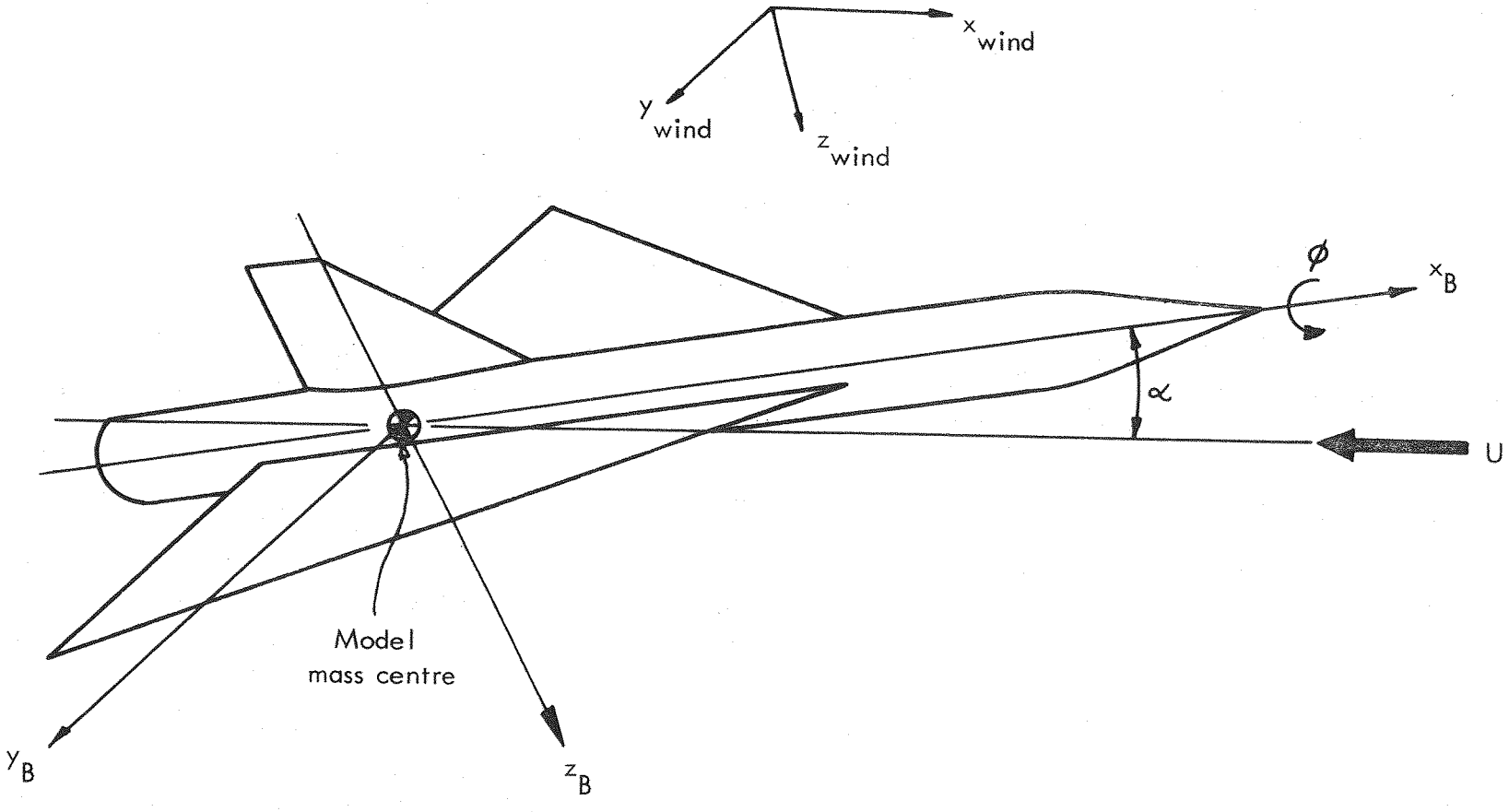

FIG. 3.9. THE MODEL AXES SYSTEM

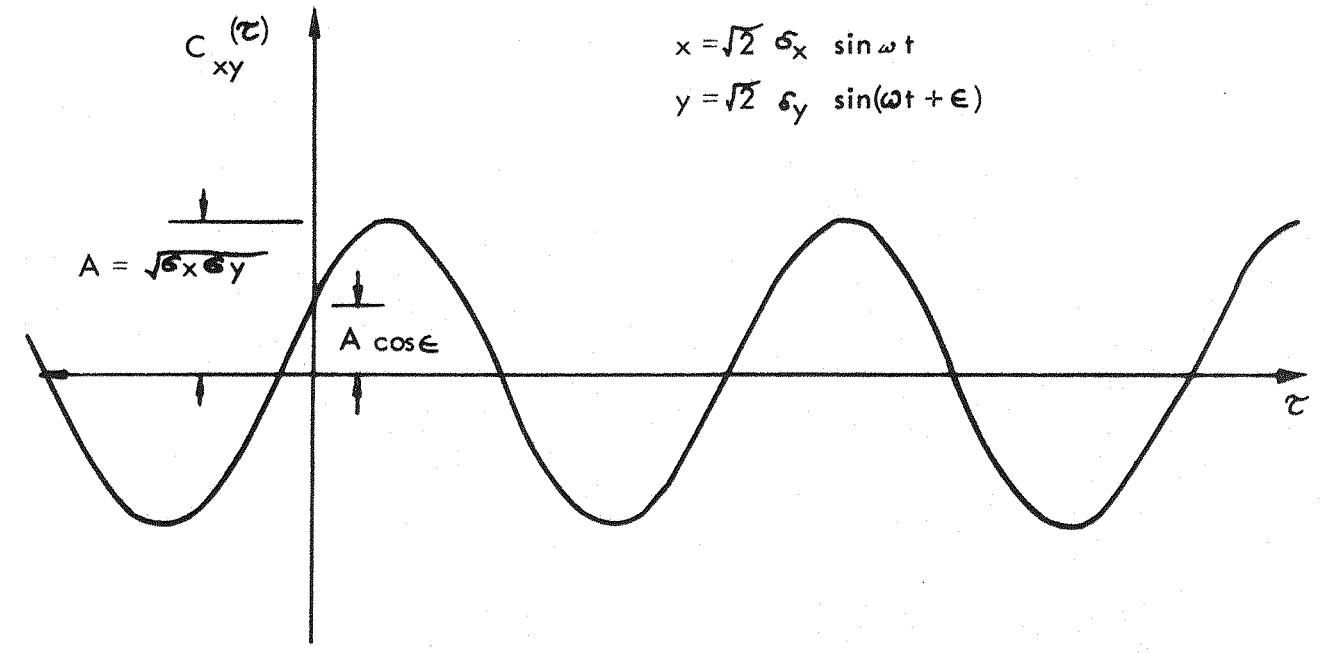

COVARIANCE FUNCTION

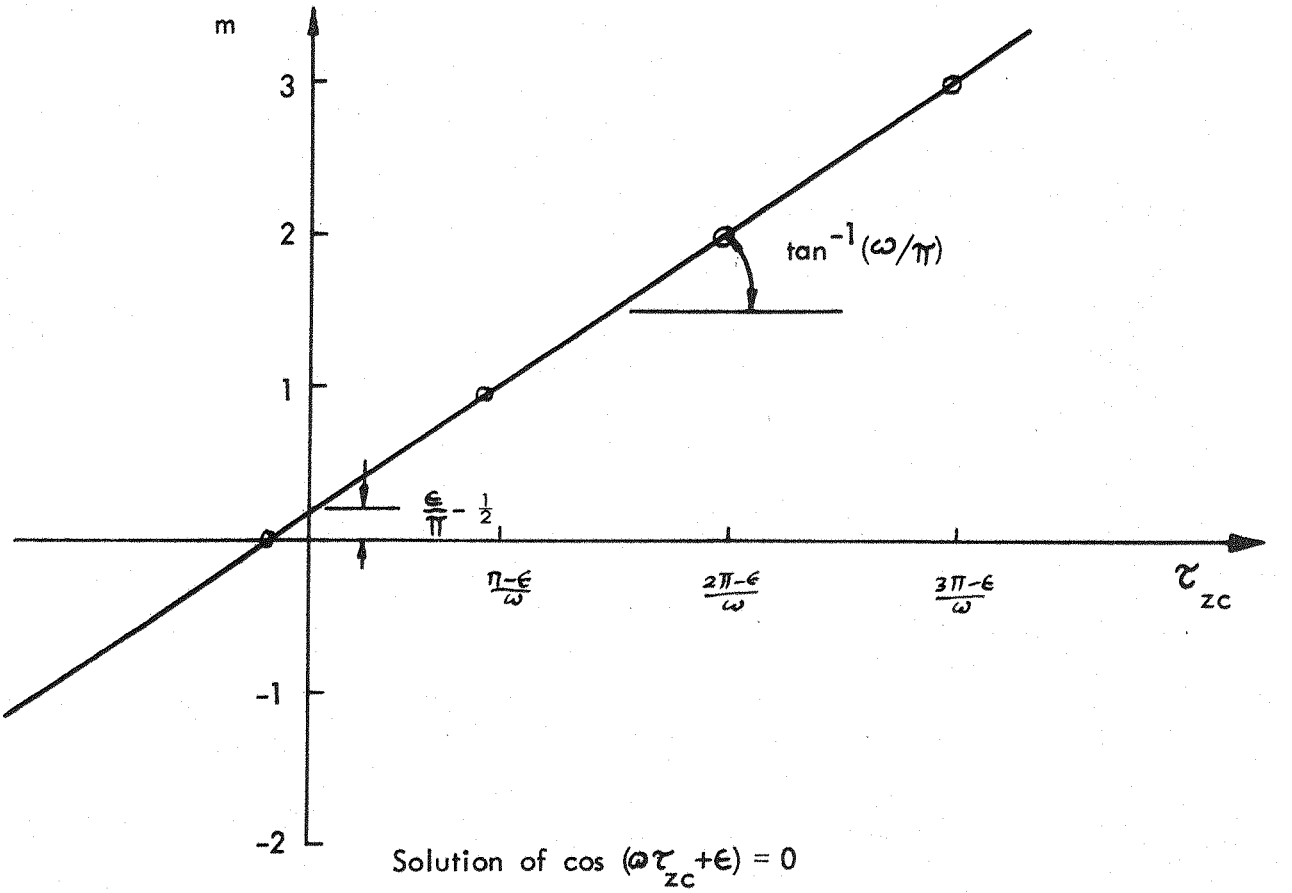

Solution of $\cos(\omega\tau_{zc} + \epsilon) = 0$

FIG. 3.10 . ZERO CROSSINGS OF THE COVARIANCE FUNCTION OF TWO SINUSOIDS.

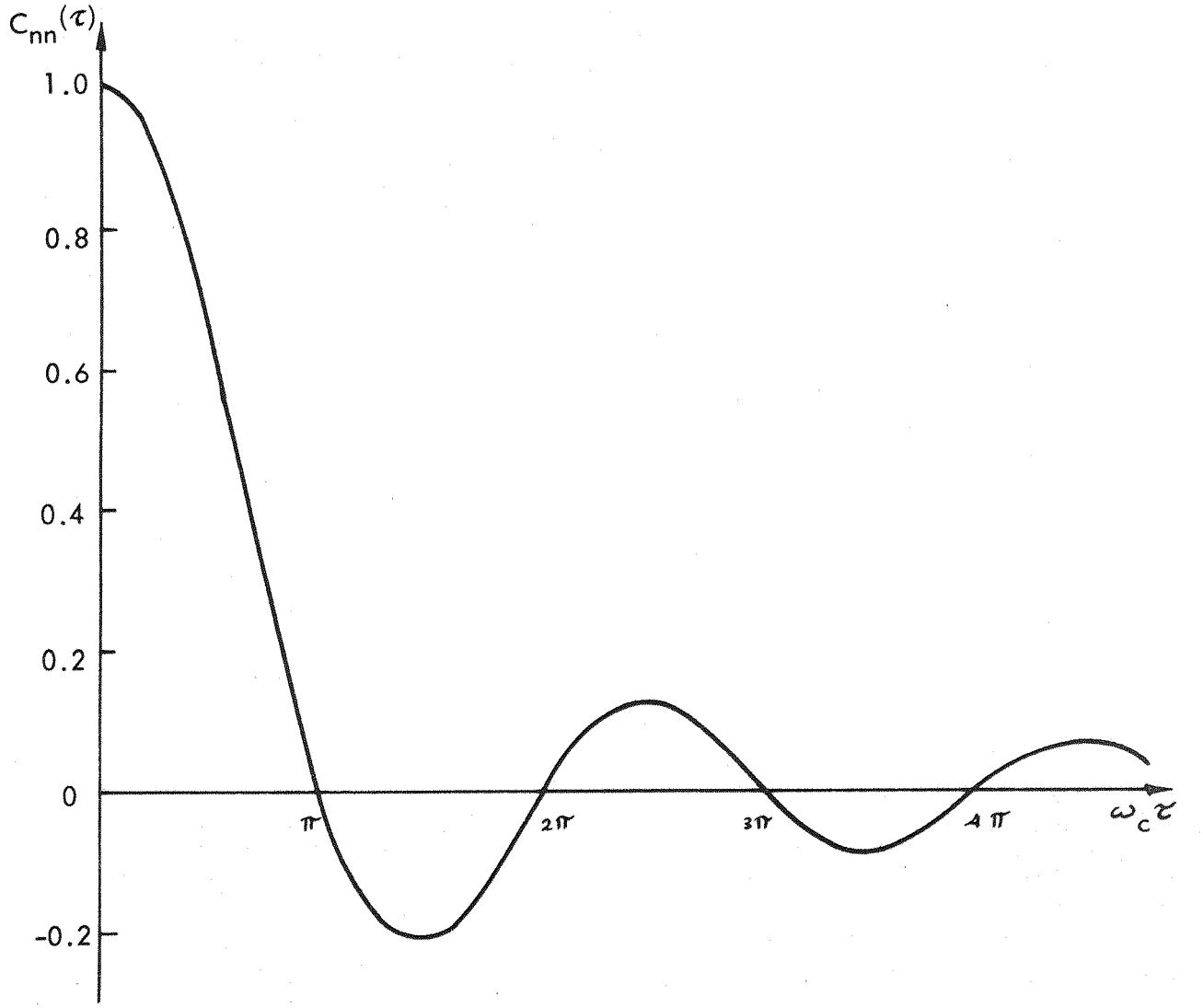

FIG. 3.11. THE AUTO-COVARIANCE FUNCTION OF BAND LIMITED (BANDWIDTH ω_c) WHITE NOISE.

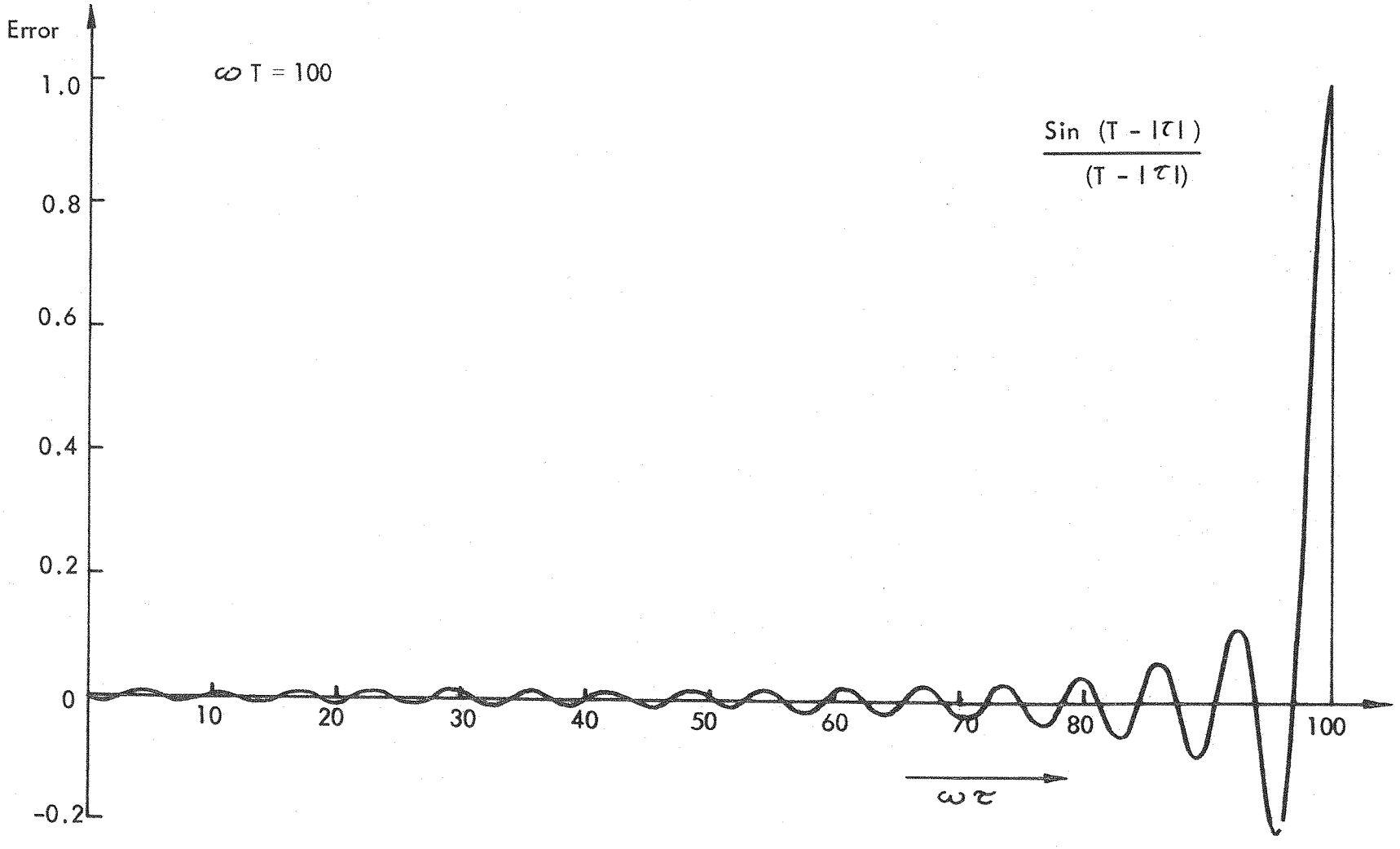

FIG. 3.12. VARIATION OF SIN| (T - |τ|) |/ (T - |τ|) WITH FOR ωT = 100

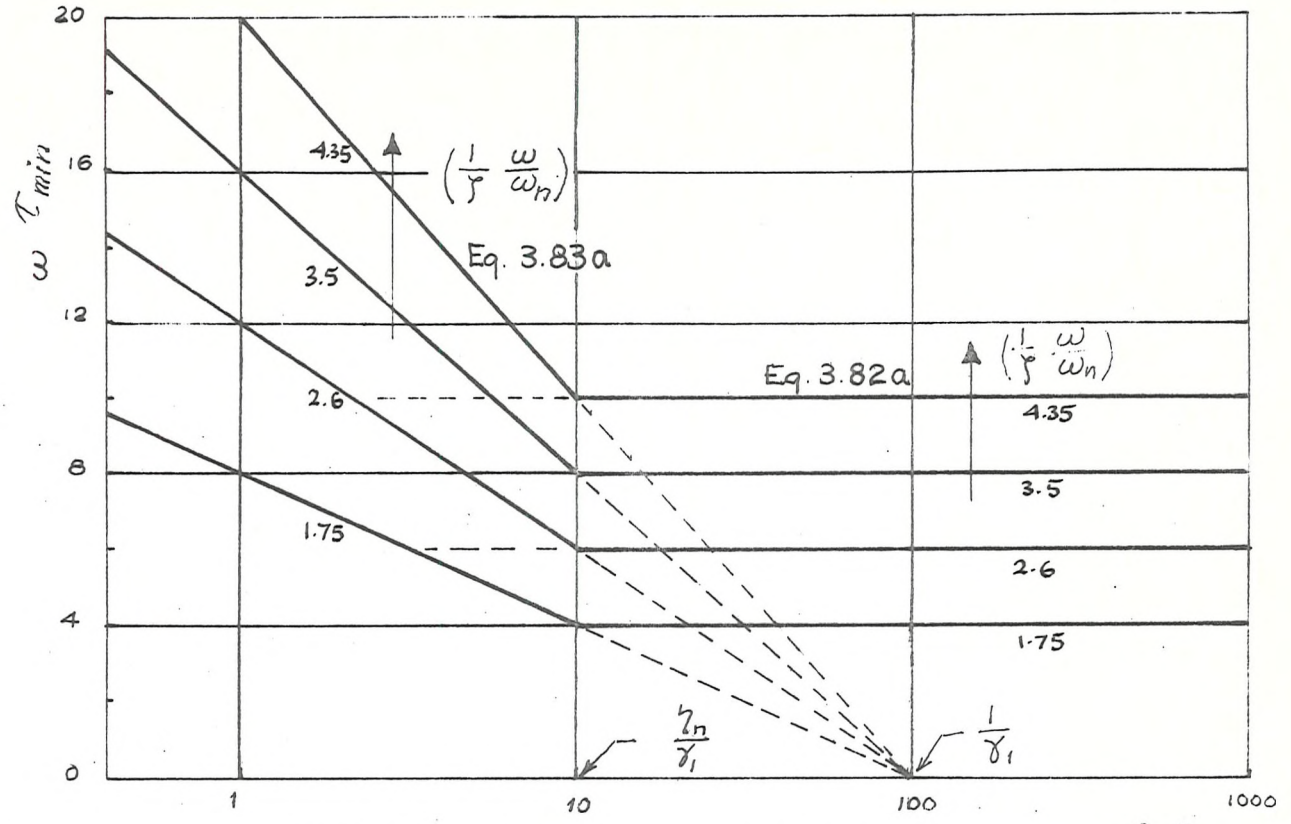

FIG. 3.13a MINIMUM LAG VALUES
$\eta_n = .1\ ,\ \gamma_1 = .01$

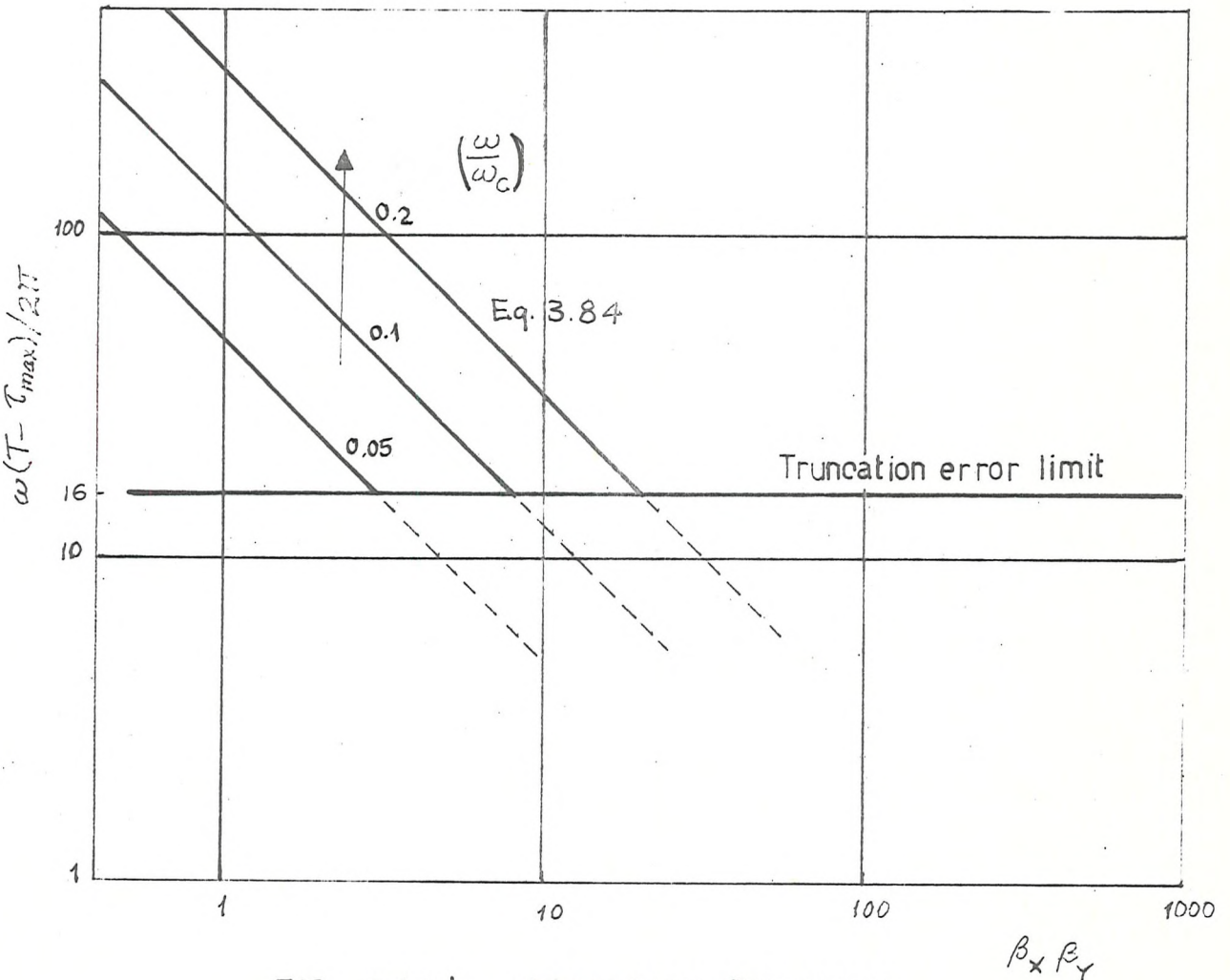

FIG. 3.13b SEPARATION BETWEEN
MAX. LENGTH AND MAX. LAG. USED, $\gamma_2 = .01$

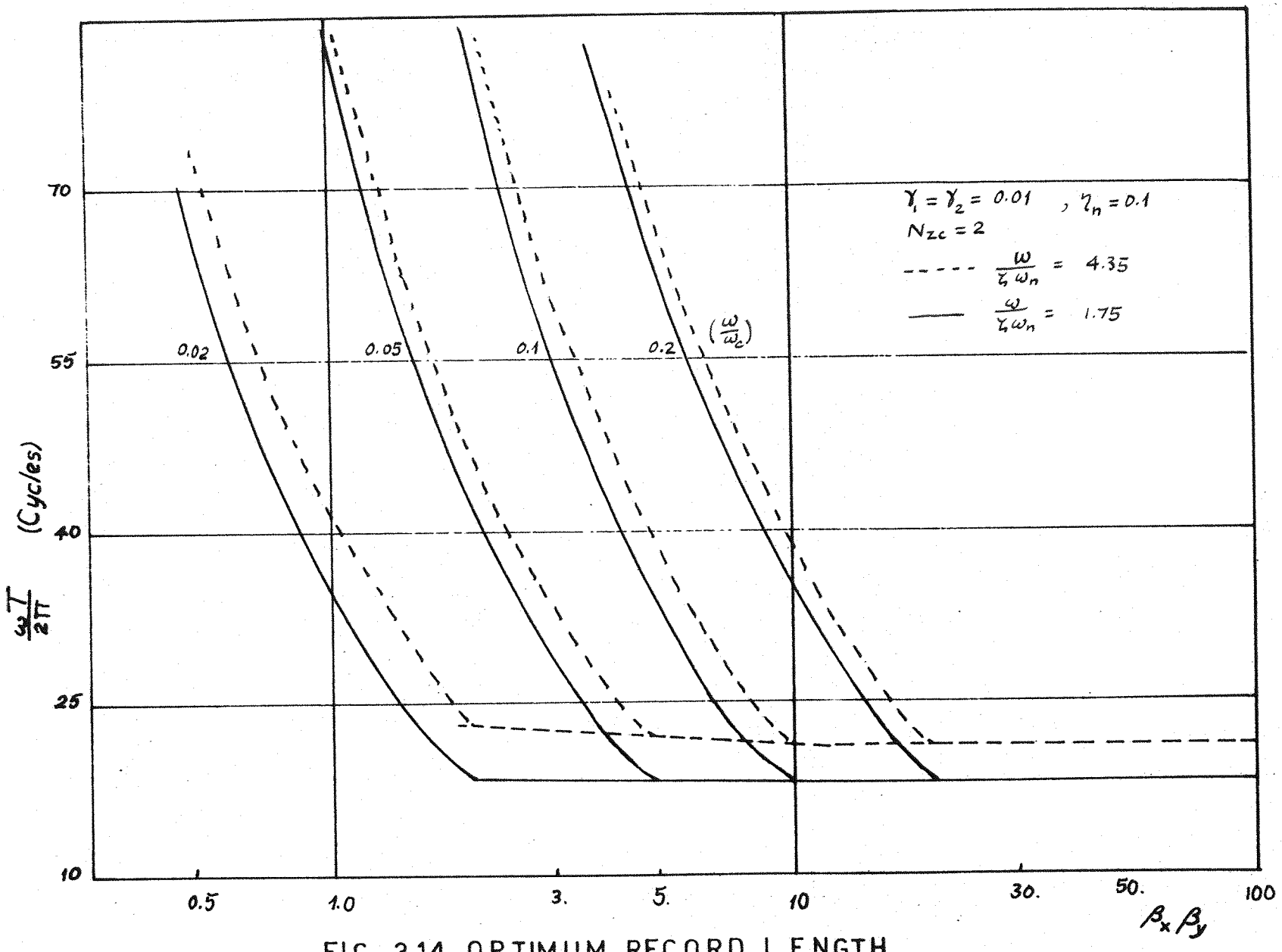

FIG. 3.14 OPTIMUM RECORD LENGTH

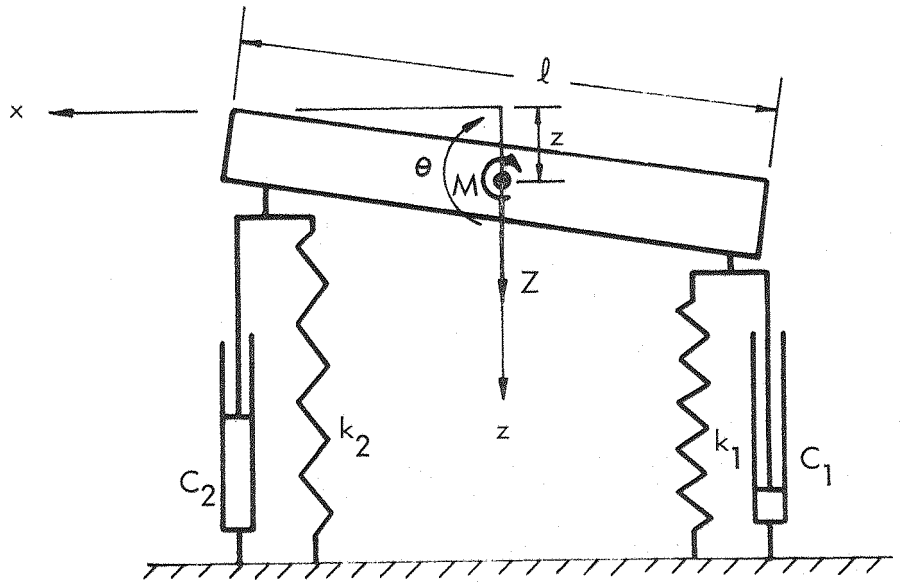

FIG. 3.15. TWO-DEGREE OF FREEDOM SYSTEM

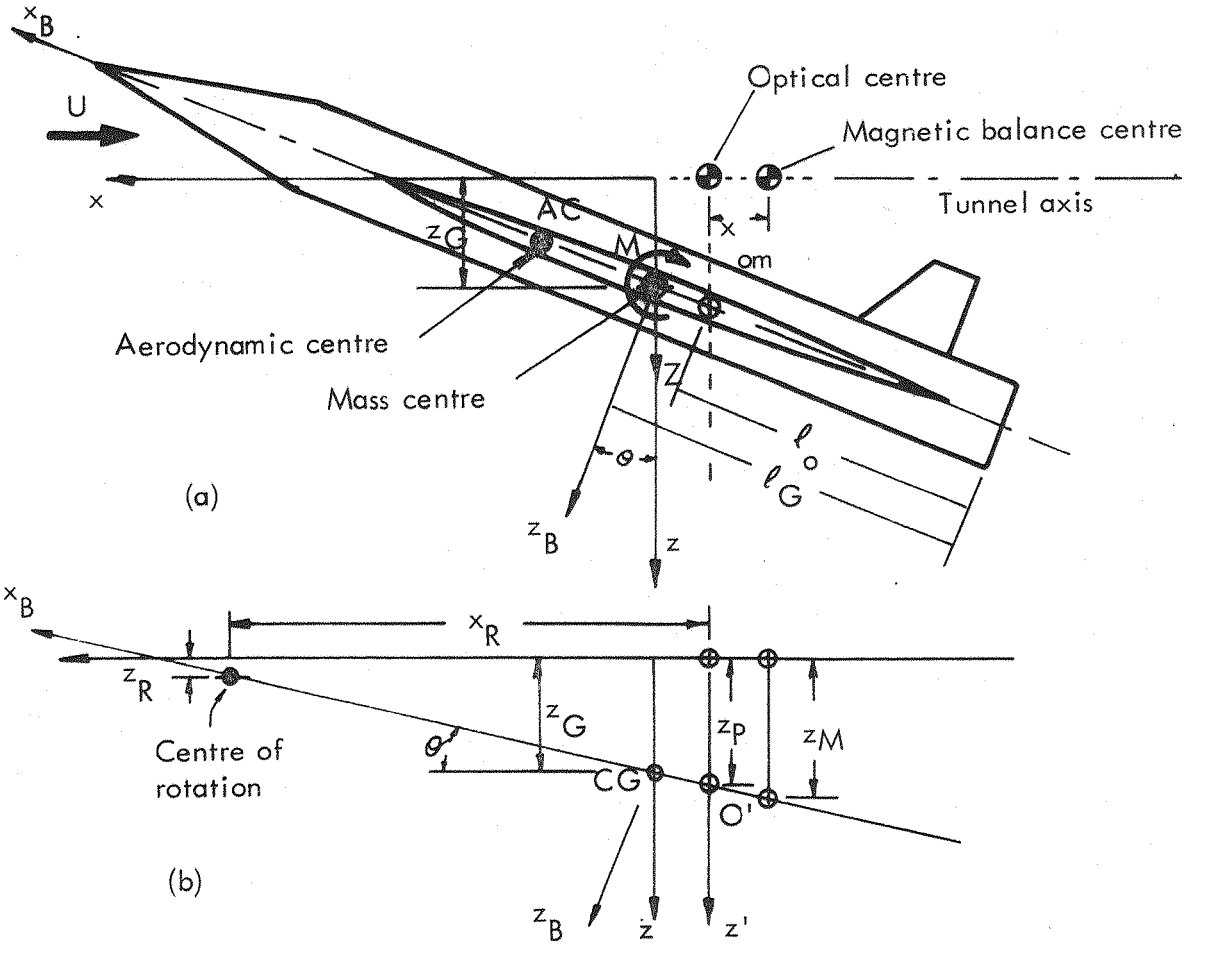

FIG. 3.16. MODEL AND COORDINATE SYSTEM.

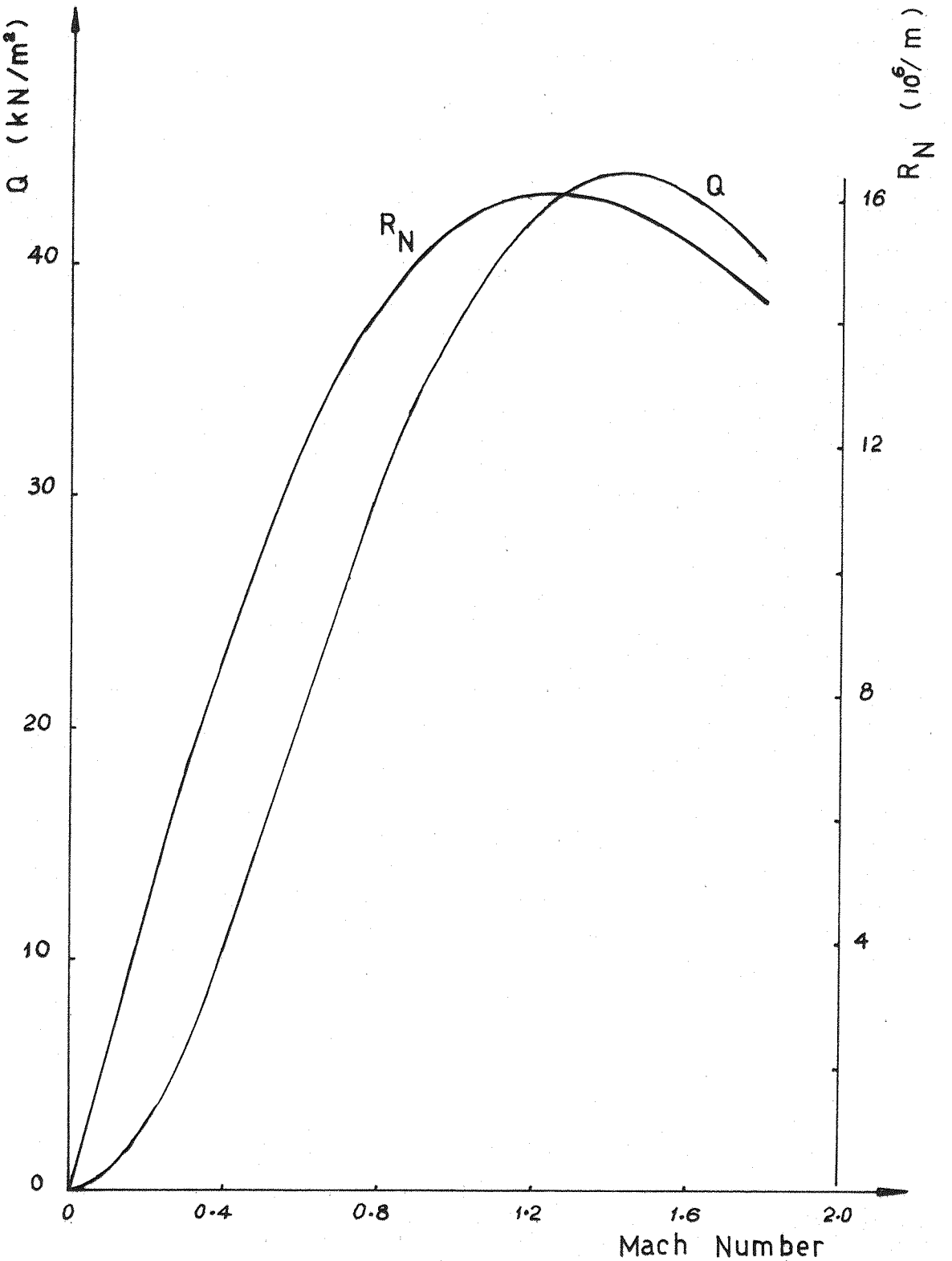

FIG. 4.1 VARIATION OF DYNAMIC HEAD & REYNOLDS NUMBER WITH MACH NUMBER

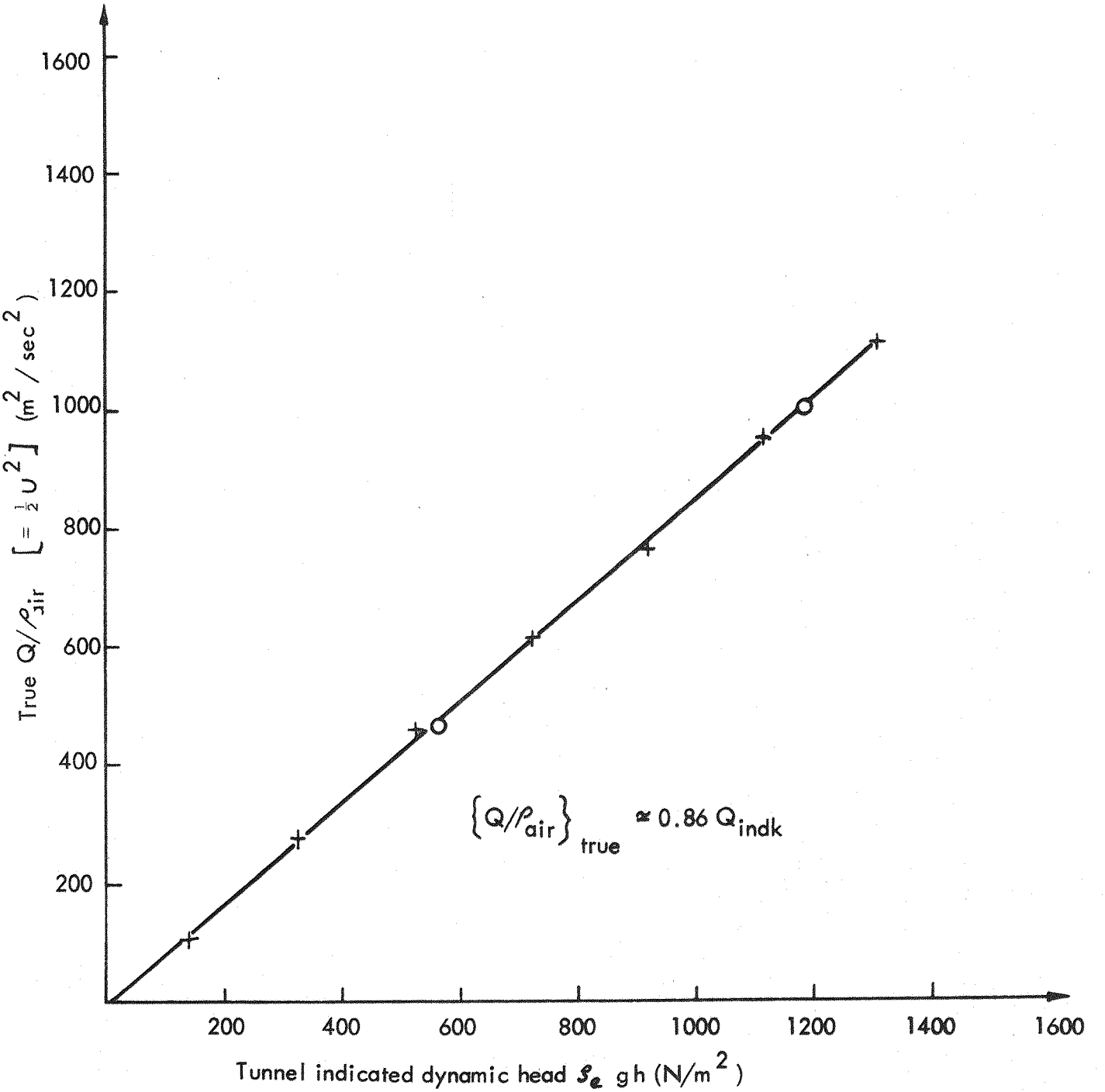

FIG. 4.2. WIND TUNNEL DYNAMIC HEAD CALIBRATION.

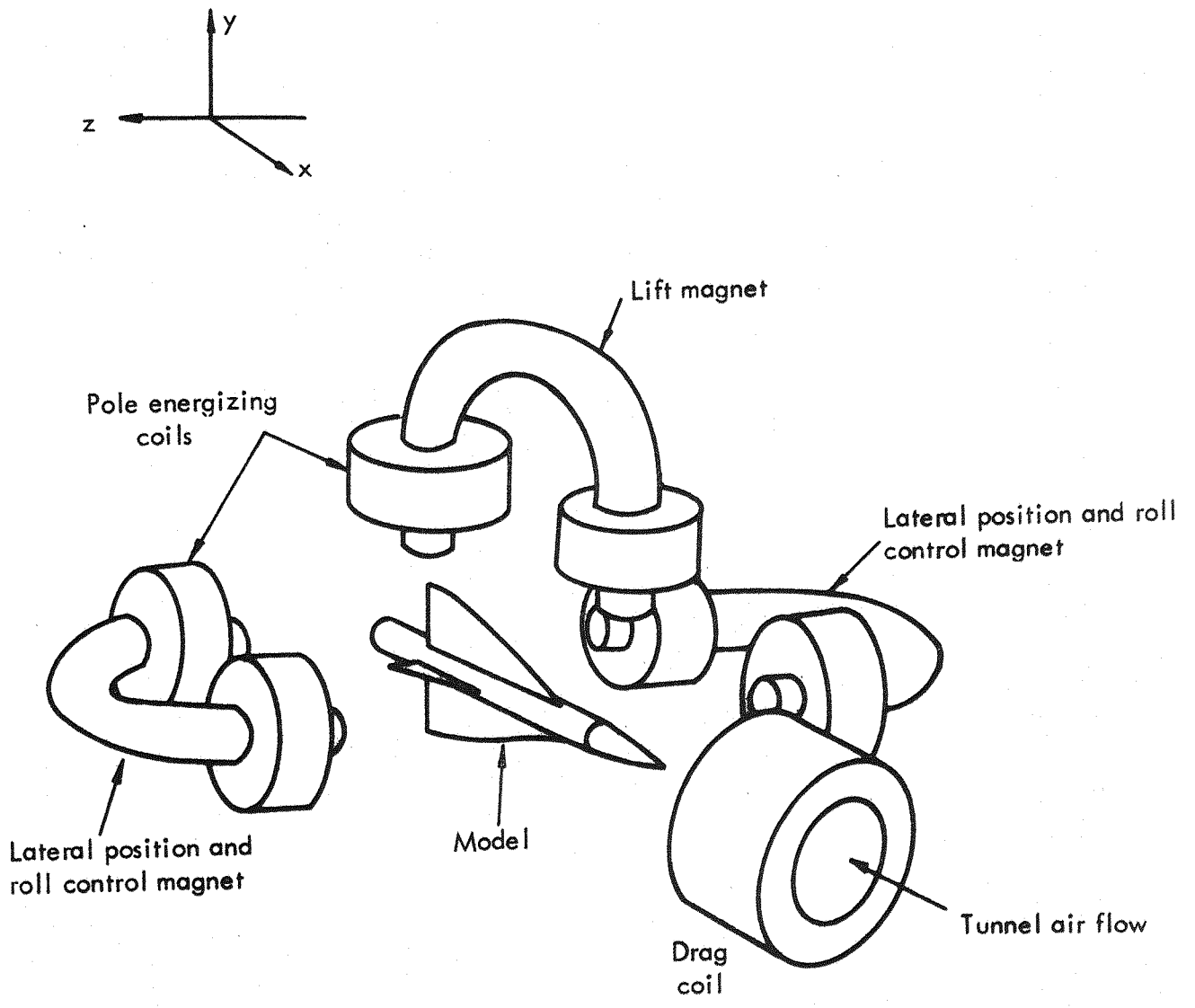

FIG. 4.3. A SCHEMATIC DIAGRAM OF THE SUSPENSION MAGNET ARRAY OF THE SIX COMPONENT MAGNETIC SUSPENSION AND BALANCE SYSTEM OF SOUTHAMPTON UNIVERSITY.

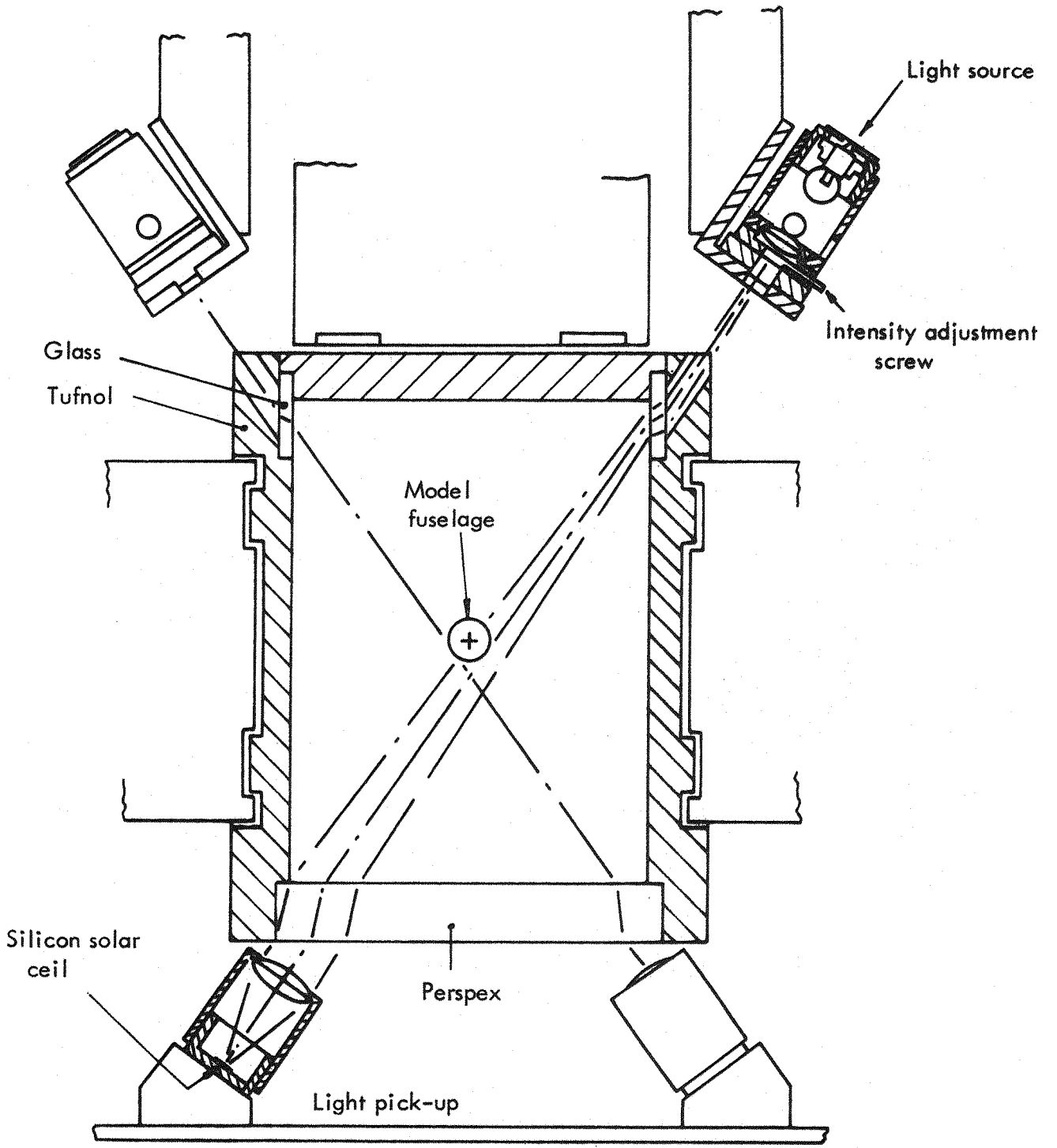

FIG. 4.4. A CROSS SECTION THROUGH THE WIND TUNNEL WORKING SECTION SHOWING THE OPTICAL SYSTEM MONITORING VERTICAL AND HORIZONTAL MOTIONS OF ONE END OF MODEL.

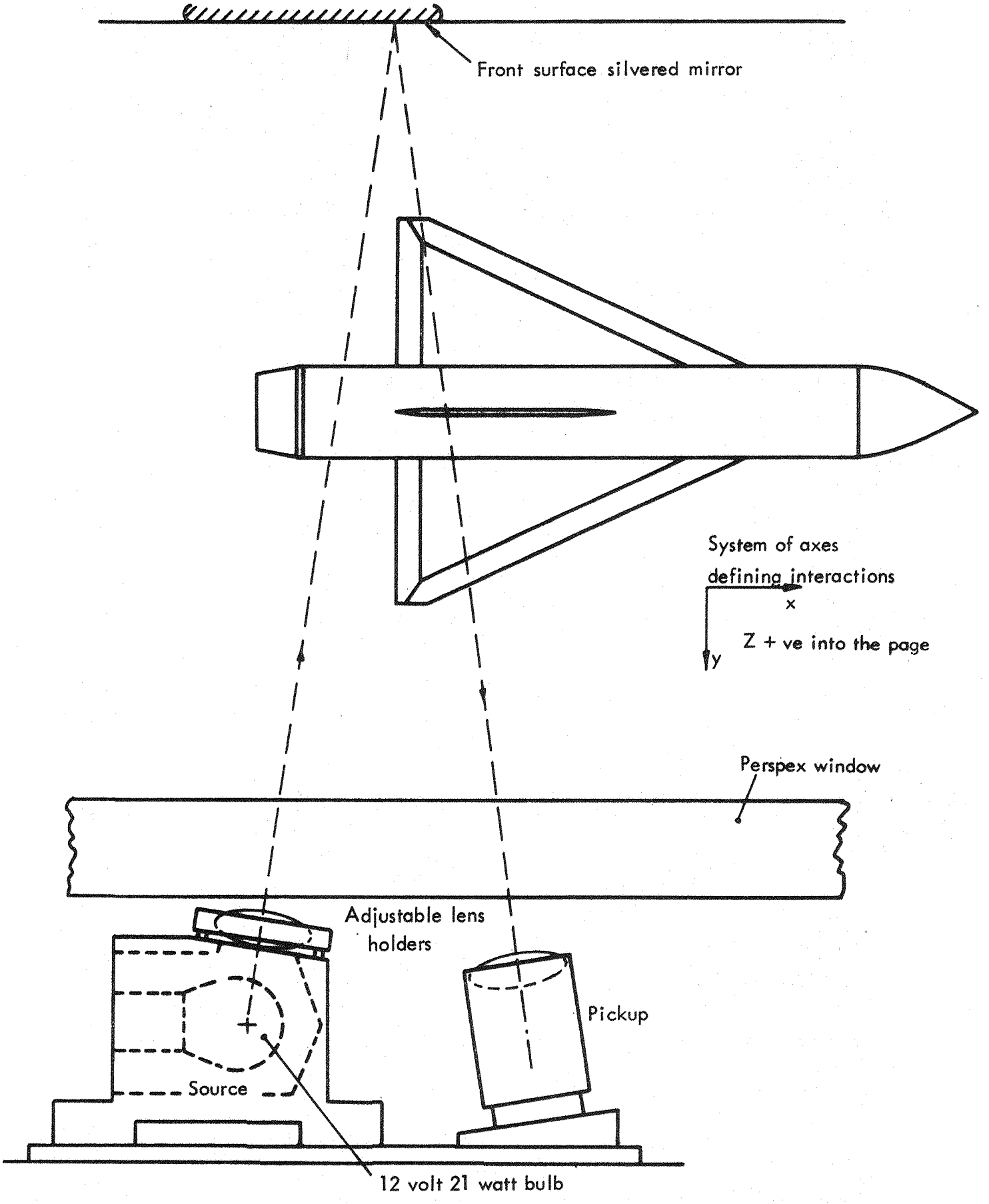

FIG. 4.5. A SIDE VIEW OF A SECTION THROUGH THE WIND TUNNEL WORKING SECTION SHOWING THE ROLL OPTICAL SYSTEM AND BEAM PATH.

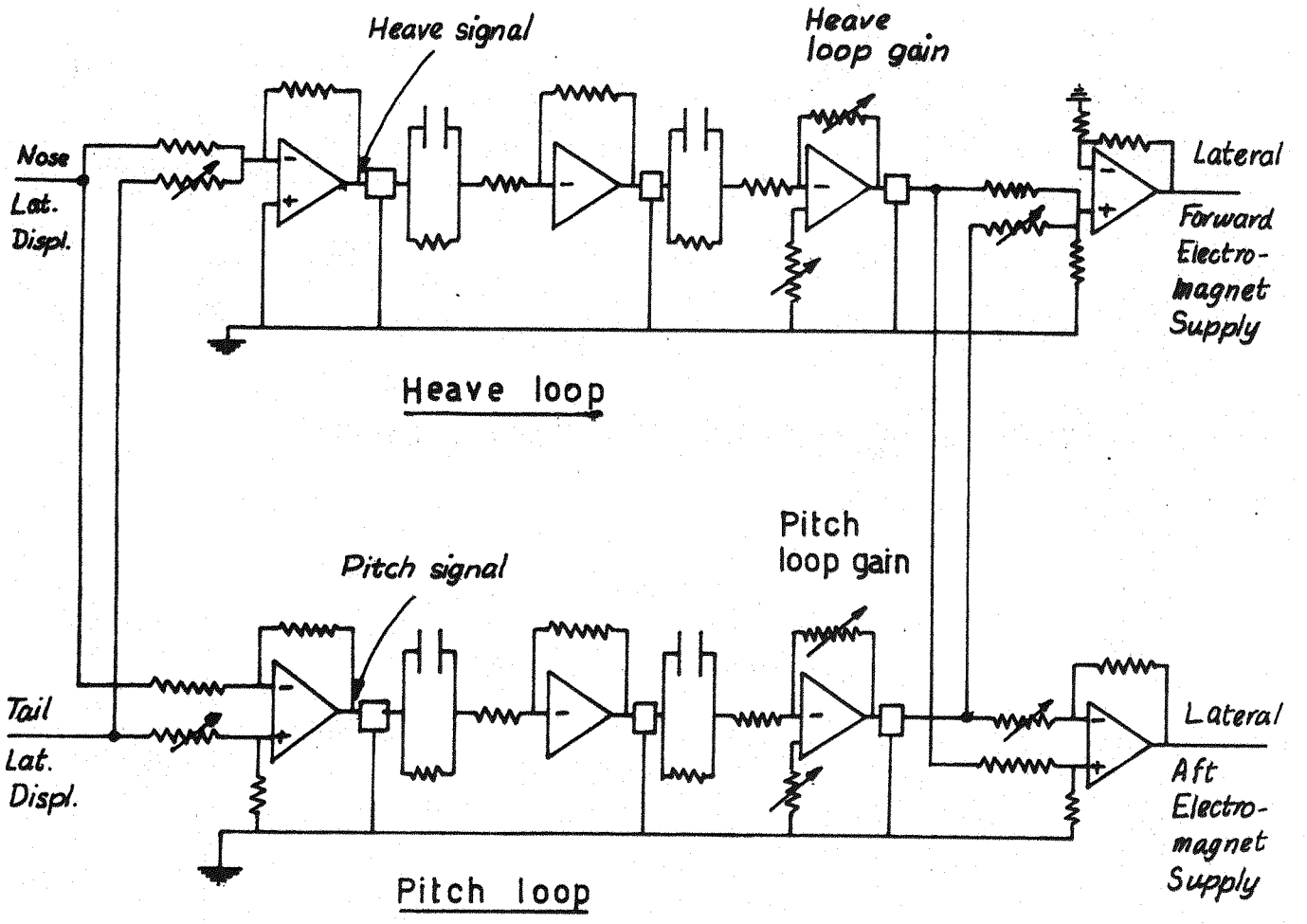

FIG. 4.6. LATERAL LOOP FEEDBACK CIRCUIT

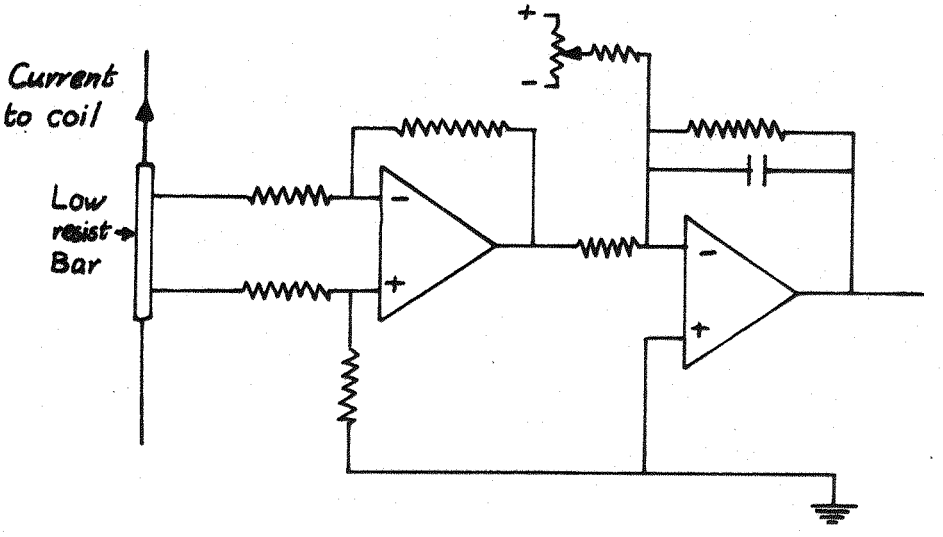

FIG. 4.7 CURRENT SIGNAL AND CONDITIONING CIRCUIT

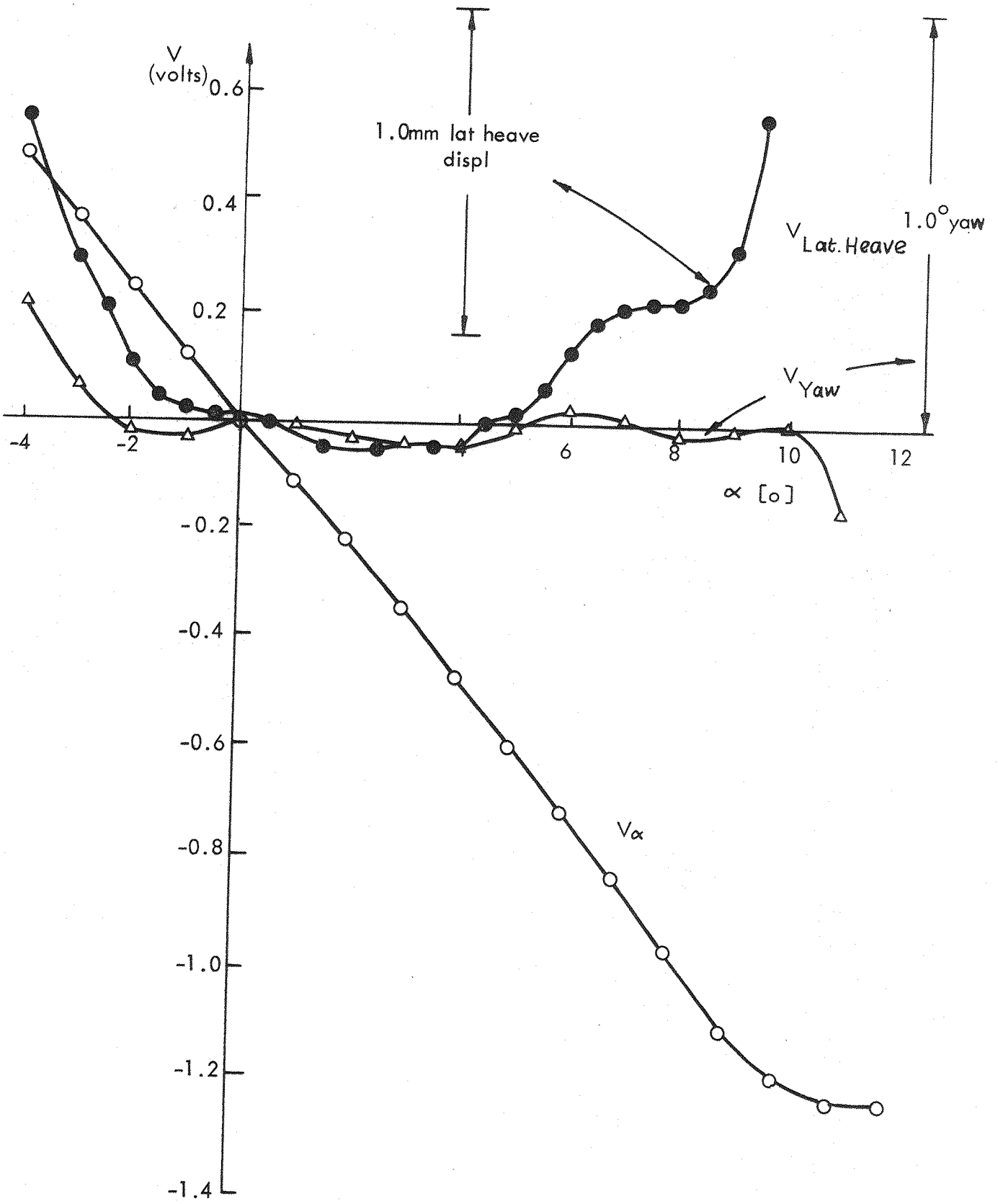

FIG. 4.8. IMPORTANT POSITION OPTICAL SYSTEM CALIBRATION.

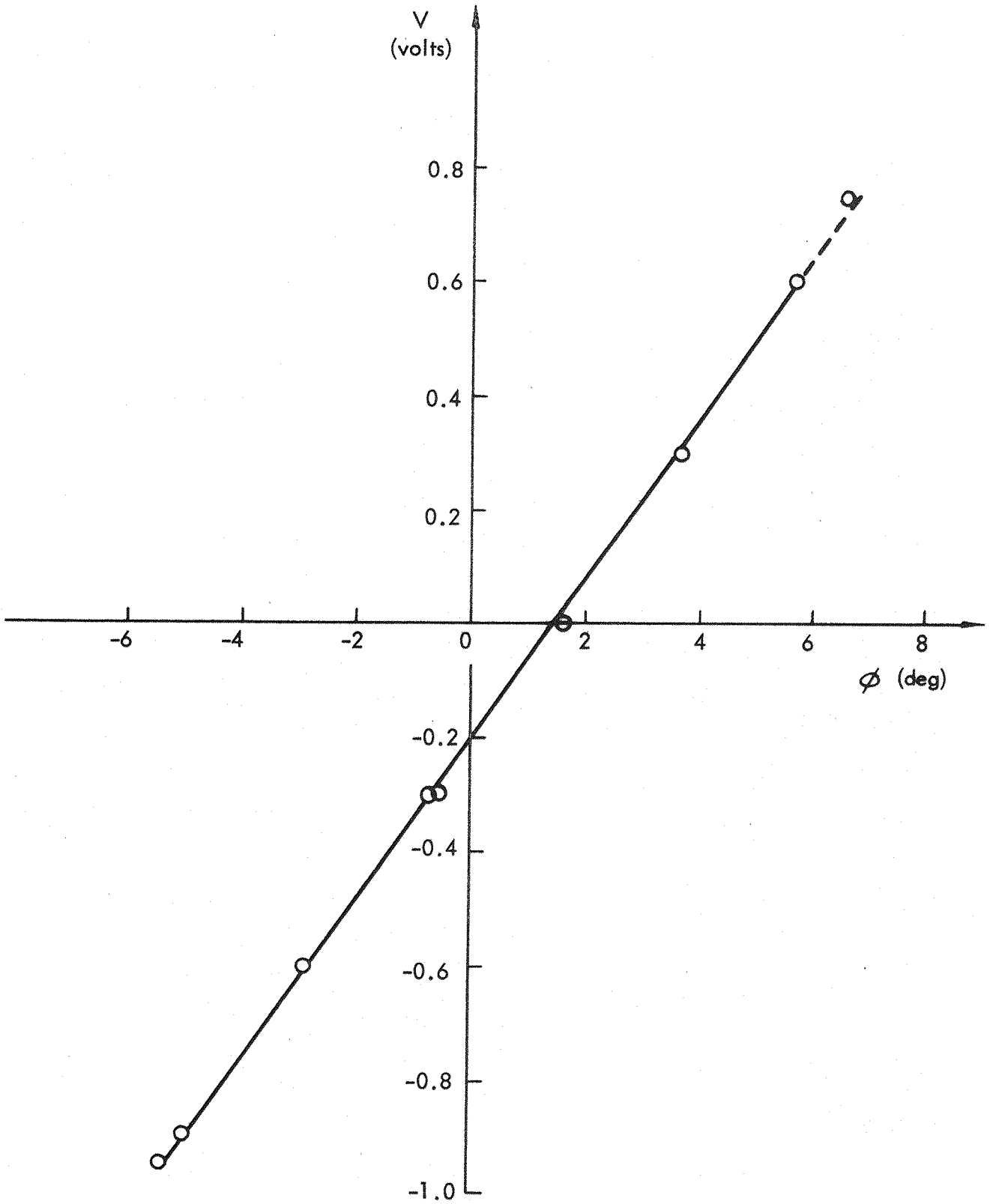

FIG. 4.9. ROLL POSITION CALIBRATION.

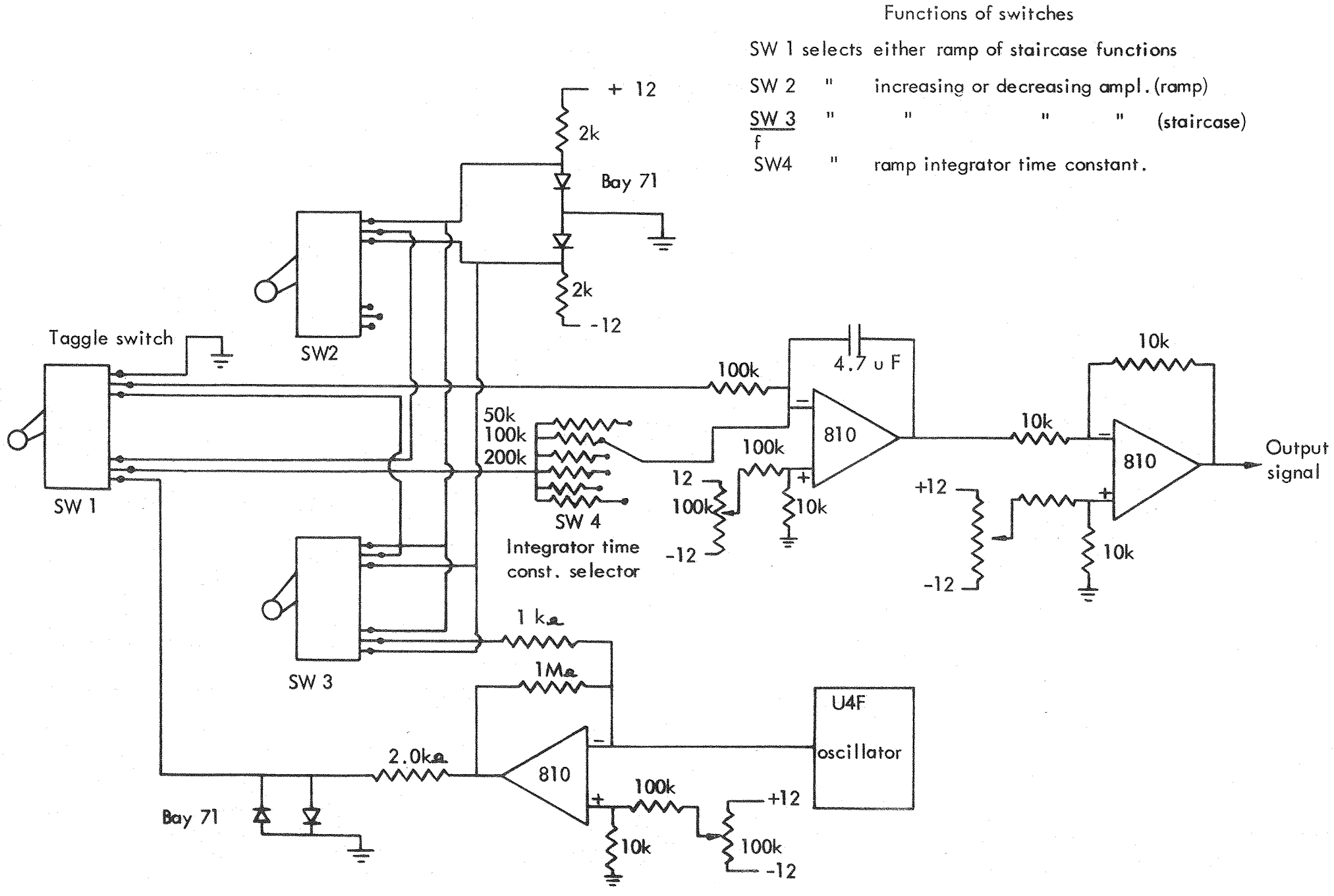

FIG. 4.10. THE BUILT IN CIRCUIT FOR RAMP/STAIRCASE FUNCTION GENERATION.

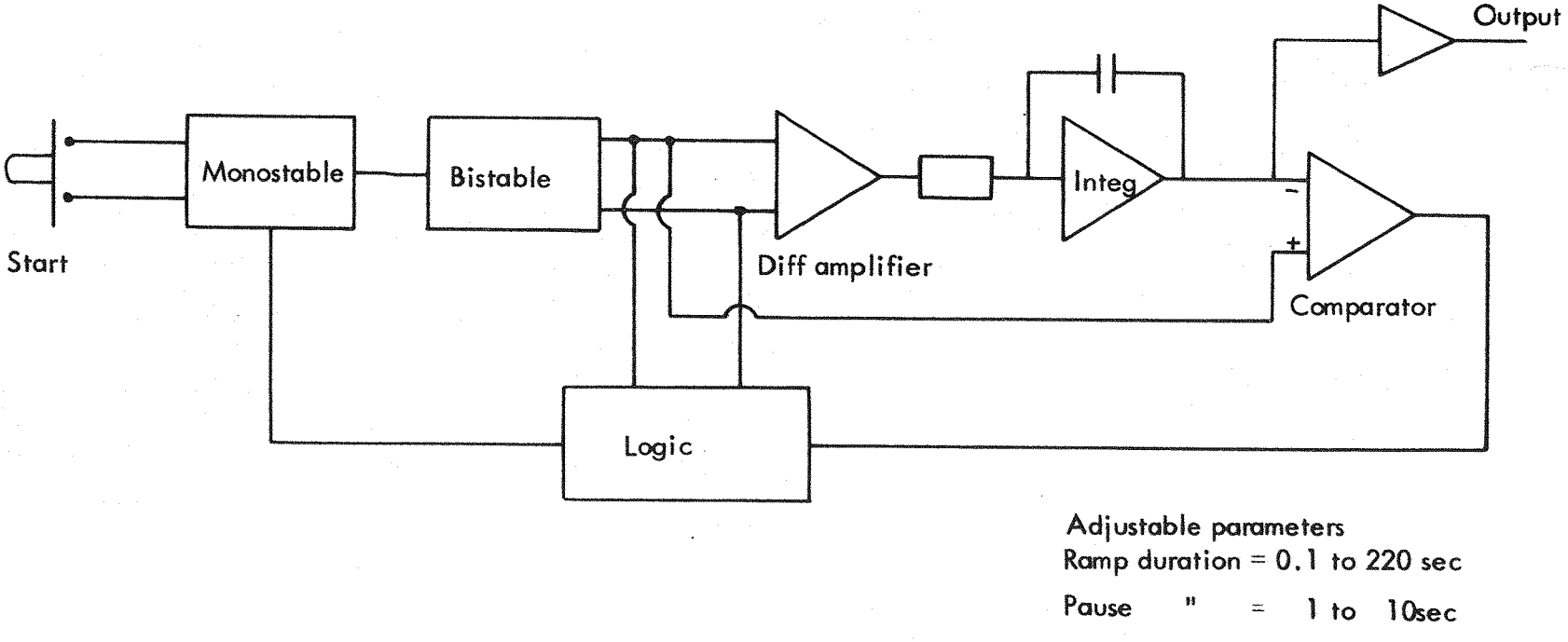

FIG. 4.11. SIMPLIFIED CIRCUIT OF PORTABLE RAMP FUNCTION WAVEFORM GENERATOR.

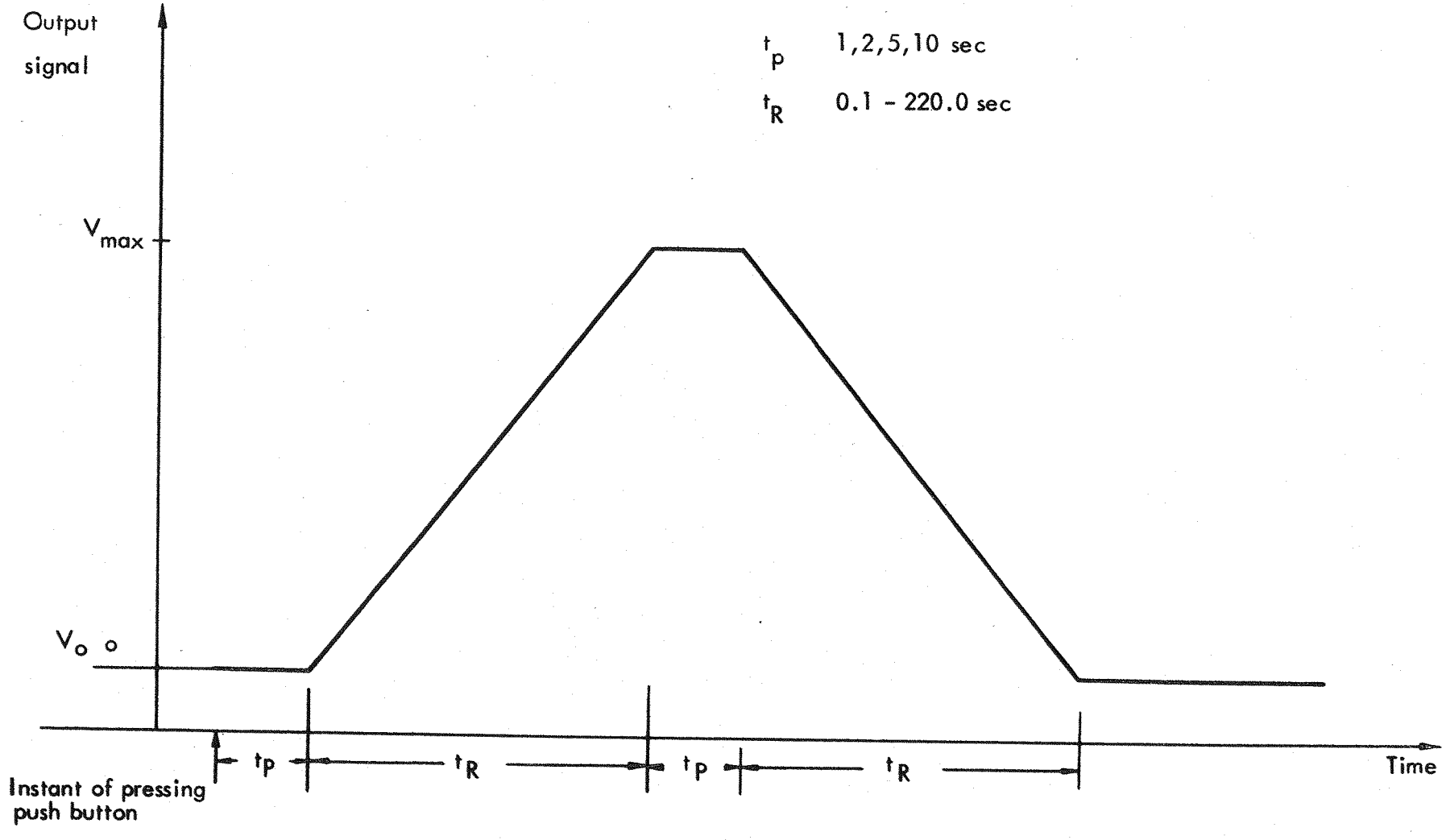

FIG. 4.12. THE VOLTAGE OBTAINED FROM THE RAMP FUNCTION GENERATOR.

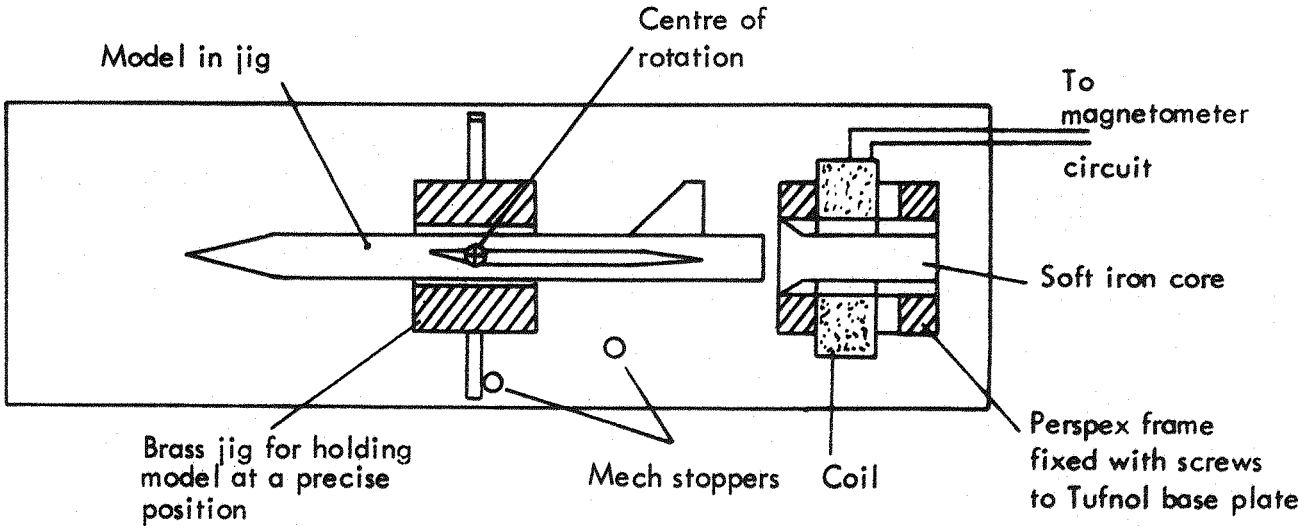

MAGNETOMETER LAYOUT

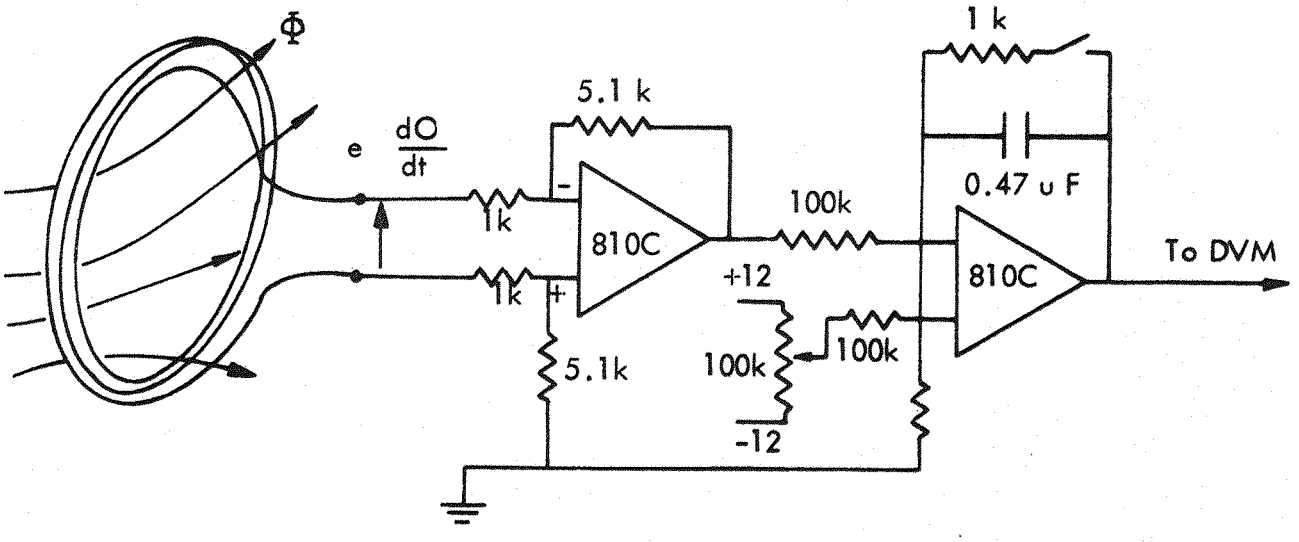

MAGNETOMETER CIRCUIT

FIG. 4.13. MAGNETOMETER LAYOUT AND CIRCUIT.

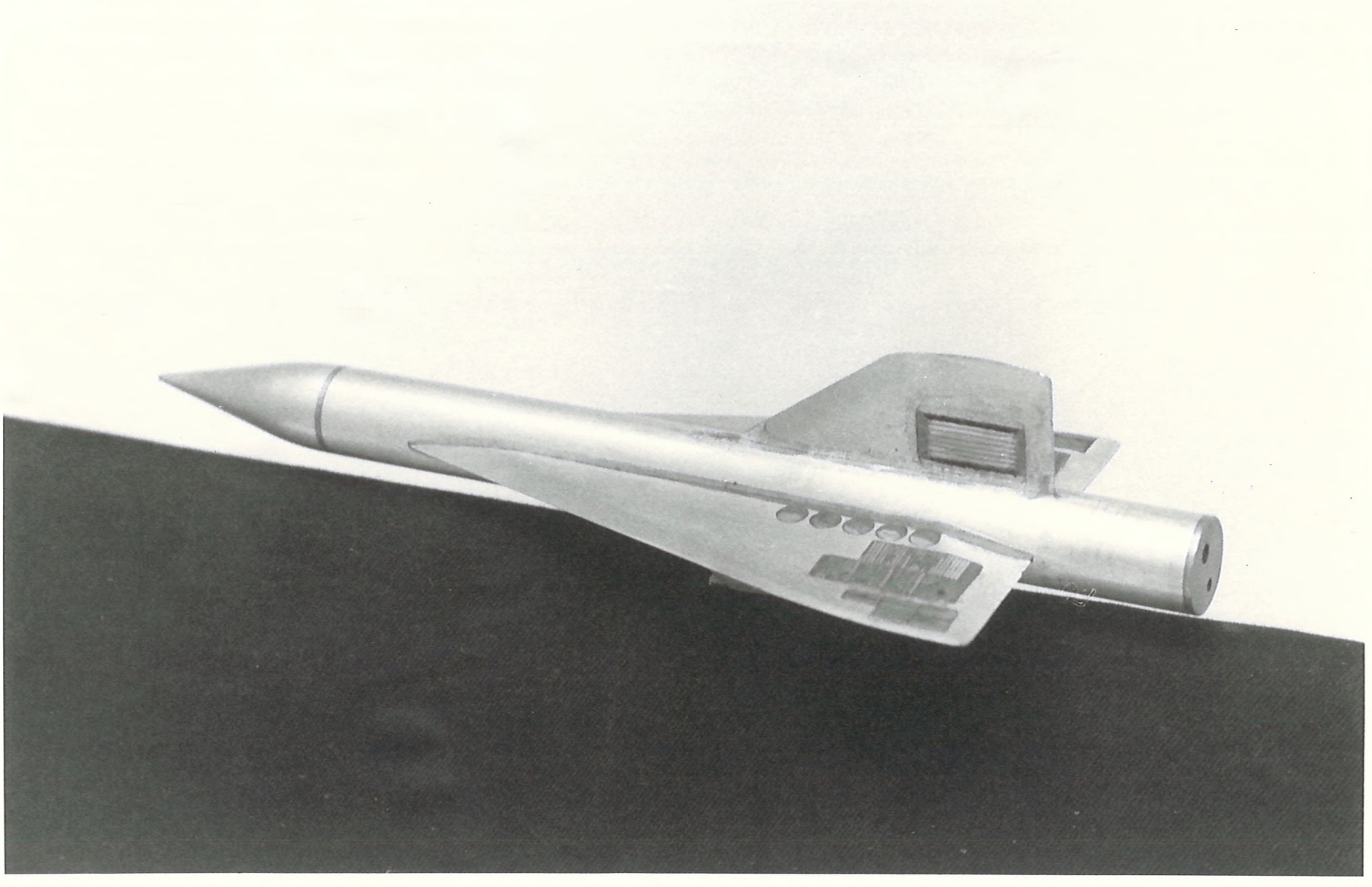

FIG. 5.1 MAIN MODEL - APPROX. AGARD-G

Transition strips, when present are, 3mm wide and 20mm streamwise behind wing L.E.

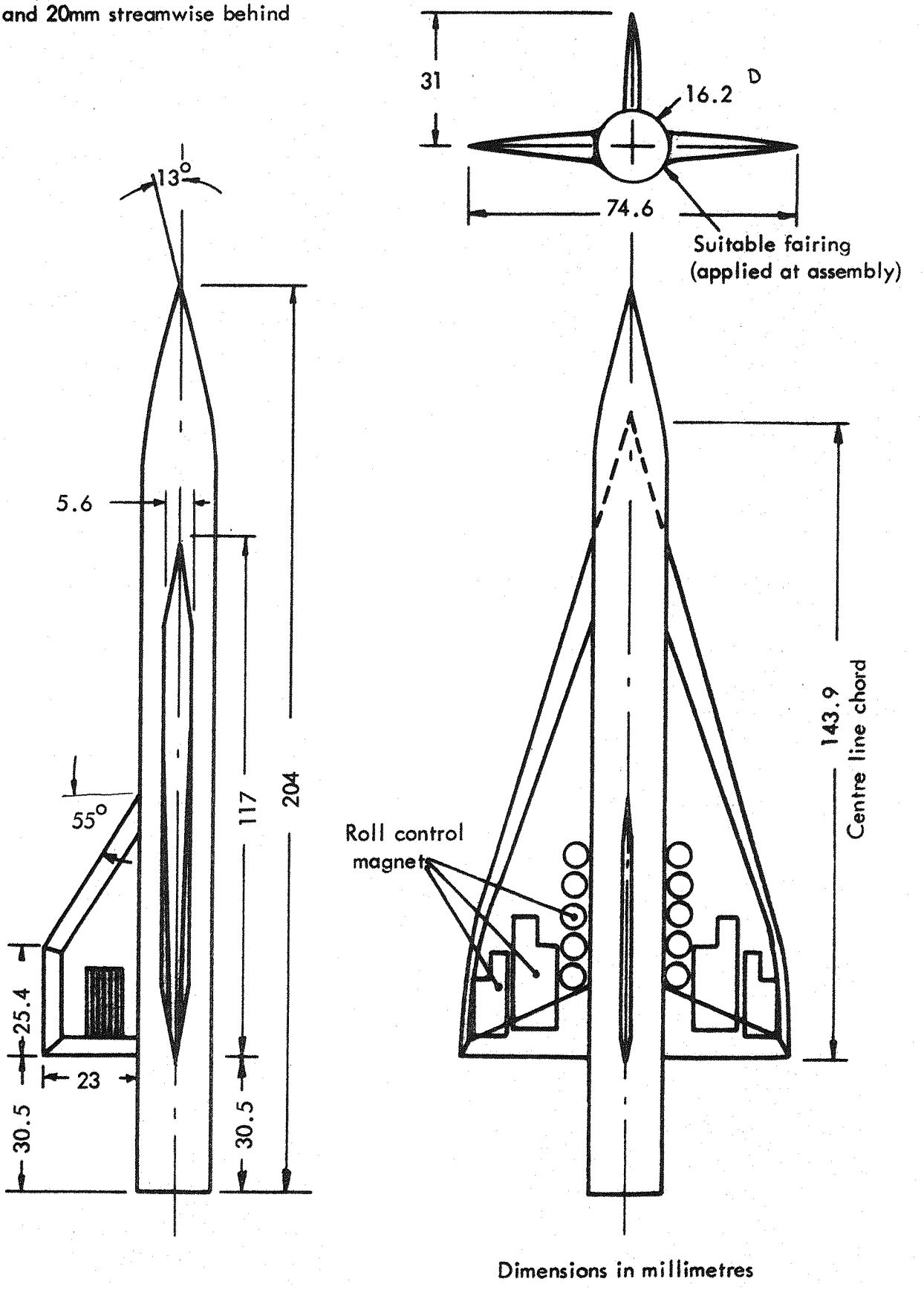

FIG. 5.2. AGARD -G WINGED MODEL.

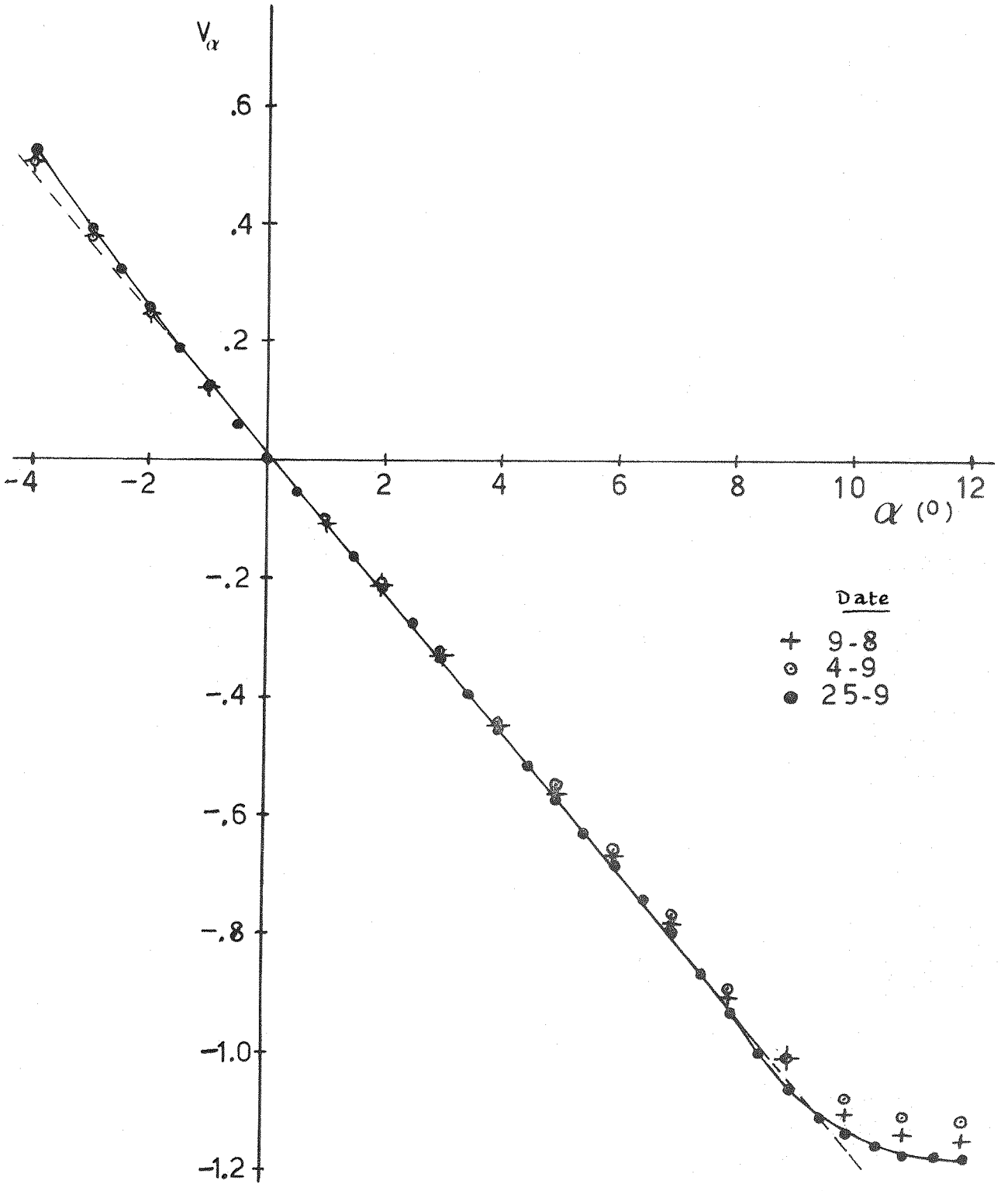

FIG. 5.3 INCIDENCE CALIBRATION

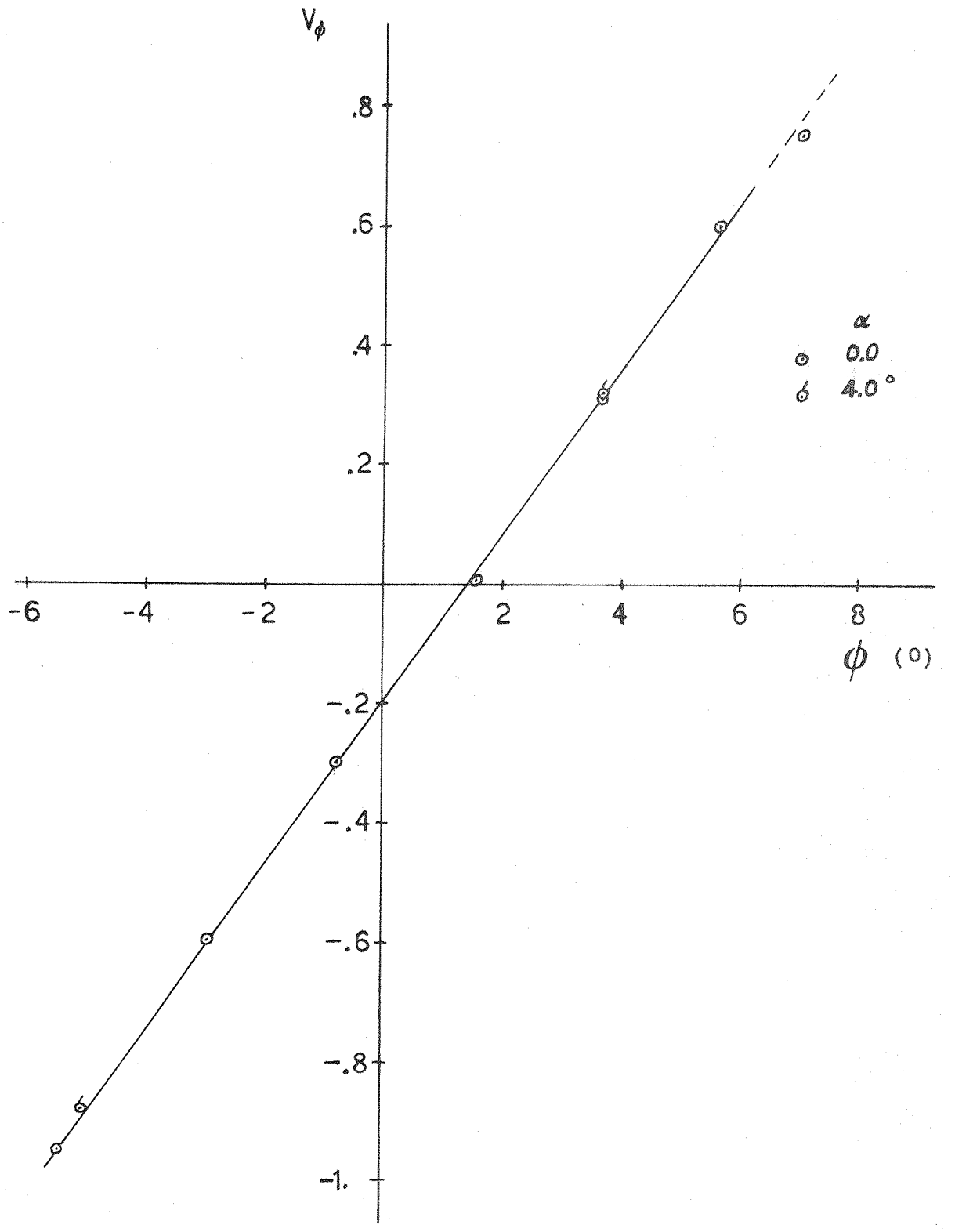

FIG. 5.4 ROLL DISPLACEMENT CALIBRATION

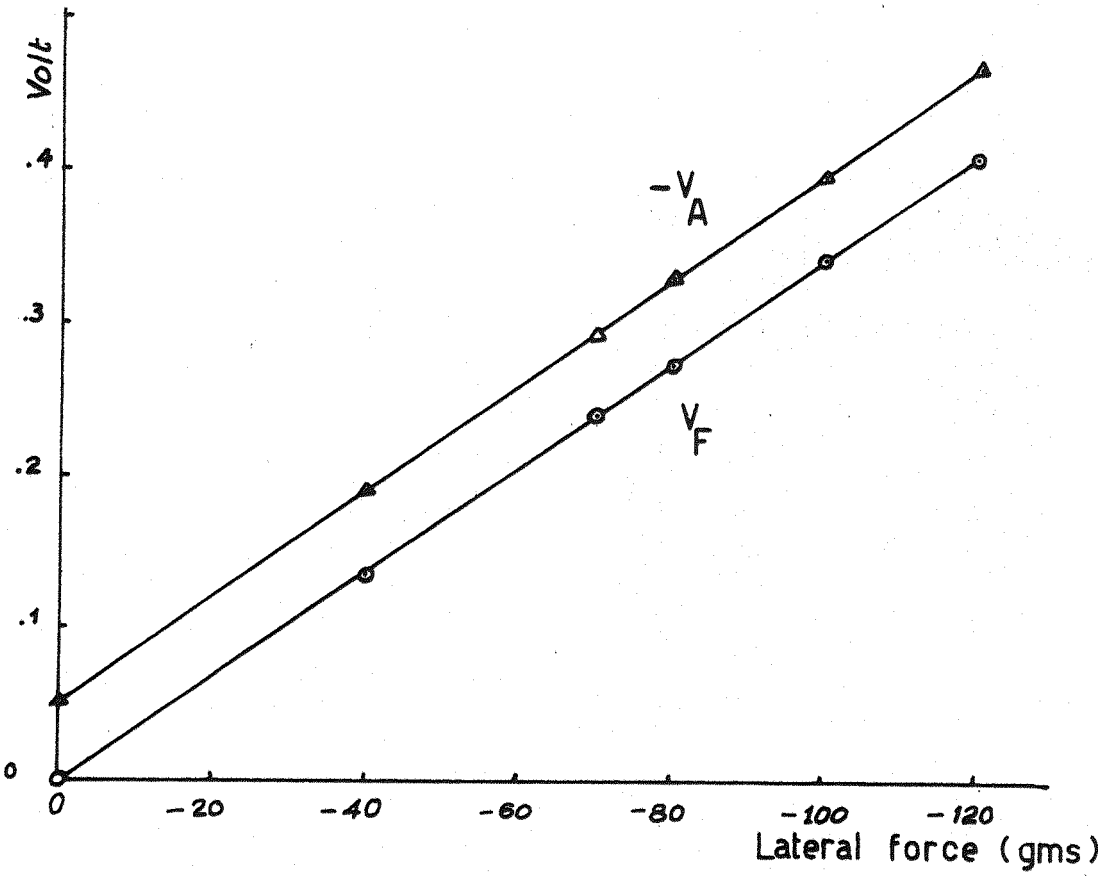

FIG. 5.5 LATERAL FORCE CALIBRATION

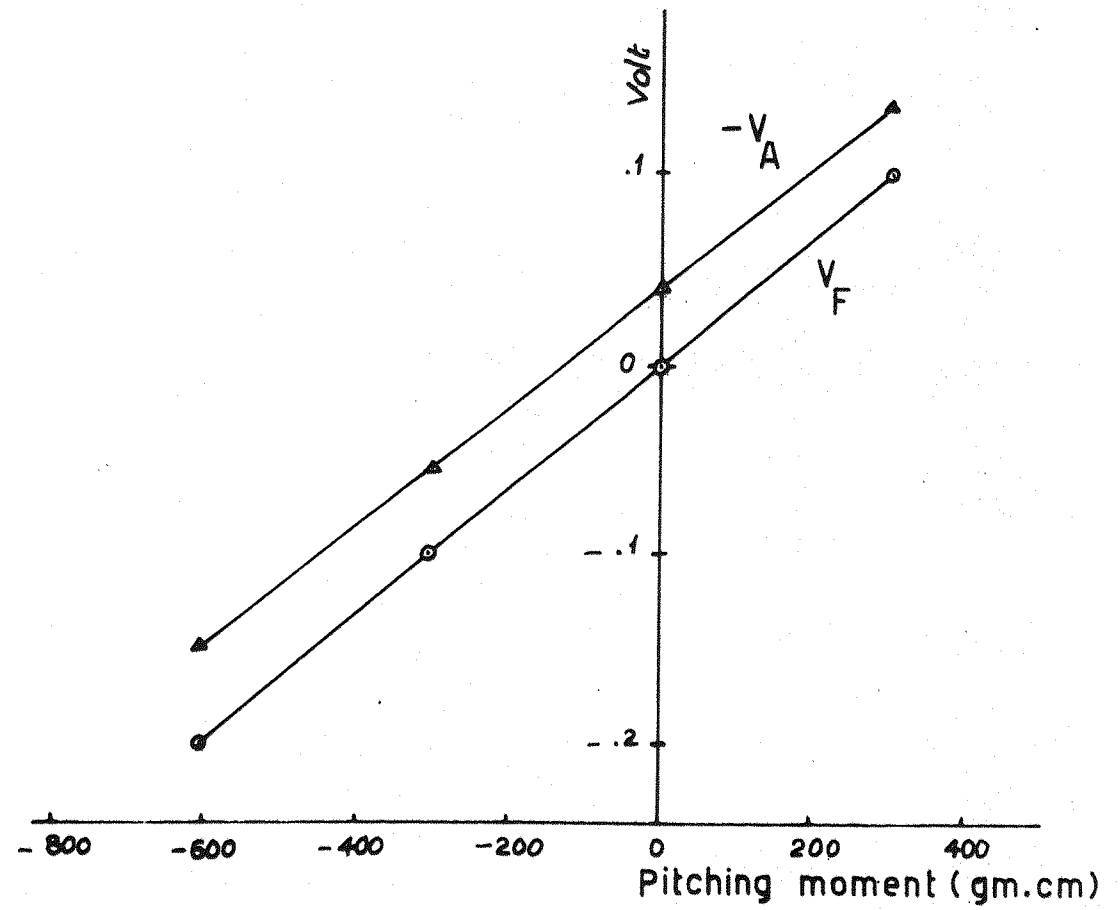

FIG. 5.6 PITCHING MOMENT CALIBRATION

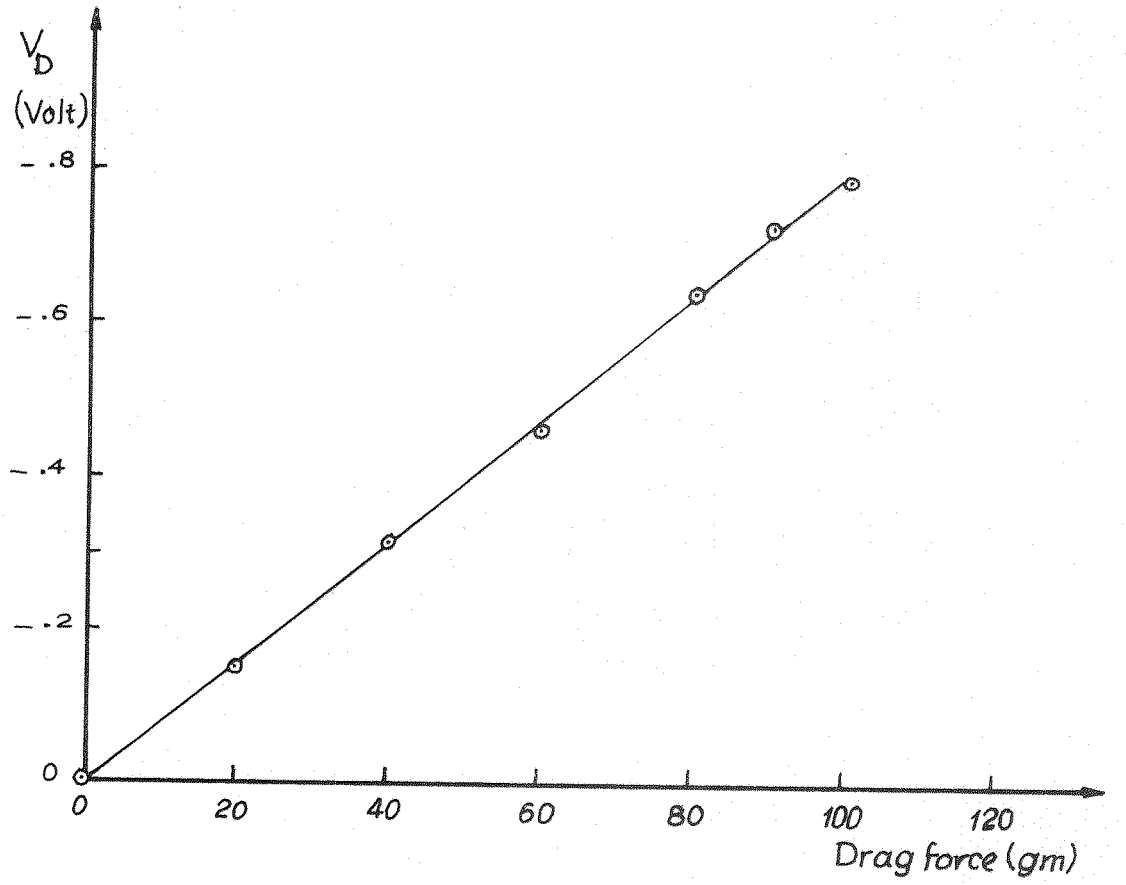

FIG. 5.7 DRAG FORCE CALIBRATION

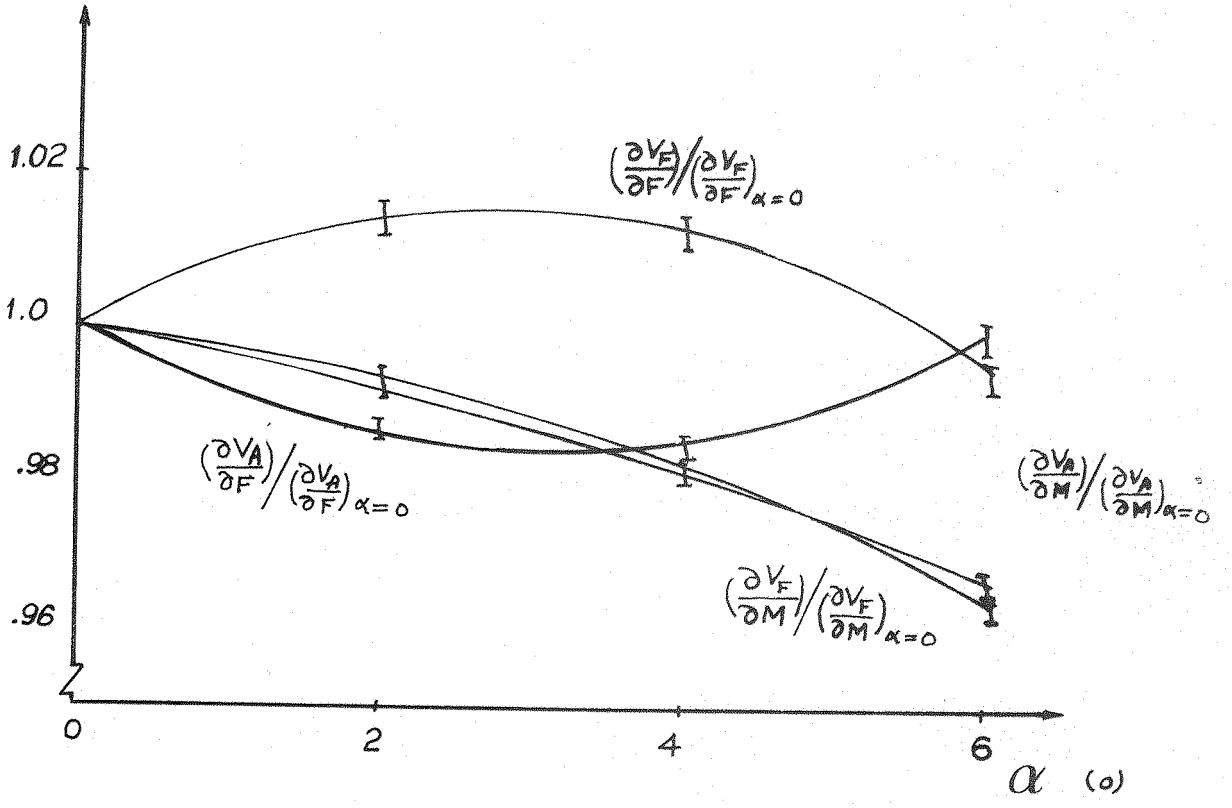

FIG. 5.8 VARIATION OF FORCE & MOMENT CALIBRATION CONSTANTS WITH α

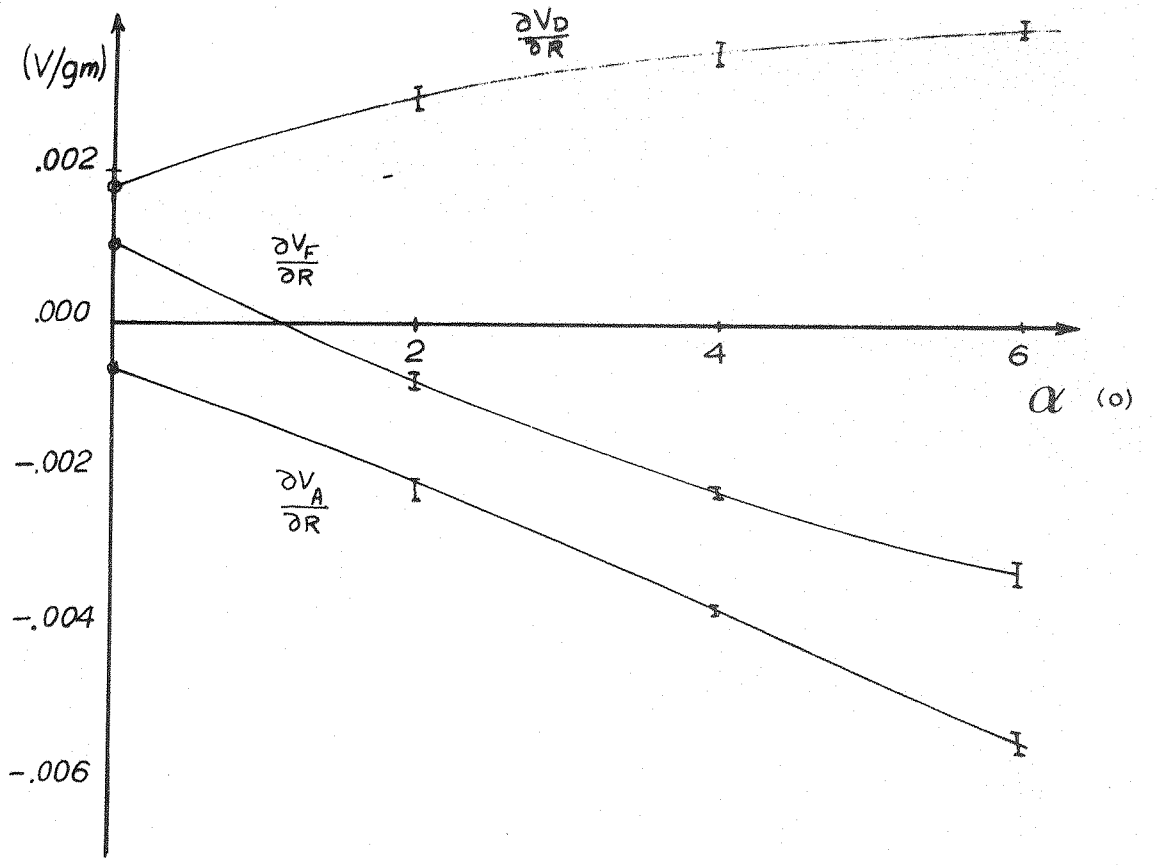

FIG. 5.9 VARIATION OF ROLL INTERACTION CALIBRATION CONSTANTS WITH α

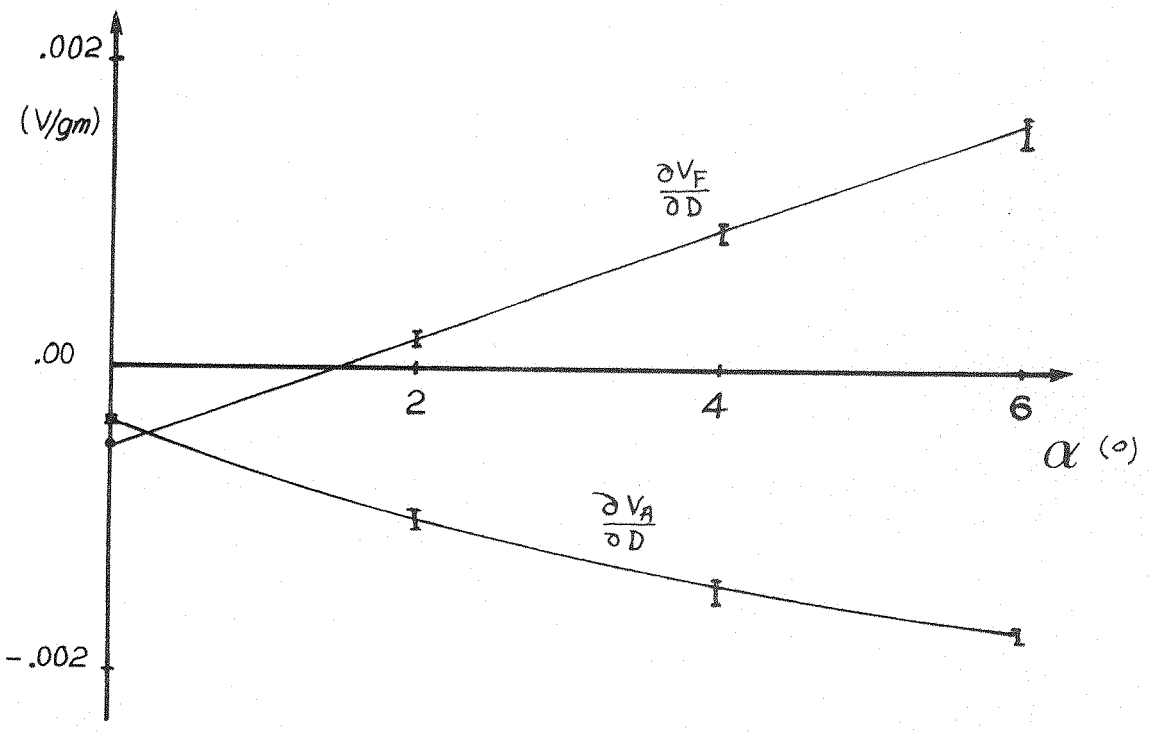

FIG. 5.10 VARIATION OF DRAG INTERACTION CALIBRATION CONSTANTS WITH α

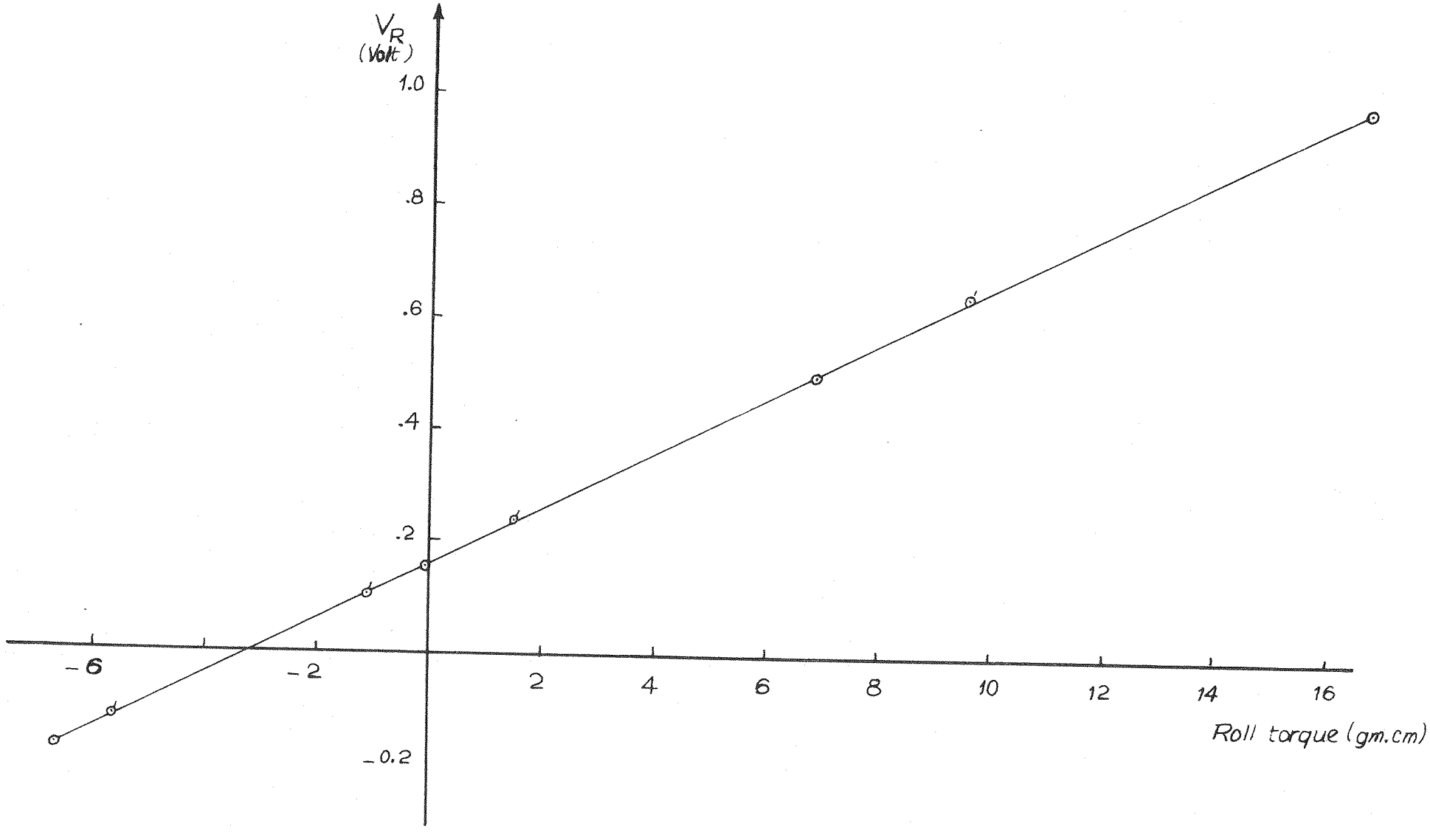

FIG. 5.11 ROLL TORQUE CALIBRATION

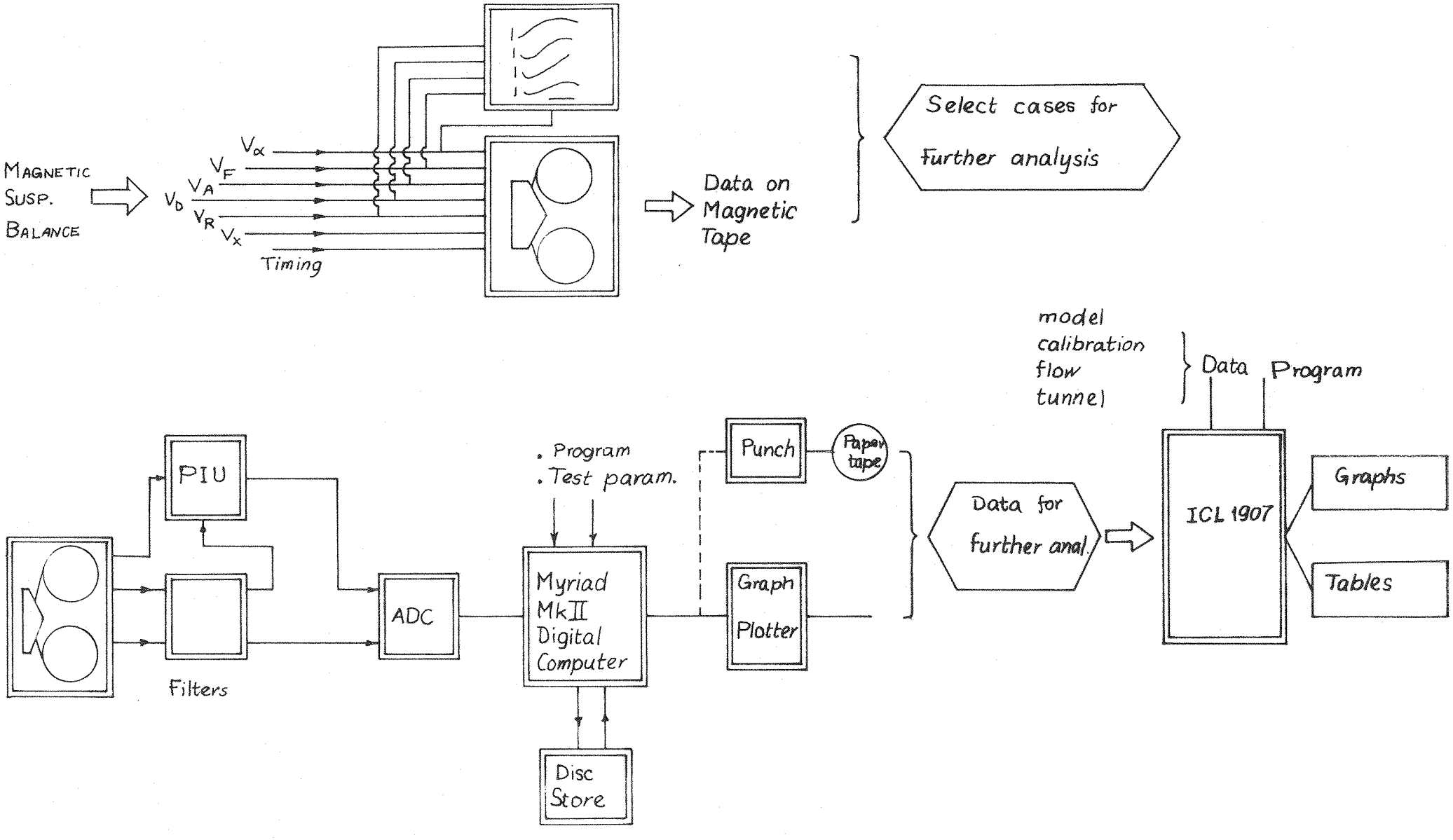

FIG 6.1 STEADY AERODYNAMIC ACQUISITION AND REDUCTION

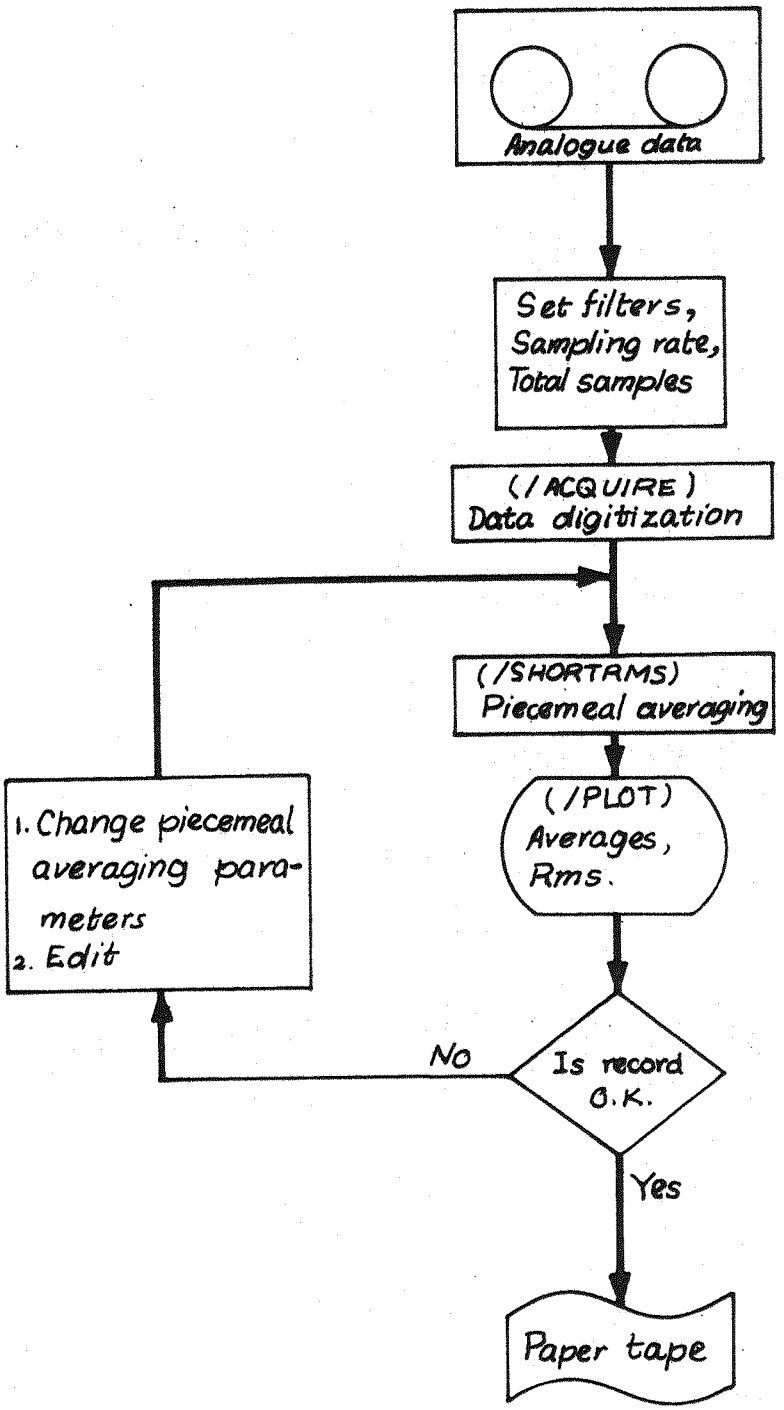

FIG. 6.2 DATA REDUCTION ON MYRIAD COMPUTER

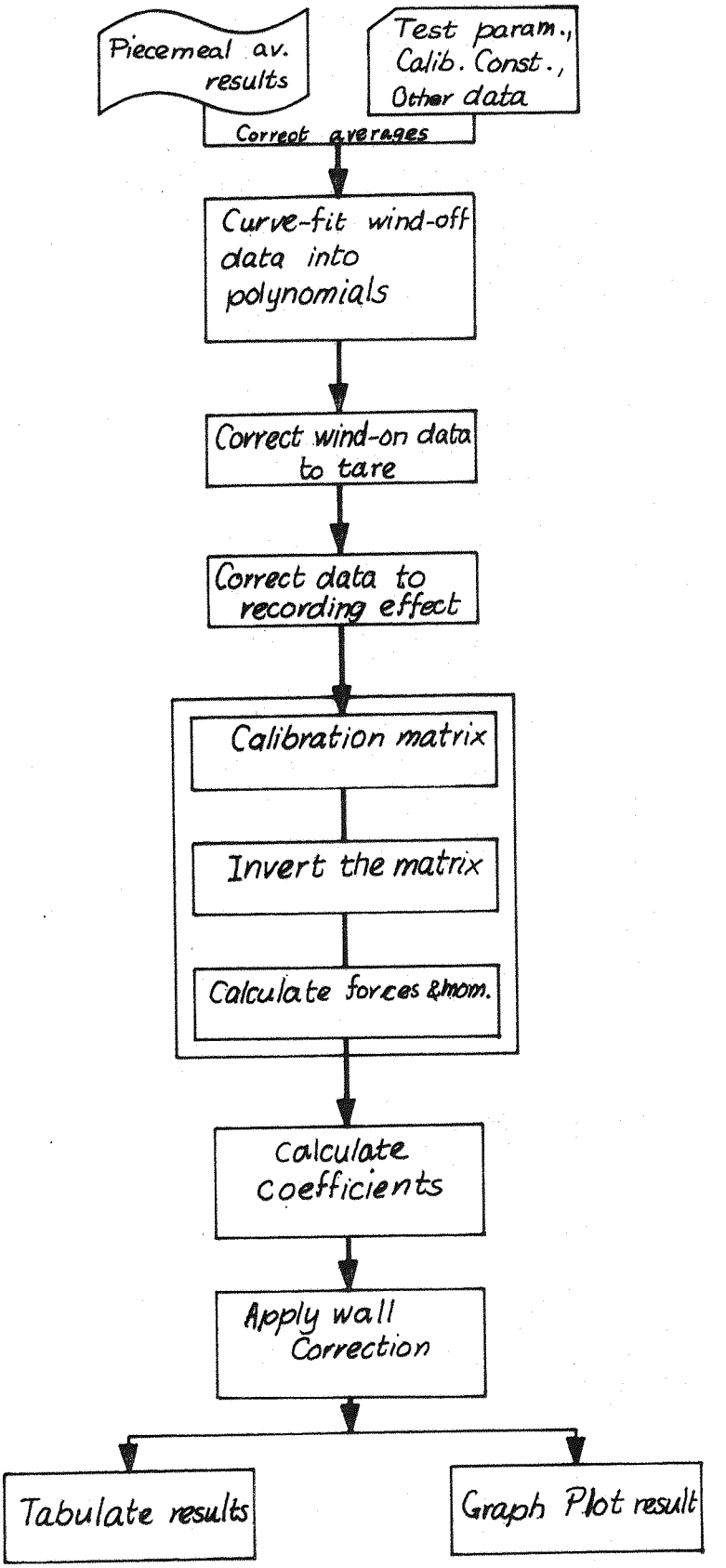

FIG. 6.3 FLOW CHART OF MAIN PROGRAM

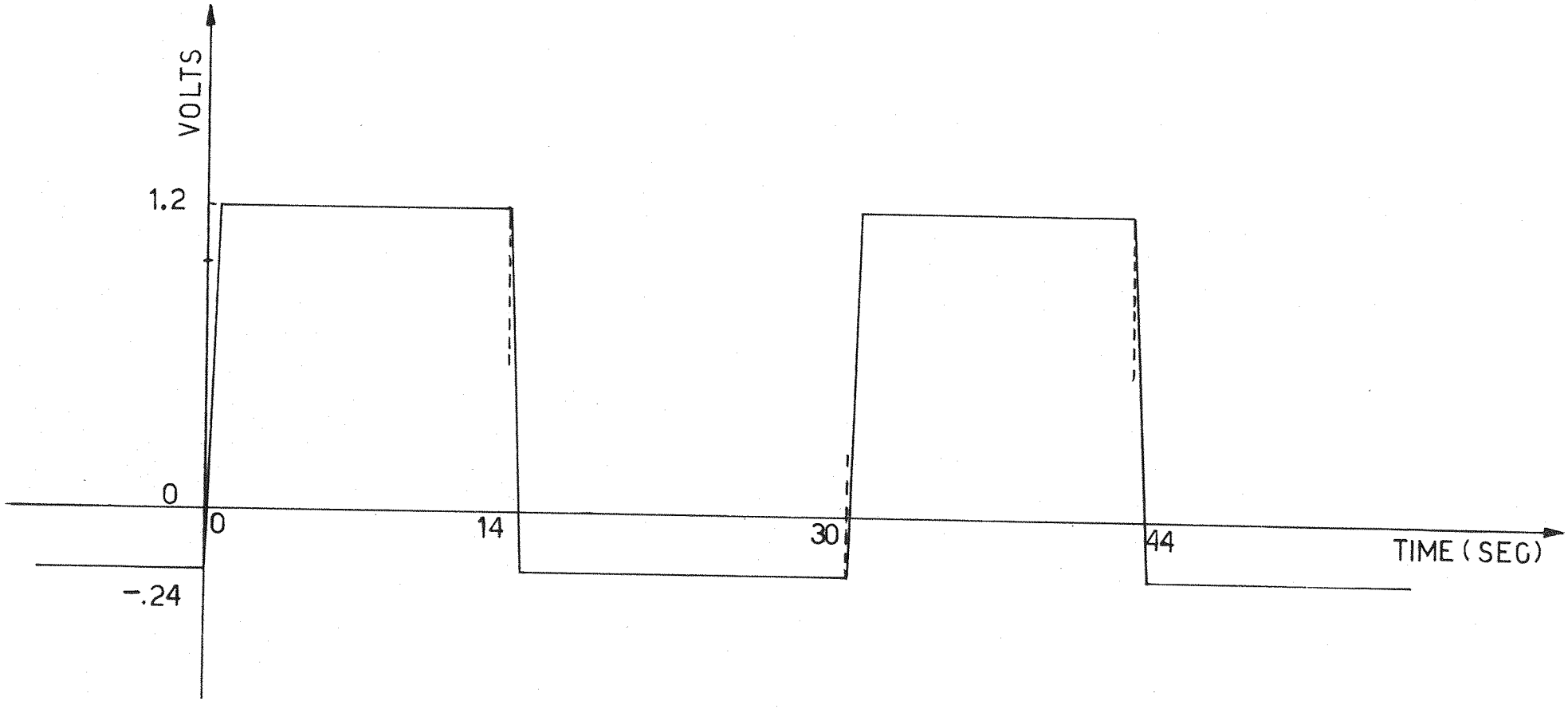

FIG. 6-4 TAPE RECORDER D-C CALIBRATION SIGNAL

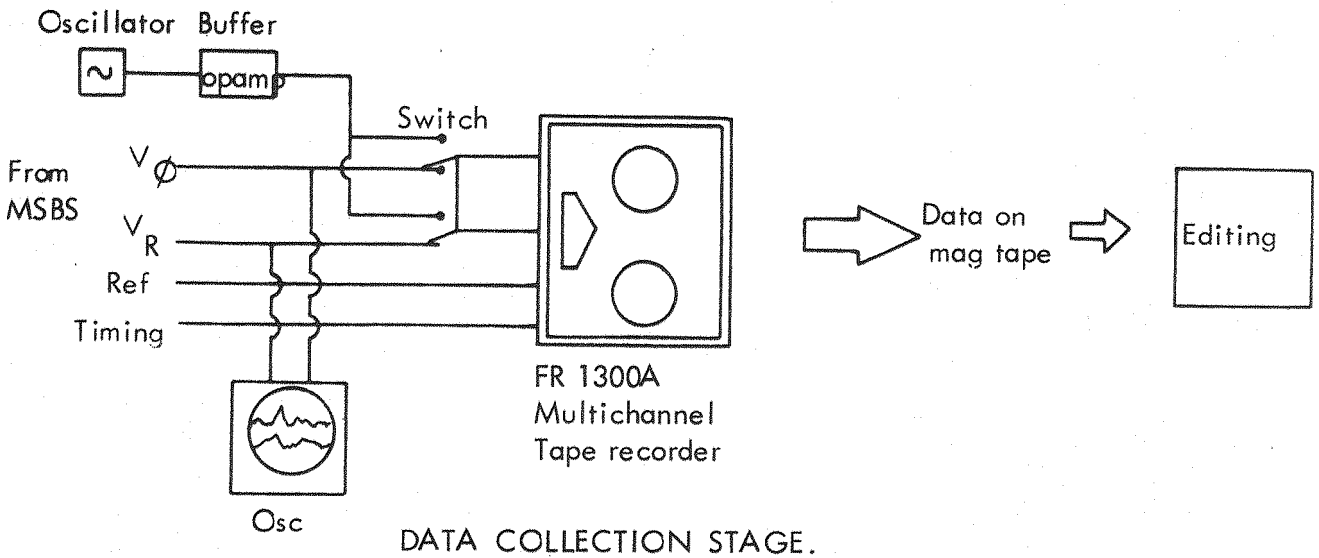

DATA COLLECTION STAGE.

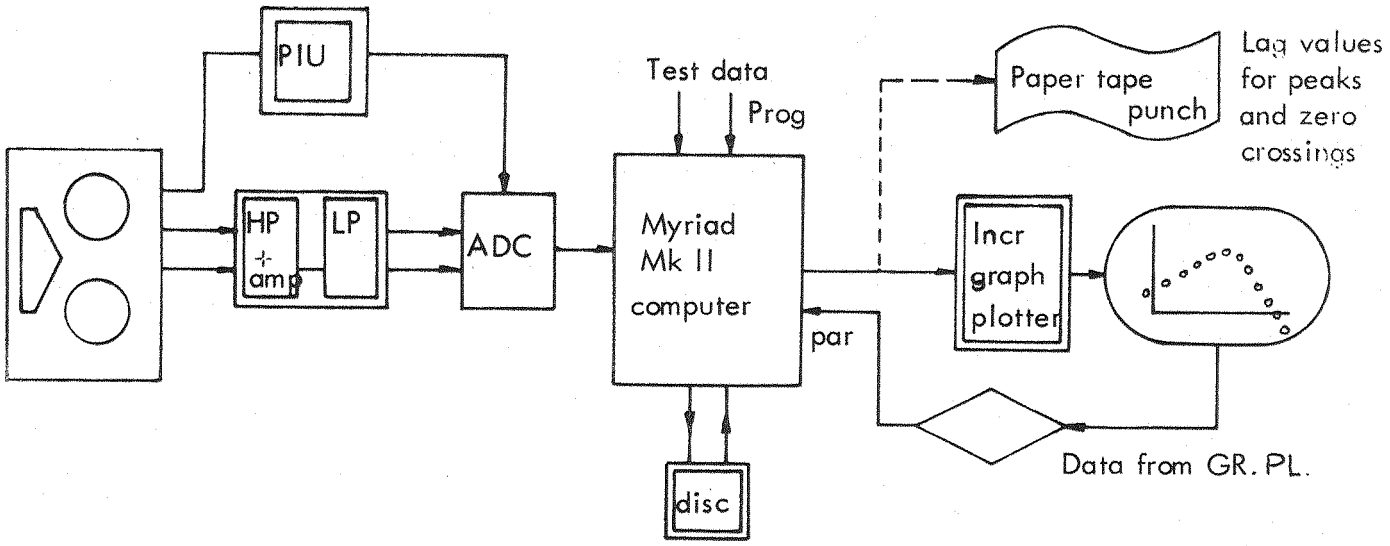

DATA REDUCTION AND ANALYSIS STAGE

FIG. 6.5. DATA COLLECTION , REDUCTION AND ANALYSIS , DYNAMIC TESTING.

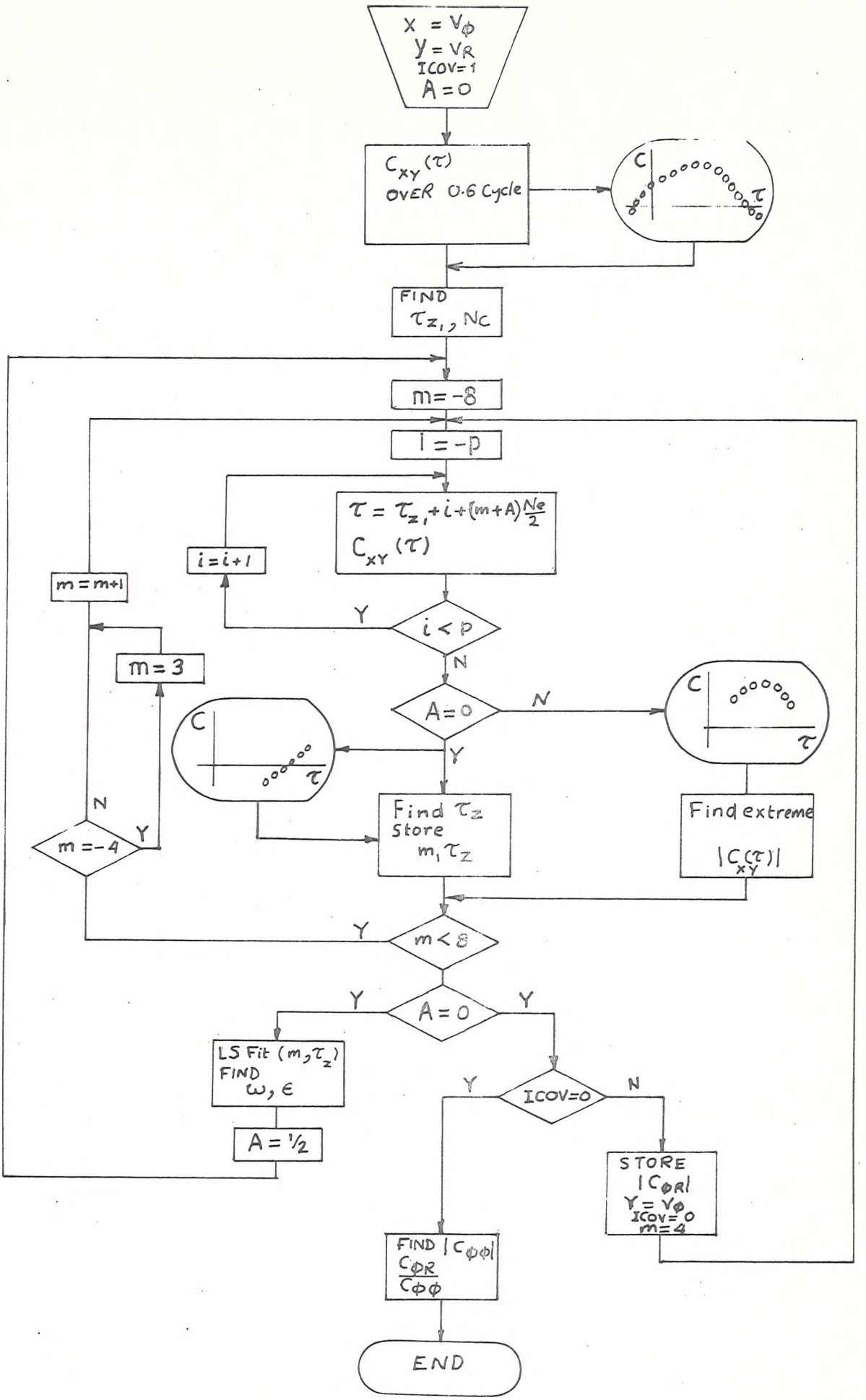

FIG. 6.6 DETAIL FLOW CHART OF ZEROCROSSING COVARIANCE METHOD OF TWO SIGNALS.

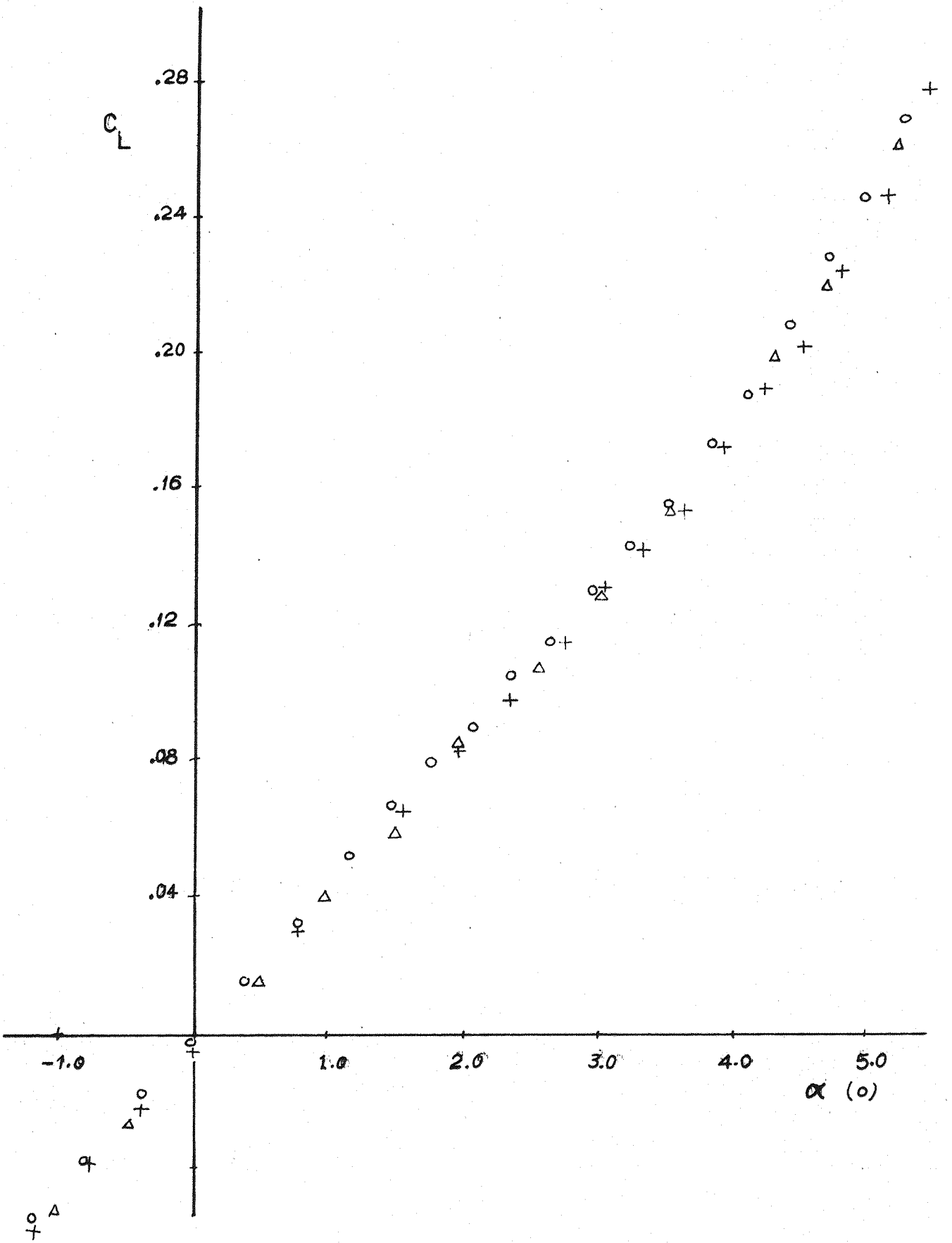

FIG. 7.1a A REDUCTION USING POINT BY POINT MEASUREMENT MODEL (i)

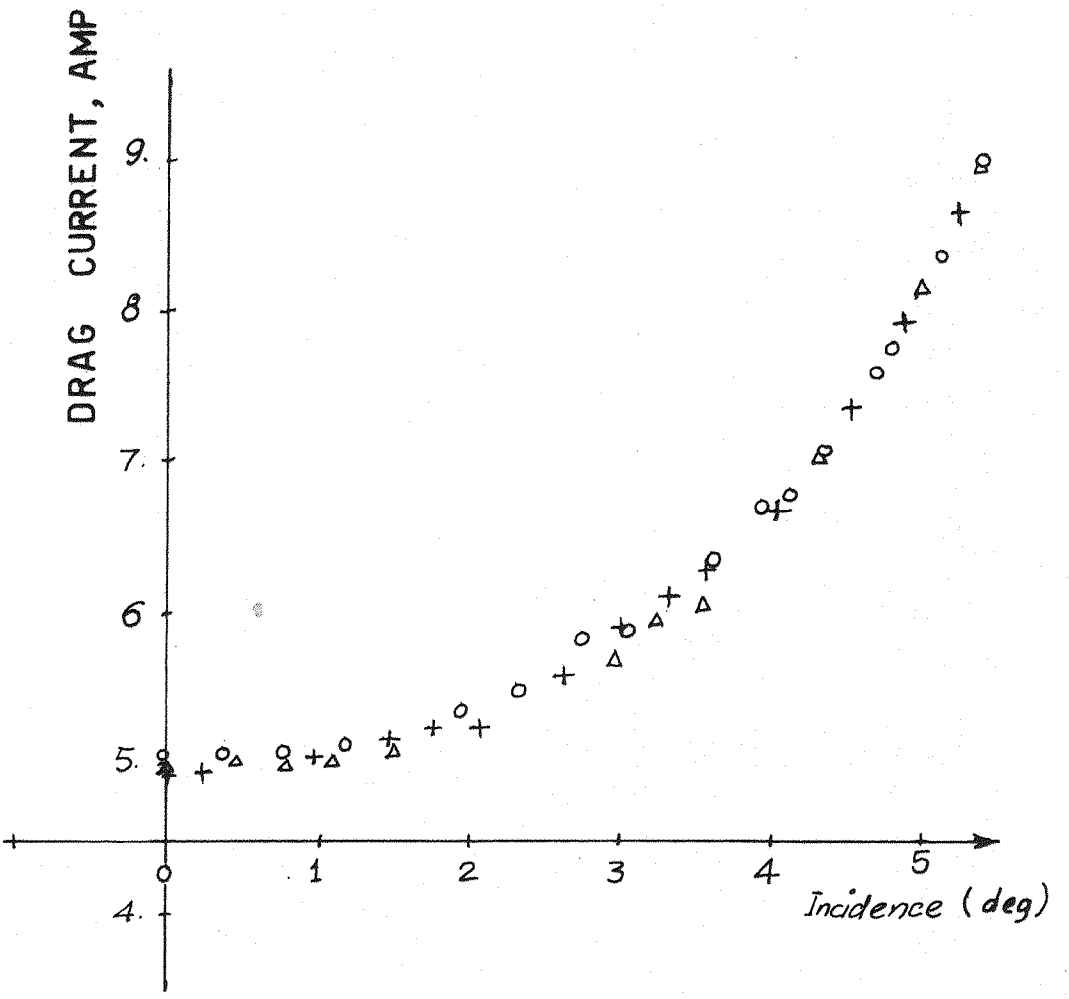

FIG. 7.1 b VARITION OF DRAG CURRENT WITH INCIDENCE
MODEL (*i*) WIND-ON

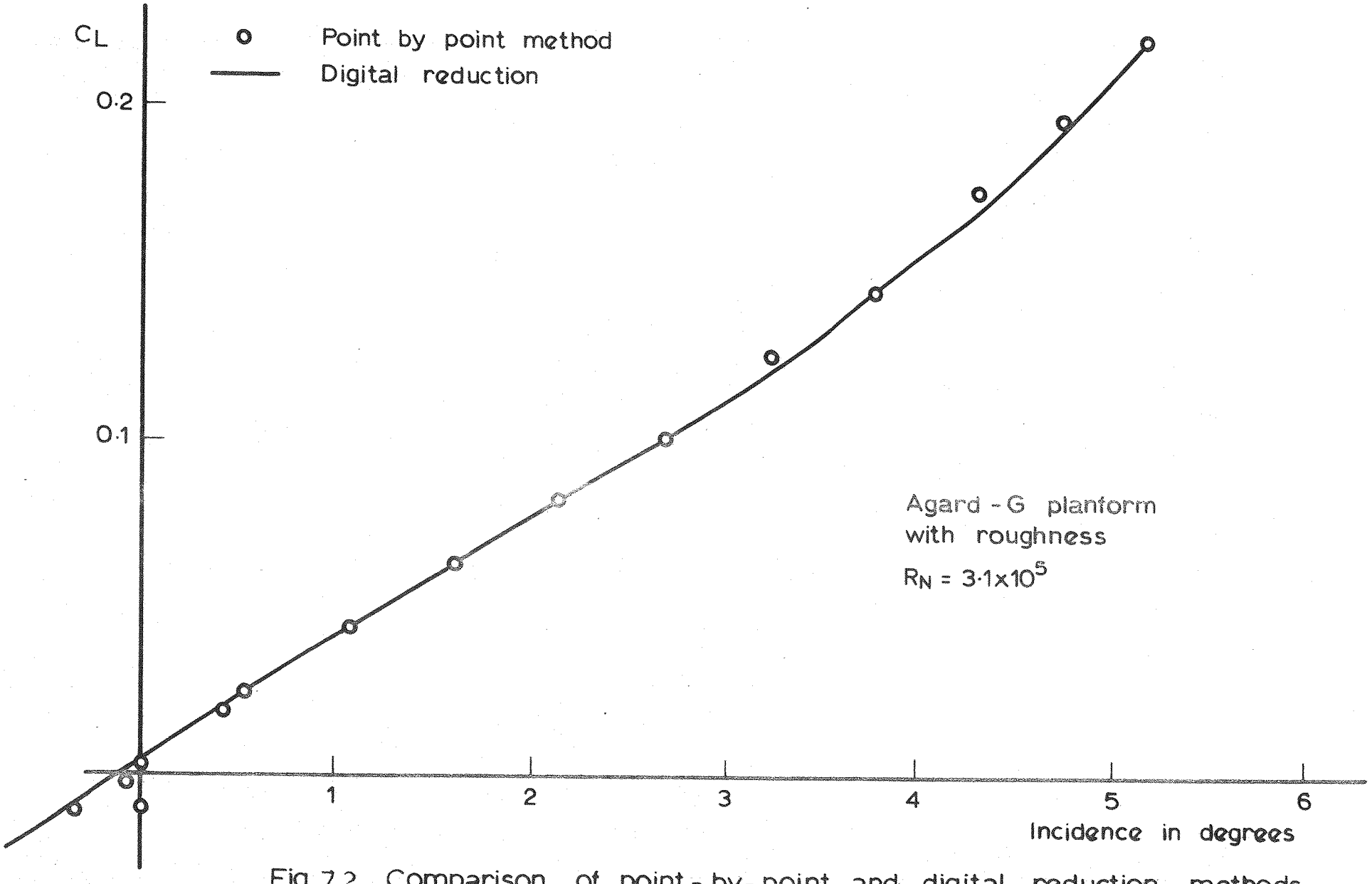

Fig 7.2 Comparison of point - by - point and digital reduction methods

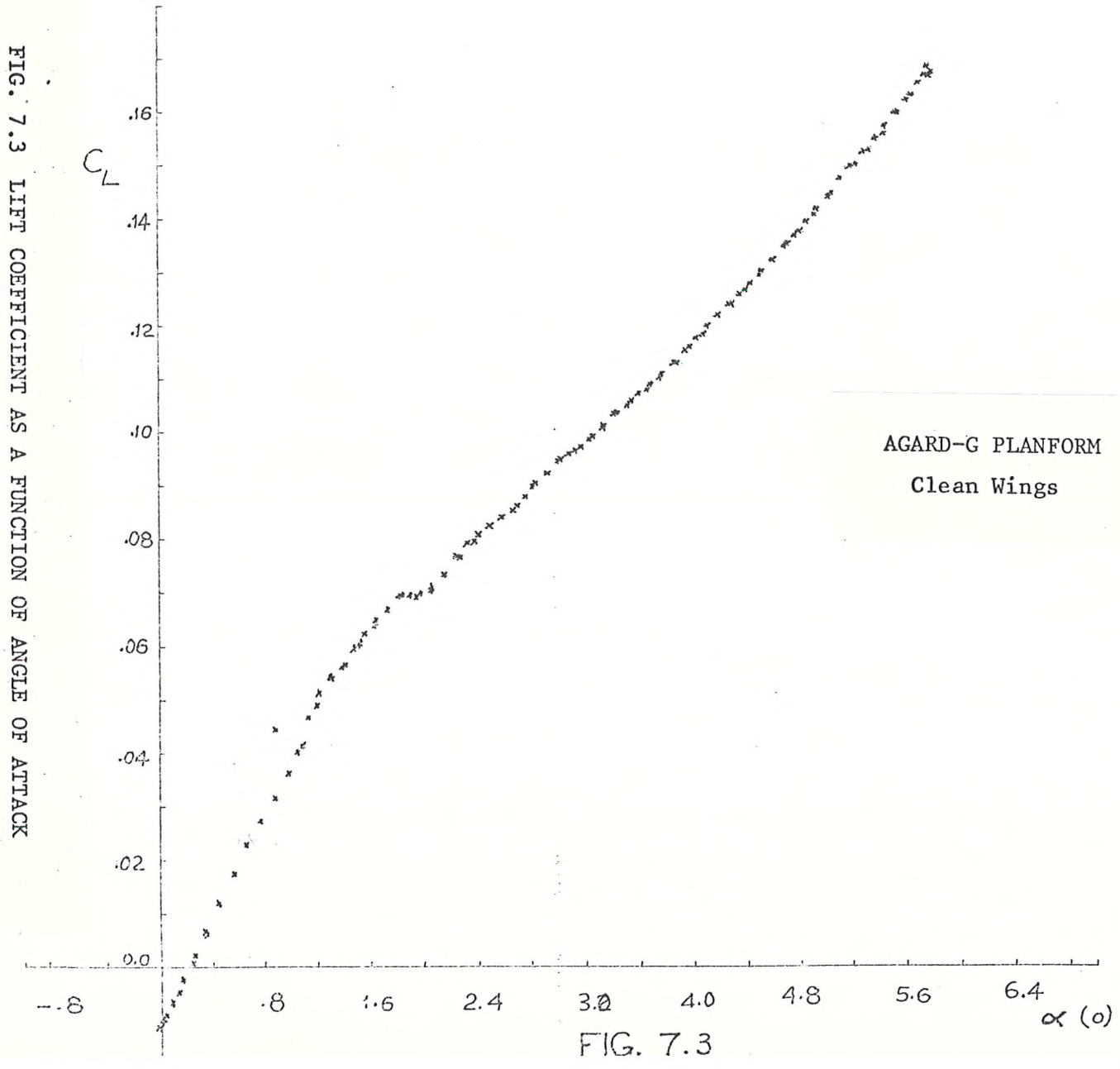

FIG. 7.3 LIFT COEFFICIENT AS A FUNCTION OF ANGLE OF ATTACK

CONTINUOUS SWEEP METHOD WITH PIECEMEAL AVERAGING.

FIG. 7.3

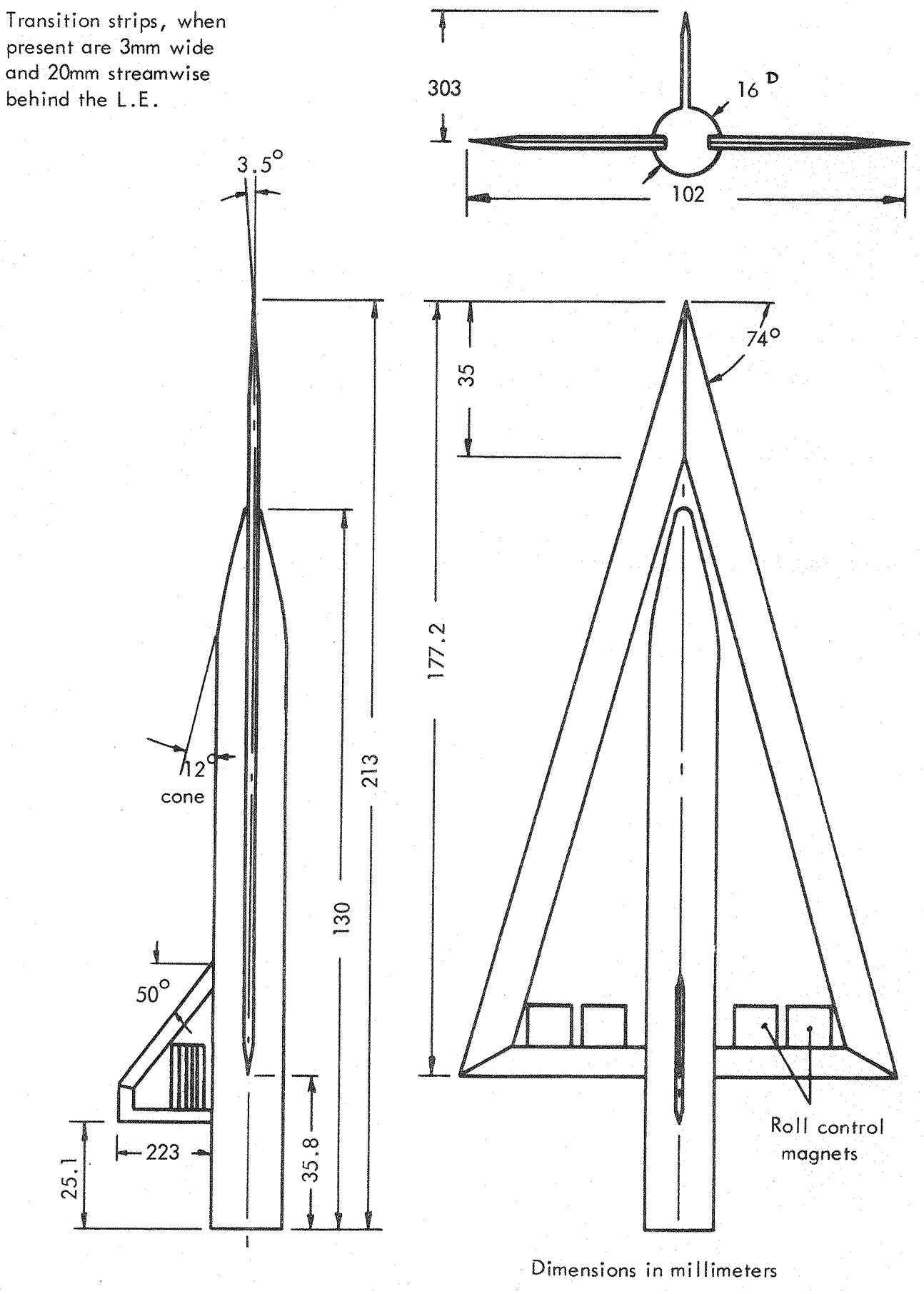

FIG. 7.4. RAK FLAT PLATE DELTA WING MODEL (REF DRWNG NASA LC 934847)

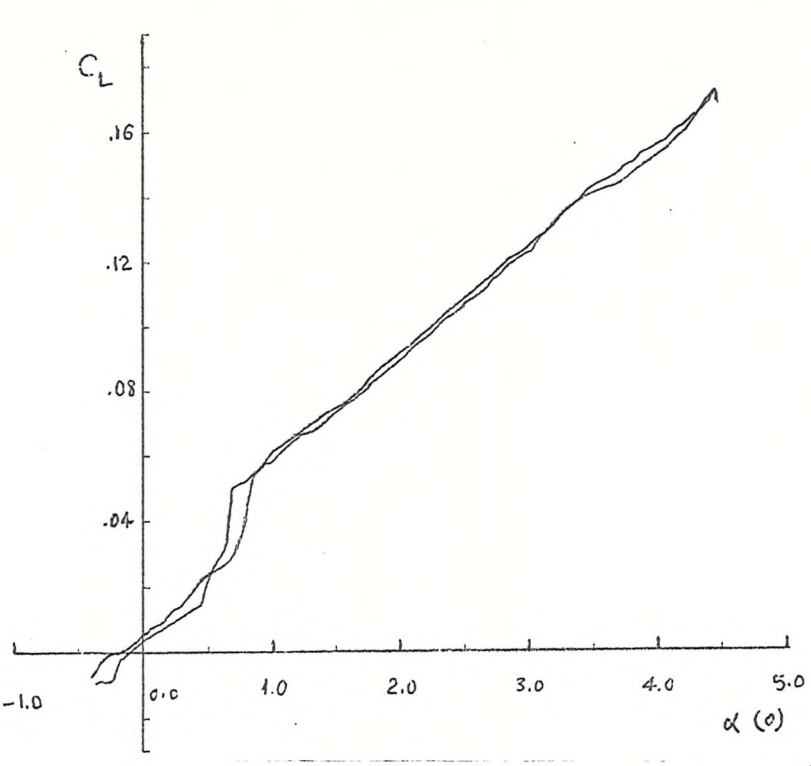

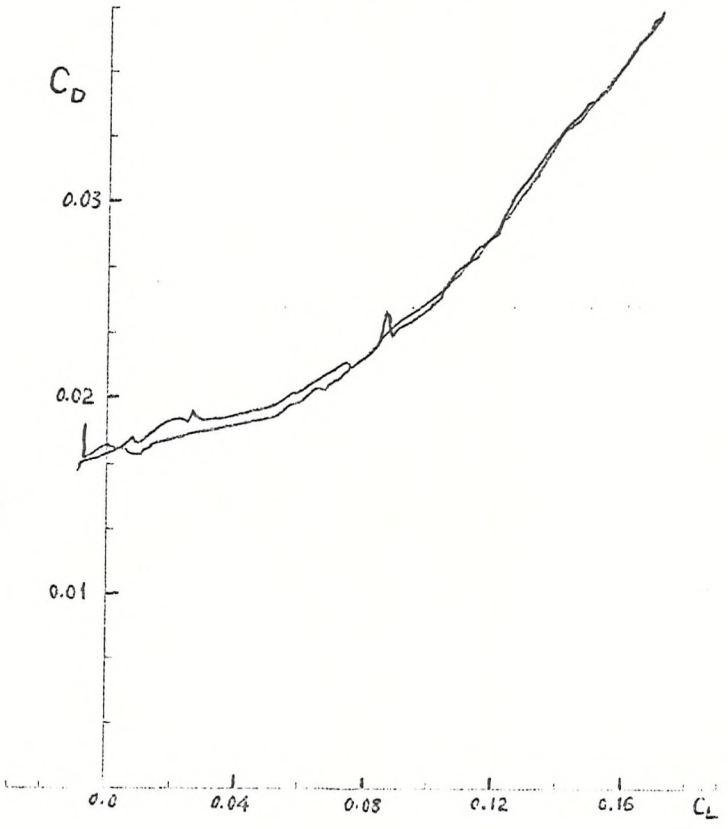

FIG. 7.5 RAK MODEL RESULTS, CLEAN WINGS

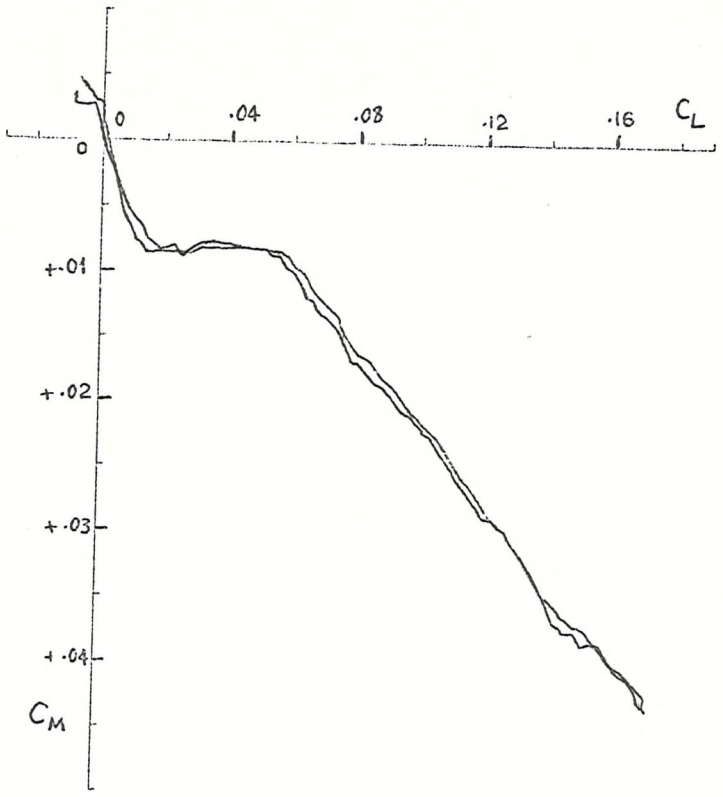
0
.04
.08
.12
.16
C_L
0
+.01
+.02
+.03
+.04
C_M

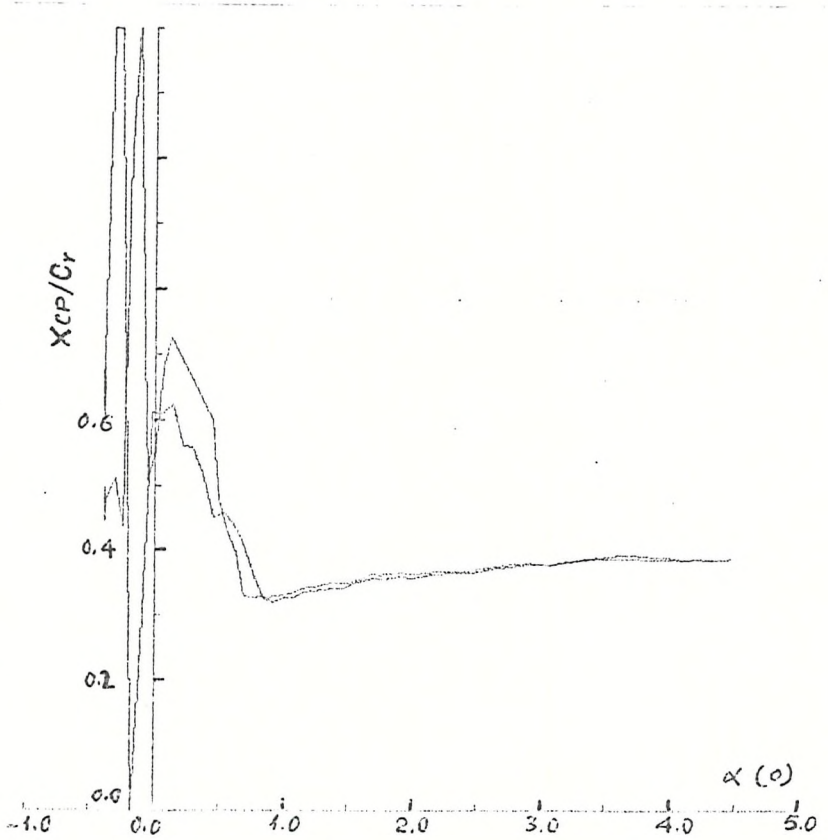
X_{CP}/C_r
0.6
0.4
0.2
0.0
α (0)
-1.0
0.0
1.0
2.0
3.0
4.0
5.0

FIG. 7.5 (Cont)

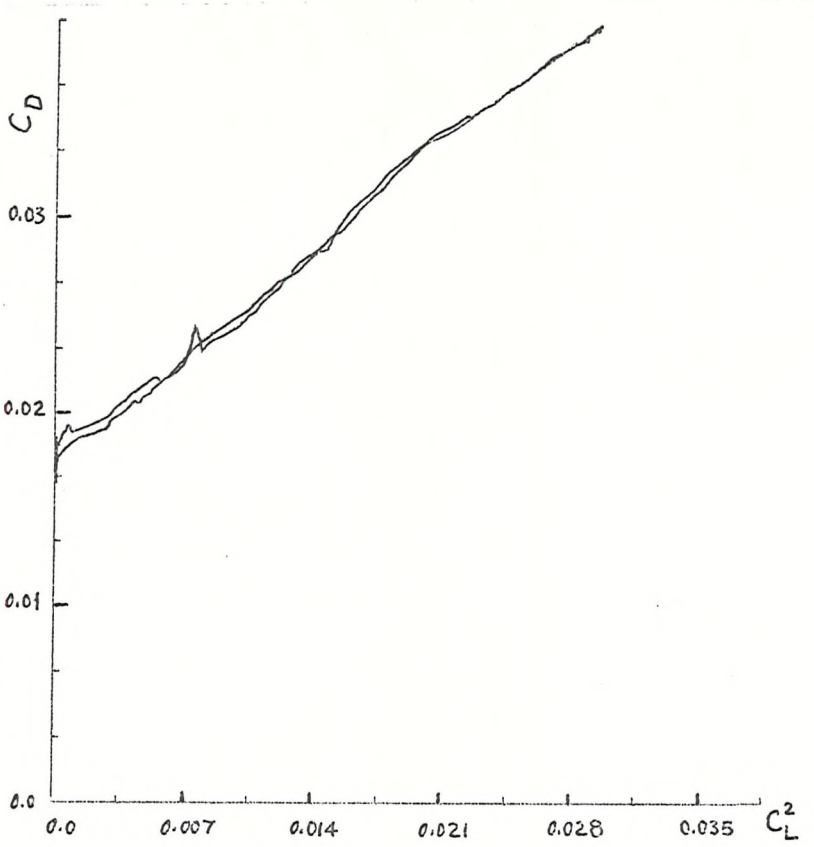
C_D
0.03
0.02
0.01
0.0
0.0
0.007
0.014
0.021
0.028
0.035
C_L^2

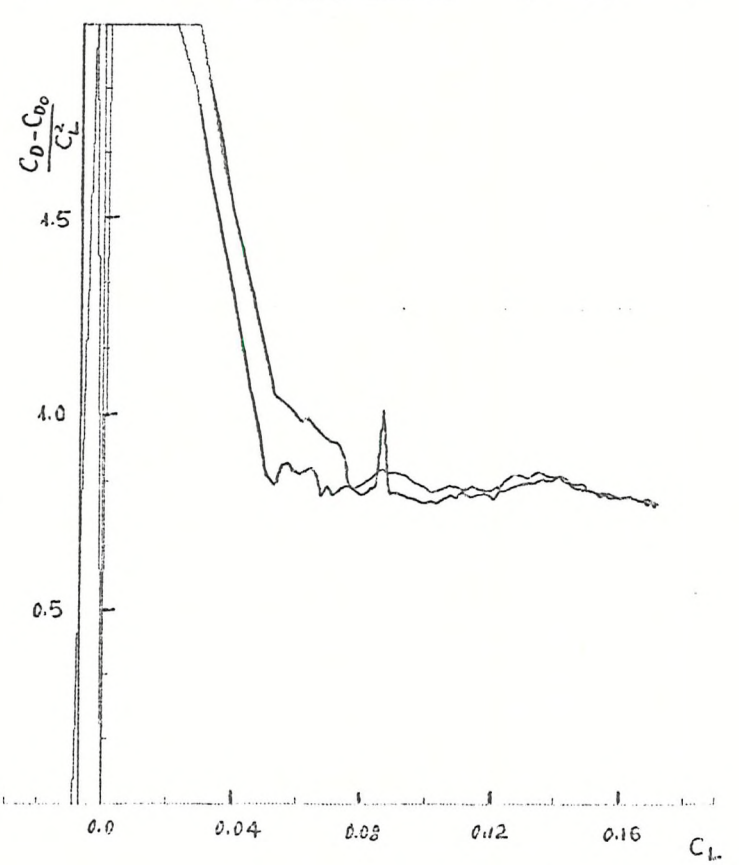
$\frac{C_D - C_{D_0}}{C_L^2}$
1.5
1.0
0.5
0.0
0.04
0.08
0.12
0.16
C_L

FIG. 7.5 (Cont.)

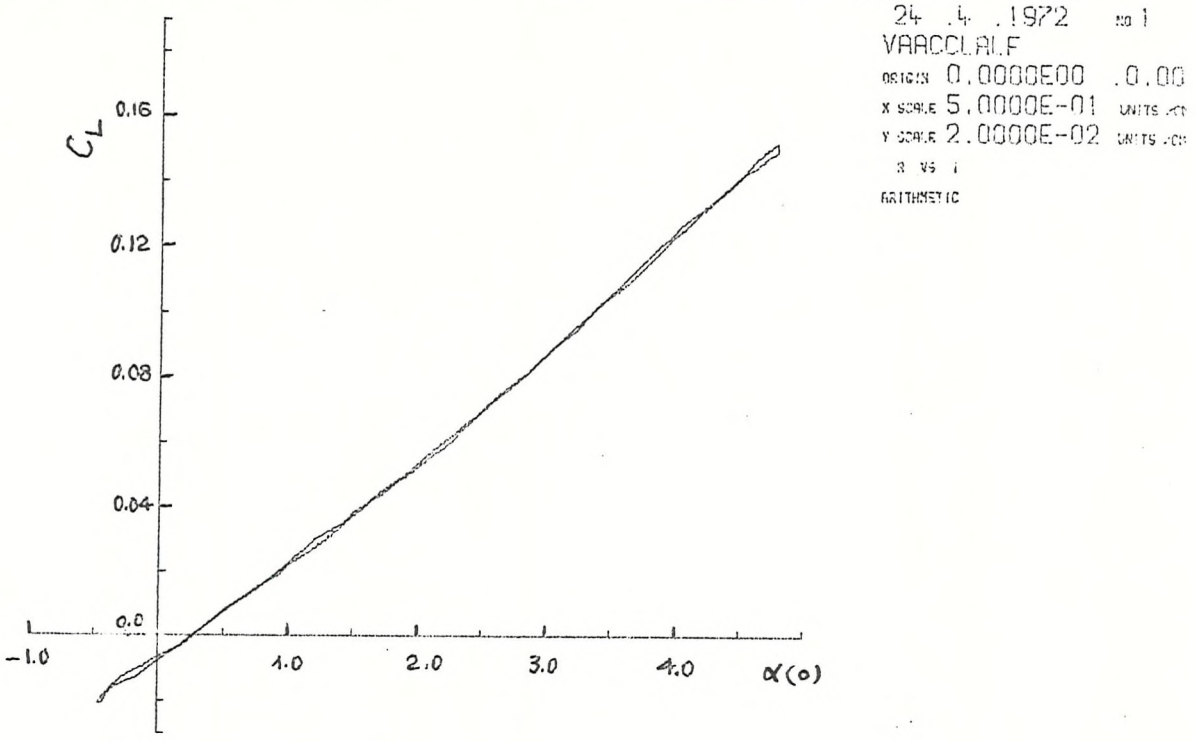

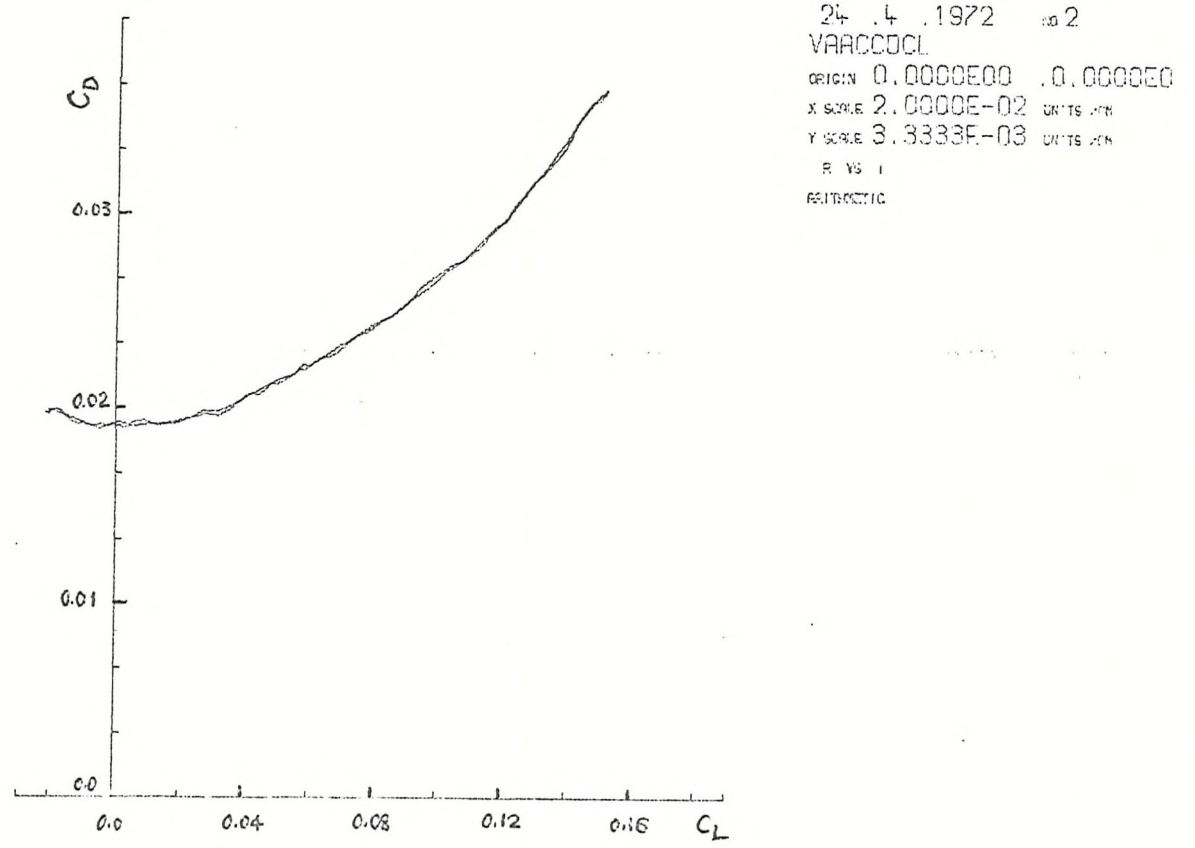

FIG. 7.6 RAK MODEL RESULTS, WINGS WITH TRANSITION STRIPS

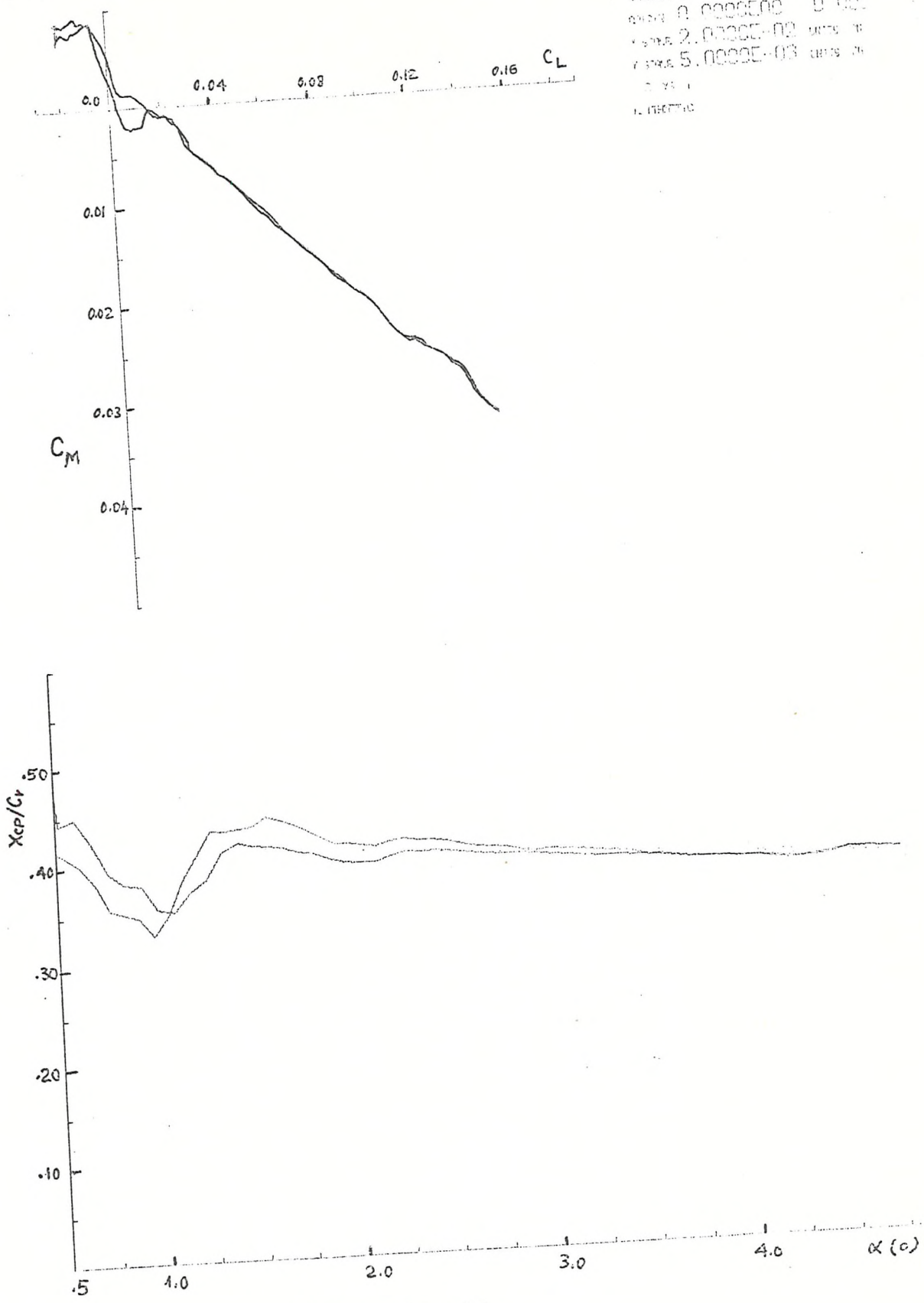
0.0
0.04
0.08
0.12
0.16
C_L
0.01
0.02
0.03
C_M
0.04
X_{CP}/C_r
.50
.40
.30
.20
.10
.5
1.0
2.0
3.0
4.0
α (°)

FIG. 7.6 (Cont)

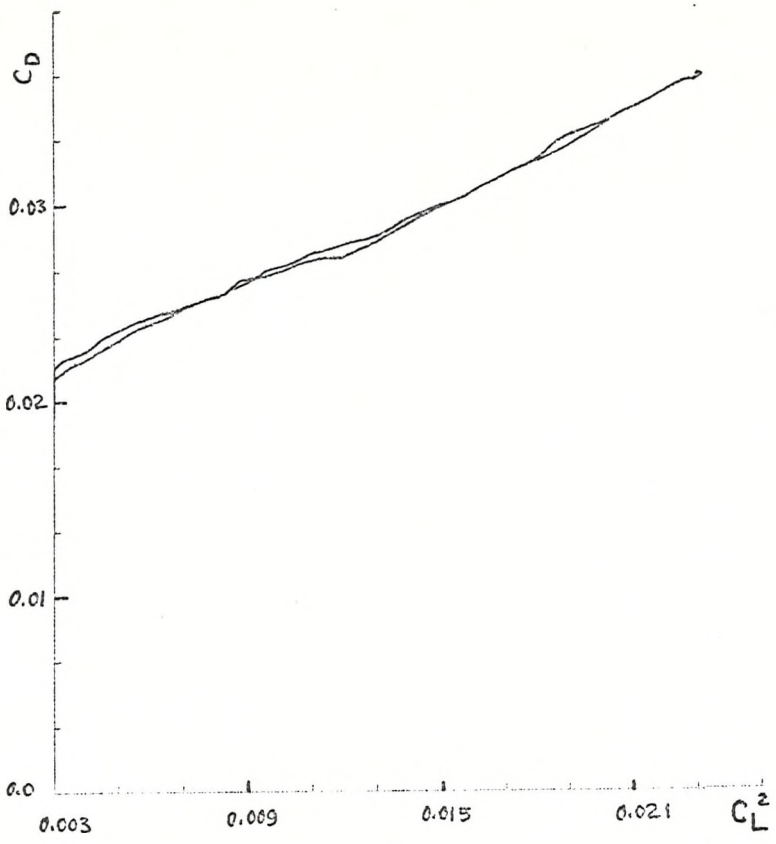
C_D
0.03
0.02
0.01
0.0
0.003
0.009
0.015
0.021
C_L^2

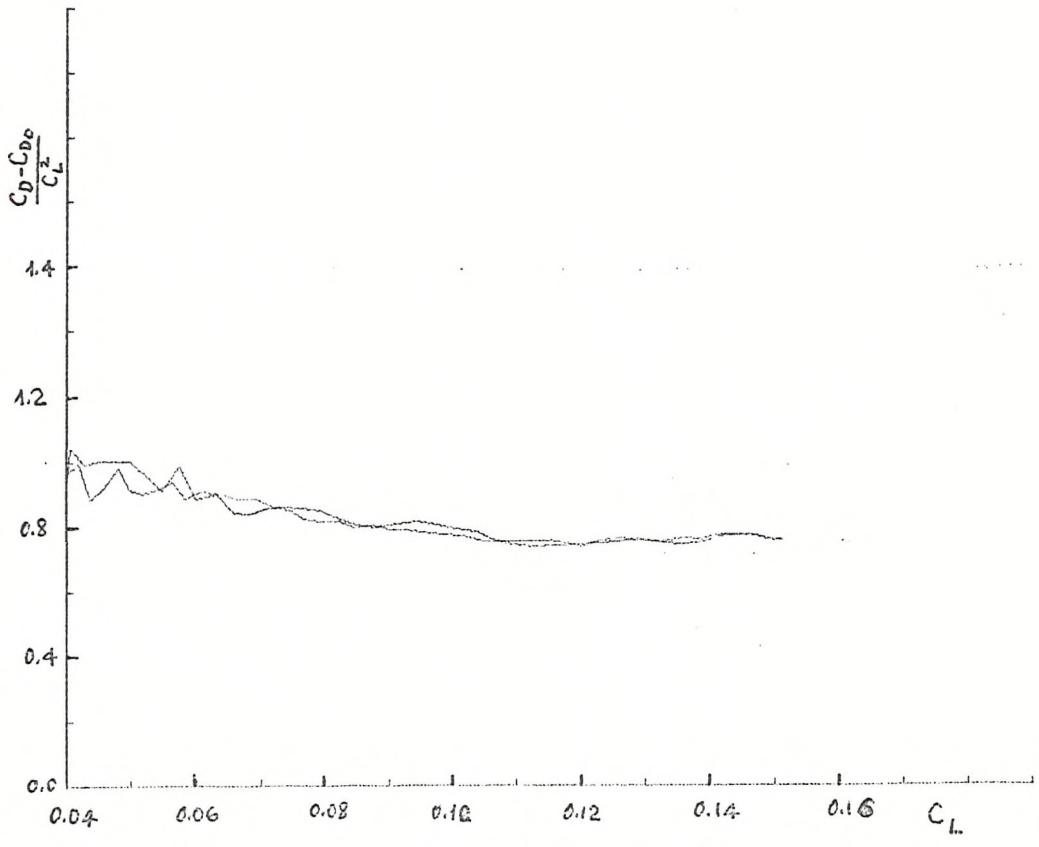
$\frac{C_D - C_{D_0}}{C_L^2}$
1.4
1.2
0.8
0.4
0.0
0.04
0.06
0.08
0.10
0.12
0.14
0.16
C_L

FIG. 7.6 (Cont)

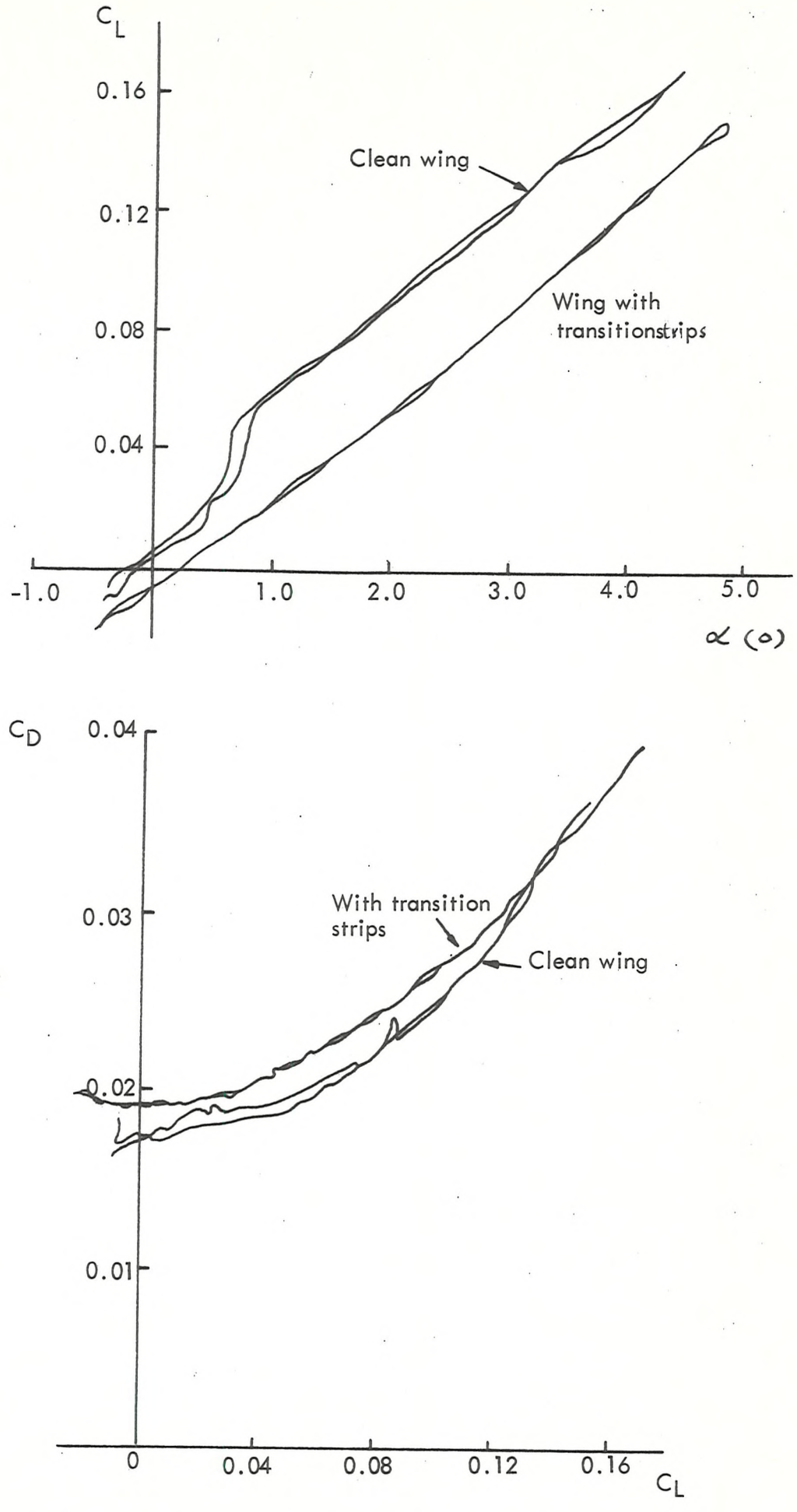

FIG. 7.7. EFFECT OF BOUNDARY LAYER TYPE ON C_L & C_D OF RAK MODEL.

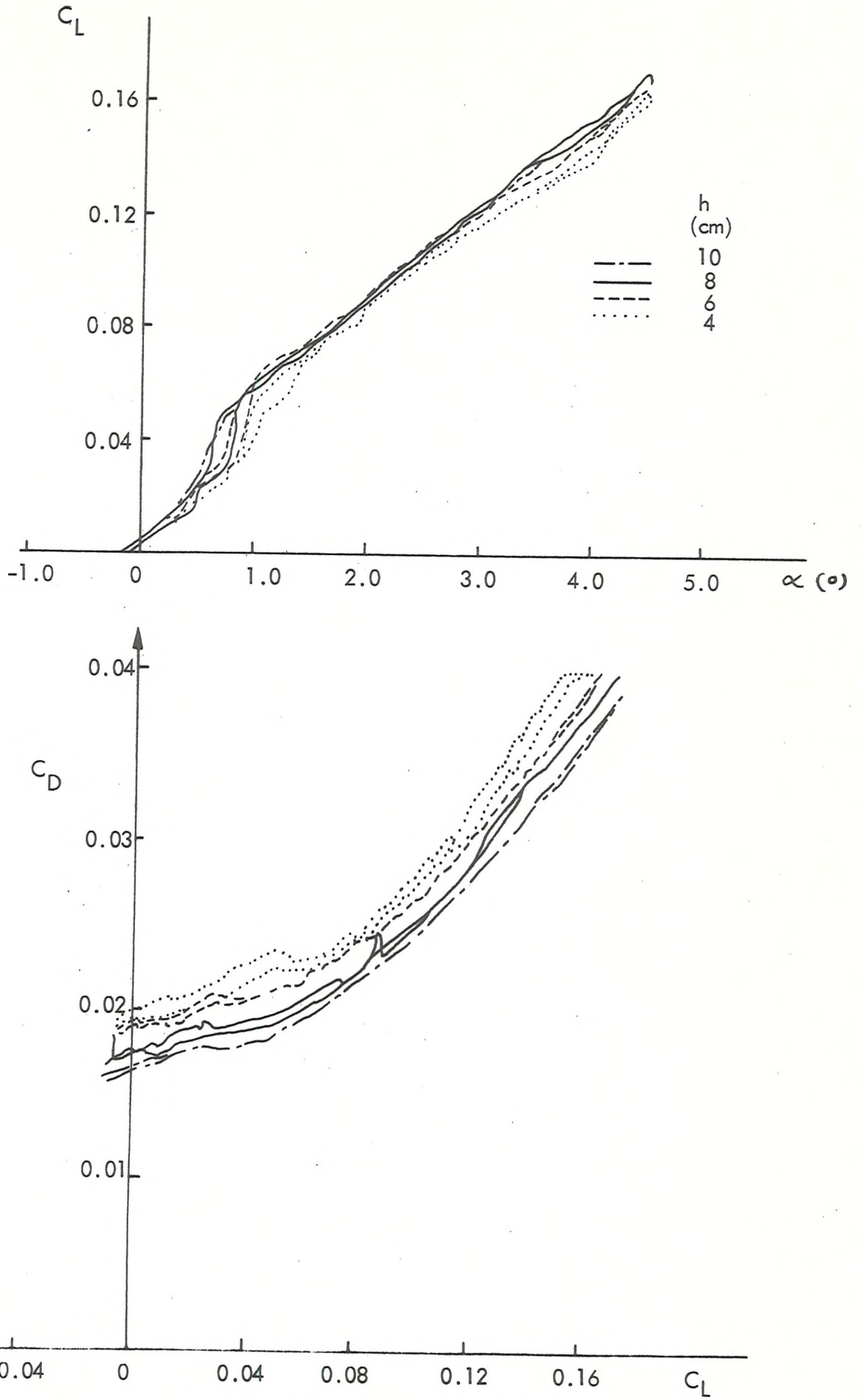

FIG. 7.8. EFFECT OF R_N ON C_L & C_D FOR RAK MODEL

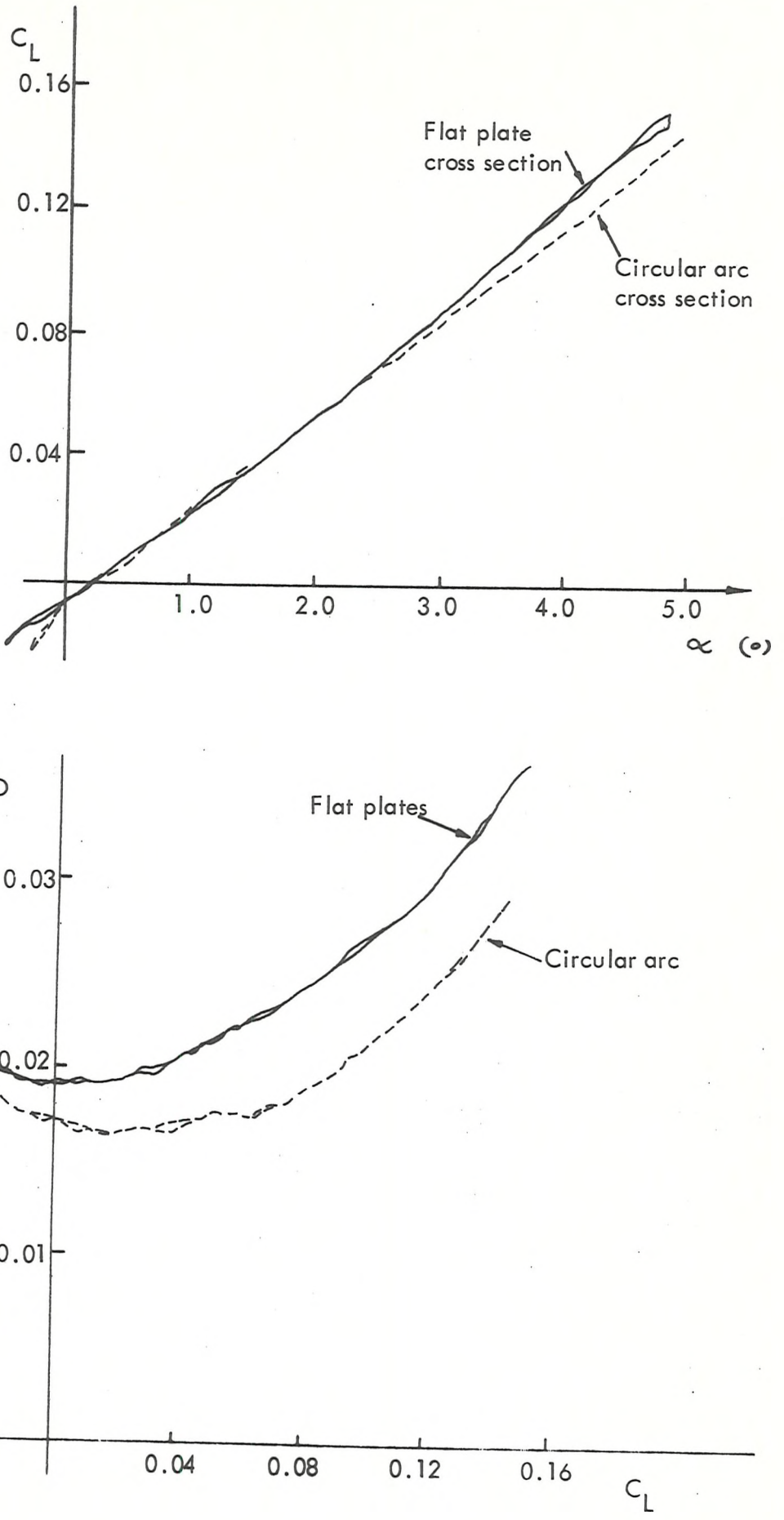

FIG. 7.9. EFFECTS OF THICKNESS FORM ON AERODYNAMICS OF PAK MODEL.

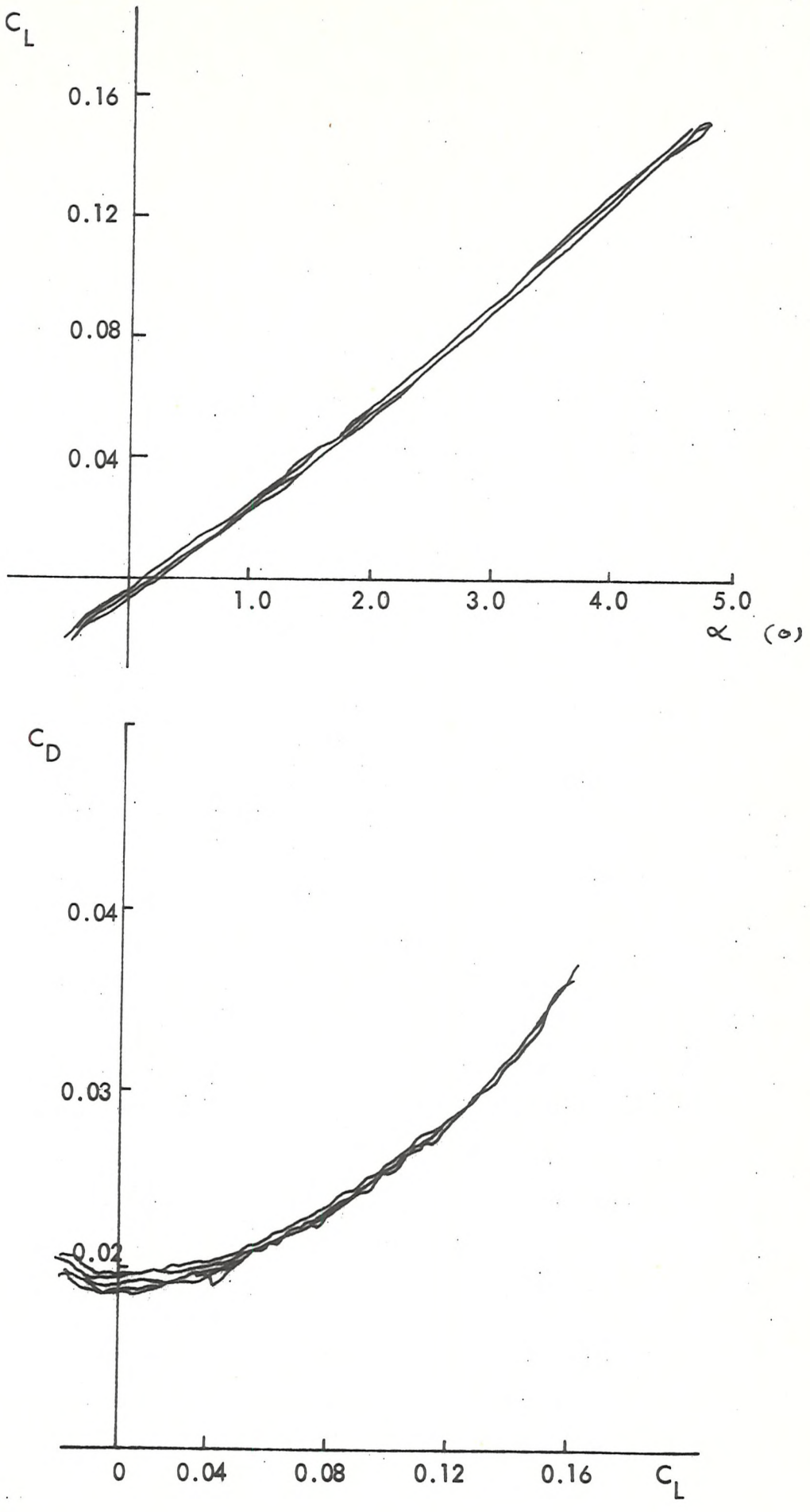

FIG. 7.10. REPEATABILITY OF C_L & C_D RAK MODEL 4 DIFFERENT RUNS.

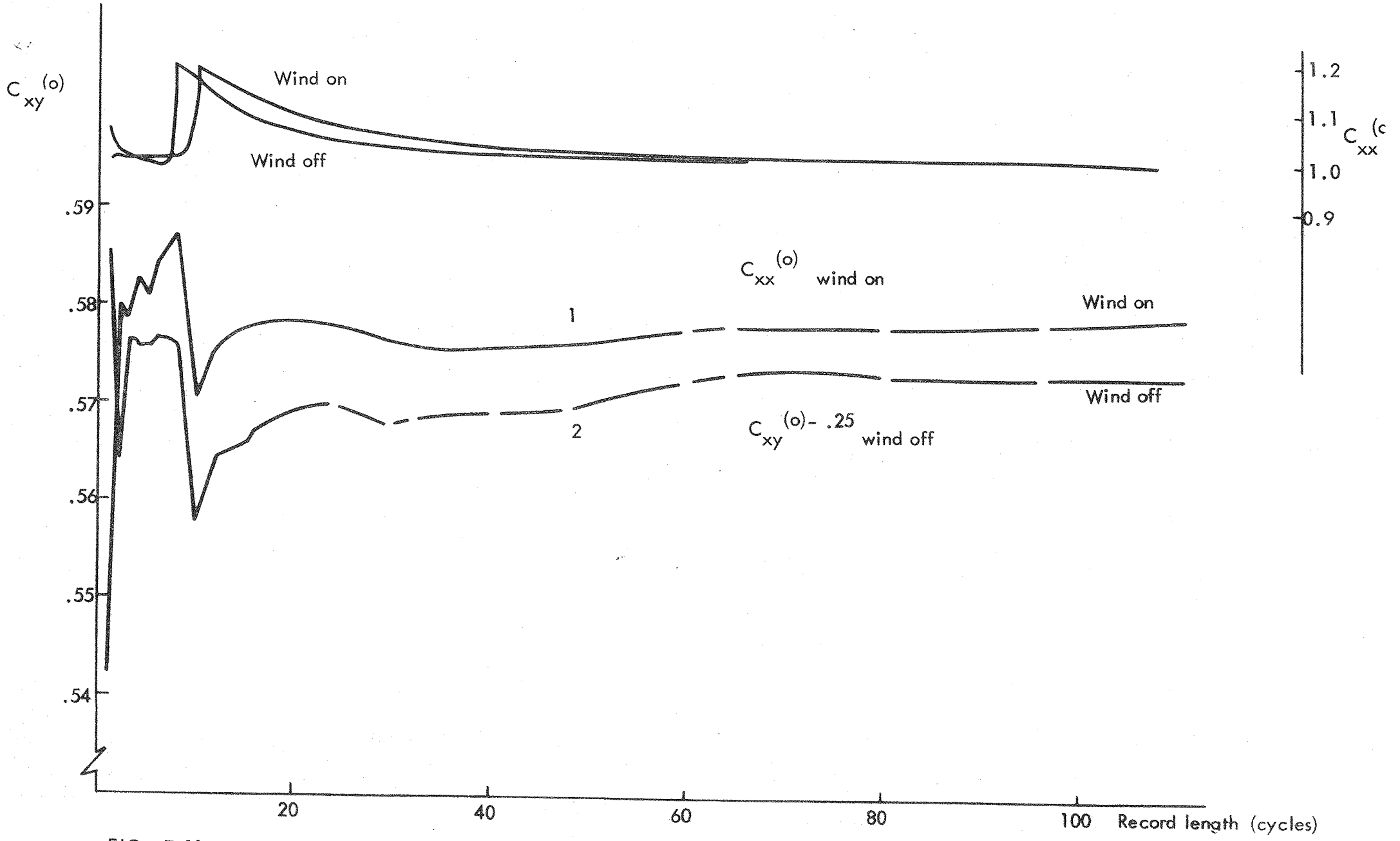

FIG. 7.11. EFFECT OF RECORD LENGTH ON ZERO LAG COVARIANCE ESTIMATE.

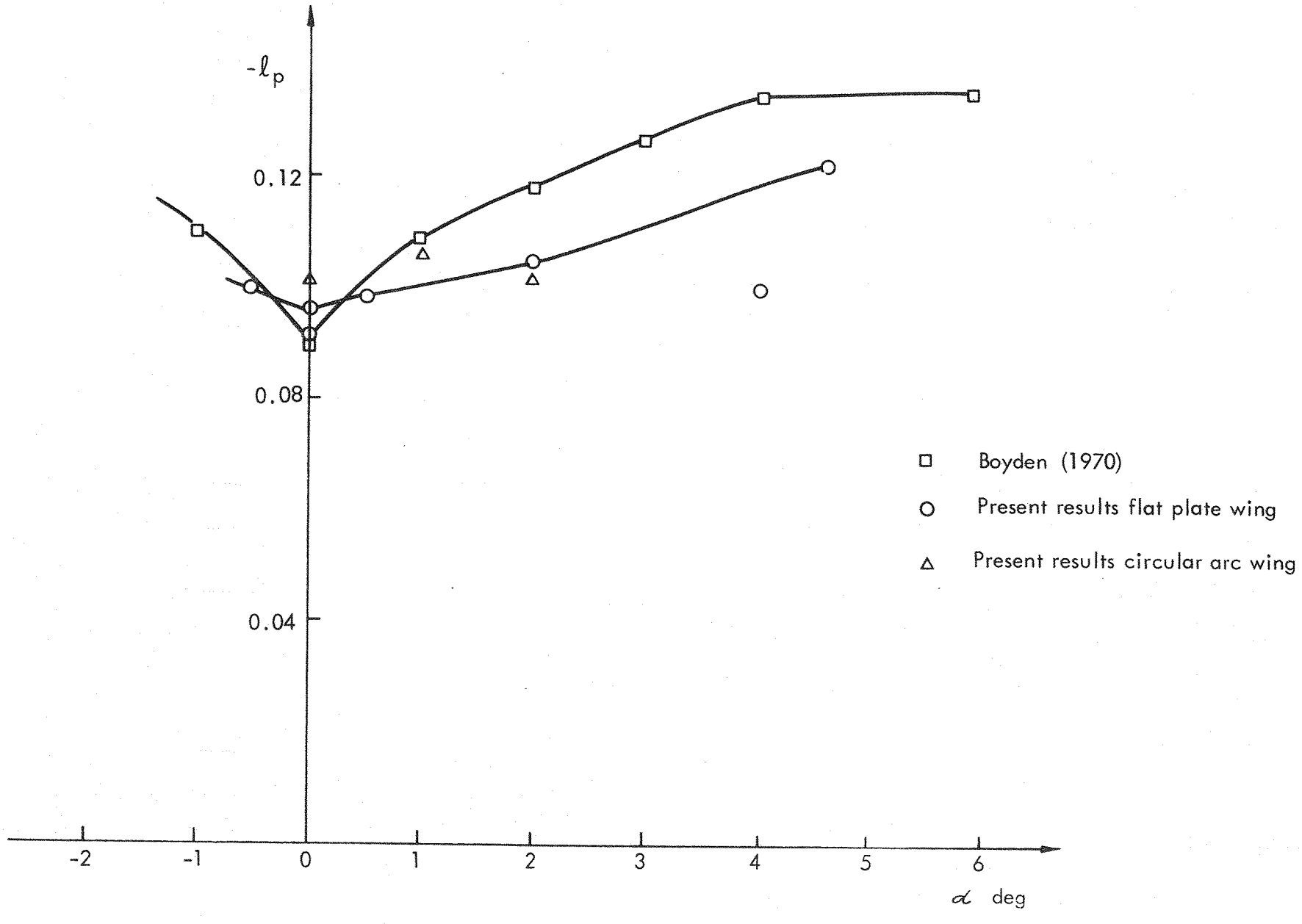

FIG. 7.12. OSCILLATORY ROLL DAMPING DERIVATIVE FOR RAK MODEL

Scales time = .2 sec/div , V_α , V_F , V_M , V_D = .2 V/div

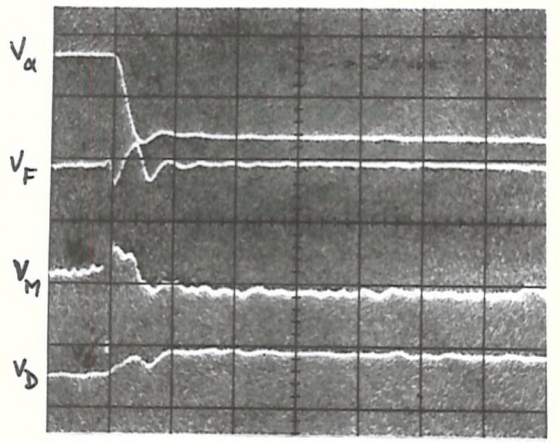

a) $\alpha_o = 0^\circ$
$\Delta\alpha = 1.1^\circ$
h = 0

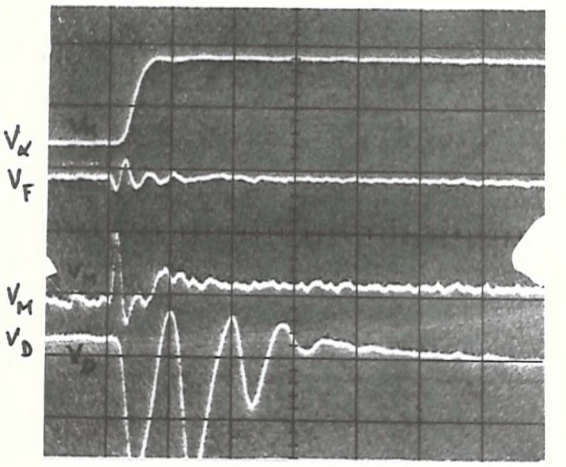

b) $\alpha_o = 0^\circ$
$\Delta\alpha = -1.1^\circ$
h = 0

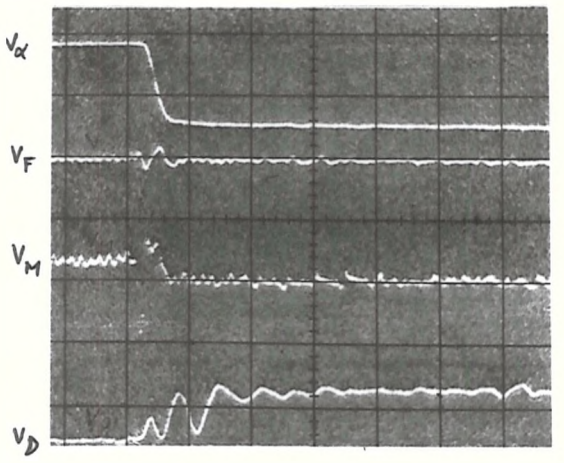

c) $\alpha_o = 2.1^\circ$
$\Delta\alpha = 1.1^\circ$
h = 0

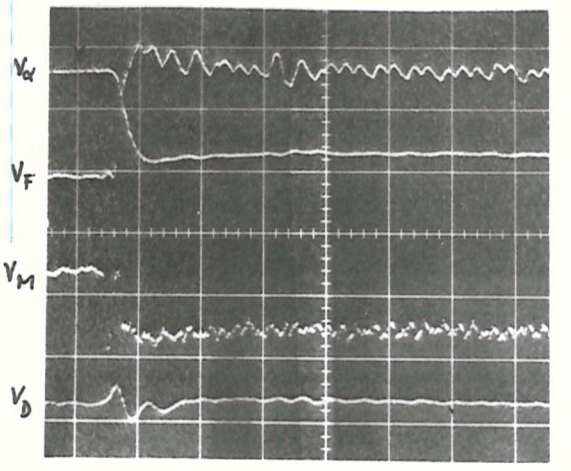

d) $\alpha_o = 0^\circ$
$\Delta\alpha = 1.1^\circ$
h 937 N/m²

Fig. 7.13 Storage scope oscillograms of the step response of a model in MSBS

Scales same as Fig 7.13

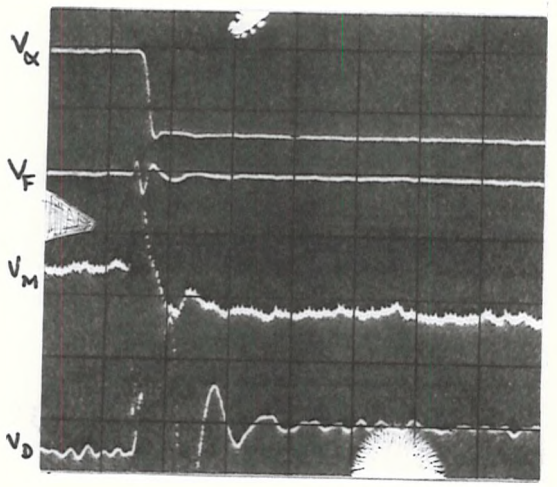

a) $\alpha_0 = 3.1^\circ$
$\Delta\alpha = 1.1^\circ$
$h = 0$

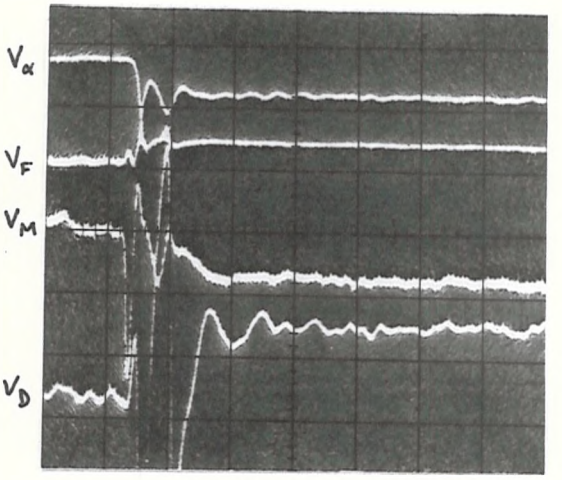

b) $\alpha_0 = 3.1^\circ$
$\Delta\alpha = 1.1^\circ$
$h = 937\ N/m^2$

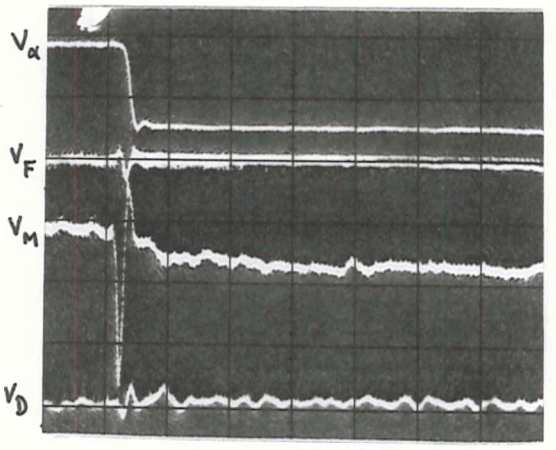

c) $\alpha_0 = 4.1^\circ$
$\Delta\alpha = 1.1^\circ$
$h = 0$

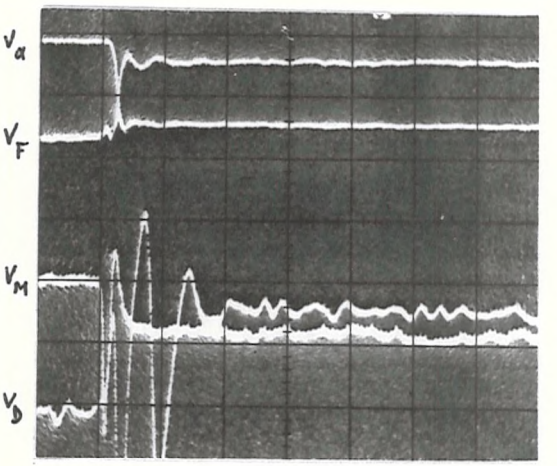

d) $\alpha_0 = 4.1^\circ$
$\Delta\alpha = 1.1^\circ$
$h = 937\ N/m^2$

Fig. 7.14 Storage scope oscillograms of the step response of model in MSBS

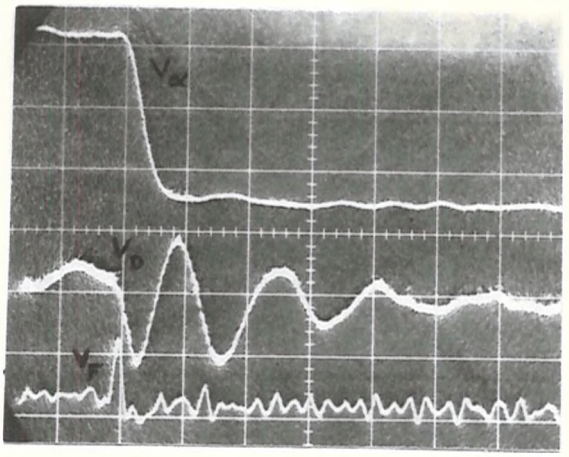

a) $\Delta\alpha = -0.7°$
h = 0

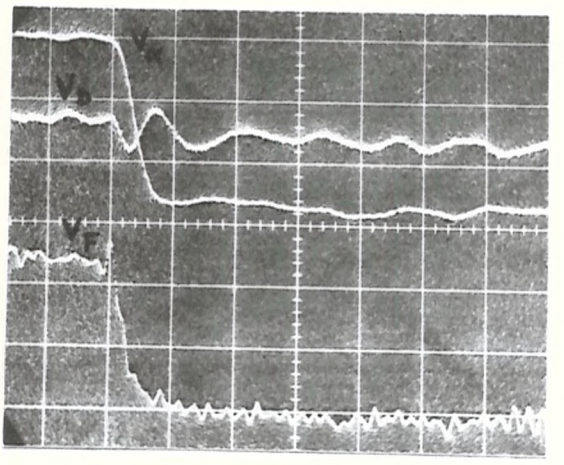

b) $\Delta\alpha = -0.7$
h = 1400 N/m²

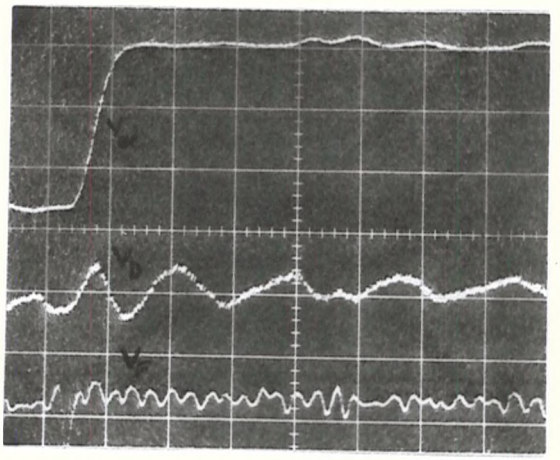

c) $\Delta\alpha = +0.7$
h = 0

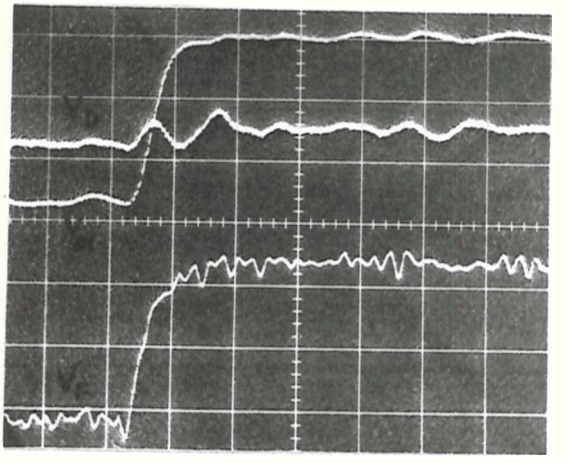

d) $\Delta\alpha = 0.7°$
h = 1400 N/m²

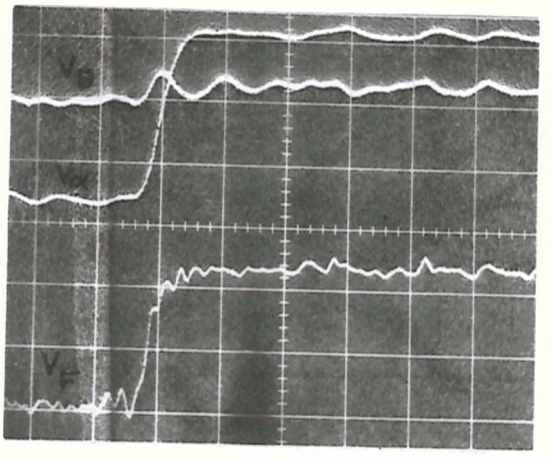

d) $\Delta\alpha = 0.7$
h = 1400 N/m²

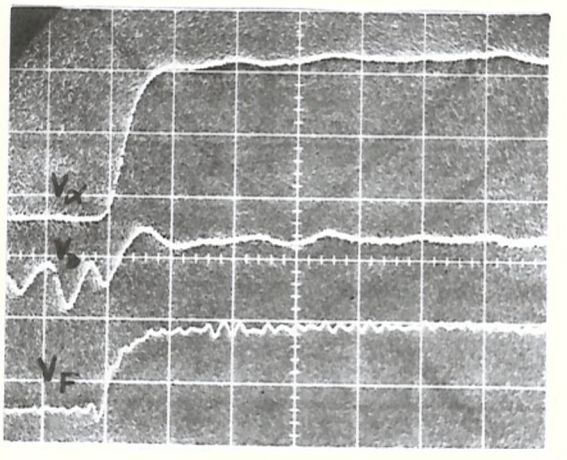

e) $\Delta\alpha = 0.7$
h = 1250 N/m²

Fig. 7.15 Storage scope oscillograms of the step response of a model in MSBS

Scales : time - .1 sec/div V - .1 V/div

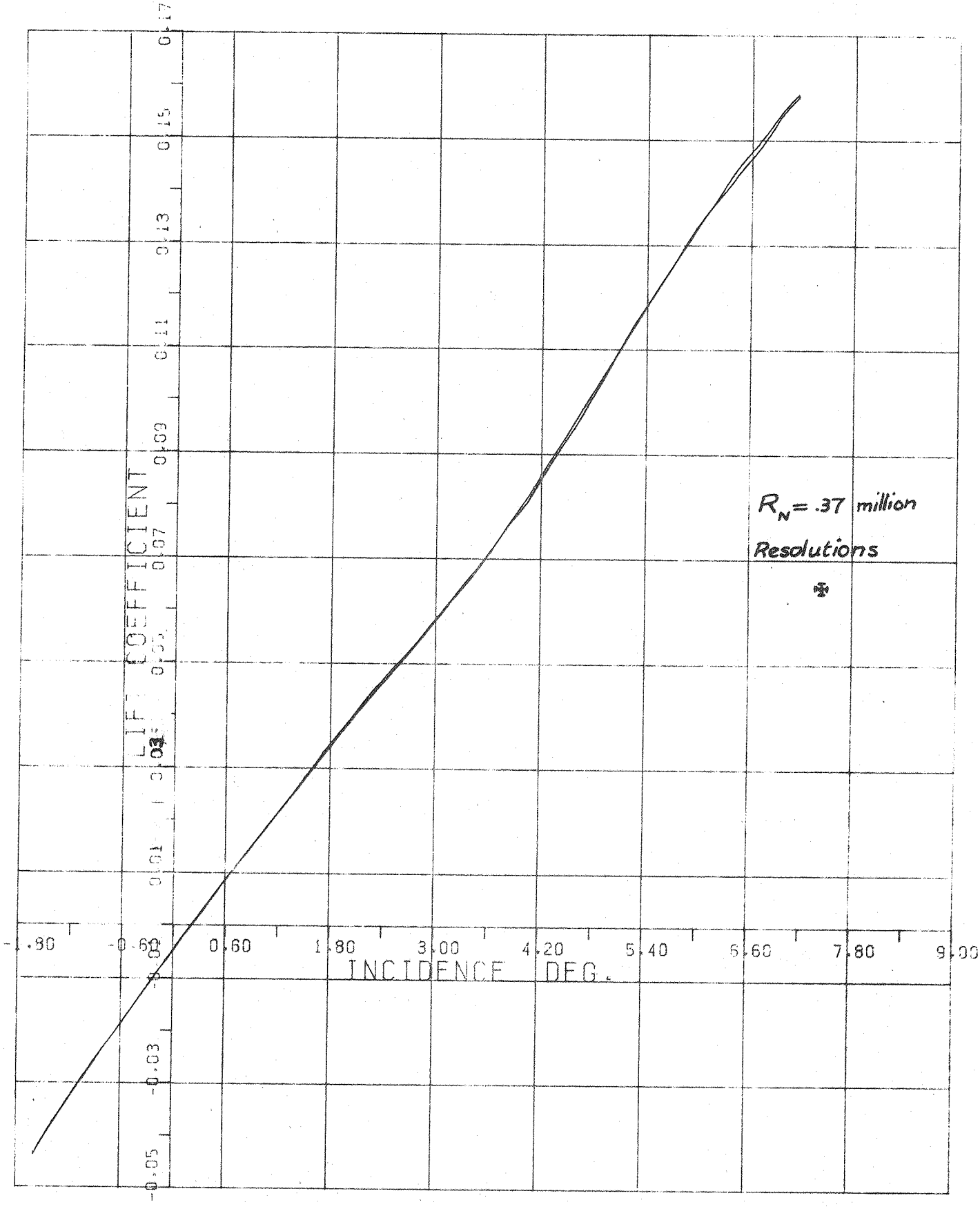

(α)

FIG. 7.16 - AERODYNAMIC LIFT VARIATION WITH INCIDENCE

PITCH RATE (DEG/SEC) = 0.125

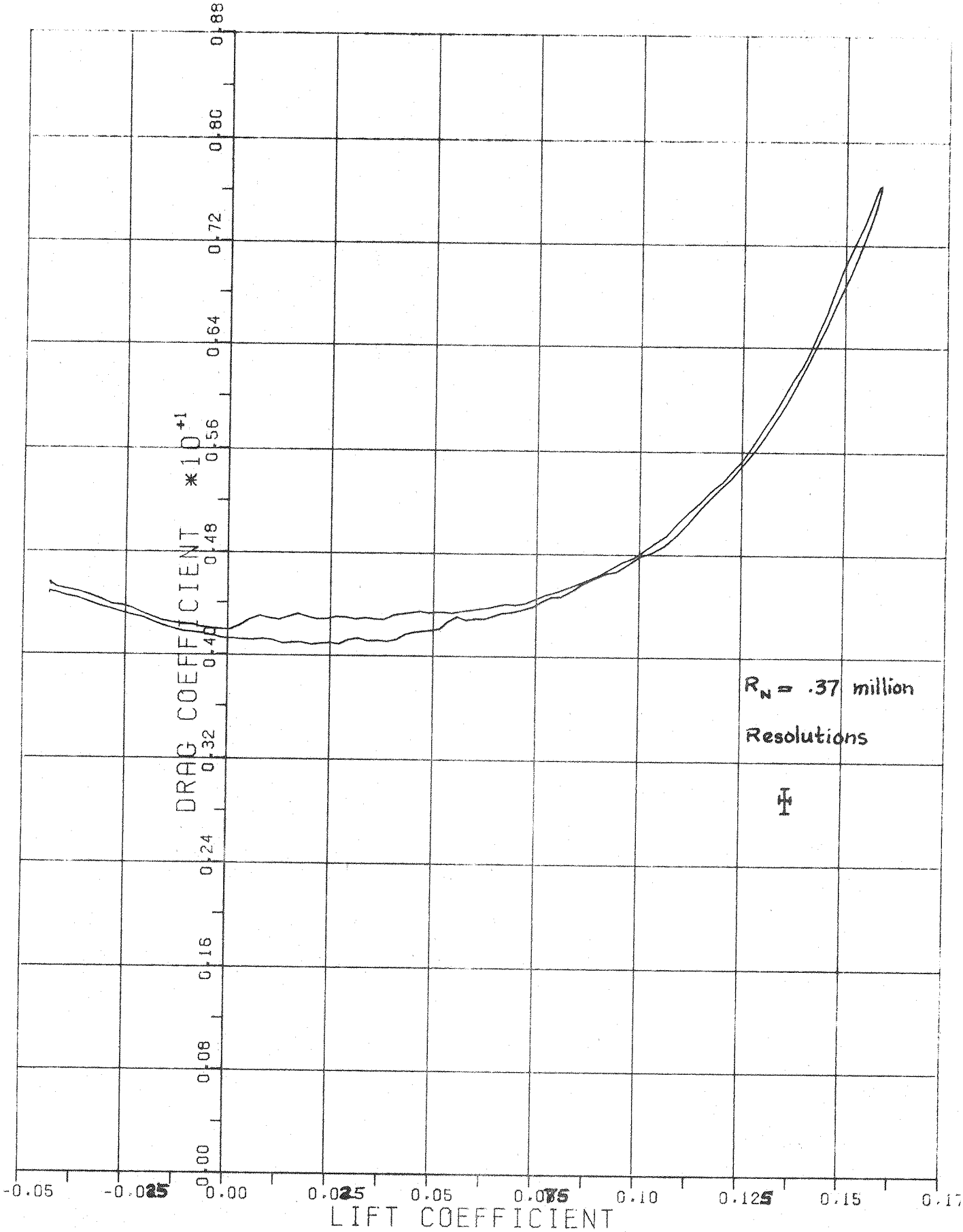

(b)

FIG. 7.16 - DRAG VARIATION WITH LIFT

PITCH RATE (DEG/SEC) = 0.125

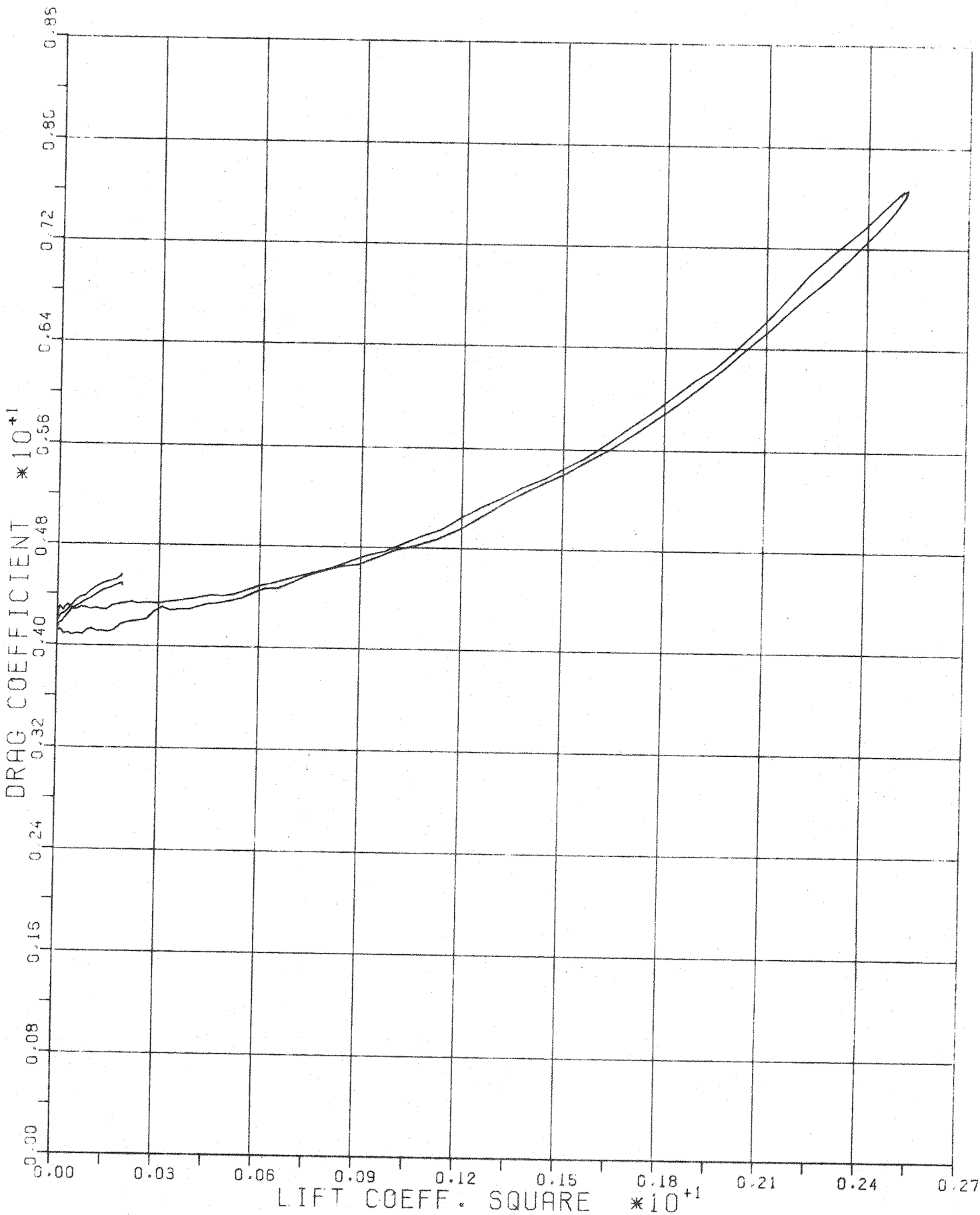

(c)

FIG. 7.16 - DRAG VARIATION WITH SQUARE OF LIFT

PITCH RATE (DEG/SEC) = 0.125

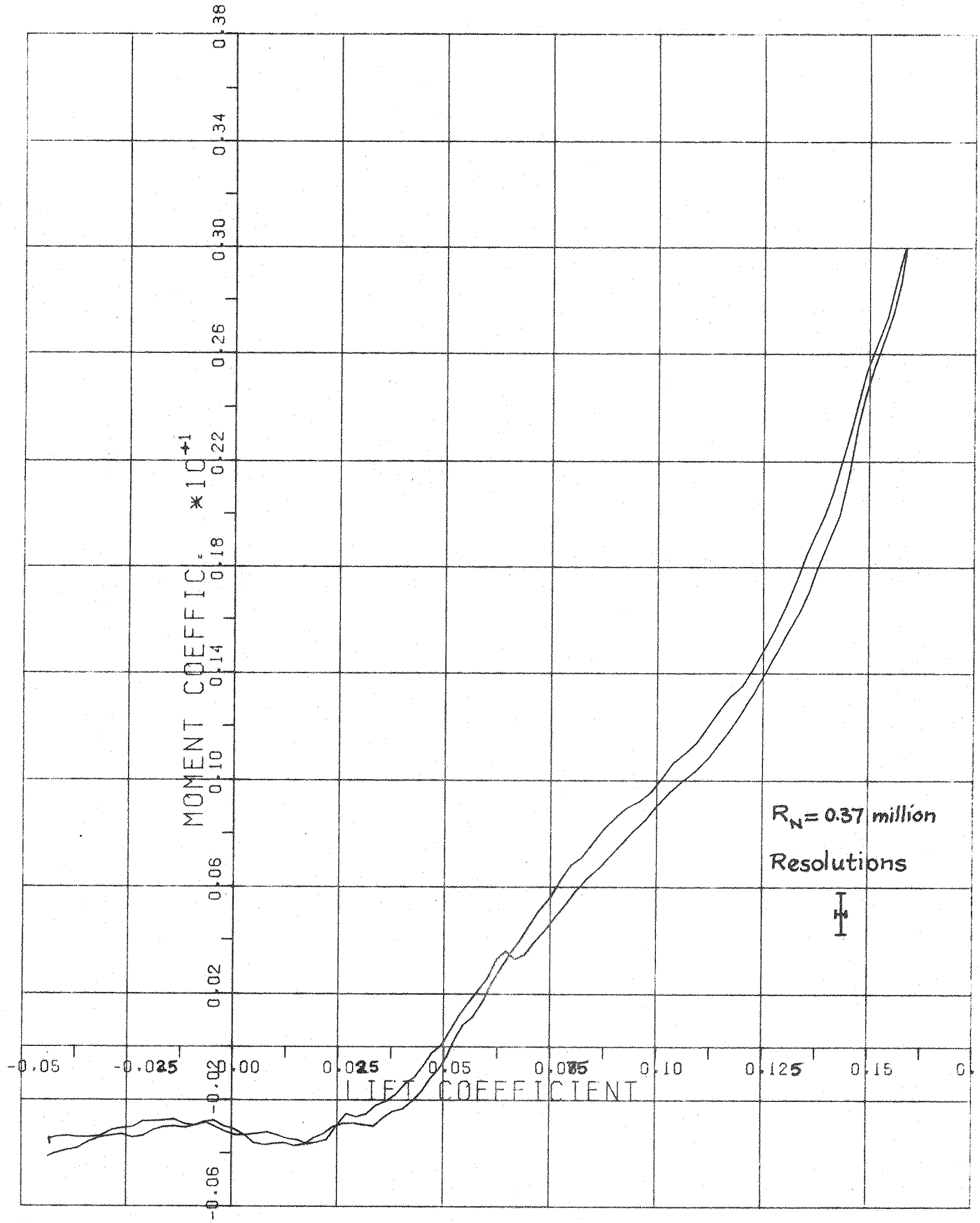

(a)

FIG. 7.16 - PITCHING MOMENT (ABOUT WING CR/2) VARIATION WITH LIFT

PITCH RATE (DEG/SEC) = 0.125

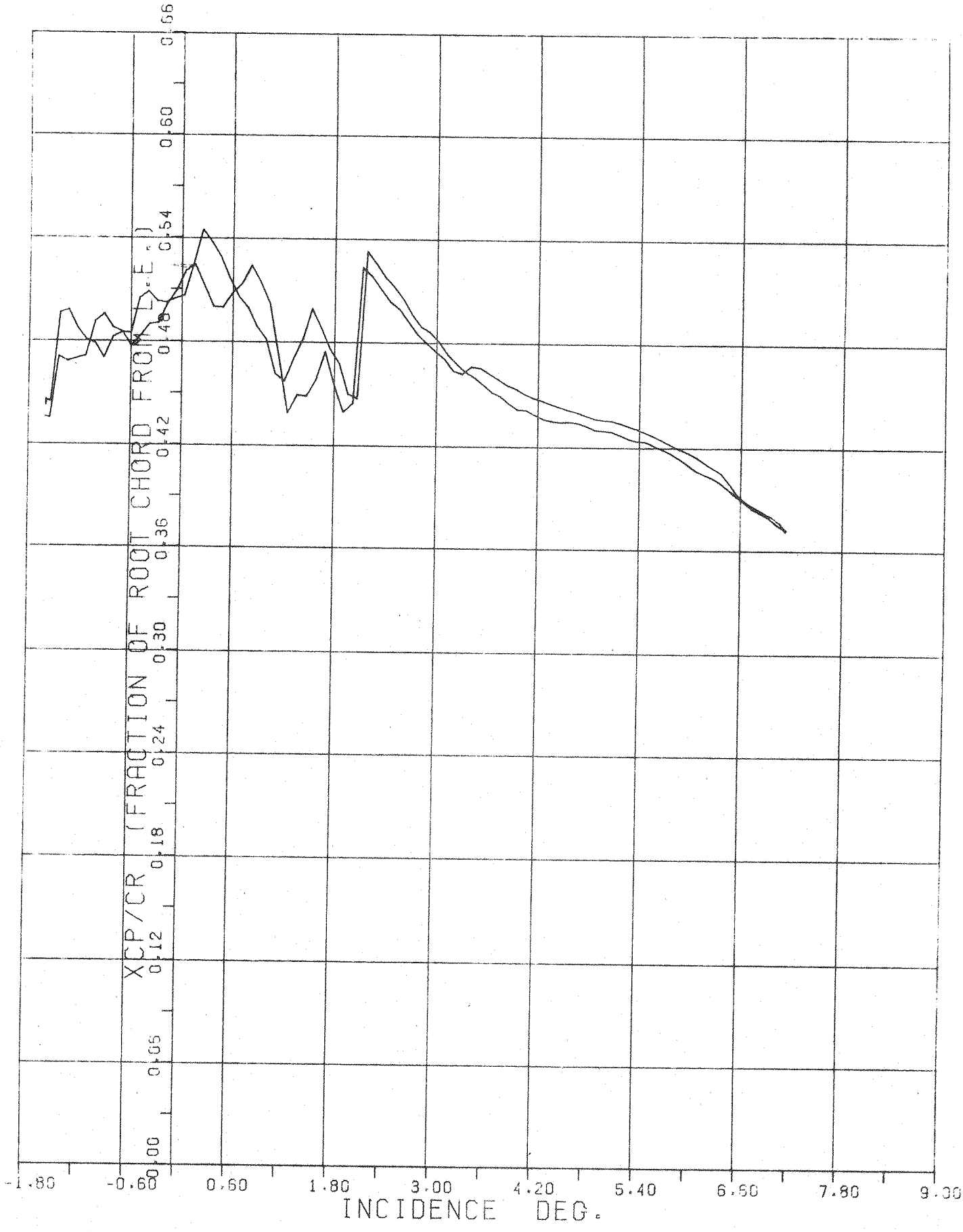

(e)

FIG. 7.16-CENTER OF PRESSURE LOCATION (% OF ROOT CHORD) BEHIND L. E. OF ROOT CHORD

PITCH RATE (DEG/SEC) = 0.125

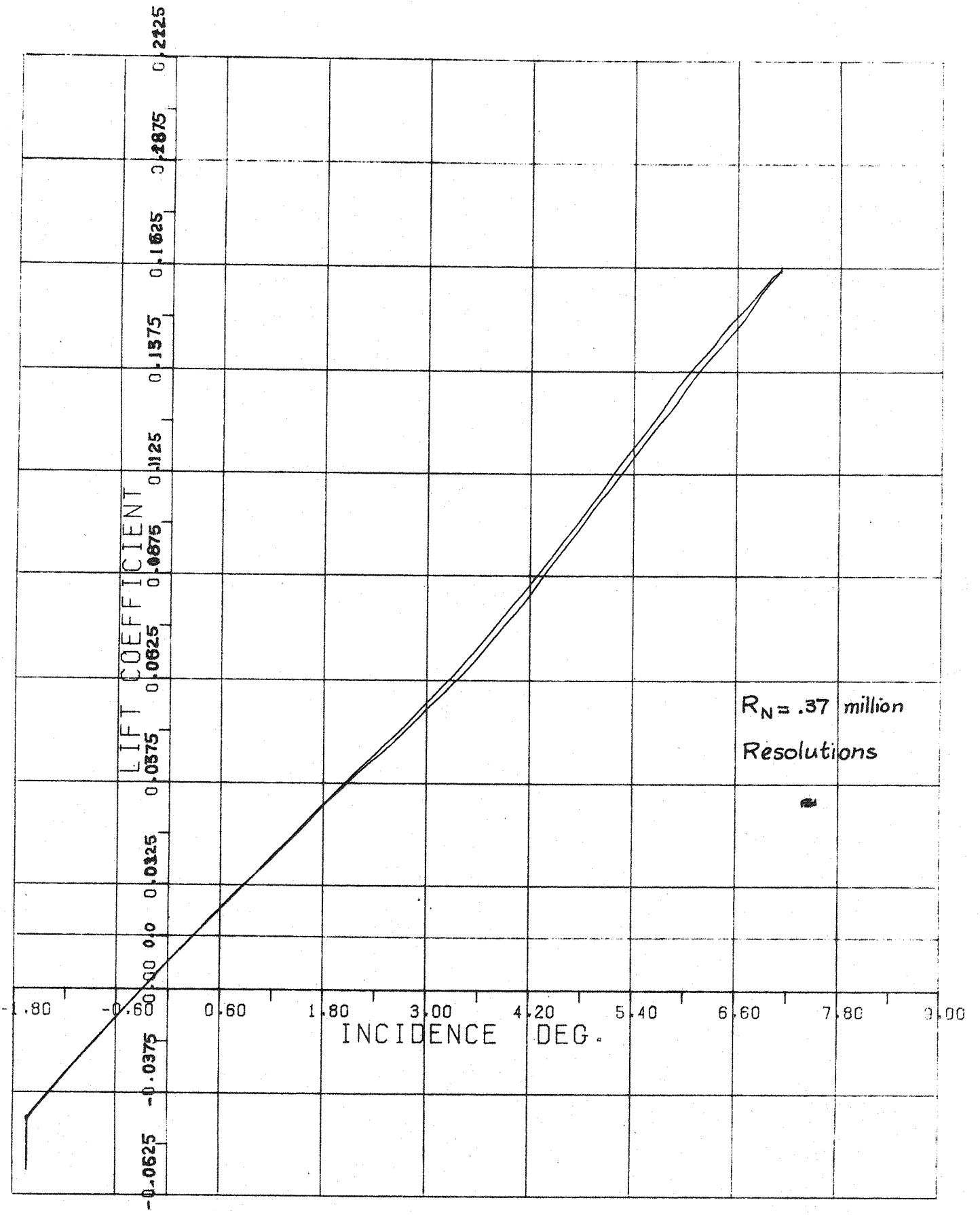

(a)

FIG. 7.17 - AERODYNAMIC LIFT VARIATION WITH INCIDENCE

PITCH RATE (DEG/SEC) = 0.25

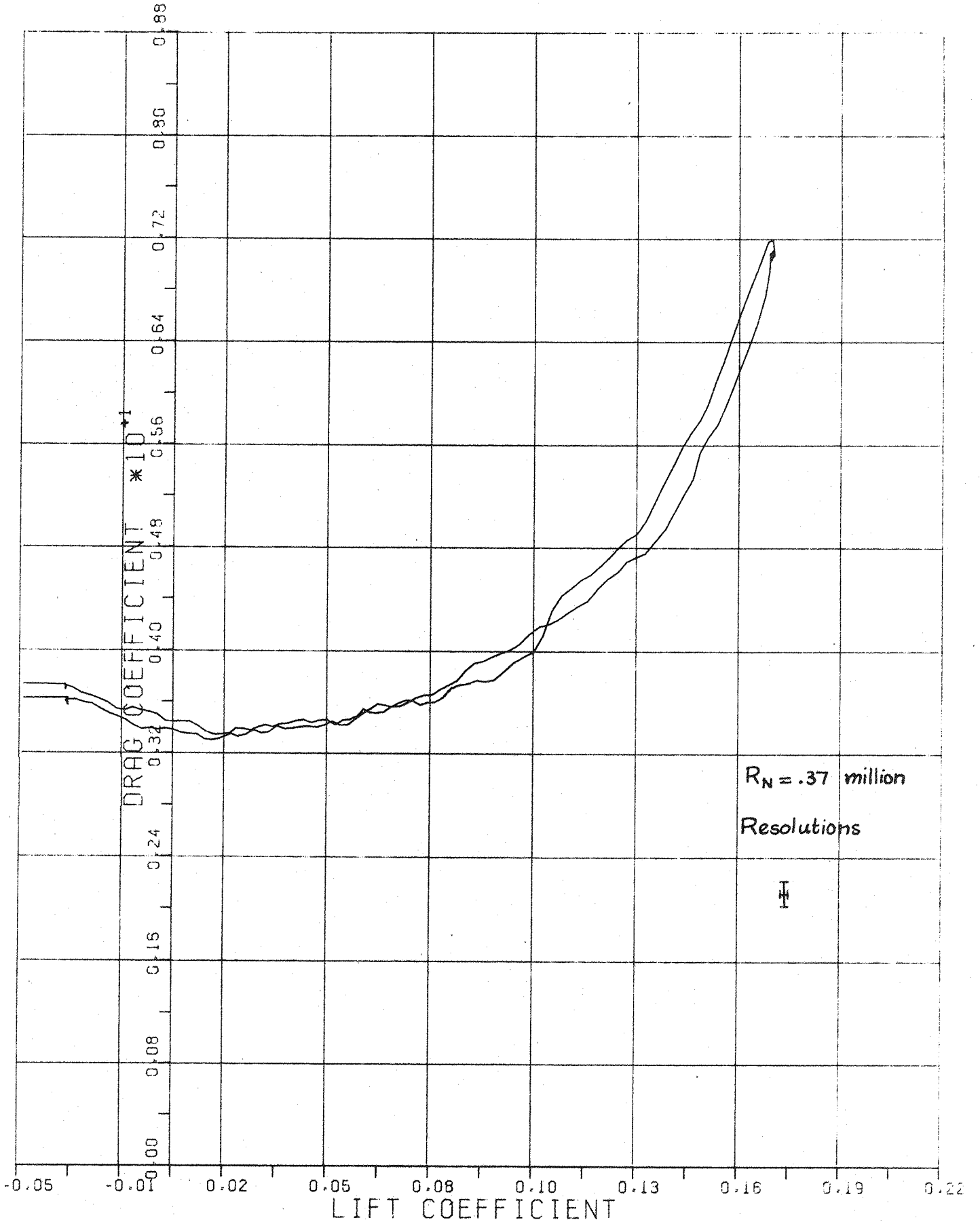

(b)

FIG. 7.17 - DRAG VARIATION WITH LIFT

PITCH RATE (DEG/SEC) = 0.250

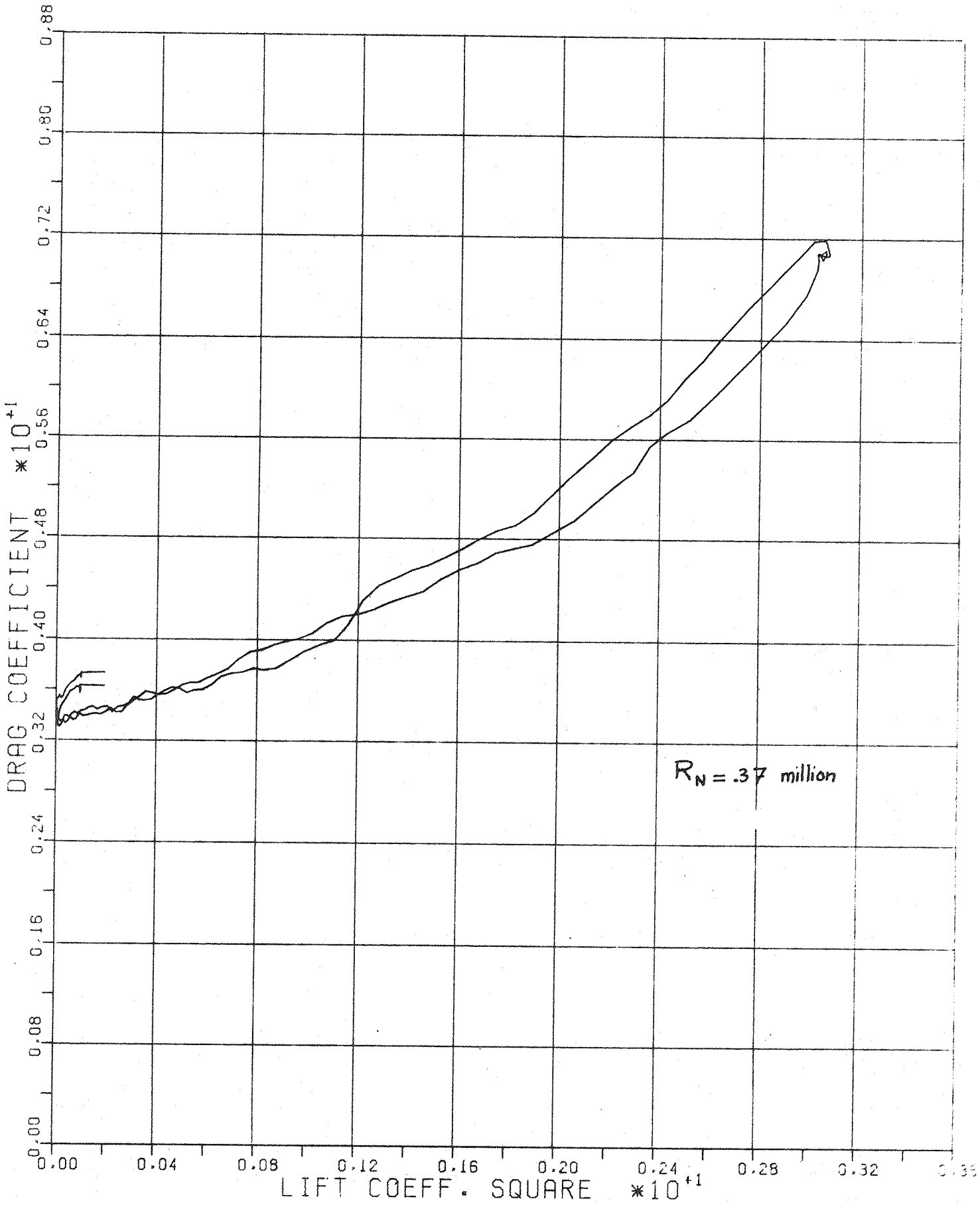

(c)

FIG. 7.17 - DRAG VARIATION WITH SQUARE OF LIFT

PITCH RATE (DEG/SEC) = 0.250

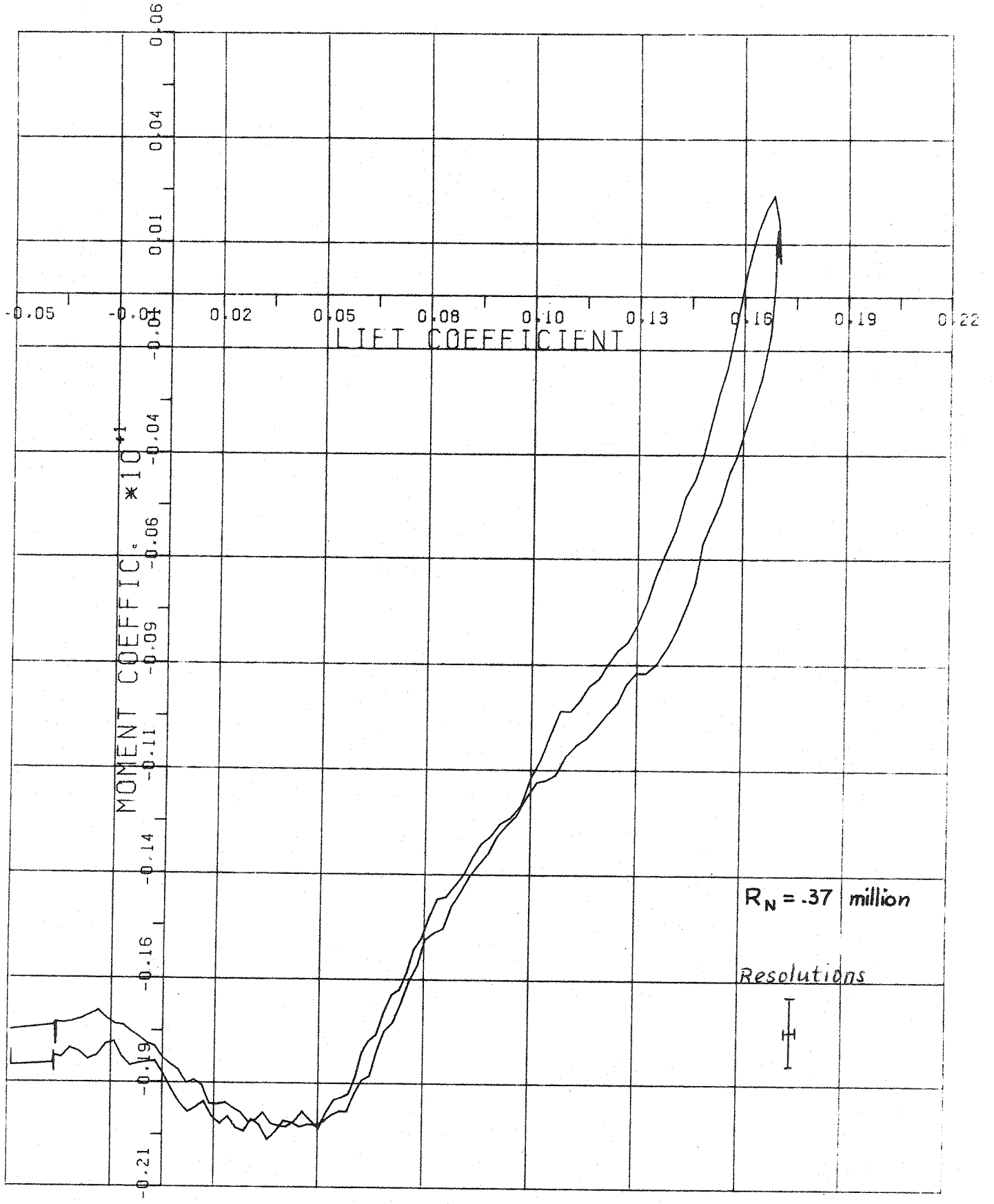

(d)

FIG. 7.17-PITCHING MOMENT (ABOUT WING CR/2) VARIATION WITH LIFT

PITCH RATE (DEG/SEC) = 0.250

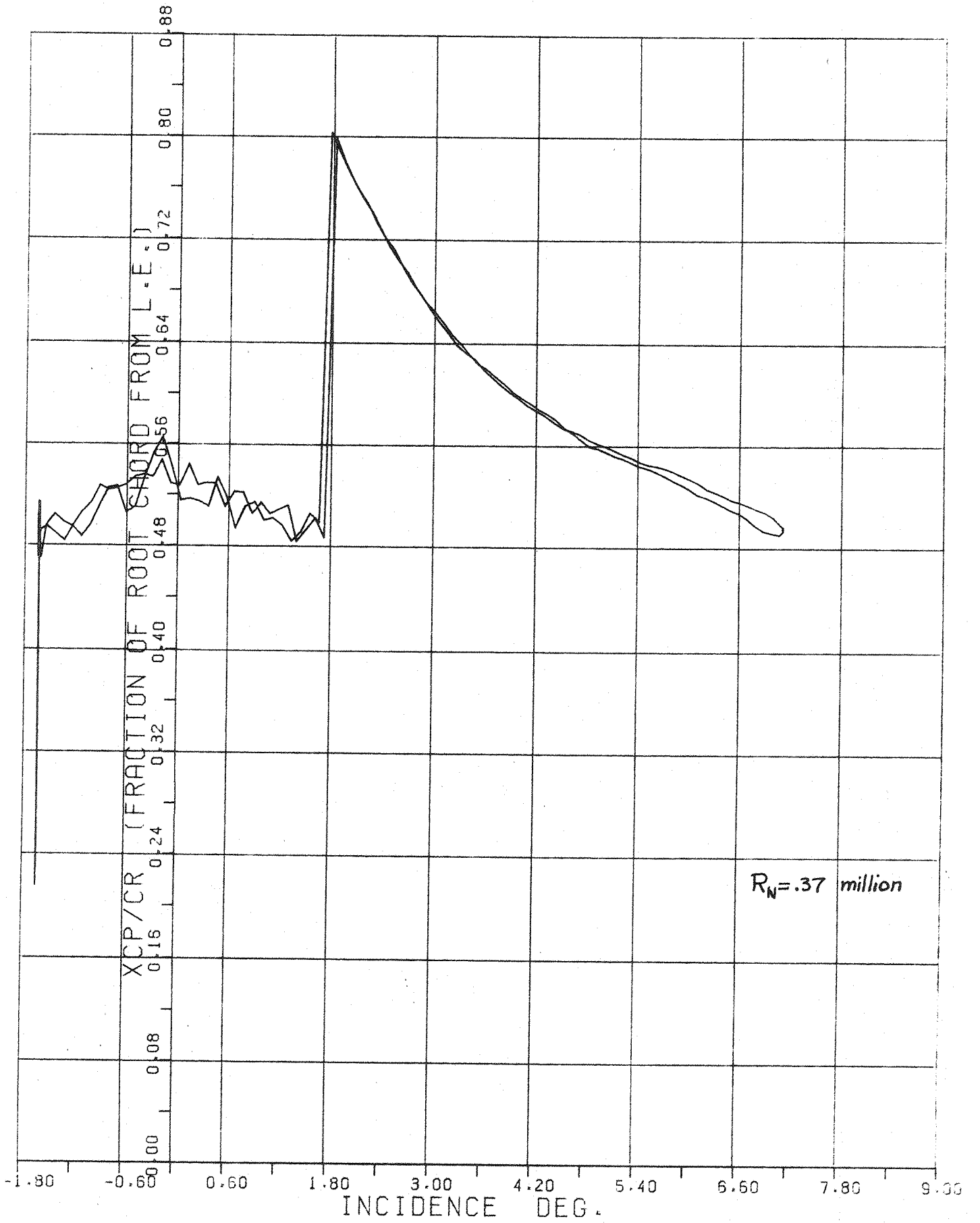

(e)

FIG. 7.17 CENTER OF PRESSURE LOCATION (% OF ROOT CHORD) BEHIND L. E. OF ROOT CHORD

PITCH RATE (DEG/SEC) = 0.250

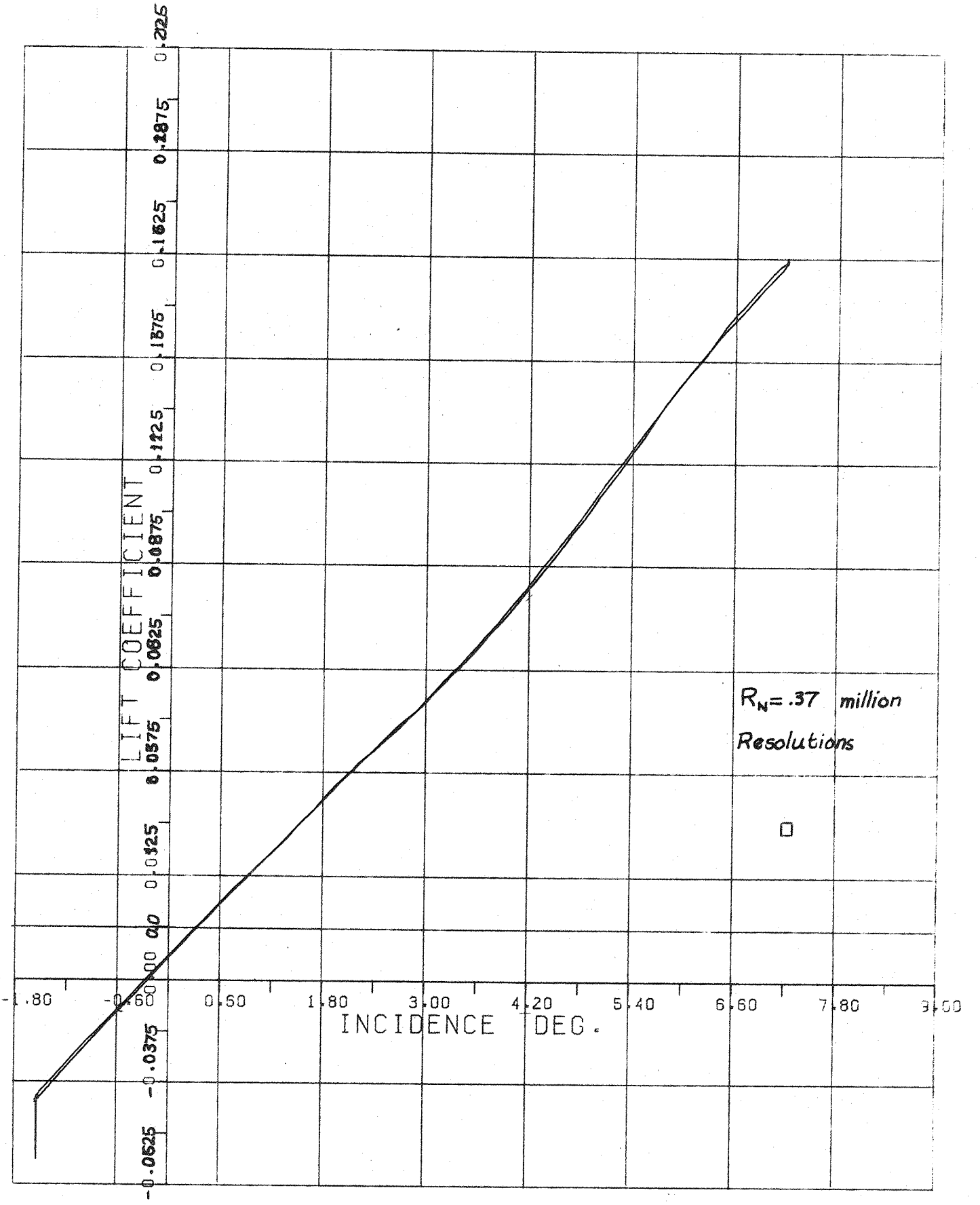

(a)

FIG. 7.18-AERODYNAMIC LIFT VARIATION WITH INCIDENCE

PITCH RATE (DEG/SEC) = 0.500

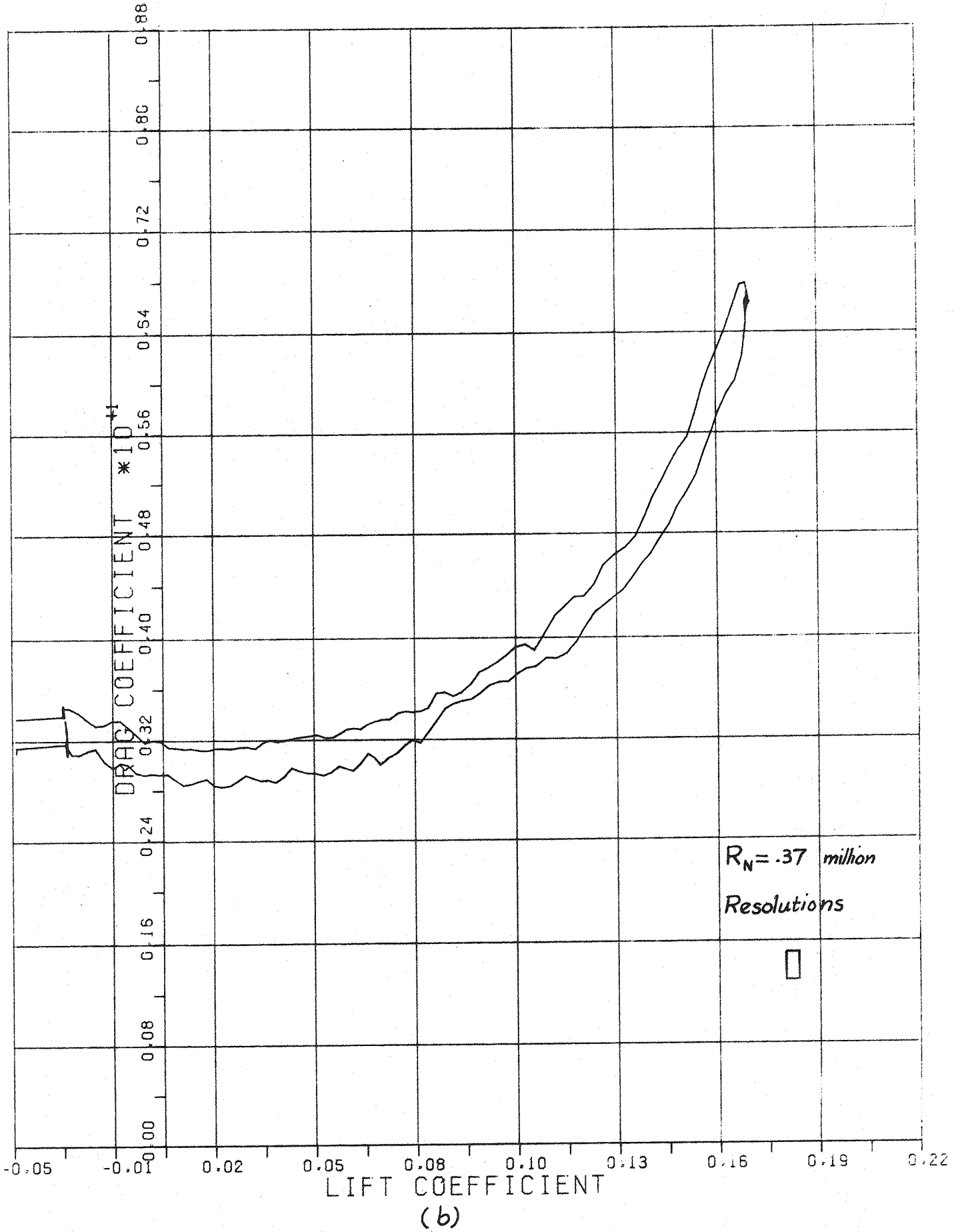

(b)

FIG.7.18-DRAG VARIATION WITH LIFT

PITCH RATE (DEG/SEC) = 0.500

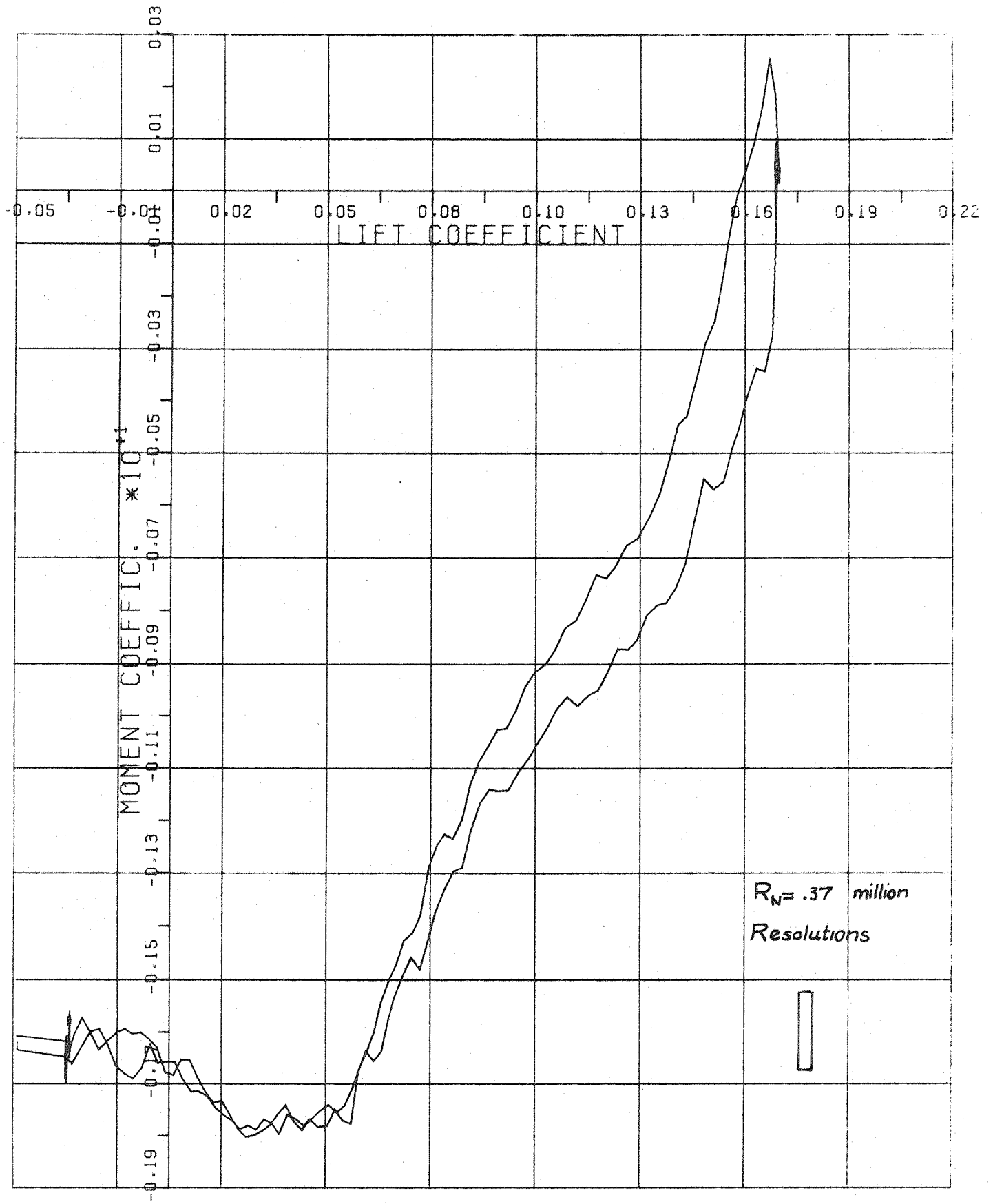

(c)

FIG.7.18-PITCHING MOMENT (ABOUT WING CR/2) VARIATION WITH LIFT

PITCH RATE (DEG/SEC) = 0.500

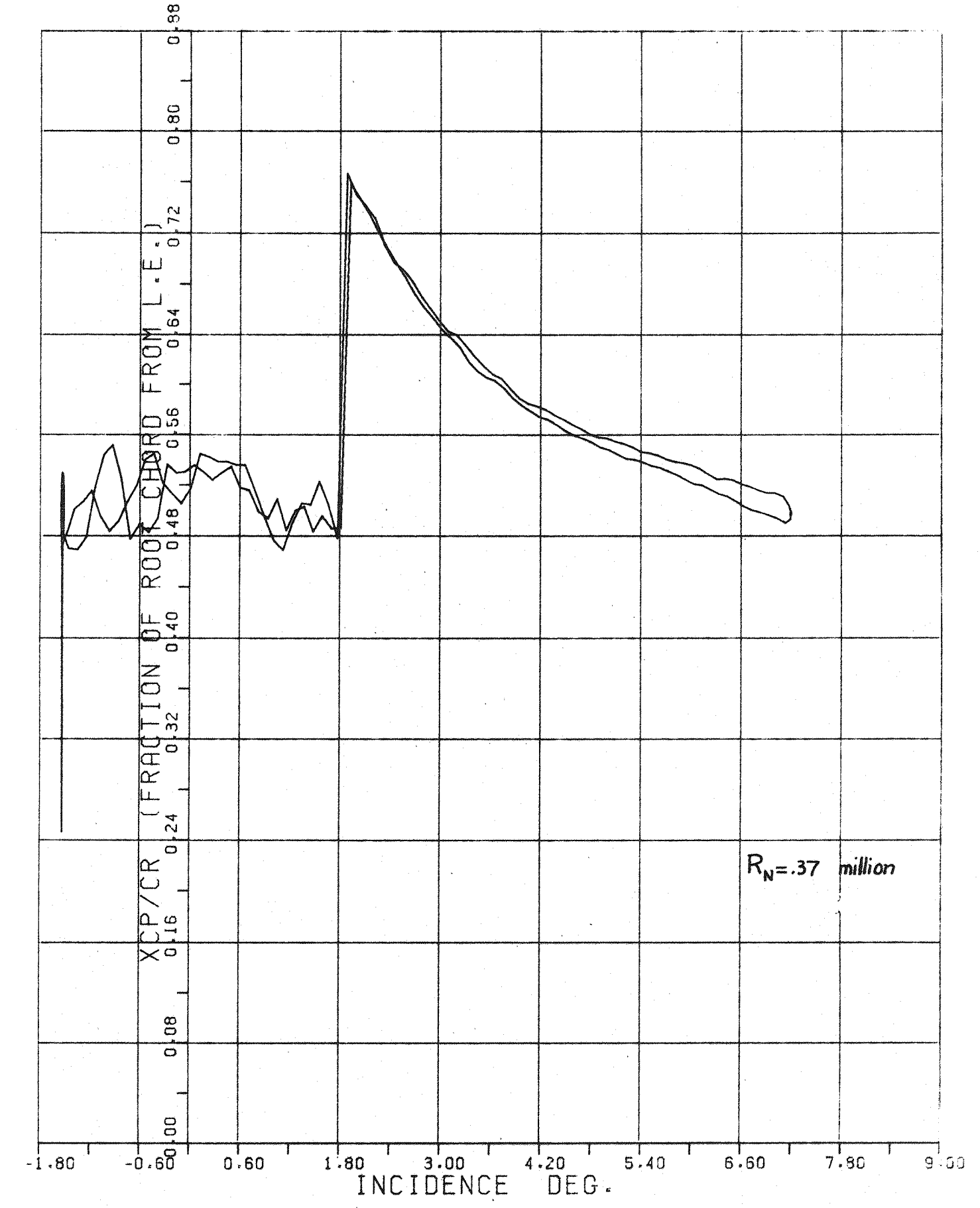

(d)

FIG. 7.18 CENTER OF PRESSURE LOCATION (% OF ROOT CHORD) BEHIND L. E. OF ROOT CHORD

PITCH RATE (DEG/SEC) = 0.500

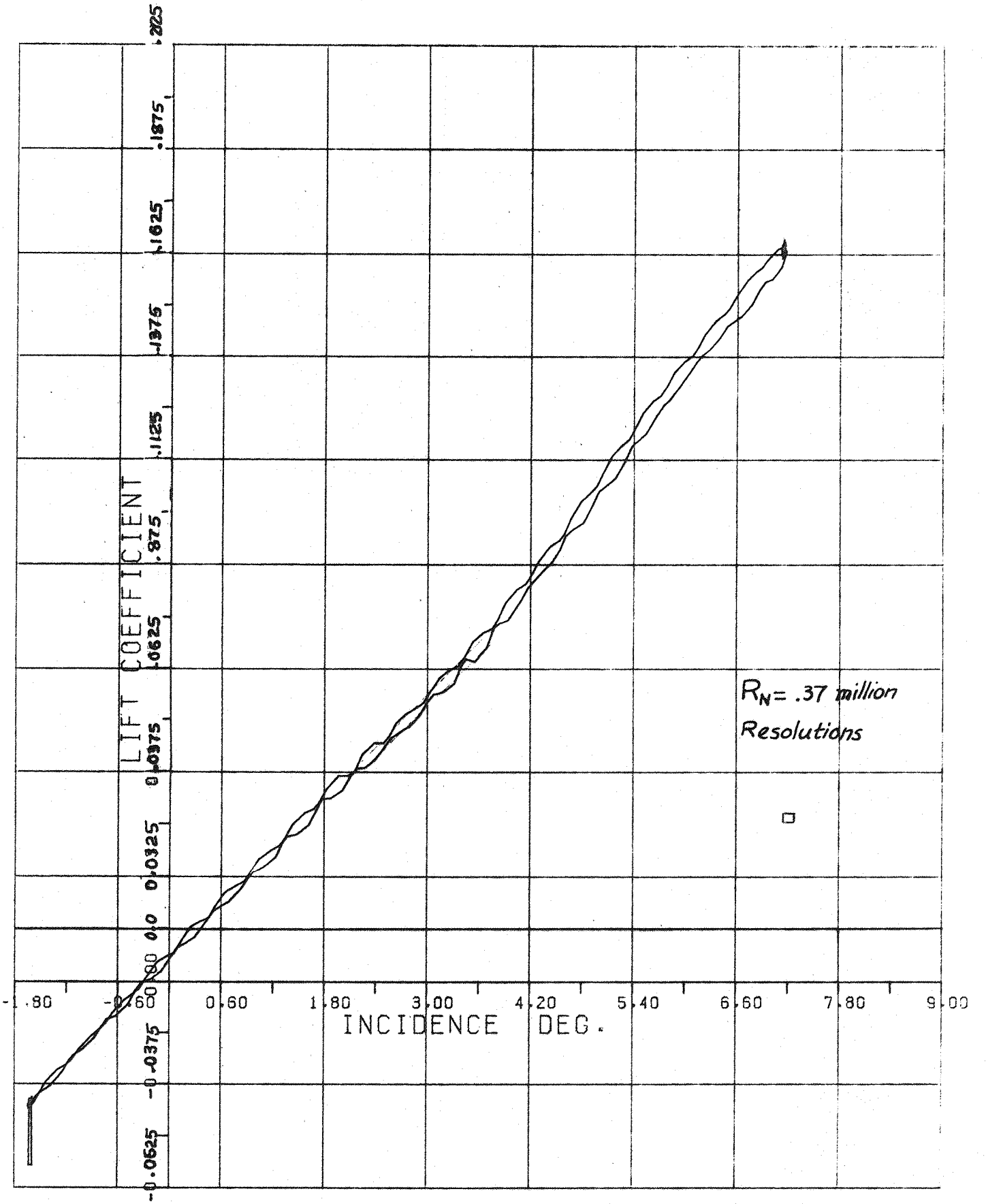

(a)

FIG 7.19 - AERODYNAMIC LIFT VARIATION WITH INCIDENCE

PITCH RATE (DEG/SEC) = 1.000

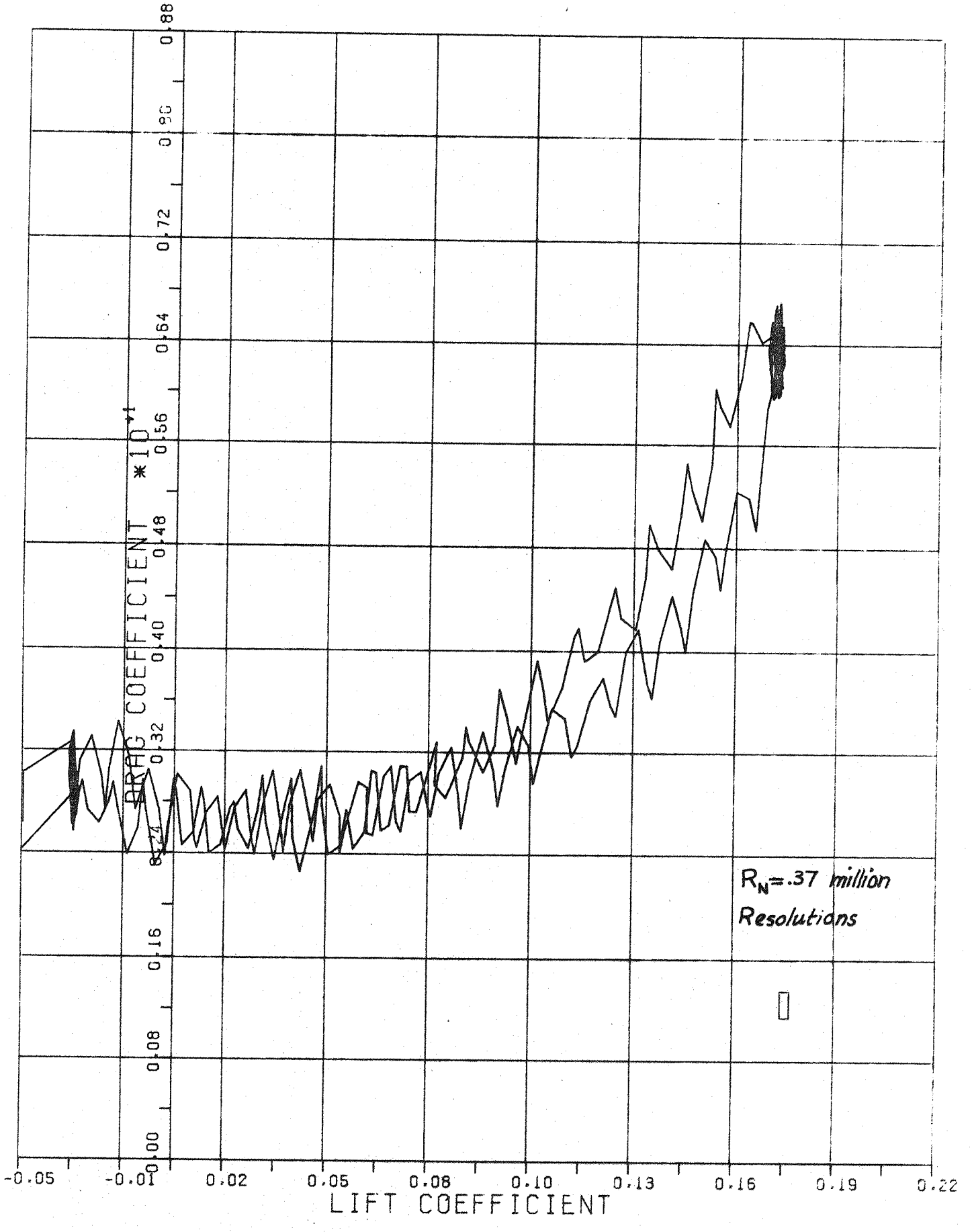

(b)

FIG 7.19 -DRAG VARIATION WITH LIFT

PITCH RATE (DEG/SEC) = 1.000

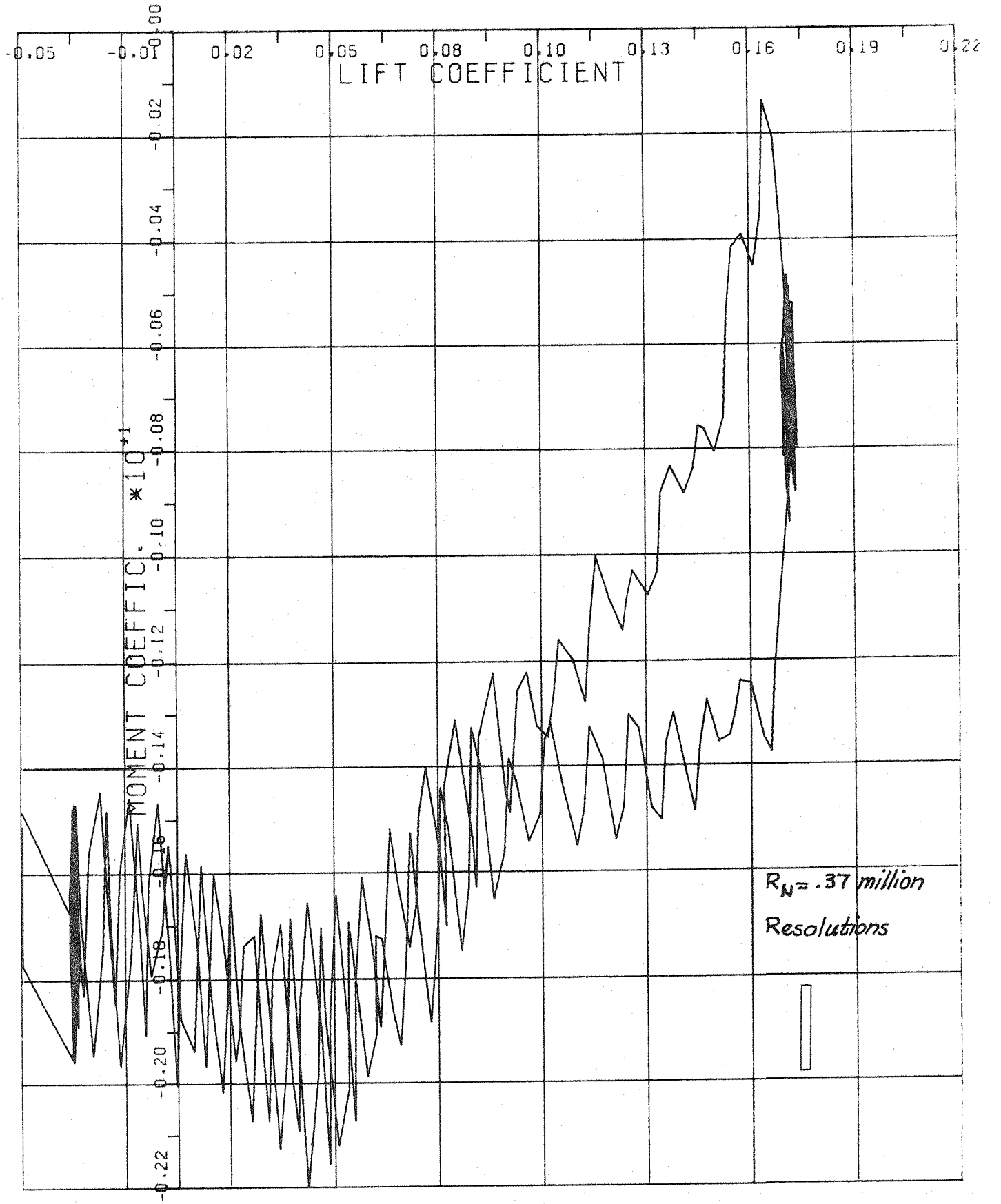

(c)

FIG.7.19-PITCHING MOMENT (ABOUT WING CR/2) VARIATION WITH LIFT

PITCH RATE (DEG/SEC) = 1.000

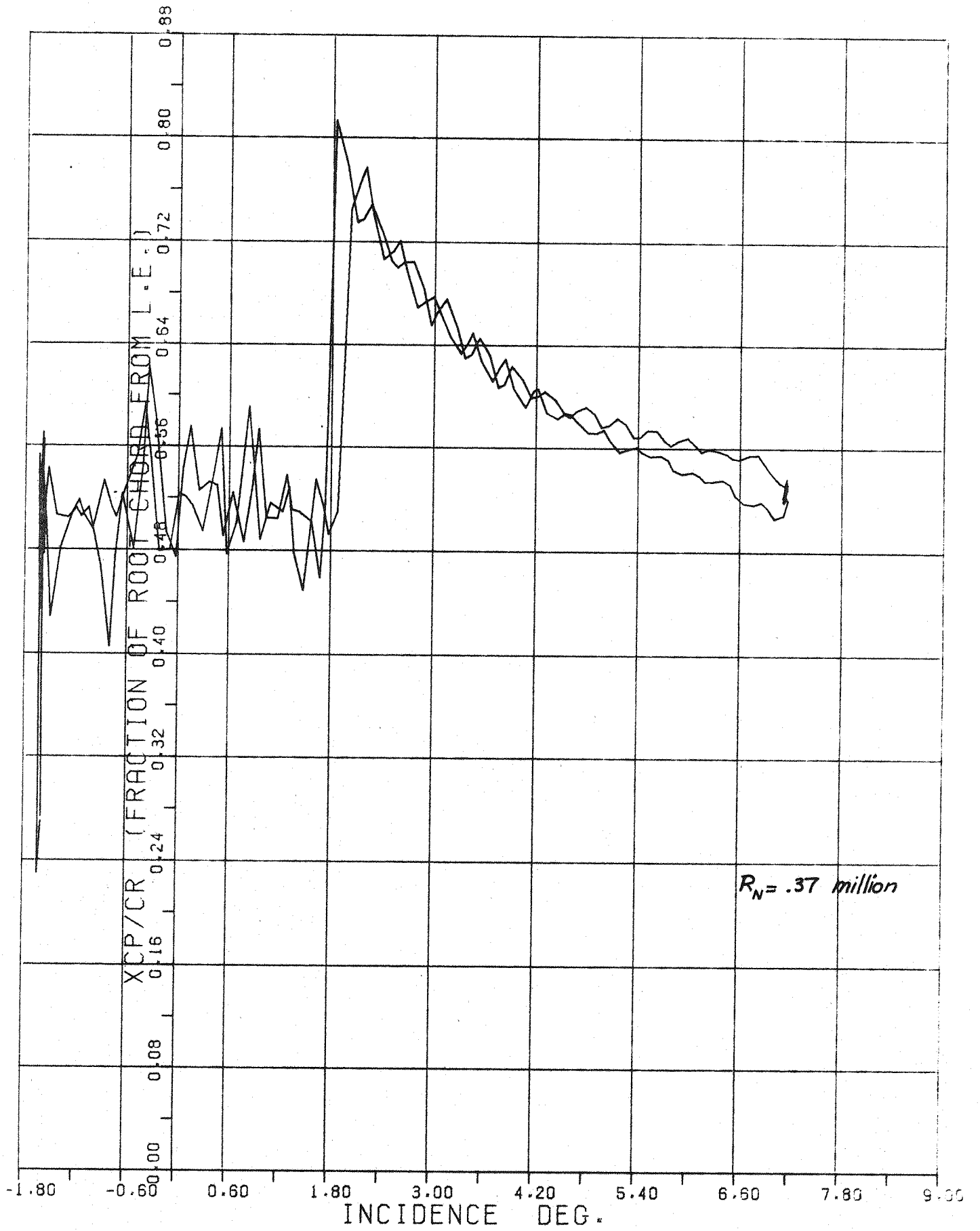

(d)

FIG. 7.19 - CENTER OF PRESSURE LOCATION (% OF ROOT CHORD) BEHIND L. E. OF ROOT CHORD

PITCH RATE (DEG/SEC) = 1.000

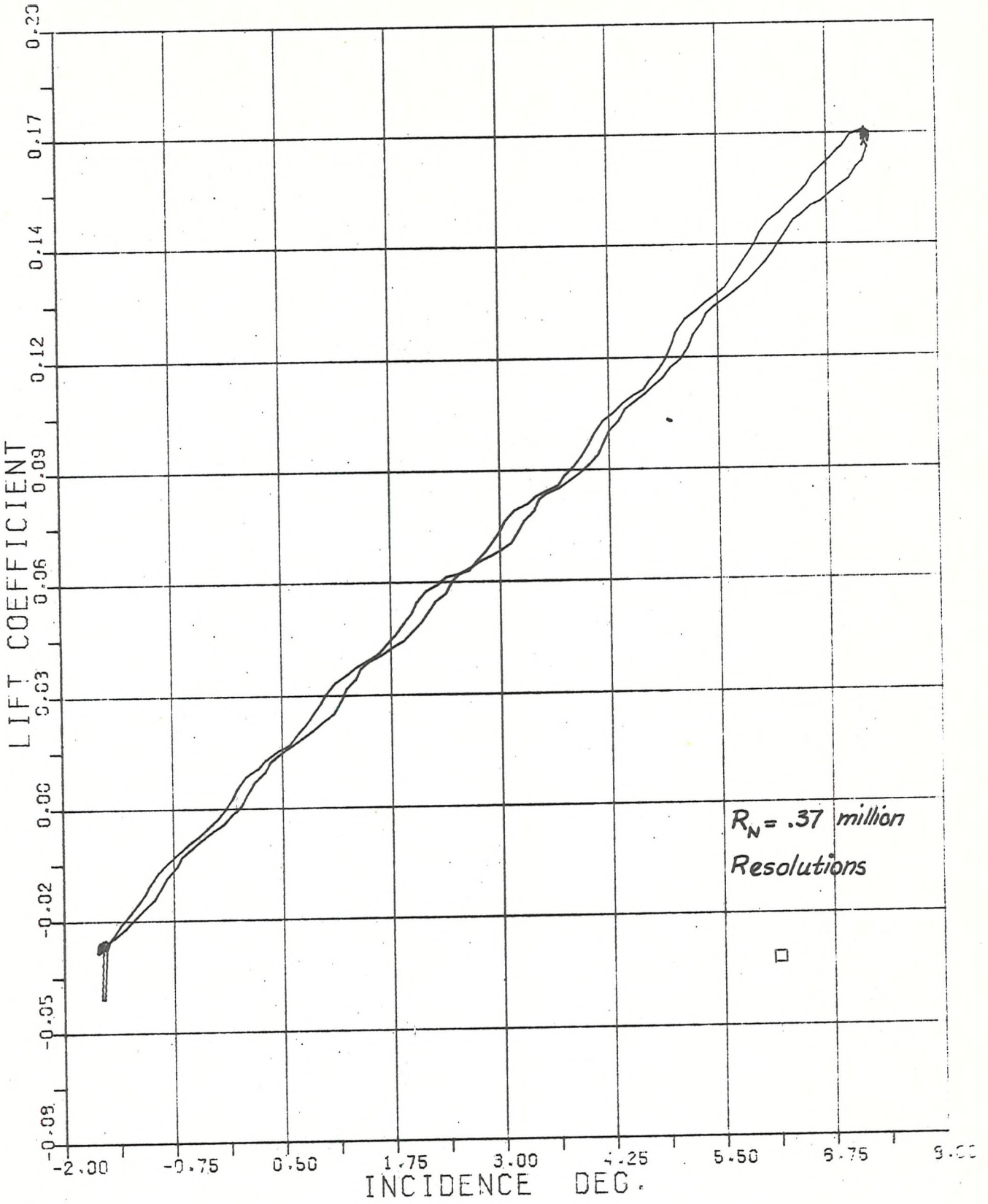

(a)

FIG. 7.20 - AERODYNAMIC LIFT VARIATION WITH INCIDENCE

PITCH RATE (DEG/SEC) = 2.500

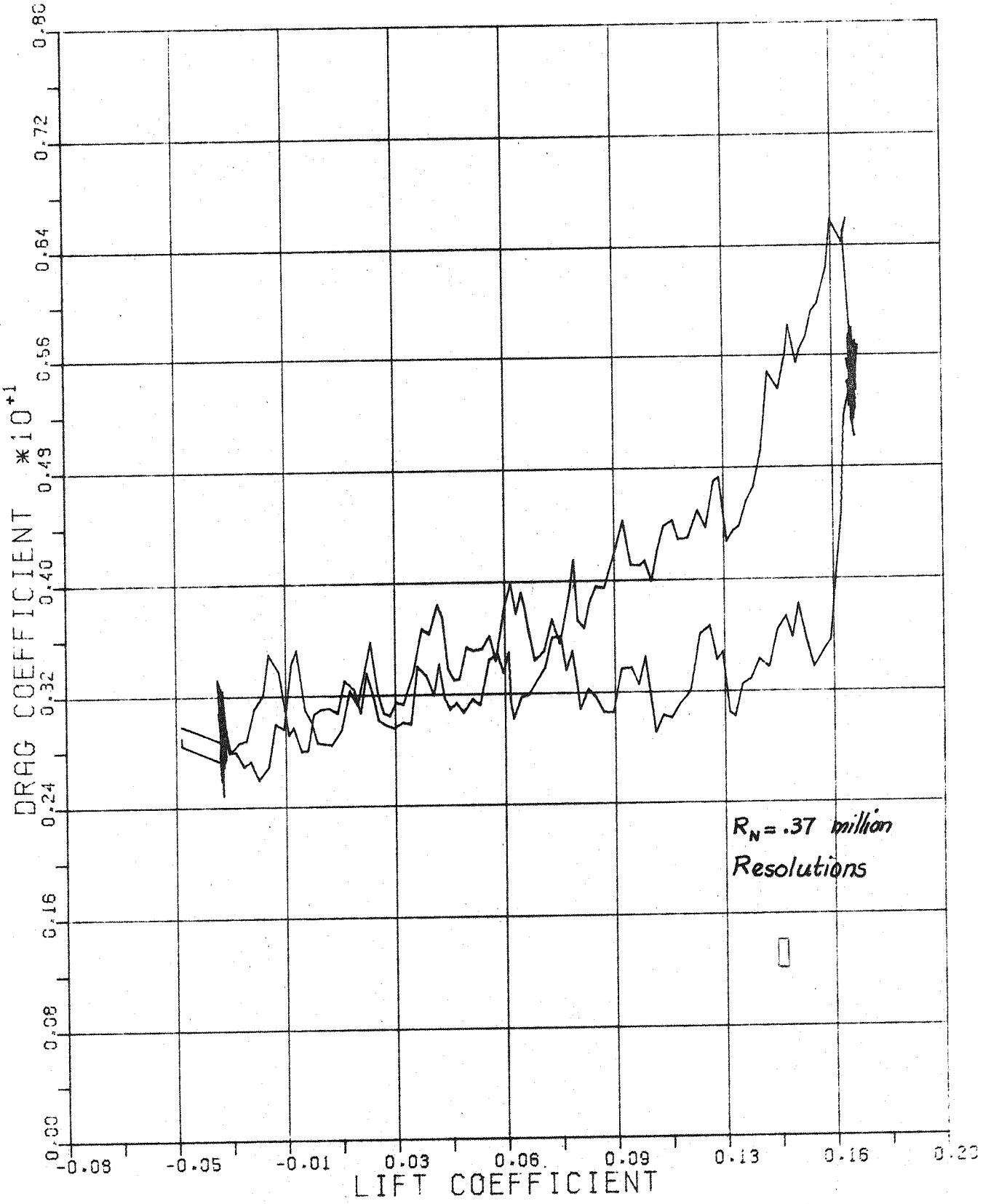

(b)

FIG 7.20 -DRAG VARIATION WITH LIFT

PITCH RATE (DEG/SEC) = 2.500

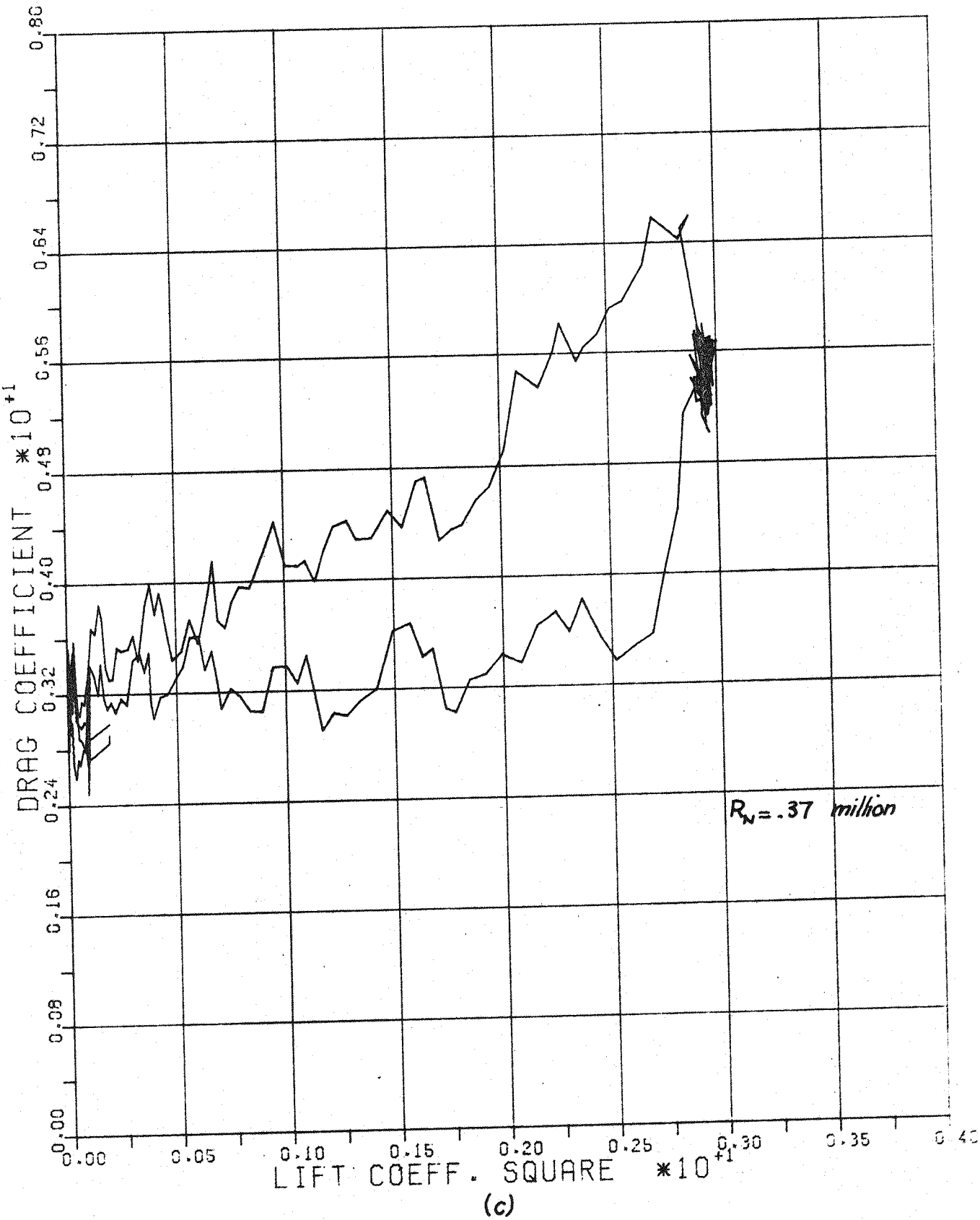

FIG. 7.20 - DRAG VARIATION WITH SQUARE OF LIFT

PITCH RATE (DEG/SEC) = 2.500

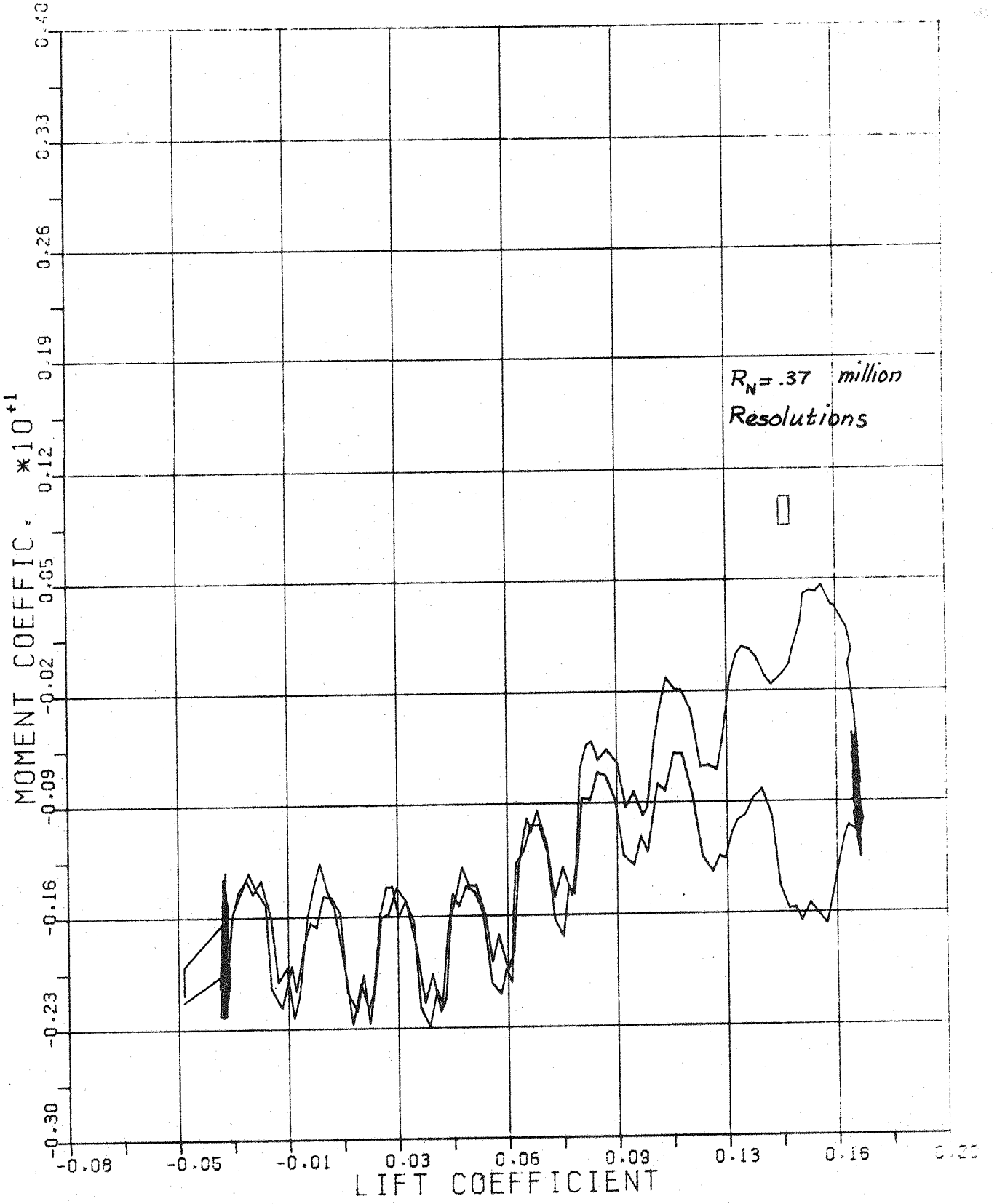

(d)

FIG. 7.20-PITCHING MOMENT (ABOUT WING CR/2) VARIATION WITH LIFT

PITCH RATE (DEG/SEC) = 2.500

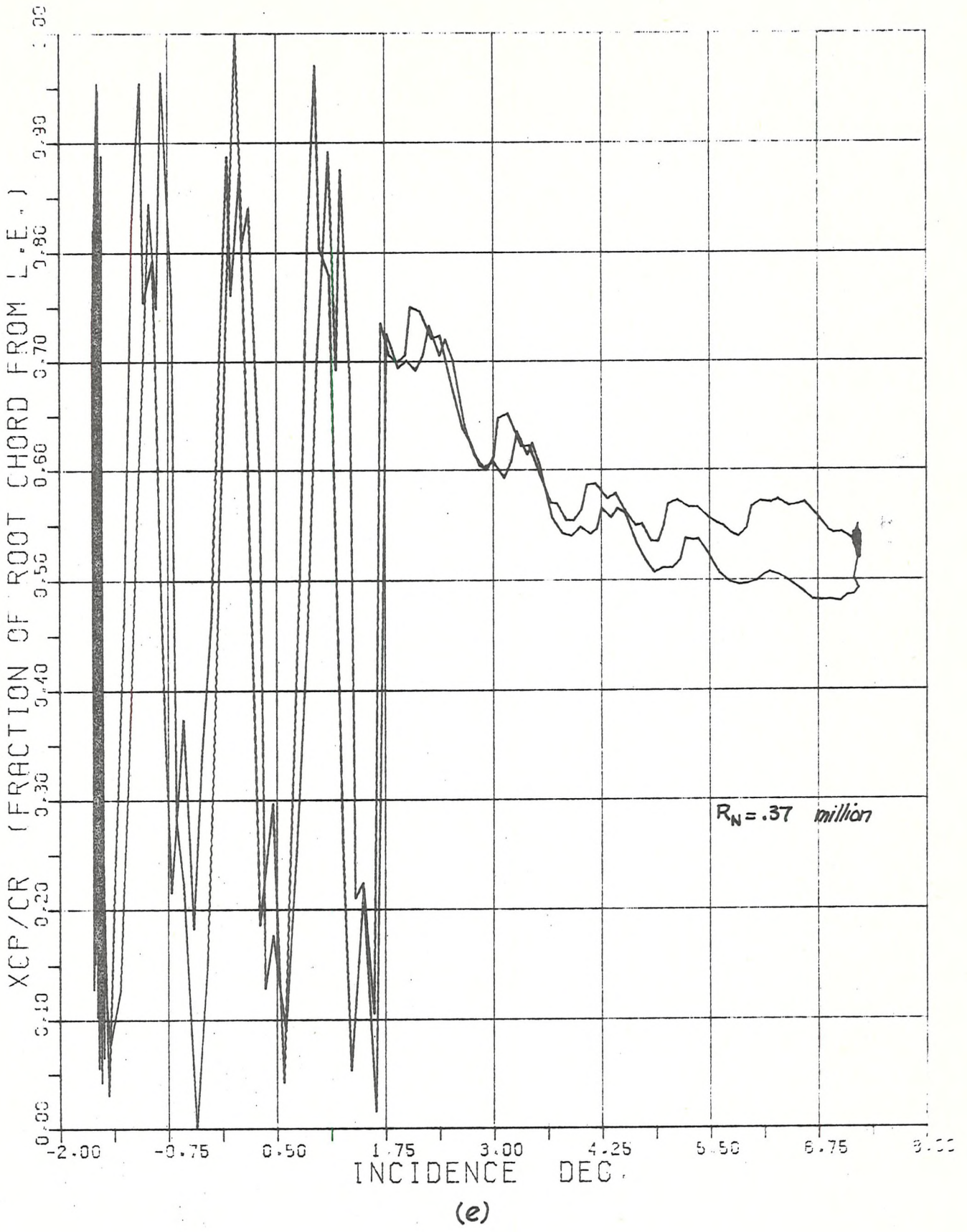

(e)

FIG 720 CENTER OF PRESSURE LOCATION (% OF ROOT CHORD) BEHIND L. E. OF ROOT CHORD

PITCH RATE (DEG/SEC) = 2.500

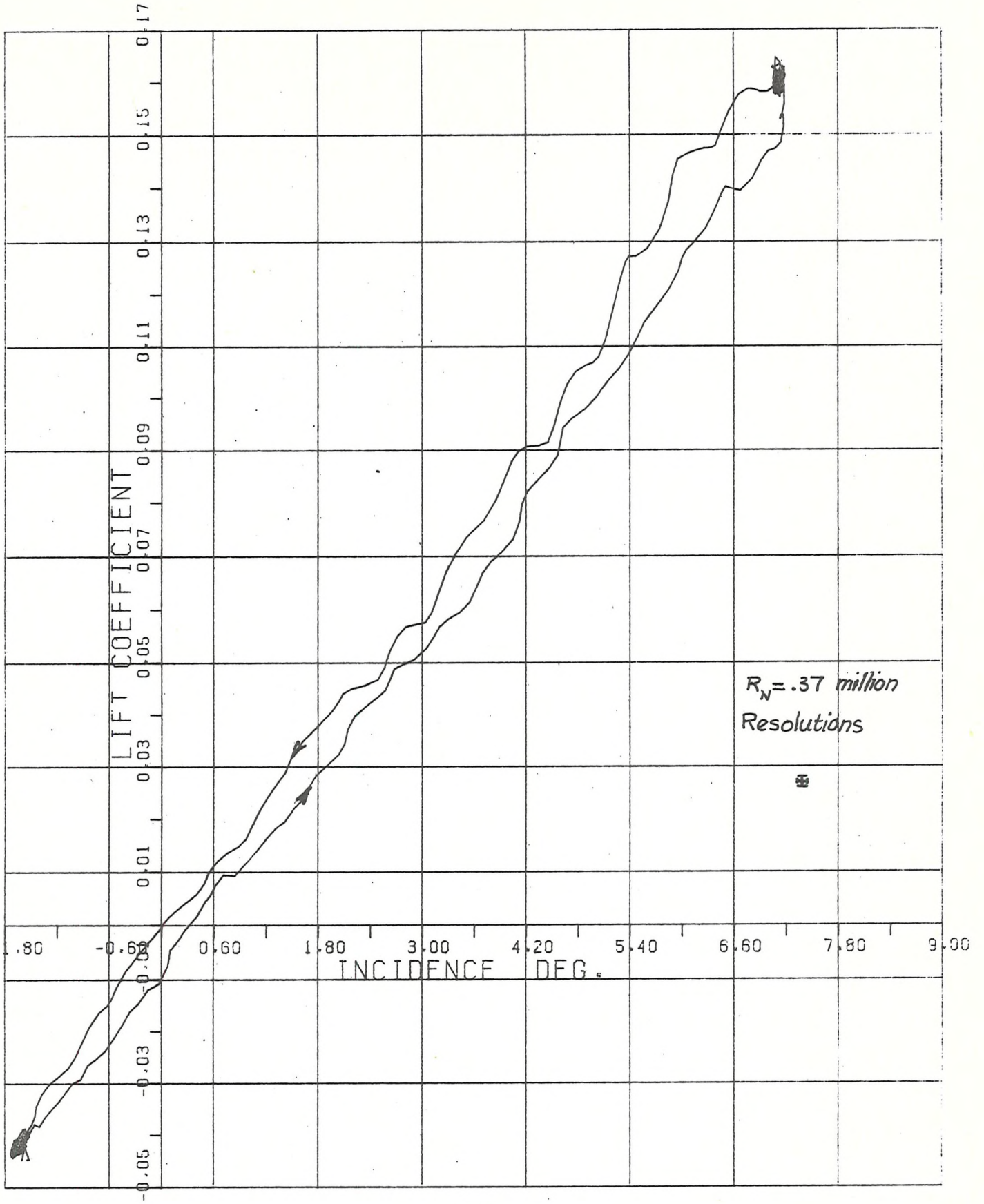

(a)

FIG.7.21-AERODYNAMIC LIFT VARIATION WITH INCIDENCE

PITCH RATE (DEG/SEC) = 5.000

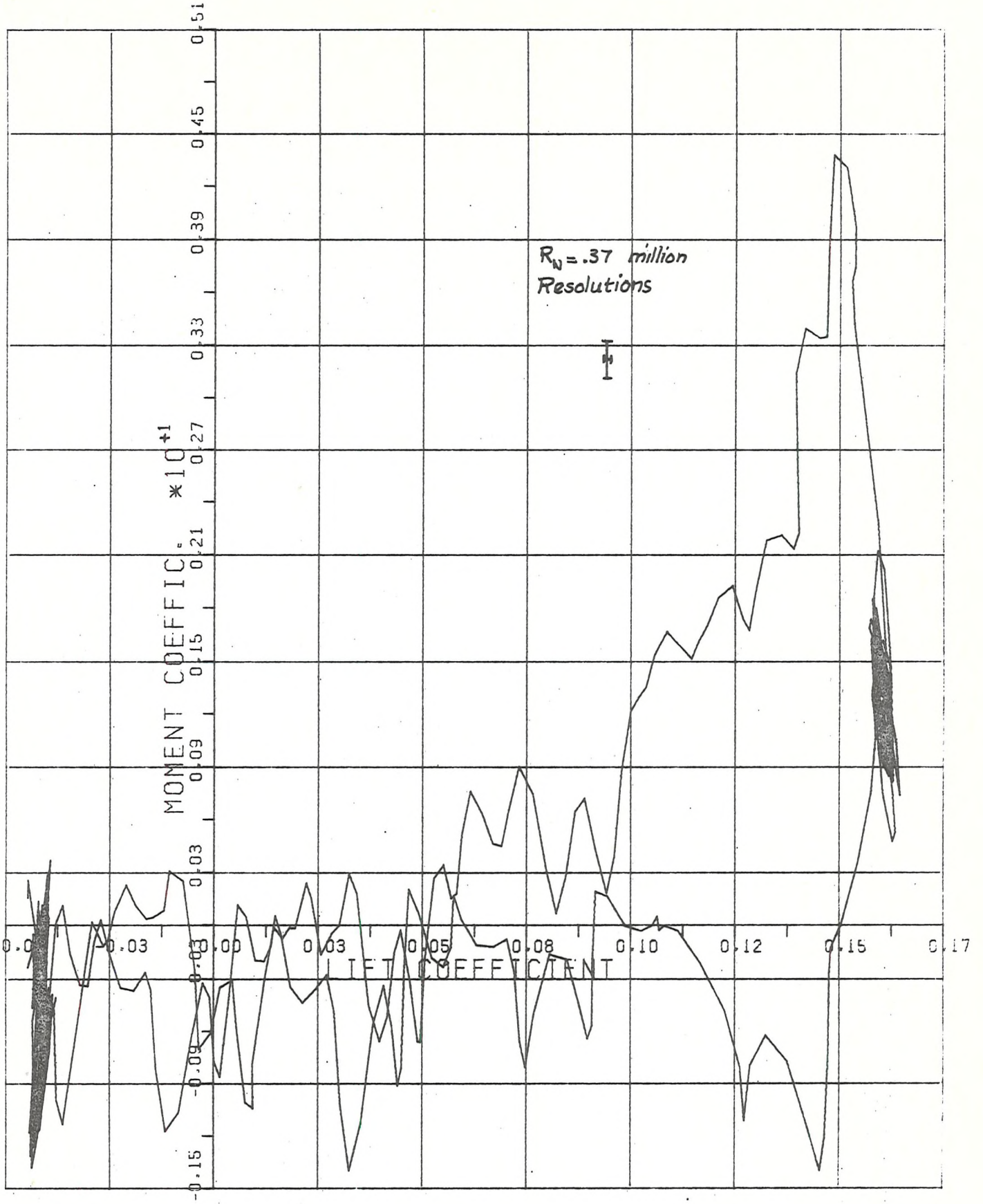

(d)

FIG.7.21-PITCHING MOMENT (ABOUT WING CR/2) VARIATION WITH LIFT

PITCH RATE (DEG/SEC) = 5.000

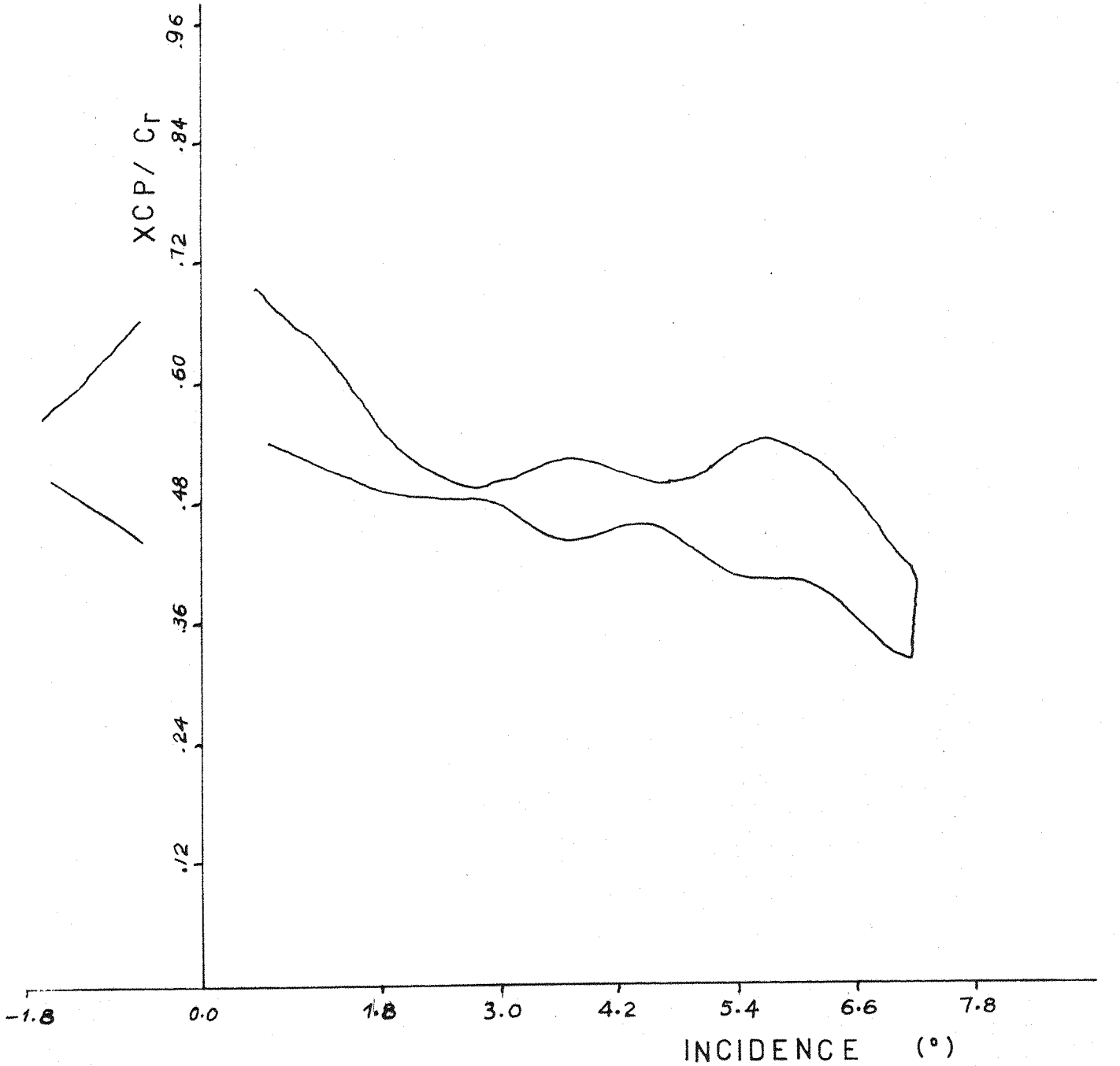

(c)

FIG. 7.21 CENTRE OF PRESSURE LOCATION
(% OF ROOT CHORD) BEHIND APEX
PITCH RATE (°/sec) = 5.00

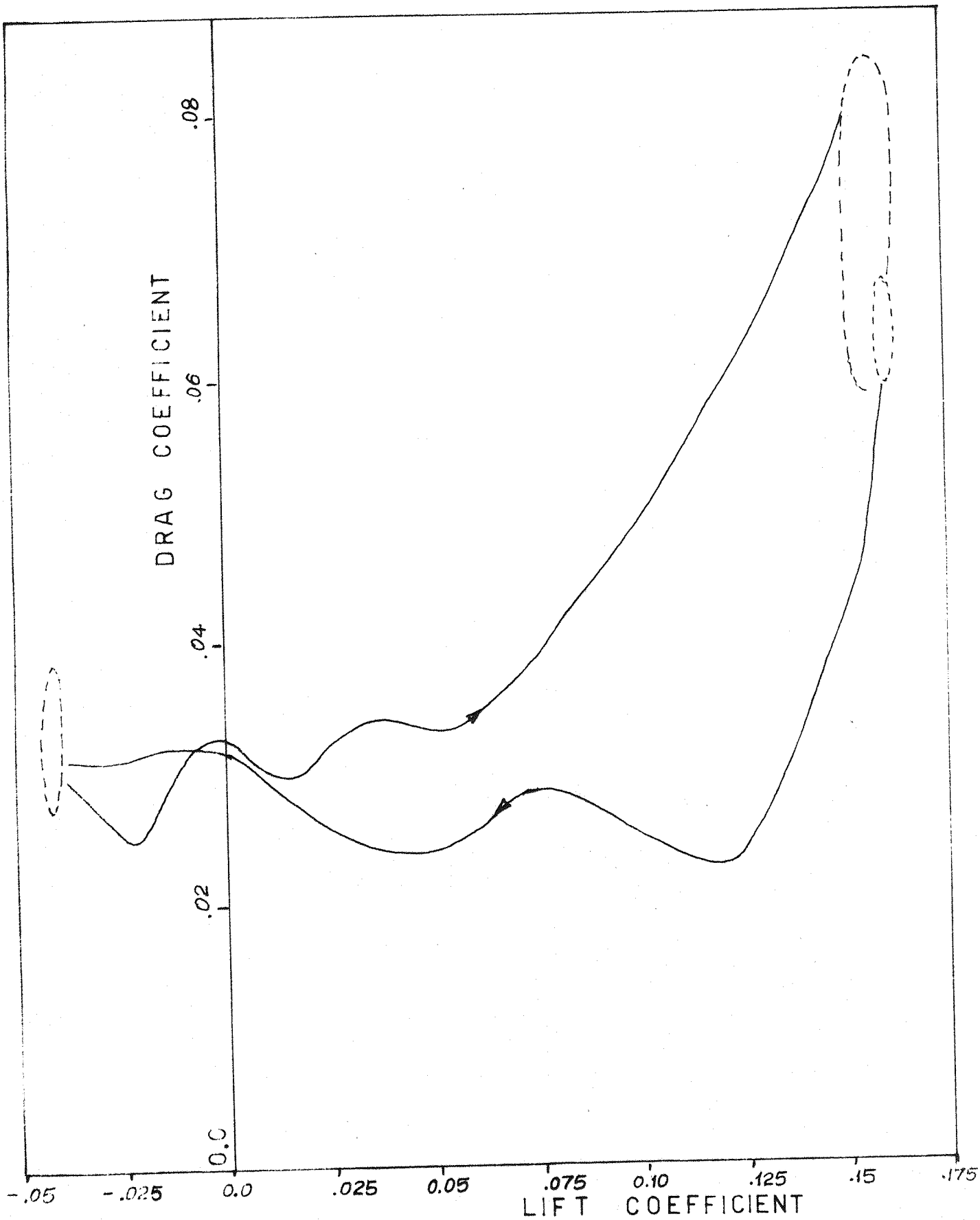

(b)

FIG. 7.21 DRAG VARIATION WITH LIFT
PITCH RATE (°/sec) = 5.00

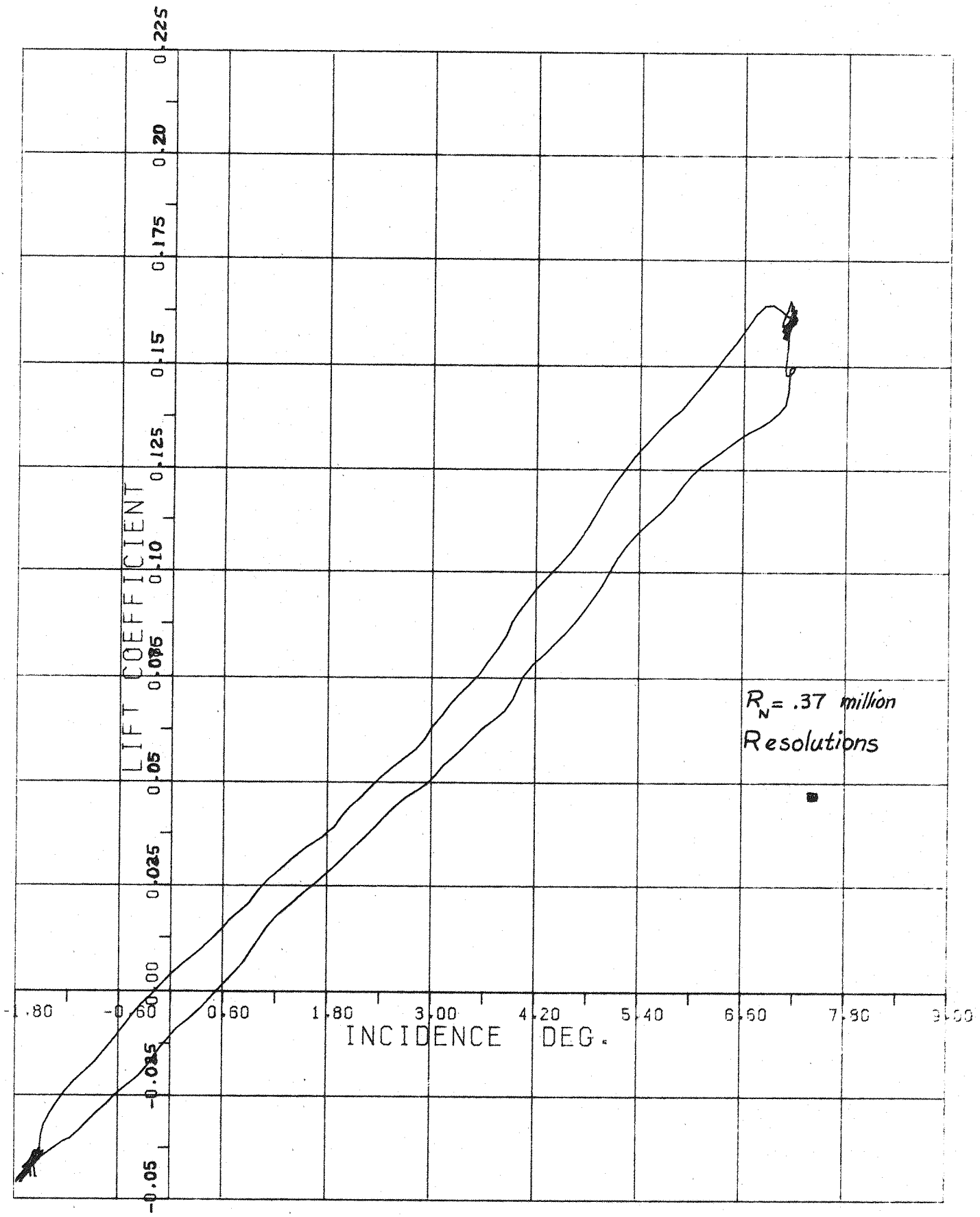

(a)

FIG. 7.22 - AERODYNAMIC LIFT VARIATION WITH INCIDENCE

PITCH RATE (DEG/SEC) = 10.000

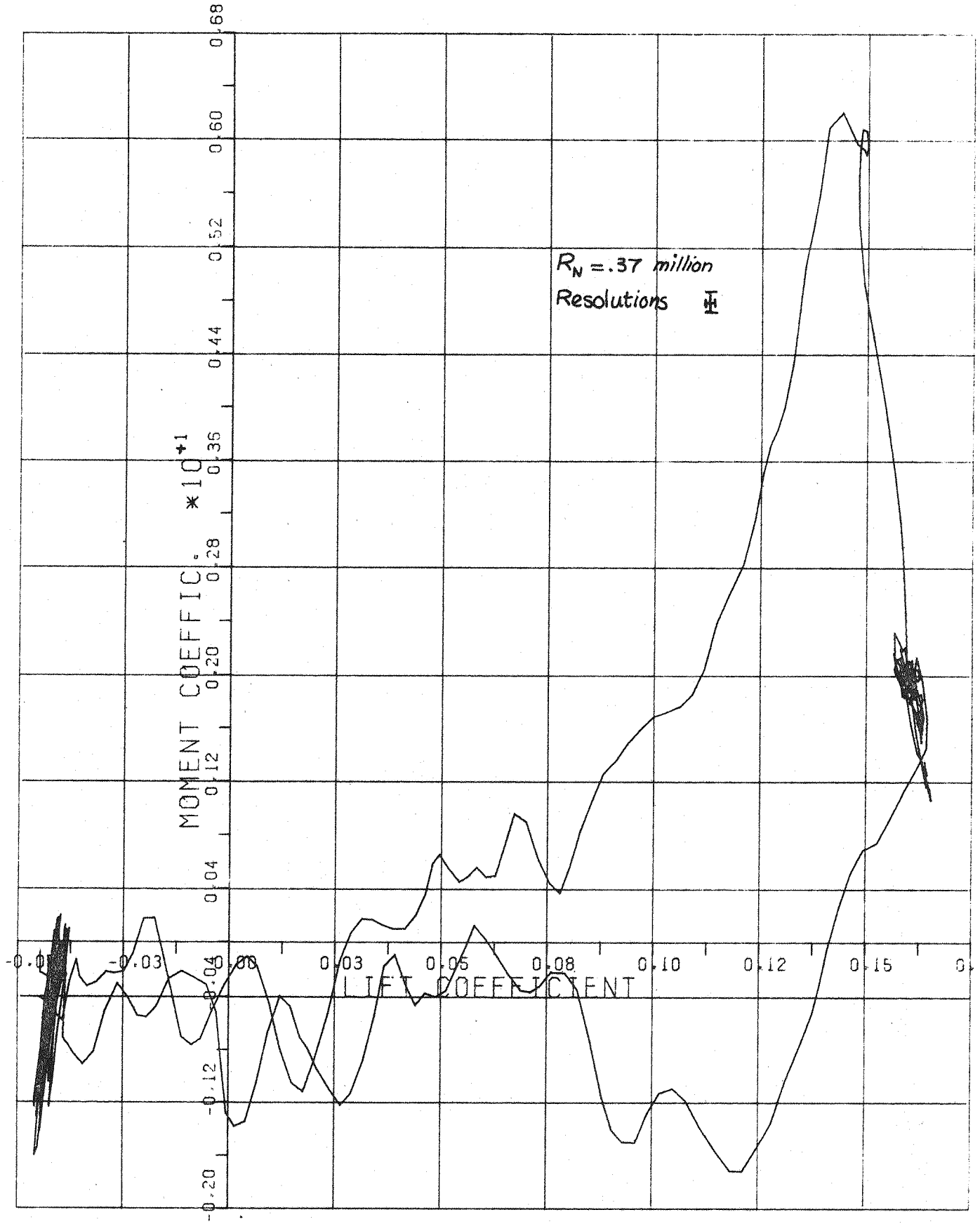

(b)

FIG 7.22 -PITCHING MOMENT (ABOUT WING CR/2) VARIATION WITH LIFT

PITCH RATE (DEG/SEC) = 10.000

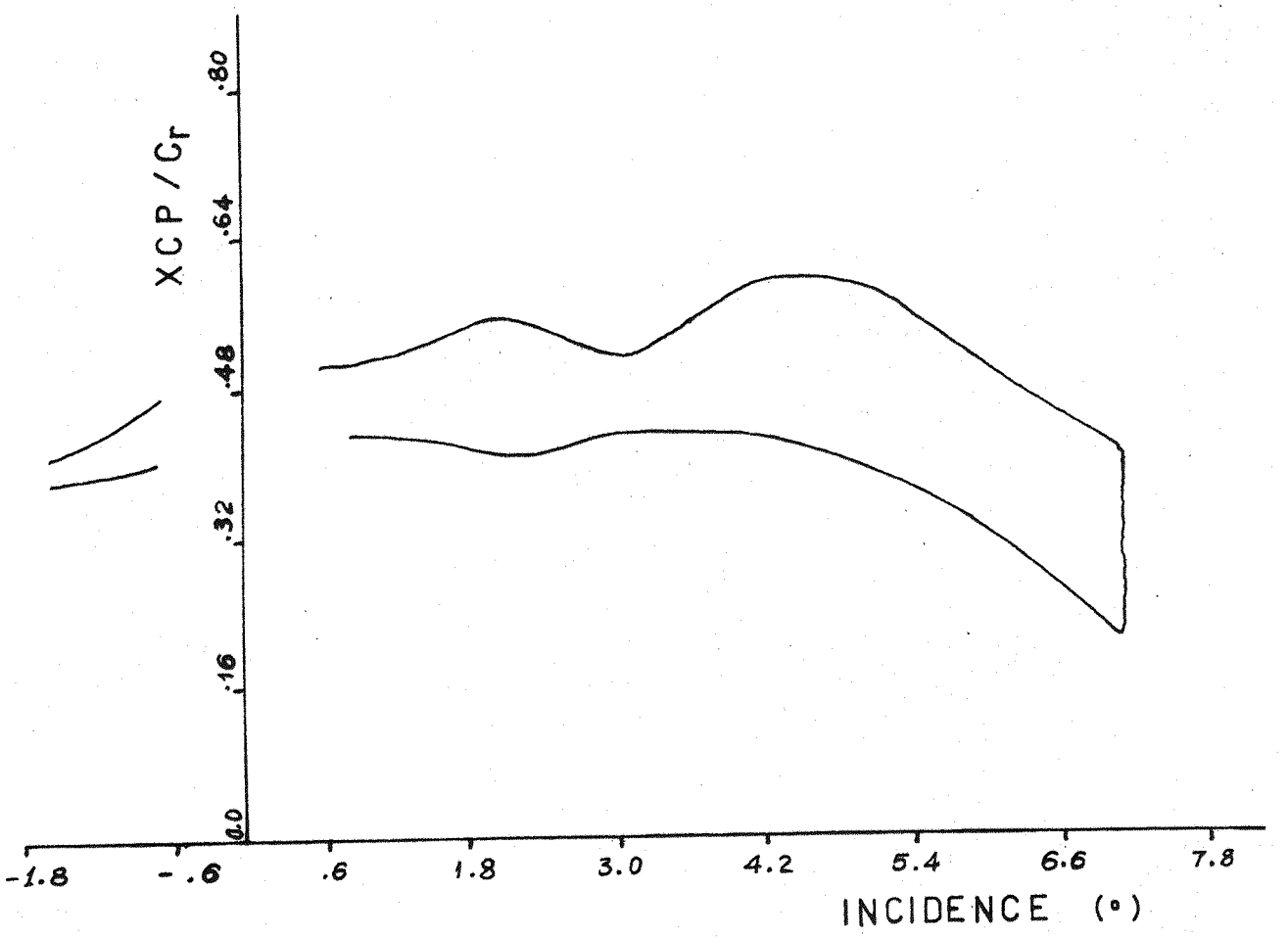

(c)

FIG. 7.22 CENTRE OF PRESSURE LOCATION (% OF ROOT CHORD) BEHIND APEX
PITCH RATE (°/sec) = 10.00

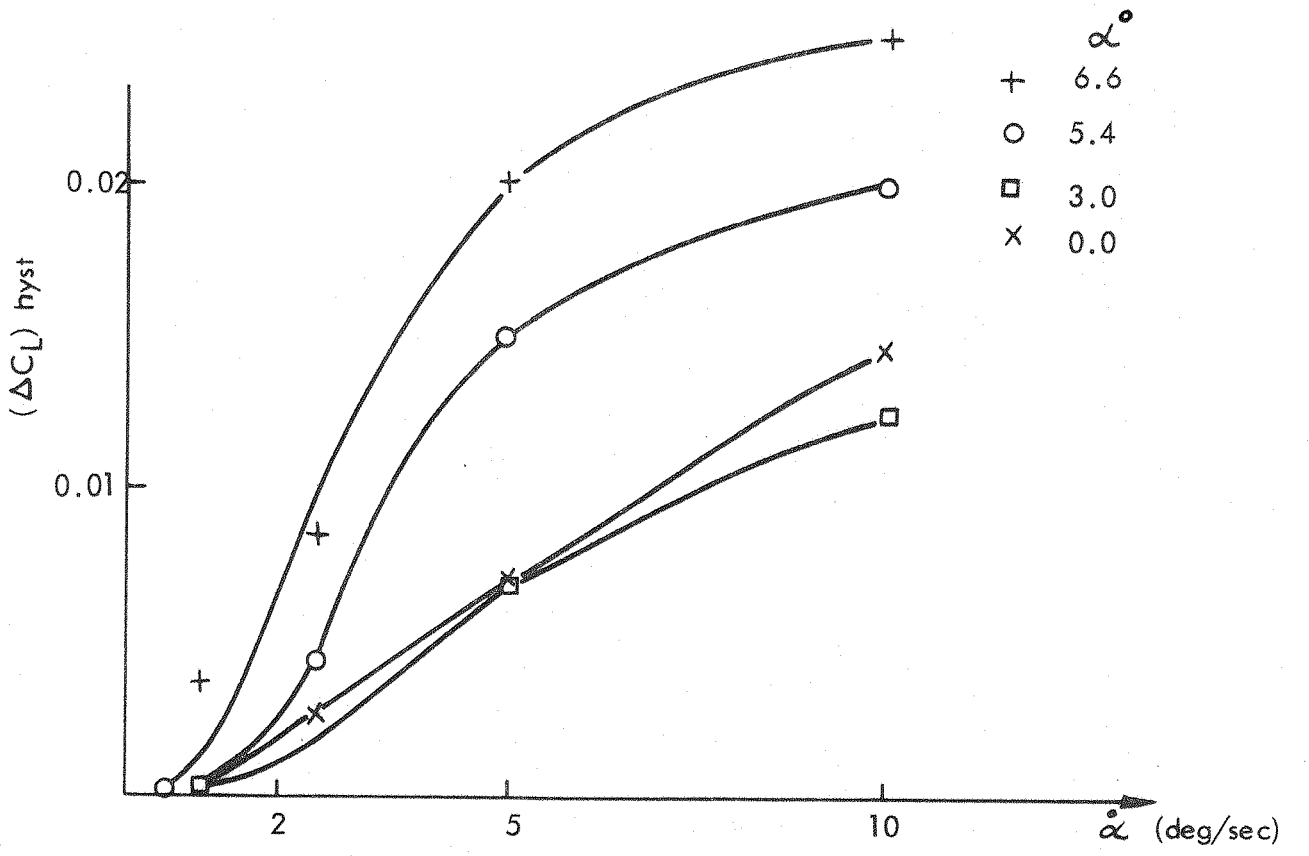

FIG. 7.23. VARIATION OF HYSTERETIC LIFT COEFFICIENT WITH RAMP RATE.

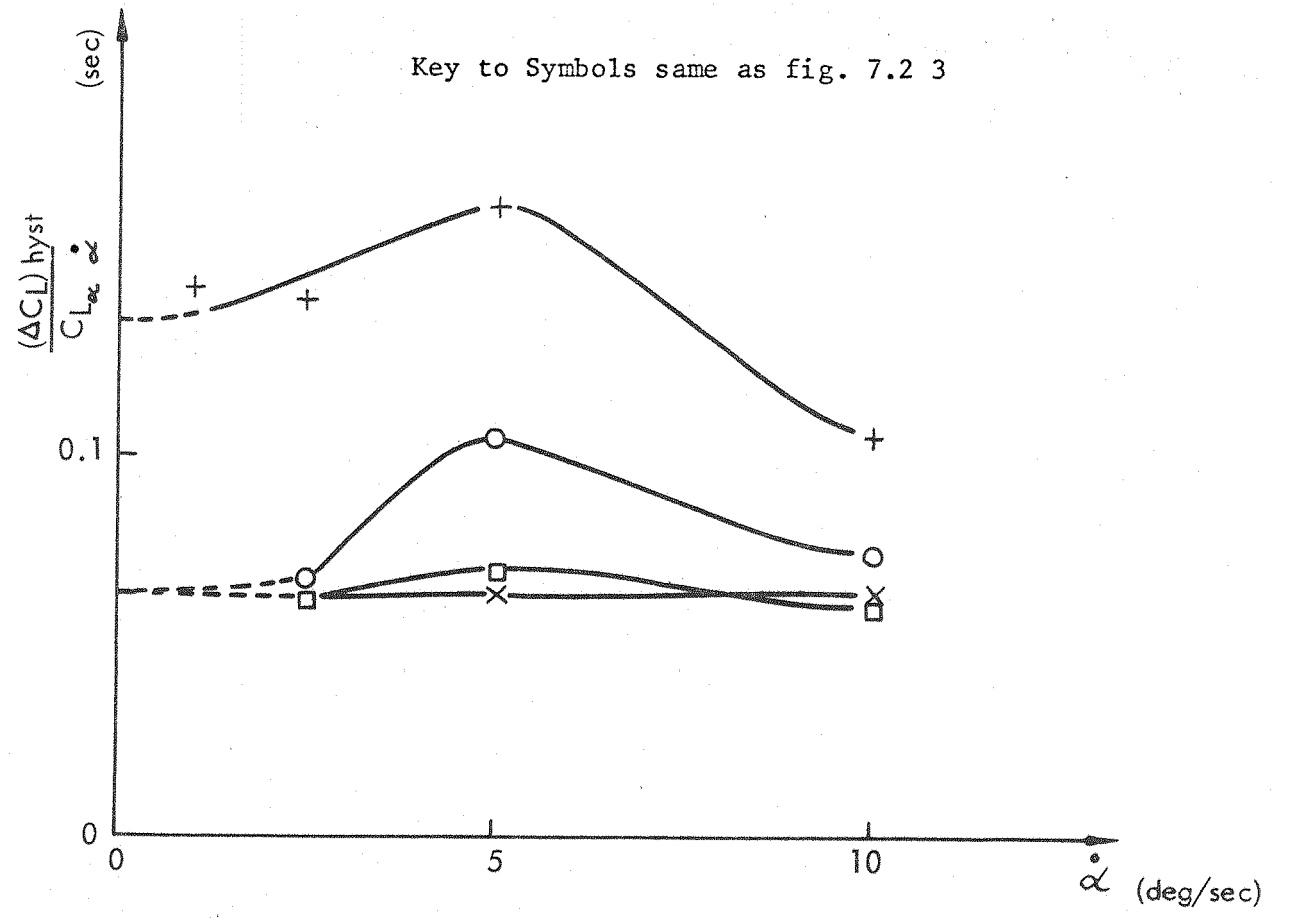

FIG. 7.24. VARIATION OF LIFT PARAMETER WITH RAMP RATE.

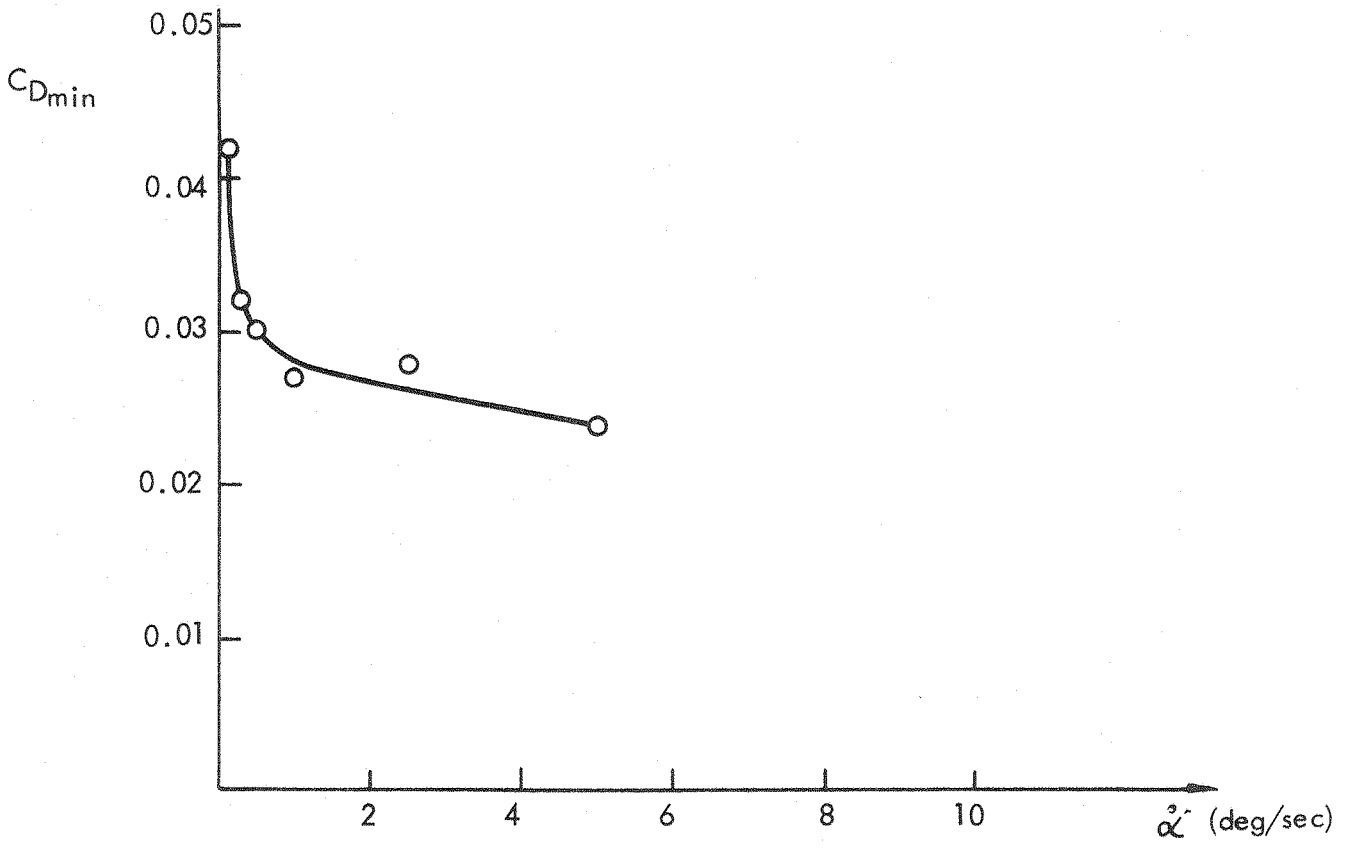

FIG. 7.25. VARIATION OF MINIMUM DRAG COEFFICIENT WITH $|\dot{\alpha}|$

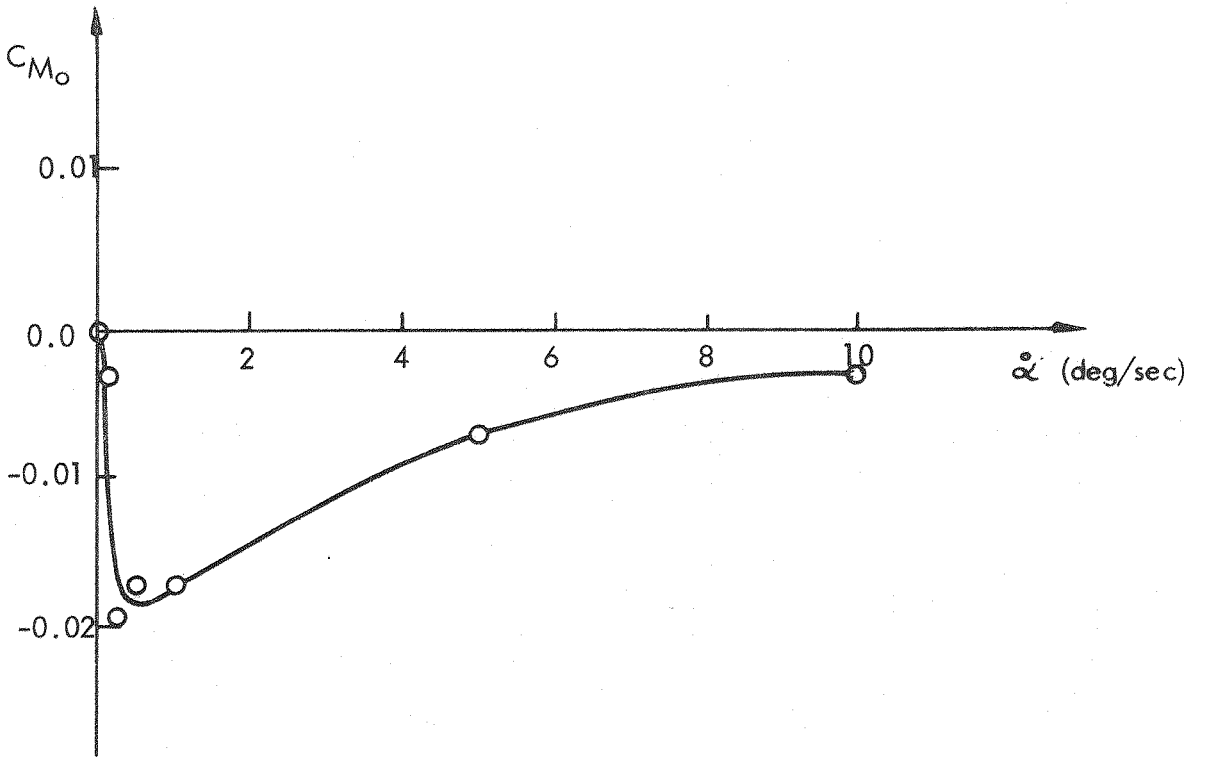

FIG. 7.26. VARIATION OF PITCHING MOMENT COEFFICIENT ABOUT MID-CHORD POINT WITH $|\dot{\alpha}|$

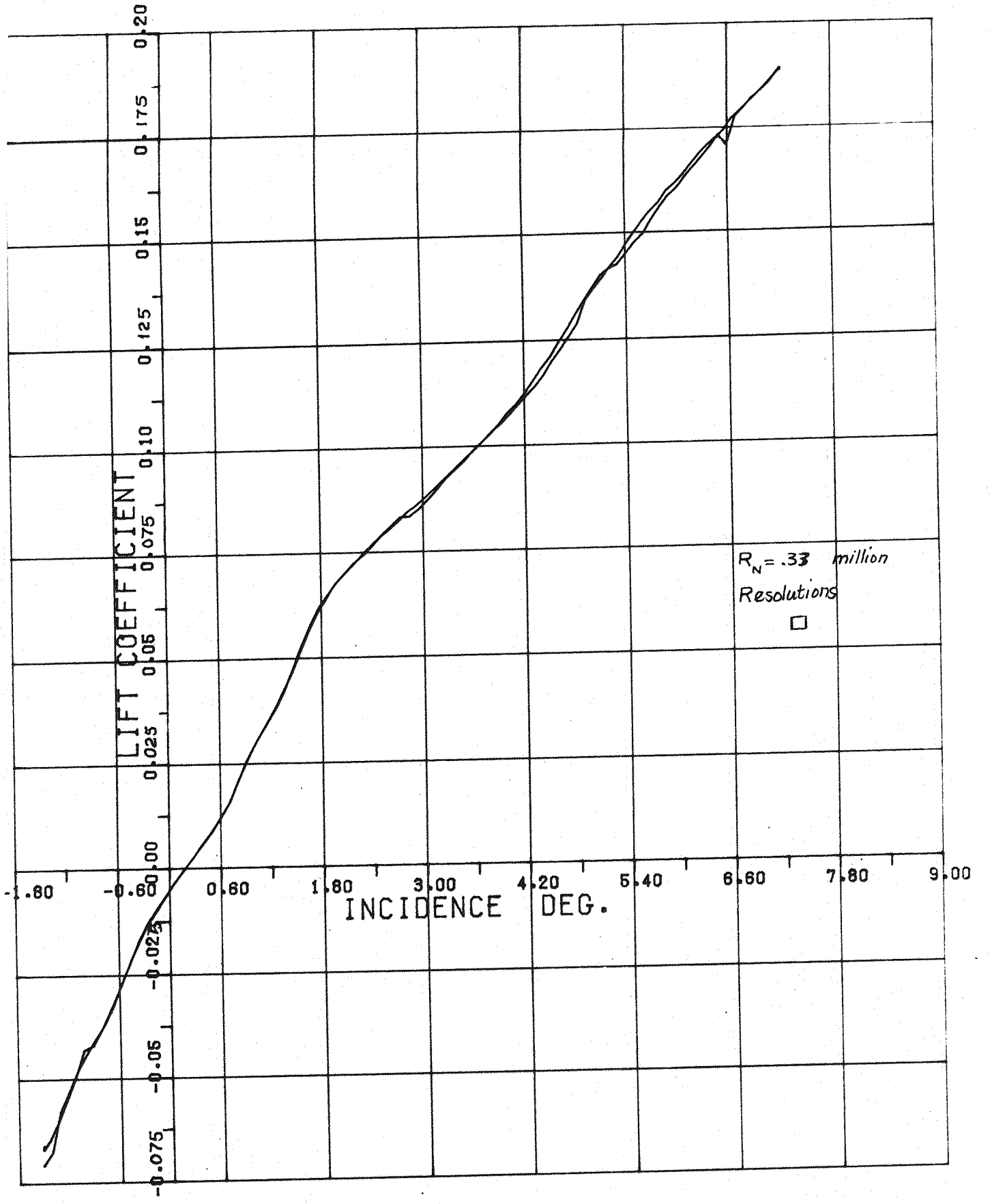

(a)

FIG.7.27-AERODYNAMIC LIFT VARIATION WITH INCIDENCE

PITCH RATE (DEG/SEC) = 0.05

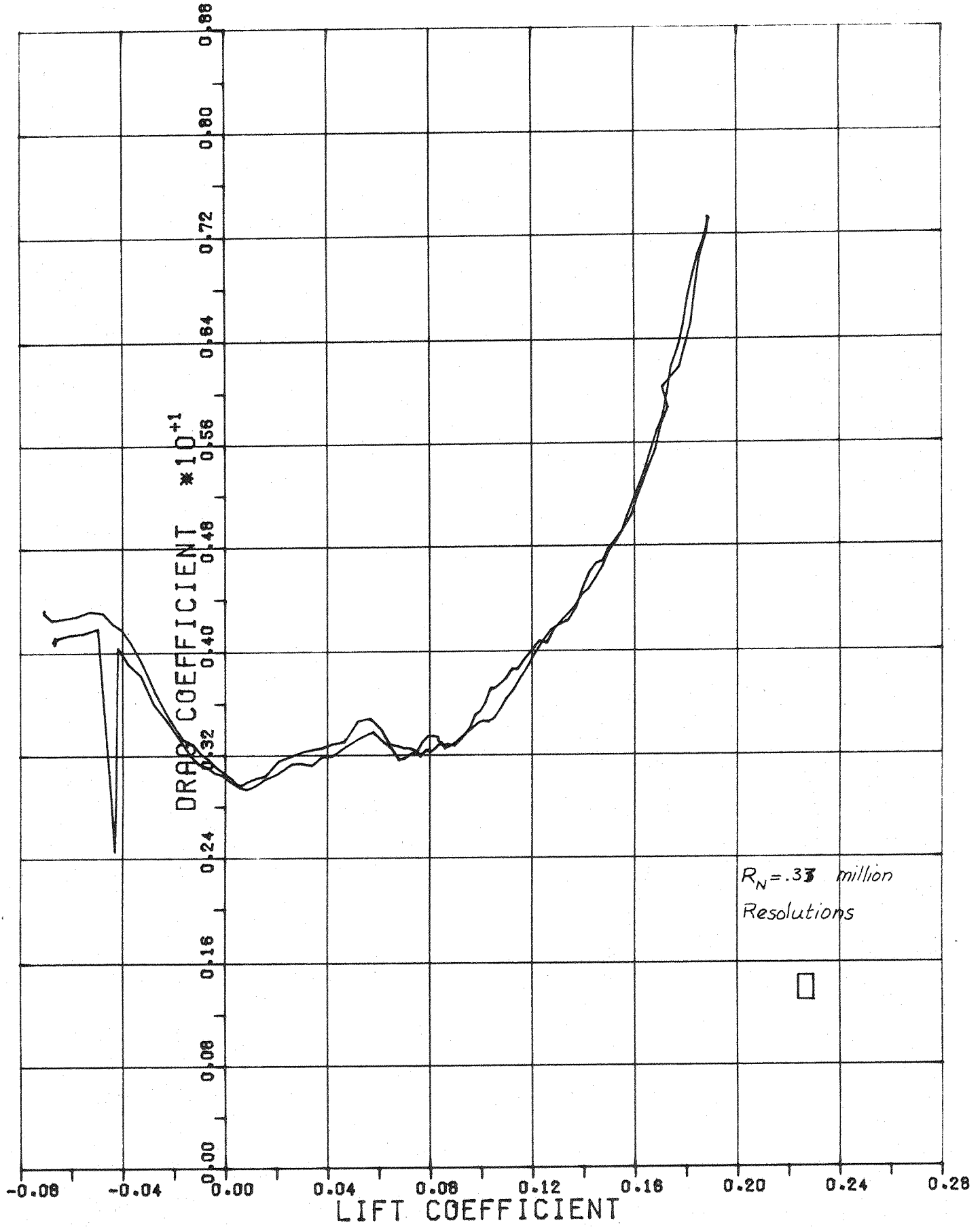

(b)

FIG.7.27-DRAG VARIATION WITH LIFT

PITCH RATE (DEG/SEC) = 0 .05

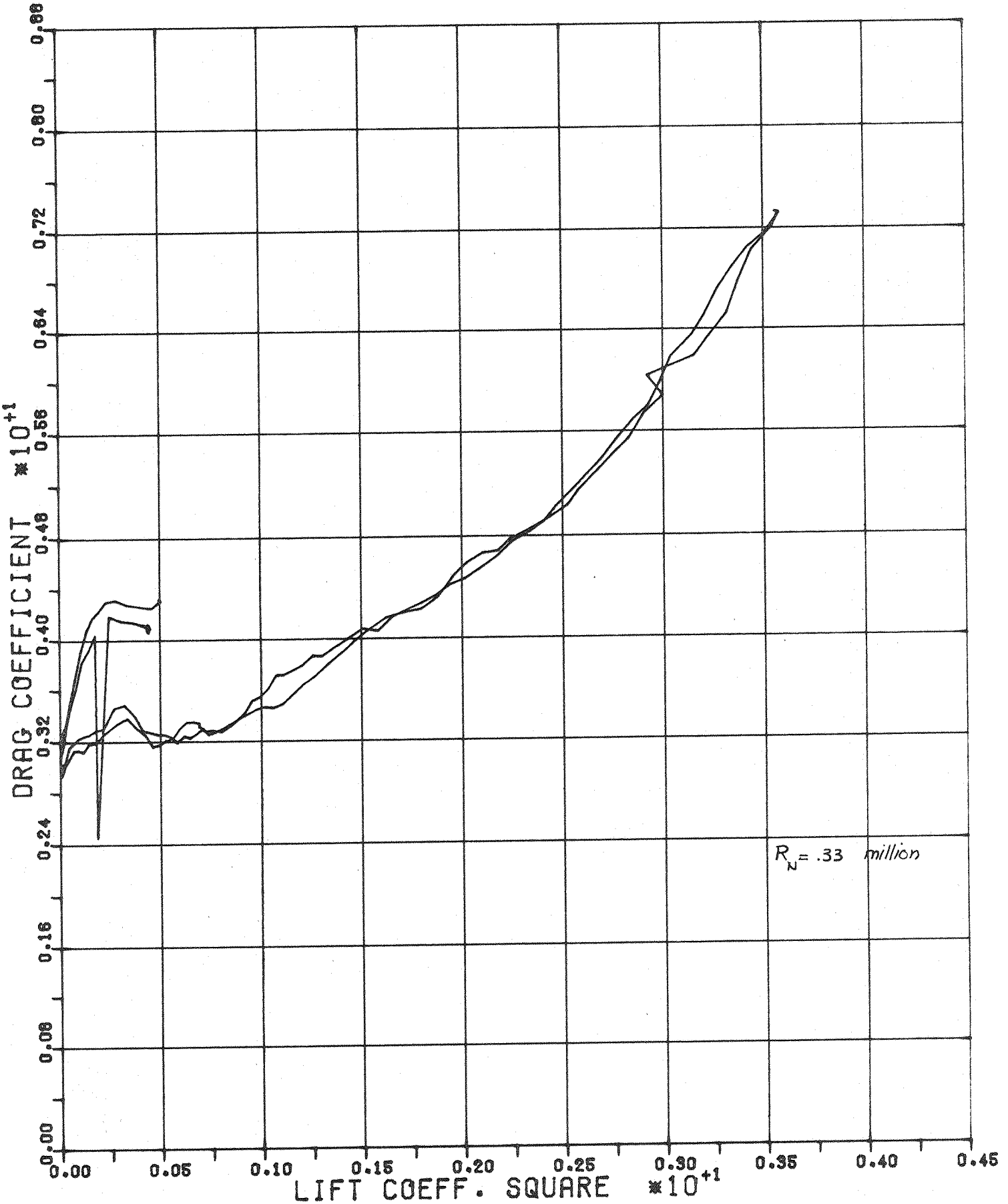

(c)

FIG.7.27-DRAG VARIATION WITH SQUARE OF LIFT

PITCH RATE (DEG/SEC) = 0 .05

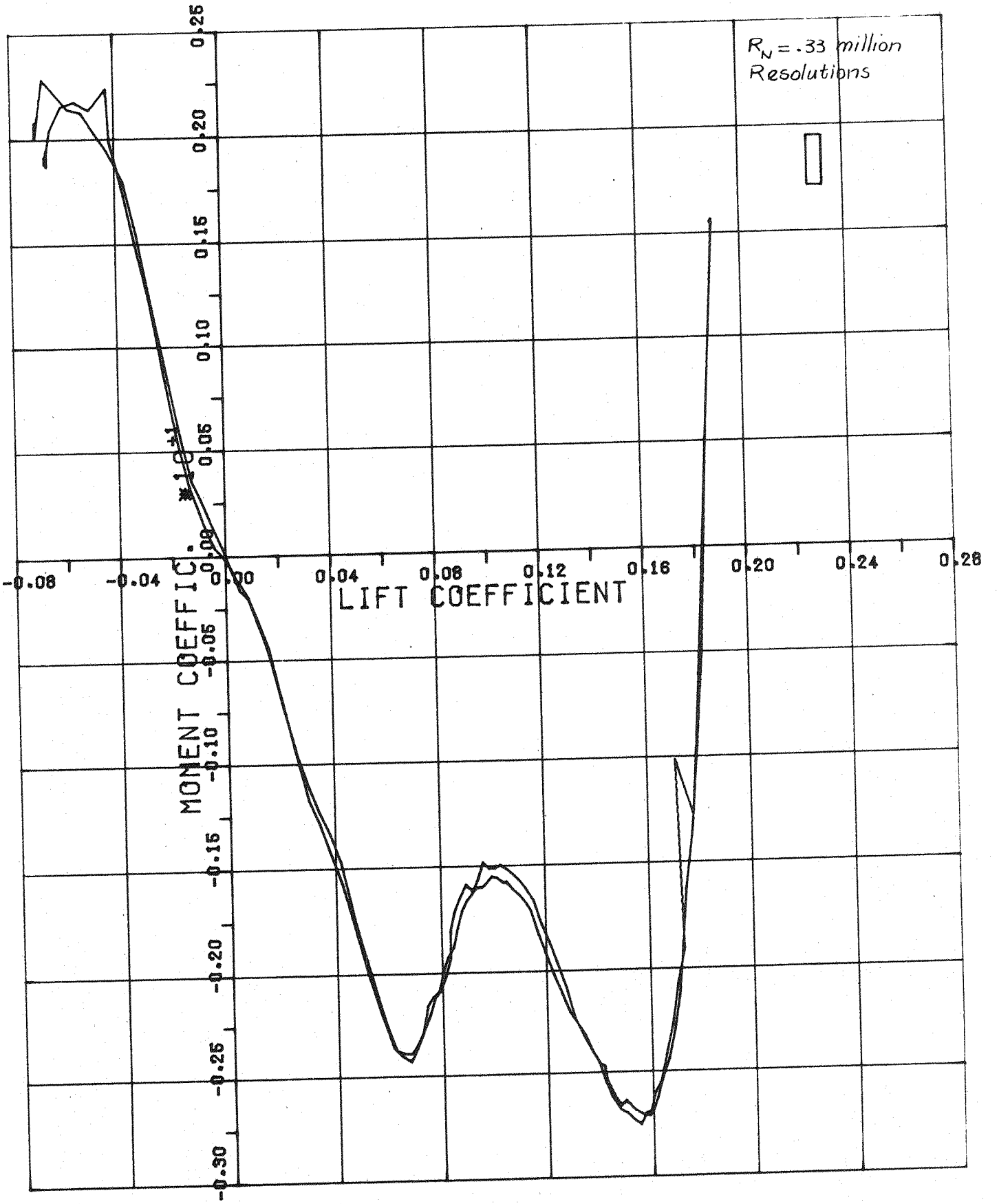

(d)

FIG. 7.27 - PITCHING MOMENT (ABOUT WING CR/2) VARIATION WITH LIFT

PITCH RATE (DEG/SEC) = 0.05

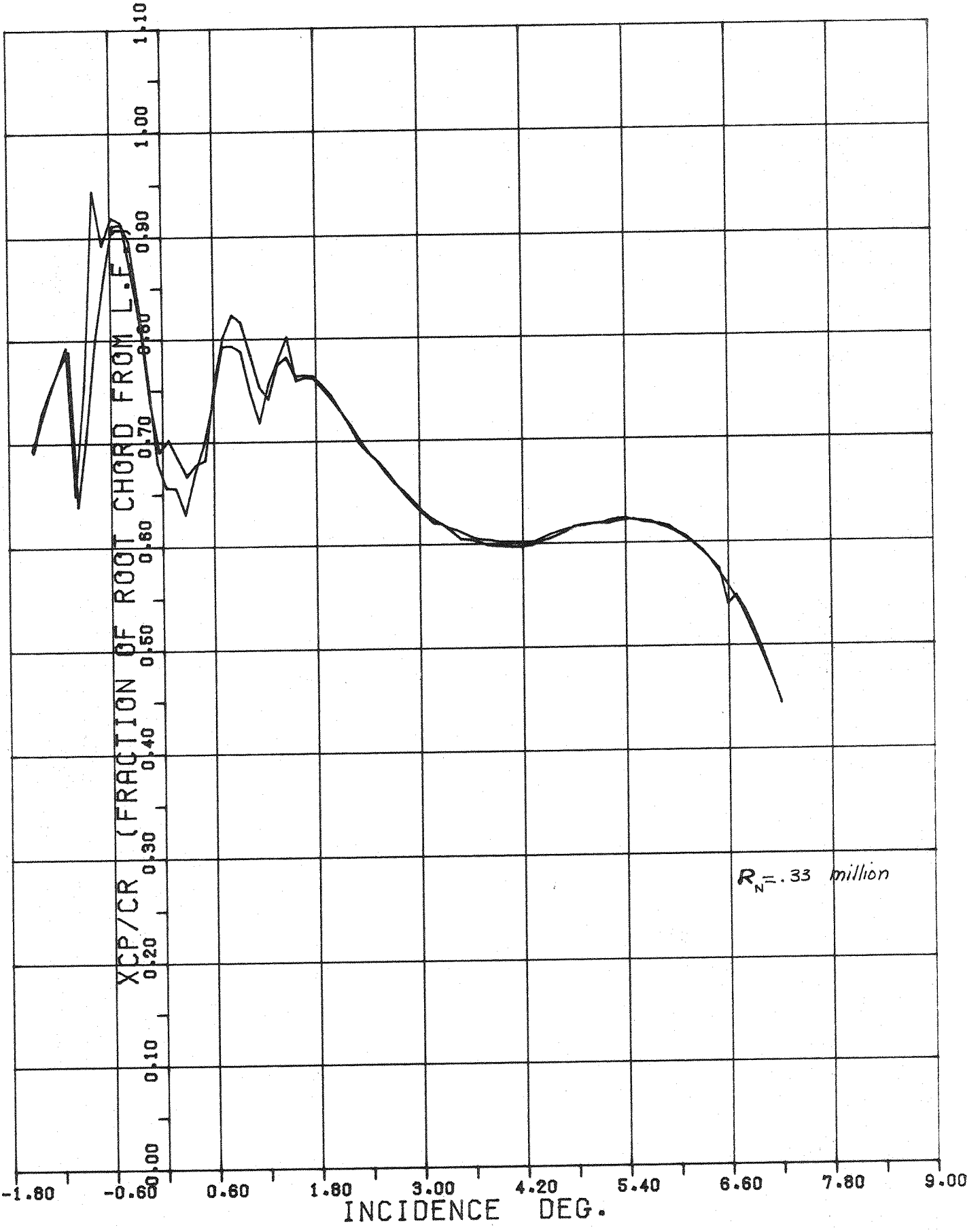

(e)

FIG. 72 - CENTER OF PRESSURE LOCATION (% OF ROOT CHORD) BEHIND L. E. OF ROOT CHORD

PITCH RATE (DEG/SEC) = 0.05

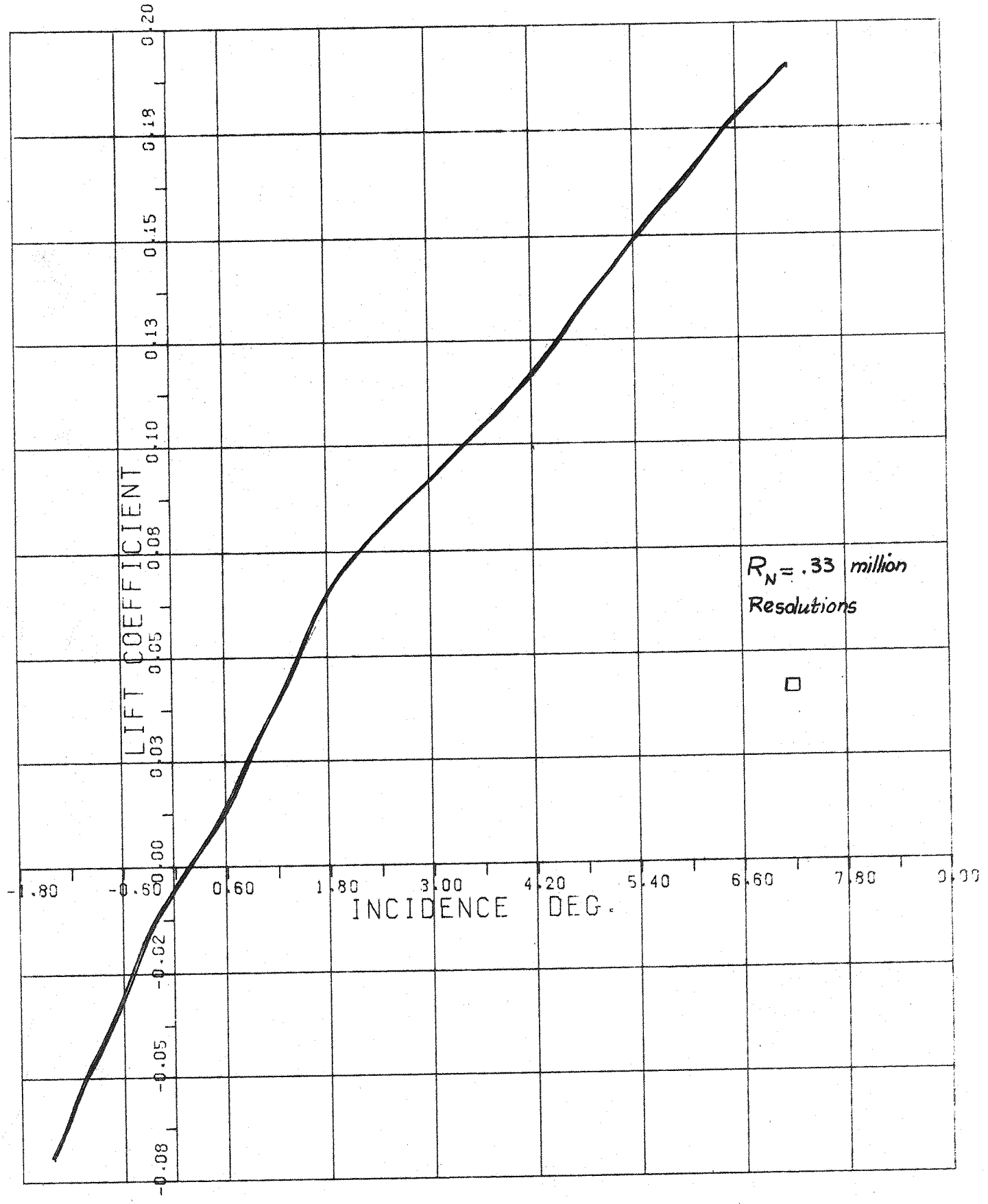

(a)

FIG. 7.28 - AERODYNAMIC LIFT VARIATION WITH INCIDENCE

PITCH RATE (DEG/SEC) = 0.125

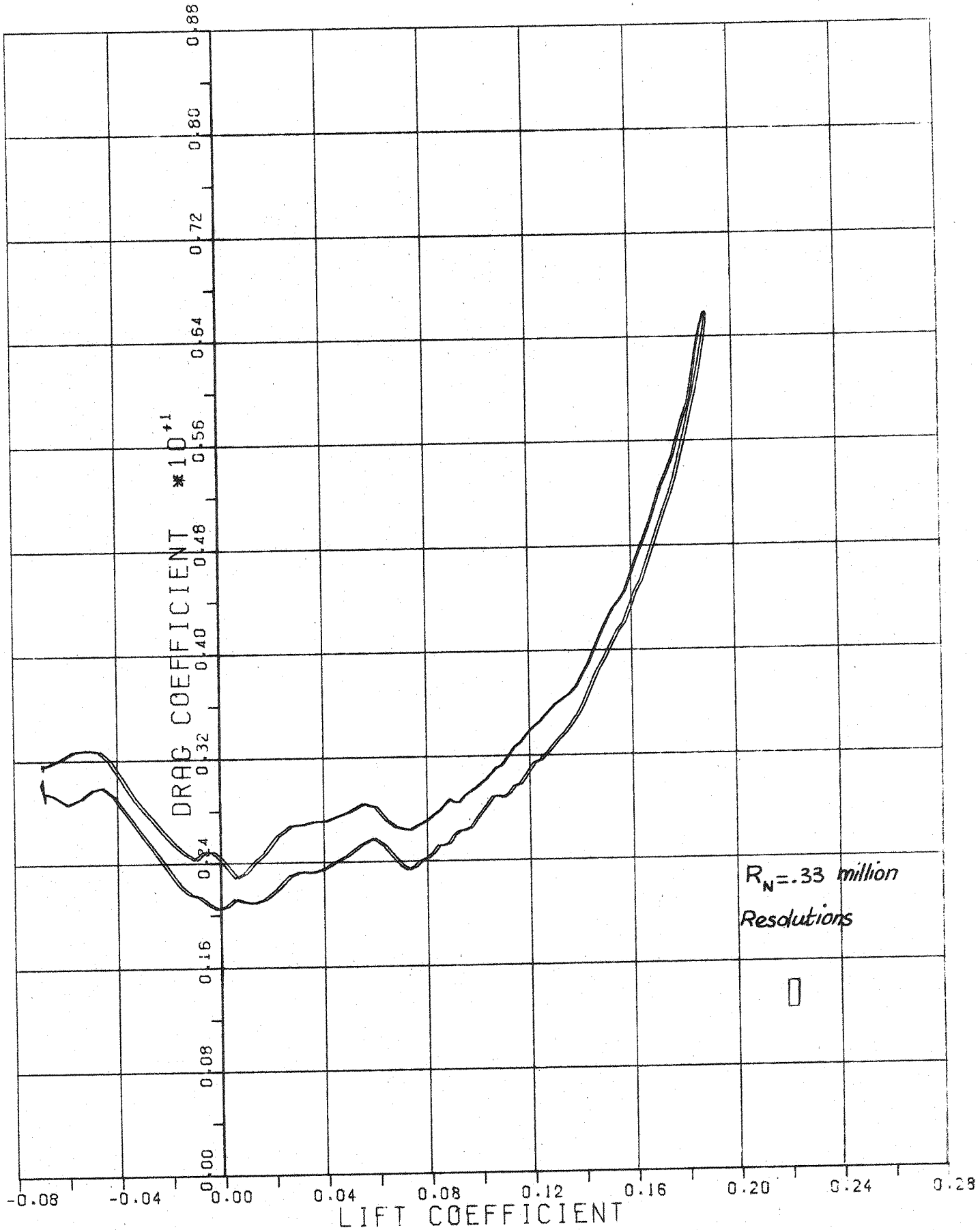

(b)

FIG.7.28-DRAG VARIATION WITH LIFT

PITCH RATE (DEG/SEC) = 0.125

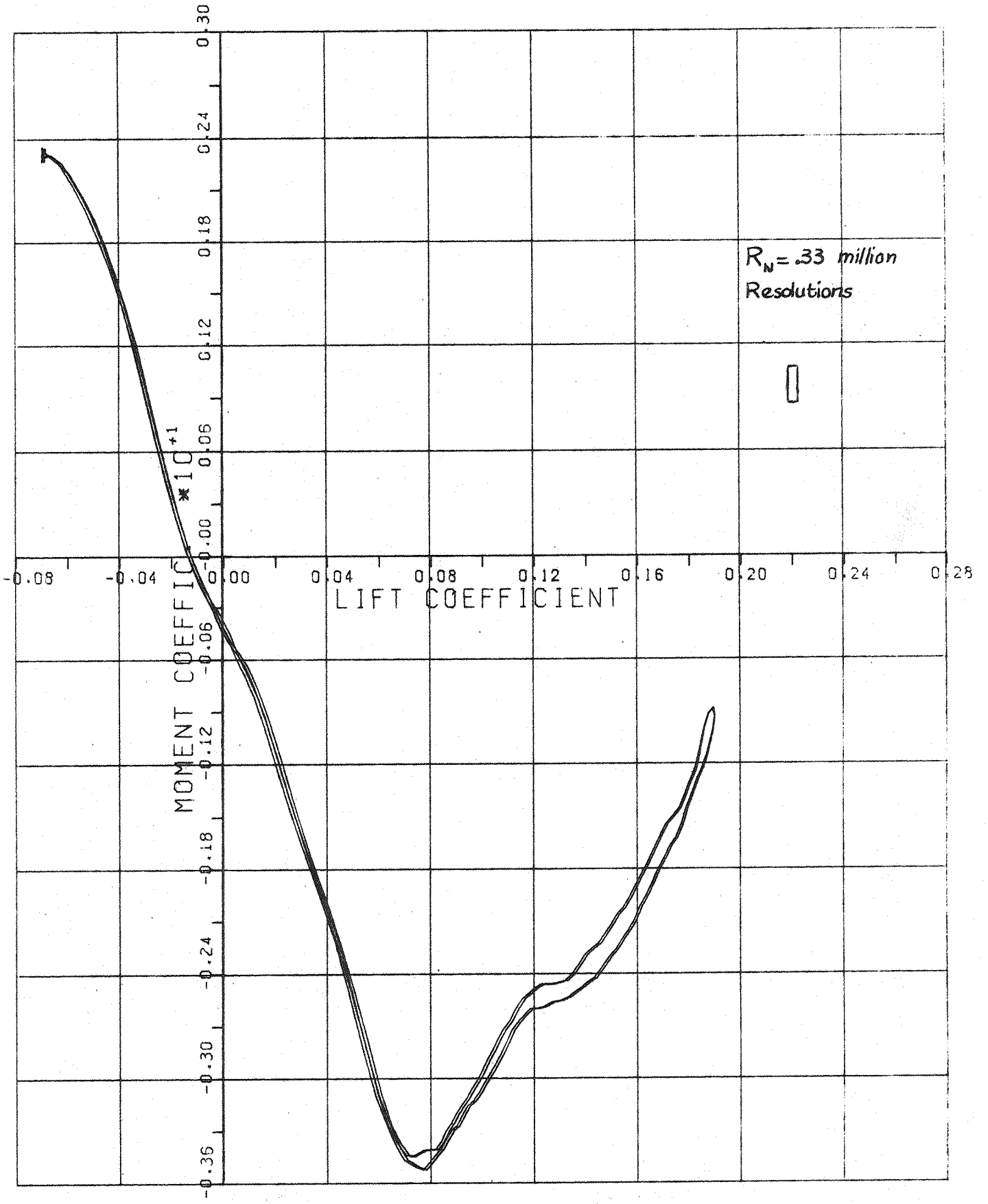

(c)

FIG. 7.28 - PITCHING MOMENT (ABOUT WING CR/2) VARIATION WITH LIFT

PITCH RATE (DEG/SEC) = 0.125

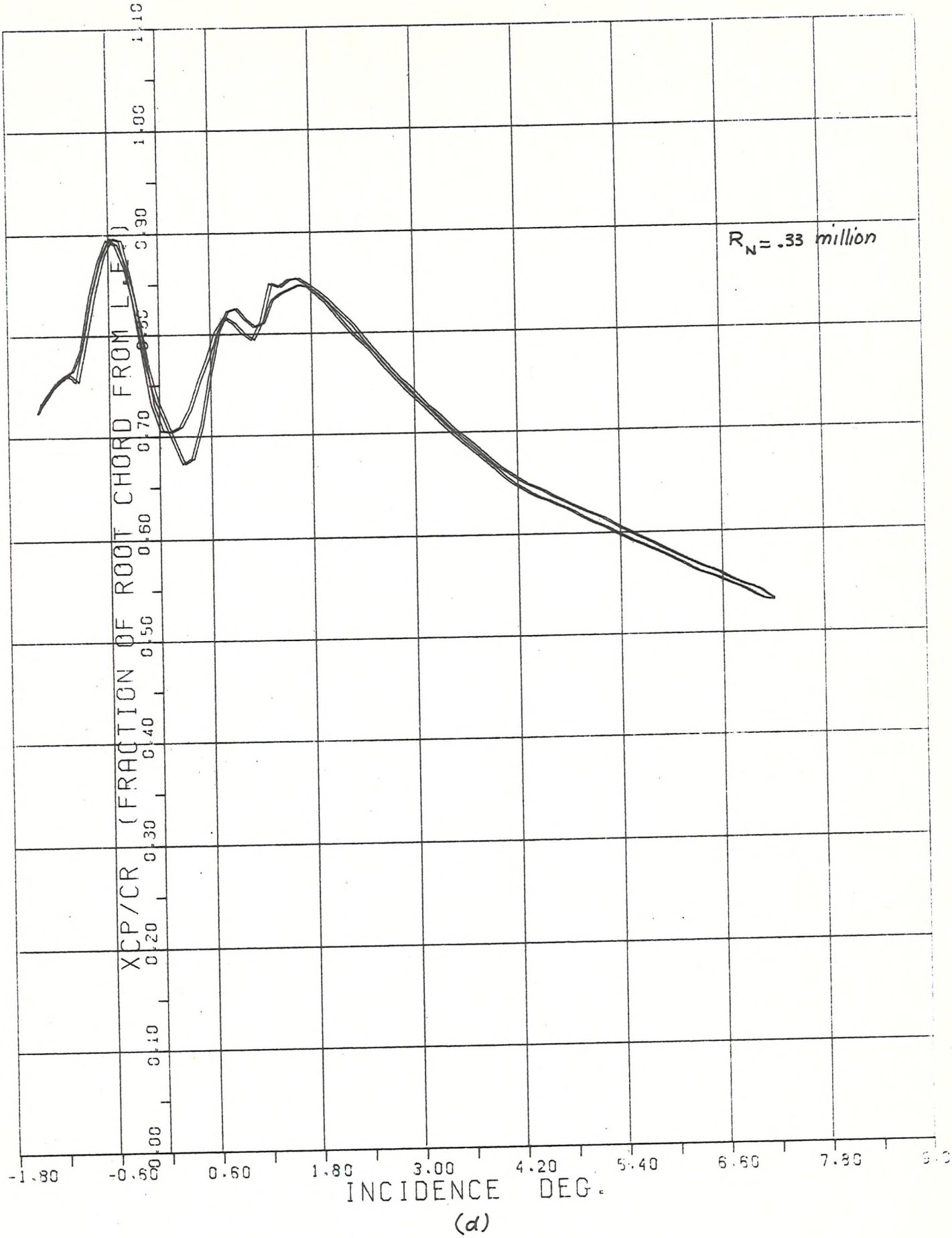

FIG. 7.28 CENTER OF PRESSURE LOCATION (% OF ROOT CHORD) BEHIND L. E. OF ROOT CHORD

PITCH RATE (DEG/SEC) = 0.125

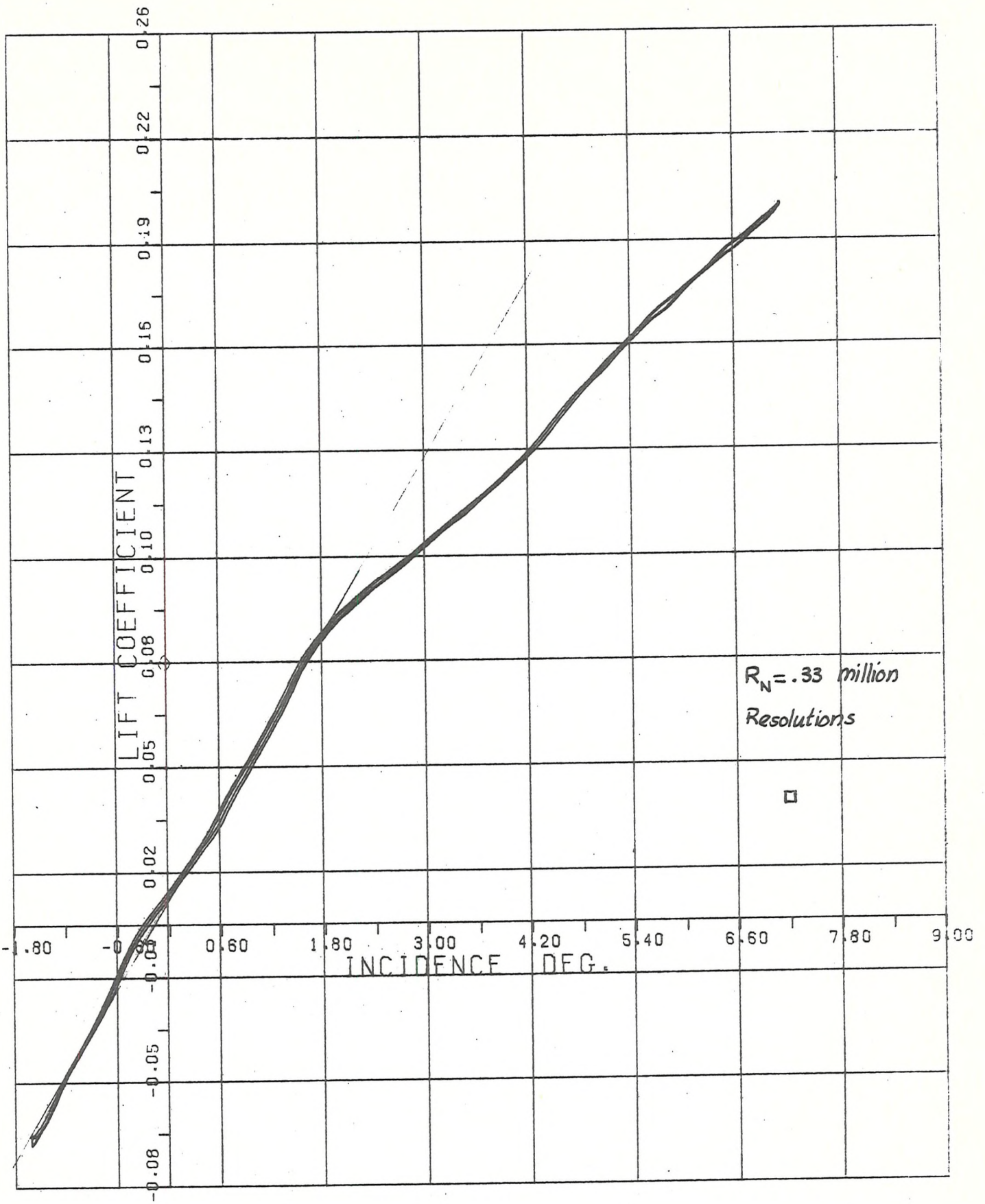

(a)

FIG.7.29-AERODYNAMIC LIFT VARIATION WITH INCIDENCE

PITCH RATE (DEG/SEC) = 0.250

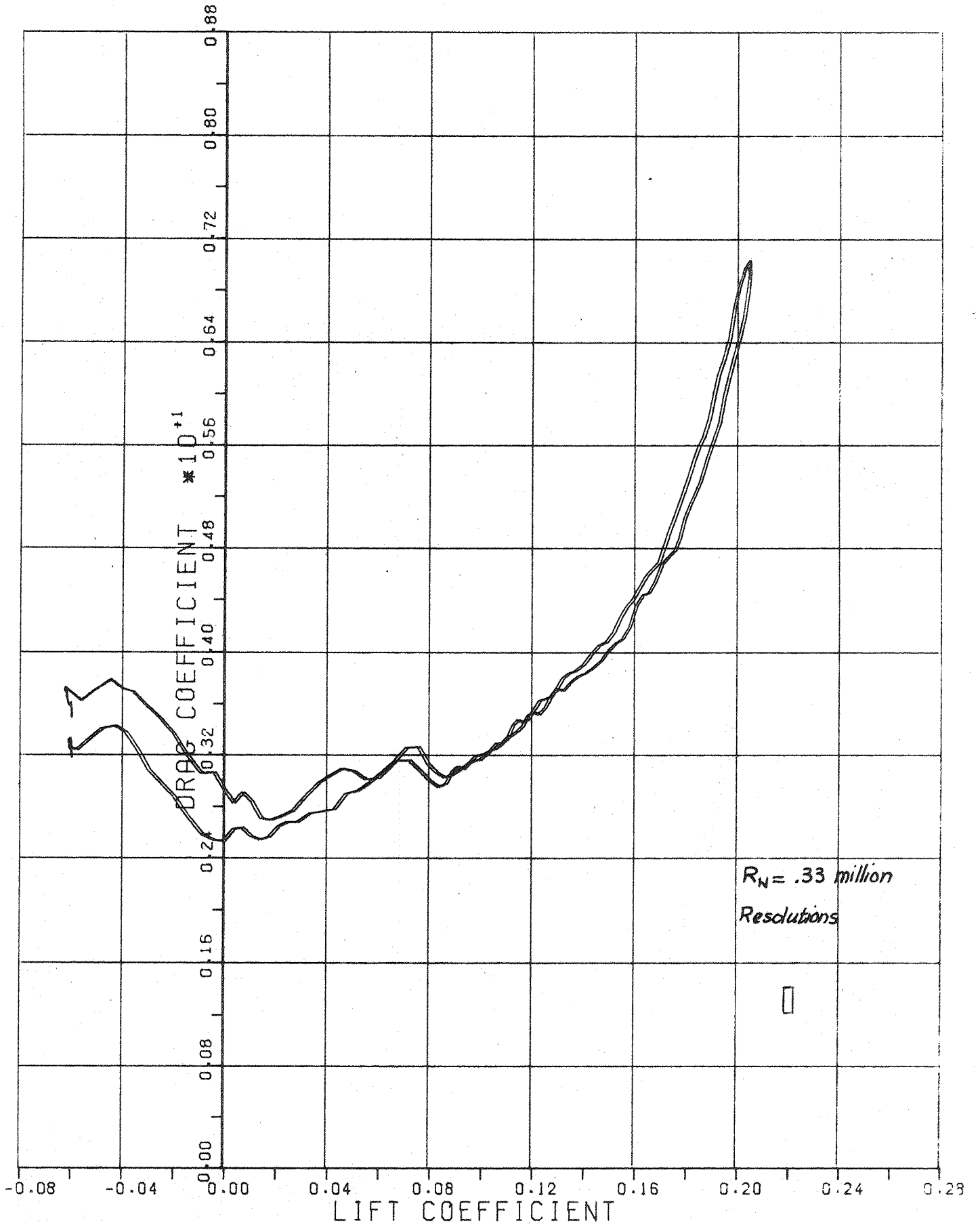

(b)

FIG. 7.29 - DRAG VARIATION WITH LIFT

PITCH RATE (DEG/SEC) = 0.250

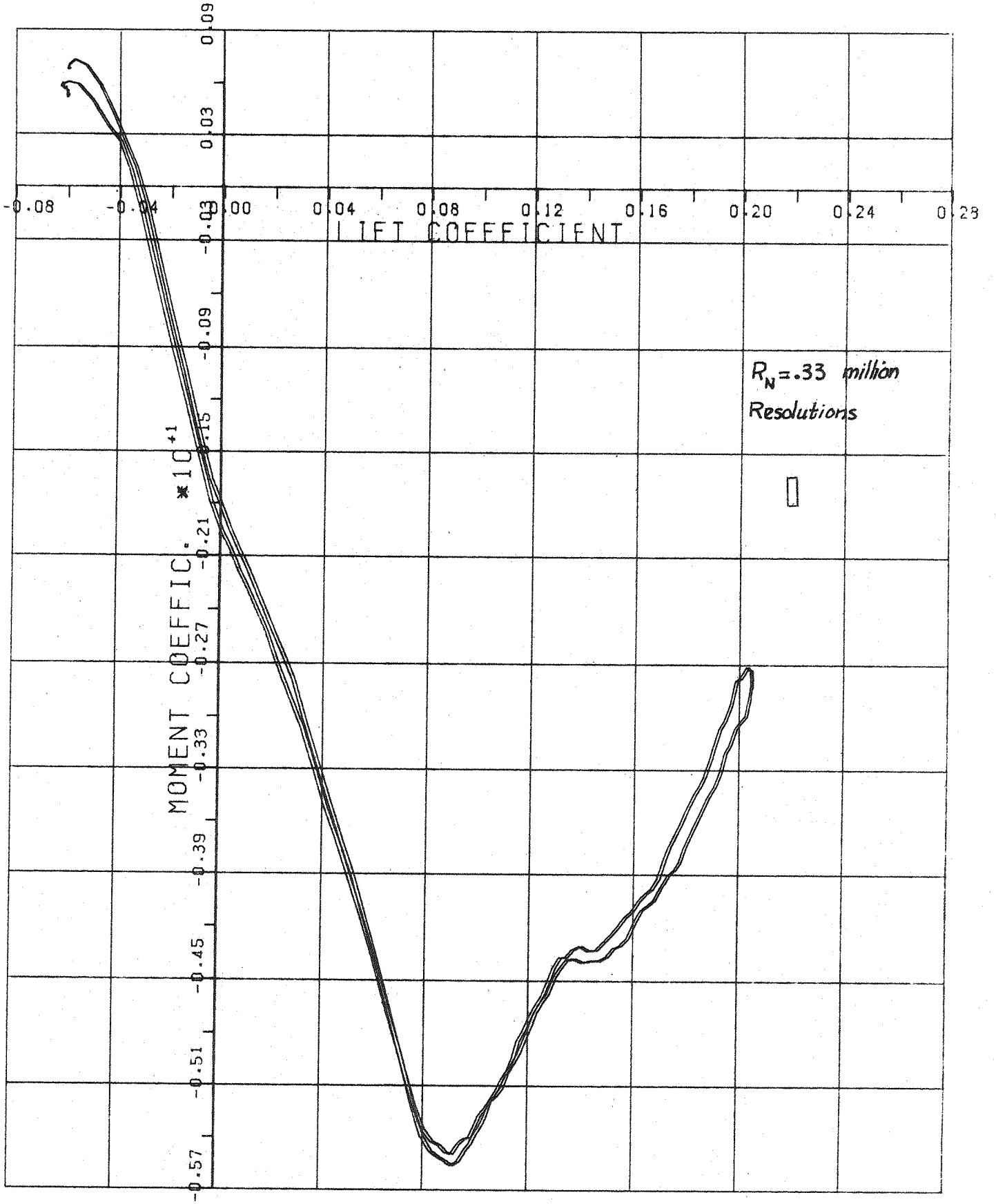

(c)

FIG 7.29 - PITCHING MOMENT (ABOUT WING CR/2) VARIATION WITH LIFT

PITCH RATE (DEG/SEC) = 0.250

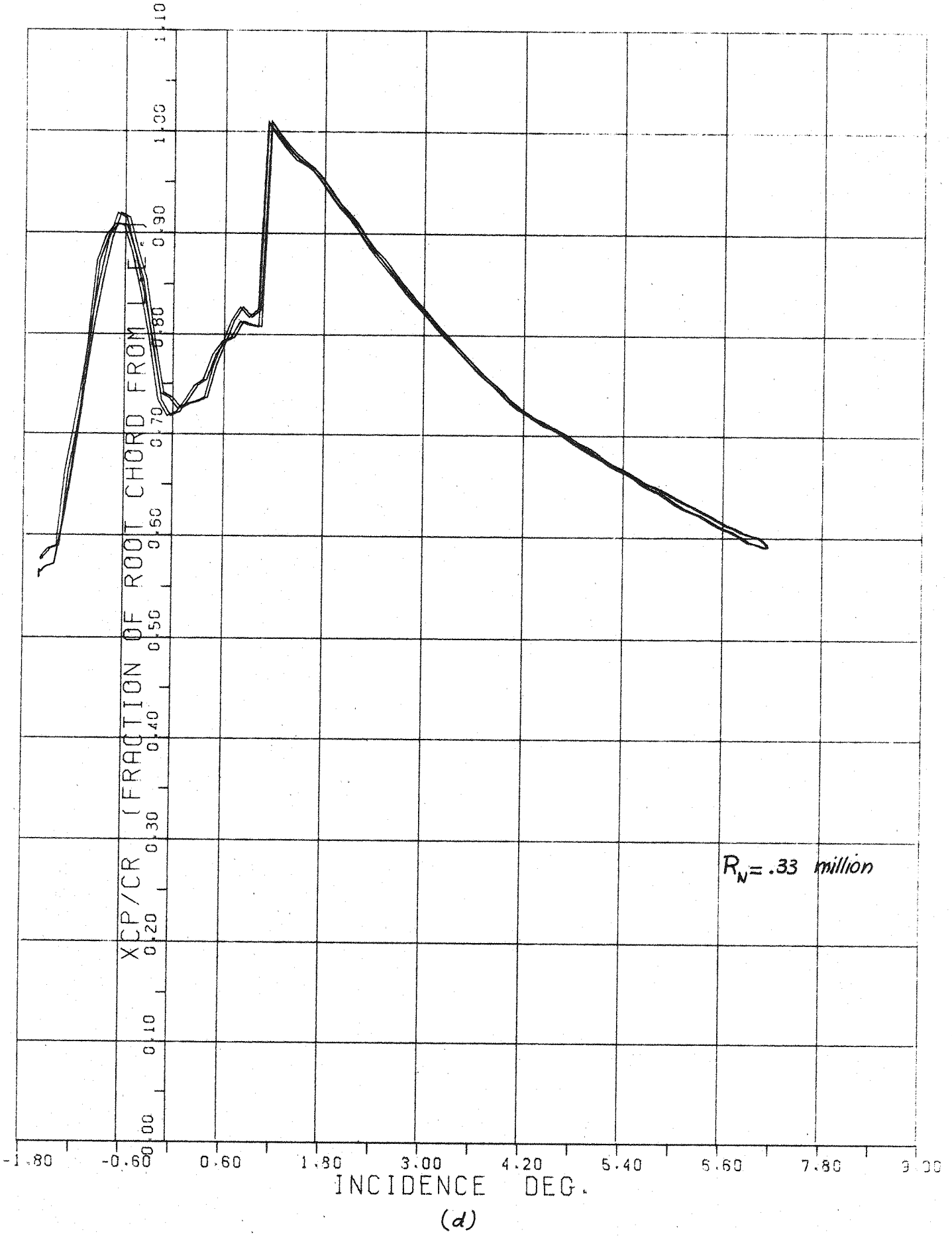

FIG 7.29 CENTER OF PRESSURE LOCATION (% OF ROOT CHORD) BEHIND L. E. OF ROOT CHORD

PITCH RATE (DEG/SEC) = 0.250

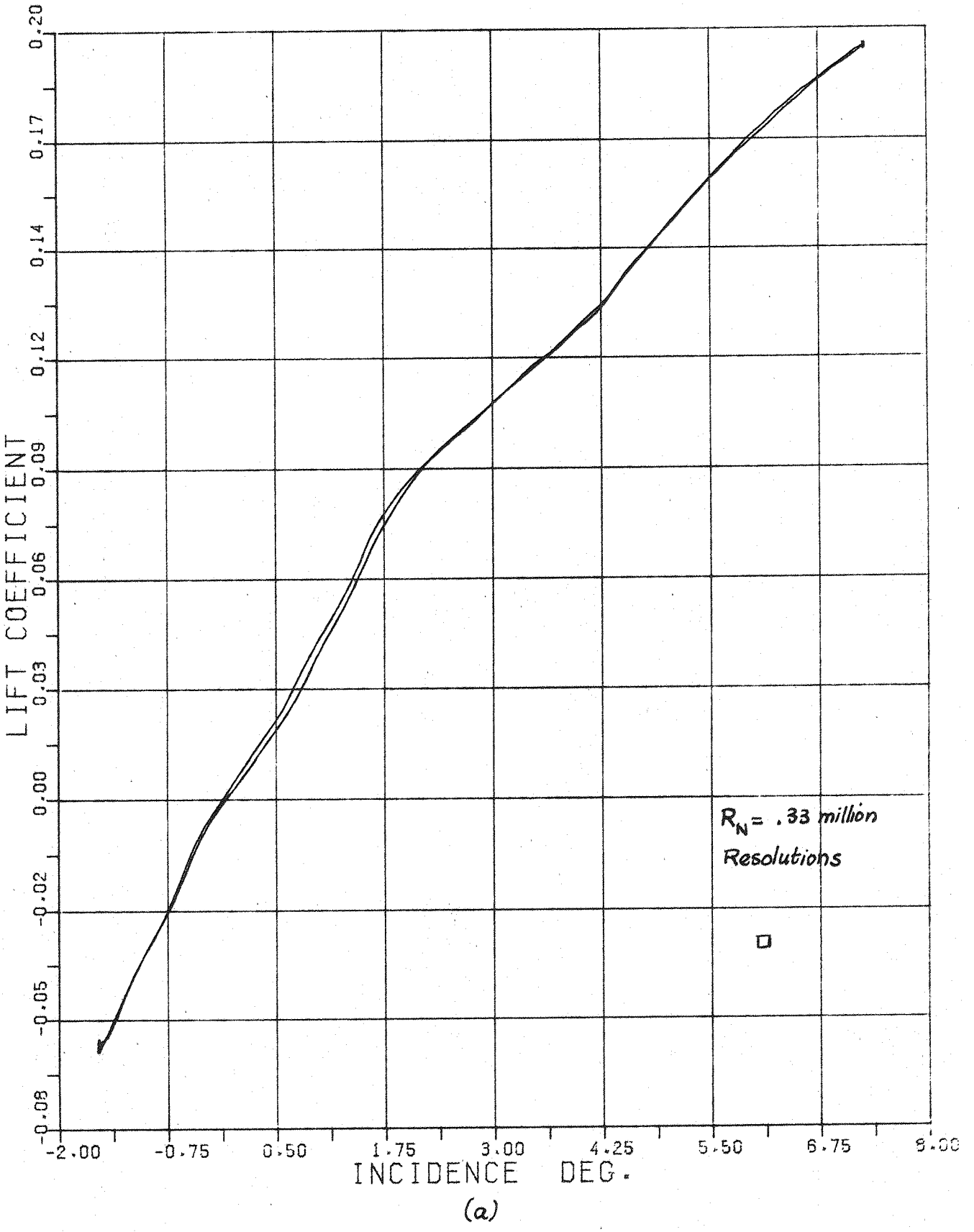

(a)

FIG 7.30 - AERODYNAMIC LIFT VARIATION WITH INCIDENCE

PITCH RATE (DEG/SEC) = 0.500

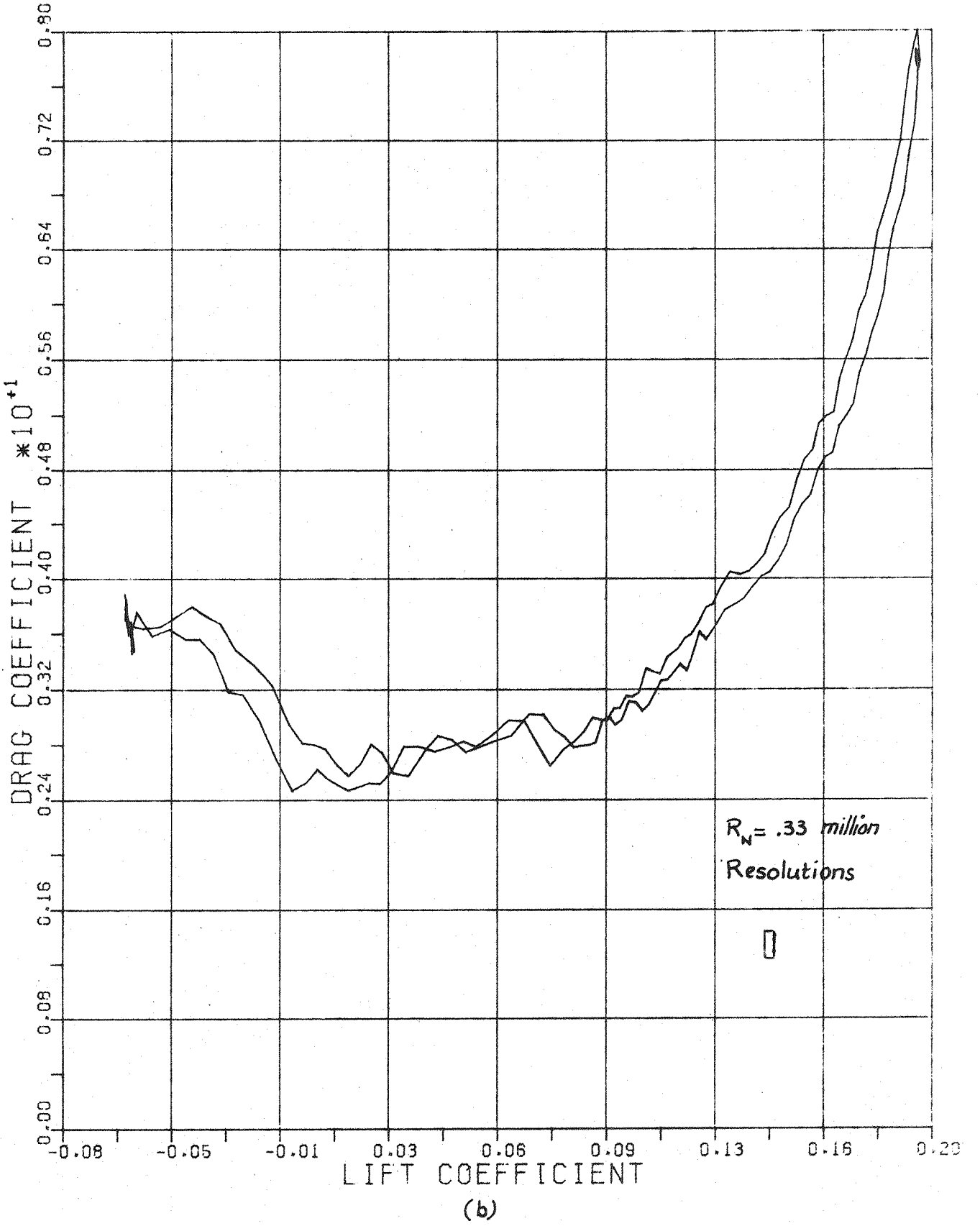

(b)

FIG .7.30 - DRAG VARIATION WITH LIFT

PITCH RATE (DEG/SEC) = 0.500

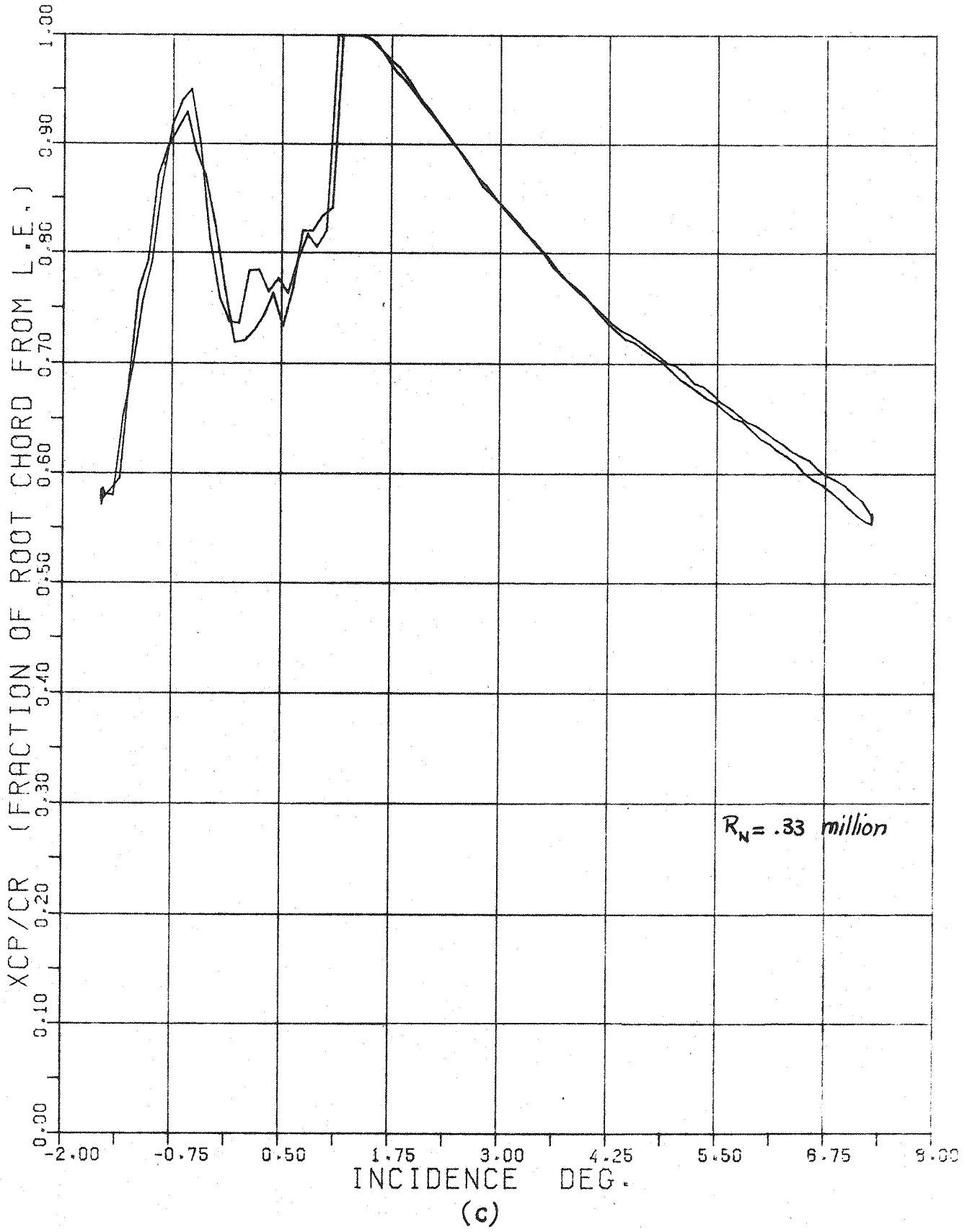

FIG 730-CENTER OF PRESSURE LOCATION (% OF ROOT CHORD) BEHIND L. E. OF ROOT CHORD

PITCH RATE (DEG/SEC) = 0.500

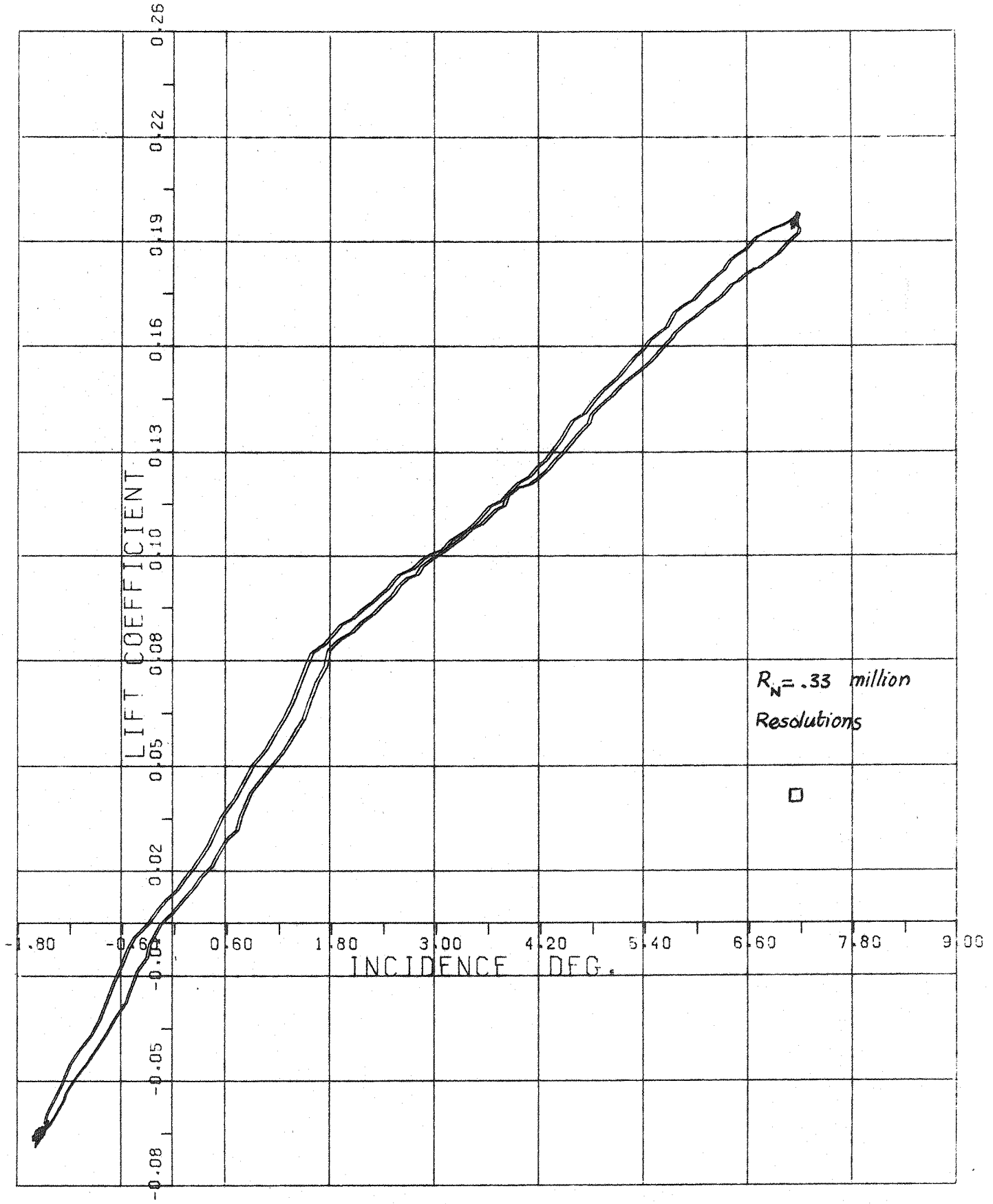

(a)

FIG.7.31-AERODYNAMIC LIFT VARIATION WITH INCIDENCE

PITCH RATE (DEG/SEC) = 2.500

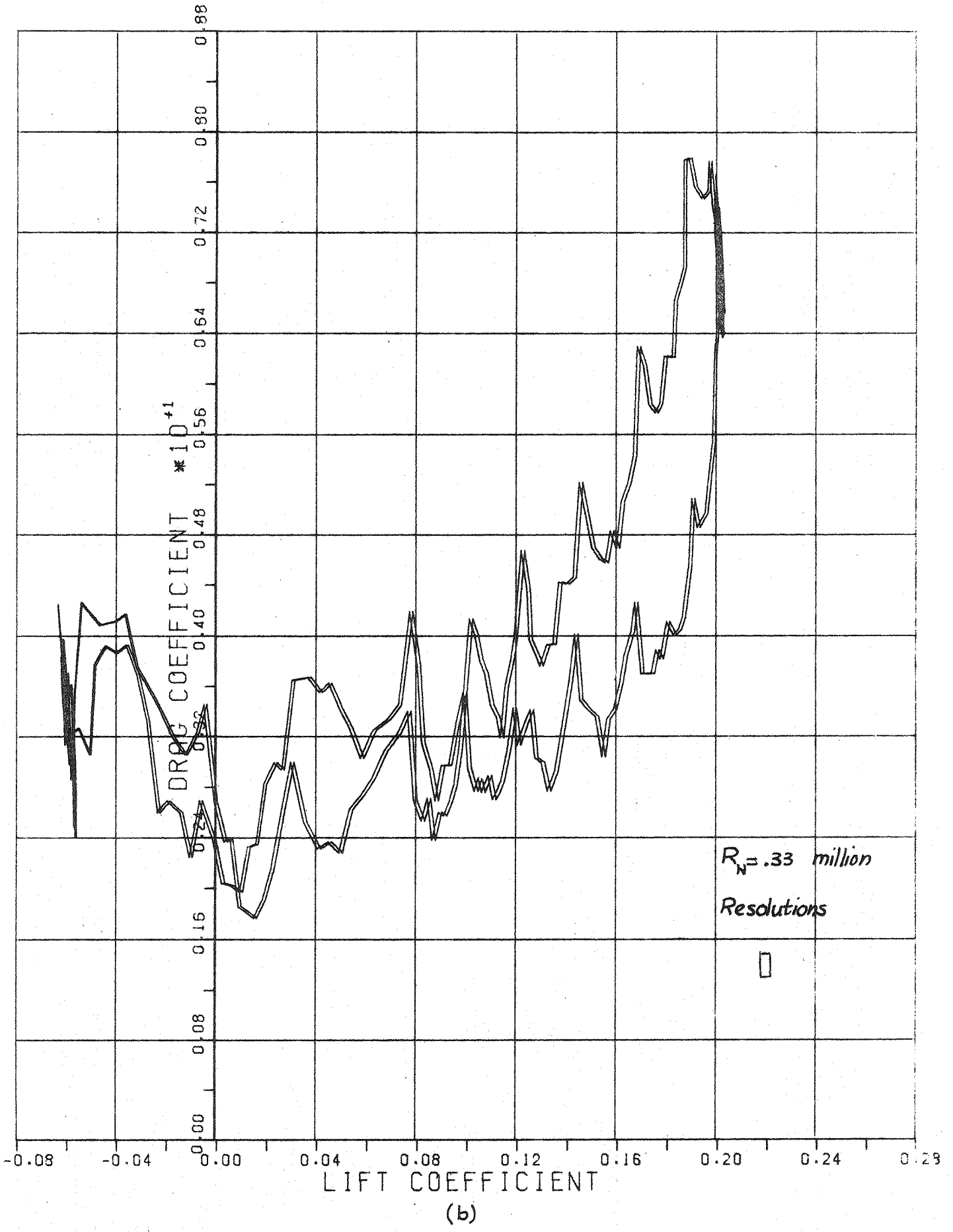

(b)

FIG.7.31 - DRAG VARIATION WITH LIFT

PITCH RATE (DEG/SEC) = 2.500

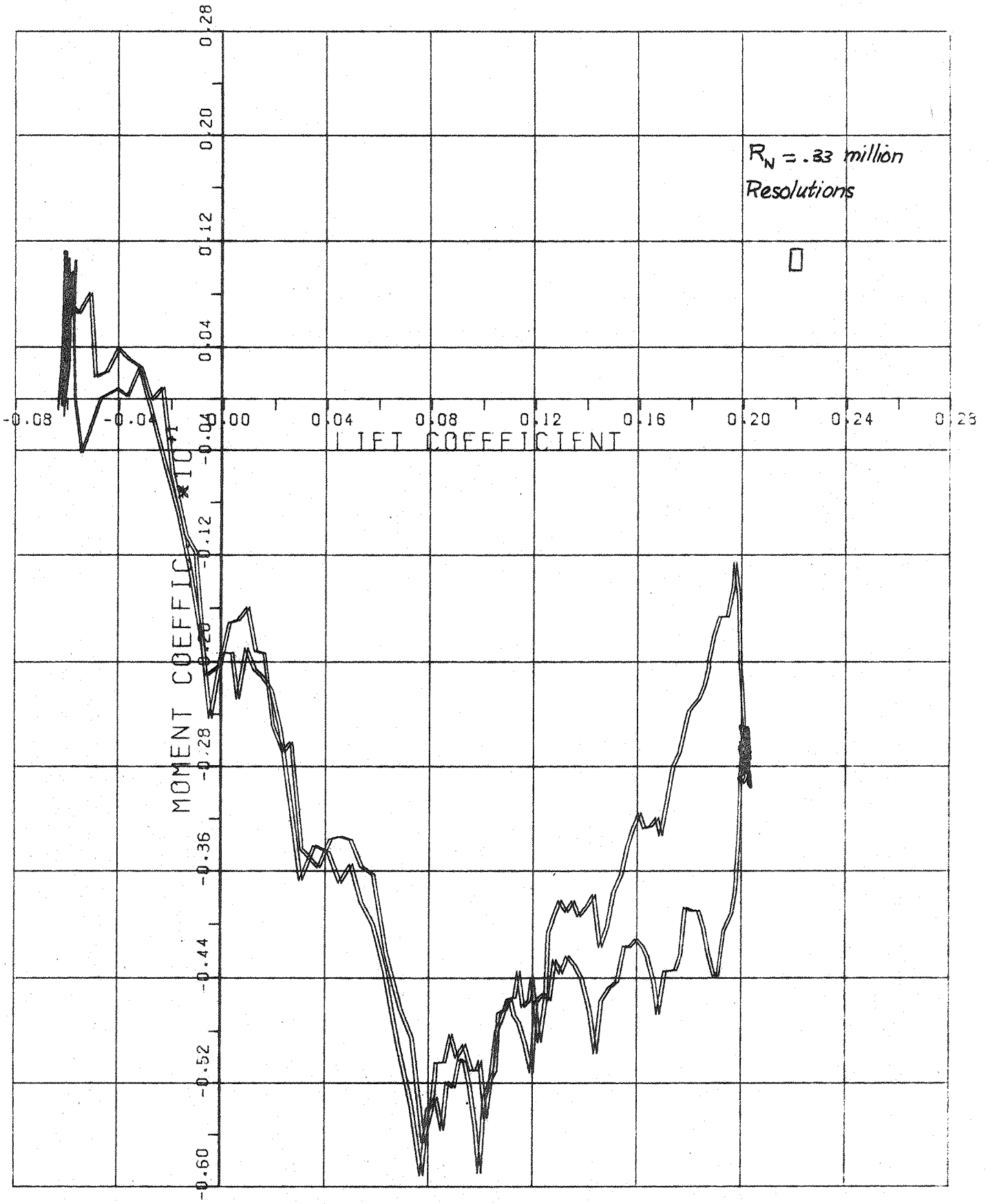

(c)

FIG 7.31-PITCHING MOMENT (ABOUT WING CR/2) VARIATION WITH LIFT

PITCH RATE (DEG/SEC) = 2.500

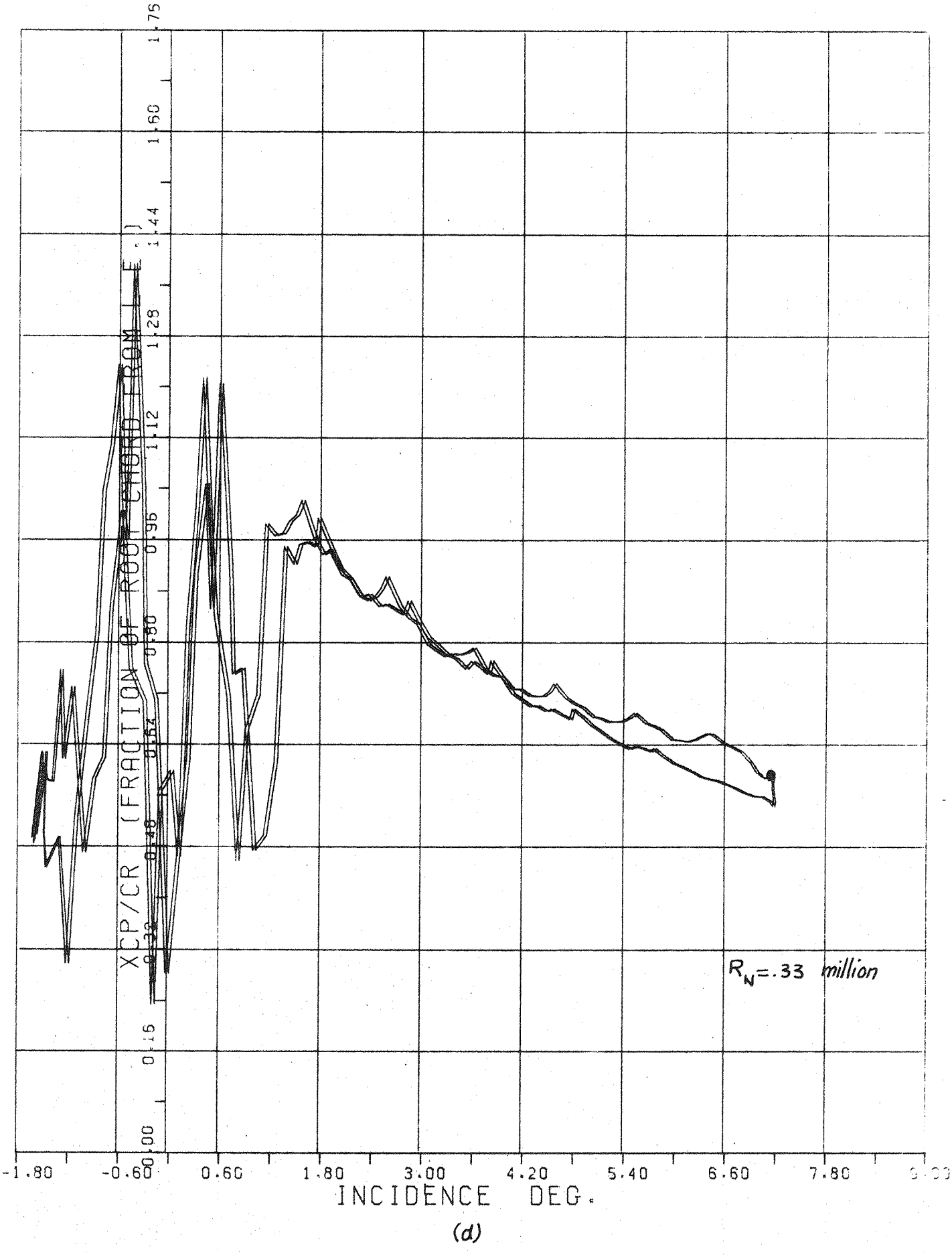

(d)

FIG. 7.31 - CENTER OF PRESSURE LOCATION (% OF ROOT CHORD) BEHIND L. E. OF ROOT CHORD

PITCH RATE (DEG/SEC) = 2.500

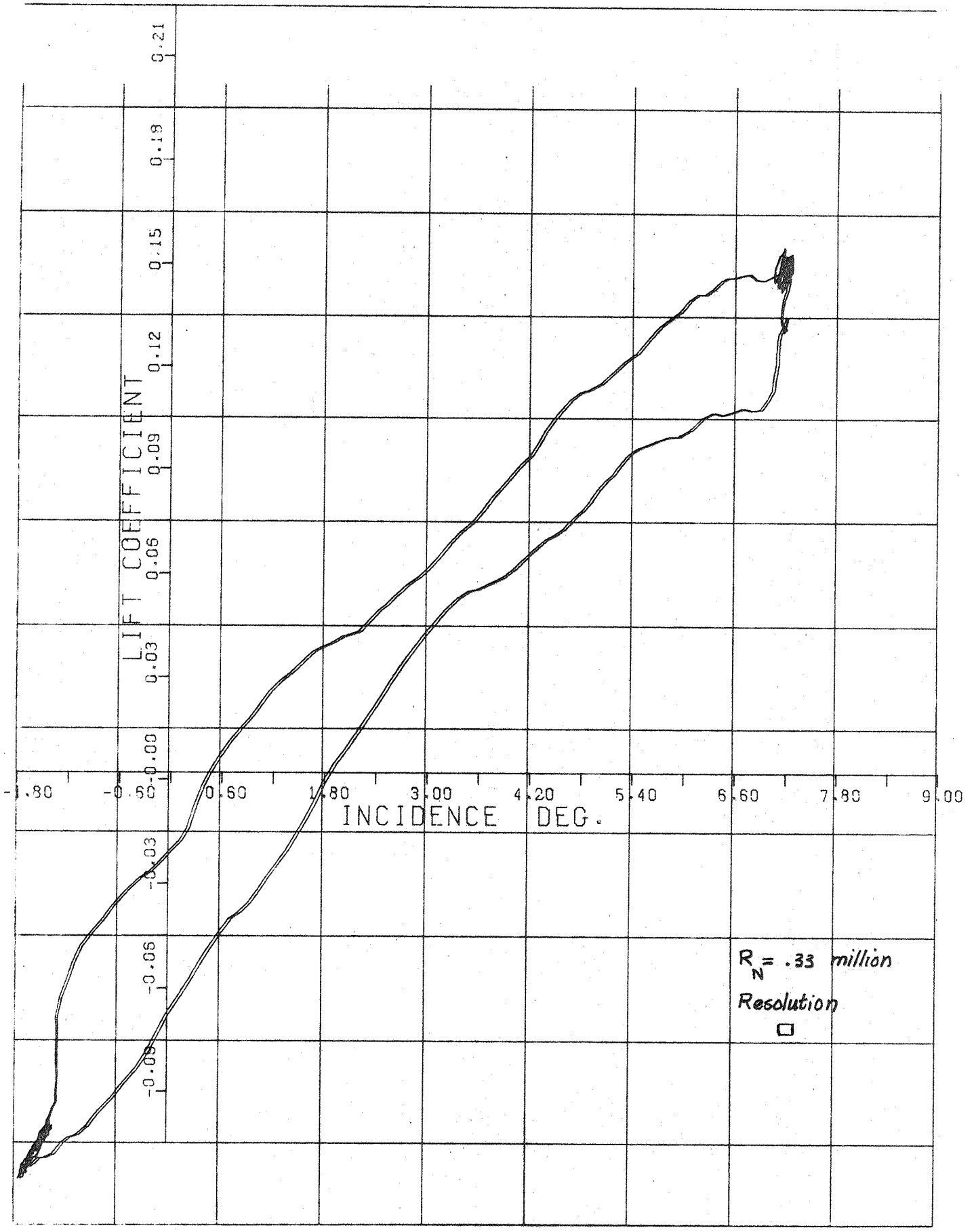

(a)

FIG. 7.32 - AERODYNAMIC LIFT VARIATION WITH INCIDENCE

PITCH RATE (DEG/SEC) = 20.000

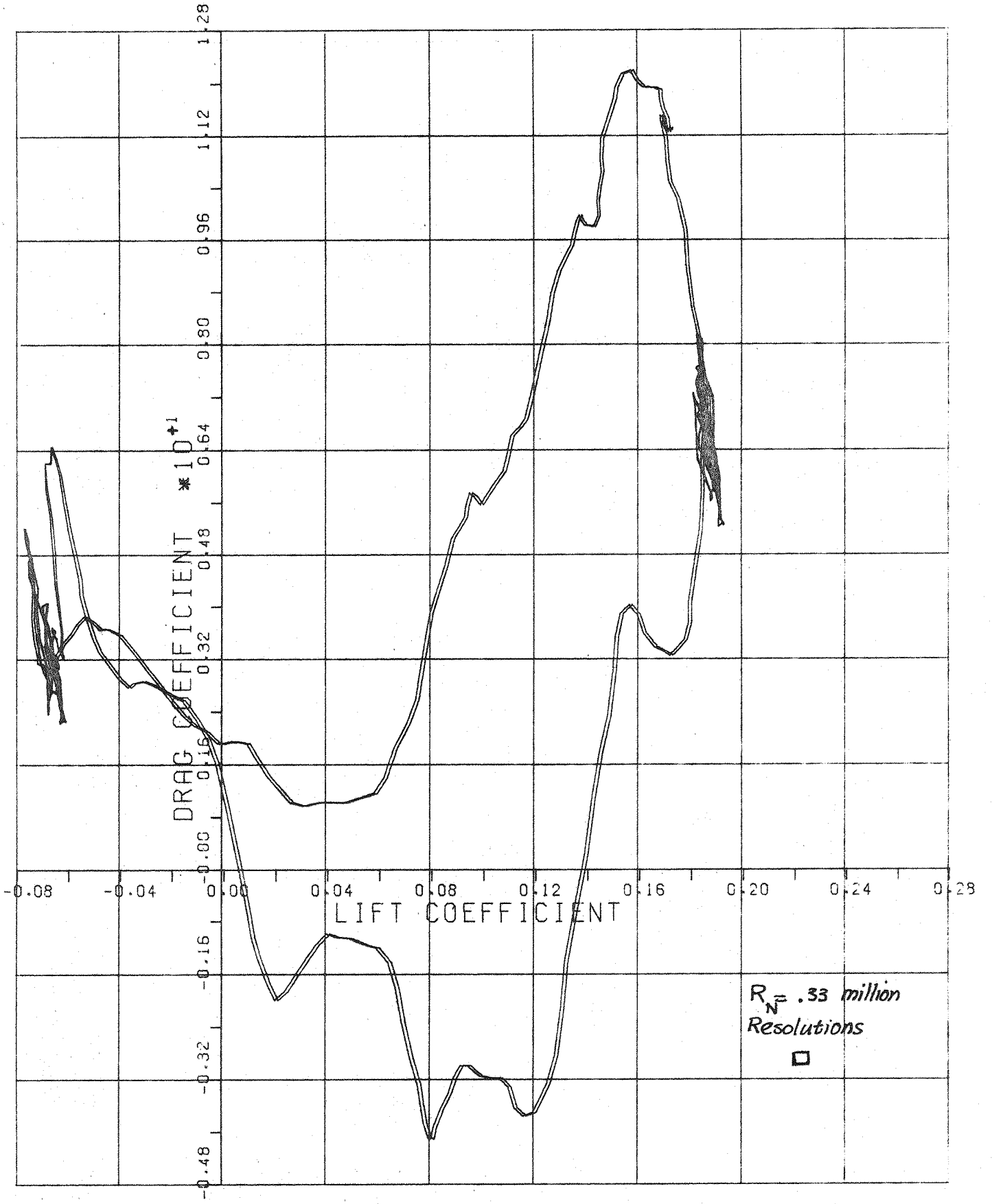

(b)

FIG 7.32 - DRAG VARIATION WITH LIFT

PITCH RATE (DEG/SEC) = 20.000

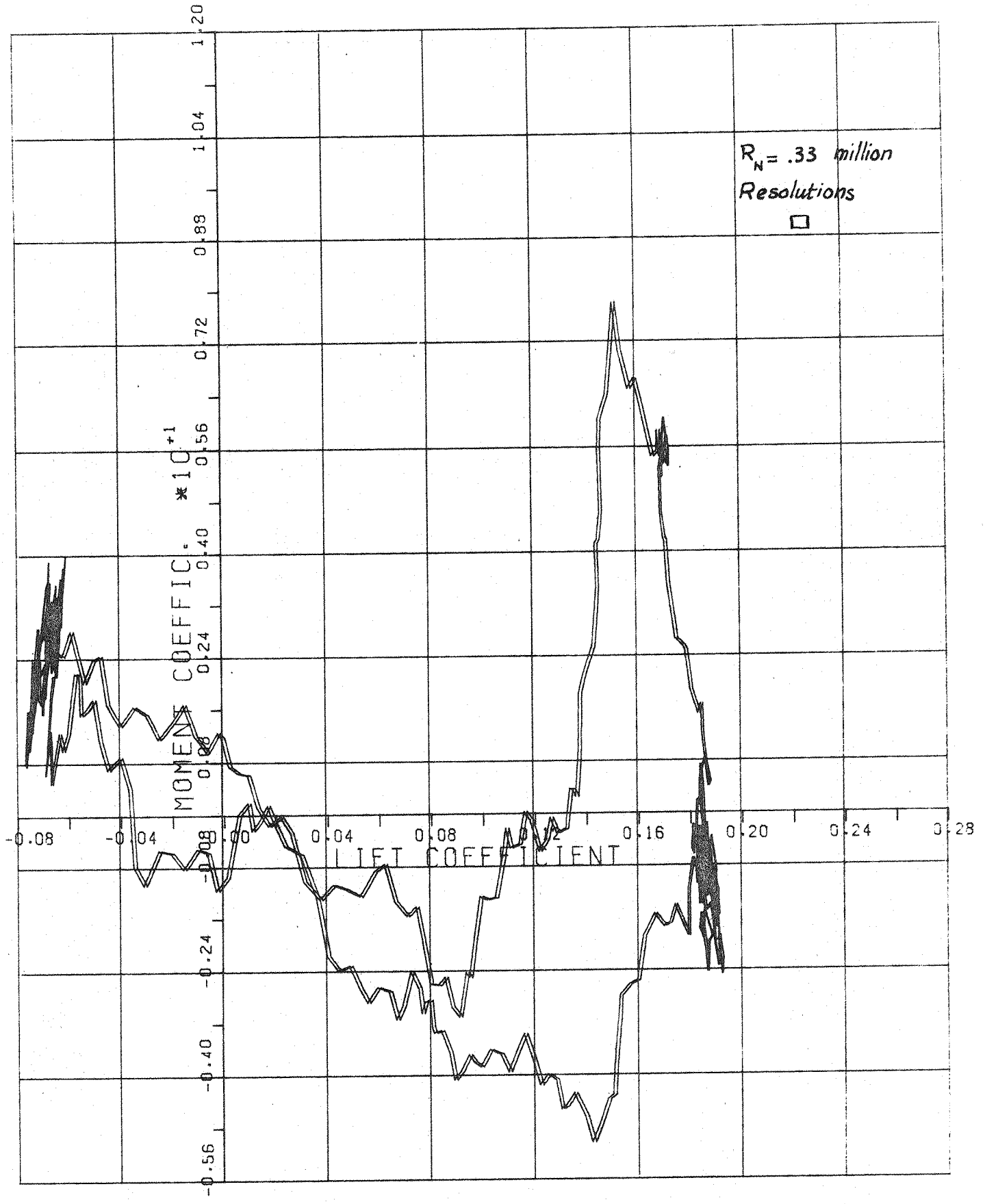

(c)

FIG 7.32-PITCHING MOMENT (ABOUT WING CR/2) VARIATION WITH LIFT

PITCH RATE (DEG/SEC) = 20.000

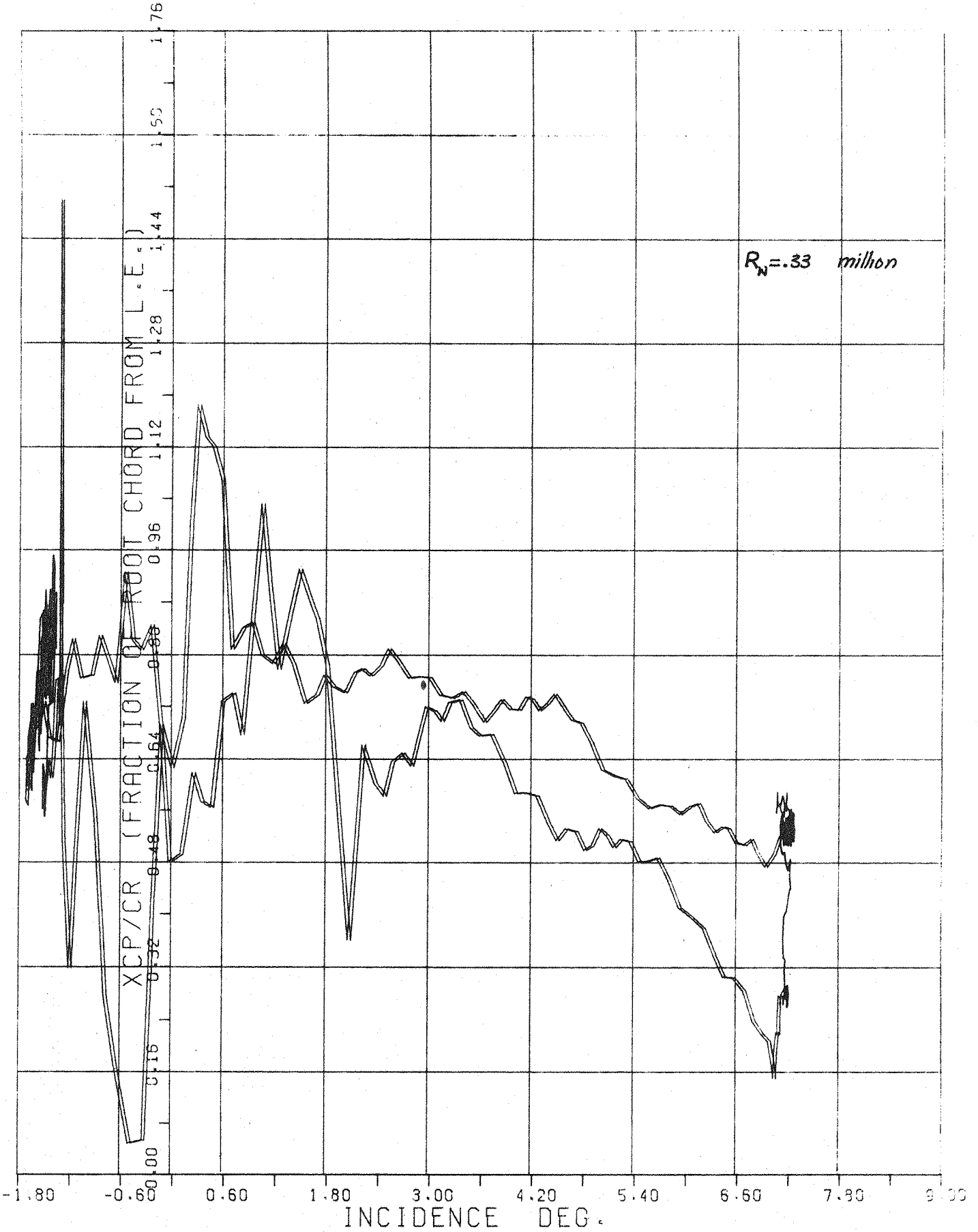

(d)

FIG 7.32 CENTER OF PRESSURE LOCATION (% OF ROOT CHORD) BEHIND L. E. OF ROOT CHORD

PITCH RATE (DEG/SEC) = 20.000

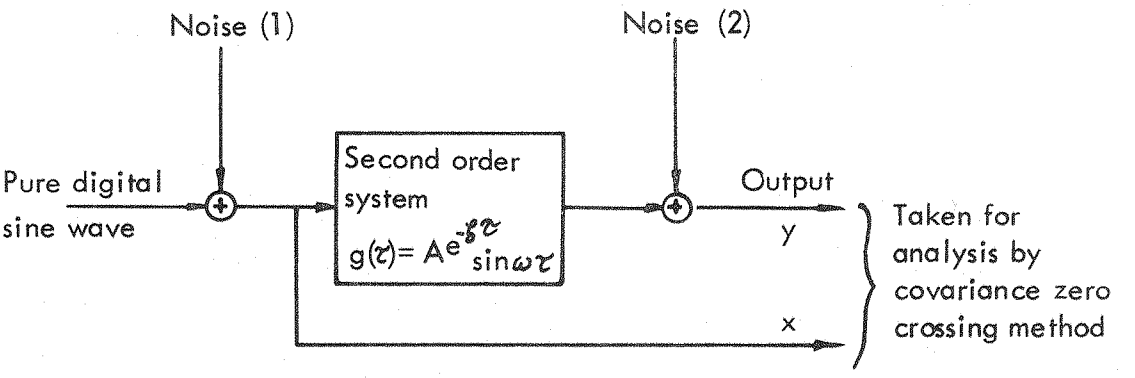

FIG. 7.33. DIGITAL SIMULATION OF NOISE EFFECT ON MEASURED PARAMETERS OF A 2nd ORDER SYSTEM.

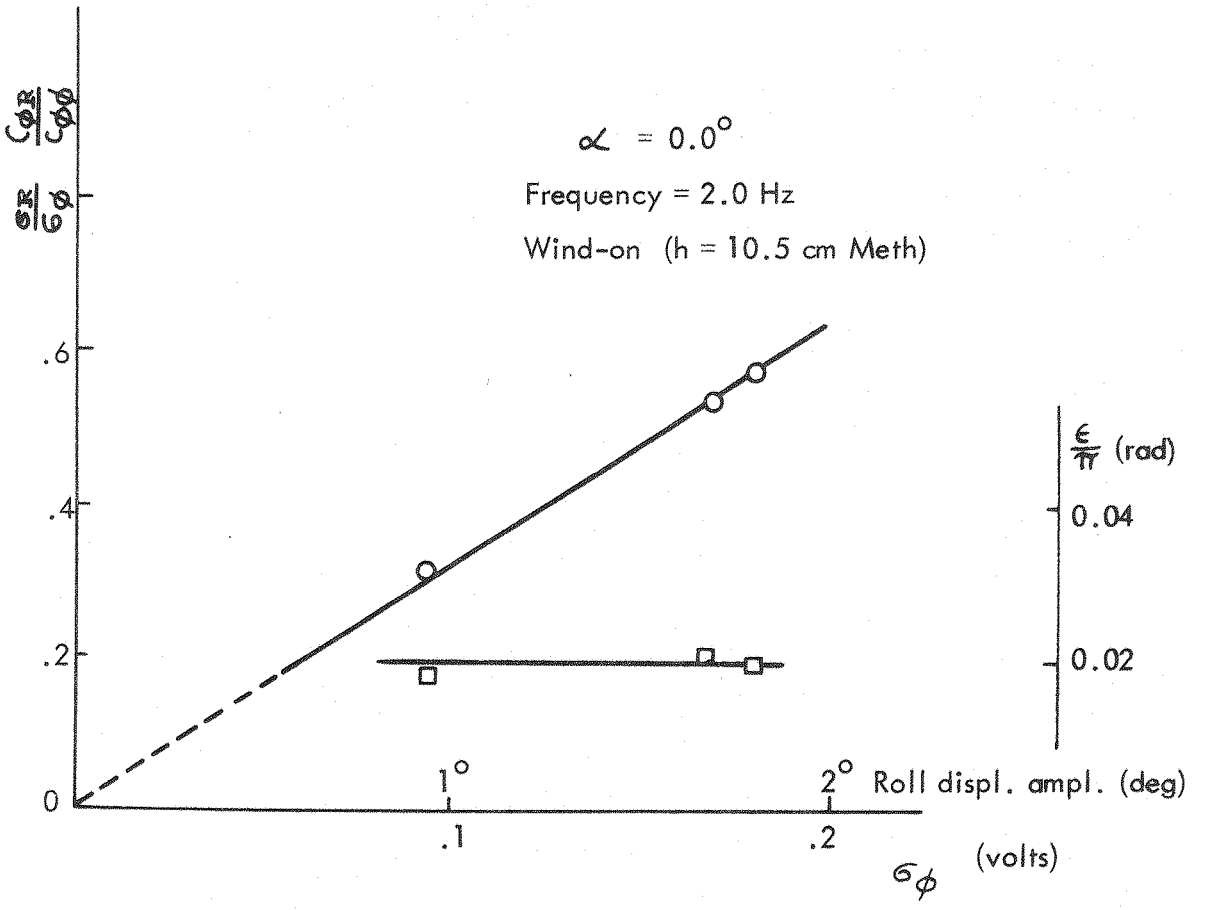

FIG. 7.34. LINEARITY OF THE OSCILLATION AMPLITUDE.

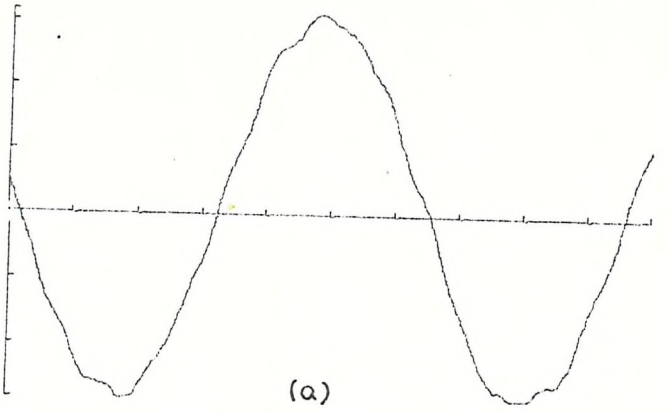

(a)

(b)

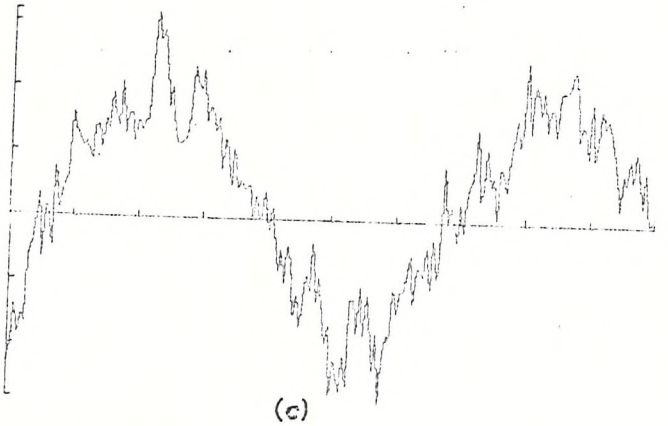

(c)

FIG. 7.35 TYPICAL ROLL OSCILLATIONS
a) Displacement signal
b) Current signal + heavy noise
c) " " + noise + distortion

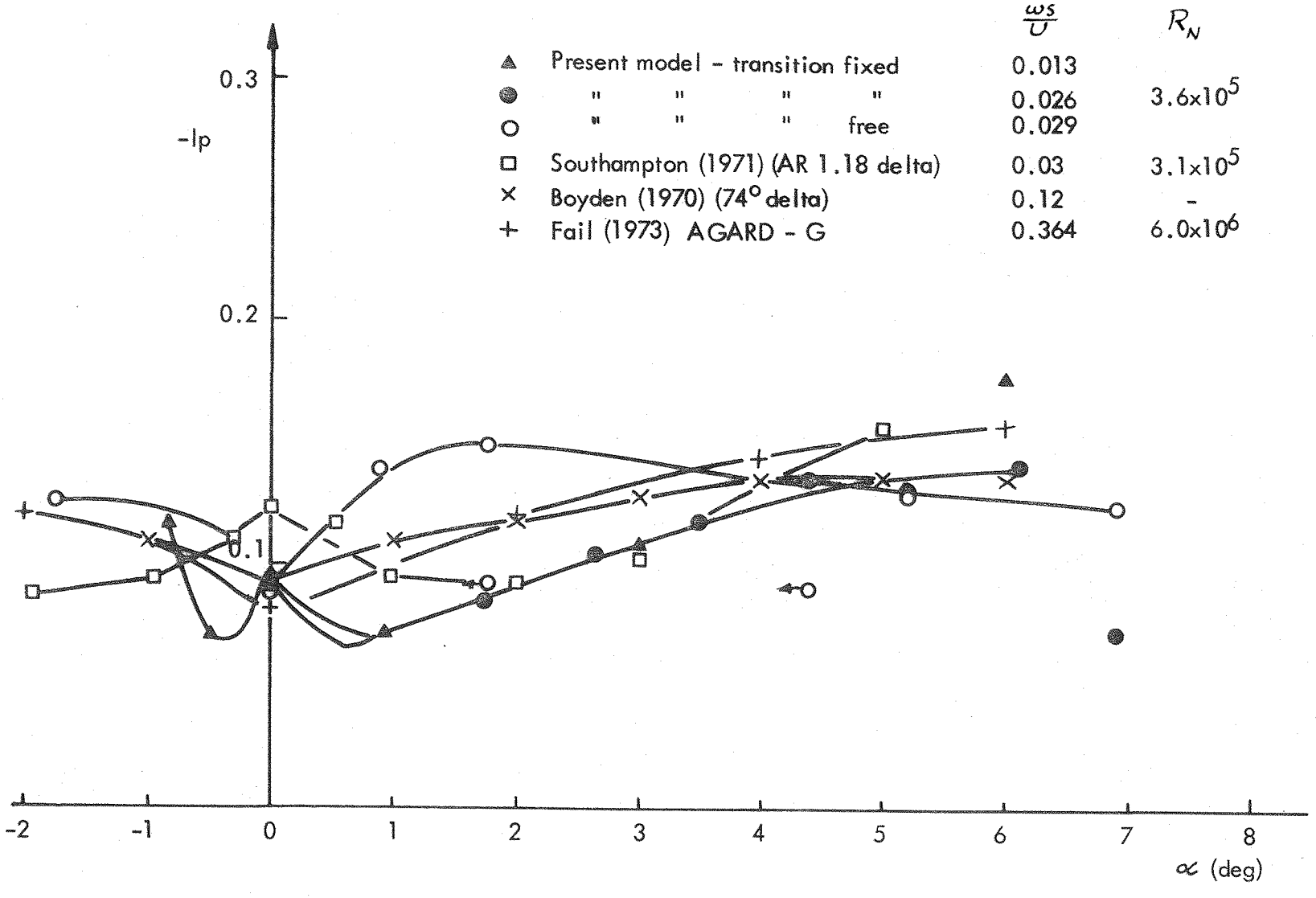

FIG. 7.36. ROLL DAMPING DERIATIVE MEASURED AT CONSTANT INCIDENCE.

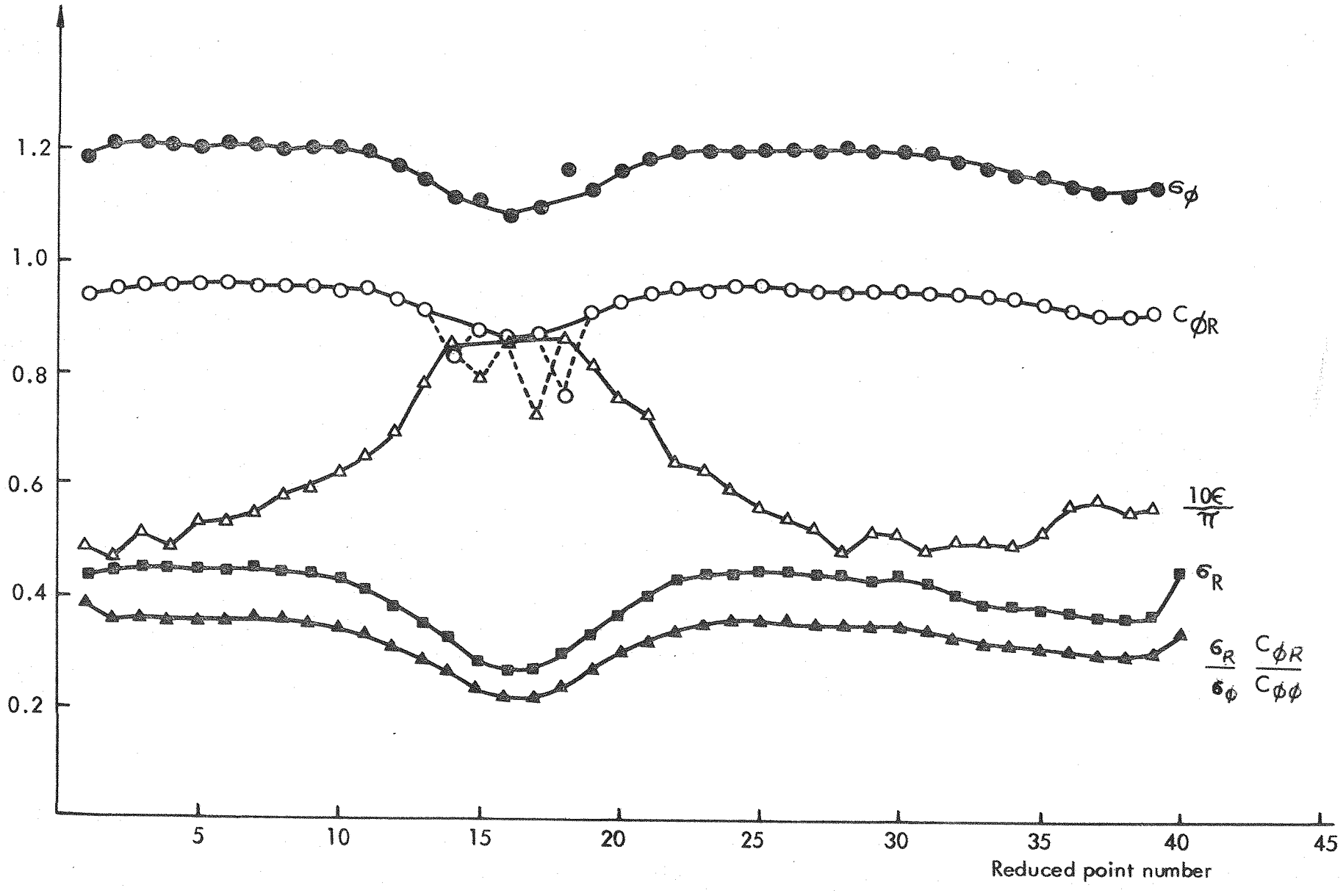

FIG. 7.37. INTERMEDIATE RESULTS FOR THE COMBINED ROLL FORCED OSCILLATION AND RAMPED INCIDENCE.

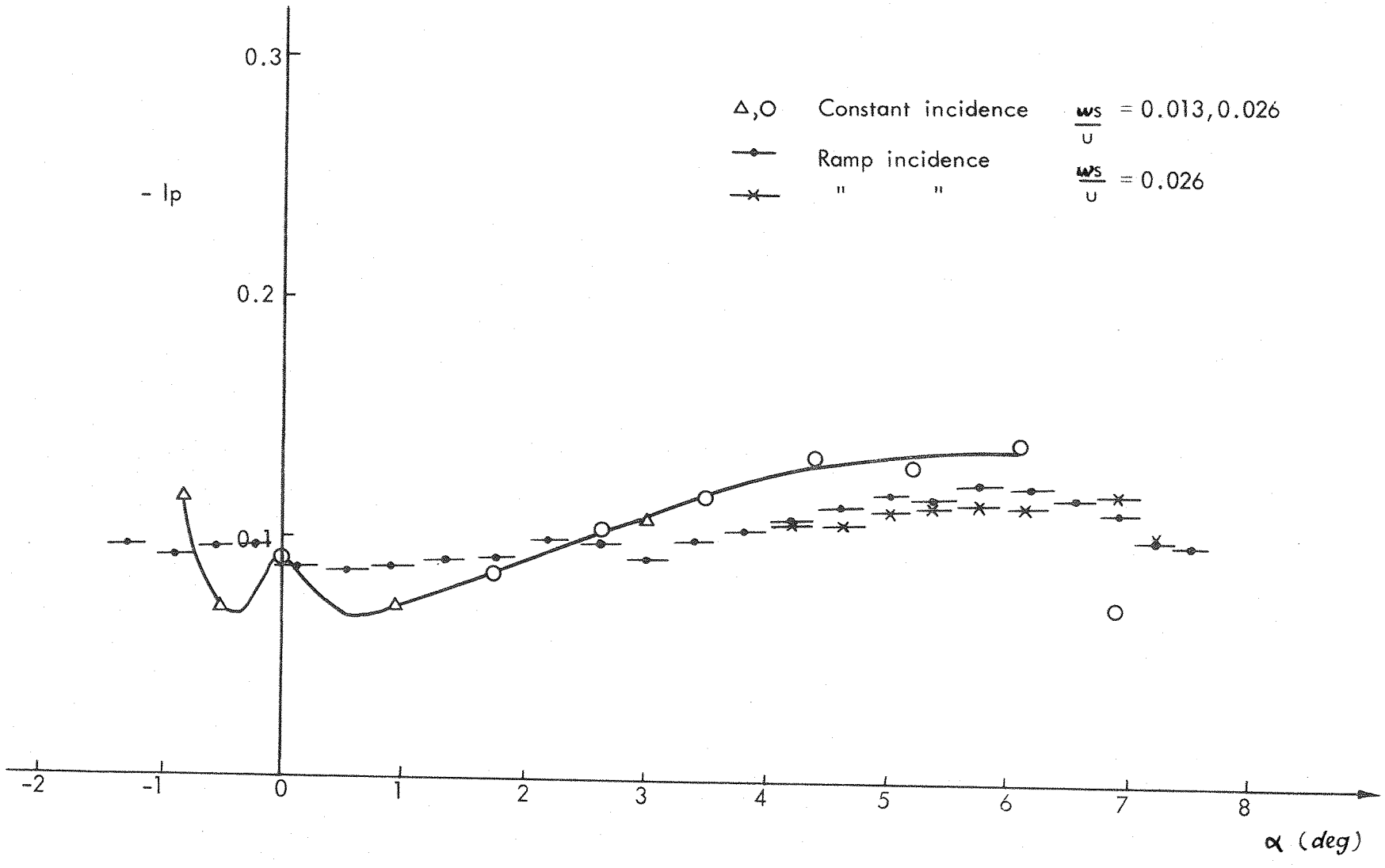

FIG. 7.38. ROLL DAMPING DERIVATIVE COMPARISON OF CONSTANT INCIDENCE WITH RAMPED INCIDENCE MEASUREMENT.

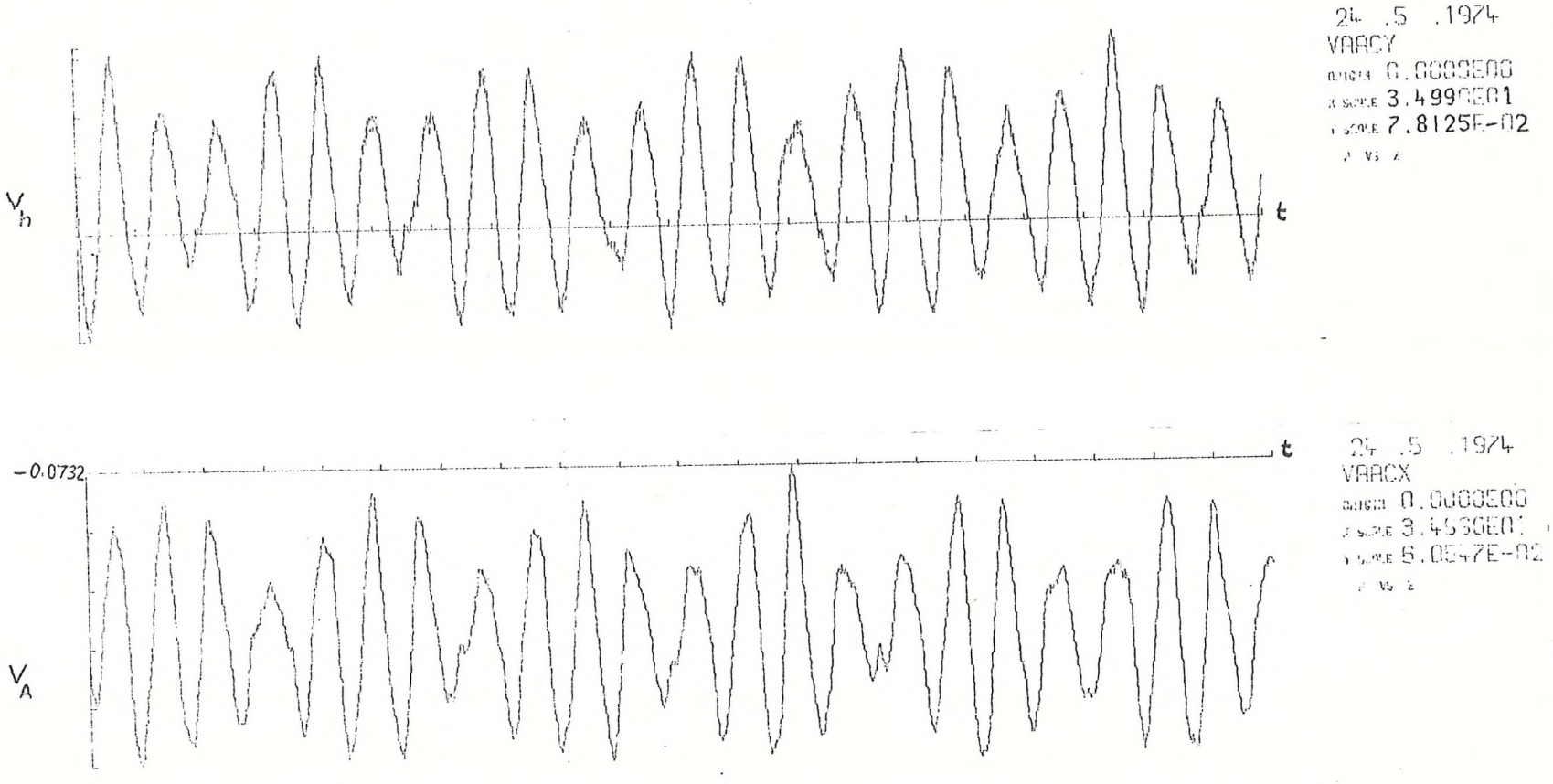

FIG. 7.39 COMBINED PITCH & HEAVE OSCILLATION SIGNALS

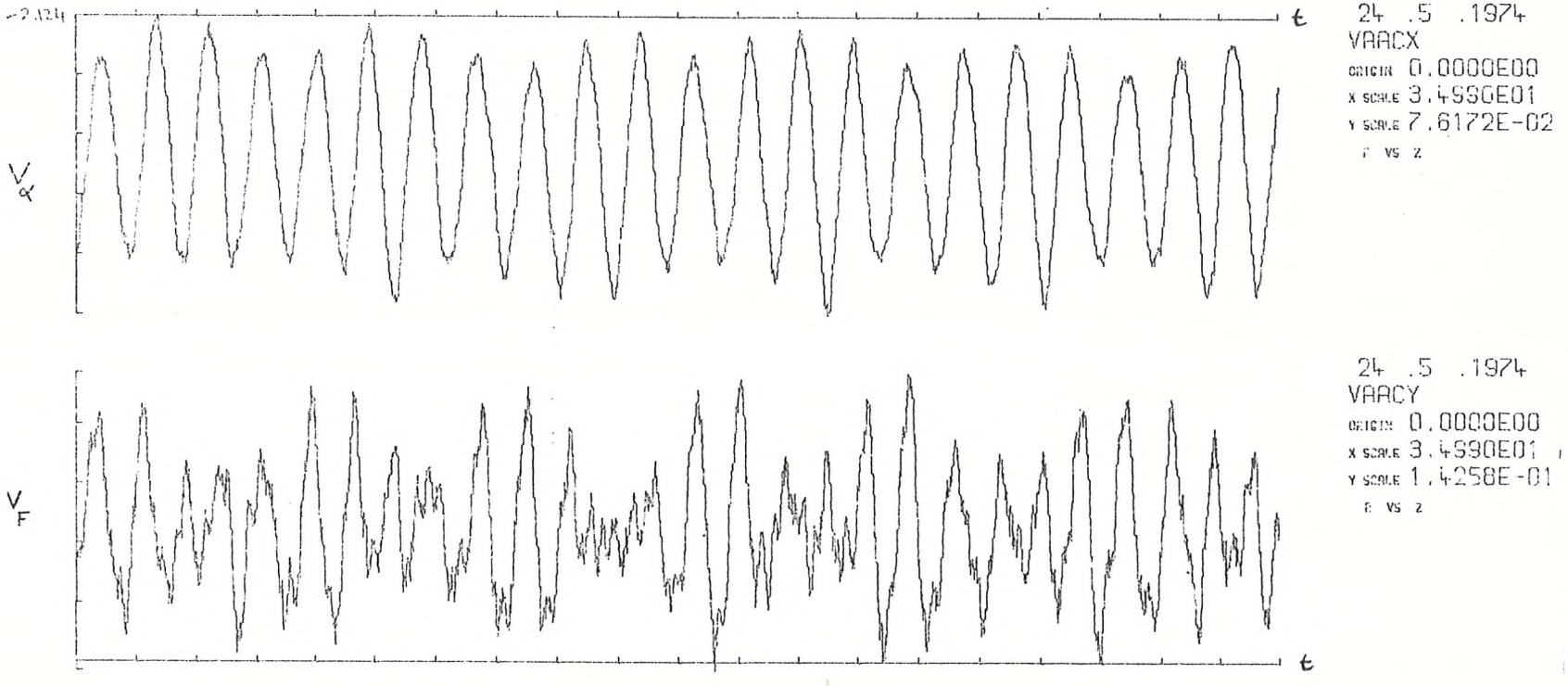
t
24 .5 .1974
VARCX
ORIGIN 0.0000E00
X SCALE 3.4590E01
Y SCALE 7.6172E-02
Y VS X
V_x
24 .5 .1974
VARCY
ORIGIN 0.0000E00
X SCALE 3.4590E01
Y SCALE 1.4258E-01
Y VS X
V_F
t

FIG. 7.39 (Cont.)

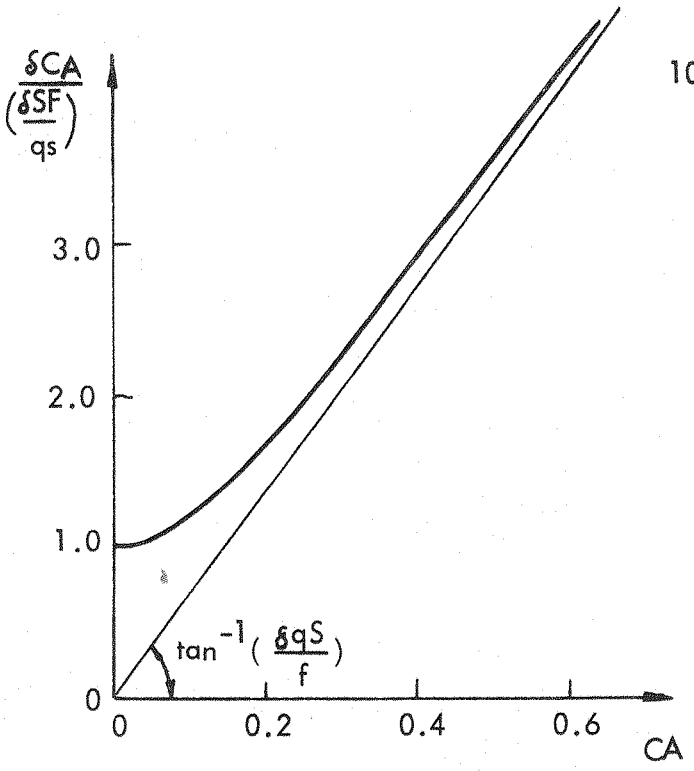

(a)

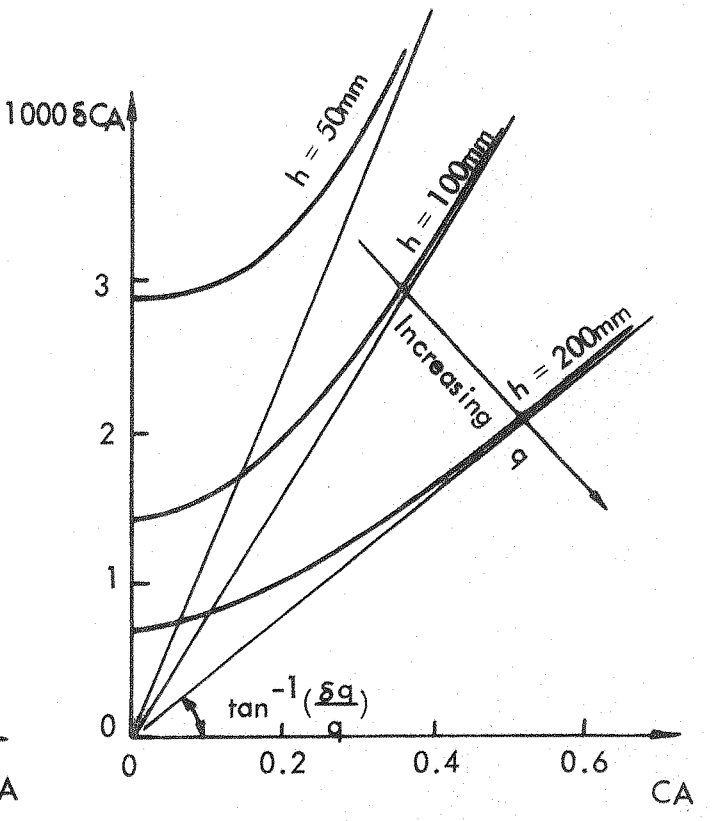

(b)

(h is flow manometer head methylated spirit)

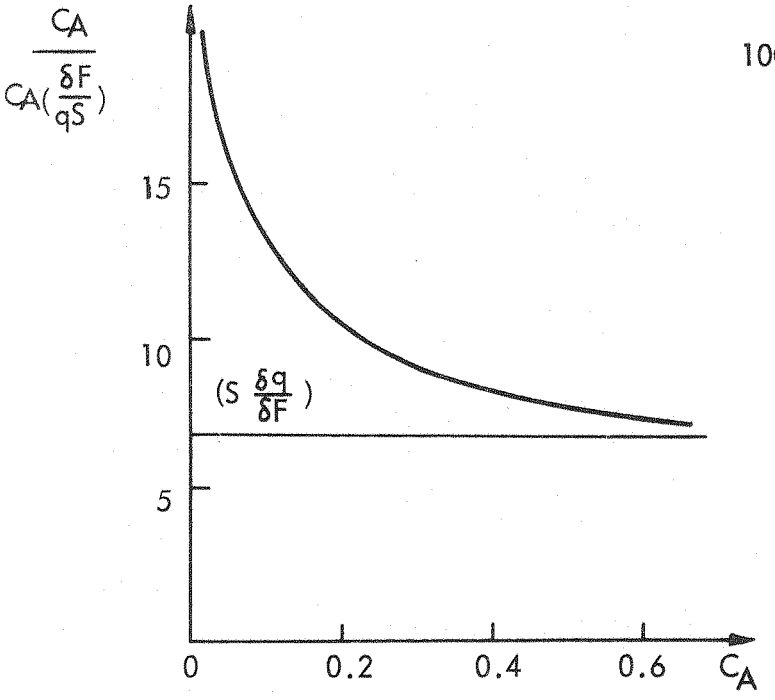

(c)

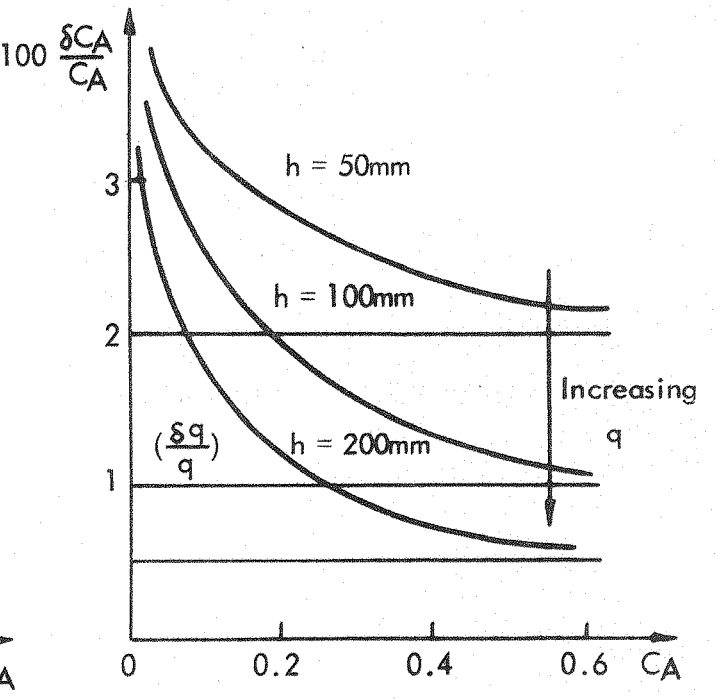

(d)

FIG. 7.40 VARIATION OF ERROR IN MEASURED AERODYNAMIC COEFFICIENT
$\delta q = 10\ N/m^2$, $\delta F = 0.01$ N.